

FOR REFERENCE ONLY

28 JAN 1999

ProQuest Number: 10290275

All rights reserved

INFORMATION TO ALL USERS

The quality of this reproduction is dependent upon the quality of the copy submitted.

In the unlikely event that the author did not send a complete manuscript and there are missing pages, these will be noted. Also, if material had to be removed, a note will indicate the deletion.



ProQuest 10290275

Published by ProQuest LLC (2017). Copyright of the Dissertation is held by the Author.

All rights reserved.

This work is protected against unauthorized copying under Title 17, United States Code
Microform Edition © ProQuest LLC.

ProQuest LLC.
789 East Eisenhower Parkway
P.O. Box 1346
Ann Arbor, MI 48106 – 1346

BL DLG
✓ 15/2/17

**THE USE OF ACOUSTIC EMISSION
TO MONITOR THE DEFORMATION OF A SOIL BODY**

JOHN GERARD KAVANAGH

**A thesis submitted in partial fulfilment of the
requirements of The Nottingham Trent University
for the degree of Doctor of Philosophy**

May 1997

10273091

40 0675707 9



To Mum & Dad

**The Use of Acoustic Emission
to Monitor the Deformation of a Soil Body**

**A thesis submitted in partial fulfilment of the
requirements of The Nottingham Trent University
for the degree of Doctor of Philosophy**

John Gerard Kavanagh

Abstract

This study has demonstrated that the phenomenon of acoustic emission can be used to detect and monitor first time deformation characteristics in stiff, heavily-overconsolidated clay soils.

The results from two field studies are presented and discussed with the aim of identifying the mechanisms responsible for the generation of acoustic emission. The first study, conducted at the Building Research Establishment's test site at Cowden (Humberside), was a section of cliff, naturally eroded by sea action. The second study, conducted in a 'moth-balled' brick-pit in Arlesey (Bedfordshire), was a large scale test in which instability was induced in a cut slope (in the Gault Clay) by cutting away at the toe. A number of different designs of *wave guide* were installed at both sites in order to determine the relative performance of each and, also, to provide further insight into the generation mechanisms. Some consideration has also been given to the effect of alternative data processing techniques.

The results obtained indicate that the *active* wave guide model is the more appropriate in explaining the occurrence of acoustic emission and this finding is supported by the results of laboratory tests designed to replicate the perceived role of the wave guide in the field. In itself, identification of the generation mechanism is a result but, more importantly, understanding of the mechanics enables the design of monitoring systems which are suited to particular geotechnical conditions.

Some comparison is also made between acoustic emission and standard methods of deformation monitoring. It is observed that acoustic emission can detect and clearly indicate disturbances at the same time as standard methods record such small magnitudes of movement as to be indistinguishable from instrument error.

Additionally, a number of triaxial shear tests were conducted on a selection of soils which illustrates that different soils do exhibit different acoustic characteristics.

Finally, this study demonstrates the feasibility of envelope processing using analogue to digital signal conversion both in the field and laboratory.

Four published papers pertaining to work described within this thesis are appended.

Acknowledgements

The research described herein was conducted at The Nottingham Trent University (where I was employed as a research assistant) and was jointly funded by the University and the Engineering and Physical Sciences Research Council (EPSRC).

I would like to thank my supervisors, Dr Neil Dixon (Department of Civil & Structural Engineering) and Dr Roger Hill (Department of Chemistry & Physics), for all the help, guidance, information and enthusiasm they have conveyed. In particular, Neil has played a very active role in the research. Apart from having acquired much relevant literature and equipment prior to my arrival at Nottingham Trent, he has also been the source of abundant 'drive'. Through his contact with Professor Eddie Bromhead, at the University of Kingston, he obtained a loan of their Traveller 30 rotary drilling rig which we used to install instruments at the BRE site and thanks are due, both to Professor Bromhead and the University of Kingston, for this.

In particular, thanks are due to Neil Dixon and John Cole for their tremendous efforts in helping to install instruments at the BRE test site and, without whom, installation would have been impossible. Thanks are also given to the Building Research Establishment for permitting us to use their site, the Royal Air Force for granting us access and to the Station Commander, George Phillips.

Thanks are due to Butterley Brick for permitting us to use their site at Arlesey and to Shanks & M^cEwan for allowing us access to it. Of particular help were Andy Cawley and Peter Naughton of Butterley Brick Ltd. and 'Melvyn' of Shanks & M^cEwan. The test could not have been conducted without the aid of a mechanical digger and, in this respect, thanks are due to Blackwell (the contractor working for Butterley Brick) and to the various drivers 'Dave', 'Dave' and 'Doug'. Thanks also to those colleagues who helped to install the instruments - Neil Dixon, John Cole and Ian Froggatt.

During the term of the project much help was forthcoming from many of the technicians employed by The Nottingham Trent University but particular thanks are due to Mr Rob Stickney, Mr Pete Langley, Mr Nick Howard and Mr Larry Wilson. I would also like to thank Miss Ann-Marie Priston (former research colleague at the Department of Chemistry & Physics, The Nottingham Trent University) for the many useful conversations concerning acoustic emission we shared.

Finally I would like to thank my friends Chris Benn (for his help at the BRE site) and John O'Brien and Pete Devito for their help in scanning a number of documents now contained within this thesis.

List of Contents

	Page
Dedication	i
Abstract	ii
Acknowledgements	iii
List of contents	iv
List of tables	viii
List of figures	ix
Chapter 1 Introduction	
1.1 Evolution of Acoustic Emission Monitoring Applied to Soil	1
1.2 Soil Behaviour and Acoustic Emission	2
1.3 Programme of Work	4
1.4 Original Contribution to Knowledge	5
1.5 Outline of Chapter Contents	6
Chapter 2 Literature Review	
2.1 Introduction	11
2.2 Acoustic Emission Measurement Criteria	11
2.3 Laboratory Investigations of Soil-AE Relationship	12
2.4 Soil-AE Fundamentals	
2.4.1 Frequency Content of Emission	19
2.4.2 Signal Attenuation	21
2.4.3 Wave Velocity & Prediction of Emission Magnitude	23
2.4.4 Relationship between Physical Characteristics & Soil-AE	25
2.4.5 Investigations of the Wave Guide	27
2.5 Applications of AE Strain Monitoring to Soil Masses in the Field	29
2.6 Other Geotechnical Applications of AE Monitoring	36
2.7 Literature Review Summary	37
Chapter 3 Acoustic Emission Instrumentation	
3.1 Introduction	76
3.2 Electronic Hardware & Software	
3.2.1 Transducer	76
3.2.2 Filter & Preamplifier	77
3.2.3 AET Model 204GR	77
3.2.4 Signal Enveloping Circuit	77
3.2.5 Analogue-to-Digital Conversion Board	78
3.2.6 The DacPac	79
3.2.7 The Computer	79
3.2.8 Software	79
3.3 The Wave Guide	79
3.4 Monitoring Philosophy	81
(i) Available Time	81
(ii) Electrical Power	81

	(iii) Hard-Disc Capacity	82
	(iv) Representative Sample	82
	(v) Signal Detail	82
3.5	Monitoring Procedure	83
3.6	Measurement Criteria	83
3.7	The Data	86
3.8	Data Set Problems	86
3.9	Acoustic Emission Instrumentation Summary	87
Chapter 4	Cowden Field Test	
4.1	Introduction	100
4.2	Site Description	100
4.3	Site Instrumentation	
4.3.1	Site Instruments	102
4.3.2	Instrument Installation	102
4.3.3	Borehole Logs	103
4.3.4	The Control Wave Guide	104
4.4	Instrument Monitoring	
4.4.1	Evolution of AE Monitoring Technique	104
4.4.2	Inclinometer Monitoring	106
4.4.3	Instrument Monitoring History	108
4.4.4	AE Analysis Database	114
4.5	Field Instrument Data Analysis	
4.5.1	Inclinometer Data	115
4.5.2	Acoustic Emission Data	
	(i) Introduction	117
	(ii) Wave Guides 1, 2 & 3	117
	(iii) Wave Guides 4, 5 & 6	118
	(iv) Wave Guides 8, 9, 10 & 11	119
	(v) Wave Guides 7 & 12	119
	(vi) Alternative Data Processing Techniques	119
4.5.3	Summary of AE & Inclinometer Field Data	120
Chapter 5	The Arlesey Large Scale Test	
5.1	Introduction	150
5.2	Site Description	150
5.3	Site Instrumentation	
5.3.1	Site Instruments	151
5.3.2	Instrument Installation	151
5.3.3	The Control Wave Guide	152
5.4	The Test	
5.4.1	The Test Site	153
5.4.2	Instrument Monitoring	
	(i) Arlesey Standard Monitoring Routine	154
	(ii) The Inclinometers	154
5.4.3	The Test - A Chronology	155
5.4.4	Instrument Monitoring History	156
5.5	Inclinometer Data Analysis	157

5.6	Analysis and Interpretation of Field Acoustic Emission Data	159
5.6.1	Introduction	160
5.6.2	Effect of Wave Guide Design	161
	(i) Wave Guide Backfill	162
	(ii) Wave Guide Length	162
	(iii) Arlesey Wave Guide 4 - Solid Steel Driven Bar	162
	(iv) Arlesey Inclinator 1 - Use as Wave Guide	162
5.6.3	Effect of Data Processing Technique	166
5.6.4	Signal-Time Relationship - A Closer Look	166
5.6.5	The Control Wave Guide	167
5.6.6	Background Noise	168
	(i) Airborne	168
	(ii) Electronic	168
	(iii) Constructional	169
Chapter 6	Implications of Cowden and Arlesey Results for AE Monitoring in the Field	
6.1	Introduction	214
6.2	The Nature of the Emission	214
6.3	The Active Wave Guide Model	
	6.3.1 Evidence for the Active Wave Guide Model	216
	6.3.2 Pedogenic Acoustic Emission	217
6.4	Application of Acoustic Emission to Deformation Monitoring	219
6.5	Data Processing Technique	221
6.6	Summary of Field Acoustic Emission Results	222
Chapter 7	The Laboratory Test Programme	
7.1	Introduction	238
7.2	Triaxial Test Apparatus	
	7.2.1 The Acoustic Emission Triaxial Testing System	239
	7.2.2 Relationship between the Principle Stresses and the Lower Chamber Pressure	240
	7.2.3 Axial Strain Generation	240
	7.2.4 Axial Ram Friction	241
7.3	Computer Interface with Triaxial Tests	
	7.3.1 Standard Laboratory Acoustic Emission Monitoring Routine	242
	7.3.2 Triaxial Cell Control and Monitoring	243
7.4	Test Soils	244
7.5	Triaxial Test Procedures	
	7.5.1 Soil Sample Formation	245
	7.5.2 The Triaxial Test Procedure	246
7.6	Consolidation Test Procedure	248
7.7	Box Tests	248
7.8	Introduction to Triaxial Apparatus Test Results	249
7.9	Results of Triaxial Shear Tests	
	7.9.1 Drained Triaxial Tests conducted on Leighton Buzzard Sand	250
	7.9.2 Change in Sample Volume due to Drainage	251
	7.9.3 Drained, Undrained & Consolidated Undrained Triaxial Shear Tests conducted on Leighton Buzzard Sand	254

7.9.4	Triaxial Shear Tests conducted on Leighton Buzzard, 'Arlesey' & 'Red' sands	256
7.9.5	Triaxial Shear Tests Conducted on Clays	257
7.10	The Consolidation Test	259
7.11	Box Tests	260
7.12	Laboratory Test Programme - Summary of Results	
7.12.1	Triaxial Test Results	262
7.12.2	Box Test Results	263
Chapter 8	Conclusions	
8.1	Field Investigations	333
8.2	Laboratory Investigation	335
8.3	Future Work	335
References		337

List of Tables

Table	Title	Page
4.1	BRE coastal cliff section instrumentation	122
4.2	Cowden instrument borehole logs	123
4.3	Summary of Cowden inclinometer & wave guide monitoring history	124
4.4	Data sets available for AE slope instability analysis	125
5.1	Arlesey test site instrumentation	170
5.2	Size by volume of the six Arlesey test cuts	170
5.3	AE & inclinometer monitoring history	171
7.1	Determination of axial ram friction	265
7.2	Test sand parameters from PSD curves	265
7.3	Individual conditions & results of tests using triaxial test arrangement	266
7.4	Summary of all tests using triaxial test arrangement by test type & material	271
7.5	Estimation of pore water pressures in samples at failure	273
7.6	Description of box tests	274

List of Figures

Figure	Title	Page
1.1	Title of first soil study by FD Beard	8
1.2	Generation of 'apparent' cohesion	9
1.3	Idealised model of soil generated acoustic emission	10
2.1	AE measurement criteria	38
2.2	Model slope test results	39
2.3	Relationship between AE and moisture content	40
2.4	Relationship between AE and soil grading	40
2.5	Earth dam model & results	41
2.6	Bearing capacity test model & results	42
2.7	Relationship between strain rate and AE	43
2.8	Prediction of failure time using AE	43
2.9	Relationship between energy and AE	44
2.10	AE in cyclic loading test	45
2.11	Strain-controlled triaxial test results	46
2.12	Stress-controlled triaxial test results	47
2.13	Triaxial test results and AE	48
2.14	Peak amplitude distributions with strain	48
2.15	Energy moment distribution	49
2.16	AE peak amplitude distribution	50
2.17	Improved AE peak amplitude distribution	50
2.18	Improved 'b-value'	51
2.19	Frequency distribution of clayey silt soil	52
2.20	Frequency distribution of silty sand soil	52
2.21	Frequency distribution of silty sand soil under compression	53
2.22	Frequency distribution of kaolinite clay	53
2.23	An example of frequency emission content	54
2.24	Frequency distribution of sand, silt & clay near failure	55
2.25	Attenuation for dry sand at various densities & frequencies	56
2.26	Relationship between signal level & source-receiver distance	56
2.27	Frequency vs attenuation of dry granular soils	57
2.28	Attenuation in clayey silt of 1kHz signal	57
2.29	Attenuation of different soil types with rock, coal, iron & steel	58
2.30	Collation of attenuation data	59
2.31	Comparison of AE amplitudes of different soil types	60
2.32	Frequency response vs wave guide length	61
2.33	Idealised function of wave guide	62
2.34	Noise rates vs displacement at Thornton Bluffs	63
2.35	Diagram of AE monitored earth dam	64
2.36	Settlement monitoring test set-up	65
2.37	Time-settlement-AE relationship	65
2.38	Schematic of slope failure field test	66
2.39	Results of slope failure field test	67

2.40	AE measurements prior to soil slip	68
2.41	AE response in dug trench test	69
2.42	Embankment AE monitoring - schematic & results	70
2.43	Slope AE monitoring - results	71
2.44	Relationship between AE & rainfall	72
2.45	Time series & power spectrum of AE event	73
2.46	Structure of AE monitoring rod	74
2.47	Relationship between deflection & AE of rod	75
2.48	AE distribution and bending moment of rod	75
3.1	Schematic representation of system	88
3.2	Sensor calibration curve	89
3.3	Notebook, DacPac & AET model 204GR	90
3.4	Measurement criteria	91
3.5	Wave guide and transducer attachment	92
3.6	Segment of standard data set	93
3.7	Wave envelope generated by 100 data points	94
3.8	Wave envelope generated by 100 data points, showing points	95
3.9	AET 'warming-up' problem	96
3.10	High data sets	97
3.11	Null data sets	98
3.12	Shifted data sets	99
4.1	Geographical location of BRE coastal cliff section	126
4.2	Soil profile at the Cowden site	126
4.3	Schematic diagram of the failure mechanism	127
4.4	Cowden instrument positions as at 11 November 1993	128
4.5	Schematic representation of inclinometer data	129
4.6	Tension crack around WG8 at 11 February 1994	130
4.7	Slip development at 10 March 1994	131
4.8	Cowden instrument array as at 11 November 1993 showing extent of slip surface as at 16 June 1994	132
4.9	Cowden instrument array as at 11 November 1993 showing relationship with slip surface as at 16 June 1994	133
4.10	Cowden instrument array depicting change in position between 11 November 1993 and 16 June 1994	134
4.11	Landslip as at 27 May 1994	135
4.12	WG11 as at 27 May 1994	136
4.13	Cowden inclinometer 1 change in mean deviation	137
4.14	Cowden inclinometer 2 change in mean deviation	138
4.15	Cowden inclinometer 1 displacement profile	139
4.16	Cowden inclinometer 2 displacement profile	140
4.17	Cowden inclinometers rates of movement	141
4.18	Dipped water levels in inclinometer casings	142
4.19	AE mean signal value WG's 1, 2 & 3 & 12	143
4.20	AE mean signal value WG's 4, 5, 6 & 12	144
4.21	AE mean signal value WG's 8, 9, 10, 11 & 12	145
4.22	AE mean signal value WG's 7 & 12	146
4.23	Alternative data processing techniques	147

4.24	Dipped water level and movement rate inclinometer 1	148
4.25	AE mean signal value WG's 1 & 9 and 5 & 10	149
5.1	Geographical location of Arlesey, Bedfordshire	172
5.2	Perspective view of site	173
5.3	Test slope showing instruments & cuts, plan view	174
5.4	View of site illustrating very wet conditions	175
5.5	Test slope with cross-section, plan view	176
5.6	Site profile	177
5.7	Test cuts 1-6, 3-D schematic	178
5.8	Test slope profiles	179
5.9	View of test slope and five marked test cuts	180
5.10	Illustration of test cut 2 in progress of being made	181
5.11	Debris from slope collapse	182
5.12	Spoil levelling following test cut 6	183
5.13	Change in mean deviation inclinometer 1	184
5.14	Change in mean deviation inclinometer 2	185
5.15	Displacement profile inclinometer 1	186
5.16	Displacement profile inclinometer 2	187
5.17	Change in mean deviation (I1 @ 1.5m & I2 @ 0m)	188
5.18	Displacement profile (I1 @ 1m & I2 @ 0m)	189
5.19	AE mean signal value WG's 1 & 7	190
5.20	AE mean signal value WG's 2 & 7	191
5.21	AE mean signal value WG's 3 & 7	192
5.22	AE mean signal value WG's 4 & 7	193
5.23	AE mean signal value WG's 5 & 7	194
5.24	AE mean signal value WG's i & 7	195
5.25	AE mean signal value WG's 1, 2 & 3	196
5.26	AE mean signal value WG's 1, 2 & 3 & I1 displacement profile at 1.0m depth for period cut 5 - cut 6	197
5.27	AE mean signal value WG's 1, 2 & 3 & I1 displacement profile at 1.0m depth for period following cut 6	198
5.28	AE mean signal value WG's 2 & 5	199
5.29	AE standard deviation WG's 2 & 5	200
5.30	AE mean signal value, standard deviation & root means square WG2	201
5.31	AE standard deviation WG's 1, 2 & 3	202
5.32	AE mean signal value, post threshold WG's 1 & 2	203
5.33	AE standard deviation, post-threshold WG's 1 & 2	204
5.34	AE mean signal value bulk & standard deviation post-threshold WG2	205
5.35	AE standard deviation post-threshold WG's 4 & 7	206
5.36	AE response-cut relationship cuts 1 & 2	207
5.37	AE response-cut relationship cuts 3 & 4	208
5.38	AE response-cut relationship cut 5	209
5.39	AE response-cut relationship cut 6	210
5.40	Effect of wave guide covers	211
5.41	AE mean signal value electronic noise & WG 7	212
5.42	AE standard deviation post-threshold electronic noise & WG 7	213

6.1	AE mean signal value bulk data WG's 1 & 2	227
6.2	AE standard deviation bulk data WG's 1 & 2	228
6.3	AE mean signal value post-threshold WG's 1 & 2	229
6.4	AE standard deviation post-threshold WG's 1 & 2	230
6.5	Average no. data points per event vs total no. data points Arlesey	231
6.6	No. of events vs \log_{10} no. data points Arlesey	232
6.7	Average no. data points per event vs total no. data points Cowden	233
6.8	Average no. data points per event vs total no. data points Arlesey & Cowden	234
6.9	Comparison of Arlesey & Cowden control wave guide response	235
6.10	Event mean magnitude distribution WG's 1 & 2, days X1 & X7	236
6.11	AE standard deviation bulk & post-threshold data WG 2	237
7.1	Schematic of AE monitoring system & triaxial test apparatus	275
7.2	Schematic of Bishop & Wesley triaxial cell	276
7.3	GDS digital controller	276
7.4	PSD curves for 'Red', 'Arlesey' & Leighton Buzzard sands	277
7.5	Box test equipment cross-section & plan view	278
7.6	q vs axial strain for drained tests conducted on Leighton Buzzard Sand	279
7.7	Mohr stress circles for drained tests conducted on Leighton Buzzard Sand	280
7.8	q_{\max} vs p' for drained tests conducted on Leighton Buzzard Sand	281
7.9	q_{\max} vs work for drained tests conducted on Leighton Buzzard Sand	282
7.10	AE mean, standard deviation & root means square vs p' for drained tests conducted on Leighton Buzzard Sand	283
7.11	AE mean, standard deviation & root means square vs work for drained tests conducted on Leighton Buzzard Sand	284
7.12	Event map (mean magnitude) for tests TR50, 51, 54, 59 & 60	285
7.13	Mean event magnitude frequency distribution for tests TR50, 51, 54, 59, 60	286
7.14	Change in sample volume for drained tests conducted on Leighton Buzzard Sand	287
7.15	q vs axial strain for unconsolidated undrained tests conducted on Leighton Buzzard Sand	288
7.16	Mohr stress circles for unconsolidated undrained tests conducted on Leighton Buzzard Sand	289
7.17	q_{\max} vs p' for drained, consolidated undrained & unconsolidated undrained tests conducted on Leighton Buzzard Sand	290
7.18	q_{\max} vs p' for drained, consolidated undrained & unconsolidated undrained tests conducted on Leighton Buzzard Sand	291
7.19	AE mean vs work for drained, consolidated undrained & unconsolidated undrained tests conducted on Leighton Buzzard Sand	292
7.20	Number of counts vs events for drained, consolidated undrained & unconsolidated undrained tests conducted on Leighton Buzzard Sand	293
7.21	AE mean vs number of events for drained, consolidated undrained & unconsolidated undrained tests conducted on Leighton Buzzard Sand	294
7.22	Mean magnitude frequency distribution for tests TR56, 60 & 62	295
7.23	q vs axial strain for tests conducted on 'Arlesey' sand	296
7.24	q vs axial strain for tests conducted on 'Red' sand	297
7.25	Mohr stress circles for undrained tests conducted on 'Arlesey' sand	298
7.26	Mohr stress circles for undrained tests conducted on 'Red' sand	299
7.27	q_{\max} vs work for tests conducted on Leighton Buzzard, 'Arlesey' & 'Red' sands	300

7.28	AE mean vs work for tests conducted on Leighton Buzzard, 'Arlesey' & 'Red' sands	301
7.29	Number of counts vs events for tests conducted on Leighton Buzzard, 'Arlesey' & 'Red' sands	302
7.30	AE mean vs number of events for tests conducted on Leighton Buzzard, 'Arlesey' & 'Red' sands	303
7.31	Number of events vs work for tests conducted on Leighton Buzzard, 'Arlesey' & 'Red' sands	304
7.32	Mean magnitude frequency distribution for 'Arlesey' sand	305
7.33	Mean magnitude frequency distribution for Leighton Buzzard, 'Arlesey' & 'Red' sands	306
7.34	q vs axial strain for tests conducted on Gault Clay & Mercia Mudstone	307
7.35	Mohr stress circles for tests conducted on Gault Clay & Mercia Mudstone	308
7.36	q _{max} vs moisture content for tests conducted on Gault Clay & Mercia Mudstone	309
7.37	Work vs moisture content for tests conducted on Gault Clay & Mercia Mudstone	310
7.38	q _{max} vs work for tests conducted on Gault Clay & Mercia Mudstone	311
7.39	AE mean vs work for tests conducted on Gault Clay & Mercia Mudstone	312
7.40	AE mean vs number of events for tests conducted on Gault Clay & Mercia Mudstone	313
7.41	Number of counts vs events for tests conducted on Gault Clay & Mercia Mudstone	314
7.42	q _{max} vs work for 48 tests conducted on sands & 17 on clays	315
7.43	AE mean vs work for 48 tests conducted on sands & 17 on clays	316
7.44	Number of counts vs events for 48 tests conducted on sands & 17 on clays	317
7.45	Event distribution (mean magnitude) for 4 consolidation cycles	318
7.46	Event distribution (counts) for 4 consolidation cycles	319
7.47	Cumulative count for 4 consolidation cycles	320
7.48	Box tests B4 & B5 by event mean magnitude	321
7.49	Box tests B4 & B5 by number of data points per event	322
7.50	Cumulative count for Box tests B4 & B5 vs time	323
7.51	Box tests B7 & B8 by event mean magnitude	324
7.52	Box tests B7 & B8 by number of data points per event	325
7.53	Cumulative count for Box Tests B7 & B8 vs time	326
7.54	Cumulative count for Box test B8 vs time	327
7.55	Box test B10 by event mean magnitude	328
7.56	Box test B10 by number of data points per event	329
7.57	Cumulative count for Box test B10 vs time	330
7.58	Box tests B8 & B10 by event mean magnitude	331
7.59	Event map & q vs axial strain for triaxial shear test TR11	332

Chapter 1

Introduction

1.1 Evolution of Acoustic Emission Monitoring Applied to Soil

The phenomenon of acoustic emission (AE) generated by a deforming body of soil evolved from comparative studies in rock where it was observed that failure, such as collapse or rock bursts, was often preceded by an audible emission. Initially, investigations were concerned with mining and tunnelling applications but were extended to include cut and natural slopes; the predominant constituent geologic material of interest being rock. However, once investigations started to focus on surface material, the application of the technique to soil stability was only a logical step.

The earliest work accredited to having specifically investigated soil (as opposed to rock) was entitled 'Predicting slides in cut slopes'. Appearing in a publication called 'Western Construction' it described the successful use of the 'Seismitron', an instrument designed to detect microseisms (acoustic emission), and the article proudly announced 'First results are highly promising'. The item, written by FD Beard (figure 1.1), was published in September 1961!

However, even this work was primarily concerned with rocks and, concerning soil, Beard would only concede that ...

"Certain soft materials such as sand, clay, mud, etc., do not produce microseisms that are clearly definable".

It was more fundamental field and laboratory investigations conducted in the USA (by researcher's such as Koerner, Lord and Hardy) in the 1970's and 1980's which clearly established the link between the acoustic emission and the type of soil being examined and the process affecting it. Additionally, by the middle of the 1970's Japanese workers (primarily Tanimoto) had also started to play an increasingly important role in this area of research.

Although chapter 2 details the findings of past works and presents an appraisal of them, it should be appreciated that a good deal more work pertaining to AE in a geologic environment than is discussed in chapter 2 exists. However, it is considered that much of this is largely peripheral to this research (particularly studies in rock) and is not, therefore, referred to. For those interested in the broader perspective, Hardy (1989) reviews research, relating to the geotechnical field application of AE, being conducted in nineteen countries and Hardy (1994) presents an historical review of similar studies conducted at the Pennsylvania State University.

It should be made clear at the outset that this investigation is wholly concerned with soil; with a granular medium consisting of discrete particles and not with rock where a substantial contribution to the material's strength may be derived from an element of true inter-particle cohesion. Specifically, attention has been focused on the detection of first-time deformation processes in stiff clay soils.

1.2 Soil Behaviour and Acoustic Emission

Soil is a granular material consisting of solid particles and fluid filled voids; the fluid usually being air and/or water. When subjected to a change in the stress regime a soil body responds by straining and, because the soil is an assemblage of discrete particles, this involves some reorganisation of the constituent particles. For example, simply subjecting a soil sample to an all round pressure (in the drained state) forces the soil grains to come into closer contact with one another. Although this investigation is primarily concerned with modes of shear deformation (soil being weak in tension) the important point is that soil strain involves *relative* particle movement. However, exactly how the soil responds to a particular change in the stress regime is governed by its nature and stress history.

When a differential exists between the principal stresses acting on a soil body then shear stresses are generated. The shear stresses strain the soil and the strain *mobilises* soil shear strength. Coulomb (1766) formulated the following equation to describe the strength envelope of a soil (which has been modified in order to describe shear strength in terms of effective rather than total stresses):-

$$\tau = c' + \sigma' \tan \phi'$$

where τ is the shear strength, c' is the *apparent* cohesion, σ' is the normal effective stress and ϕ' is the angle of shearing resistance. 'Cohesion' does not usually refer to a genuine component of soil strength but is used to describe the intercept of the failure envelope with the τ axis on a $\tau - \sigma'$ plot (figure 1.2). Hence the soil's resistance to shear is dependent upon the effective stress (i.e. after allowing for any pore water pressures) and the parameter ϕ' . Note that ϕ' is a true soil parameter and its value is dependent upon the nature of the soil. In particular, it reflects volume change, occurring in the shear zone, as a soil responds to shear stresses.

A model which explains the behaviour of soil, after an increment of shear stress has been applied, as particles sliding past one another under pressure, is attractive when attempting to explain the generation of AE. It can be envisaged that the AE produced is the sum effect of the frictional characteristics of the soil grains, the total particle surface area involved in sliding (related to volume change) and the normal effective stress. Of greater consequence to this investigation, however, is that the emission is generated as a result of the strain and, in effect, provides a means of strain monitoring and measurement.

Figure 1.3 is a schematic representation of the model showing the relationship between an applied shear stress (F), the mobilised shear strength (τ) and the normal effective stress (σ'). Clearly the magnitude of the contact area, the normal effective stress and the frictional characteristics of the material will all contribute to the generation of the AE.

It is emphasised that this is only intended as a simple consideration of factors which might be significant in the generation of AE from soil. The behaviour of soil particles under shear is more complicated than described above and the mechanisms responsible for the generation of AE in field situations is still a subject of debate. For reasons which will become evident, in field applications of AE, it is necessary to utilise a *wave guide*. This is essentially an instrument which facilitates the capture of field generated AE and is, in itself, a subject of some research. Wave guides are discussed further in section 2.4.5, section 3.3, chapter 4, chapter 5 and chapter 6.

This research is principally concerned with the application of acoustic emission to the monitoring of soil slope stability. All slopes are inherently unstable structures in which a differential in the principal stresses is tending to bring the body to failure. In many circumstances the soil or rock body can mobilise enough strength to resist these tendencies and

maintain equilibrium but in many circumstances it cannot, especially where the stresses are changing due to, for example, erosion of a natural slope or construction of an earth embankment.

Slope failure can be classified into three main groups - slides, falls and flows. This investigation is wholly concerned with slides as this is the most commonly encountered mechanism. Although it is tempting to visualise blocks of sliding soil generating frictional noise, clearly pre-failure deformation is of more interest as there can be little point in developing monitoring systems without some element of intended prediction or forewarning of failure.

Current methods of slope deformation monitoring measure the *macroscopic* effects of instability. Extensometers determine the change in width of surface tension cracks. Inclinometers (section 4.4.2) determine the change in lateral position of various points at depth in the slope. However, the fact that such macroscopic defects are observable indicates that much deformation has already taken place. AE is produced by (or as a result of) the *microscopic* response of the soil and it is this aspect which makes the phenomenon so potentially useful in detecting and measuring pre-failure deformation.

1.3 Programme of Work

This research project, which commenced in September 1992, comprises three basic work units - two field studies and a laboratory test programme. The first field study centred on a section of coastal cliff at the Building Research Establishment's test site, based at Cowden in Humberside, and which is naturally eroded by sea action. This was the main focus of attention between September 1993 and May 1994. The second field study consisted of a large scale test conducted on a cut slope in a 'moth-balled' brick-pit in the Bedfordshire town of Arlesey and this was the main focus of attention between September 1994 and May 1995. The main laboratory test programme occupied the final three months of the project, from July 1995 to September 1995.

It should be borne in mind that the above two sites were only subsequently selected after considering (in the first study) a number of other coastal locations in Yorkshire and Norfolk, and (in the second study) a brick-pit in Nottinghamshire. Additionally, a considerable part of the first year was spent in assembling and assessing components for the AE monitoring system.

Furthermore (during the three year period) the literature search was completed, a number of presentations on the work were given and a number of conference papers published.

1.4 Original Contribution to Knowledge

This research has clearly demonstrated the feasibility of using acoustic emission to detect and monitor first time deformation characteristics (i.e. shear zone development) in heavily-overconsolidated clay soils. It has also demonstrated the feasibility of envelope processing using analogue to digital signal conversion both in the field and laboratory. In particular, it has also achieved the following:-

- (i) The production of a model which describes the mechanisms responsible for the generation of acoustic emission in the field. In particular, evidence acquired at the field sites suggests that the *active* wave guide model (as opposed to the passive) is the more appropriate in explaining the nature and occurrence of a field emission. This contention has also been supported by the results of a number of laboratory based tests designed to replicate the perceived role of the active wave guide in the generation of a field emission. This should not be interpreted as meaning that pedogenic AE is non-existent or not detected by the monitoring system. However, there is no evidence to suggest that any such pedogenic AE is significant.
- (ii) The determination that the constructional features of a wave guide may be responsible for the generation of emission.
- (iii) The determination, in the laboratory, that increased acoustic activity is due to the generation of a greater number of similarly sized events rather than the generation of events of increased magnitude.
- (iv) The identification of two different field AE characteristics related to two different modes of generation. The first, consisting of relatively large magnitude emission generated over a short duration of time, is considered to arise as a result of a sudden disturbance to the soil mass. The second, consisting of relatively small magnitude

emission generated over a more sustained period, is considered to arise in response to a more gradual, longer-term, deterioration in slope stability.

- (v) Two case histories illustrating the potential use of acoustic emission in the detection of first-time deformation mechanisms in stiff, heavily-overconsolidated clay soils, have been provided. The effects of different wave guide design and different signal processing techniques have been explored and a *control* wave guide (section 3.3) has been introduced for the first time.

1.5 Outline of Chapter Contents

Chapter 2 contains the literature survey which presents a review of all relevant material. It concentrates on works centred on field and laboratory investigations which examine the relationship between AE and soil in a state of strain. Some mention is also made of the application of AE to other geotechnical situations such as seepage monitoring and penetration tests. The review is divided into six sections. The first is an introduction and the second describes some of the means of measuring acoustic emission, of which some knowledge is necessary in order to understand the literature review. Of the last four sections, the first deals with general laboratory soil-AE investigations, the second deals with studies of fundamental properties of soil-AE, the third with field soil-AE investigations and the fourth with other geotechnical AE applications.

Chapter 3 details the components of the AE monitoring system. It describes the function of each component and discusses the role of the wave guide in field applications. Consideration is also given to monitoring philosophies. Monitoring procedures are detailed and AE measurement criteria stated.

Chapter 4 concerns the Cowden field study. It describes the site and details instrumentation, instrument installation, site monitoring and presents the results. It also includes a detailed section concerning the use of *inclinometers*; explaining the data acquired and the relevance of the various processing techniques. As Cowden was the first field study, the evolution of the AE monitoring routine is also outlined.

Chapter 5 concerns the Arlesey large scale test. It describes the site and details instrumentation, instrument installation and the structure of the test. It also describes site monitoring and presents the results. The effects of wave guide design and data processing technique are analysed and special consideration is given to the topics of background acoustic noise and the control wave guide. Where necessary, results from the Cowden field study are drawn on and used to aid analysis.

Chapter 6 examines the findings of the Cowden and Arlesey field studies (jointly) in an attempt to ascertain the mechanisms responsible for AE generation and to present a descriptive model. It discusses the application of AE to deformation monitoring and makes qualitative recommendations concerning the suitability of particular instrument designs and data processing techniques to particular geotechnical situations.

Chapter 7 deals with the laboratory test programme. It details for each test type (triaxial shear, consolidation and 'box' tests) test equipment, test procedure, monitoring routine and results. Inference is made concerning the mechanisms responsible for AE generation and (where possible) the laboratory test results are used to support the field test results.

Chapter 8 summarises the findings of this research and makes some recommendations concerning future work.

Predicting slides in cut slopes

An instrument called the Seismitron, used for years in mines and tunnels to give advance warning of failures, is now being tried on surface excavations. First results are highly promising.

**By F. D. BEARD
Senior Engineer
Liberty Mutual Insurance Co.
San Francisco, California**

Figure 1.1 Title of first accredited study into soil generated AE by FD Beard in Western Construction, September 1961

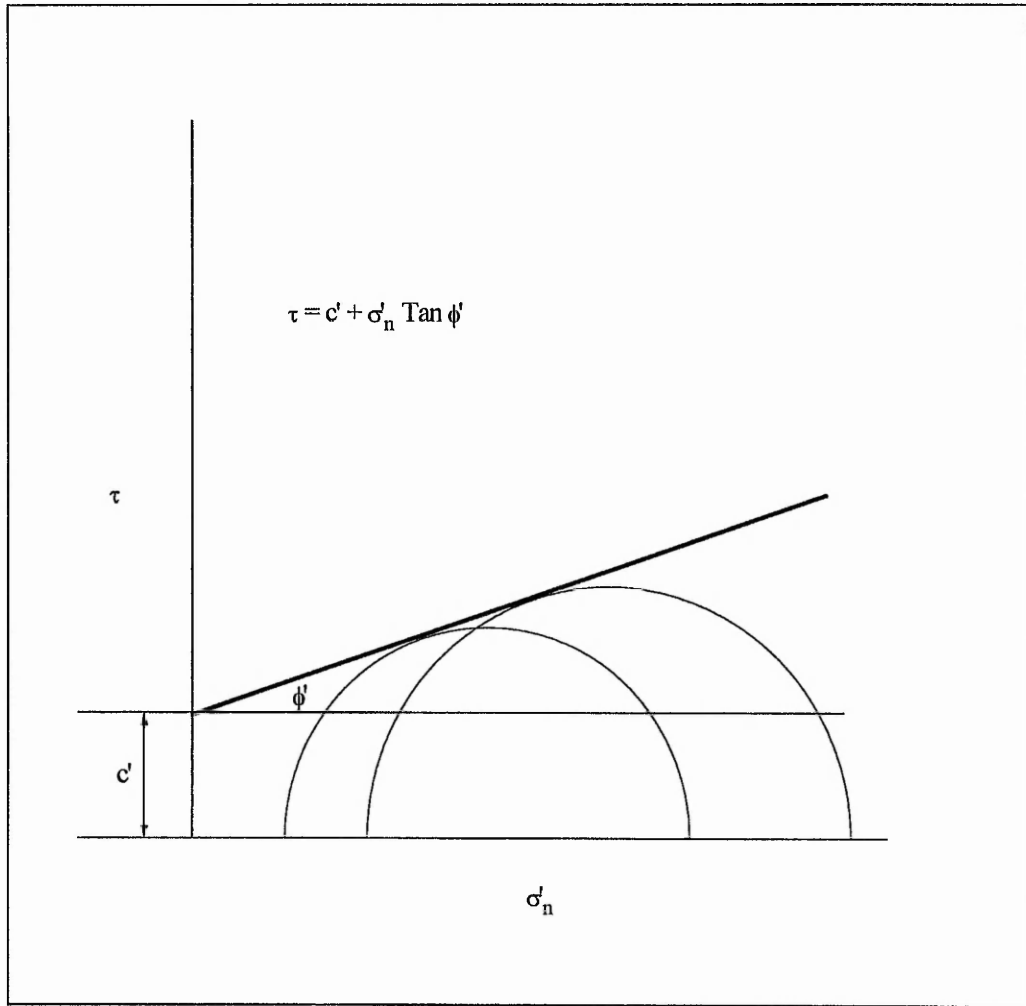


Figure 1.2 Generation of apparent cohesion (c') by extending the failure envelope to intercept the y-axis (t).

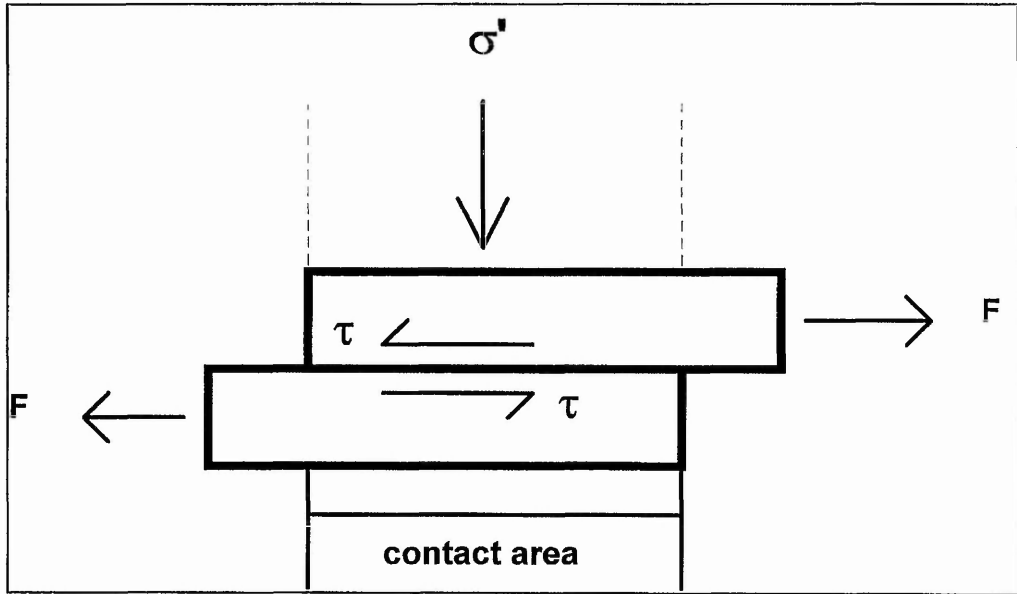


Figure 1.3 Idealised model depicting factors responsible for the generation of acoustic emission from a soil body.

Chapter 2

Literature Review

2.1 Introduction

Before proceeding with the review of past works, it is necessary to have some understanding of the various methods used to quantify an acoustic emission and section 2.2 describes some of the commonly used parameters. The literature review itself is sub-divided into four sections. Section 2.3 details general laboratory based tests designed to investigate the relationship between soil (under various conditions) and any generated acoustic emission. Section 2.4 examines soil acoustic emission fundamentals. These include (for example) wave velocity and attenuation in soil as an acoustic medium. Literature relating to investigations of the wave guide is also included in this section, as this is considered to be a fundamental requirement for monitoring acoustic emission in the field. Section 2.5 examines field investigations, and large scale tests, of acoustic emission to detect instability in soil masses. Section 2.6 briefly examines literature relating to other geotechnical applications of acoustic emission such as the development of in-situ pressuremeter testing equipment and seepage detection.

2.2 Acoustic Emission Measurement Criteria

Resonant sensors used to detect an acoustic emission respond by producing a decaying transient sinusoidal signal. Such a typical response is illustrated in figure 2.1 and a number of alternative methods by which the wave form can be quantified are shown. The traditional AE measurement parameters are the *ringdown* count and event count. A ringdown count is simply an upward crossing by the signal (rising edge) of some threshold value pre-determined to eliminate background noise (section 3.3). Figure 2.1 shows nine counts constituting a single event. Two event describing parameters, peak amplitude and rise time, are also shown and defined on the figure.

It is important to appreciate that (considering narrow band transducers as used in this investigation) all measurement criteria relate to the sensor's *response* to an emission and not to

the emission's actual wave form propagating through the soil. An introduction to AE sensors and measurement criteria is given by Nakamura (1977). Although dealing with a particular application, Dixon *et al.* (1994) also provides a general introduction to the use of AE (but from a broader perspective) and provides some historical background. Further detail of the sensor used in this investigation is given in section 3.2.1.

Finally, it should be noted that the signal described in figure 2.1 is (in this investigation) further processed before being analysed. This step is dealt with in section 3.2.4.

2.3 Laboratory Investigations of Soil-Acoustic Emission Relationship

One of the earliest laboratory based investigations of soil generated AE, by Cadman & Goodman (1967), consisted of a series of tests in which small slopes of saturated sand were brought to failure by tilting. Four Rochelle-salt, bender, crystal transducers were installed within the sand as the 45° slopes were constructed. The aim of the investigation, to locate the source of the emission (which was calculated by consideration of differences in arrival times of individual events at each sensor), was reasonably successful as figure 2.2 illustrates.

Koerner & Lord jnr (1972) published the first of many fundamental works on soil-AE relationships with a study of a medium plasticity clay. Samples of the soil, at different moisture contents, were subjected to unconfined compression tests and the emission monitored in terms of counts. The sensor used was an accelerometer described as having a response which was 'flat from a few hertz to about 6,000Hz'. The accelerometer was mounted to the sample in one of three different fashions, reflecting the different soil properties due to the varying moisture contents. Two of the methods involved inserting the sensor, either partially or totally, into the sample and it is possible that this intrusive method may have resulted in some noise being generated as a result of soil-sensor interaction - particularly under load. Never-the-less, the results (figure 2.3) illustrated that the level of recorded emission increased as axial stress increased and moisture content decreased.

Lord jnr & Koerner (1974) examined the response of five dry soils with different gradings. The soils were formed by 'blending' specific proportions of two 'parent' soils, one a sand and the other a clayey silt. The samples were tested in unconfined compression using the same

accelerometer as Koerner & Lord jnr (1972) but with the addition of a short wave guide which was inserted into the sample. The results indicated that the greater the proportion of sand particles present the greater the level of emission, as recorded in terms of counts and these are illustrated in figure 2.4. The authors also used equipment which is responsive to high frequencies to determine that soil generated AE is 'well below' 100kHz.

Koerner & Lord jnr (1974) subjected a number of samples of a clayey silt, at varying moisture contents, to a series of isotropic consolidation and triaxial shear compression tests. Again, the results demonstrated that increasing levels of stress generated a greater magnitude of emission (measured in counts). This is probably the first documented use of acoustic emission monitoring in triaxial shear.

Koerner *et al.* (1975) described (among other aspects) two laboratory experiments designed to replicate soil failure mechanisms in the field. The first experiment utilised a large box with an adjustable segmented base upon which was constructed a model earth dam. The soil used in the construction was described as a clayey silt and a number of tests were conducted using different moisture contents. After the dam had been constructed, failure was induced by lowering the segmented base. Acoustic emission was monitored with a Columbia 476 accelerometer which was described as having a reasonably flat response from a few Hz to 5000Hz. The authors found that most of the emission was generated immediately after the deformation was initiated and that the total number of acoustic emission counts reached a peak when the soil recorded its optimum moisture content (figure 2.5). This they reasonably explained as being due to more inter-particle contact occurring at maximum density. The authors also commented upon the low number of counts generated which they attributed to the lack of confining pressure.

The second experiment consisted of a steel plate being vertically pressed into a sample of dry Ottawa sand in order to generate a bearing capacity type failure mechanism within the sand. The results, depicted in figure 2.6, indicate that there is a good relationship between the load-deflection and load-AE curves.

Tanimoto & Noda (1977), who were particularly interested in the prediction of failure, conducted a series of stress and strain controlled drained triaxial shear tests on saturated samples of well graded sands. Using a 40kHz transducer, they identified two AE processes in which the emission (measured as a count rate in counts per minute) first climbed to a peak value and then

remained constant at that value until failure. The authors showed that the count rate during this second, or 'steady-state', process was directly proportional to the strain rate (figure 2.7). In an attempt to remove the effects of confining pressure (cell pressure), the authors defined an emission rate R as being the result of the total number of counts in the first thirty seconds of the steady-state process divided by the total number of counts in the first process. Additionally, this was plotted against failure time which, for each test, was defined as the time from the test start to failure point. Figure 2.8 plots the results, which indicates a good linear correlation between failure time and $\log R$, for strain controlled tests. A similar relationship was found to exist for stress controlled tests.

Tanimoto *et al.* (1978) extended the investigations of the previous work to include a wider range of soils and test parameters (using a 40kHz transducer). Again the authors generated a good linear correlation between failure time and $\log R$ which appeared to be independent of the cell pressure, strain rate, moisture content, dry density of the sample, sensitivity of the sensor and the threshold employed. They also introduced the concept of calculating the work done in deforming the soil sample by consideration of applied stresses and measured strains. Figure 2.9 depicts the authors' results for a number of tests which indicate a good linear correlation. Note that energy (E) is plotted against cumulative counts (N) and that figures for both the first process only and for the test totals are shown (E_1 & N_1 - first process, E_T & N_T -totals). The authors also describe a repetitive loading test, in which the point of maximum previous stress is identified using the *Kaiser effect*, and comment themselves that the emission 'can be monitored only in the virgin state of loading'. The authors' results are illustrated in figure 2.10.

Tanimoto & Nakamura (1981a) further extended the previous two works by improving the triaxial apparatus. This, essentially, amounted to measuring the volume of water flowing into or out of the cell in order to determine volumetric strain. Additionally, the authors switched from using the 40kHz transducer in the previous investigations to using a transducer described as having a flat response from 4Hz to 17KHz in this investigation. One test sand was employed and similar relationships as previously determined were illustrated again. Figure 2.11 depicts deviator stress, emission count rate and volumetric strain plotted as a function of axial strain. The figure indicates that the change from an increasing to a constant count rate occurs at the point where sample contraction changes to dilation.

It must be commented that it is difficult to understand the emphasis being put upon the conducting of both stress and strain controlled tests. It is widely accepted by Tanimoto and his various co-workers that the acoustic emission is generated by inter-particle friction. It seems only too reasonable, therefore, that there ought to be a relationship between the rate of strain and the count rate (i.e. faster strain rates produce greater count rates because there is more movement per unit time). Use of stress controlled tests merely masks this fundamental relationship. Consider figure 2.12 which depicts the results of such a stress controlled test as reported by Tanimoto & Nakamura (1981a) in the same form as that in figure 2.11. At the point identified as ϵ_i by the authors, both tests indicate that axial strain of approximately 2% corresponds with a deviator stress of 600kPa (all other test parameters being equal). However, at this point, the strain controlled test records a count rate of approximately 1500 counts per minute compared with the stress controlled test's equivalent figure of approximately 300 counts per minute. The difference lies in the strain *rates*, which both Tanimoto & Noda (1977) and Tanimoto & Nakamura (1981a) identified as being directly proportional to the count rate (in the 'steady state' process). In the strain controlled test, the rate used was 0.6% per minute, implying that ϵ_i had been reached after some three to four minutes of testing. In the stress controlled tests the rate used was 70.4kPa per minute, implying that ϵ_i had been reached after some eight or nine minutes which corresponds to a strain rate of approximately 0.25% per minute. Clearly, therefore, it would be expected that the stress controlled test would exhibit a lower count rate than the strain controlled test. Furthermore, this can be used to explain the apparent difference between the constant response of the strain controlled test in the 'steady state' process and the increasing response of the stress controlled test. In the former, a constant strain rate infers a specific magnitude of movement in unit time and, therefore, a constant count rate. In the latter although the soil hardens in response to strain, it does so at a reducing rate. As the deviator stress is applied at a constant rate (in terms of kPa per minute) this will obviously result in greater magnitudes of strain being generated in unit time and also, therefore, greater count rates. Nevertheless, the point ϵ_i does demarcate two distinct physical processes.

Mitchell & Romeril (1984) tested two clay and two sand soils by bringing them to passive failure in a special box with a hinged wall. The authors recorded acoustic emission (in terms of volts and cumulative events), angle of wall rotation and the average wall stress. It was concluded that the emission was 'stronger' and the rate of acoustic emission events 'higher' in course grained soils than in fine grained soils.

Koerner *et al.* (1984a) was the first of three papers to specifically investigate the potential use of acoustic emission to predict pre-consolidation pressure in the field and it reported a laboratory-based investigation of granular soils. Using a consolidometer, the authors first loaded and then completely unloaded a soil sample before reloading it. During the reload cycle deformation and acoustic emission were both measured. A series of eighty tests were conducted, on five different granular soils, using four different degrees' of saturation and four different pre-load pressures. Using a 175kHz transducer, the authors concluded that both AE and deformation techniques were capable of predicting the pre-consolidation pressure to within approximately 5%; the only exception being that for the lowest magnitude of pre-consolidation pressure for which the error was 12.9%. However, the authors appear to have calculated these figures by simply averaging the error's for each test at a particular pre-consolidation pressure, regardless of soil type or degree of saturation.

The second paper in the series, by Koerner *et al.* (1984b), reported a laboratory investigation of fine grained ('cohesive') soils. Using a similar procedure to that described previously, the authors used a 30kHz transducer to detect emission from six soils, at each of three different moisture contents and four different pre-consolidation pressures; in all seventy-two tests were conducted. The authors concluded that it should be feasible to predict in-situ pre-consolidation pressures to within approximately 10%. The third paper in this series of three is referenced in section 2.6.

Garga & Chichibu (1990) subjected three different sands to a series of drained triaxial shear tests, studying frequencies in the range 500Hz to 30kHz, with the aim of investigating a number of acoustic emission parameters. These were event count, ring down count, rise time, duration time, peak amplitude, AE energy and energy moment.

AE energy, E , is defined as

$$E = \int_{t_s}^{t_e} a^2 dt$$

and energy moment, Tem , is defined as

$$Tem = \frac{1}{E} \left(\int_{t_s}^{t_e} a^2 t dt \right)$$

Figure 2.13 depicts what the authors described as a typical result and it illustrates the traits of a number of AE parameters as well as the stress-strain relationship through the course of a test. As the authors concluded, whereas energy rate and ring down count rate increased with increasing strain the event rate remained constant. This implies that the size of an event, as strain increases, must also be increasing (in terms of counts). Also, the event count rate is quoted in units of $\times 10^8$ in a ten minute period which equates to a rate of event generation in the order of 10^5 per second! Unless the figure is being misinterpreted this seems rather high.

The authors also considered peak amplitude distribution by plotting AE count as a function of peak amplitude on a log-log basis and from which a parameter 'm', equivalent to the gradient of the line, was obtained. Figure 2.14 illustrates that the magnitude of 'm' decreases as the strain increases although, the authors noted, there was a tendency for 'm' to at first increase when strains were small.

Finally, a plot of energy moments as a function of strain for all three sands (figure 2.15) illustrates that, at low strains, the energy moment exhibited one peak whereas, at high strains, the energy moment exhibited two peaks. The authors associated the first with particle reorganisation and the second with a sliding mechanism and noted that this characteristic is the same for all sands irrespective of density. However, examination of the figure reveals that magnitudes of the 'high' strain values considered vary between 16.8% and 22.1%. It is, therefore, possible that the second peak may be due to other test related factors.

Shiotani *et al.* (1994) derived an improved 'b-value' (I_b) parameter, based on the original 'b-value' (b) parameter as defined by Gutenberg and Richter. The original b-value was derived from an examination of earthquake magnitude and frequency. It is calculated by plotting the logarithmic cumulative frequency of earthquake magnitude (or peak amplitude) and calculating the gradient of the descending portion of the curve. Figure 2.16 illustrates such a plot. Note that M is magnitude, $n(M)$ is frequency and $N(M)$ is defined by the authors' as (although this appears to 'weigh' the frequency by the magnitude):-

$$N(M) = \int_M^{\infty} n(M) dM$$

The authors improved the original b-value by considering data generated by a test on a 60° model slope constructed from sand and into which had been imbedded five 150kHz resonant AE sensors. The slope was brought to failure by loading the top. They observed that, by optimising the number and the range of the amplitude data set considered, that the b-value could be improved. It should be noted that, whereas the adjustment to the number of data appears to be somewhat arbitrary, the adjustment to the range is based upon the arithmetic mean and standard deviation of the set. Figure 2.17 illustrates such cumulative plots at various times during the test and the demarcated zone using the mean and standard deviation. Figure 2.18 depicts calculated Ib-values and load as a function of displacement obtained from four of the AE sensors for the first 7mm of deformation. Note that, in figure 2.18, the sensors are numbered one through four and were vertically spaced at 5cm intervals in the slope with sensor one at the top. It is interesting to observe, as the authors do, the general tendency of the maximum Ib-value to correlate with increasing displacement at increasing depth.

The frequency distribution (not cumulative) shown in figure 2.16 is a schematic of the typical form of amplitude distribution exhibited by soils in a state of shear. Other examples can be found both in this work (see, for example, figure 7.17) and in work by Jackson (1986). The main characteristic of the real distributions is that only one peak exists and this lies within the range of available amplitudes. In fact both this work and Jackson (1986) further demonstrate that this distribution is 'right skewed', i.e. the peak is situated nearer to the left boundary of the distribution than the right. As part of an investigation into the AE response of sand (with particular reference to the identification of the yield point), Jackson (1986) attempted to provide a parametric description of soil-AE by fitting a curve to this frequency distribution using the β -probability density function. This has the form of

$$f(x) = k(x - a)^\alpha (b - x)^\beta$$

where

a	lower bound of distribution
b	upper bound of distribution
k, α, β	parameters derived from the range, mean and standard deviation of the data

Unfortunately, the author found that the variation in the parameters α and β (calculated for a number of tests) was too large to make characterisation feasible, except in the most general case. The only conclusion which appears to be drawn from such a distribution is that the single peak is indicative of a single generation mechanism.

Amplitude distribution's were also considered by Garga & Chichibu (1990) from which, as already discussed, values were derived for the parameter 'm'. However, as figure 2.14 illustrates, the amplitude distribution forms one straight line of a negative gradient, which appears contradictory to the findings discussed in the above paragraphs. It is possible that what the authors described as 'AE count' is cumulative, however there would then be little to distinguish the parameter 'm' from the 'b-value' other than the former is derived from a log-log plot and the latter from a semi-log plot (but both of essentially the same data).

2.4 Soil-Acoustic Emission Fundamentals

2.4.1 Frequency Content of Emission

This section considers investigations which specifically examined the frequency content of acoustic emission. As described in section 2.2, actual measurements of AE are derived from the sensor's response to the emission rather than the actual wave form propagating through the soil body. It should be appreciated, therefore, that frequency contents are also derived from the sensor's response.

Lord jnr *et al.* (1977) used a Bruel and Kjaer 4344 accelerometer as part of a system in which detected AE was recorded and then played back through an octave filter in order to establish the frequency content of the emission. The whole system was described as having a response 'to be quite flat up to 15kHz'. Sands, clays, silts and combinations of these three soils were subjected to unconfined compression and triaxial compression shear tests. The authors found that, for both a clayey silt soil and a silty sand soil tested in unconfined compression, the predominant frequencies were in the 1 and 2kHz bands (figures 2.19 and 2.20). However the results of one triaxial shear test, conducted on a silty sand soil with a confining pressure of 10psi (69kPa), showed that the dominant frequencies had shifted up to the 4 and 8kHz bands (figure 2.21).

Koerner *et al.* (1976) summarised the AE characteristics of granular soils. Although this is a good paper which details the relationship between AE and various soil descriptive parameters (as well as reviewing more fundamental works), it includes no new data pertaining to emission frequency content.

Koerner *et al.* (1977) summarised the AE characteristics of 'cohesive' soils. This complemented the previous work but also included some new investigations into the emission frequency content of clay soils. Samples of kaolinite clay were subjected to unconfined compression tests and AE detected using a Bruel and Kjaer type 6366 accelerometer described as having a 'flat response from 1,000Hz to 40,000Hz' and a 'resonant frequency of 119,000Hz'. Despite the wide bandwidth of the accelerometer, the authors discovered that the predominant frequencies were in the 2 and 3kHz range. This was found to be independent of moisture content and the results (shown in figure 2.22) were the same for moisture contents of between 22% and 38%. No mention is made in the text of the nature of the response above 20kHz. Although the authors noted that the upward shift in frequency which occurred in compression tests on granular soils did *not* occur in 'cohesive' soils, they do not detail any such tests as having been conducted.

Tanimoto *et al.* (1978) also examined frequency content of the emission. Using a 40kHz transducer to detect AE during a series of triaxial shear tests conducted on sandy soils, the authors noted that the dominant frequency was in the range of 0 - 13kHz. The result is depicted in figure 2.23, from which it is noted that the largest recorded amplitudes lie in the range of 12kHz. As already discussed, Lord *et al.* (1977) demonstrated an upward shift in frequency content when tests were conducted with a confining pressure. It was found that using a cell pressure of 10psi (69kPa) increased the dominant frequency range from the 1 - 2kHz region to the 4 - 8kHz region. This work has indicated a dominant frequency of approximately 12kHz and was conducted under a cell pressure of 1.0kgcm^{-2} . In fact, as 10psi corresponds to approximately 69kPa and 1.0kgcm^{-2} corresponds to approximately 98kPa, these results are consistent and appear to confirm the finding that increased confining pressure increases the frequency content of the emission. Note, however, that for the 40kHz transducer used by Tanimoto *et al.* (1978), nothing is known about its frequency response. Koerner *et al.* (1976) suggested that 'shifting' might be caused by higher cell pressures causing densification of the soil which, in turn, causes higher frequencies to be less *attenuated*.

Koerner *et al.* (1981a), in a state-of-the-art review paper, summarised and extended their previous findings. Using a transducer with a resonant frequency of about 130kHz, the authors subjected three soils (a well-graded angular beach sand, a river-transported clayey silt and a commercially obtained kaolinite clay) to a series of direct shear box tests. Each soil was tested, under a normal load of 76 kNm⁻², by the application (in turn) of blocks of shear stress which were not incremented until activity had ceased. The stresses were 9, 18, 36 and 72 kNm⁻²; all samples failed following application of the final shear stress increment.

It was demonstrated that for all soil types that the dominant frequency range (near failure) was in the order of 0 - 10kHz. However, for silt and sand soils, the authors noted, increased activity was also detected in the region of about 100kHz. The results are illustrated in figure 2.24.

The authors also cited work conducted by Hakuno *et al.* (1968) who found that emission frequency content was related to sand density, with a maximum magnitude of approximately 6000Hz.

2.4.2 Signal Attenuation

Owing to the loss in the acoustic stress wave amplitude, or *attenuation*, a signal suffers as it propagates through a medium, it is possible that an emission at source may have completely dissipated by the time it has reached an AE sensor. It is, therefore, useful to have some idea of the magnitude of the attenuation affecting an emission.

With regard to AE in soil material, this area of research is the most ancient with the first, and probably most comprehensive, study being conducted by Nyborg *et al.* (1950). The authors measured the magnitude of attenuation suffered by a sand and a silty loam, both dry and saturated, with varying density and over a frequency range of between 10 and 100kHz.

The test set up, for dry soils, essentially consisted of a sound source (which was a whistle) and a sensor, separated by varying thicknesses of a soil sample. Attenuation was measured in the order of 2dbcm⁻¹ for 'nodulous, loose soils' to greater than 25dbcm⁻¹ for 'finely divided soils and sand'. Figure 2.25 illustrates some of the results obtained for a sand. Note that the authors also considered the d.c. flow resistivity of the material and this is plotted on the graph.

For saturated soils, the authors considered the test set up used for dry soils to be unsuitable owing to the large reflection losses which they felt would occur at the air-mixture boundary. As a result, a source and a number of receiver hydrophones were placed within the soil sample. The magnitude of the attenuation was found to be highly dependent on the proportion of air, probably in the form of bubbles, in the mix. Attenuation, measured in air-free soil samples (i.e. a saturated soil in which the voids are filled with water from which all the air has been removed - deaired water) proved 'too small to be measurable - probably less than 2dbcm^{-1} .' For one sample prepared in the presence of air, attenuation was measured from between 26dbcm^{-1} at 10kHz to 64dbcm^{-1} at 30kHz , although one test resulted in an attenuation of 74dbcm^{-1} at 35kHz being recorded. Figure 2.26 depicts the relationship between signal level and distance travelled for a number of frequencies in a medium consisting of a mix of 'field soil' and water.

The authors pursued the effects of air on attenuation in soil-water mixes by monitoring samples immediately after preparation and again after having left the sample standing for a number of days. An increase in signal level with time was noted, which the authors attributed to air bubbles going into solution. Furthermore, the authors observed that whereas the silty loam would, if disturbed by stirring, record a reduced signal level, that the signal level recorded through a sand was unaffected by this.

The results indicated that, generally, saturated soil samples (using deaired water) produced the lowest attenuation, air-water mix samples the highest and dry samples somewhere in between. However, it must be noted that the mechanisms of noise generation employed bear little resemblance to genuine mechanisms of generation. The authors acknowledged that the sound was probably transmitted through the voids and this would explain increasing attenuation with increasing density. However, in reality, emission generation will occur as a result of inter-particle friction and will, therefore, be generated and initially propagated through the solid soil material. This may explain why these results appear to contradict the findings of section 2.4.1, where an upward frequency 'shift' with the imposition of confining pressure was explained in terms of greater density leading to a *reduction* in attenuation.

Lord jnr *et al.* (1977) added to these findings by consideration of an extensive theoretical and practical investigation of damping in sands by Hardin (1965). Using this work Lord jnr *et al.* (1977) deduced an attenuation of 0.007dbcm^{-1} at 200Hz for sand. The authors also extended the range of available data by conducting a number of 'pulse' tests using a mechanical hammer to

strike a soil sample within which a number of sensors had been imbedded. A number of different soils were tested but, in particular, the attenuation recorded for a dry silty sand was 1.3dbcm^{-1} at approximately 1kHz. The authors also developed testing apparatus along the lines of that described by Nyborg *et al.* (1950) in which a soil sample was placed between a microphone and a loud-speaker continuously emitting sound. Results were similar to those obtained by Nyborg *et al.* (1950) including the increasing effect the presence of air had on the recorded attenuation.

Koerner *et al.* (1976) deduced from Cadman & Goodman (1967) an attenuation of 0.09dbcm^{-1} at 500Hz for a moist sand. The authors also reported attenuation of 5dbcm^{-1} at 4kHz and 10dbcm^{-1} at 16kHz in dry silty sand obtained using the 'loud-speaker' apparatus described above.

Koerner *et al.* (1977) reiterated findings published by Lord jnr *et al.* (1977) in which it was demonstrated that attenuation of a 1kHz signal in a clayey silt decreases as moisture content increases. This is consistent with previous findings assuming that any air present is in solution.

Koerner *et al.* (1981a) presented a general summary of the results of investigations into soil attenuation to date.

Figure 2.27 combines a number of the results from investigations into attenuation in soil and figure 2.28 illustrates the recorded variation in attenuation due to varying moisture content in a clayey silt. Figure 2.29 compares attenuation in soil with attenuation in other materials and figure 2.30 collates the majority of the published soil attenuation data into a single graph. Note that the three sets of twinned data denoted as 'Nyborg *et al.* 1950 - dry sand' each occur due to variations in sample density with the higher points in each pair corresponding to the greater density. Also note that the set denoted as 'Koerner *et al.* 1976 - dry sand' consists of a number of results obtained by different researchers using different techniques as outlined in that paper and is a reproduction of the data plotted in figure 2.27.

2.4.3 Wave Velocity and Prediction of Emission Magnitude

A knowledge of frequency content and attenuation are obviously pertinent to any study interested in utilising acoustic emission as a means of strain measurement as they both have implications for the monitoring system employed. Although not as important, some discussion of

wave velocity has also appeared in the literature. Lord jnr *et al.* (1977) and Koerner *et al.* (1976) both referred to an in-depth study of the subject by Hardin & Richart (1963) where samples of Ottawa sand, crushed quartz and crushed quartz silt were tested using the resonant column method. The effect on wave velocity of confining pressure, moisture content, void ratio and grain characteristics were examined although, the authors concluded, void ratio was the most significant factor; other factors only exhibiting an effect on wave velocity by virtue of their effect on void ratio. It was found that wave velocity in sand varied with approximately the $\frac{1}{4}$ power of the confining pressure.

Lord jnr *et al.* (1977) and Koerner *et al.* (1976) both related an experiment used to determine wave velocity by mechanically generating an impulse in a large tank of silty sand within which two sensors had been placed. The authors obtained velocities of between 120 - 240ms⁻¹ depending on density and moisture content and regarded these values as being consistent with the findings of Hardin & Richart (1963).

The only attempt to derive an expression for the magnitude of an emission appears to be that by Lord jnr and Koerner (1979) which is also summarised in Koerner *et al.* (1981a). Assuming elastic soil deformation, the authors developed the following relationship between the magnitude of an emission at source and it's magnitude at a receiver:

$$a_{\max} = \sqrt{\frac{\pi f^2 e^2 V R c}{2 \Delta t r}}$$

where

a = acceleration

c = wave velocity

f = frequency

Δt = time

e = elastic strain

r = distance from source

V = volume

R = radiation efficiency

2.4.4 Relationship between Physical Characteristics of Soil and Acoustic Emission

The effect various soil characteristics have on the nature of the acoustic emission is a consideration of many of the works already reviewed. In particular, Koerner & Lord jnr (1972, 1974), who considered the effects of moisture content, and Lord jnr & Koerner (1974), who examined the effects of different gradings, have already been discussed in section 2.3.

Lord jnr *et al.* (1977) reported the results of a number of triaxial shear tests conducted on glass beads and clearly demonstrated that increasing confining pressure generated an increasing magnitude of emission.

Koerner *et al.* (1976) conducted a comprehensive study of the AE behaviour of granular soils in which the authors subjected four different sands to a series of drained isostatic and triaxial shear tests. Each sand was fully described in the paper in terms of particle shape, coefficient of uniformity (grading) and effective size. The authors commented, based on the results of the isostatic tests, that those soils containing the rounder particles tended to regain equilibrium and, hence, cease generating emission, 'much' before those soils consisting of angular particles. It was also remarked that the angular and sub-angular samples were 'significantly more' emissive than the rounded particles 'in both the initial and final stages of triaxial testing.' The authors were less certain about the effects of the coefficient of uniformity despite the fact that an increase in the magnitude of this parameter was accompanied by an increase in the detected emission. This was because the more angular soils also had the highest coefficient's of uniformity, leading the authors to conclude that the 'actual cause of greater emission may therefore be a combined effect.'

Koerner *et al.* (1977) investigated the AE behaviour of 'cohesive' soils using four clays for which full descriptions (including liquid limit, plastic limit and optimum moisture content) are provided. However, initially, two sand samples used in the investigation by Koerner *et al.* (1976) and a sample of kaolinite clay, were each subjected to triaxial testing in order to compare the resulting emission. The sensor, a Columbia 476-R accelerometer was embedded within the sample, and a confining pressure of 34kNm^{-2} applied. As figure 2.31 illustrates, the sands tended to be more emissive than the clay and, at about 80% of the failure stress, whereas the magnitude of the emission generated by both sands tends to dramatically increase, that of the clay reduces. The authors explained this by suggesting that the soil particles have become aligned with the

shear plane. It was also demonstrated, using two of the 'cohesive' soils in triaxial shear, that increasing confining pressure generated emission of increasing magnitude.

All four 'cohesive' soils were also compacted in order to achieve a void ratio of 0.89 and then each subjected to a series of triaxial shear tests. It was subsequently shown that there was a good correlation between the level of generated emission and the plasticity index.

All works concerning fundamental soil-AE relationships are collected together in the state-of-the-art paper by Koerner *et al.* (1981a). However, a brief summary of the main findings is given below:-

Confining Pressure - When generating an increase in the effective stress, an increase in the confining pressure *always* results in an increase in the level of detected emission.

Mineralogy - The emission, which is considered to be the result of inter-particle friction, is related to the frictional characteristics of the soil minerals. (Although this is not specifically mentioned in any of the works reviewed, it is considered to be a logical extension of the findings so far obtained).

Particle Shape - Angular particles are more emissive than rounded particles.

Coefficient of Uniformity - A measure of a soil's grading, the evidence is, unfortunately, inconclusive. The level of AE appears to increase with an increasing coefficient of uniformity (i.e. the soil is tending to become well-graded) but of the soils examined, those with the higher coefficients of uniformity were also the most angular.

Effective Size - Inconclusive.

Moisture Content - For a saturated soil, increasing moisture content implies a decrease in shear strength and detected emission.

Plasticity Index - A 'strong correspondence' exists between the plasticity index and the level of detected emission. However, as the index is dependent upon soil mineralogy and grading, this is not unreasonable.

2.4.5 Investigations of the Wave Guide

Although the beneficial use of wave guides (both in the field and laboratory) in facilitating the capture of acoustic emission has long since been appreciated, surprisingly little work has been focused on wave guides themselves. The earliest investigation appears to have been by Koerner *et al.* (1975), who examined the effect of the wave guide on a signal propagating through it. This was achieved by generating a specific signal which was made to propagate through wave guides of varying design before being detected by an accelerometer. The wave guides were constructed from various lengths and two diameters (1/8 & 1/2 inch) of steel rod.

The authors drew the following conclusions which are taken *verbatim* from the paper:-

- Longer wave guides lower the frequency of first resonance of the detector system.
- Different diameter rods do not appear to influence the first resonant frequency of the system.
- Different surface conditions (threaded versus smooth) do not appear to affect the location of the first resonance.
- The method of connecting one rod to another does not appear to influence the resonances, so long as such connections are solid and firm in their metal to metal contact.

Figure 2.32 illustrates the relationship between the frequency of first resonance and wave guide length.

Additionally, the authors also examined the effect of the surrounding medium on a signal propagating through a wave guide. A number of tests (as described above) were conducted on a 4ft section of 1/2 inch diameter steel rod which was variously surrounded by a silty sand soil at different moisture contents. It was concluded that 'the influence of the soil mass around the wave guide is negligible on the detector's frequency response but does reduce its sensitivity to a certain extent'.

Lord jnr *et al.* (1982) expanded on the previous investigation using a similar experimental set-up. A signal, consisting of frequencies between 1 and 8kHz was 'pulsed' through a 2m long section of 12mm diameter steel bar which was surrounded by either Ottawa sand or Kaolinite Clay at different moisture contents. At either end of the bar an accelerometer was used to detect the emission both before and after propagating the length of the wave guide section. The difference between the magnitudes of the two signals (thought to be due to absorption by the soil) was referred to by the authors as the soil covering loss (SCL).

It was found that the soil covering loss, for longitudinal waves, varied between 0 and 6dB. These values were described as being higher than for steel alone but lower than for soil alone. The equivalent range for transverse waves was 10 to 17dB which, the authors noted, was close to that of soil alone and from which it was concluded that transverse waves are attenuated much more than longitudinal waves. It was also found that (a) increased moisture content increased the soil covering loss but not significantly, (b) greater soil density produces higher attenuation and (c) the resonant frequencies of the rod were only altered some 0.05 - 0.1kHz due to the presence of the soil.

The authors described a model in which emission, propagating from a source and through the soil, was collected by the wave guide. This has subsequently been described as the *passive* model and, as figure 2.33 illustrates, the authors derived a relationship which implies that the volume of soil sensed is cone shaped. They also claim that use of the wave guide increases the volume of soil sensed by a factor of 30 and the depth of soil sensed by a factor of 60.

Styles *et al.* (1988) also made clear the importance of 'acoustic coupling' between the soil and the wave guide. As is common in the physical world, energy propagating through one medium is both reflected and refracted at the boundary when crossing into another. This is illustrated by an

example in which it is demonstrated that, whereas only 30% of acoustic energy travelling in a soil medium will cross a soil:steel boundary, 85% will cross a soil:water boundary.

A number of investigations of wave guides have also been carried out by Hardy and various co-workers, for example Hardy *et al.* (1989) and Hardy (1992). However as they are wholly concerned with applications in rock, they are not considered further.

Finally, an interesting development of the wave guide was described by Nakajima *et al.* (1995). In this investigation a wave guide formed from glass fibre and resin was used in conjunction with two AE transducers to detect emission. However, as the arrangement was used in the monitoring of a landslide, discussion of this work is deferred until section 2.5.

2.5 Applications of Acoustic Emission Strain Monitoring to Soil Masses in the Field

In what is largely accredited as being the first work to specifically investigate soil, Beard (1961) reported the use of AE to predict the onset of failure in a soil mass. Although dealing mainly with rock slopes (as opposed to soil), the author described an instrument called the 'Seismitron' and its operation in detecting field generated AE. Concerning rocks, the instrument recorded higher magnitudes of emission as instability increased. When applied to soil, however, it unfortunately appears to have been somewhat less than successful. As already stated in section 1.1, the only reference made of the AE behaviour of soil is ... '*Certain soft materials such as sand, clay, mud, etc., do not produce microseisms that are clearly definable*'. It is also interesting to note that background noise and characterisation of an emission (which is referred to as a 'microseism') were already established phenomena.

Fisher & Yorke (1964) investigated three existing landslides in soil material using a geophone with a resonant frequency of 1kHz. Monitoring was achieved by lowering the geophone to the bottom of a borehole which traversed the shear zone, although use was also made of 'reference' (or control) boreholes placed outside the 'unstable area'. There do not appear to have been any deformation measurements made using conventional techniques and instability is indicated by a disparity between the AE readings obtained from boreholes in and out of the 'unstable area'. The authors also comment on various sources of background noise.

Goodman & Blake (1966) examined existing slides and cut slope failures using, initially, a single channel system which was upgraded to four channels. This enabled background noise to be separated out from genuine emission and also enabled the location of the source to be identified. The authors did not relate the sensitivity of the geophone used in the investigation but commented that such emission consisted of frequencies in the range of between 0.1 -1kHz. 'Blast' experiments, in which the positions of the instruments and source were previously determined, were conducted in the field in an attempt to verify the source location technique. Unfortunately, the authors only noted that 'extreme velocity variations' and 'attenuation of the high-frequency portion of the blast energy' occurred in soft materials. This was due to the many problems encountered with the instrumentation. The authors did, however, conclude that '*Rock noise monitoring does forewarn of accelerated movements in landslides and rockslides*'.

McCauley (1977) described the successful use of AE monitoring to forewarn of reduced stability at two sites. The first, a 41m high cut slope in differentially weathered granite, was situated in Kern Canyon, California. After cracks had appeared on the surface of the cut it was decided to monitor stability both using AE and, also, by driving pairs of nails into the ground either side of a crack and regularly measuring the distance between them. Transducers were located in six positions (five of the six being buried in shallow hand-augered holes) and data was acquired in fifteen minute recordings. The authors reported that increased AE activity, in conjunction with the other deformation measurements, 'strongly influenced' the decision to take remedial action.

The second site (consisting of poorly consolidated marine sand, silt and clay) was situated at Thornton Bluffs, California. As before, AE was monitored at six locations and deformation measurements made by regularly monitoring the distance separating pairs of nails either side of a crack. The transducers were housed in shallow hand-augered holes into which a length of piping had been placed. The author noted that a dramatic increase in detected AE pre-empted a sizeable change in the deformation as recorded by more traditional methods. Figure 2.34 illustrates these results. Note that 'SARN SI-3' is the measured AE in counts per minute whereas 'NAIL POINT #6' and 'SI-3 AT 95' represent measured displacement.

Lord jnr & Koerner (1975) reported four earth dams instrumented for acoustic emission but only gave details of one (which was designated 'Neb. 200'). This dam, which was 67ft tall, was instrumented with four 'sets' of wave guides. Each set comprised three wave guides (or 'rods') of varying length (constructed from 3/8 inch diameter reinforcing rods) and were arranged

horizontally, one above the other, with the longest rod at the bottom and the shortest at the top. This is illustrated in figure 2.35. The aim appears to have been to detect settlement. Although the authors noted some success in the level of emission detected between rods within a set (i.e. the longest being noisiest), there were differences between sets which they were unable to explain.

Koerner *et al.* (1978a) reported seventeen field studies being conducted but detailed only three. The first, designated as 'Pa-PIA', was essentially a compressibility test in which a surcharge induced settlement in a foundation soil. Wave guides were used to monitor the generated acoustic emission and the authors noted that the time in which the AE dissipated (5 - 15 days) was in better agreement with theoretical predictions than the 2 - 3 days observed from the measured settlement. Figure 2.36 illustrates the test set-up and figure 2.37 illustrates the time-settlement-AE response.

The second study, designated 'NJ-NLI', revolved around a series of holding ponds for chemical waste fluids constructed from 2.4 - 6.1m high embankments and founded on extremely poor soils. Using twelve wave guides at depths of up to 6.1m below the foundation soil, the authors could only conclude that 'count rates vary considerably'. The third study, designated 'Pa-DSP2', was a large scale test conducted in a stockpile for highway fill and this also forms the major consideration of Koerner *et al.* (1978b).

Using the same piezoelectric transducer (described as having a 'relatively flat frequency response from about' 0.5 to 5kHz) as Koerner *et al.* (1978a), Koerner *et al.* (1978b) described a test in which an earth stockpile was artificially brought to failure by cutting away at the toe. Consisting of a well-graded silty sand with an approximate 17% clay content, the stockpile was originally 18m long and 4.6m high. It was brought to failure by making five cuts with a large front end loader and these are illustrated in figure 2.38. Instrumentation consisted of (a) surface stakes for surveying purposes, (b) soil strain gauges, (c) slope inclinometers and (d) steel rod wave guides. The AE response to each of the cuts, together with a 'cut summary', is shown in figure 2.39. The authors commented on the typical AE response to each cut in which initially high readings were followed by an approximate exponential decay. The only exception was the response following cut five where the decay in the level of the emission was abruptly interrupted by a rapid increase occurring some thirty minutes after the cut was made. These AE readings compared with an average movement of 0.51cm recorded by the surface stakes following cut

three. The authors also noted that heavy rain during the test period had the affect of temporarily causing large increases in the level of AE recorded.

Evans (1984) investigated a soil failure problem surrounding the construction of a lagoon adjacent to a high-pressure steel gas pipeline and a canal. Although the exact nature of the problem appears to be unclear, it manifested itself in the form of bubbles (determined to be air) rising from the bottom of the canal and was considered to be due to the additional load of the filled lagoon. Using the steel pipeline as a wave guide and an AE monitoring system with a frequency bandwidth of between 20 and 100kHz, the author recorded the effects of increased instability and, subsequently, of remedial works. A soil slip, producing heave in the bottom of the canal, also occurred and the recorded AE is shown in figure 2.40. The author noted that there was a general decrease in the level of emission (associated with the corrective work) and that, ultimately, recorded values of AE became 'acceptable'. The author also commented on the existence of a relationship between water level readings obtained from piezometers and the recorded AE. A number of triaxial shear tests were also conducted and reported on.

In their state-of-the-art paper, Koerner *et al.* (1981a) summarised many of the works so far considered but also discussed some others which have not. One concerns a water reservoir which had been drained too quickly with the net result that a very high water table was left in the surrounding slopes generating, in turn, a seepage-induced failure. Monitoring commenced after mobilisation of the failure plane and lasted for approximately one month. It was noted that initially high rates of AE were associated with increasing settlement rates but, as settlement rates became 'steady', AE rates decreased.

A second study concerned the use of AE to detect lateral movement in trench walls as a result of stress relief. However, three separate AE monitoring systems were employed and the main aim of this investigation appears to have been to provide an inter-comparison of the three.

Penning *et al.* (1983) described a field experiment in which a trench (in material described as medium to coarse graded sand) was dug out in stages and the resulting AE monitored. Instrumentation consisted of seven 4m long steel rod wave guides (placed perpendicularly to the line of the trench) which were monitored using two separate AE systems. Figure 2.41 illustrates the results obtained by one of the systems monitoring the wave guide nearest the trench edge (a distance of 0.3m). The authors noted the correlation between the level of emission and the depth

of the trench as well as the tendency of the AE to stabilise with time after each cut. A number of triaxial shear and plate bearing tests were also reported.

Yuda *et al.* (1984) described AE monitoring of existing landslips (in weathered rock material) and noted the existence of two types of event. The first, with a frequency of about 1kHz, occurred at the toe of slope and was (according to the authors) associated with inter-particle action close to the wave guide. The second, thought to be generated by the slip-plane, had a frequency of about 200Hz. The authors noted both spatial and temporal variations in the emission, which was captured using a system with a frequency bandwidth of between 1.6Hz and 7kHz and 1 to 2m long carbon steel wave guides.

Chichibu *et al.* (1989) reported a slope failure (in material described as 'Clayey rock') caused by a road cutting and which occurred after a displacement stake, installed to monitor deformation, had recorded less than 5mm of movement. Subsequently, a 20m high embankment was constructed as a counterweight to prevent further movement and a number of other instruments to monitor the slip were also installed. Note that both the counterweight embankment and the slope were monitored in the study.

The embankment was instrumented with a driven 5.5m section of 32mm diameter steel rod (as a wave guide) and a deformation stake to monitor both vertical and horizontal displacements. The results are illustrated in figure 2.42. Initially rates of movement and AE were high and it was decided to construct an additional embankment to support the first. This was completed on 14 - 15 November and, as figure 2.42 shows, both AE and movement almost ceased. Heavy rain then caused further activity which diminished within two weeks. The authors commented that there was a good correlation between the AE and the horizontal movement of the stake. They also suggested that the source of the AE may be inter-particle friction or an inter-action between the soil and the wave guide.

The natural slope was monitored using a borehole inclinometer, a ground surface displacement meter and a 17m section of 25mm diameter reinforcing rod (as a wave guide). Figure 2.43 illustrates the results. Note that 'A' and 'B' refer to ground surface displacement and that underground movements were recorded at a depth of 14.5m. The authors noted that the high rates of AE recorded over February were accompanied by very small rates of measured displacement. This, they claimed, implies that 'microcracks', which themselves cannot be

detected by the displacement meter, generated AE which can be acquired. However, owing to a diminishing AE rate, with effect from 1 March the authors decided to change the AE monitoring point and they lowered a water-proofed sensor down the inclinometer borehole to a depth of 20m. This is marked in figure 2.43 and clearly illustrates that high rates of AE were recorded as a precursor to any significant magnitudes of recorded movement. The authors also commented that, once displacements became significant, AE activity decreased.

Styles *et al.* (1988), Rouse *et al.* (1991a) & Rouse *et al.* (1991b) reported work carried out on two large, existing, landslips and the geology of the area was extensively detailed. Four Bruel and Kjaer 8318 accelerometers (with a relatively flat response up to approximately 6kHz) and an O.A.S. 281 hydrophone were used to capture AE which was subsequently recorded onto analogue tape. Unfortunately, the recorder was identified as a source of noise which had a frequency content described as being 'partially coincidental with the signal bandwidth of acoustic emission, 0.25 to 8kHz, as defined by Koerner *et al.* (1981a)'. The authors, therefore, recorded system noise on a separate channel in order to subtract this element from signals captured via the accelerometer and hydrophone. Monitoring was performed (on one site) subsequent to a major failure and (on another) during slow continuous movement but never *before* a major failure. Apart from natural slippage, the authors also conducted tests in which a twenty ton load was placed on the backscar of one of the slips and this was found to generate AE. A good correlation between periods of high rainfall and increased AE activity was also established, as figure 2.44 illustrates. However the authors' primary result was the identification of four types of 'pedogenic' AE event, the descriptions of which are as follows (after Rouse *et al.*, 1991a):-

Type A are multicyclic, burst type signals that usually have a small amplitude of emission with one or two specific frequencies present within the signal. Comparison of the noise channel and signal channel is very important with low power events of this nature. Figure 2.45 illustrates an example of a Type A event, after noise removal, and indicates peaks at 4.2, 4.9 and 5.5kHz.

Type B events consist of two frequencies: a lower monocyclic negative going pulse that has a frequency of between 200 to 500Hz and a higher multicyclic pulse that can range in frequency from 2.5 to 8kHz. Their amplitude is larger than that of Type A.

Type C events have only been recorded at one of the sites and are multicyclic with a characteristic frequency of 1.2 to 2.0kHz.

Type D are particularly rare and consist of very short mono/di-cyclic events with a frequency of approximately 6.5kHz.

Nakajima *et al.* (1995) described a very interesting new wave guide design and its application in the monitoring of active landslides. The wave guide, illustrated in figure 2.46, was formed from a composite of resin and glass fibre encased in a steel pipe. Two Marubun M568 accelerometers, with a frequency response of between 0.3 and 5kHz, were attached either end of the assemblage which was then placed into a section of PVC piping. The steel and PVC pipes were separated by nylon rings in order to reduce the effect of damping on the propagating signal. The authors claimed that this reduced the damping factor from about 0.84dBm^{-1} (for a wave guide in contact with a borehole) to about 0.07dBm^{-1} . The wave guide was subjected to a number of laboratory tests prior to its deployment in the field. Figure 2.47 illustrates the results of applying a constant deflection rate to the wave guide and, despite the variance in the AE count rate, it is fairly evident that there is a good linear correlation between the number of accumulated events and the deflection. Additionally, as illustrated in figure 2.48, the dual accelerometer configuration makes it possible (by using arrival times) to identify the source of AE events. This, in turn, can relate which section of the wave guide has been most active and, therefore, suffered greatest deformation.

The authors monitored two locations in active landslides. The first AE monitoring rod, at the head of the slope, was installed to a depth of 40.4m and the second, located mid-slope, was installed to a depth of 45.9m. Pipe strains were monitored by a series of strain gauges attached to the PVC piping and ground water levels were also recorded. At the head of the landslide, the authors detected AE activity which they related to an earthquake which had occurred some 650km from the monitoring site. Using the relationship derived for AE and deformation, they deduced that rates of movement equivalent of up to 38myear^{-1} had been generated. By contrast, the mid-slope AE only corresponded to movement rates of up to 10mmyear^{-1} .

The most impressive aspect, however, was the identification of the sliding surface in the mid-slope. The total number of events per 0.2m length of wave guide was plotted and compared with displacement (as recorded by the strain gauges) for monitoring periods of 16, 23 and 58 days.

Initially (after 16 and 23 days) distinct levels of AE were recorded only at a depth of 35m but displacement (according to the strain gauges) was negligible measuring, at most, 0.001mm. After 58 days, however, although AE activity was still greatest at a depth of 35m, additional activity was recorded at depths of between 7 and 24m. The strain gauges (for the first time) recorded a distinct displacement, which occurred at a depth of 35m, but even this was in the region of only 0.005mm. As the authors concluded, the acoustic emission monitoring rod appears to have successfully identified the active location long before any conclusive evidence was available from the strain gauges.

Details of field studies conducted as part of this investigation are reported by Dixon *et al.* (1994, 1996a, 1996b) and Hill *et al.* (1994).

2.6 Other Geotechnical Applications of Acoustic Emission Monitoring

In this section it is not intended to describe any of the works concerned but simply to present a list of appropriate references.

Much work has concentrated on the use of acoustic emission in the testing of soils in-situ and in the development of in-situ AE testing apparatus. Relevant works are by Tanimoto & Nakamura (1984), Tanimoto *et al.* (1981), Villet *et al.* (1981), Lord jnr & Koerner (1983, 1985), Deutsch *et al.* (1989) and Naemura *et al.* (1990)

The use of acoustic emission in the detection of sub-surface seepage has also received some attention and relevant works include Koerner *et al.* (1979, 1981a, 1981b) & Blystra (1990, 1994).

Other studies include the use of AE to monitor rock and soil grouting - for example Huck & Koerner (1981) and Koerner *et al.* (1981a) - and its use in monitoring subsidence - for example Koerner (1986) and Wood & Harris (1990).

2.7 Literature Review Summary

The study of acoustic emission and soils is very broad-based with both physicists and engineers having contributed works over the past forty-six years. Soil-AE fundamentals (such as emission frequency content, signal attenuation, wave velocity and wave magnitude) have been investigated. Many laboratory tests have demonstrated that generated AE is related to the type of soil being examined and the degree of strain it has suffered. Other laboratory tests have sought to develop and improve data processing techniques. In the field AE has been used to detect movement in existing landslides but only two field tests aimed at the detection of first time deformation characteristics, Penning *et al.*(1983) and Koerner *et al.* (1978b) (both in granular material), appear to have been conducted. A wide range of detection equipment has been employed and AE sensors, sensitive to frequencies of between a 'few Hz' to 130kHz, have been used. Wave guide design and behaviour has been investigated and they exist in the form of simple metal rods driven into the ground or more complex designs such as described by Nakajima *et al.* (1995). It has also been shown that AE monitoring can be applied to many other forms of geotechnical processes such as seepage monitoring, detection of subsidence and the in-situ testing of soils. A very large volume of work, investigating AE monitoring of rock, is also in existence.

The research described within this thesis adds to the body of knowledge by the provision of two case histories which demonstrate the use of AE in the detection and monitoring of first time deformation characteristics in stiff, heavily-overconsolidated clay soils. Additionally, it details the use of an analogue-to-digital conversion board to capture soil generated AE both from the field and laboratory.

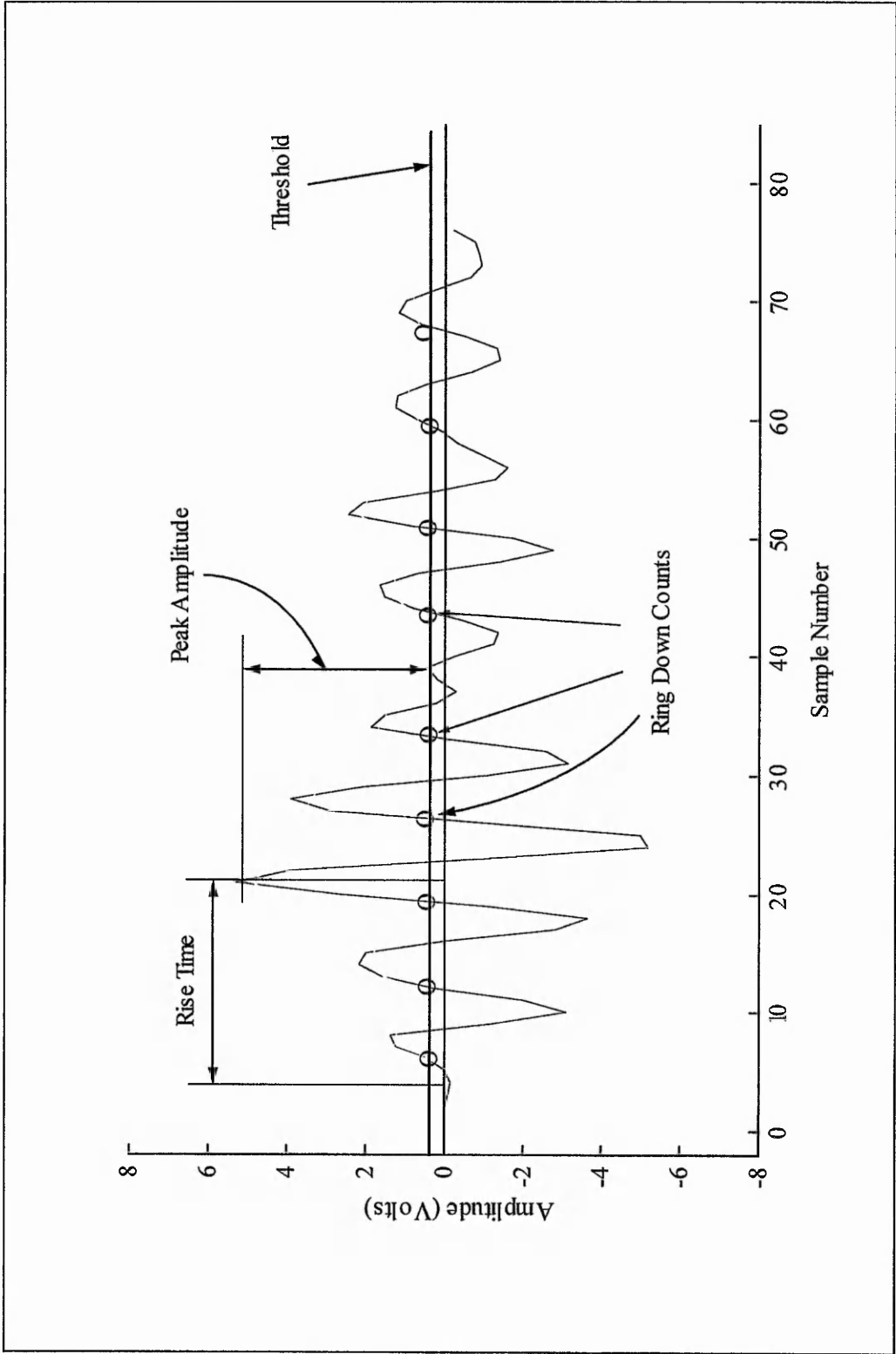


Figure 2.1 AE measurement criteria

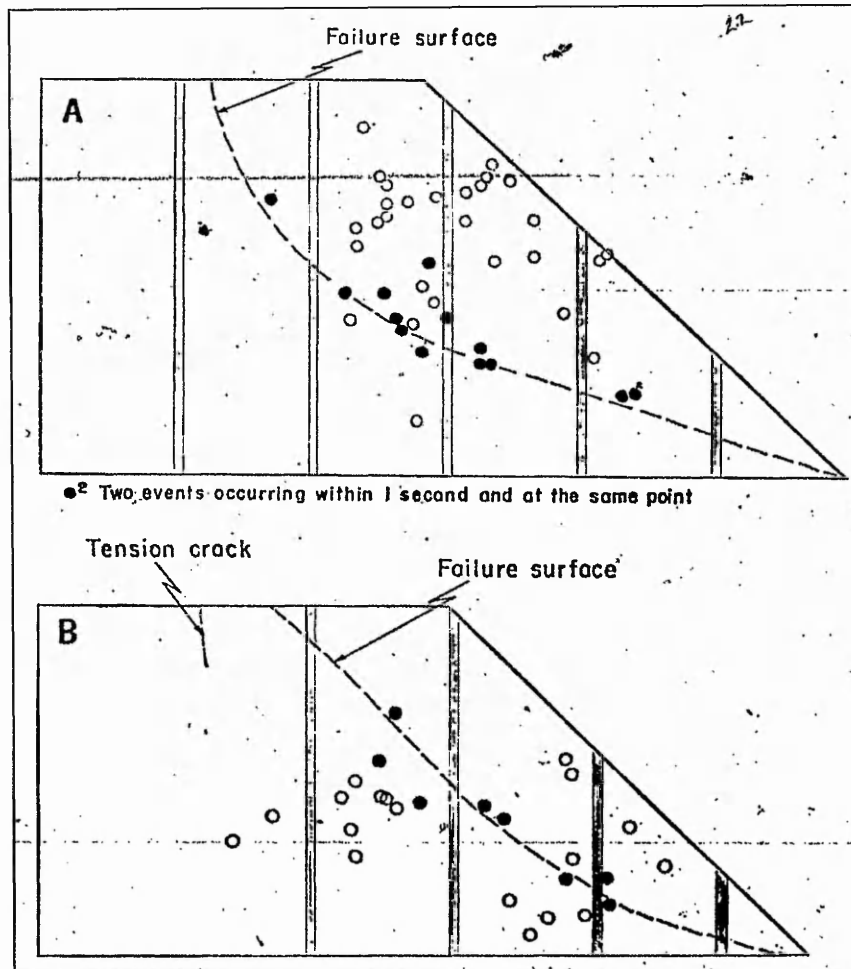


Figure 2.2 (A) Profile of a thick slide developed in a tilting box in the laboratory, showing the location of the noises generated at high factors of safety (open circles), lying mostly within the slide. The noises at low factors of safety (black circles) lie close to the failure surface. (B) Profile of a thinner slide, showing most of the very early events lying behind the failure surface and probably associated with the tension crack. The noises generated just before failure again plot close to the failure surface. Gray verticals are layers of red sand.

(After Cadman & Goodman, 1967)

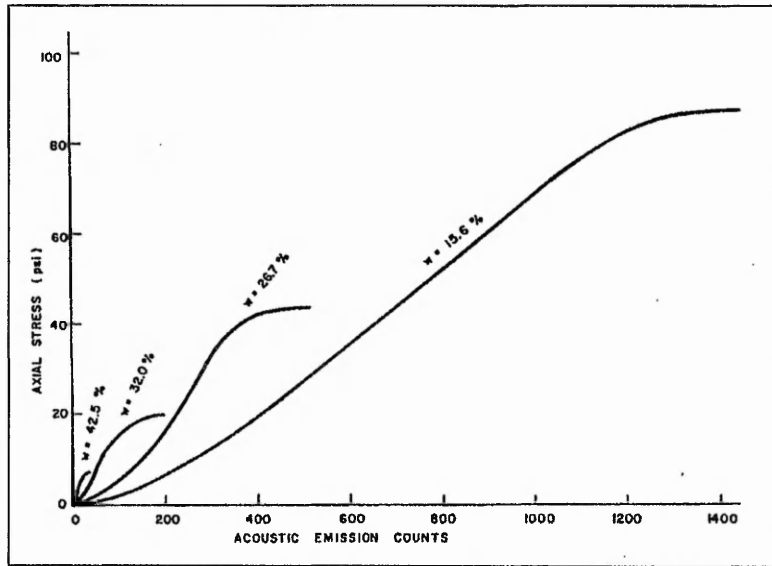


Figure 2.3 Axial stress as a function of cumulative AE count for four soil samples at varying moisture contents.

(After Koerner & Lord, 1972)

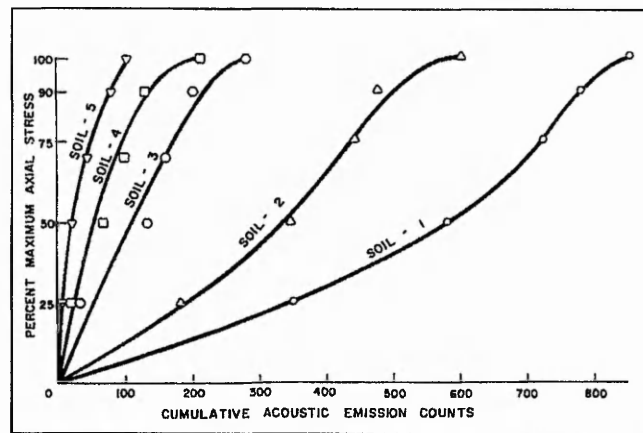


Figure 2.4 Axial stress (as a % of maximum axial stress) as a function of cumulative AE count for five differently graded soils.

(After Lord & Koerner, 1974)

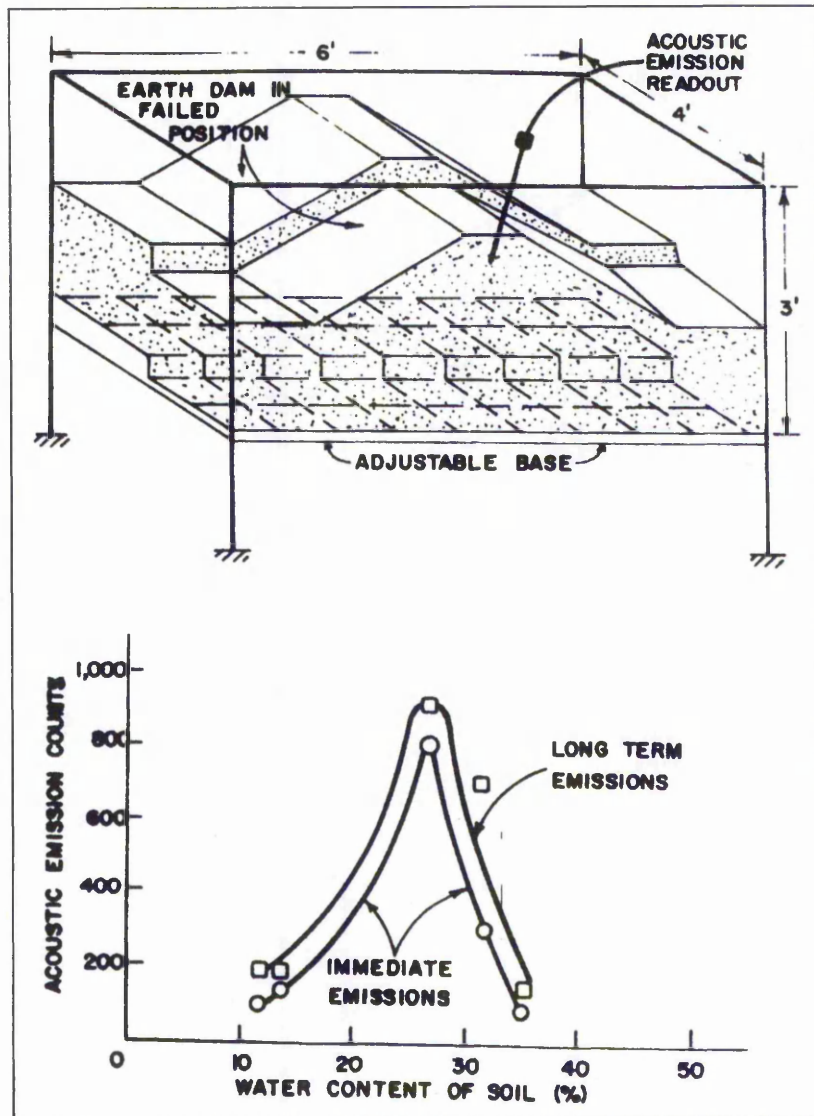


Figure 2.5 Earth dam model shown schematically in its failed position (transverse crack) and the results for a series of tests at various moisture contents.

(After Koerner *et al.*, 1975)

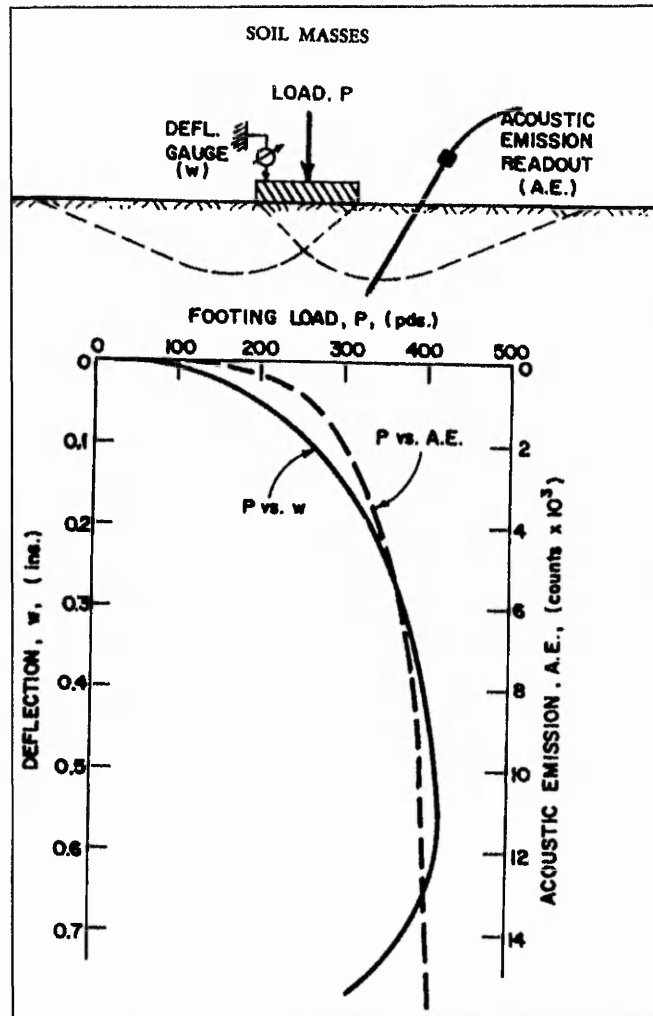


Figure 2.6 Bearing capacity model test showing schematic of test setup and the deflection and acoustic emission response curves.

(After Koerner *et al.*, 1975)

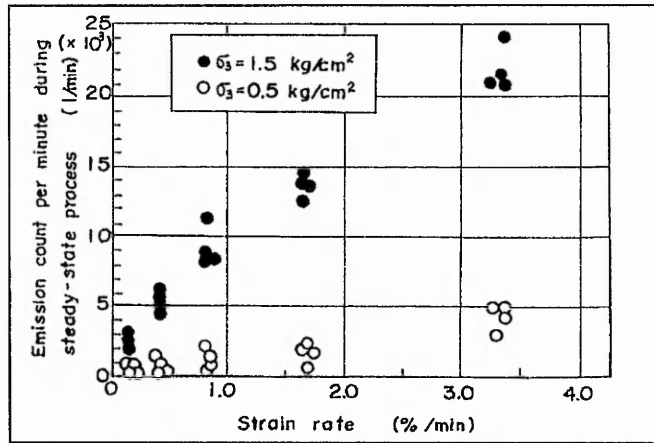


Figure 2.7 Relationship between strain rate and emission count per minute monitored during steady-state process of strain control tests.

(After Tanimoto & Noda, 1977)

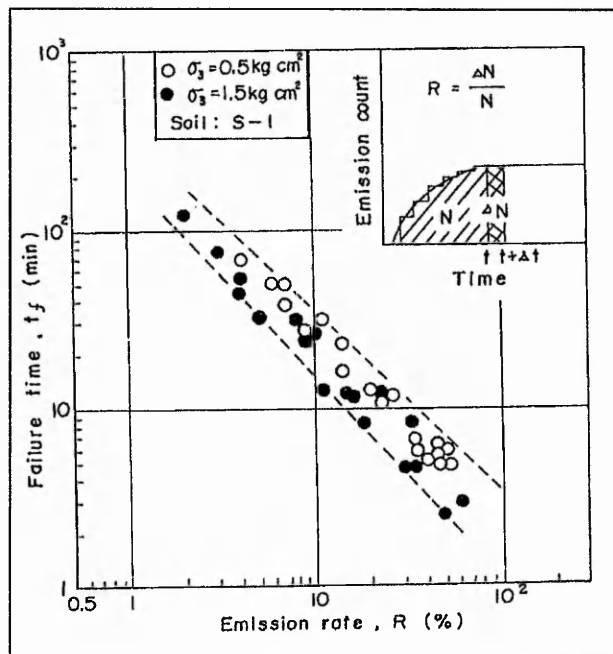


Figure 2.8 Prediction of failure time by emission rate in strain control tests.

(After Tanimoto & Noda, 1977)

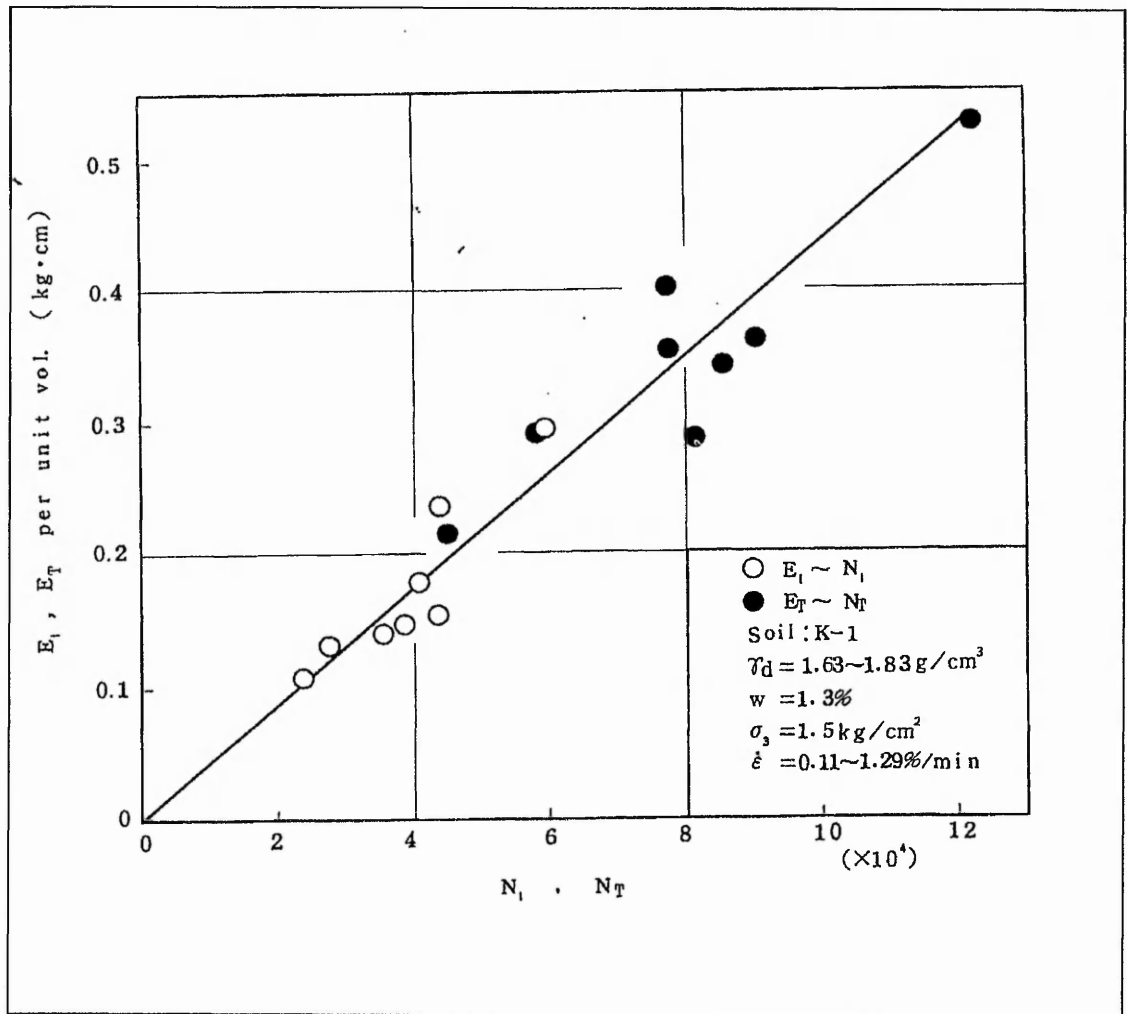


Figure 2.9 $E_i - N_i$ relationship and $E_T - N_T$ relationship

(After Tanimoto *et al.*, 1978)

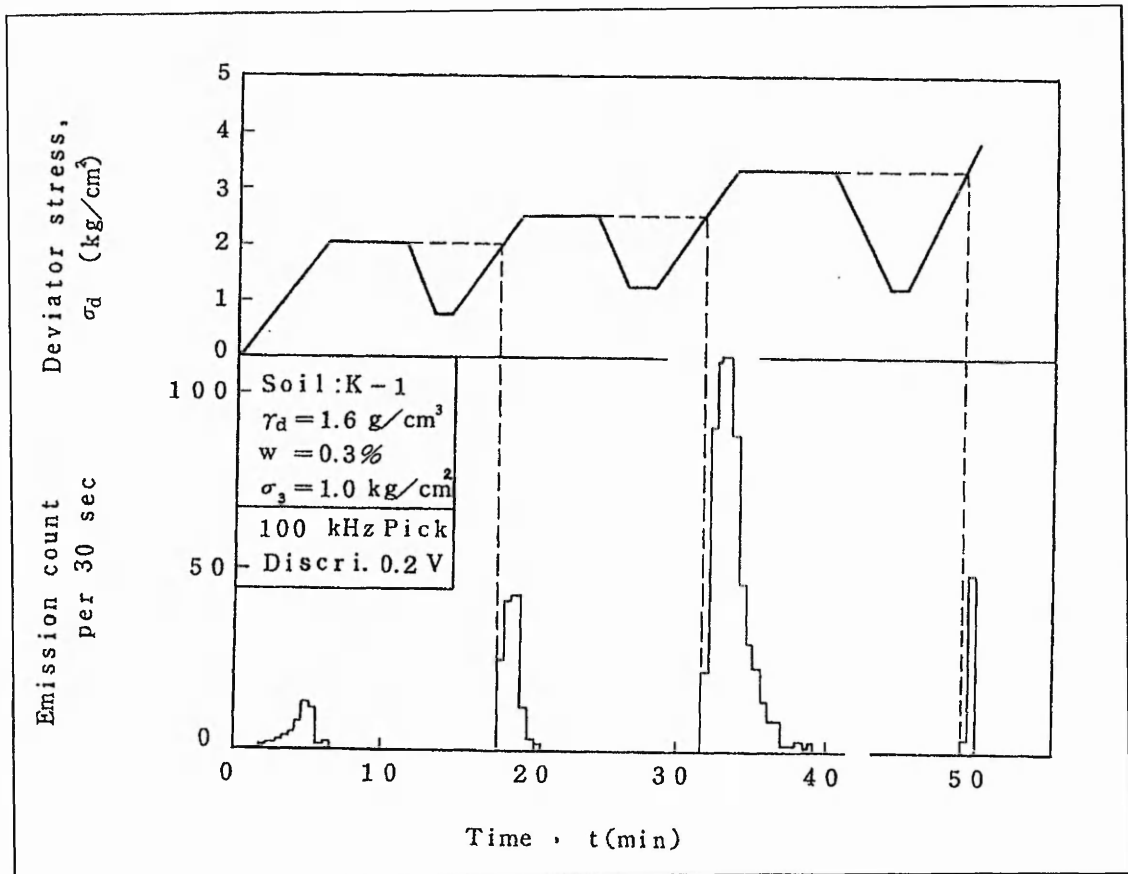


Figure 2.10 Emission count in repetitive loading test (*demonstration of Kaiser effect*).

(After Tanimoto *et al.*, 1978)

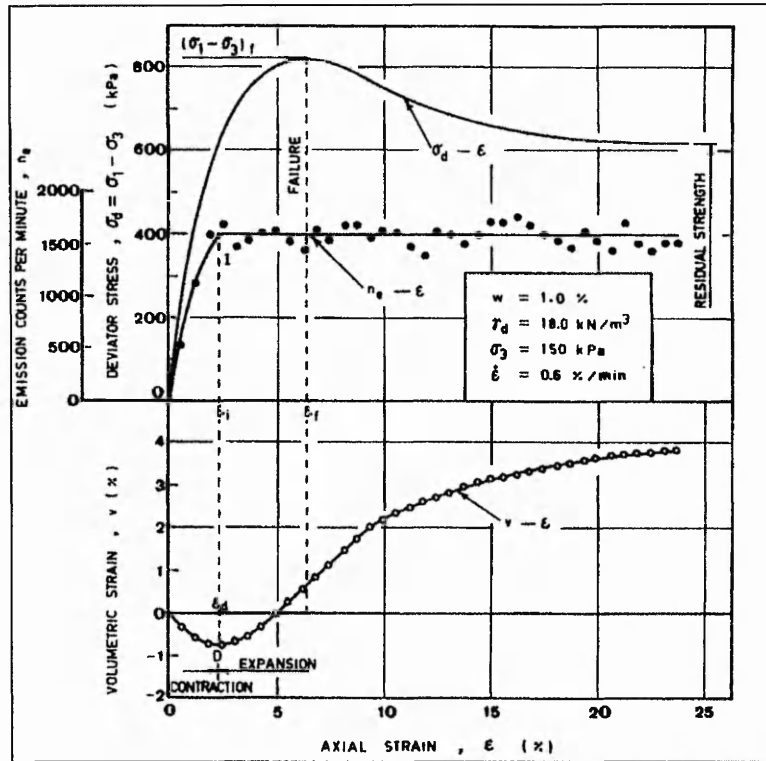


Figure 2.11 Emission counts, volumetric strain, deviator stress and axial strain relationships in strain-controlled test.

(After Tanimoto & Nakamura, 1981a)

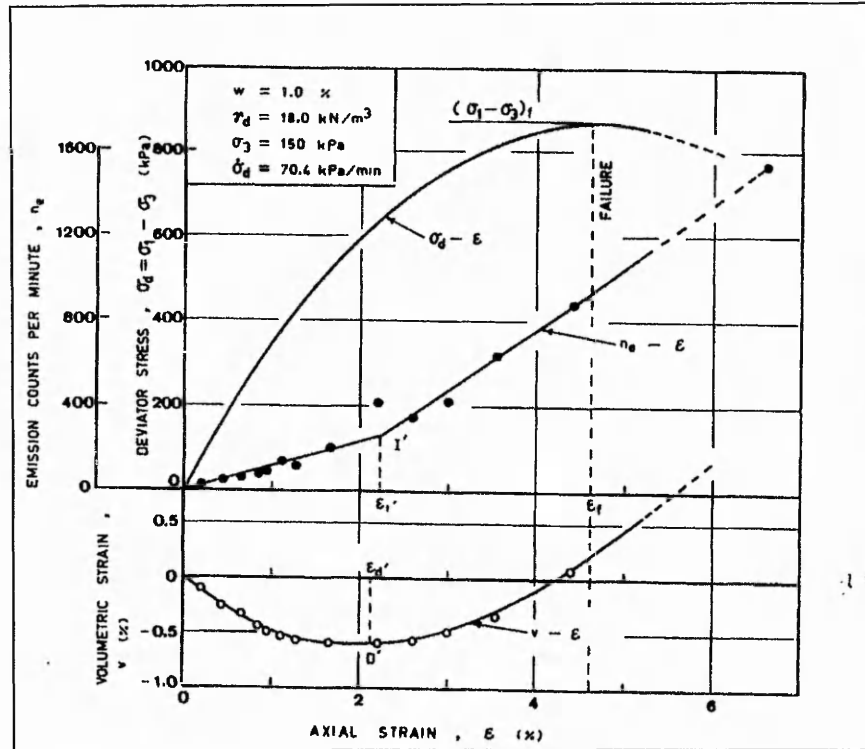


Figure 2.12 Emission counts, volumetric strain, deviator stress and axial strain relationships in stress-controlled test.

(After Tanimoto & Nakamura, 1981a)

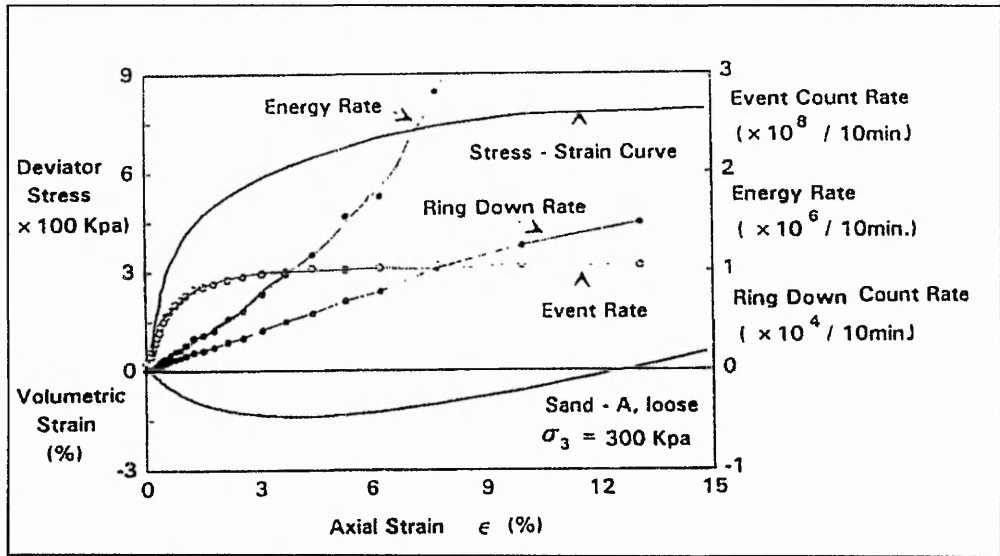


Figure 2.13 Relationships between energy rate, ring down count rate, event count rate, deviator stress, volumetric strain and axial strain in a typical result.

(After Garga & Chichibu, 1990)

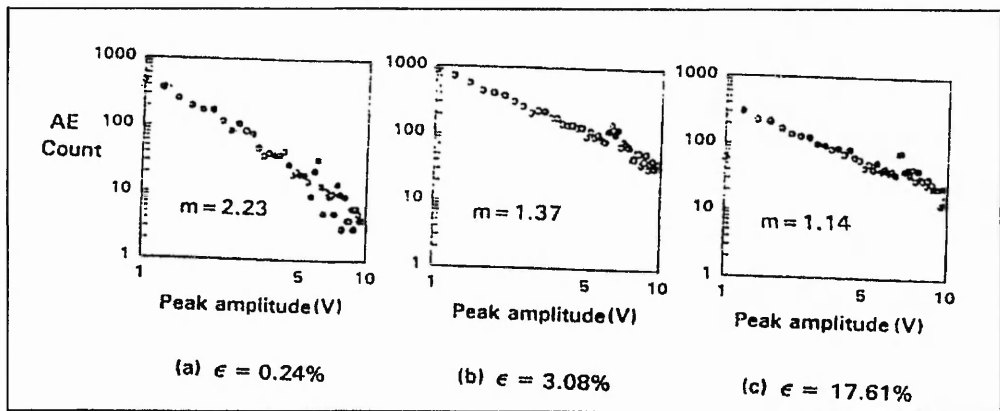


Figure 2.14 Changes of peak amplitude distribution with axial strain growth.

(After Garga & Chichibu, 1990)

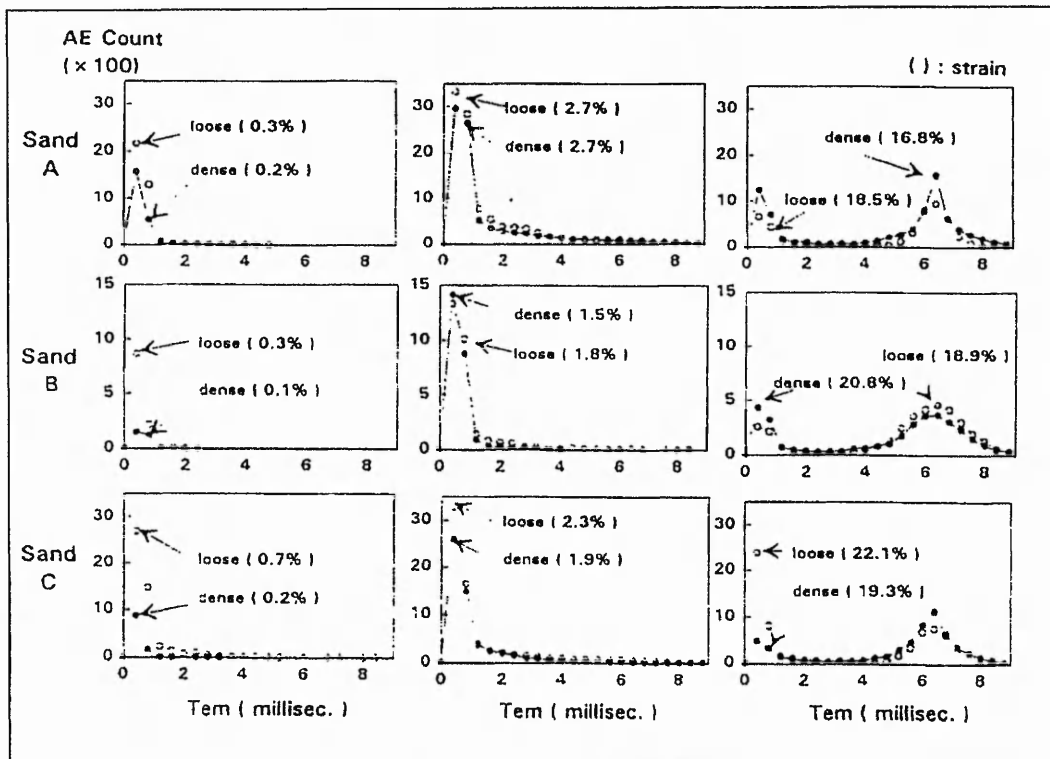


Figure 2.15 Energy moment distribution with AE count.

(After Garga & Chichibu, 1990)

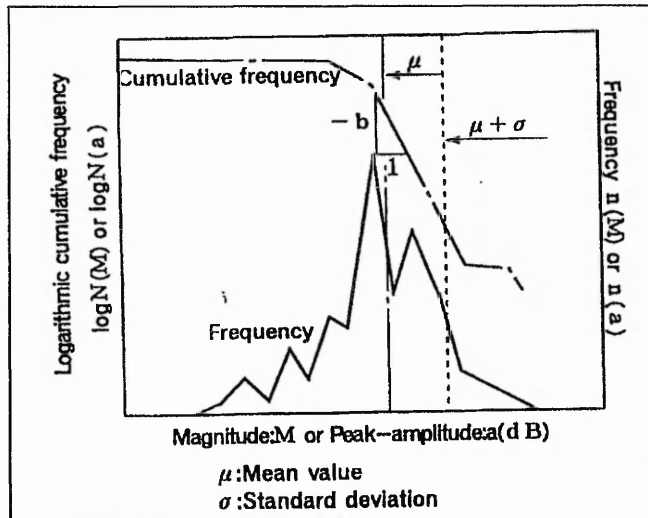


Figure 2.16 Schematic representation for AE peak amplitude distribution.

(After Shiotani *et al.*, 1994)

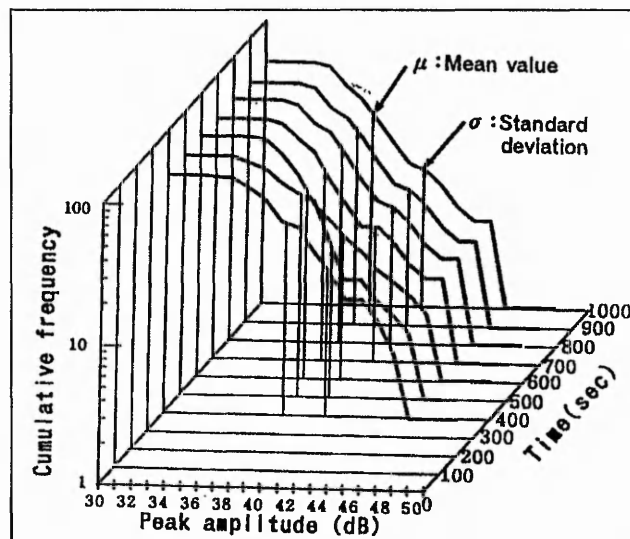


Figure 2.17 AE peak amplitude distribution based on 50 data points.

(After Shiotani *et al.*, 1994)

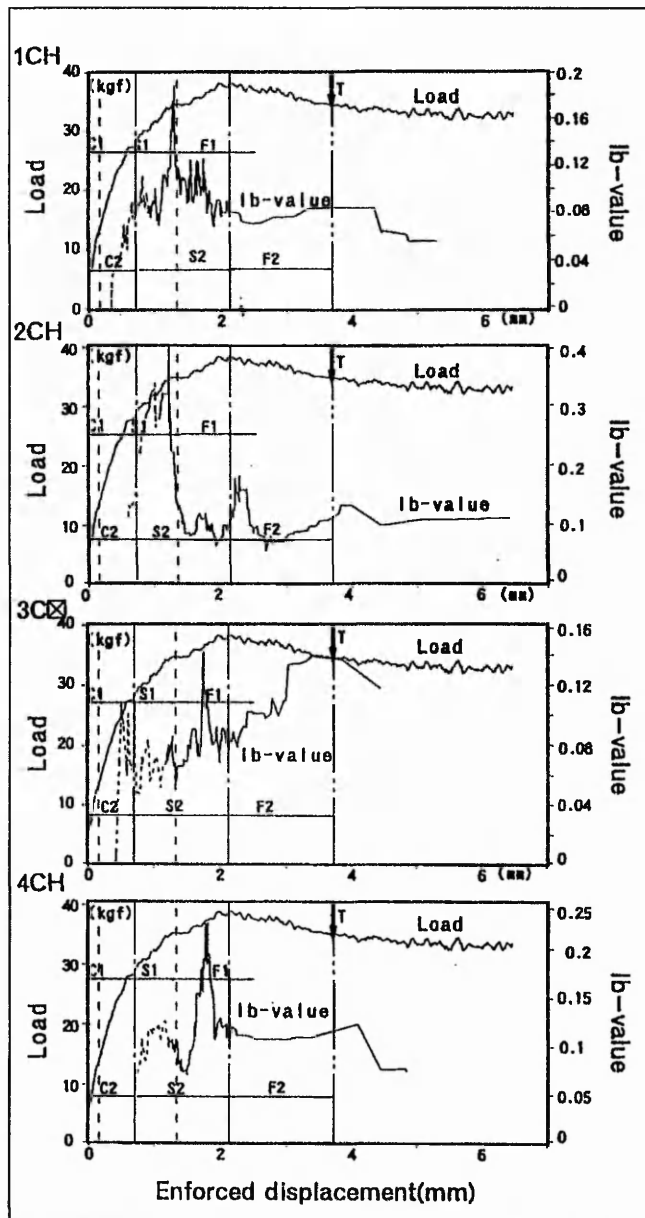


Figure 2.18 Change with enforced displacement in improved 'b-value' calculated from data acquired from four sensors.

(After Shiotani *et al.*, 1994)

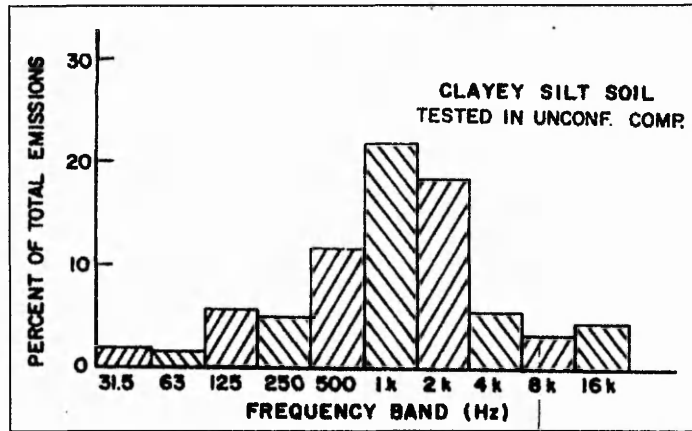


Figure 2.19 Frequency distribution of acoustic emission resulting from an unconfined compression test on a clayey silt soil.

(After Lord Jnr *et al.*, 1977)

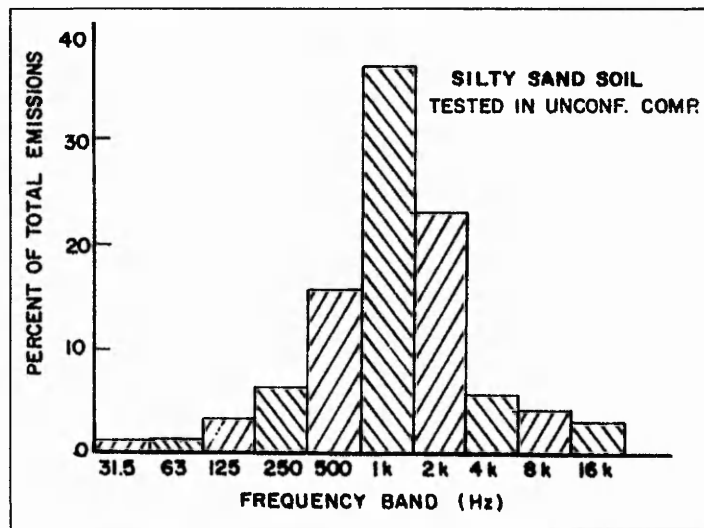


Figure 2.20 Frequency distribution of acoustic emission resulting from an unconfined compression test on a silty sand soil.

(After Lord Jnr *et al.*, 1977)

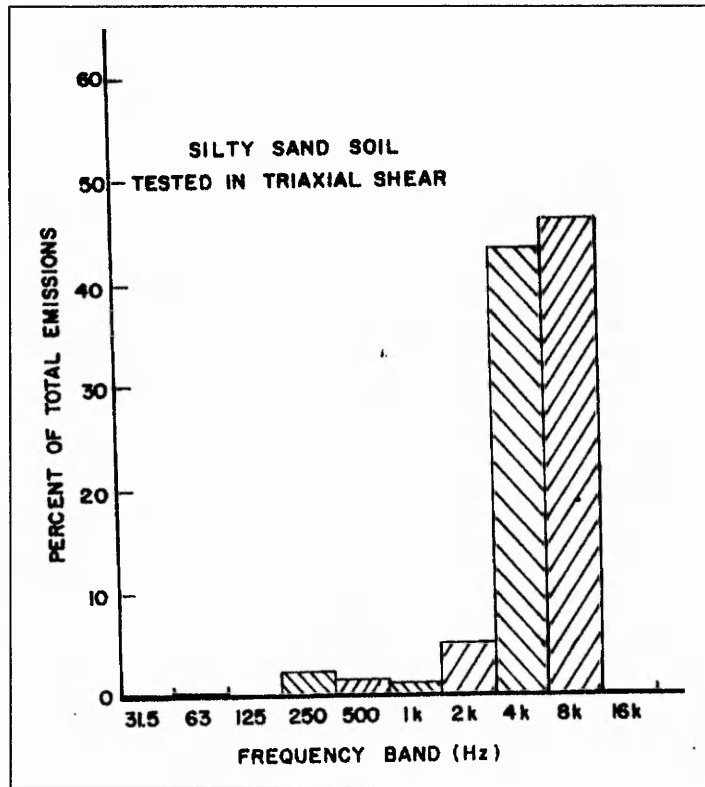


Figure 2.21 Frequency distribution of acoustic emission resulting from a triaxial compression test at 10psi confining pressure on a silty sand soil at 17% water content.

(After Lord Jnr *et al.*, 1977)

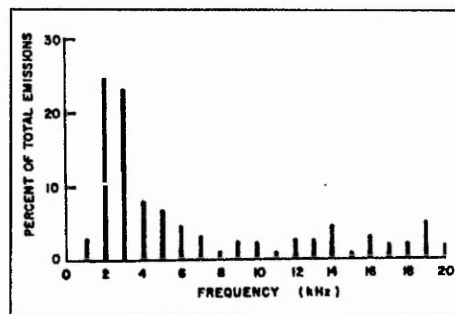


Figure 2.22 (bottom) Frequency distribution of acoustic emission from kaolinite clay at 33% moisture content tested in unconfined compression

(After Koerner *et al.*, 1977)

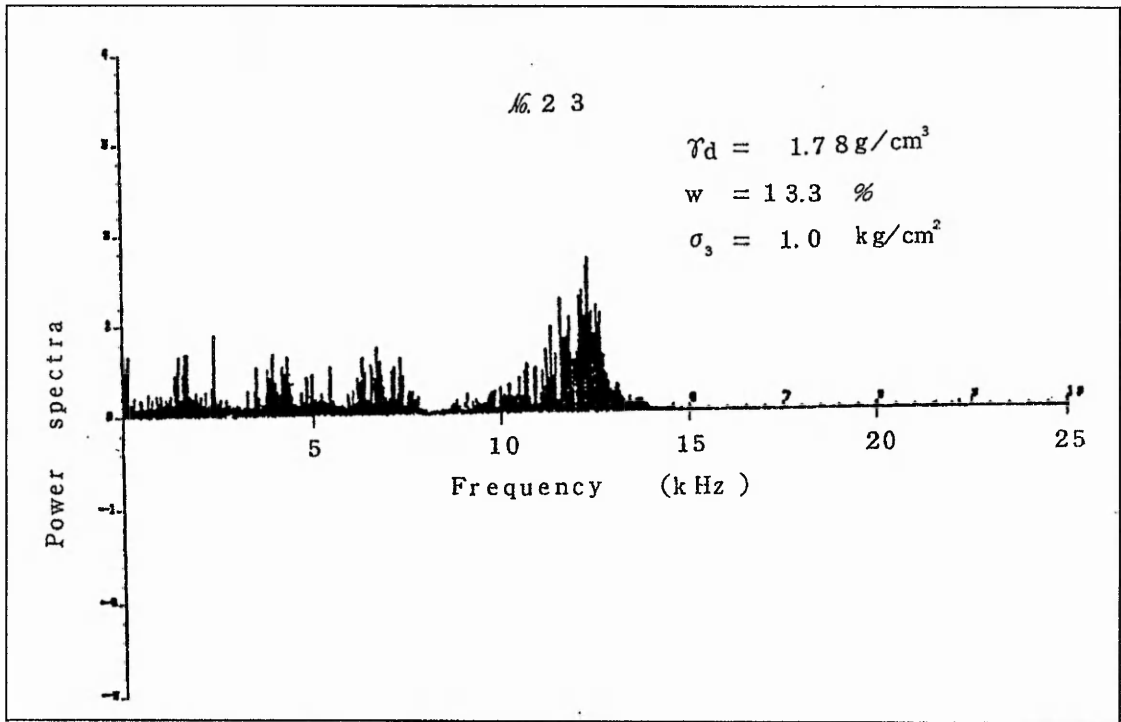


Figure 2.23 An example of frequency emission content.

(After Tanimoto *et al.*, 1978)

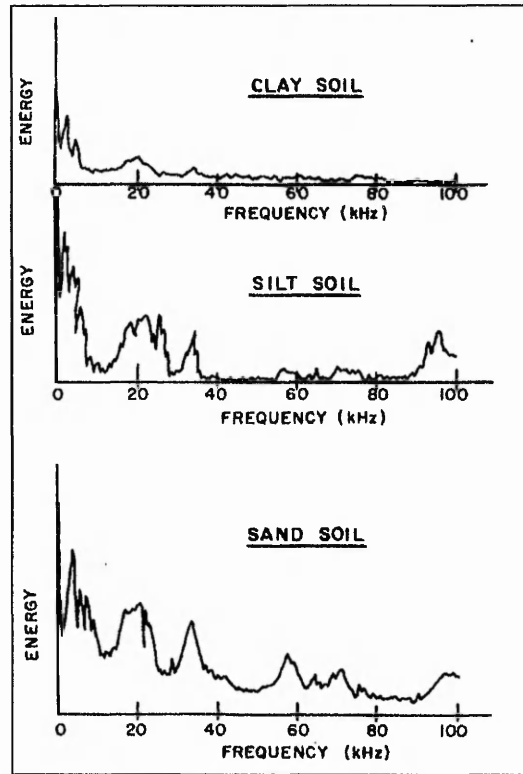


Figure 2.24 Frequency content of emission from sand, silt and clay (near failure) tested in direct shear.

(After Koerner *et al.*, 1981a)

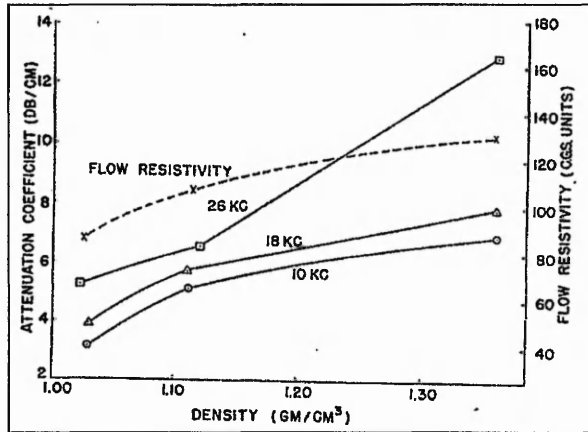


Figure 2.25 Attenuation and flow resistivity for a dry sand at various densities and frequencies.

(After Nyborg *et al.*, 1950)

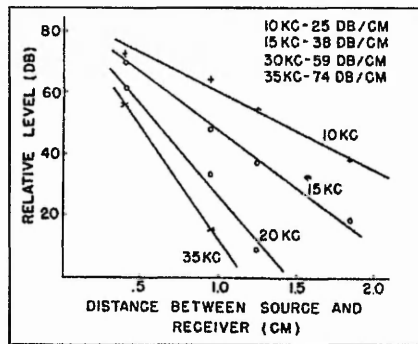


Figure 2.26 Relationship between signal level and source-receiver distance.

(After Nyborg *et al.*, 1950)

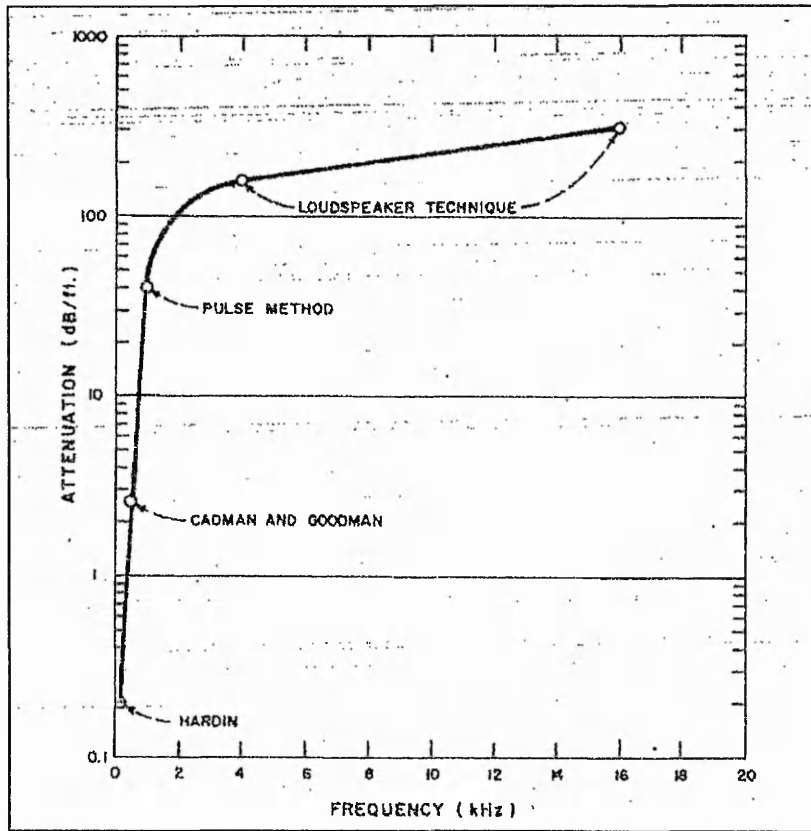


Figure 2.27 Frequency vs attenuation response of dry granular soils using techniques indicated.

(After Koerner *et al.*, 1976)

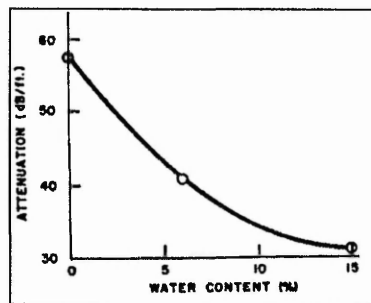


Figure 2.28 Attenuation of acoustic emission in clayey silt at varying water contents at frequency of about 1kHz.

(After Koerner *et al.*, 1977)

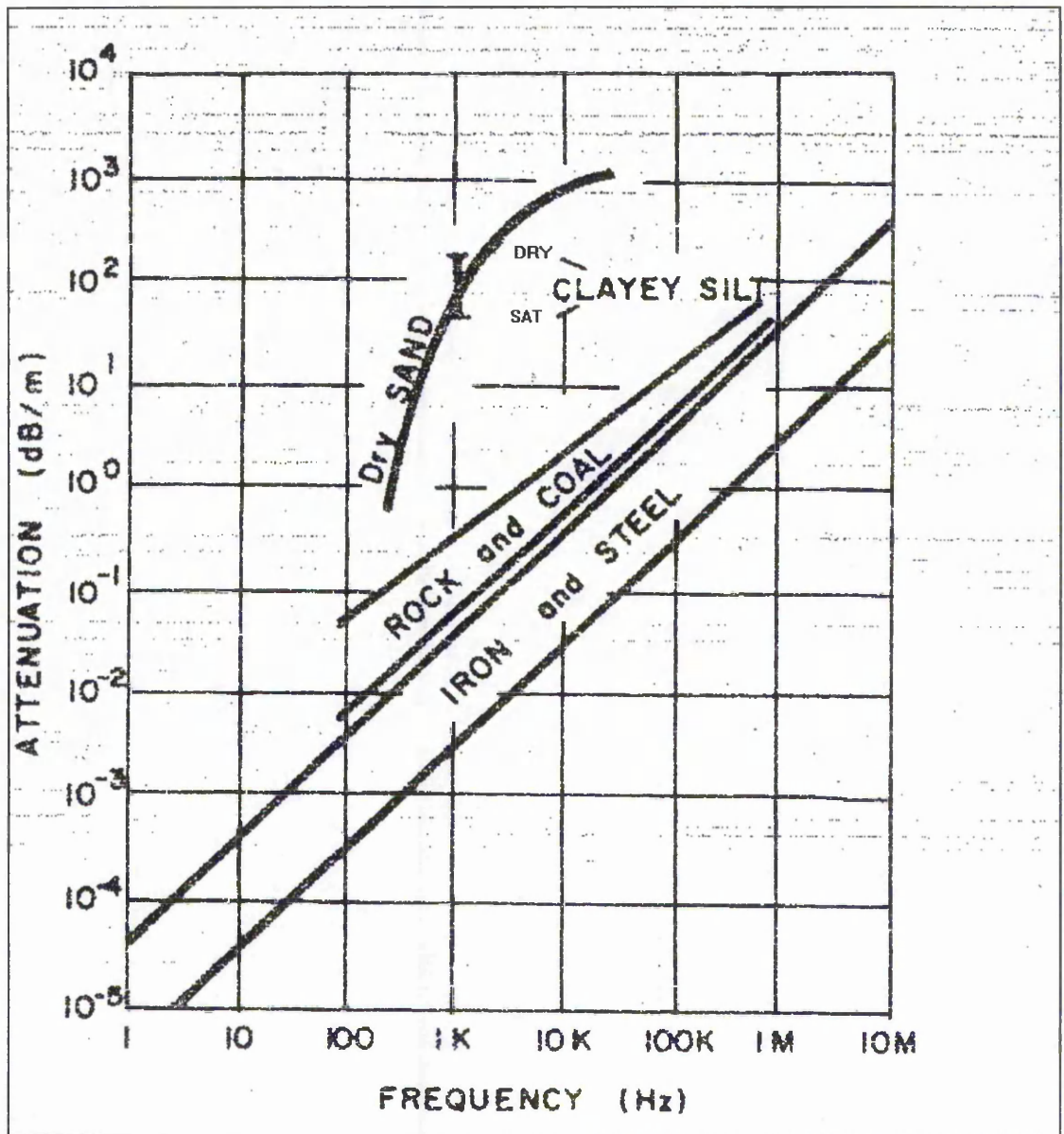


Figure 2.29 Attenuation response of different soil types contrasted to rock/coal and iron/steel.

(After Koerner *et al.*, 1981a)

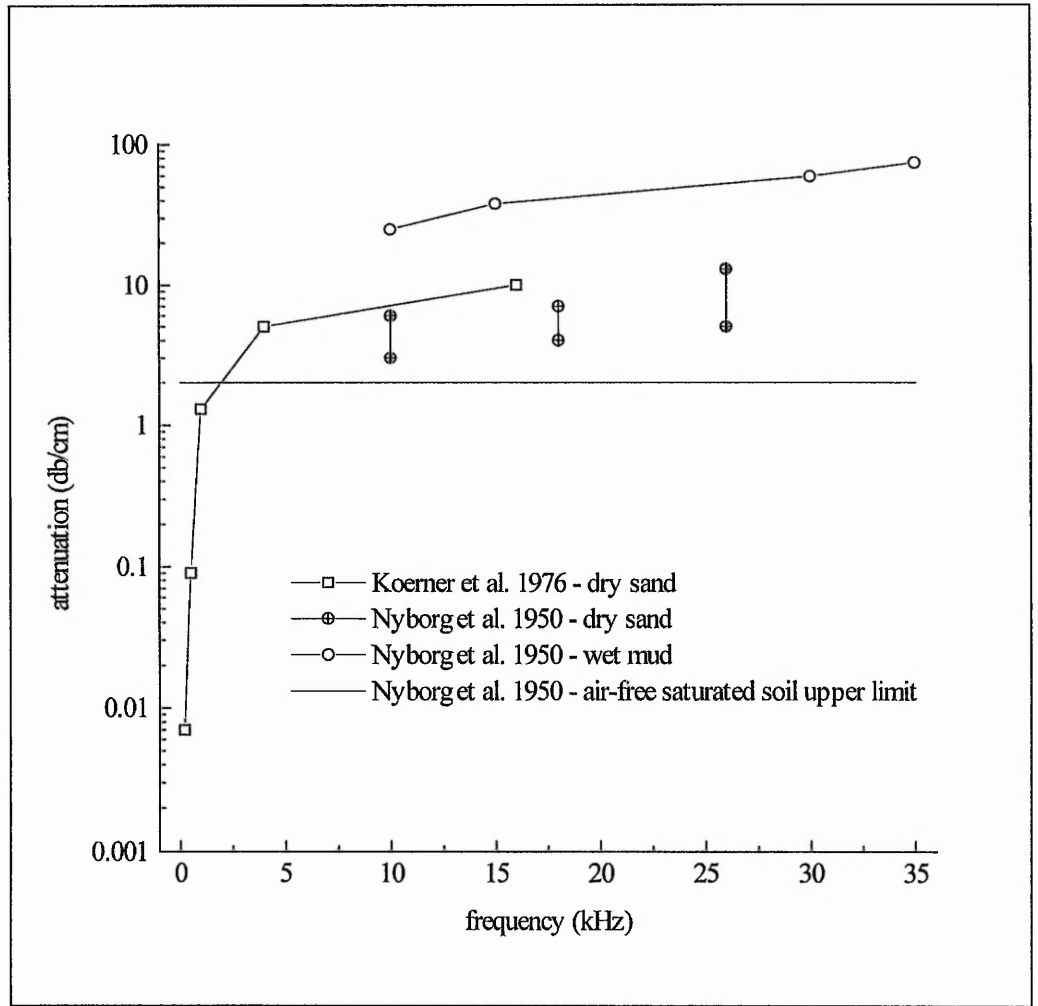


Figure 2.30 Collation of majority of published data relating to attenuation in soils.

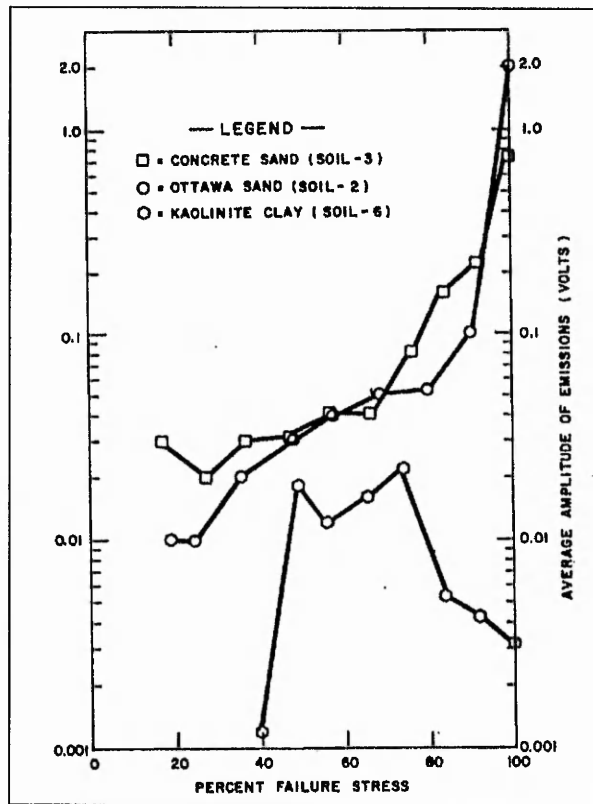


Figure 2.31 Average amplitude of acoustic emission (measured as peak signal voltage output) for various soils as function of percentage failure stress in triaxial creep at 34kNm⁻² confining pressure.

(After Koerner *et al.*, 1977)

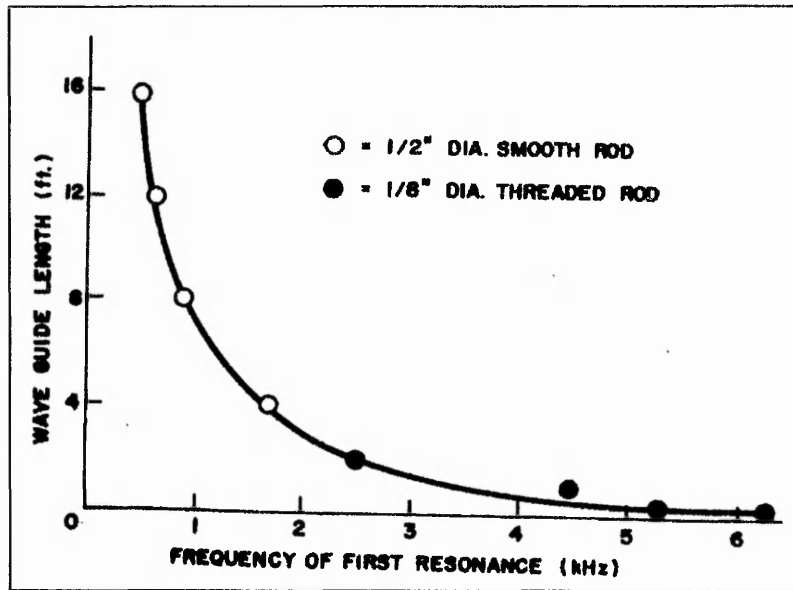


Figure 2.32 Influence of various lengths and diameter of steel rod wave guides on acoustic emission response.

(After Koerner *et al.*, 1975)

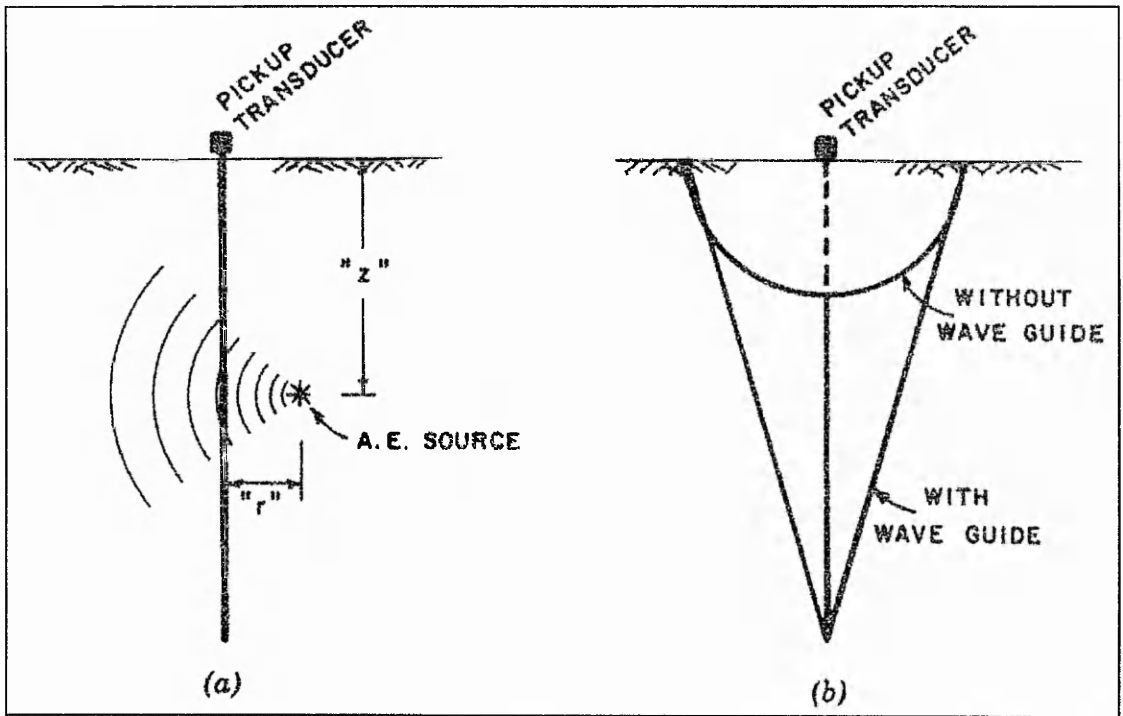


Figure 2.33 Idealised configuration of soil volume sensed by AE method using steel rod wave guides: (a) model ; (b) volume of soil sensed

(After Lord jnr *et al.*, 1982)

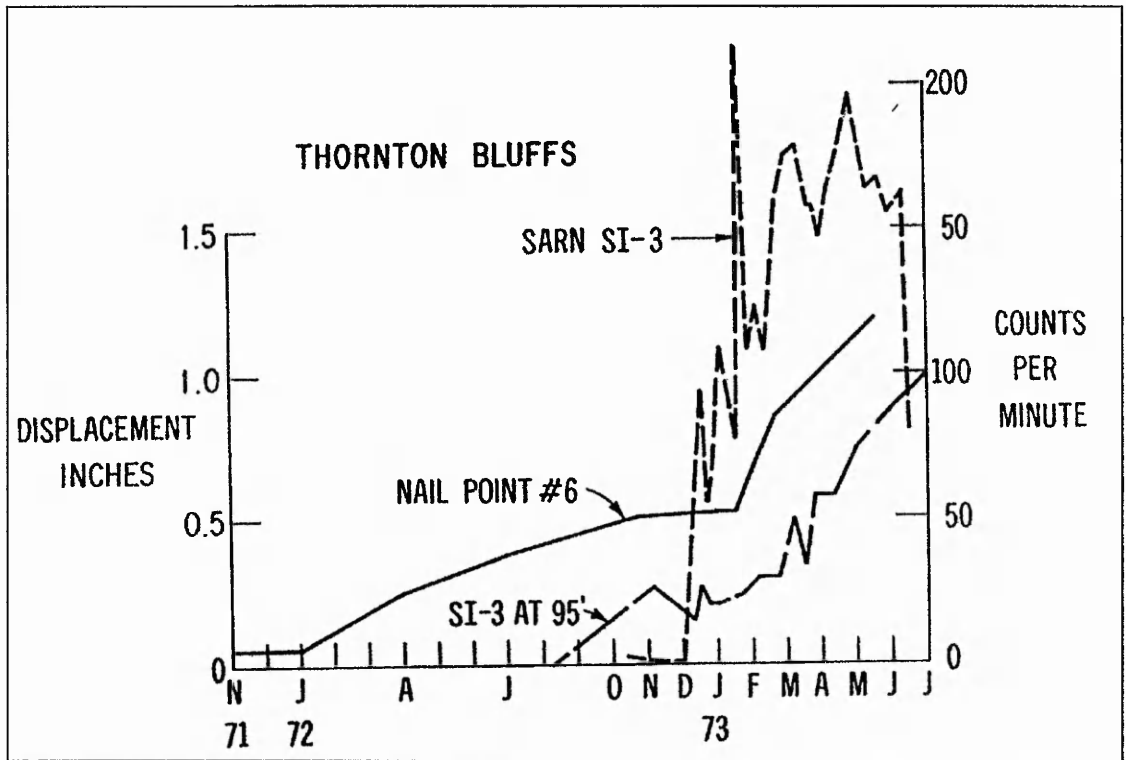


Figure 2.34 Noise rates and displacements at Thornton Bluffs field site.

(After McCauley, 1975)

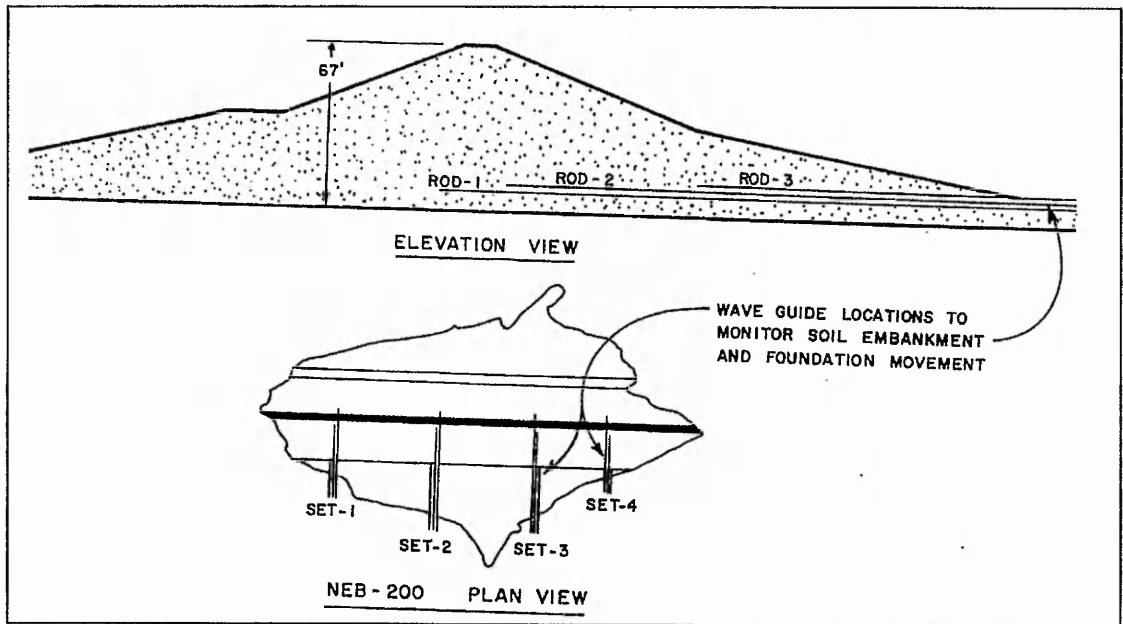


Figure 2.35 Elevation and plan view of acoustically monitored earth dam in Nebraska, showing wave guide locations

(After Lord jnr & Koerner, 1975)

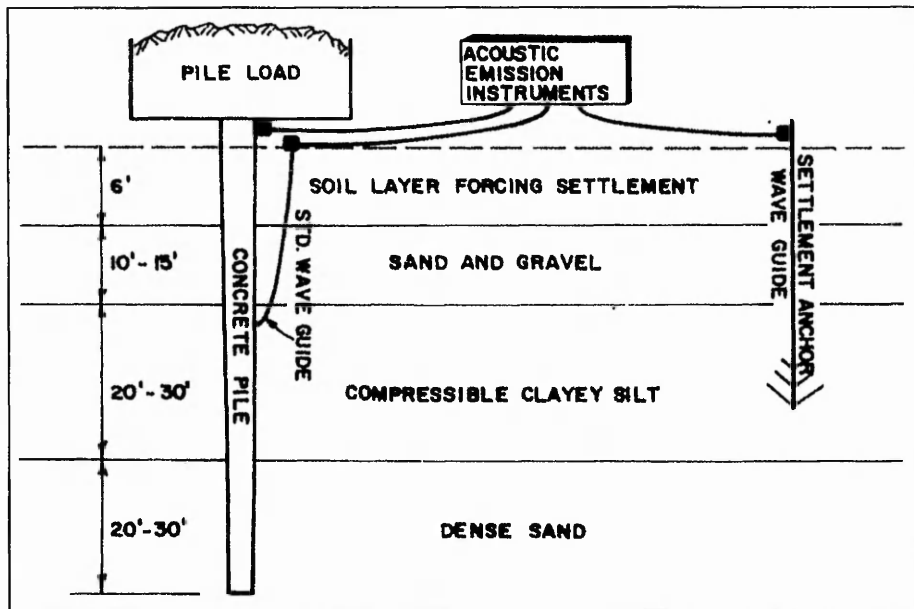


Figure 2.36 Settlement monitoring test set-up

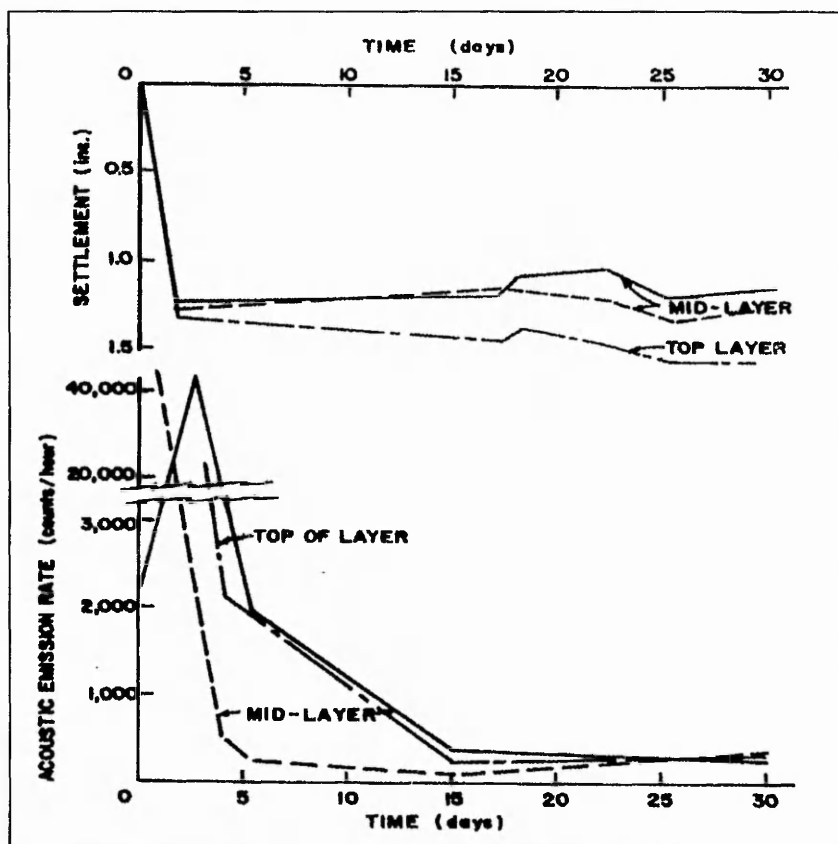


Figure 2.37 Time-settlement-AE relationship after test depicted in figure 2.36
Both figures after Koerner *et al.* (1978a)

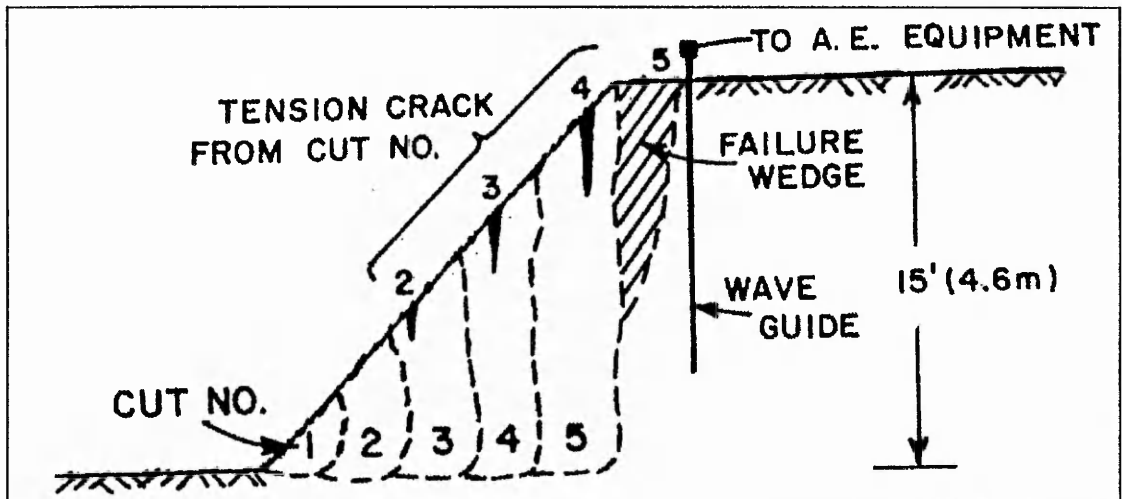


Figure 2.38 Schematic diagram of site 'PA-DSP2' showing approximate boundaries of five cuts made.

(After Koerner *et al.*, 1978b)

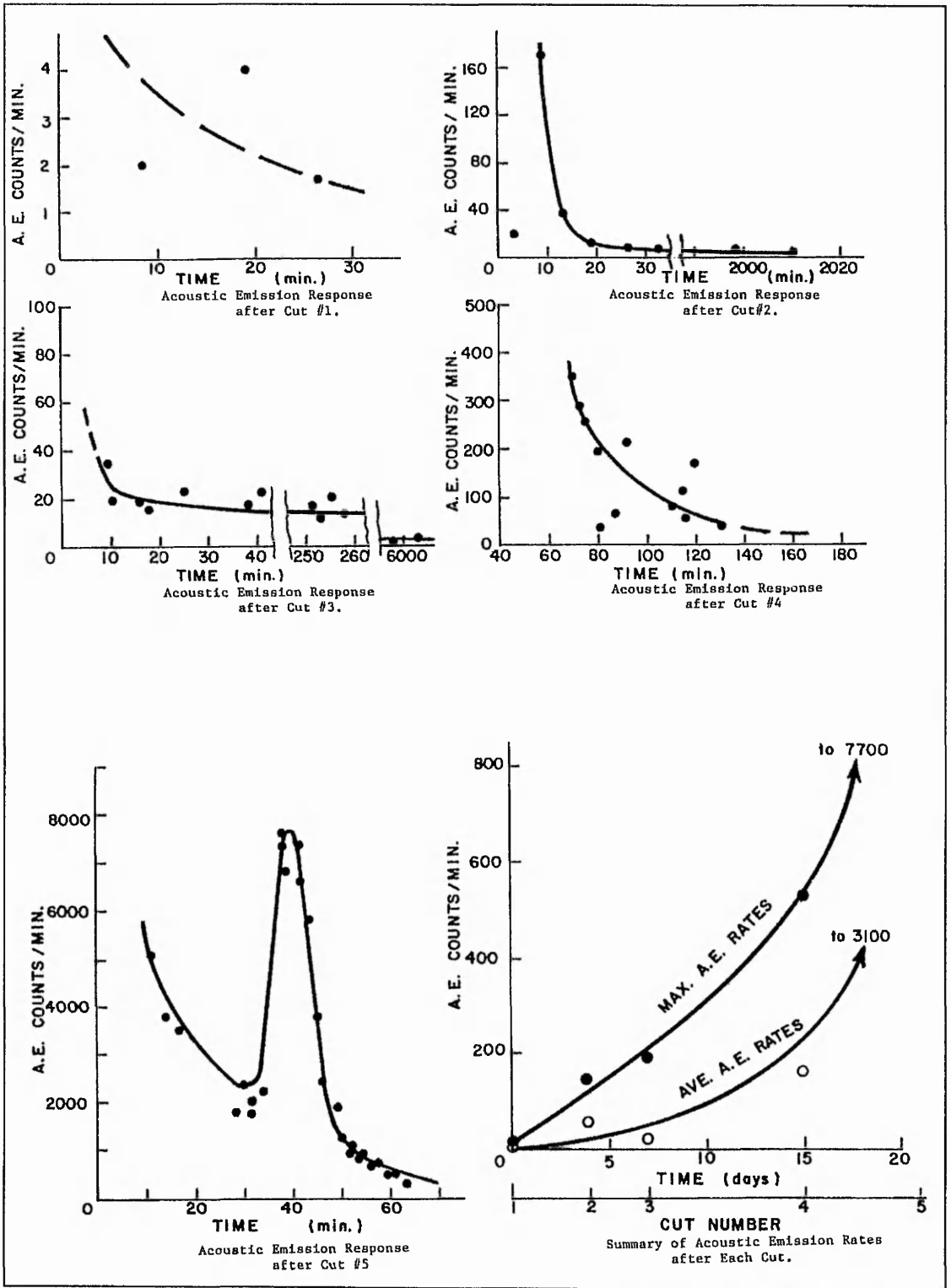


Figure 2.39 Response to cuts made in test conducted at site 'PA-DSP2'.
(After Koerner *et al.*, 1978b)

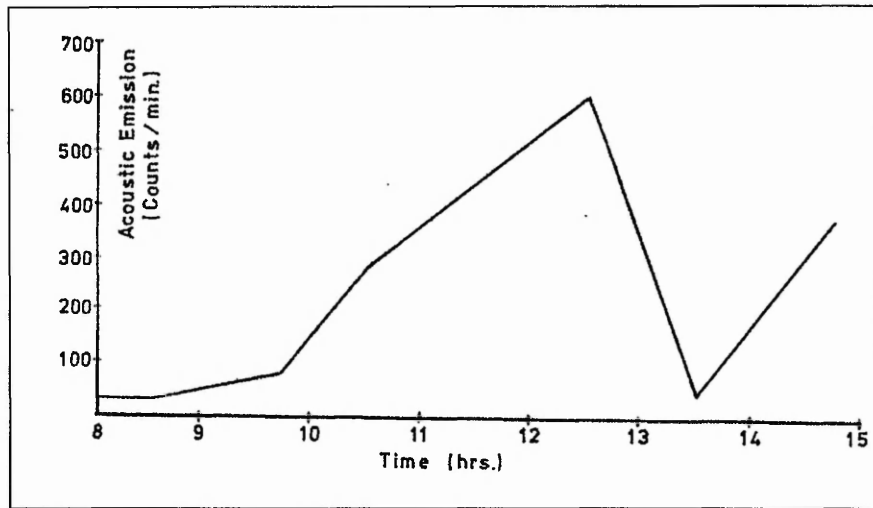


Figure 2.40 Acoustic emission measurements prior to soil slip

(After Evans, 1984)

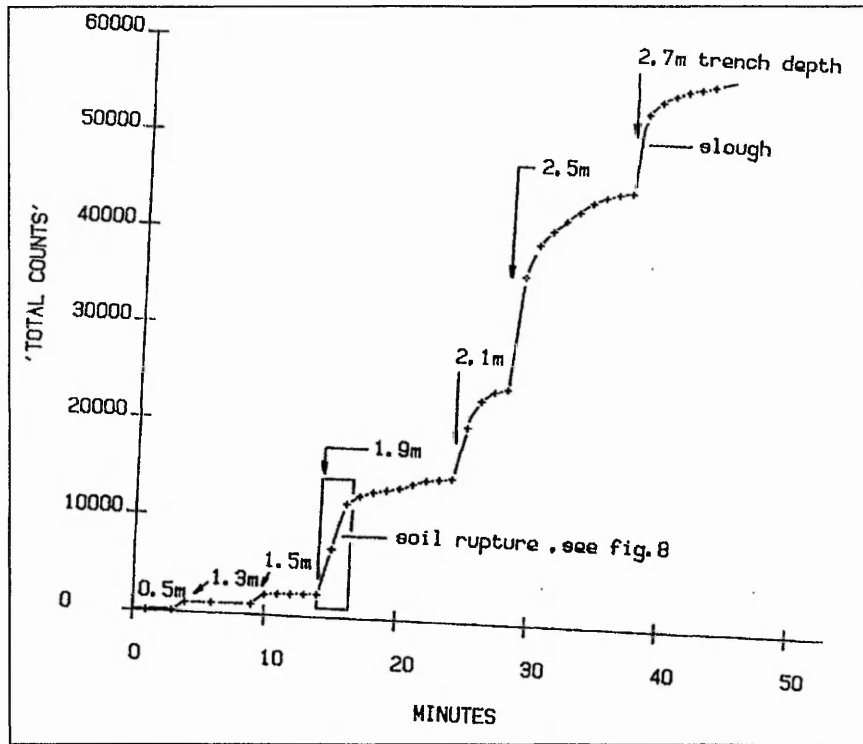


Figure 2.41 AE versus time for each cut made in trench up to failure

(After Penning *et al.*, 1983)

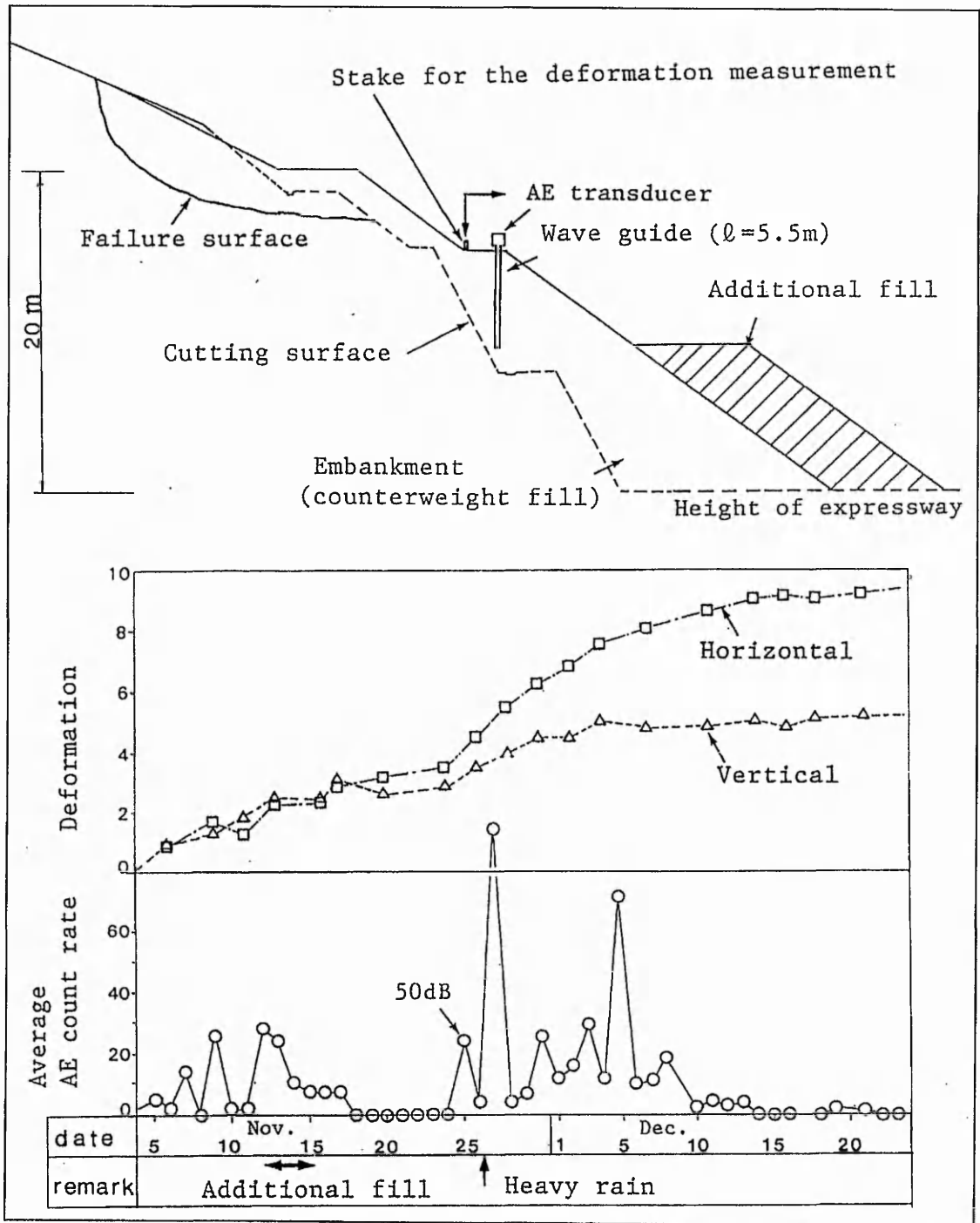


Figure 2.42 Sketch of embankment and results of monitoring. AE is measured in terms of counts per 10 minute period and displacements are given in cm.

(After Chichibu *et al.*, 1989)

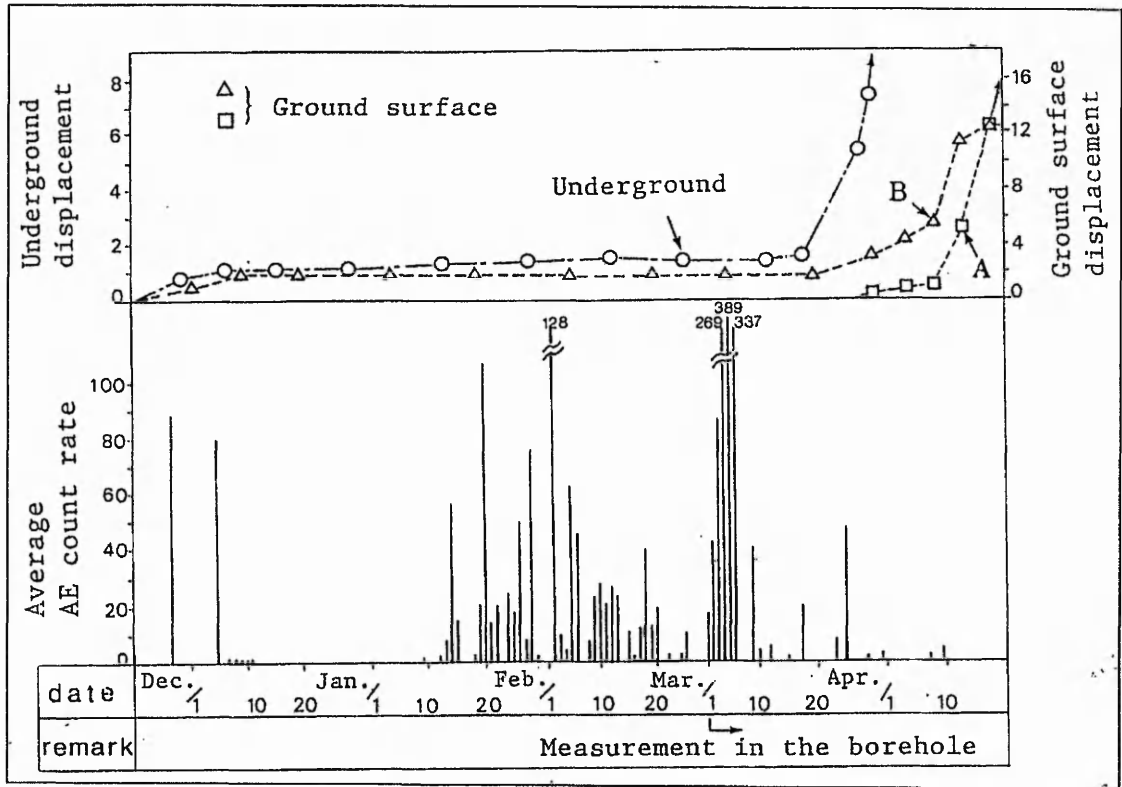


Figure 2.43 Results from monitoring of the natural slope. AE is measured in terms of counts per 10 minutes period. Underground displacement is given in mm and surface displacement in cm.

(After Chichibu *et al.*, 1989)

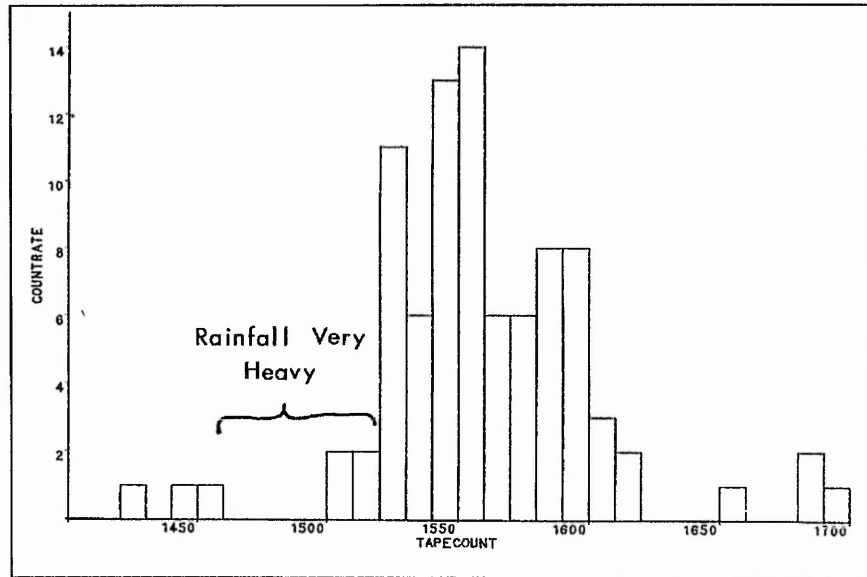


Figure 2.44 Relationship between rainfall and AE

(After Rouse *et al.*, 1991b)

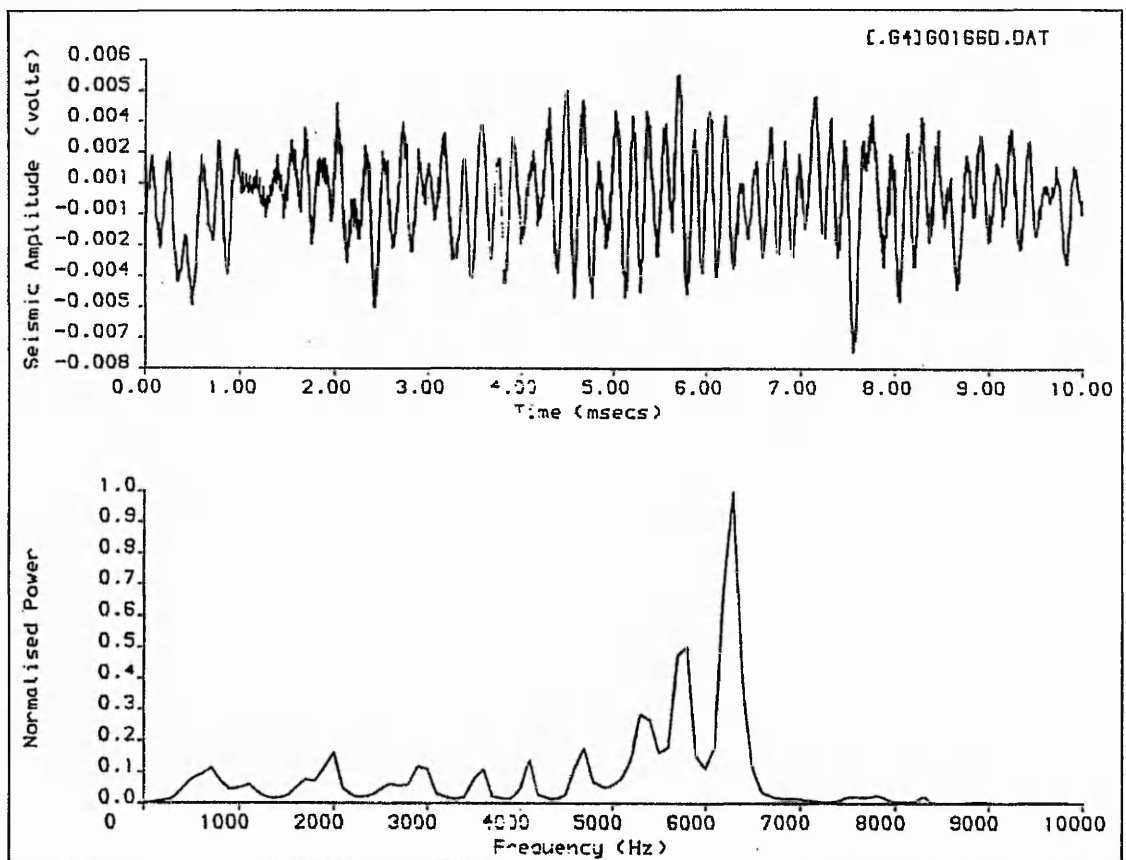


Figure 2.45 Time series and power spectrum of Type A events.

(After Rouse *et al.*, 1991a)

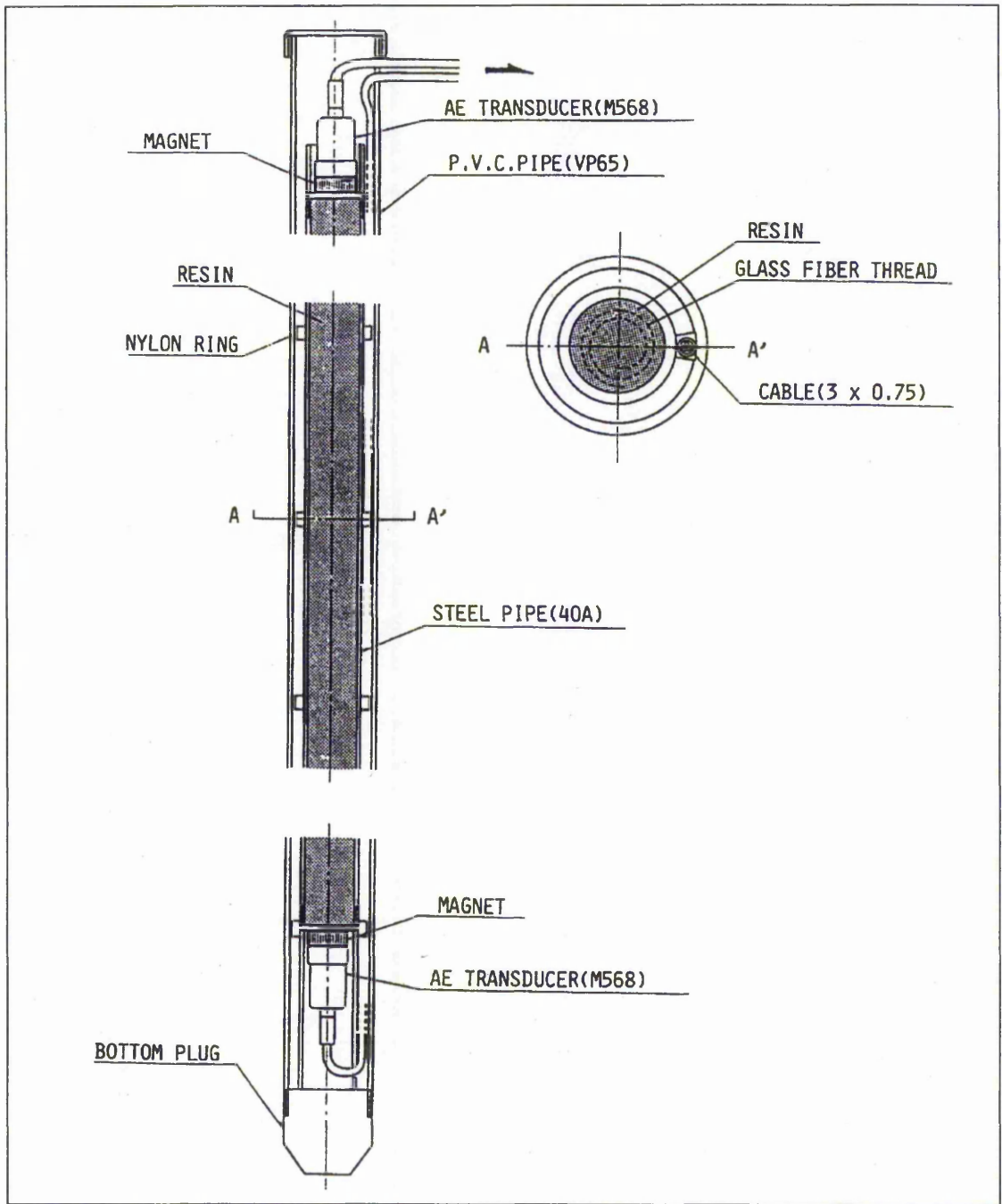


Figure 2.46 Structure of the acoustic emission monitoring rod

(After Nakajima *et al.*, 1995)

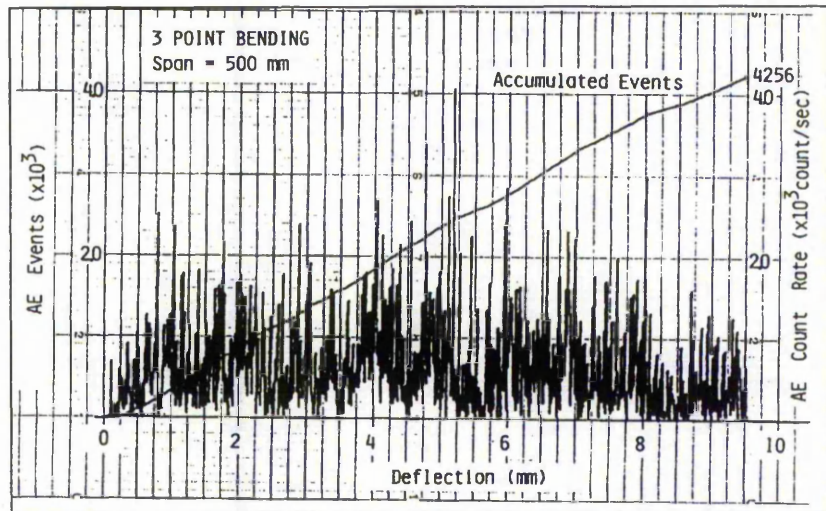


Figure 2.47 Relation between acoustic events and deflection of the monitoring rod

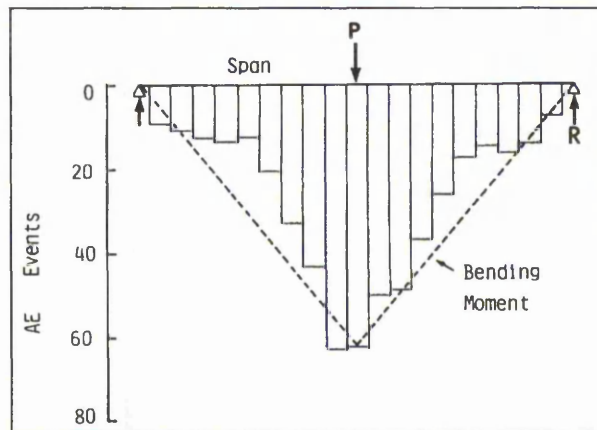


Figure 2.48 Location histogram of acoustic events on span and diagram of bending moment

(Both figures 2.47 & 2.48 after Nakajima *et al.*, 1995)

Chapter 3

Acoustic Emission Instrumentation

3.1 Introduction

This chapter discusses the instrumentation used to capture acoustic emission in this investigation and section 3.2 details both the electronic hardware and software employed. Note that individual data capture and processing routines are not covered in this chapter as these have varied between each of the field sites and the laboratory. (Particular capture routines used at Cowden, Arlesey and in the laboratory can be found in section's 4.4.1, 5.4.2(i) and 7.3.2 respectively). An integral part of any field monitoring system, section 3.3 discusses the wave guide and outlines two of the models used to describe its role. Section 3.4 discusses monitoring philosophy and highlights five considerations on field data acquisition which are imposed through the use of the system employed. Section 3.5 describes the field monitoring procedure, which was common to both Cowden and Arlesey. Following on from section 2.2, section 3.6 discusses measurement criteria in more detail and includes the effects of one further step of pre-capture processing (the signal enveloping circuit) not yet considered. It also includes some relevant formulaic definitions. Section 3.7 examines the nature of the captured emission and, finally, section 3.8 looks at some of the problems encountered with field acquired data and outlines the remedial techniques used.

3.2 Electronic Hardware and Software

Figure 3.1 presents a schematic representation of the components of the instrumentation system, each of which is detailed as follows:-

3.2.1 Transducer

The sensor used was an Acoustic Emission Technology (AET) 30kHz peak resonance piezoelectric acoustic transducer. This converts mechanical disturbances into an electrical voltage in the order of micro-volts (10^{-6} volts). Figure 3.4 shows a typical transducer response, which is called an *event* or *transient*, and its rectified envelope (section 3.2.4). Figure 3.2

illustrates a sensor calibration curve for a 30kHz transducer, indicating the sensitivity of its response at various frequencies. The choice of a 30kHz resonant transducer is something of a compromise between the desire to monitor at as low a frequency as possible (in order to reduce the effects of acoustic attenuation) and the need to minimise background acoustic noise (achieved by monitoring at as high a frequency as possible).

3.2.2 Filter and Preamplifier

Combined into one unit, this AET product is a narrow band preamplifier with a bandwidth of 15 - 45kHz and amplifies the signal by 40dB (x100).

3.2.3 The AET 204GR

This is a ruggedized battery operated acoustic emission monitoring system designed to measure and process AE data arising from field applications. It operates within a bandwidth of 30Hz to 200kHz and can provide measurements of AE in terms of total ring down counts, total events, count rates, event rates and signal strength (Root Mean Square). It can sample up to eight channels consecutively and amplifies the signal between 10 and 68dB in steps of 2dB. Together with the transducer and preamplifier this forms an AE monitoring system in itself. The only output is an LED counter, which relates the current value of the chosen parameter, or a connector through which the amplified signal is available. The AET only operates from a battery supply and will work for approximately twenty-four hours on one full charge. In this investigation the unit was used solely to amplify the signal prior to being further processed as outlined below.

3.2.4 Signal Enveloping Circuit

The purpose of the signal enveloping circuit is to reduce the number of data points required to describe the response of the transducer to an emission. The circuit achieves this by processing the a/c signal generated by the transducer to produce its rectified envelope. Figure 3.4 illustrates such an a/c signal with its rectified envelope. The circuit basically consists of three electronic

components - a diode, a capacitor and a potentiometer (variable resistor). The diode permits charge of only one polarity to pass (thus eliminating half the original wave form) and this is stored by the capacitor. The capacitor then discharges over a period of time dependent upon the product of the capacitance and resistance (the time constant) used in the circuit. The potentiometer, therefore, permits final refinements to be made to the form of the envelope until the desired output is obtained.

Although this involves some loss of resolution of the AE event, acquiring a smaller number of data points does generate a number of advantages. In this research it resulted in the use of a half-sized analogue-to-digital (A-to-D) conversion board (section 3.2.5) instead of a full-sized one. This immediately involved savings in terms of both cost and consumption of electrical energy, the latter being of considerable importance in field applications. Additionally, a reduction in the number of data points required to describe an event enables more events to be stored on a computer hard disc of finite capacity. Note that this unit, logically positioned between the main amplifier and A-to-D conversion board, is not shown in figure 3.1.

Figure 3.4 is explained more fully in section 3.6 which deals with measurement criteria.

3.2.5 Analogue-to-Digital Conversion Board

The board is a *Keithley DAS1402* capable of sampling at a maximum rate of 100kHz. It is a half-sized board with sixteen single-ended or eight differential input channels. The A-to-D board, under instruction from the computer, is responsible for the sampling and digital conversion of the analogue voltage. An important aspect, which has implications for the data capture routines, is the fact that the board is *not* capable of triggering on the event. Although this is a useful and efficient way of eliminating unwanted noise, it does require the judicious selection of a 'threshold' value below which data is discarded. Too high a threshold may involve the loss of valuable data. Owing to the DAS 1402's inability to trigger on the event, this was not a problem and details of the various data sampling routines used can be found in sections 4.4.1, 5.4.2(i) and 7.3.2.

3.2.6 The DacPac

The DacPac is a specially manufactured expansion box which houses the A-to-D board. Rechargeable batteries within the DacPac power the board for about six hours of field acquisition from one full charge.

3.2.7 The Computer

The notebook computer is a *Dual* 486DX 33MHz clock speed, 8 MB RAM, 250MB hard disc. It has its own on-board battery power source but, due to problems concerning an adequate ground connection (section 4.4.1), was invariably run from a Landrover battery using the vehicle's chassis as ground. The notebook, DacPac and AET model 204GR are illustrated (in use in the field) in figure 3.3. (Note that the DacPac is the slim unit under the notebook and on top of the AET 204GR).

3.2.8 Software

Data acquisition (and much of the processing) was controlled by the high-level, Keithley-produced programming language called *Viewdac*. It consists of powerful single commands or *tasks* which can control, or be controlled by, any other task (within certain rules). This means that programmes can be formulated whereby the usual top-to-bottom flow of logic can be dispensed with. Also, as more than one task may be active at any one time, the language is capable of exhibiting *pseudo multi-tasking* (there is still only one CPU).

A number of additional data processing routines were written in FORTRAN and QBASIC.

3.3 The Wave Guide

The wave guide usually consists of some form of metal tubing which is inserted into the ground and to which the transducer is attached. Generated noise propagates along the length of the wave guide and is detected by the transducer. There are two suggested models which attempt to

explain the role of the wave guide and the mechanisms responsible for the generation of the emission. In the first, or passive, model (passive wave guide) it is assumed that noise generates in, and propagates through, the body of soil (and therefore suffers attenuation in the soil) before striking the wave guide. (Note that AE generated in this manner, as the result of soil particle interaction, is also known as *pedogenic* acoustic emission). This model has already been discussed in section 2.4.5 (and illustrated in figure 2.33) when work by Lord jnr *et al.* (1982) was considered. The second, or *active*, model (active wave guide) assumes that noise is generated as a result of some interaction between the wave guide and surrounding material, with the deformation of the soil body acting as a driving force. As such the emission only propagates through the metal of the wave guide (and, possibly, the wave guide backfill as well) and not the soil body. (In fact, it has already been stated, both in the abstract and section 1.4, that the *active* wave guide model is considered the most likely explanation of wave guide behaviour in this investigation).

It is evident (for both wave guide models) that the position of the wave guide *relative to a zone of deformation* is highly important. Any wave guide must, therefore, be *designed and positioned* to take account of the prevailing geotechnical conditions in order to ensure that it is capable of responding to deformation.

With both models it is also possible to envisage a wave guide which is positioned such that it is unable to relay deformation-related AE to the transducer (e.g. it is situated well back from the face of a slope) and this leads to the concept of the *control* wave guide. At both field test sites control wave guides were employed in order to determine the level of *background noise* (section 5.6.6), which is the portion of a captured emission which arises due to mechanisms not related to deformation.

In order to distinguish between control wave guides and wave guides which are designed to detect deformation-related AE, it is appropriate to define the term *gauge wave guide*. A gauge wave guide is, therefore, defined as a wave guide which is installed into a soil body with the aim of detecting deformation-related AE, irrespective of the particular design of the wave guide or whether the intention is to generate active AE or capture pedogenic AE.

Specific details relating to the design, construction and installation of wave guides at both Cowden and Arlesey are dealt with in sections 4.2 and 5.3 respectively.

3.4 Monitoring Philosophy

Although, by design and construction of dedicated circuitry, it is possible to monitor a wave guide continuously and indefinitely, there is (as yet) insufficient information upon which any such design could be based. Also, as an investigation of this type would involve leaving an amount of expensive experimental monitoring and data capture equipment in the field, it is clearly not feasible at the moment. It is, at any rate, evident from the description of the monitoring hardware that this research was based upon periodic site visits and acquisition of data. It is highly likely, therefore, that much deformation-related emission was not captured simply because no operator was present when it was generated.

Once a system based on periodic site visits was chosen, important constraints were placed upon how and when the field data was acquired. Five major constraints, which are interrelated although dealt with separately, have been identified as follows:-

(i) Available Time

Both Cowden and Arlesey were, coincidentally, almost exactly 110 miles by road from The Nottingham Trent University and both sites were on private property which opened and closed at specific times. Although arriving too early was rarely a problem, the fact that both sites closed at approximately 5.00pm was. Generally all the Arlesey wave guides were monitored but at Cowden, where there were twelve wave guides and two inclinometers, this was not usually achieved.

(ii) Electrical Power

Before problems concerning grounding of the system (section 4.3.1) were discovered the notebook was operated using its own battery supply. This permitted approximately one hours use in the field. However, on purchase of an adapter from which the notebook could be powered using a vehicle's battery, this ceased to be a problem. As has been discussed in section 3.2.3 and 3.2.6, the AET 204GR and DacPac were both powered using their own batteries; the former lasting approximately twenty-four hours and the latter six hours on one full charge. The DacPac

therefore presented the 'weak link' and did once, during the Arlesey test, cause monitoring to be halted prematurely when the battery became fully discharged.

(iii) Hard-Disc Capacity

The notebook has a hard-disc capacity of 250MB although much of this space was already accounted for with various software packages. This aspect was not a problem at Cowden, where available time was the predominant factor, but at Arlesey (during the test period when the researchers stayed locally permitting all day monitoring) it was. At the end of each of these test days it was necessary to compress the captured data using a shareware package called 'PKZIP' and then remove the data from the hard-disc to floppy-disc using 'MSBACKUP'. Depending upon the original data, which occupies 4 bytes per data point, typically a file would be compressed to approximately 25% of its 'normal' size. (Further information concerning the number of AE files generated and volumes of data produced are given in sections 4.3.3 and 4.3.4 for Cowden and section 5.4.4 for Arlesey). This constraint had a profound effect on acquiring a *representative sample* which is dealt with in the following section (iv).

(iv) Representative Sample

It is impossible to define exactly what a 'representative' sample is, however it is obviously desirable to obtain as large a volume of data acquired over as long a period of time, as possible. Also, because the A-to-D board was incapable of triggering on the event, it was necessary to employ capture routines which simply ran for specific time intervals. The combination of the number of wave guides on a site and the acquisition rate had, therefore, to be balanced against the length of time it was considered desirable that each wave guide should be monitored for.

(v) Signal Detail

Clearly it is advantageous to capture the emission in as much detail as possible. As the signal is generated by a 30kHz peak resonance transducer and passed through a 15 - 45kHz band pass filter, the A-to-D board was only operated on its maximum acquisition rate of 100kHz.

Individual monitoring routines (which were considered to represent the best compromise between the above five criteria) for each of Cowden, Arlesey and the laboratory test programme are outlined in sections 4.3.1, 5.4.2(i) and 7.3.2.

3.5 Monitoring Procedure

The following procedure was adopted when setting up the instrumentation system:-

- 1 The computer hardware was assembled as shown schematically in figure 3.1.
- 2 The surface of the wave guide was checked for any loose dirt or sand and cleaned. The 'U' bolt connector was dismantled and reassembled around the wave guide. Acoustic gel was applied to the wave guide and the transducer pressed into it. The 'U' bolt connector was slipped over the transducer and tightened until the transducer could not be moved by hand action (figures 3.5a & 3.b).
- 3 The inner plastic tube was placed over the wave guide assemblage ensuring that the connecting cable passed through the 'V' cut in its base and that the cable was loose within the tubing (but did not touch the wave guide). The outer plastic tubing was then placed over the inner and, after checking that no gaps existed between the wave guide covers and the ground, both plastic tubes were fitted with their own custom made lids. The whole wave guide was, in effect, 'double-glazed' (figures 3.5c & 3.5d).
- 4 The AET acoustic emission system was switched on and left for 30-60 seconds in order to allow the electronics to stabilise. The Notebook computer was then switched on and Viewdac control programme run. The appropriate sequence was activated, acquisition mode was selected and data written to disk.

3.6 Measurement Criteria

The transducer response illustrated in figure 3.4 also shows some of the alternative techniques by which the transient can be quantified. The traditional AE measurement parameters are the

ringdown count and event. A count is simply an upward crossing by the signal (rising edge) of some threshold value pre-determined to eliminate background noise (section 5.6.6). Figure 3.4 shows nine counts and, in this investigation where an event is defined as any number of consecutively acquired post-threshold data points (including one), one event.

Two other parameters which can be extracted from an electronically defined event, peak amplitude and rise time, are also shown and defined on the figure. The rectified envelope can be processed to calculate the area under the curve formed by the envelope. However, this investigation predominantly uses the statistical measurements of the arithmetic mean and standard deviation (and, to a lesser extent, the root mean square) to describe both the bulk data sets and post-threshold data. Some use of ringdown counts and events, as described above, is also made and amplitude distributions (of laboratory test data only) have been examined. Note that rise time and event duration have not been used as the resolution of the acquired wave form is not considered good enough to render measurements of sufficient precision to be meaningful. (Figure 3.8 shows wave forms captured at Cowden).

Peak amplitude distributions have been used to attempt to differentiate between alternative mechanisms responsible for the generation of AE within a particular system as well as indicating changes in the nature of an emission with time (e.g. Jackson, 1986; Garga & Chichibu, 1991; Shiotani *et al.*, 1994 - section 2.3). As has been stated in the abstract and section 1.4, the mechanism considered most likely to generate AE in the field is that described by the *active* wave guide model. Some consideration is given to this processing technique in sections 6.6 and 7.9.1. However, it is not the peak amplitude of the event which is considered but the mean magnitude of its constituent data points.

Use of the statistical measurements of the arithmetic mean and standard deviation (a measure of the 'spread' about the mean) to describe an AE data set is not without precedent (Jackson (1986) & Shiotani *et al.* (1994) - section 2.3). As will become evident in Chapter's 4 and 5, comparison between the arithmetic means and standard deviations of 'bulk' and 'post-threshold' data sets can provide some insight into the mechanisms of AE generation.

The arithmetic mean, standard deviation and root mean square are defined as follows:-

For a set of N data points $X_1, X_2, X_3, \dots, X_N$

a) The Arithmetic Mean

$$\bar{X} = \frac{1}{N} \sum_{j=1}^{j=N} X_j$$

b) The Standard Deviation

$$s = \sqrt{\frac{1}{N-1} \sum_{j=1}^{j=N} (X_j - \bar{X})^2}$$

c) The Root Mean Square (RMS)

$$RMS = \sqrt{\frac{1}{N} \sum_{j=1}^{j=N} X_j^2}$$

It is appropriate to include here the definition used for signal amplification - the decibel (dB)

$$dB = 20 \log_{10} \left(\frac{V_{out}}{V_{in}} \right)$$

Where V_{in} is the reference or input voltage and V_{out} is the voltage resulting after some form of processing has been performed on the signal. Processing, for example, could be the amplification

made to the voltage generated by the transducer or it could be the attenuation suffered by the signal as it propagates through a medium.

3.7 The Data

One of the advantages of the capture system employed in this investigation is that the acquired data may be examined on the computer's screen (and thus enabling the operator to assess its validity) prior to it being written to hard disk. This form of visual check is very difficult, if not impossible, to accomplish with a numeric display as would have been used by earlier workers. This has led to the identification of a number of problems which are dealt with in section 3.8.

An example of genuine field acquired AE data is shown in figure 3.6 which depicts a sample of 20,000 data points captured at the Cowden site. This also indicates how captured data would appear on screen to an operator. Figure 3.7 depicts just 100 data points of the same sample. Figure 3.8 is the same as figure 3.7 but with the acquired data points indicated.

3.8 Data Set Problems

A number of different problems were encountered in data acquisition. These are outlined below and illustrated in the appropriate figures.

- (a) It was noted at Cowden that monitoring immediately after switching on the AET produced a low level signal which gradually increased (over approximately fifteen seconds) to the 'normal' level. Figure 3.9 illustrates such an increasing signal. The problem was not, therefore, allowed to occur at Arlesey. However, for those data sets where it did occur, it was dealt with simply by excluding the affected portion of the wave form. Reduced data sets were then expanded to the standard size for Cowden (section 4.3.1) by duplicating unaffected portions of the wave.
- (b) A number of data sets acquired at Arlesey suffered from a threshold shift, an example of which is shown in figure 3.10. These were adjusted by reducing the affected data set to the

'zero' position by considering the level of other data acquired on the same day and data trends with time.

- (c) Groups of 'null' data points were found in a number of data sets acquired at Arlesey. An example of this is illustrated in figure 3.11. It transpired that these were due to a faulty connection in one of the co-axial cables. Substitute files were collected immediately after the main acquisition and these were then used to replace the null sets.
- (d) A problem related to (b) above was the generation of files within which portions of the acquired data appeared to suffer from a threshold shift. An example of this is illustrated in figure 3.12. Again, a corrected data set was generated by reducing the affected portion of the wave form to the 'zero' position, as described in (b).

Fortunately few data sets suffered any of these problems. The 'rising signal level' problem affected five Cowden files, null data sets were found in ten Arlesey files and the shifted threshold data set problem occurred in four Arlesey files.

3.9 Acoustic Emission Instrumentation Summary

This chapter has described the components of the AE monitoring system and qualified the effect each has on a signal. It has also included some discussion on the role of the wave guide and outlined the field monitoring procedure. Limitations of the system have placed a number of constraints on data capture which have been presented as a monitoring philosophy. Post-capture data processing and measurement criteria are discussed both generally and with specific reference to this research. Finally, the format of the captured data is considered, together with a number of problems encountered in the field and the remedial techniques employed.

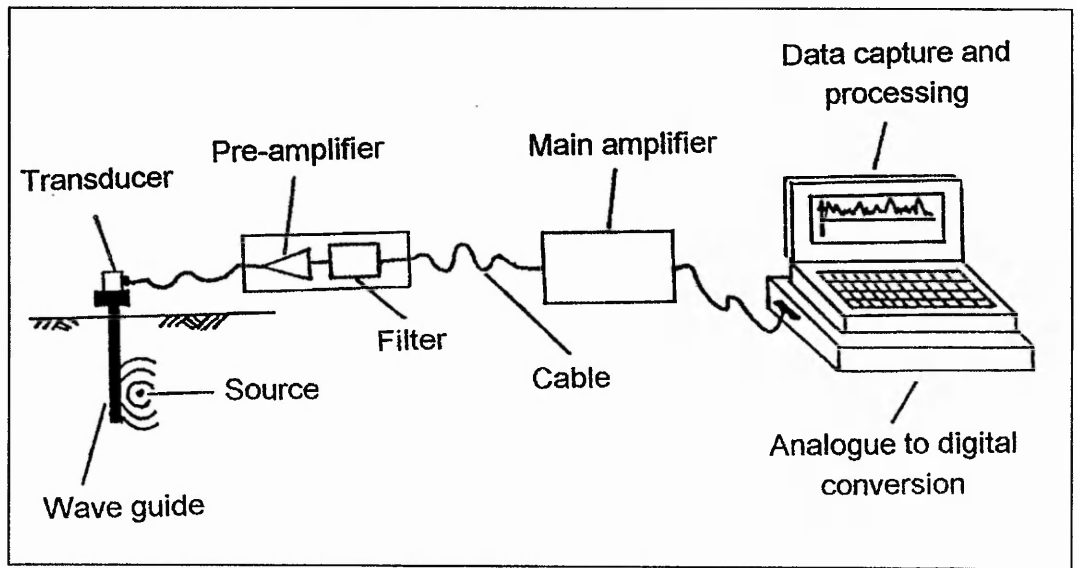


Figure 3.1 Schematic representation of system computer & electronic hardware

(After Dixon *et al.*, 1995b)

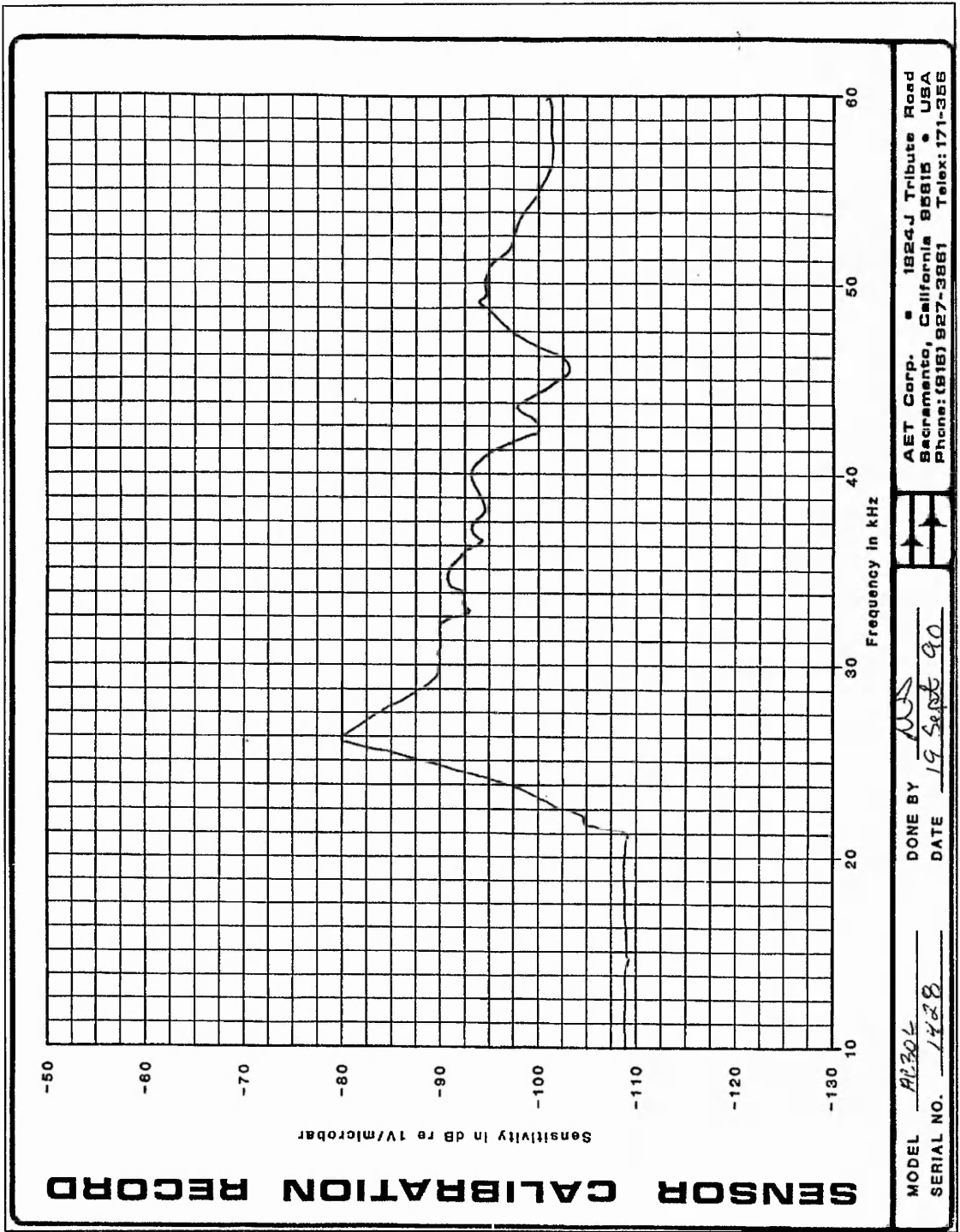


Figure 3.2 Calibration curve for AET 30kHz transducer

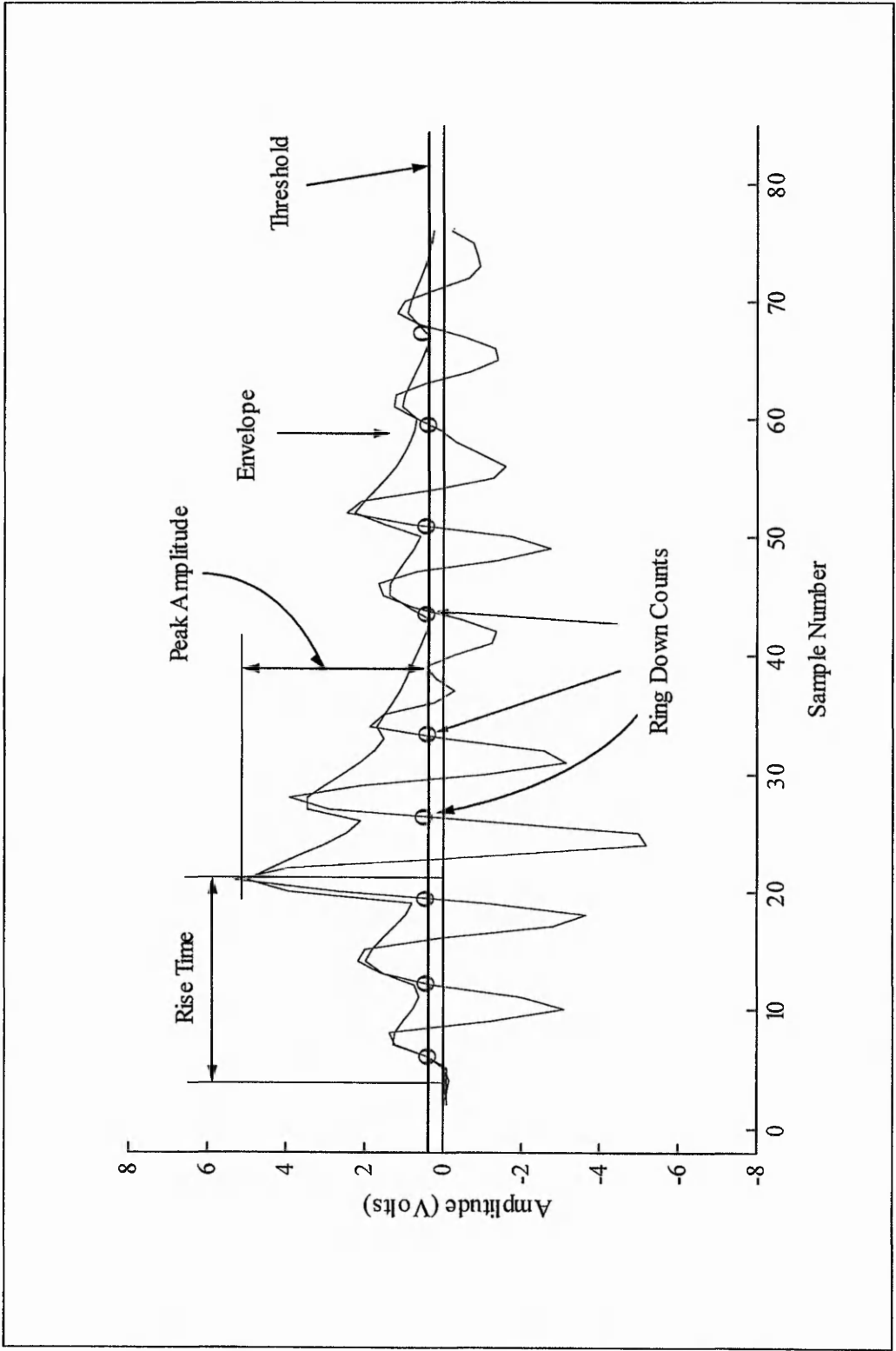
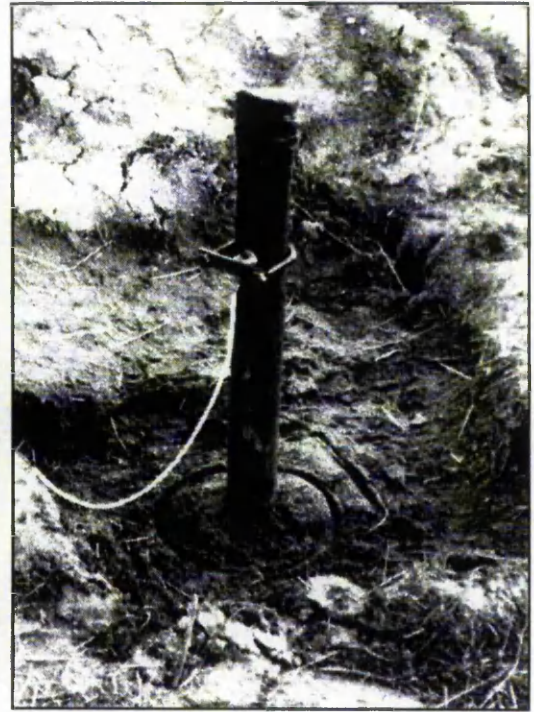


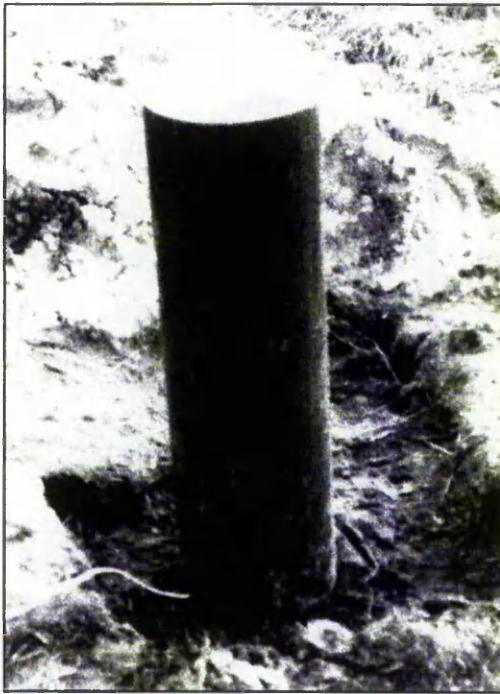
Figure 3.4 Transducer response to a transient showing its rectified envelope and measurement criteria



(a)



(b)



(c)



(d)

Figure 3.5 Field wave guide and transducer attachment - (a) transducer clamped to wave guide with 'U-bolt' connector, (b) perspective view of transducer and wave guide, (c) inner wave guide cover in place & (d) outer wave guide cover in place

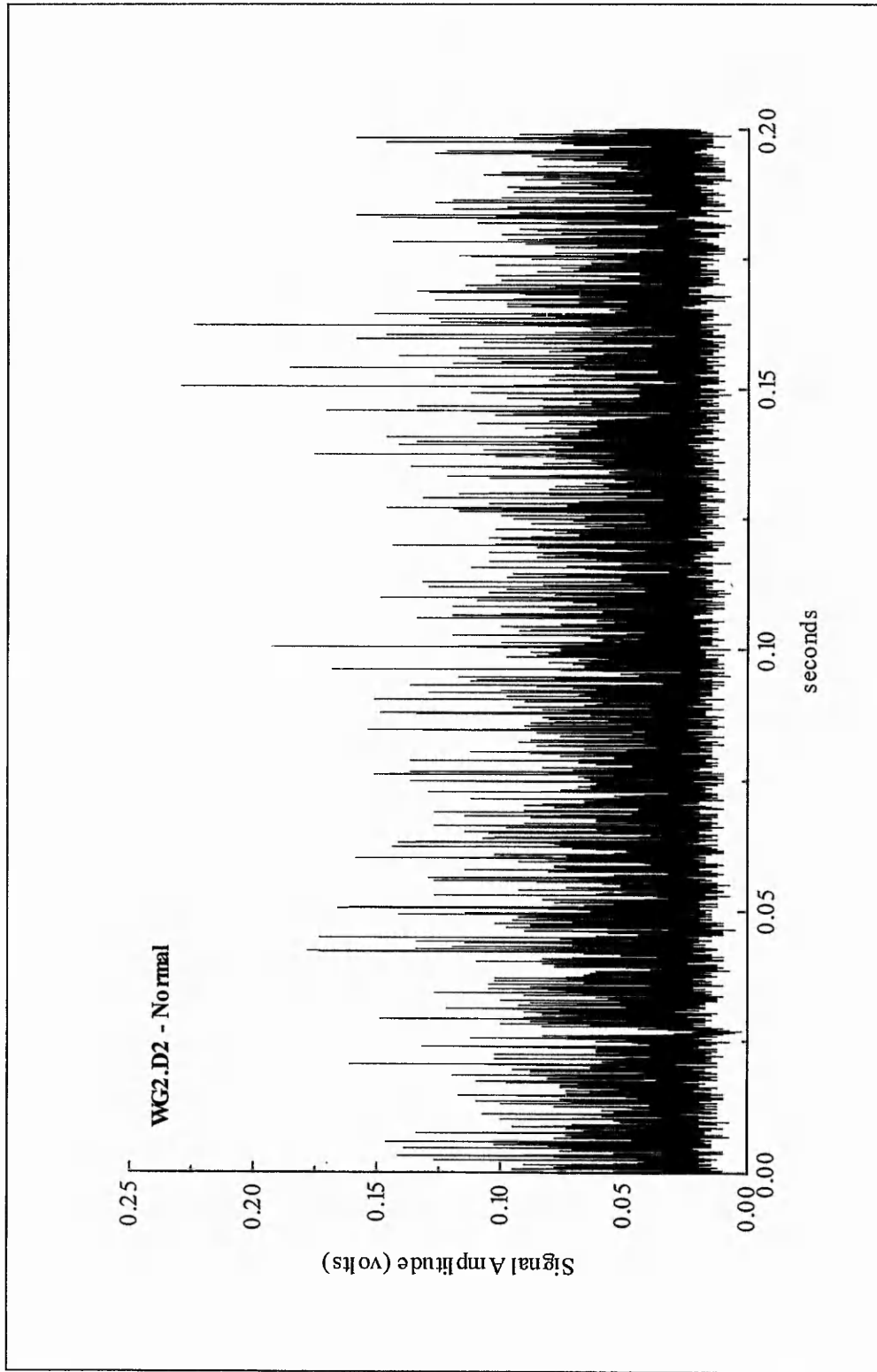


Figure 3.6 Segment of a standard data set depicting 20,000 data points

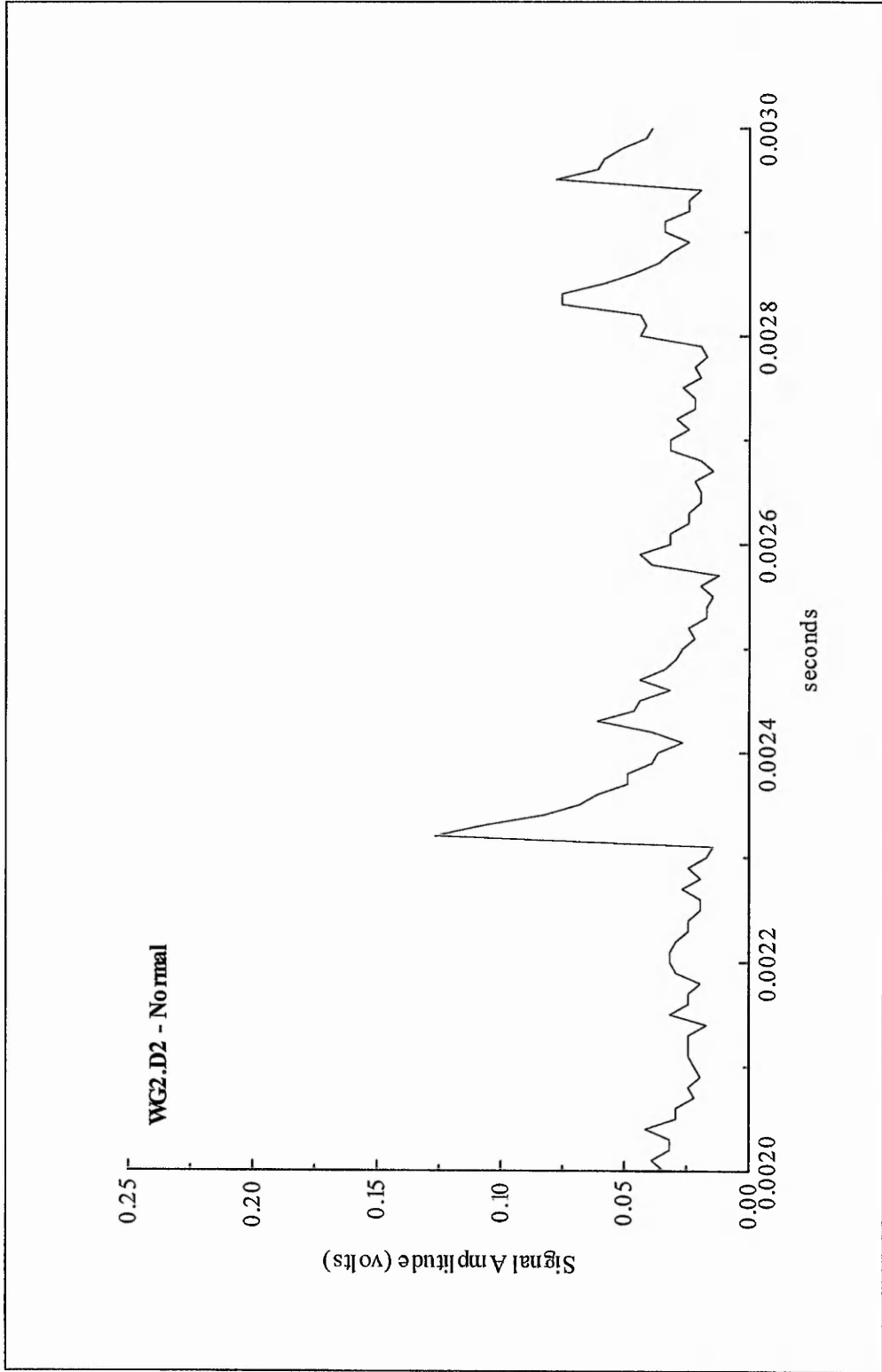


Figure 3.7 Wave envelope generated by 100 captured data points

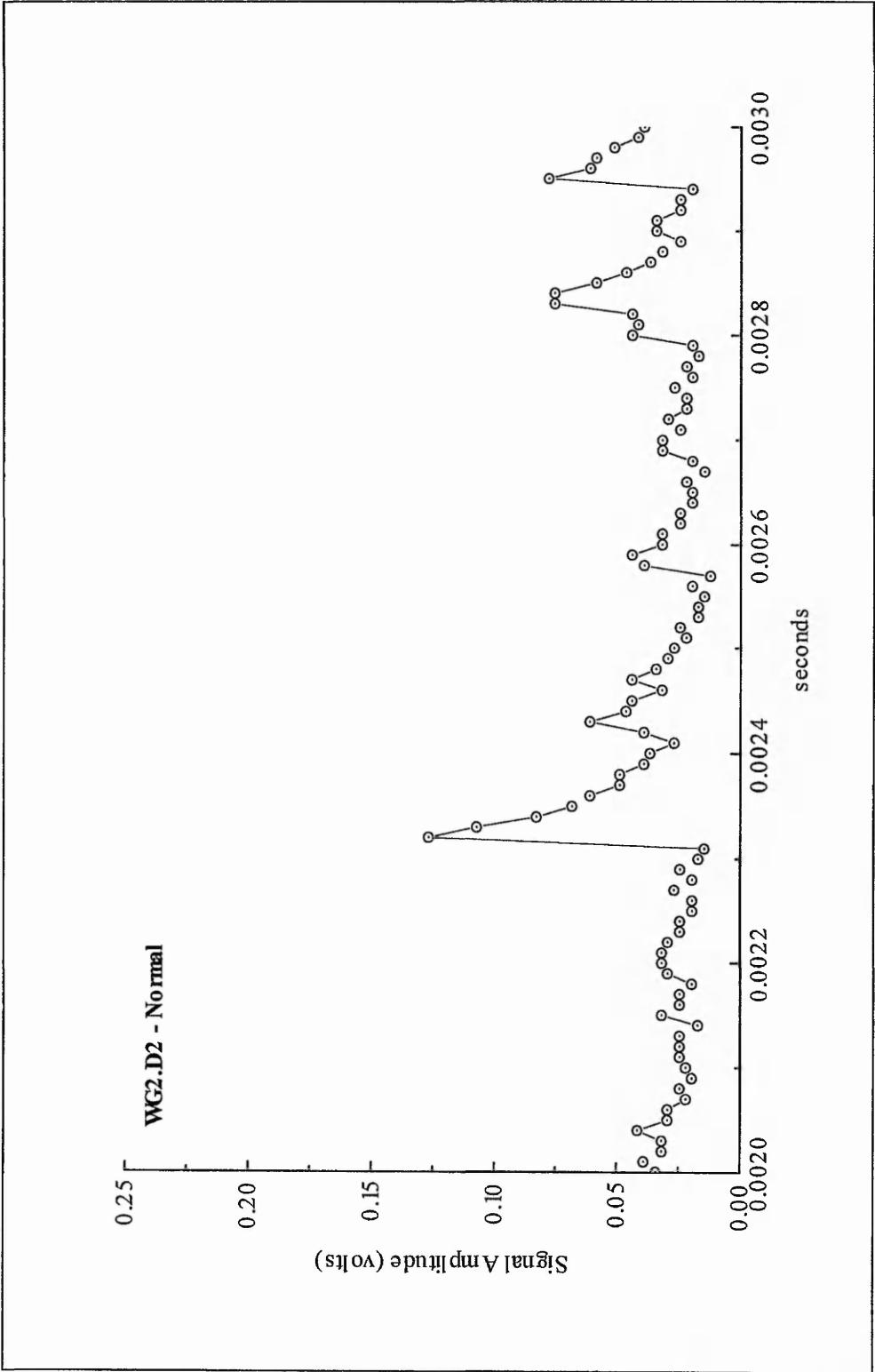


Figure 3.8 Wave envelope generated by 100 captured data points indicating the data points

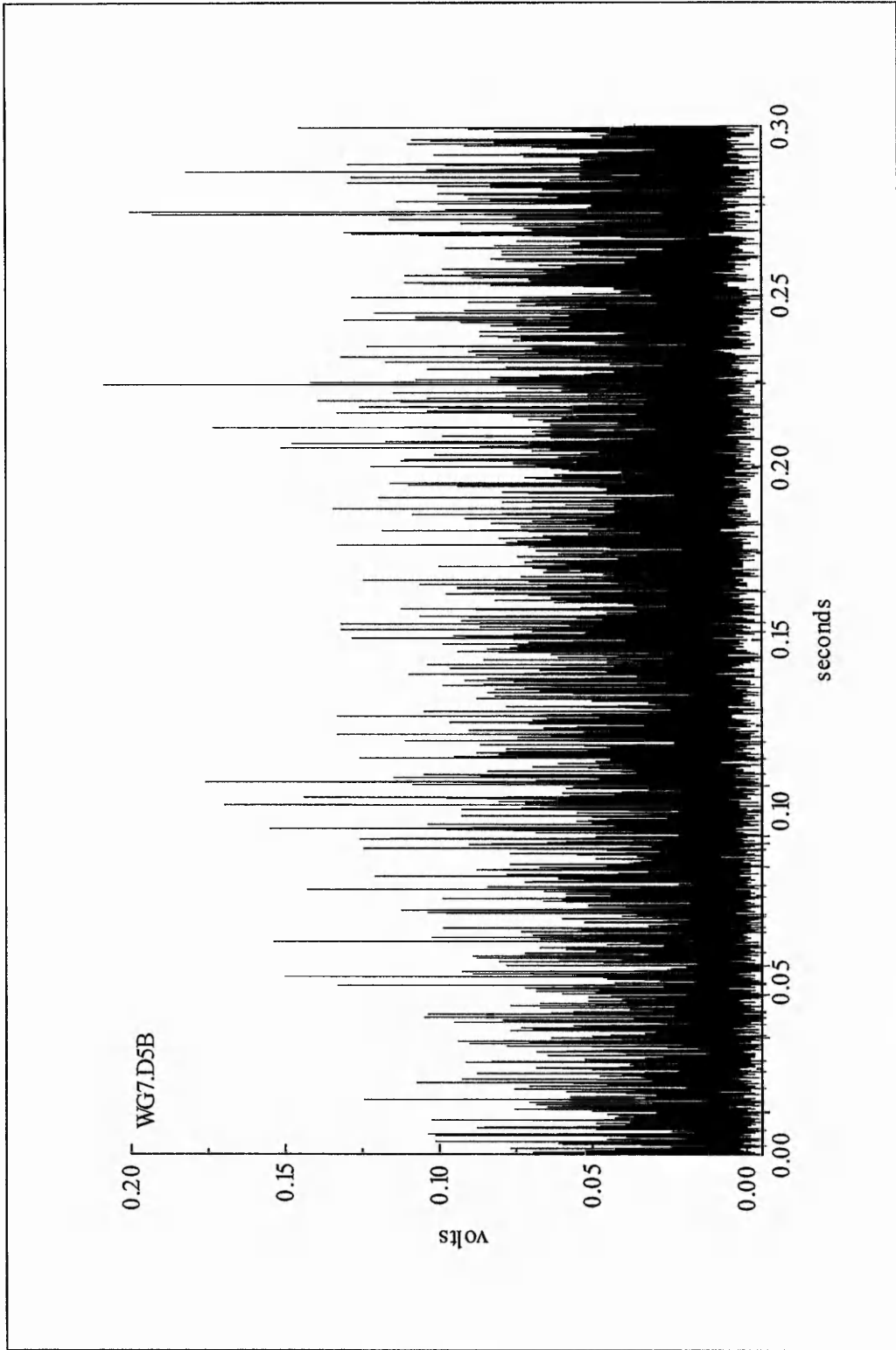


Figure 3.9 AET 'warming-up' problem

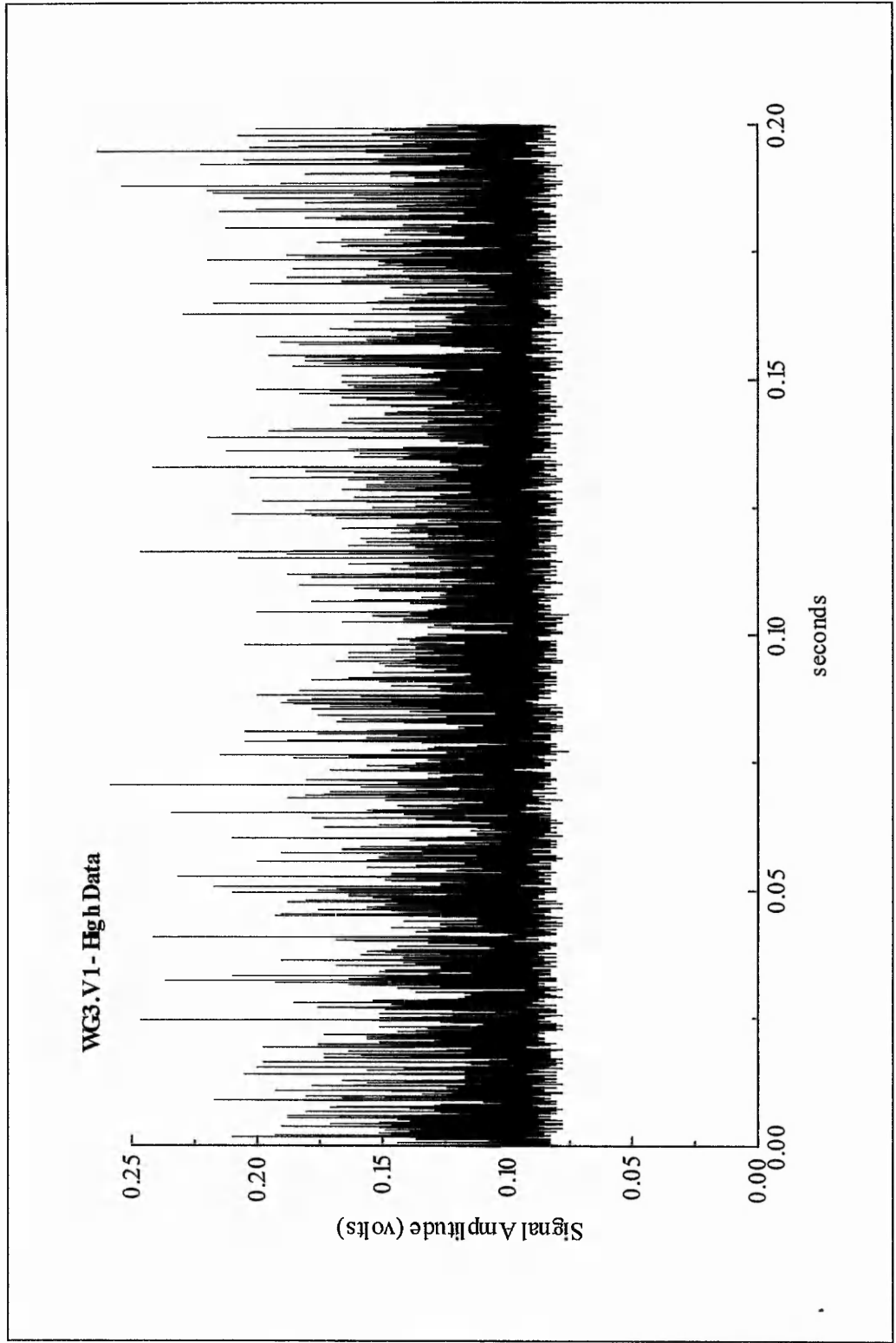


Figure 3.10 Abnormally high data set

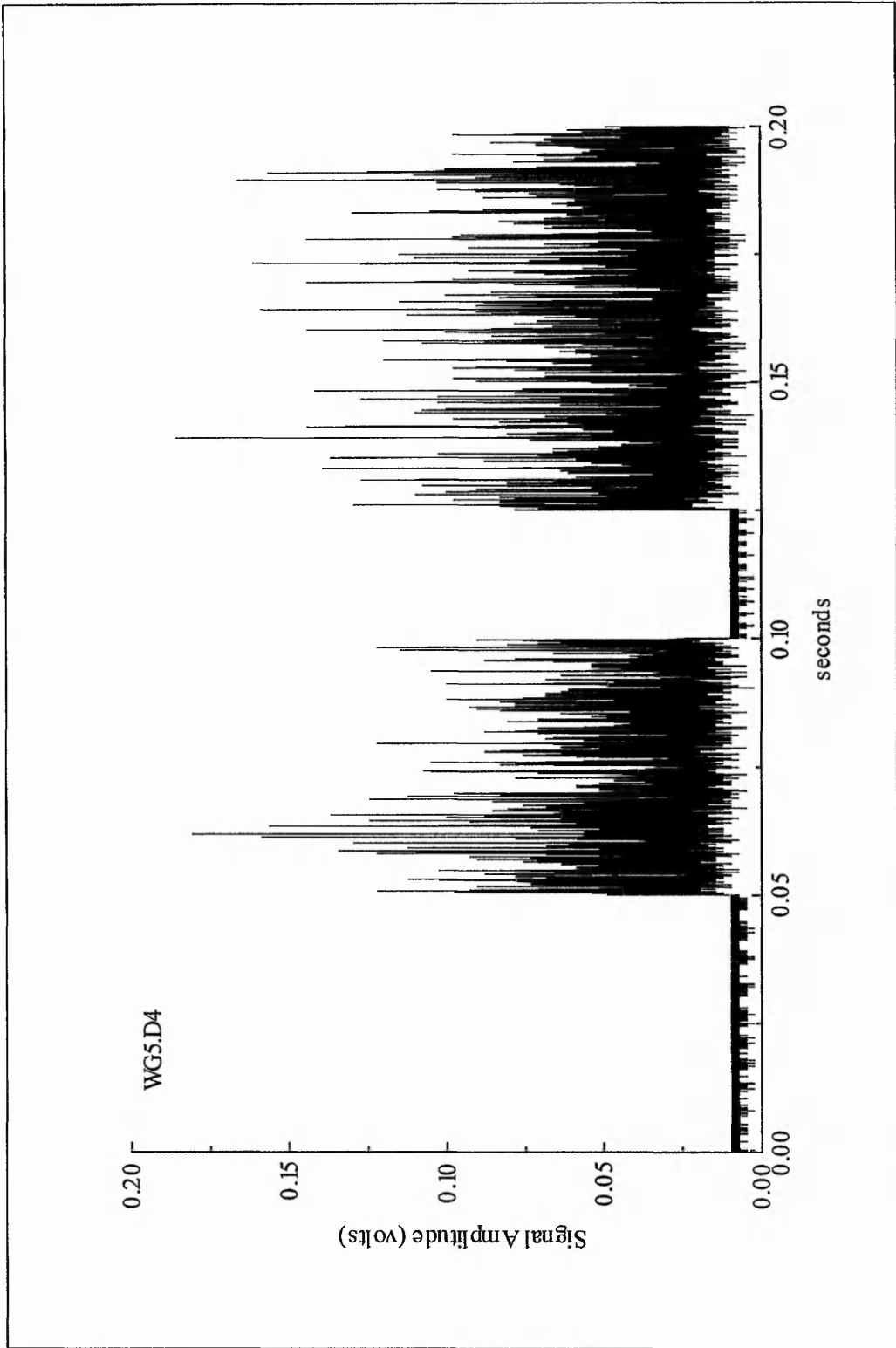


Figure 3.11 Sample of captured data showing inclusion of 'null' sets

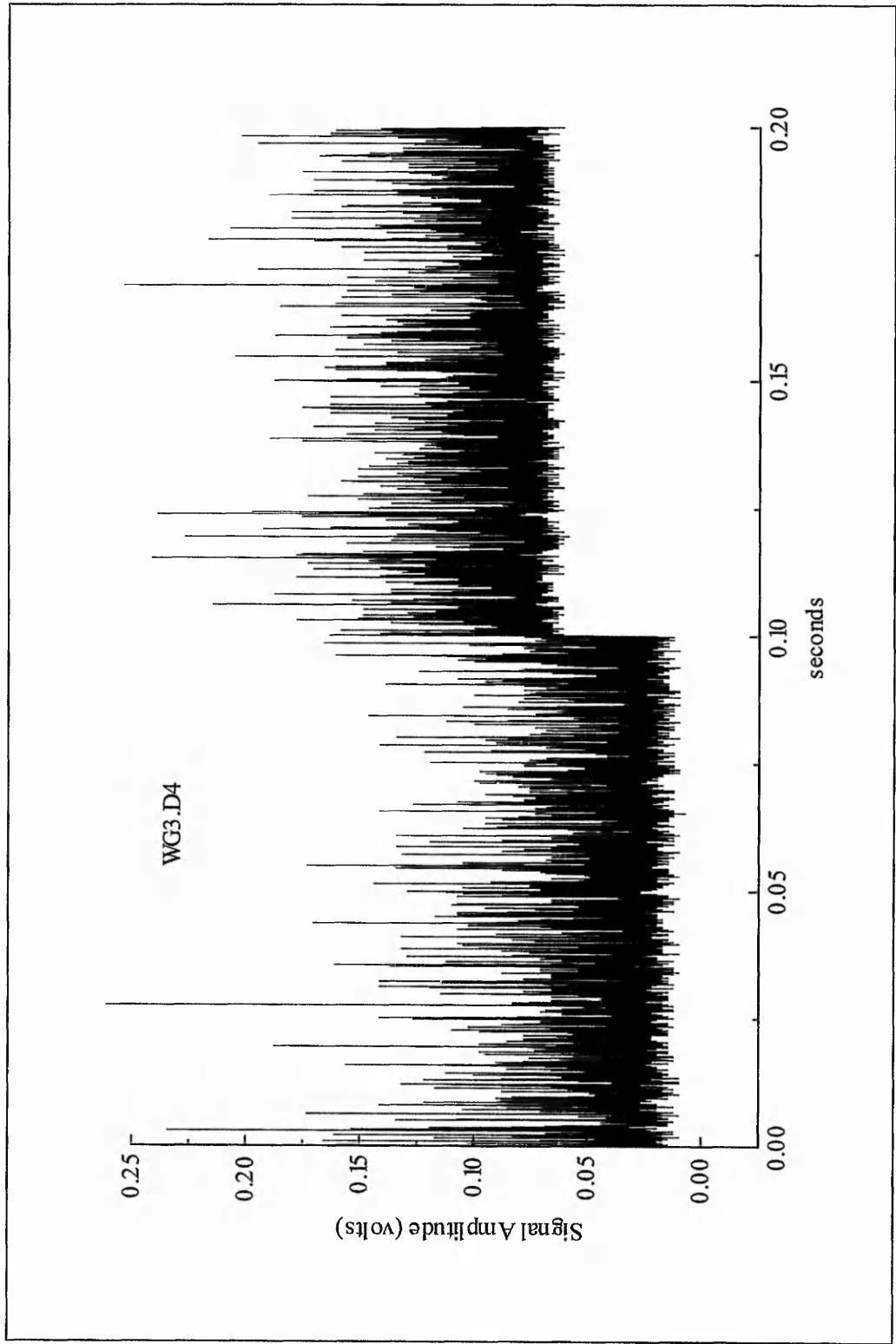


Figure 3.12 Captured data showing 'shifted' sets

Chapter 4

The Cowden Field Test

4.1 Introduction

The aim of the Cowden field test was to install a number of wave guides of varying design into a section of initially stable cliff and then to monitor the onset and development of failure as it occurred naturally using AE. It was intended to use the acquired data from alternative wave guide designs to make inferences about the mechanics of AE generation and to make some qualitative decisions about the relative merits of each design. Additionally, the acquired AE was compared with deformation measurements which were obtained from two inclinometers (section 4.4.2) which had been installed into the cliff section. This part of the investigation also represented something of an evolutionary period during which data acquisition routines were developed.

4.2 Site Description

The site chosen for the Cowden field test was a section of coastal cliff situated some 800m from the Building Research Establishment's (BRE) test site at Cowden, in the Holderness Plain on the east coast of England (Grid Reference TA 253405). The geology consists of a Cretaceous chalk plateau overlain by 20 to 30 metres of glacial till deposits which are currently considered to consist of three units. From the bottom upwards these are the Basement Till, the Skipsea Till and the Withernsea Till (Bell & Forster 1991 after Madgett & Catt 1978). The latter two units date from the Late Devensian, approximately 18,000 - 13,000BP. The geotechnical characteristics of the till deposits are extensively detailed by Marsland & Powell (1985) and by Bell & Forster (1991). The geographical location of the site is illustrated in figure 4.1 and a soil profile of the cliff section at Cowden, as determined by Butcher (1991), is reproduced as figure 4.2.

The site had been selected because it was evident that the cliff face was being subjected to extensive erosion. The remnants of many previous slips were visible and the presence of rear

scarps consisting of un-weathered (and un-vegetated) material indicated that activity was recent. This was confirmed in a number of discussions with members of the local community and was also, at the time, widely reported in the media. Additionally, failures predominantly occurred in the form of slides which is, as pointed out in section 1.2, the most commonly encountered mechanism and the slip planes generally tended to cut the ground surface some 3 to 5m inland from the cliff face. (This latter point was important because a knowledge of the likely position of the failure plane aided in the design and positioning of the wave guides). The site at Cowden appeared, therefore, to present the best opportunity of monitoring a first-time slide in a stiff, heavily overconsolidated clay soil. In particular, the main instrument array was installed adjacent to a particularly steep (approximately 40° to the horizontal) section of cliff face (and, as such, no slope profile is illustrated).

The unprotected cliffs were approximately 20 metres high (relative to sea level) and the rate of erosion over the past 70 years has risen from 1.5 metres per year to 2 metres per year. The littoral drift is in a southerly direction and the construction of sea defences to the north of the cliff has been cited as a potential explanation for the increase in the rate of erosion (Butcher 1991).

The results of an extensive investigation into the degradation and failure of a section of cliff at Cowden is described by Butcher (1991). It is postulated that progressive failure is triggered in a band of high plasticity, relatively stone-free clay till (below beach level) which exhibits a large reduction in strength between peak and residual values. (In figure 4.2, this is the stratum described as 'soft brown clay till'). The trigger is considered to be the reduction in toe-loading through the removal of beach material and failure is further facilitated by rapid pore-pressure equalisation which can occur due to the underlying sand and gravel layer (labelled 'sand and gravel' in figure 4.2). Failure, therefore, is initiated with the development of a basal shear zone. Movement then causes a reduction in strength which, in turn, promotes further deformation. Figure 4.3 is a schematic diagram of the post-failure degradation of the soil mass (after Butcher, 1991).

The site forms part of RAF Cowden and was, therefore, only accessible between 8.30am and 5.00pm Monday to Friday.

4.3 Site Instrumentation

4.3.1 Site Instruments

Twelve wave guides and two inclinometers were installed at the site with the specifications as given in table 4.1. The instrument positions and cliff face are shown in figure 4.4.

The wave guides numbered 1 to 6 were used as the main wave guide array and monitored for acoustic emission. They were designed to explore the effects of wave guide length and backfill material. The length and position of the wave guides also reflected the anticipated failure mechanism based on all the available information (i.e. literature and observation). The remaining wave guides were designed to further explore the effects of size, backfill material and position relative to a zone of deformation.

The gravel used as a backfill was graded and this revealed that more than 82% of its particles were greater than 6.3mm. Unfortunately no such grading was available for the sand. However, it should be appreciated that, as the sand and gravel used as backfills were both commercially obtained, the sand was very likely to satisfy the definition of having more than 50% of its coarse material being finer than 2mm (BS 5930).

4.3.2 Instrument Installation

Fourteen 150mm diameter boreholes were made, by the continuous flight augering technique using a Traveller 30 rotary drilling rig (borrowed from the University of Kingston, Department of Civil Engineering), to accommodate the instruments listed in table 4.1. Boreholes were either 6, 12, 18 or 21 metres deep and installation took place over a two week period in September 1993.

All wave guides were constructed from 6 metre sections of 50mm diameter steel tubing. Owing to the weight of the sections, installation was a three-man job. For boreholes deeper than 6 metres a vice was placed across the open borehole and the first section passed through the vice until most of its length was below ground. The vice was then tightened under the tubing coupler. Another section was screwed into the coupler and a chain wrench gripped around the second

section. The vice was then gently loosened and both sections allowed to slip down. This procedure was repeated until the wave guide stood on the bottom of the borehole. The wave guide was cut down (if necessary) so that only half a metre or so remained above ground level.

The boreholes were then backfilled with either sand, gravel or grout. The grout was a 4:1 bentonite:cement mix. No compaction technique was used on the sand and gravel backfills other than to tremie the fill into the borehole and to 'spiral' the wave guide in order to prevent 'bridging'.

The aluminium inclinometer casings were assembled from 3 metre sections which were riveted together via a coupler. The joints were sealed with a combination of silicon sealant and 'denzo' tape in order to prevent the influx of the grout backfill. A plug was then inserted into the base of the inclinometer and held in place with denzo tape (again to prevent the influx of grout). After insertion into their respective boreholes, the inclinometers were grouted into place. Protective caps were then placed around each inclinometer and concreted into the ground. Note that aluminium inclinometers were used (as opposed to plastic) because the intention was to investigate their potential use as wave guides.

4.3.3 Borehole Logs

The borehole logs, which are presented in table 4.2, were obtained by examining the arisings from the augers as each borehole was drilled. As such, there may be some error in the derived soil profiles. This is due partly to the difficulty in accurately measuring the depth from which a particular sample was obtained and partly to the fact that soft (or loosely consolidated) soils are likely to have become mixed with more competent strata during the extraction process.

Despite these difficulties, however, the borehole logs obtained are in reasonably good agreement with the soil profile described by Butcher (1991) and illustrated in figure 4.2. (Note that, as the final group of borehole logs presented in table 4.2 are derived from this figure, they are only approximate). All logs clearly identify three main strata. The first, described as a 'weathered brown' clay, occurs in the top 3 to 4m of the cliff. The second, described as a 'dark grey brown' clay, is found at depths of between (approximately) 6 and 10m below ground level and the third, described as a 'dark grey' clay is found at depths of between (approximately) 10 and 20m below

ground level. Note that Butcher (1991) identified two thin bands of sand and gravel separated by a layer of the 'dark grey brown' clay at a depth of between (approximately) 2.5 and 5m below ground level. This corresponds (at least in part) to a layer described (by this investigation) as 'silty fine to medium' sand. Also, the stratum described as a 'soft brown' clay was found by Butcher (1991) at depths of between (approximately) 19 and 21m below ground level. This corresponds with a layer described (by this investigation) as a 'clayey fine to medium' sand. Note, however, that this stratum was not identified in the bulk of the Cowden boreholes.

According to Bell & Forster (1991), the 'weathered brown' clay is a 'composite weathered unit of Skipsea and Withernsea Tills'. It is also likely that the 'dark grey' clay is the Basement Till but, owing to the similarities between the Skipsea and Withernsea Tills, it is impossible to distinguish between them using the available information.

4.3.4 The Control Wave Guide

Initially it was planned that wave guide 7 would be the control wave guide. However, during installation, it was noted that the borehole struck a layer of 'running sand' which made it necessary to terminate drilling at a depth of 18 metres. At this stage of the investigation the relevance of this layer in terms of 'noise' generation was not appreciated. Subsequently, therefore, it proved necessary to use wave guide 12 as the control wave guide.

4.4 Instrument Monitoring

4.4.1 Evolution of AE Monitoring Technique

It was recognised that specific methods to capture, manage and analyse acoustic emission data would need to be developed and, in this respect, the Cowden field test represented an evolutionary period.

The emission was captured using the A-to-D board's maximum sampling rate of 100kHz with each data point occupying four bytes of computer memory. At first it was attempted to initialise sampling by the upward crossing of a signal through some pre-determined threshold, known as a

trigger, but it became evident that the A-to-D board was not quick enough to do this. It was also originally intended to monitor all twelve wave guides and two inclinometers within a daily visit from Nottingham (which, owing to time restrictions, usually proved impossible). This combination of wave guide numbers and time restriction resulted in a monitoring routine which sampled 1000 data points at 100kHz every second for three minutes. This produced a data file for each wave guide consisting of 180,000 data points or 720,000 bytes.

For the first three days monitoring, an expansion box was used rather than the DacPac (section 3.2.6) as it was still awaiting delivery. As the expansion box would only operate from the mains it was also necessary to hire a portable generator for this period. With the arrival of the DacPac the AE capture system became completely independent of additional power supplies although an adapter enabled the Notebook to run from a motor vehicle's (the Nottingham Trent University's Landrover) battery. In due course it became evident that signals captured were considerably affected by which of these two power sources was used. The problem, it transpired, was to do with correct grounding. Although the exact cause of the problem was unknown, it has been suggested that, when used in isolation, the Notebook and the DacPac offered two competing grounds resulting in unintelligible signals. However when the power adapter was used a good ground was afforded through the Landrover's chassis. On occasion, when the Landrover was unavailable, good grounding was also achieved through a wire connection between the DacPac and a wave guide. The portable generator used in the first three days of monitoring also provided a good ground.

The role of the signal smoothing circuit has already been detailed in section 3.2.4. Initially the board was set to unipolar acquisition as it was expected that the sampled signal would be the positive half only. However, due to 'DC shift', although the wave-form only consisted of the wave envelope, negative values also existed. It was therefore necessary to use bipolar acquisition.

The total signal amplification of 96dB ($\times 63,096$) was arrived at by visually examining the captured wave-form. It represented a compromise between magnification of small signals and the prevention of larger signals exceeding the upper limit of the range. This range was set to -5V to +5V.

Apart from the first three days monitoring all files follow the name convention of WG#.\$ where # is the wave guide number and \$ is a file suffix representing the date the data was acquired. The first day's data saved under this convention is WG#.D2, acquired on 13 January 1994.

The *Cowden standard AE monitoring routine* can be summarised as follows:-

- The AE data consisted of 1000 envelope waveform data points collected at a 100kHz data sampling rate, every one second for three minutes - i.e. a 1% sample resulting in a file consisting of 180,000 data points (720kB) or 1.8 seconds of data
- Total AE signal amplification of 96dB (x 63,096)
- Electrical ground (earth) connection through Landrover chassis or wave guide
- Bipolar acquisition of signal envelope
- Monitoring method as outlined in section 3.5
- Threshold of 0.05V applied post-capture during data processing

4.4.2 Inclinometer Monitoring

An inclinometer is a piece of casing installed vertically into the ground and extending from the surface through all potential shear zones to a stable stratum at depth. As the slope deforms, the inclinometer deforms with it and measurements of the relative lateral displacement at points along the length of the inclinometer casing can be made using (in this investigation) a *biaxial torpedo*. (Figure 4.5 is a schematic representation of an inclinometer which is being subjected to deformation. It is shown at two separate moments in time and readings of lateral displacement are taken at two points along its length). The torpedo, which senses the deviation from true vertical, is connected to a *DataLogger* which collects and processes the data. The biaxial torpedo, so called because it is able to sense the deviation from true vertical in two orthogonal directions, travels down the inclinometer tubing by means of two sets of wheels which fit into grooves or *keyways* inside the tubing. The four keyways, set at 90° to one another, are labelled Faces A, C, B and D in a clockwise direction. The torpedo is lowered to the bottom of the tubing and senses deviation from true vertical as it is pulled back to the surface in 0.5 metre increments (initially in Faces A and C). On reaching the top of the tubing the torpedo is retracted and turned through 180° in order to read Faces B and D. This results in two sets of readings (in opposite

directions) in each of two orthogonal planes which can be used to check the accuracy of the measurements and provide an average reading or *mean deviation* from true vertical.

The angular displacement is used to calculate the mean deviation as illustrated in figure 4.5. The mean deviation, therefore, represents the difference, *in the horizontal plane*, between the top and bottom sets of wheels of the inclinometer torpedo. Inclinometer data is presented in two ways; change in mean deviation and displacement profile.

The change in mean deviation is simply the difference between two sets of mean deviations at a given depth. In figure 4.5 this would be given by (b-a) at the lower depth and by (d-c) at the higher. It should be noted that it is assumed that the base of the inclinometer remains fixed and that mean deviations, therefore, relate to the top set of wheels of the torpedo. For a 21 metre borehole the depth of the lowest reading was 20.5 metres. It should also be noted that this form of measurement necessarily assumes that the sets of wheels are located in exactly the same position every time readings are taken.

It is important to appreciate that the change in mean deviation identifies a *component* of displacement at the particular depth being considered. In the example, whereas (b-a) represents the actual distance moved through the ground at that depth, the distance (d-c) only represents the component of displacement at that depth; the actual distance moved through the ground being given by $(d+(b-(a+c)))$ or, rewriting, $(b-a)+(d-c)$. This value, which is the sum of the change in mean deviations from the base of the inclinometer to the depth in question, is called the displacement profile.

The change in mean deviation therefore indicates the relative degree of deformation suffered at each depth whereas the displacement profile provides a more accurate picture of the actual physical movement in space .

As has been stated two sets of orthogonal readings are taken; one in the A-B plane and one in the C-D plane. The processed data has amalgamated these two sets into one vectored set which specifies the deformation as one magnitude and a direction of displacement.

The inclinometers were also 'dipped' in order to ascertain the depth of water within the casings.

4.4.3 Instrument Monitoring History

The inclinometers were first read on 12 October 1993 and this date assigned as Day 0. Subsequent site visits have been allocated a value based on the number of days passing since Day 0. This number is used as the time scale for all site data. Typically site monitoring would begin about 10.30 - 11.30am and finish 3.30 - 4.30pm the same day.

The inclinometer and wave guide monitoring history is summarised in table 4.3 and a full chronology of the site monitoring (which complements table 4.3) is given below. (Also included are some notes concerning the weather, the state of the tide and the condition of the sea. These observations would have been made on arrival at the site and so, therefore, refer to that time. Further observations would only have been recorded had any significant changes occurred).

September 1993

Installation of Instruments

12 October 1993 Day 0

The inclinometers were read twice and the data averaged to produce a 'base file'. This is the file against which future inclinometer readings are compared to ascertain the magnitude of displacement. No AE readings were taken.

2 November 1993 Day 21

Both inclinometers were read to the maximum depth of 21 metres. No AE readings were taken.

11 November 1993 Day 30

The inclinometers were read to the maximum depth of 21 metres and a full survey of the site was made. The inclinometers were dipped to ascertain the level of the ground water. No AE readings were taken.

25 November 1993 Day 44

The inclinometers were dipped and read to the maximum depth of 21 metres. The weather was mild and sunny with a slight breeze. The sea was calm and the cliff profile to the immediate north of the site was becoming very steep.

1, 2 & 3 December 1993 Day 50, 51 & 52 Data File Suffix: various

The inclinometers were dipped and read to the maximum depth of 21 metres. AE readings were made for the first time. A portable generator was used to power the A-to-D board (which was housed in an expansion box) and also provided a good ground. The weather was generally mild to cold but always breezy. The sea was calm and did not reach the base of the cliff during monitoring.

22 December 1993 Day 71

Both inclinometers were dipped but only inclinometer 2 was read as considerable difficulty was experienced in removing the inclinometer caps. The weather was bright with a light breeze but there was evidence that it had been raining heavily. The tide was approximately 10 metres away from the base of the cliff.

13 January 1994

Day 93

Data File Suffix: D2

Both inclinometers were dipped and read. Inclinometer 1 could only be read to a depth of 16 metres. The sand backfill in wave guide 1 had dropped approximately 1 metre and there was some indication that it had dropped in wave guide 8 also. Noticeable gaps between the concrete caps of the inclinometers and the surrounding soil had also developed.

The weather was sunny, cold and breezy and the tide was out. AE readings were taken without a proper ground and, as a result, this data was lost.

21 January 1994

Day 101

Data File Suffix: D3

Both inclinometers were dipped and read; inclinometer 1 to a depth of 20 metres. Inclinometer 2 was read to the maximum depth of 21 metres but torpedo travel below 16 metres was lumpy. The sand backfill in wave guide 1 was still about 1 metre below ground level and was topped up. The cracks around the inclinometer caps were quite distinct; that around inclinometer 1 was in the order of 1 to 2cm wide all round and that around inclinometer 2 was about 0.5cm on the north side of the instrument only.

The weather was dry, overcast and breezy. The tide was approximately 15 metres away from the base of the slope. Some AE readings were taken using the Landrover chassis as ground for the first time and acquisition was switched to 'bipolar'.

28 January 1994

Day 108

Data File Suffix: D4

Both inclinometers were dipped and read; inclinometer 1 to a depth of 20 metres. Inclinometer 2 was read to 21 metres but the bottom of the tube seemed to be blocking very slightly. The cracks around the concrete appeared slightly bigger but the difference was minimal. The ground level around inclinometer 1 had evidently dropped as removal of the cap caused the casing and concrete to slide down around the inclinometer.

The weather was sunny, cold and quite breezy. Ice and snow were evident in inland country lanes. The sea was rough. The tide was approximately 50 metres away from the base of the cliff. AE readings were taken without a proper ground and this data was lost.

4 February 1994 Day 115 Data File Suffix: D5

Both inclinometers were dipped and read to the maximum depth of 21 metres. No discernible difference in the size of the cracks surrounding the inclinometers was noted. The weather was sunny, cold and breezy. The waves were strong but the tide was about 10 metres short of the cliff base. Some AE readings were taken using the Landrover chassis as ground.

11 February 1994 Day 122 Data File Suffix: D6

Both inclinometers were dipped and read; inclinometer 1 was read to a depth of 14 metres and inclinometer 2 to 16 metres. The crack around the concrete of inclinometer 2 had increased to 3cm wide on the south side of the instrument and 6cm on the north side. A 0.67 metre tension crack (running almost parallel to the cliff face) had developed in a northerly direction, originating from wave guide 8 (see figure 4.6). The sand backfill of wave guide 9 had dropped by approximately 0.5 metres and was re-filled.

The weather was bright but cloudy, cold and breezy. The sea was rough and the tide out. AE readings were taken without a proper ground. Hence this data was lost.

25 February 1994 Day 136 Data File Suffix: D7

Both inclinometers were dipped and read to a depth of 14 metres. Downward movement of the torpedo in inclinometer 1 was temporarily halted at a depth of 5.5 metres, suggesting a non-alignment of two sections had developed. The inclinometer protective caps could not be re-fitted (due to the inclinometers protruding through them) indicating further downward movement of the ground had occurred. The crack surrounding the concrete of inclinometer 2 had increased to 10cm on the north side of the instrument and a similar crack had developed surrounding the concrete of

inclinometer 1. Further tension cracks had developed around wave guides 6, 8 and 11. There was also a noticeable 2cm drop in the ground level just seaward of wave guide 11.

The weather was sunny and mild with a light breeze; the tide was very far out. Some AE readings were taken using the Landrover chassis as ground.

10 March 1994 Day 149 Data File Suffix: D8

Both inclinometers were dipped and read to a depth of 14 metres. There was also a noticeable dip in ground level between the lines of wave guides 1, 2, 3 and 4, 5, 6 which ran the entire length of the instrument array (see figure 4.7). As the ground surrounding wave guides 1, 2 and 3 had dropped it became impossible to cover them as the tops of the instruments protruded through the wave guide covers. The ground surface was dry.

The weather was sunny, cold and breezy; the tide was out. AE readings were taken using the Landrover chassis as ground.

24 March 1994 Day 163 Data File Suffix: D9

Both inclinometers were dipped and read to a depth of 14 metres. The dip previously identified was now a difference in ground level of some 10 - 20cm. Wave guides 1, 2 and 3 were cut down by approximately 0.5 metres. A large crack on the seaward side of wave guide 4 had also developed.

The weather was sunny, cold and breezy; the sea was about 50 metres away from the base of the cliff. The ground was dry. AE readings were taken using the Landrover chassis as ground.

7 April 1994 Day 177 Data File Suffix: X0

Both inclinometers were dipped and read. Inclinometer 2 could only be read to a depth of 3 metres. Torpedo travel on face A of inclinometer 1 was to a depth of 14 metres. However, on

attempting to read face B, the torpedo would not pass the 3 metre mark and so reading was abandoned. The dip previously identified had developed into a large, more extended, crack which ran through the instrument array and disappeared into the side of the cliff some 10 metres north of wave guide 8. The southern portion of the crack was less distinct but appeared to travel much further. The difference in ground levels was now in the region of 20 - 30cm.

The weather was overcast and mild with a gentle breeze. Some heavy rain was, however, experienced during monitoring. The tide was about 150 metres from the base of the cliff. AE readings were taken using the Landrover chassis as ground.

6 May 1994 Day 206 Data File Suffix: X1

Both inclinometers were dipped and read. The torpedo travelled to a depth of 3.5 metres in inclinometer 1 and 3 metres in inclinometer 2. However, as approximately 1 metre of each inclinometer was now above ground surface, it was decided to abandon the inclinometers altogether. The difference in ground level had now increased to about 1 metre and the southern extent of the failure was some 45 metres south of wave guide 11. Wave guides 1, 2, 3 and 10 were all located within the failure wedge and required cutting down to be covered securely by the wave guide covers.

The weather was sunny and mild with a light breeze; the tide was out. AE readings were taken using wave guides 4 and 7 as ground.

27 May 1994 Day 227 Data File Suffix: X2

It was attempted to dip both inclinometers. The probe would only travel to a depth below ground level of approximately 2.8 metres for inclinometer 2 and approximately 3.8 metres for inclinometer 1. In both cases the probe failed to reach the water table. The difference in ground level had not altered much and was still in the region of 1 metre.

The weather was cold and breezy. The tide was approximately 100 metres away from base of the cliff. AE readings were taken using wave guides 4 and 5 as ground.

Figure 4.8 depicts the instrument array (as at 11 November 1993) and the full extent of the slip surface (as at 16 June 1994). Figure 4.9 shows a 'close-up' of the instrument array (as at 11 November 1993) and the slip surface (as at 16 June 1994). Figure 4.10 illustrates the instrument array (as at 11 November 1993), the slip surface (as at 16 June 1994) and indicates the change in height of the ground level at instrument locations WG1, 2, 3, 10, I1 & I2 between the two dates.

Finally, a full survey of the site was carried out on the 16 June 1994. Figure 4.11 illustrates the landslip as of this date and figure 4.12 depicts WG11 which was situated on the slip plane.

4.4.4 AE Analysis Database

As already mentioned in section 4.4.1, a number of data files were lost due to poor grounding of the signal. Additionally a number of files were collected to assess the magnitude of amplification required, an appropriate threshold (when it was erroneously thought the board was capable of capturing an event on a trigger) and the number of samples collected on activation of a trigger. Several other forms of test files, for example to demonstrate the effect of the removal of the wave guide covers, were also collected. The result is that a much smaller number of data files, *collected on a consistent basis*, than outlined in table 4.3 are available for analysis in respect of the destabilisation of the cliff face. The full database of AE files used for analytical purposes is given in table 4.4.

The total number of files for analysis has been reduced from the original 200 (table 4.3) to 78 acquired using the standard monitoring routine as outlined in section 4.4.1. Additionally there are 14 files generated to investigate aspects of AE monitoring not connected with slope stability.

AE files captured on 1, 2 & 3 December 1993 were generated by Viewdac routines triggering off various threshold values. They are of variable length but in all other respects follow the standard AE monitoring routine (section 4.4.1).

4.5 Field Instrument Data Analysis

4.5.1 Inclinometer Data

Figure 4.8 shows the positions of the instruments with reference to the failure plane as at 16 June 1994. The slip surface is approximately 65 metres in length and, at its widest, the failure mass is about 8 metres across at the cliff top. Both inclinometers, as well as wave guides 1, 2, 3 and 10, are located within the failure wedge; wave guides 8 and 11 lie on the failure plane and all instruments are located within the northern third of the failure.

The inclinometer data (mean deviation and displacement profile) is shown in figures 4.13 - 4.16 and indicates that shearing largely occurred within a band approximately 3 to 6 metres deep but with maximum deformation occurring at a depth of about 3.5 metres.

Due to the large size of the failure wedge, the inclinometers, although separated by approximately 5 metres, occupy a similar position and this is reflected in the graphs of change in mean deviation and displacement profile. Inclinometer 1 is situated 0.7 and 13 metres away from the rear and northern ends of the slip plane respectively; inclinometer 2 is situated 1.0 and 46 metres away from the rear and southern ends of the slip plane respectively.

The greatest recorded change in mean deviation for inclinometer 1 is 46.8mm at a depth of 4 metres and for inclinometer 2 is 46.6mm at a depth of 3.5 metres. The equivalent figures for displacement profile are 148.4mm for inclinometer 1 and 138.8mm for inclinometer 2; both at a depth of 3 metres. Face errors are typically in the region of 0.1 - 0.4mm for faces A & B and 0.1 - 0.7mm for faces C & D, although towards the end of the test period some errors were as large as 1.9mm. The angles, representing the direction of the vectored displacements, indicate that movement was seaward.

The above findings are also largely in agreement with Butcher (1991) who recorded a failure with a maximum displacement of approximately 180mm (prior to the inclinometer tube shearing) at a depth of around 3.5 metres. The inclinometer concerned (identified as 'B9/10') was installed approximately 3 to 4m from the cliff face.

The plots also give an indication of when movement took place but, because readings were not always taken at a constant interval, it must be remembered that a large increase in displacement may be accompanied by an equally large time gap between monitoring periods. A much better way of determining significant changes in the displacement pattern is to consider rates of displacement. This is depicted in figure 4.17 for inclinometers 1 and 2 and is defined as the difference in successive change in mean deviation figures divided by the number of days separating the readings. For inclinometer 1 rates are based on a depth of 4 metres and, for inclinometer 2, 3.5 metres. Note that calculated rates are plotted at the end of the period to which they refer. Both graphs are very similar and indicate that displacement rates significantly increased after Day 108 (28 January 1994). The displacement profile for inclinometer 1 at 3 metres below ground level is also shown and some significant site observations are marked on the figure.

Rate of displacement is particularly suited to this study as it is postulated that noise is generated by means of the *active* wave guide model (section 3.3). It may, therefore, be reasonably expected that higher noise levels coincide with higher rates of displacement. However just because a high rate is recorded over a particular period does not necessarily mean that the AE, *which only reflects the state of stability at the time of monitoring*, will also be high.

The only inconsistency between the two inclinometers is recorded in figure 4.18 which depicts the dipped water level relative to the base of the of the inclinometer. Inclinometer 2 has remained more or less constant over the monitoring period with a recorded head of about 5 - 5.5 metres. Inclinometer 1, however, has steadily risen from a head of about 5 metres to a peak of 9.5 metres over a 50 day period before reducing to a level of some 4 - 5 metres over the following 50 to 100 days. It is not immediately obvious why the behaviour should differ so much but this is discussed further in section 4.5.3.

4.5.2 Acoustic Emission Data

(i) Introduction

Twelve wave guides of varying design (section 4.3.1) were installed into the slope in order to compare the acoustic emission data acquired from each. The design parameters were backfill type, length of wave guide and position relative to the slip plane.

The theory and function of the control wave guide have been dealt with in section 3.3.

Note that, in the following graphs, sets of AE data points are connected by lines. This is only to maintain clarity between individual sets of data points relating to different wave guides and is *not* meant to infer anything about the behaviour of the signal *between* data points.

(ii) Wave Guides 1, 2 & 3

Wave guides 1, 2 and 3 were 21 metres long and arranged in a row parallel to, and approximately 4 metres from, the cliff face. Wave guide 1 was backfilled with sand, wave guide 2 with gravel and wave guide 3 with grout. Figure 4.19 compares the recorded mean AE signal values (volts) for each wave guide and wave guide 12 (the sand backfilled, 6 metre long control wave guide) over the test period (days). It also compares the AE data with displacement rates (based on inclinometer 1) expressed in terms of mm per day over the test period (days).

There is a generally good correlation between the AE data with the control wave guide always registering the lowest values. Typically wave guide 1 recorded the best response, followed by wave guide 2 and then 3. There is also good agreement between the AE trend with time and the rate of displacement recorded by inclinometer 1. Note also, that a reduction in mean signal value from Day 149 to Day 163 (recorded by all wave guides) is accompanied by a reduction in the rate of increase of displacement recorded by inclinometer 1 (as indicated by the reduced gradient of the rate of displacement graph).

It was observed from the inclinometer data (section 4.5.1) that the shear plane was present at a depth of approximately 3.5m. Referring to figure 4.9, it is evident that wave guides 1, 2, 3 and 10 (together with both inclinometers) lay approximately in a straight line which was parallel to the shear plane (where it cut the surface). As such, it is likely that the aforementioned wave guides also passed through the slip plane.

(iii) Wave Guides 4, 5 & 6

Wave guides 4, 5 and 6 were 12 metres long and arranged in a row parallel to, and approximately 6 metres from, the cliff face. Wave guide 4 was backfilled with grout, wave guide 5 with sand and wave guide 6 with gravel.

Figure 4.20 plots the mean signal values (volts) over the test period (days) and indicates that, although the wave guides designed to detect deformation (*gauge wave guides* - section 3.3) and the control wave guide (on the whole) follow the same trend with time, the control wave guide, as before, generally recorded a lower value. The difference is not as pronounced as for wave guides 1, 2 and 3. However, this may be explained by the shorter wave guide length and positioning to the rear of the slip plane (of wave guides 4, 5 & 6). Other than the low level of activity, there is little consistency between the gauge wave guides themselves with both wave guides 4 and 5 having recorded a particular day's largest reading. However the fact that they have recorded an emission level in excess of that of the control wave guide at least provides evidence that gauge wave guides do not need to pass through the failure plane in order to detect movement.

Unfortunately no data prior to Day 115 (4 February 1994) exists for these three wave guides so it is impossible to determine whether or not the signal would have been of a reduced magnitude to complement the lower rates of displacement. However, it was possible to continue monitoring them until 27 May 1994; well beyond the termination date of 7 April 1994 for wave guides 1, 2, 3 and 10 and both inclinometers.

(iv) Wave Guides 8, 9, 10 & 11

The wave guides were positioned in pairs to the north (8 & 9) and south (10 & 11) of the main wave guide array. Wave guides 8 and 10 were 12 metres in length and 9 and 11 were 6 metres in length; all were backfilled with sand. The four were installed as supplements to the main wave guide array and were usually the last of the wave guides to be monitored. As such the monitoring record is somewhat intermittent. Also, as figure 4.9 shows, wave guides 8 and 11 were on the slip plane. The difference in ground level surrounding these wave guides made use of the wave guide covers impossible and, taking into account the data sets lost early in the test period has resulted in wave guides 8 and 11 each only being monitored twice.

As figure 4.21 shows, the mean AE signal value (volts) for each of the wave guides over the test period (days) generally follows a similar trend to that of the control wave guide although, and interestingly, of the six available readings for wave guide 9 only one plots above its equivalent control wave guide reading.

(v) Wave guides 7 & 12

As stated in section 4.3.4 originally it was intended to use wave guide 7 as the control wave guide. However it was noted on installation that it passed through a layer of 'running sand'. The significance of this in terms of AE generation was not appreciated at that time and, subsequently, it became necessary to use wave guide 12 as the control wave guide. Figure 4.22 plots the mean AE signal value (volts) of wave guides 7 and 12 over the test period (days). Although there is some correlation between the two, generally wave guide 7 records much higher levels than wave guide 12 thus vindicating the decision to use wave guide 12. The role and performance of the control wave guide is discussed more fully in section 5.6.5 where the Arlesey test control wave guide is also considered.

(vi) Alternative Data Processing Techniques

Figure 4.23(a) shows the AE recorded for wave guides 1, 2, 3 and 12 but plots the standard deviation (volts) instead of the arithmetic mean of the data sets over the test period (days).

Although the general relationship between the readings is similar there are some notable differences. In particular the dip in the mean value (figure 4.19) for wave guide 1 on Day 163 disappears and the graph of standard deviation more resembles an exponential relationship. Wave guide 3 becomes more coincident with wave guide 12 and wave guide 2 becomes a more exaggerated form of its mean equivalent. Figure 4.23(b) shows the same data which has been processed by considering the cumulative normalised area under the signal (volts vs time) above the level recorded by wave guide 12. It is possible that the different AE characteristics derived by applying alternative statistical techniques may reflect differences in the generation of the AE, which in turn, may be dependent on the design of the wave guide. The effect of alternative processing techniques is discussed more fully in section 5.6.3 and section 6.5 (and is considered in conjunction with the Arlesey test).

4.5.3 Summary of AE & Inclinometer Field Data

As discussed in section 4.5.1 the bulk of the deformation occurred at a depth of 4 metres, according to inclinometer 1, and 3.5 metres according to inclinometer 2. From the borehole data presented in section 4.3.3 this would correspond to the layer described as 'silty fine to medium sand' which is found between 4 and 6 metres below ground level (inclinometer 1) and between 3 and 6 metres below ground level (inclinometer 2).

There is considerable evidence to demonstrate that displacement rates increased dramatically after the period 28 January - 4 February 1994. Acoustic emission (particularly from wave guides 1, 2 and 3) and inclinometer data (presented in the form of displacement rates) both show a marked increase after this period. Additionally the dipped water level in inclinometer 1, which in figure 4.24 is plotted along with the displacement rate, shows that peak water levels were recorded at 28 January and 4 February 1994. In section 4.5.1 the variable behaviour of the water level in inclinometer 1 was contrasted with that in inclinometer 2 which remained more or less steady throughout the test. This may be explained by reference to the borehole data (table 4.2) which shows that while the bottom 15 metres of inclinometer 1 (including the toe) was within glacial till, the bottom 3 metres of inclinometer 2 was 'toed' into a stratum described as 'clayey fine to medium sand'. It is likely that this layer readily facilitated drainage. It is important to appreciate that, because the inclinometer was not sealed to measure pore water pressures in the same way a piezometer would be, the ground water level measured may not reflect either the

magnitude or trend of actual pore water pressures at a depth of 21 metres. However, the rapid drop in the level does coincide with increased rates of displacement (as recorded by the inclinometers) and increased levels of detected AE.

There is also some evidence that bouts of slippage along the failure plane occurred at different times along its length. Wave guides 1 and 9 were both sand backfilled and were situated on the northern side of the instrument array. Figure 4.25 shows that, over that period where both wave guides had been monitored, the AE trends (in terms of mean signal value in volts) were identical. Similarly wave guides 5 and 10 were both sand backfilled and situated on the southern side of the instrument array. Figure 4.25 shows that, as before, over the common monitoring period the AE trends were very similar (although not identical). The interesting point is that the AE trends exhibited by the wave guides on the northern and southern sides of the instrument array were different. This may suggest that movement occurred at different times along different stretches of the slip surface. There is some corroborative evidence presented in the displacement rates calculated for inclinometers 1 and 2 (figures 4.17), which were slightly different, but it is impossible to relate individual displacement rates to individual AE trends.

Further discussion of the findings of the Cowden field test are contained in chapter 5 and chapter 6, when they are considered in conjunction with the results obtained from the Arlesey large scale test.

Instrument Type	Instrument Code	Instrument Depth metres	Instrument Material	Instrument Backfill
Wave Guide	WG1	21	Steel Tubing	Sand
Wave Guide	WG2	21	Steel Tubing	Gravel
Wave Guide	WG3	21	Steel Tubing	Grout
Wave Guide	WG4	12	Steel Tubing	Grout
Wave Guide	WG5	12	Steel Tubing	Sand
Wave Guide	WG6	12	Steel Tubing	Gravel
Wave Guide	WG7	18	Steel Tubing	Sand
Wave Guide	WG8	12	Steel Tubing	Sand
Wave Guide	WG9	6	Steel Tubing	Sand
Wave Guide	WG10	12	Steel Tubing	Sand
Wave Guide	WG11	6	Steel Tubing	Sand
Wave Guide	WG12	6	Steel Tubing	Sand
Inclinometer	I1	21	Aluminium	Grout
Inclinometer	I2	21	Aluminium	Grout

Table 4.1 - BRE coastal cliff section instrumentation

1 Inclinometer 1; Wave Guides 1 - 6, 8 & 9, 11 & 12

mbgl	Description
0 - 4	weathered brown stiff gravelly CLAY: Till
4 - 6	silty fine to medium SAND
6 - 10	dark grey brown stiff gravelly CLAY: Till
10 - 21	dark grey stiff gravelly CLAY: Till

2 Inclinometer 2 & Wave Guides 10

mbgl	Description
0 - 3	weathered brown stiff gravelly CLAY: Till
3 - 6	silty fine to medium SAND
6 - 10	dark grey brown stiff gravelly CLAY: Till
10 - 18	dark grey stiff gravelly CLAY: Till
18 - 21	clayey fine to medium SAND

3 Wave Guides 7

mbgl	Description
0 - 4	weathered brown stiff gravelly CLAY: Till
4 - 6	silty fine to medium SAND
6 - 10	dark grey brown stiff gravelly CLAY: Till
10 - 18	dark grey stiff gravelly CLAY: Till
18 - 21	clayey silty fine to medium SAND: Ingress of water into borehole which collapsed back to 18 mbgl

4 Soil profile at the Cowden cliff site (after Butcher, 1991)

mbgl	Description
0 - 2.5	weathered brown stiff stoney CLAY till
2.5 - 3.0	SAND & GRAVEL
3.0 - 4.5	dark grey brown stiff stoney CLAY till
4.5 - 5.0	SAND & GRAVEL
5.0 - 10.0	dark grey brown stiff stoney CLAY till
10.0 - 19.5	dark grey stiff stoney CLAY till
19.5 - 21.0	soft brown CLAY till
21.0 - 22.0	SAND & GRAVEL
22.0 -	dark grey stiff stoney CLAY till

Table 4.2 Cowden instrument borehole logs (mbgl - metres below ground level). Note that the descriptions of strata in 4 above, are taken verbatim from the soil profile reproduced as figure 4.2 (after Butcher, 1991)

Date	Day	File Suffix	Wave Guides Monitored	No of AE Files	Notes on Data Acquisition
Sept 93	-	-	-	-	Instruments Installed
12 Oct 93	0	-		0	I
2 Nov 93	21	-		0	I
11 Nov 93	30	-		0	I
25 Nov 93	44	-		0	I
1 Dec 93	50	various		6	I,T,U,G
2 Dec 93	51	various		24	I,T,U,G
3 Dec 93	52	various		11	I,T,U,G
22 Dec 93	71	-		0	I
13 Jan 94	93	D2	2, 3, 7, 10, 11	41	I,S,U,C
21 Jan 94	101	D3	1, 2, 3, 4, 5, 6, 10, 11, 12	12	I,S,B,G,C
28 Jan 94	108	D4	1, 2, 3, 4, 5, 6, 7, 9, 12	10	I,S,B,C
4 Feb 94	115	D5	1, 2, 3, 4, 5, 6, 7, 8, 9, 10, 11, 12	18	I,S,B,G,C
11 Feb 94	122	D6	1, 7	10	I,T,B,C
25 Feb 94	136	D7	1, 2, 3, 4, 5, 6, 7, 10, 11, 12	17	I,S,B,G,C
10 Mar 94	149	D8	1, 2, 3, 4, 5, 6, 7, 8, 9, 10, 12	14	I,S,B,G
24 Mar 94	163	D9	1, 2, 3, 4, 5, 6, 7, 9, 10, 12	11	I,S,B,G
7 Apr 94	177	X0	1, 2, 3, 4, 5, 6, 7, 9, 10, 12	11	I,S,B,G
6 May 94	206	X1	5, 6, 7, 9, 12	5	I,S,B,G
27 May 94	227	X2	1, 4, 5, 6, 7, 9, 12	10	I,S,B,G

Table 4.3 - Summary of Cowden inclinometer & wave guide monitoring history

Notes on Data Acquisition

- I inclinometers I1 and I2 read except 22 Dec 93 when only I1 read
- S Viewdac routine which captures data by periodic sampling
- T Viewdac routine which captures data when activated by a *trigger*
- U unipolar data acquisition
- B bipolar data acquisition
- G signal grounded using either Landrover chassis, generator or wave guide
- C signal not grounded

Date	Day	Data File Suffix	No of AE Files	Wave Guides Monitored
1 Dec 93	50		1	1
2 Dec 93	51		12	1, 2, 3
3 Dec 93	52		4	1, 12
4 Feb 94	115	D5	12	1, 2, 3, 4, 5, 6, 7, 8, 9, 10, 11, 12
25 Feb 94	136	D7	8	3, 4, 5, 6, 7, 10, 11, 12
10 Mar 94	149	D8	11	1, 2, 3, 4, 5, 6, 7, 8, 9, 10, 12
24 Mar 94	163	D9	10	1, 2, 3, 4, 5, 6, 7, 9, 10, 12
7 Apr 94	177	X0	10	1, 2, 3, 4, 5, 6, 7, 9, 10, 12
6 May 94	206	X1	5	5, 6, 7, 9, 12
27 May 94	227	X2	5	4, 5, 6, 9, 12

Table 4.4 Data sets available for AE slope instability analysis

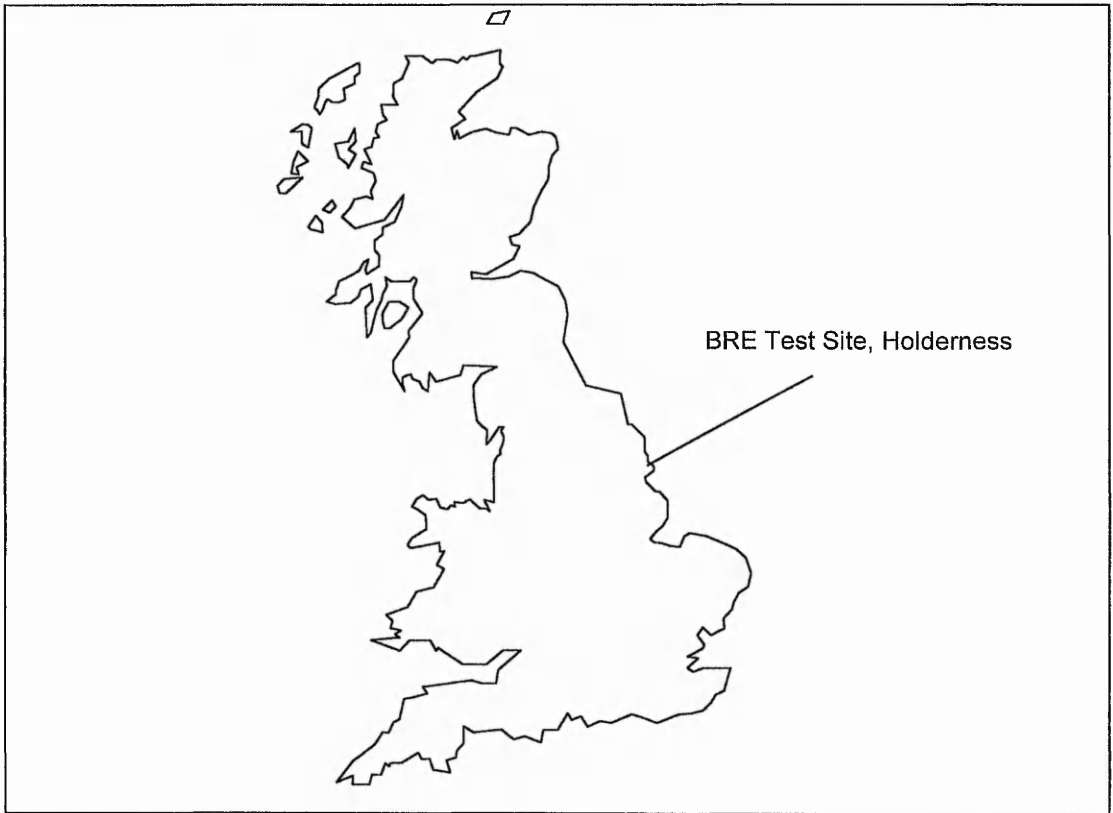


Figure 4.1 Geographical location of BRE coastal cliff section

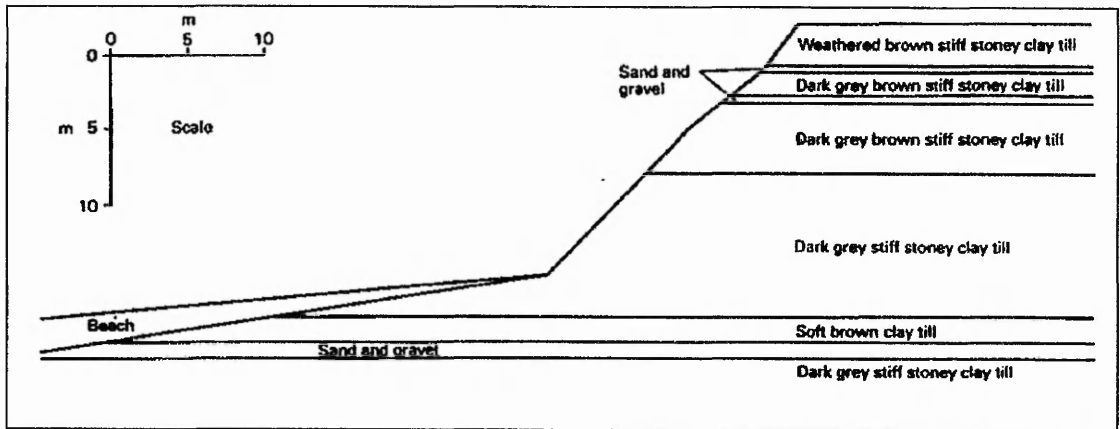


Figure 4.2 Soil profile at the Cowden site (after Butcher, 1991)

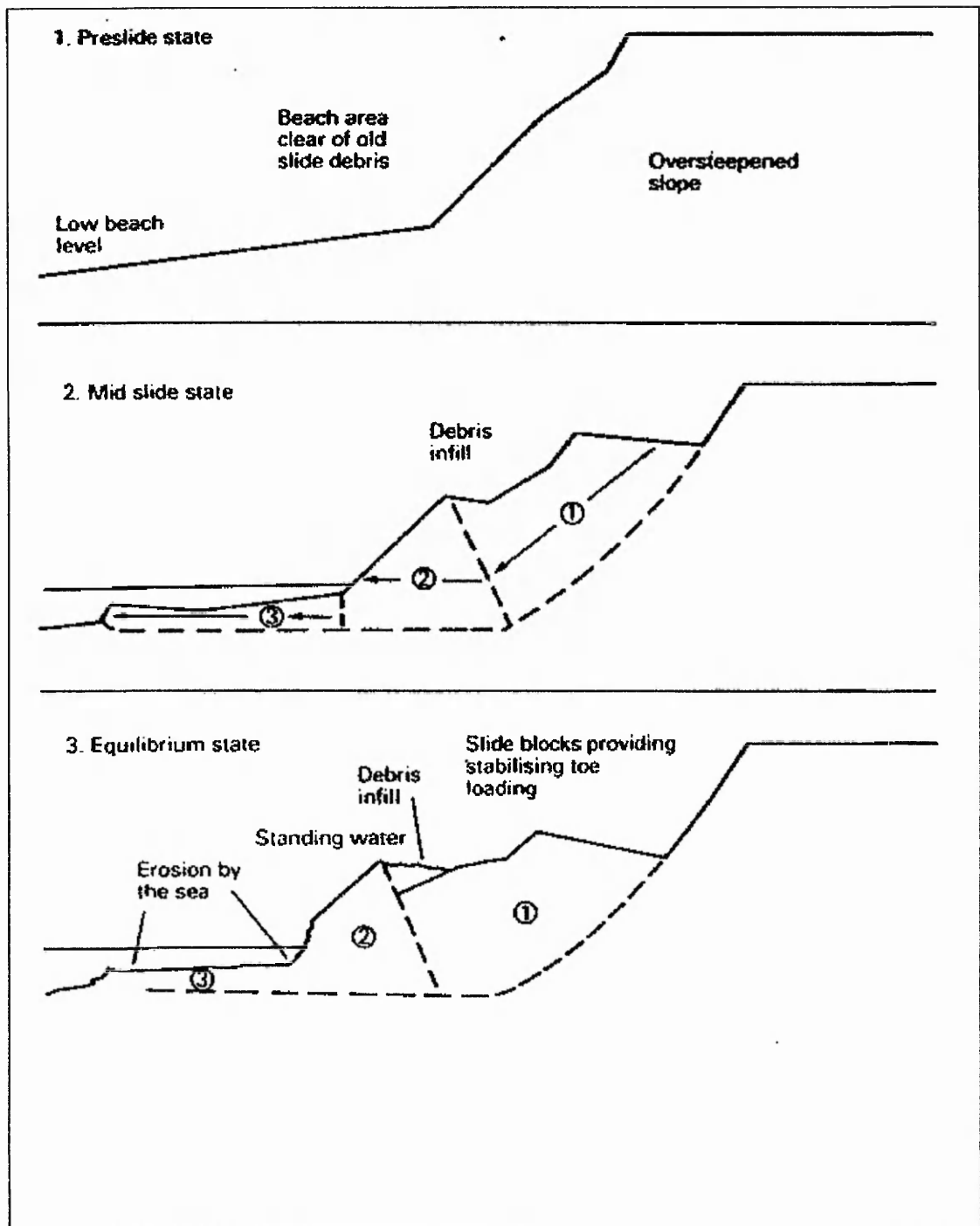


Figure 4.3 Schematic diagram of the failure mechanism (after Butcher, 1991)

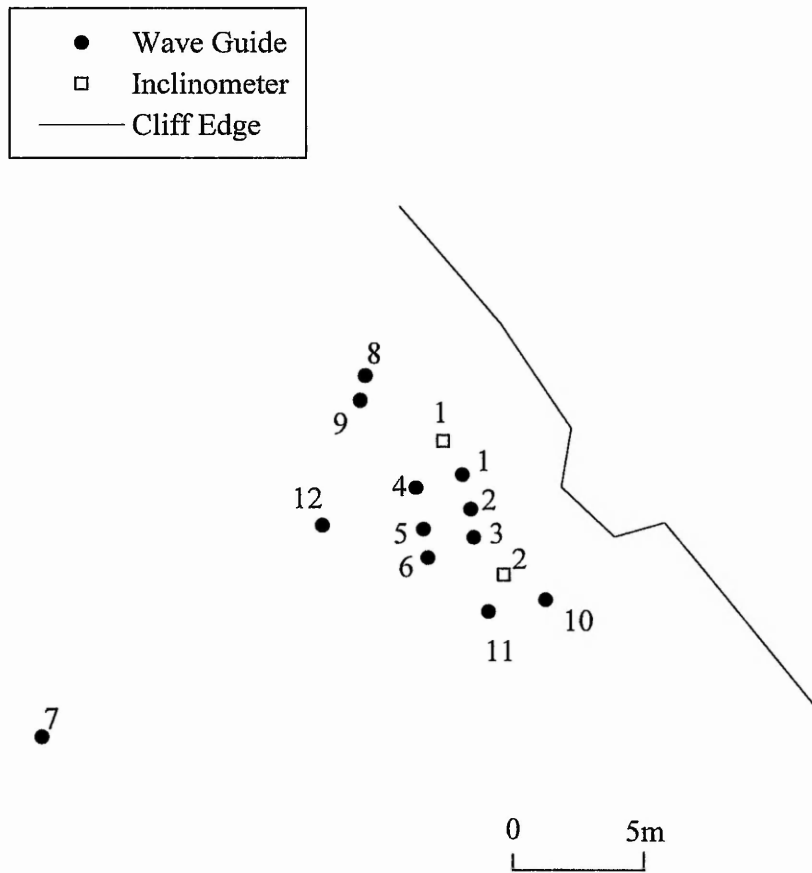


Figure 4.4 Cowden instrument positions as at 11 November 1993

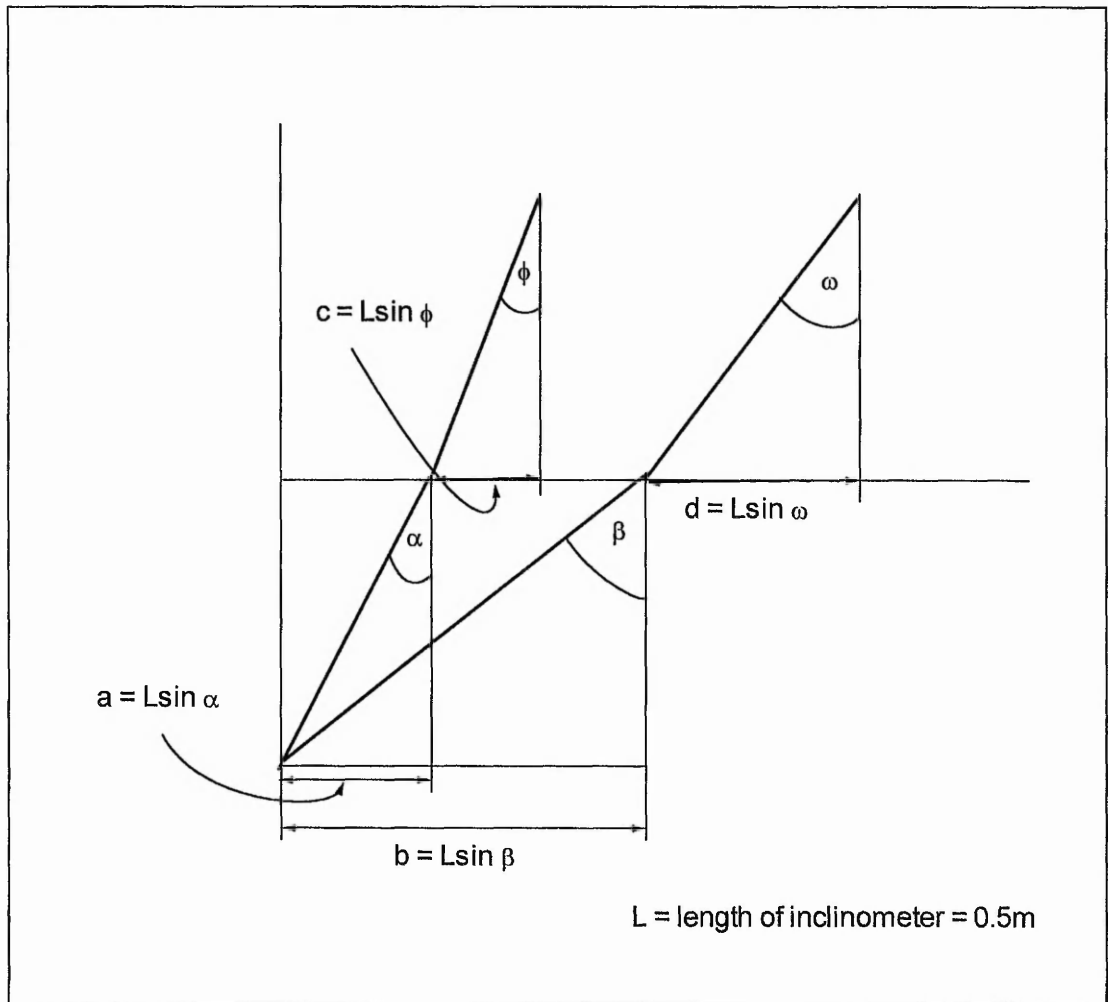


Figure 4.5 Schematic representation of inclinometer geometry



Figure 4.6 Tension crack around WG8 as at 11 February 1994

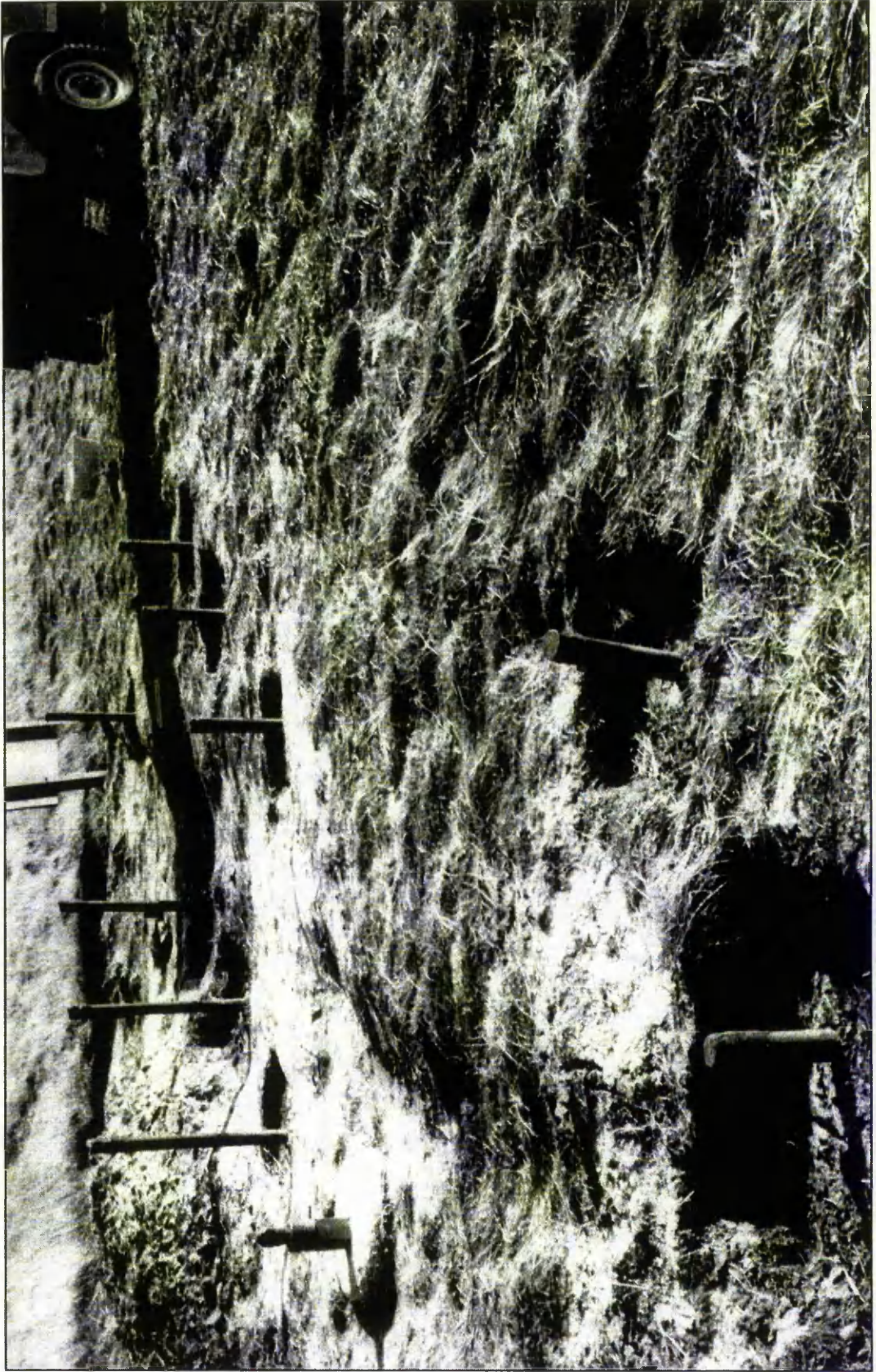


Figure 4.7 Slip development as at 10 March 1994 - WG8 is in foreground of figure

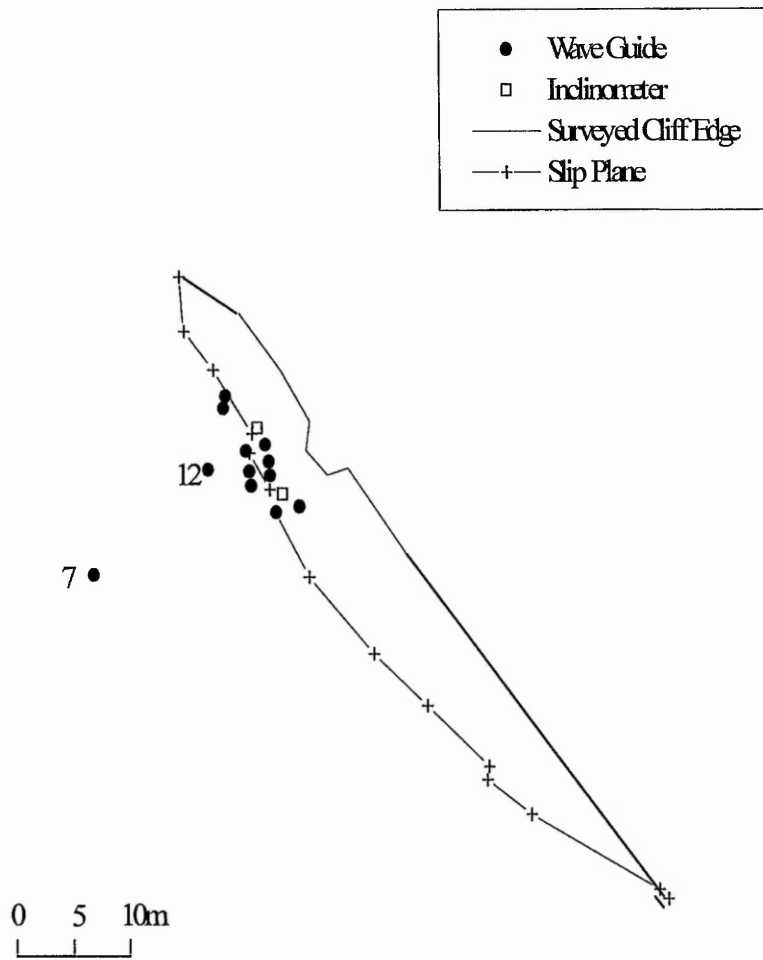


Figure 4.8 Cowden instrument array as at 11 November 1993 showing extent of slip surface as at 16 June 1994

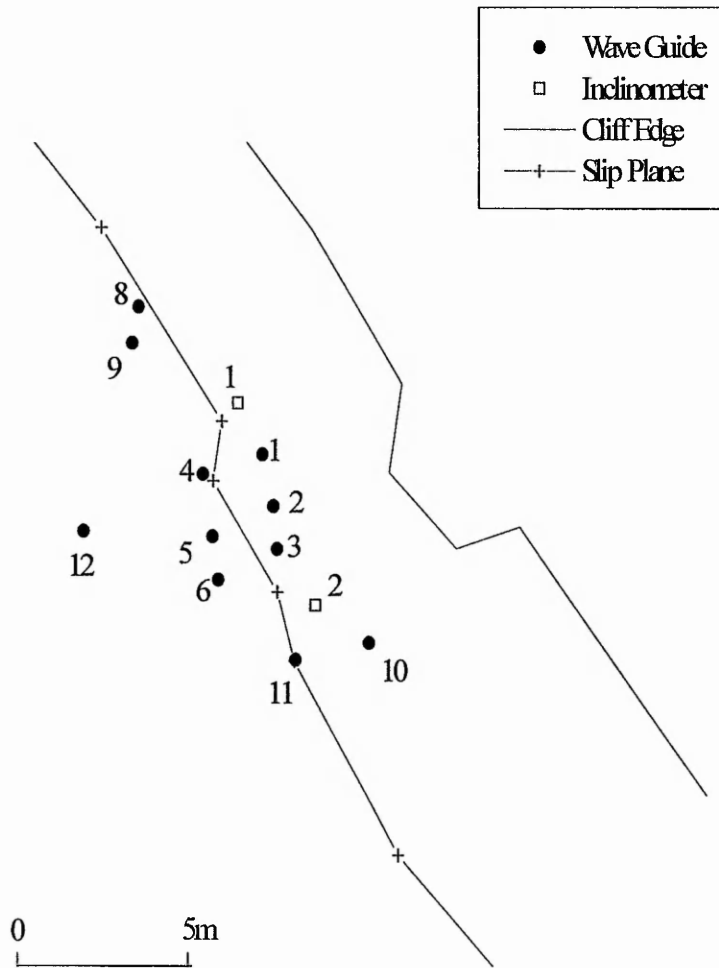


Figure 4.9 Cowden instrument array as at 11 November 1993 showing relationship with slip surface as at 16 June 1994

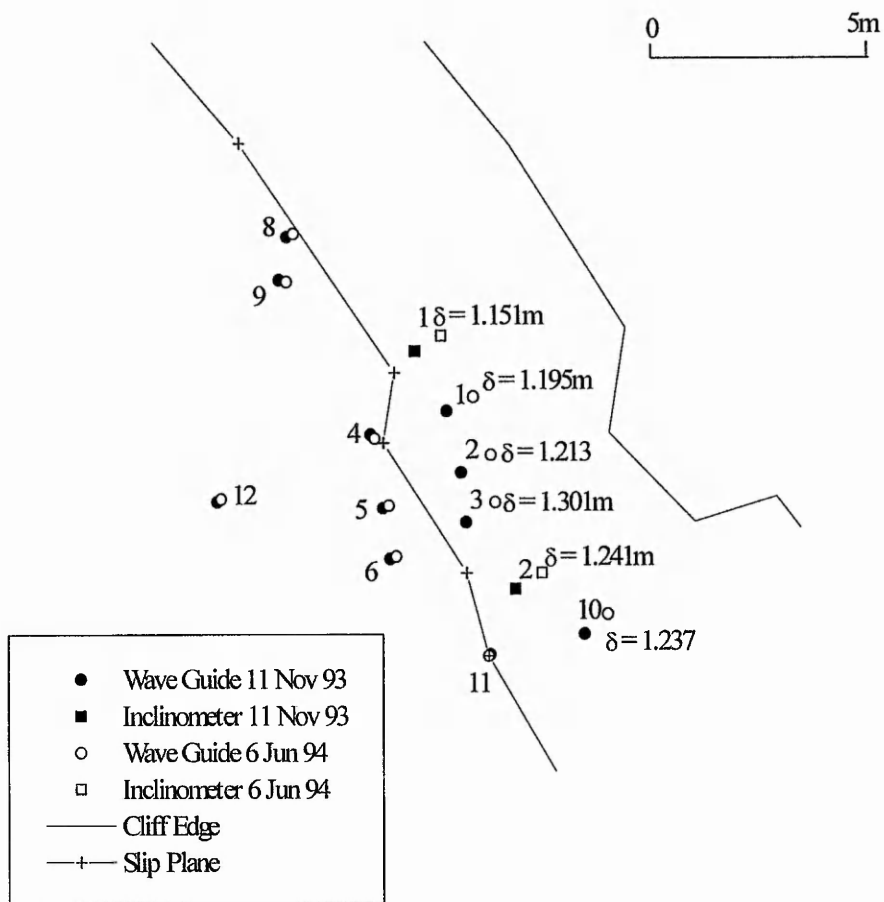


Figure 4.10 Cowden instrument array depicting change in instrument position between 11 November 1993 and 16 June 1994. Change in ground level (δ) with reference to Ordnance Datum is given for instrument locations WG1, WG2, WG3, WG10, I1 and I2

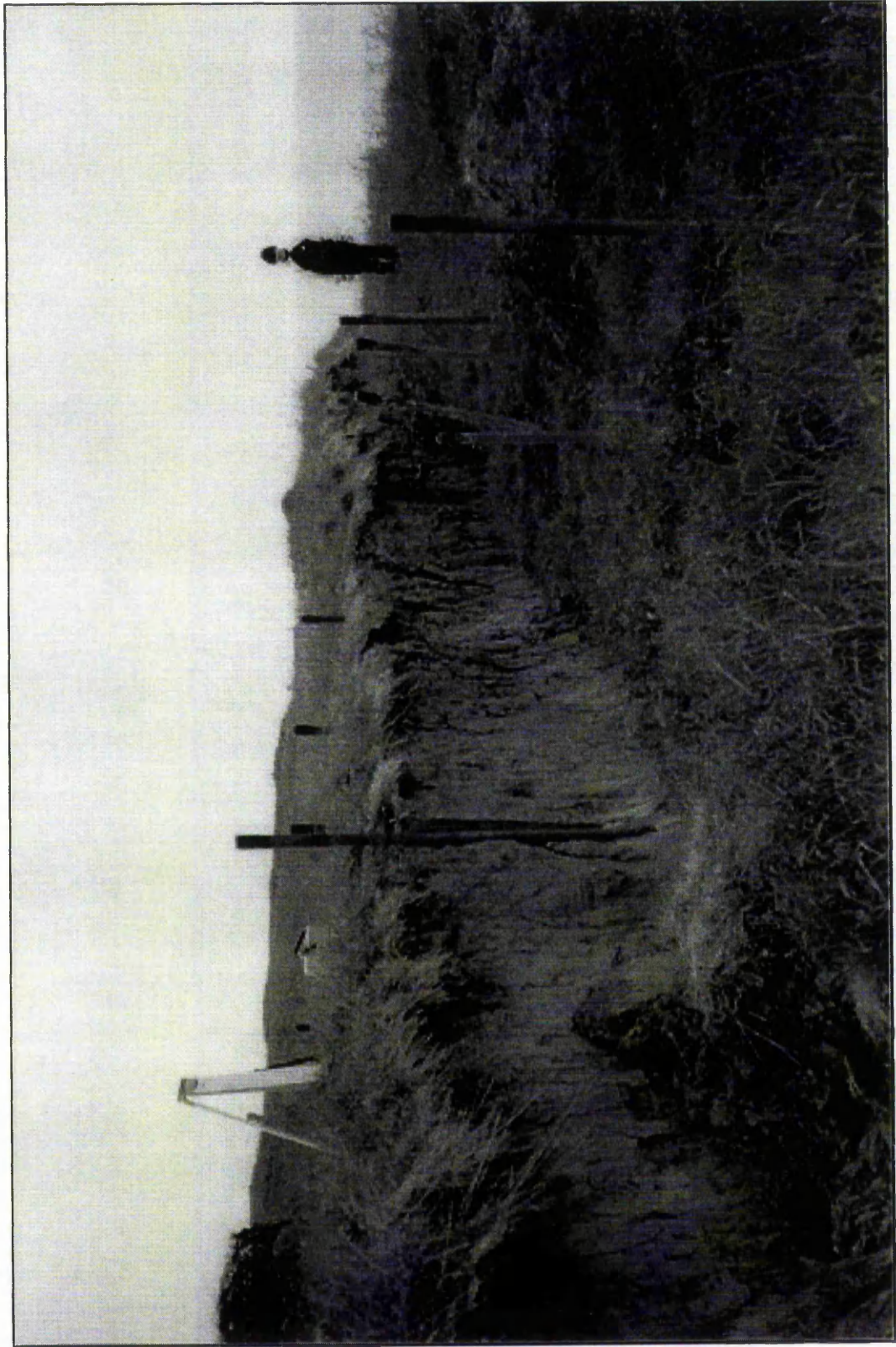


Figure 4.11 Cowden landslip (looking North) as at 16 June 1994. Note WG11 on slip plane in foreground



Figure 4.12 Cowden WG11 as at 16 June 1994

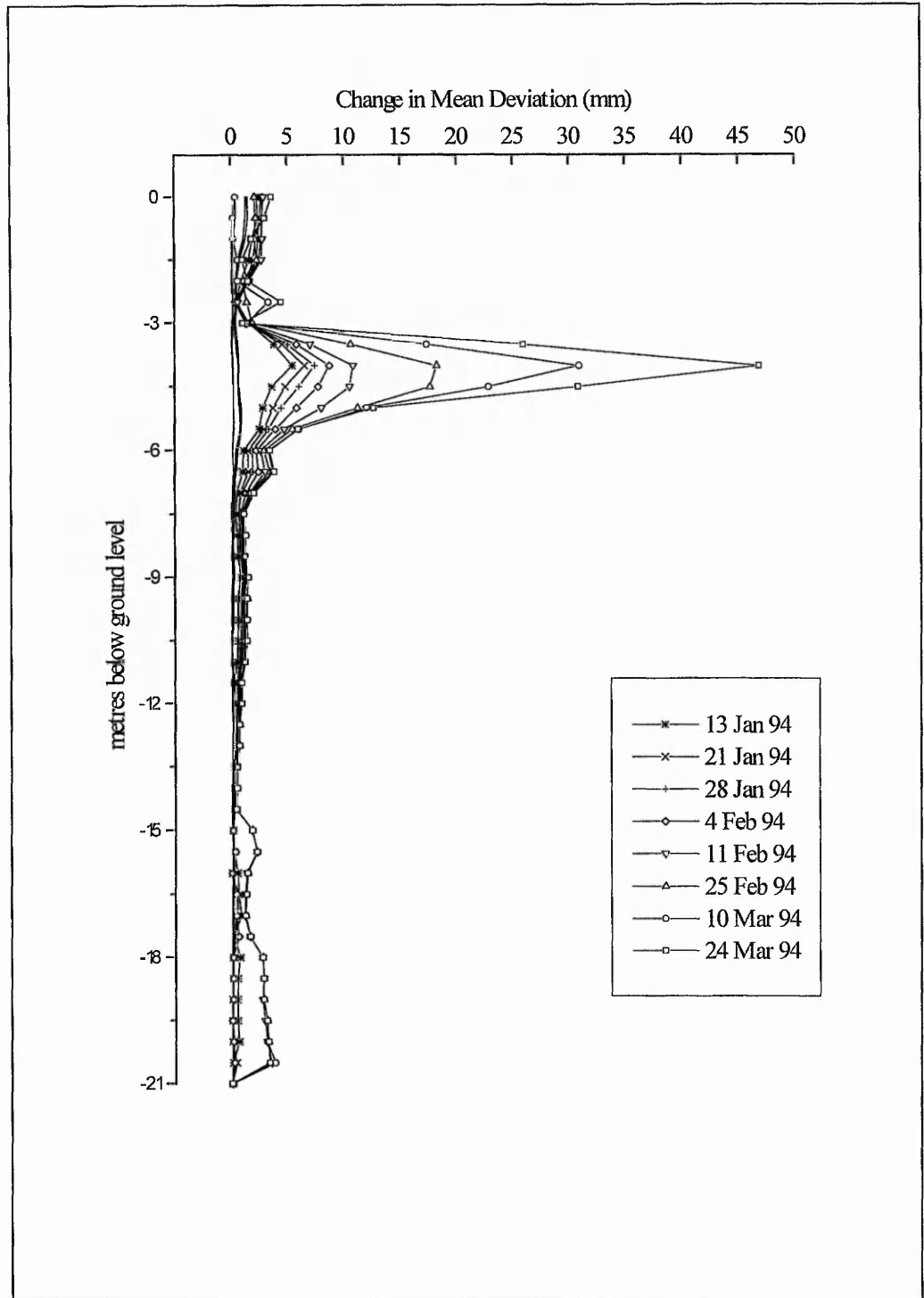


Figure 4.13 Cowden inclinometer 1 change in mean deviation

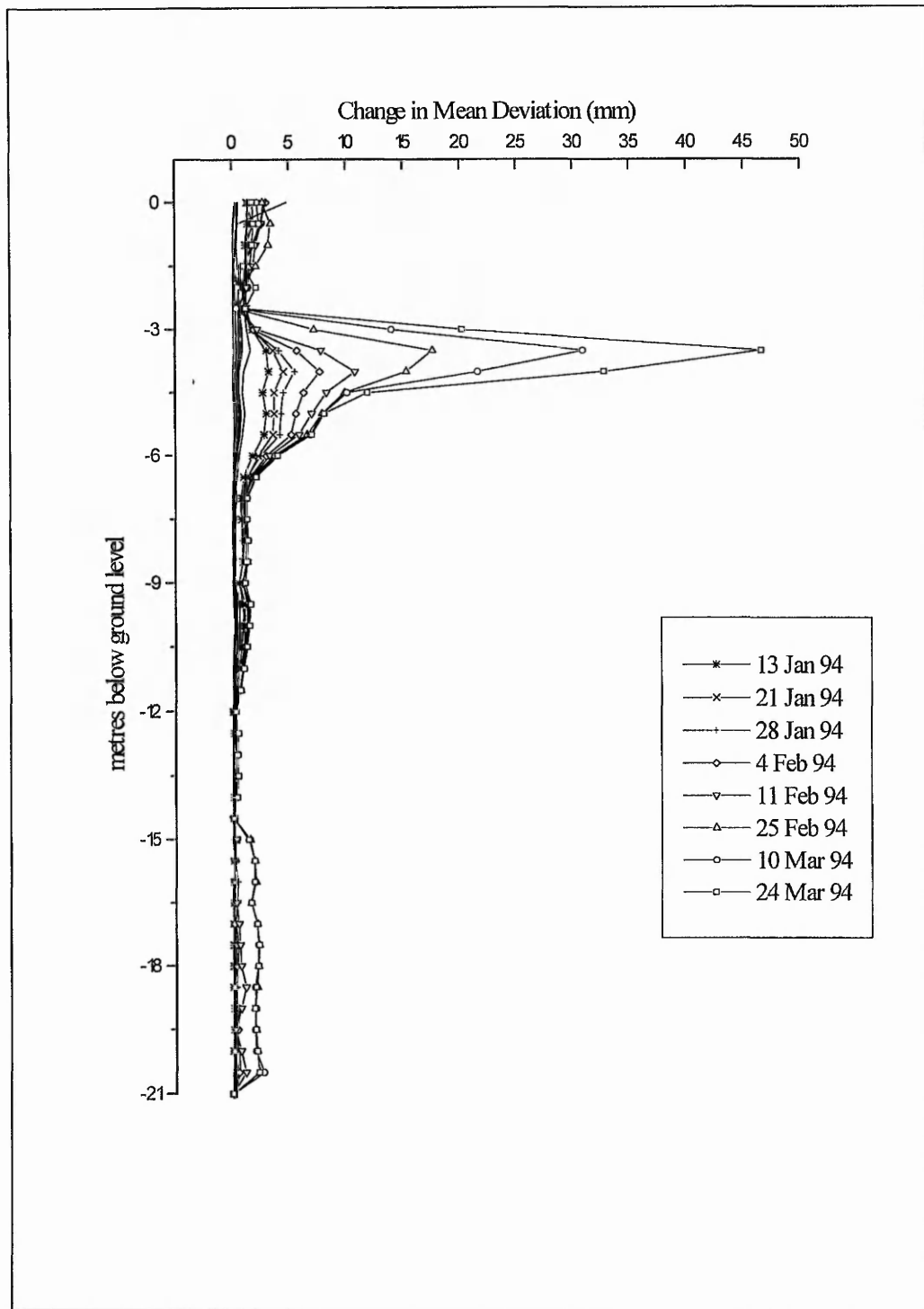


Figure 4.14 Cowden inclinometer 2 change in mean deviation

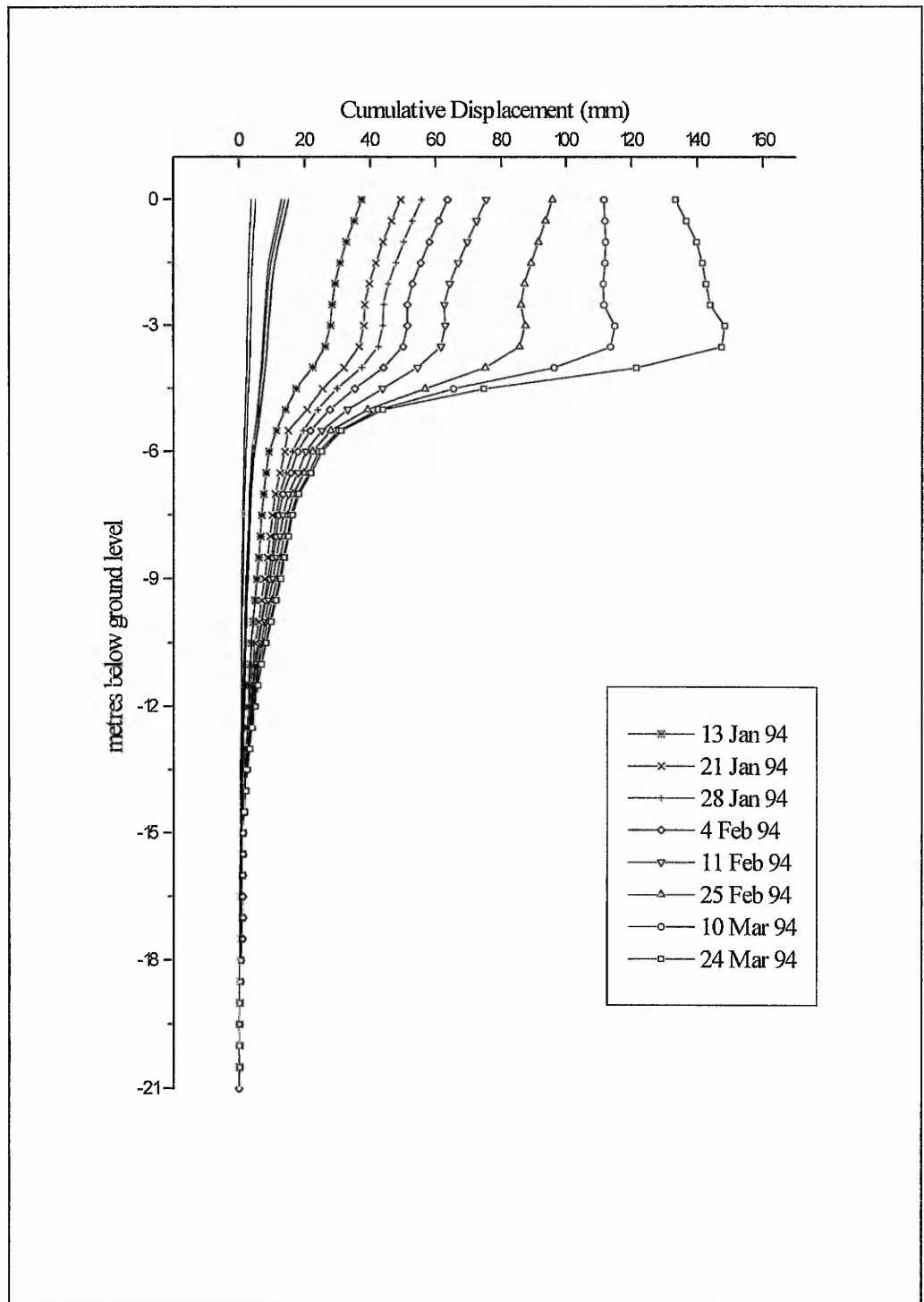


Figure 4.15 Cowden inclinometer 1 displacement profile

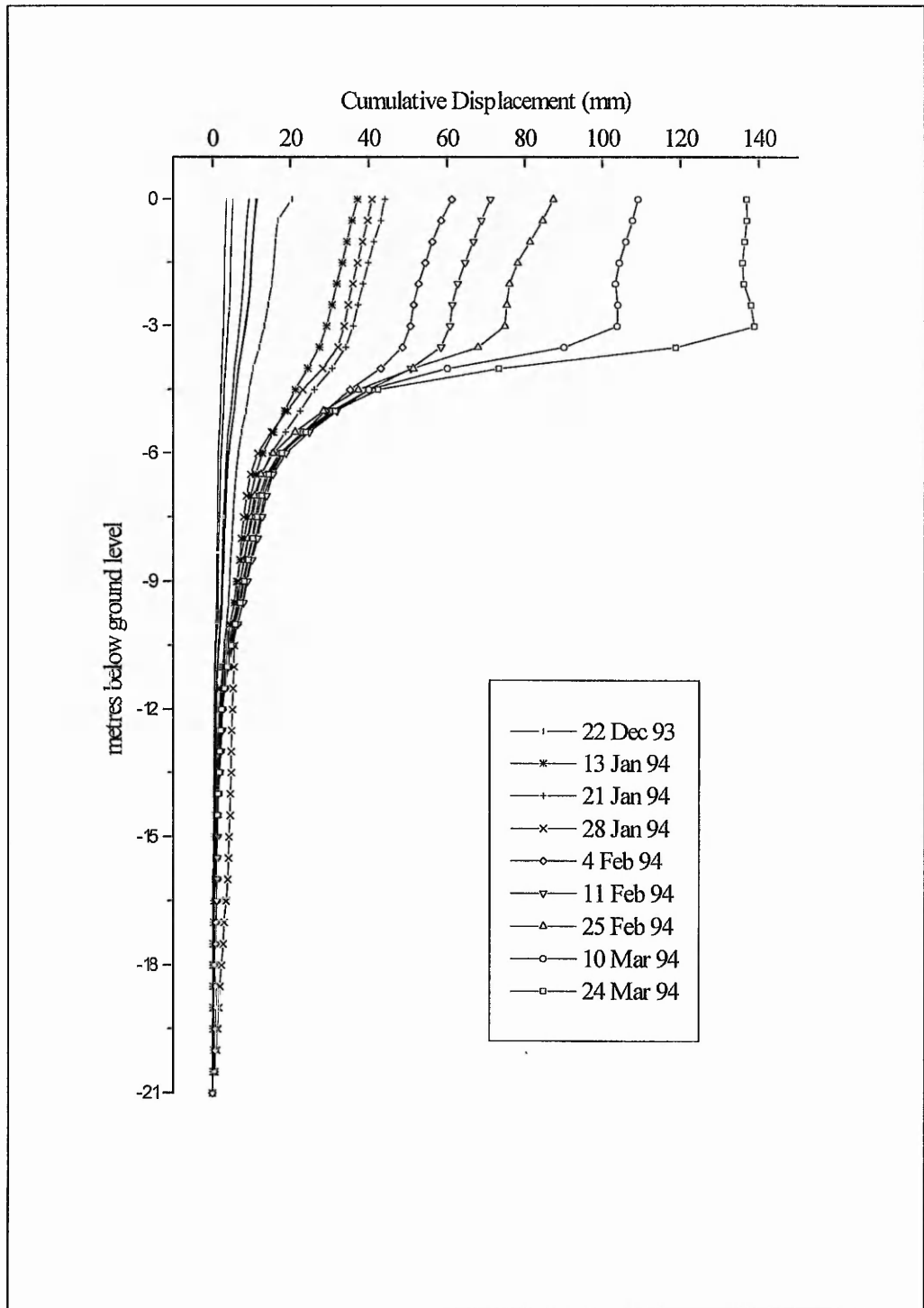


Figure 4.16 Cowden inclinometer 2 displacement profile

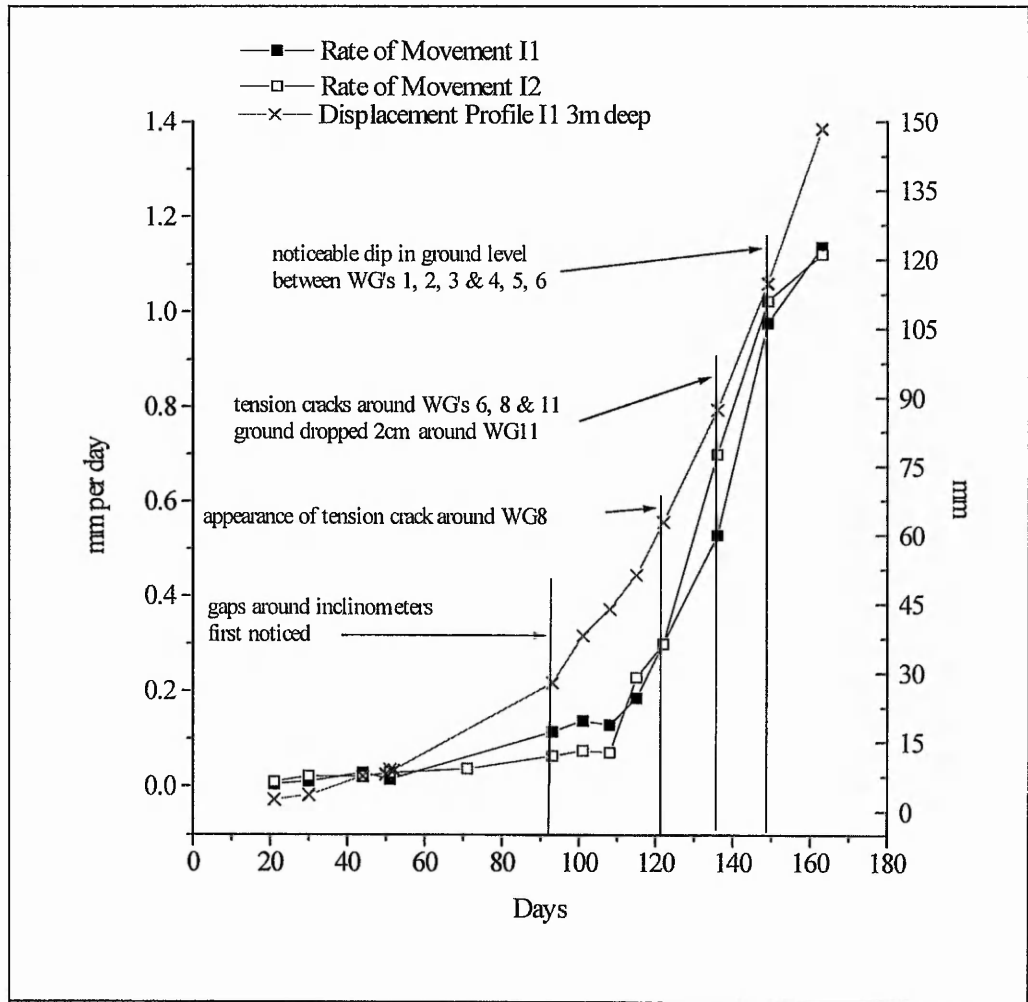


Figure 4.17 Cowden inclinometers rates of displacement

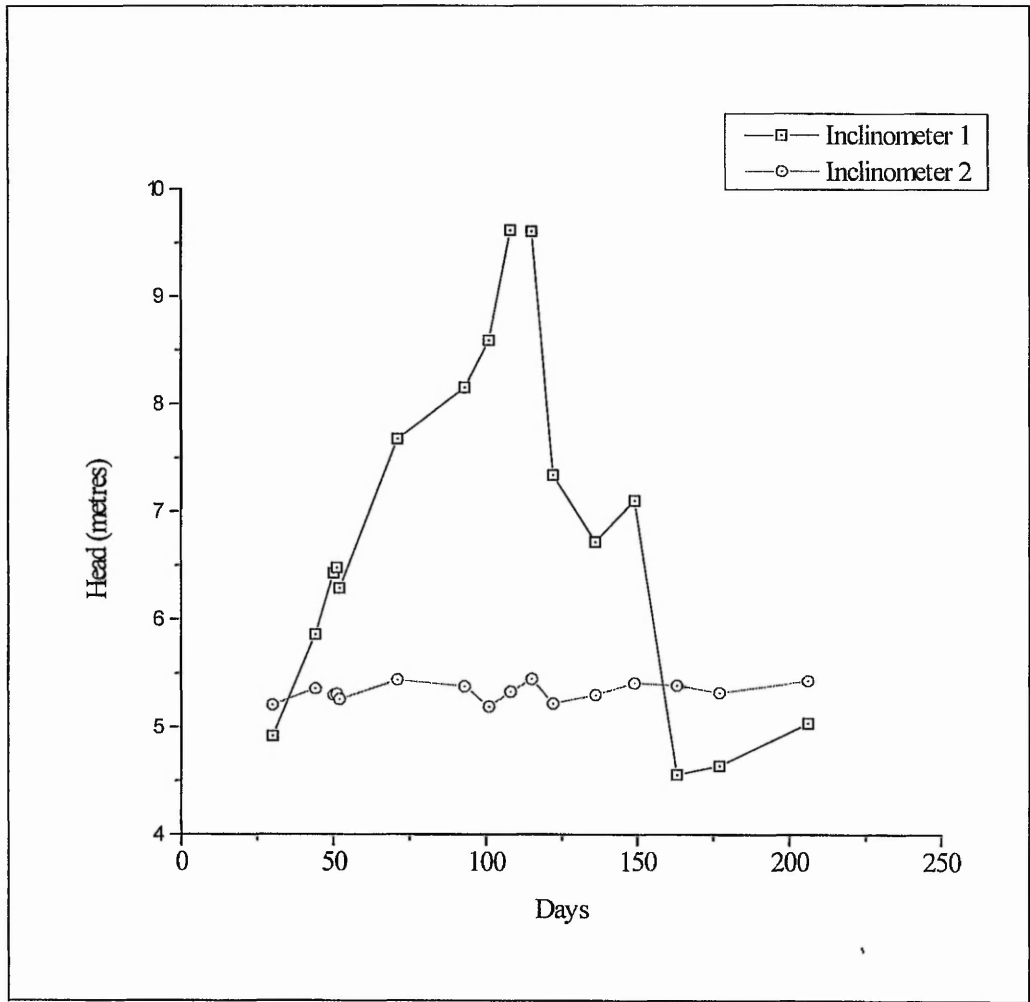


Figure 4.18 Dipped water levels in inclinometer casings (head measured relative to base of inclinometer)

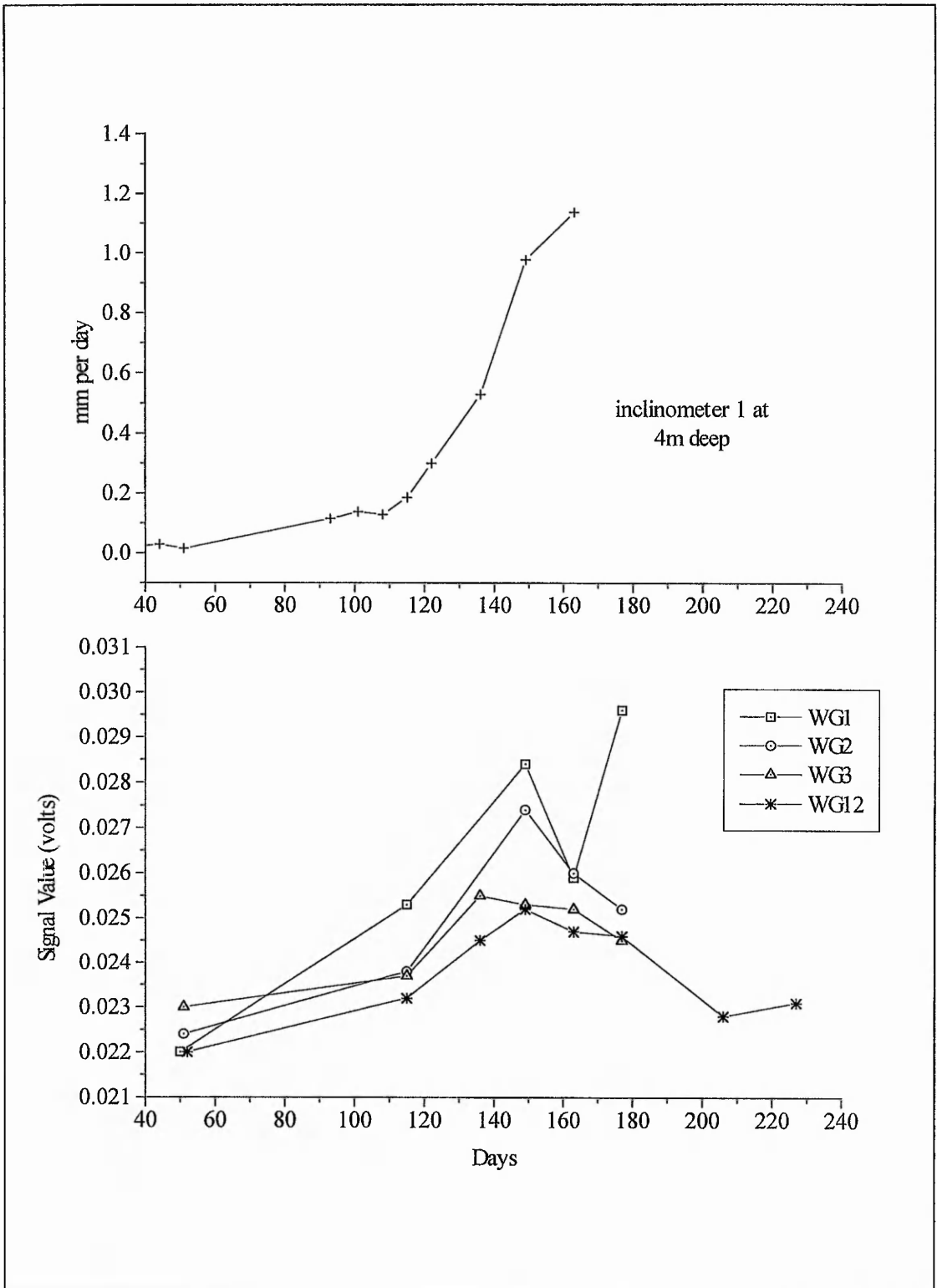


Figure 4.19 AE mean signal value WGs 1, 2, 3 & 12 and displacement rate inclinometer 1

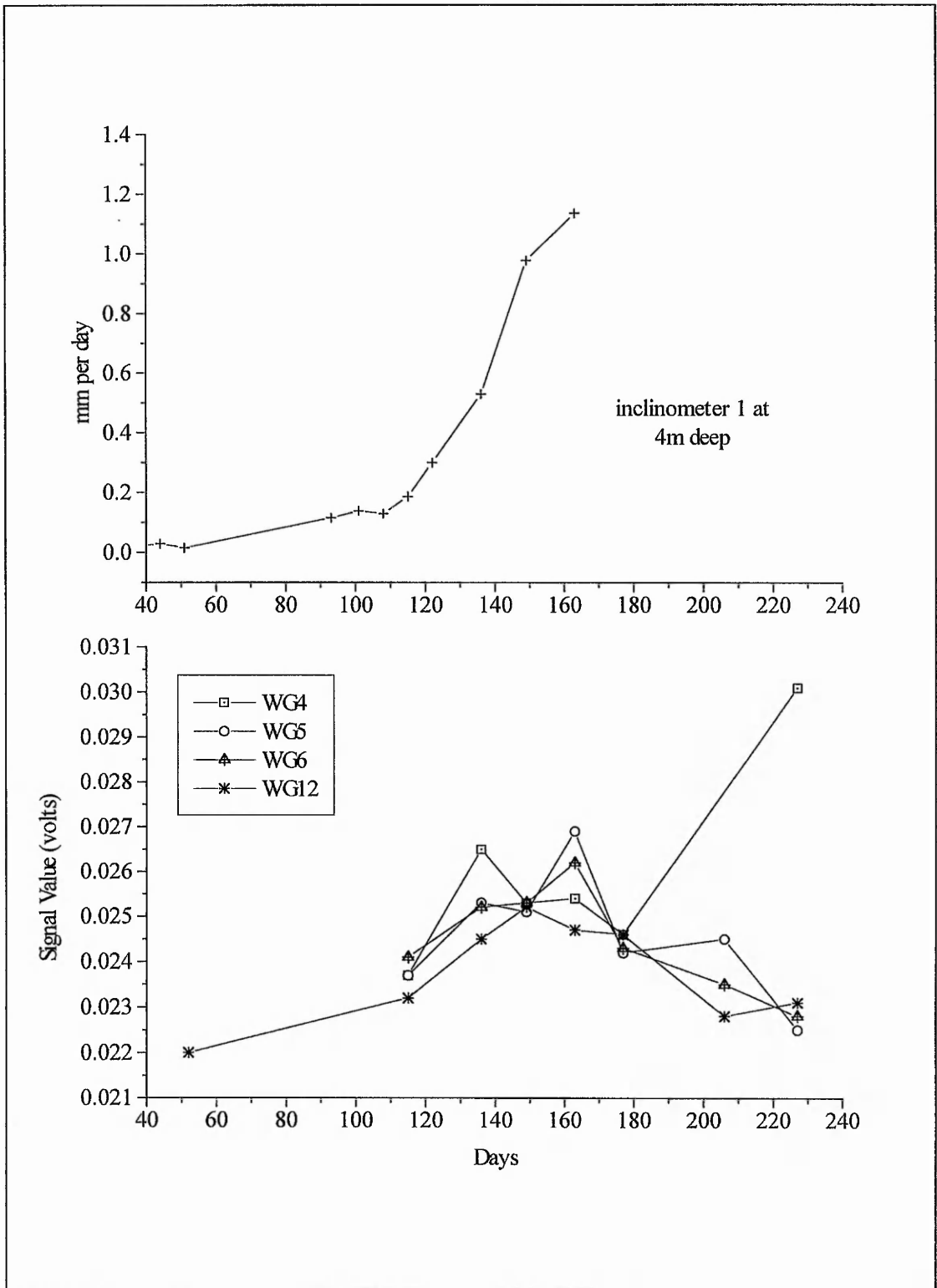


Figure 4.20 AE mean signal value WGs 4, 5, 6 & 12 and displacement rate inclinometer 1

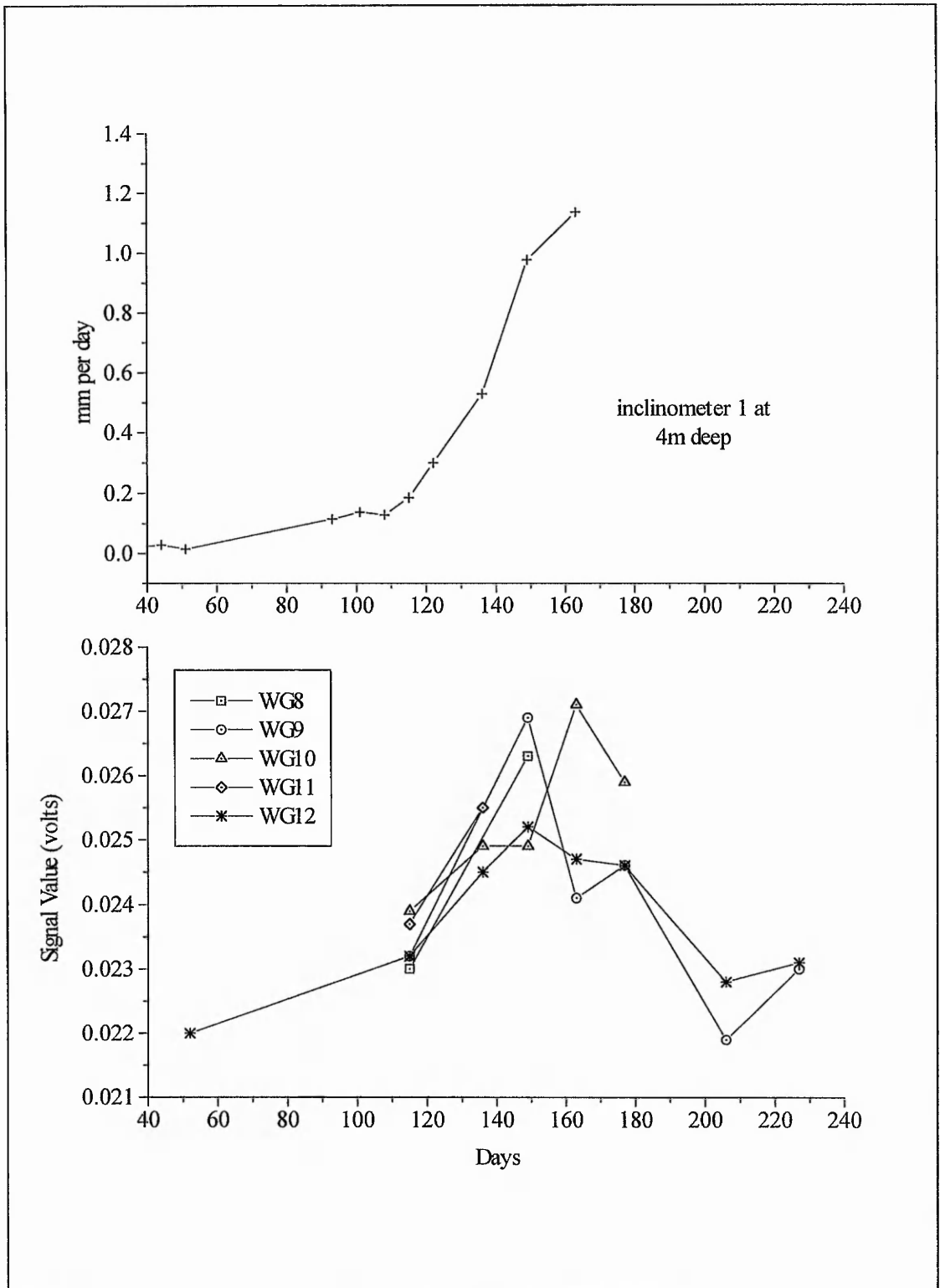


Figure 4.21 AE mean signal value WGs 8, 9, 10, 11 & 12 and displacement rate inclinometer 1

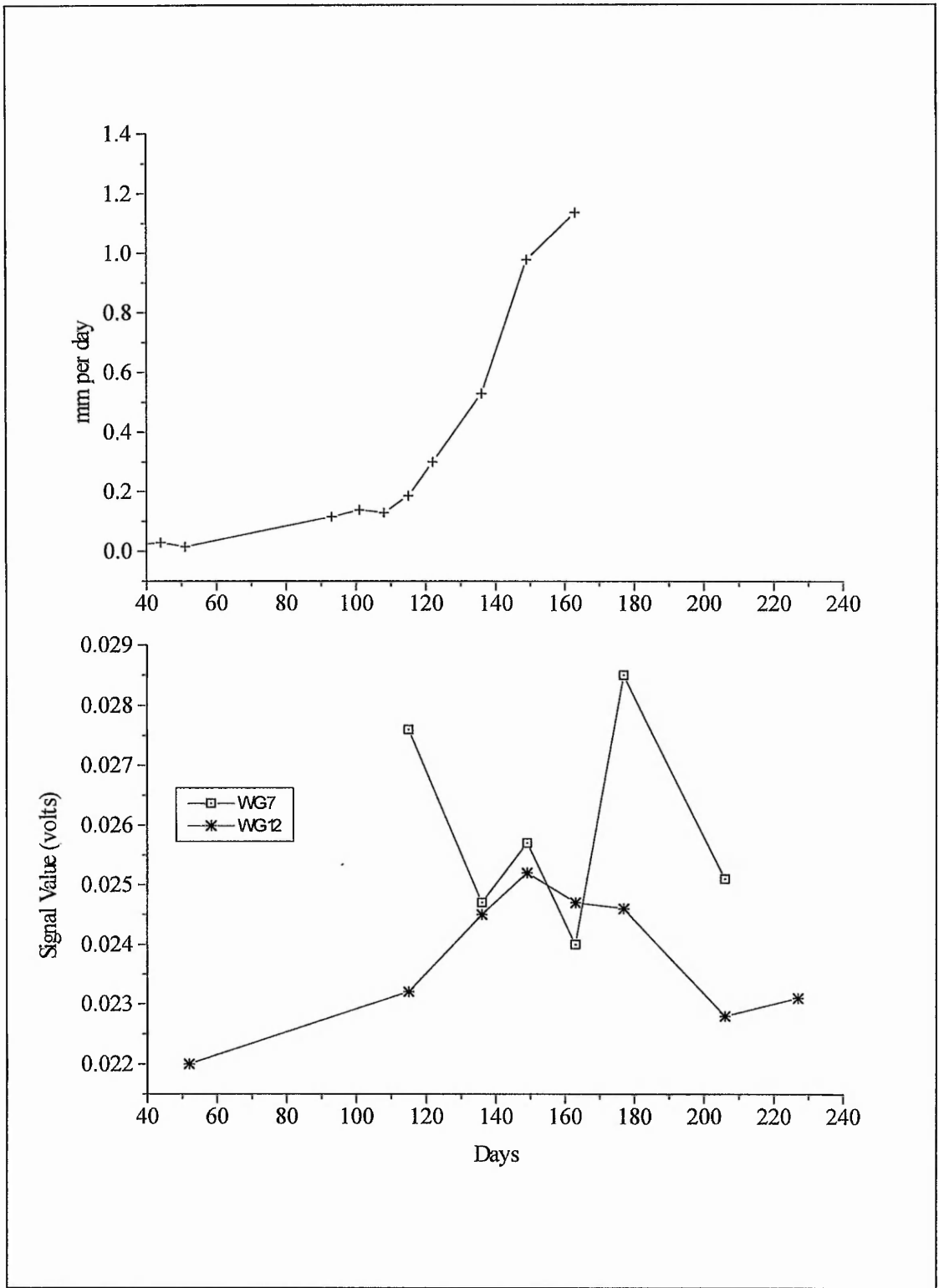


Figure 4.22 AE mean signal value WGs 7 & 12 and displacement rate inclinometer 1

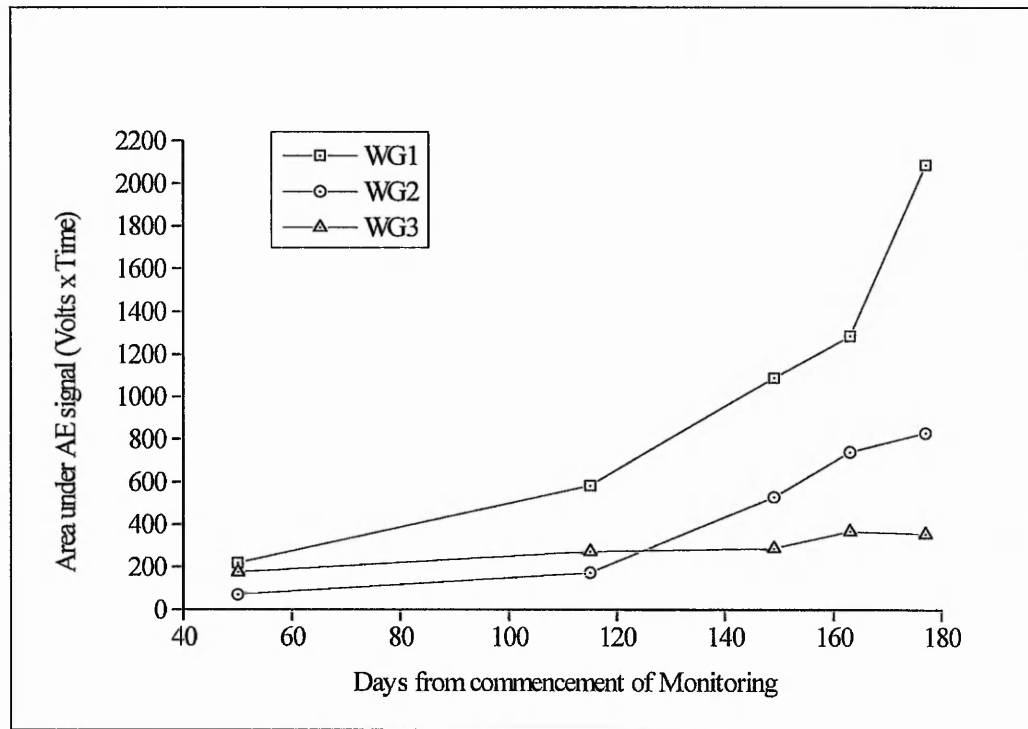
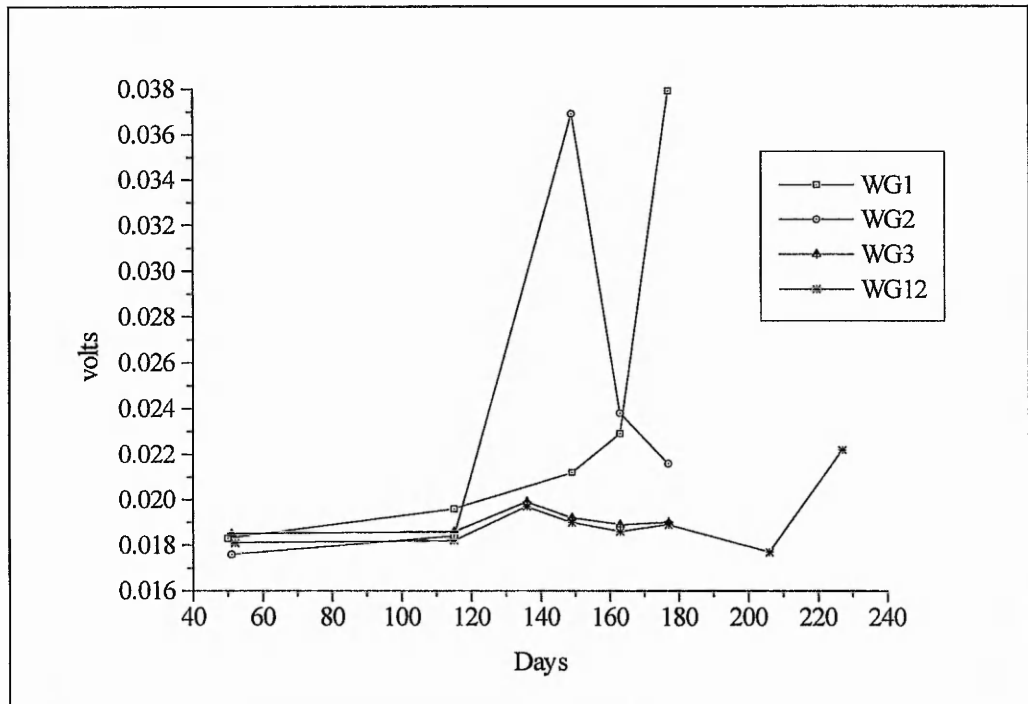


Figure 4.23 Alternative data processing techniques using (a) standard deviation of data and (b) normalised cumulative area under the curve in excess of WG12 (after Dixon *et al.*, 1994)

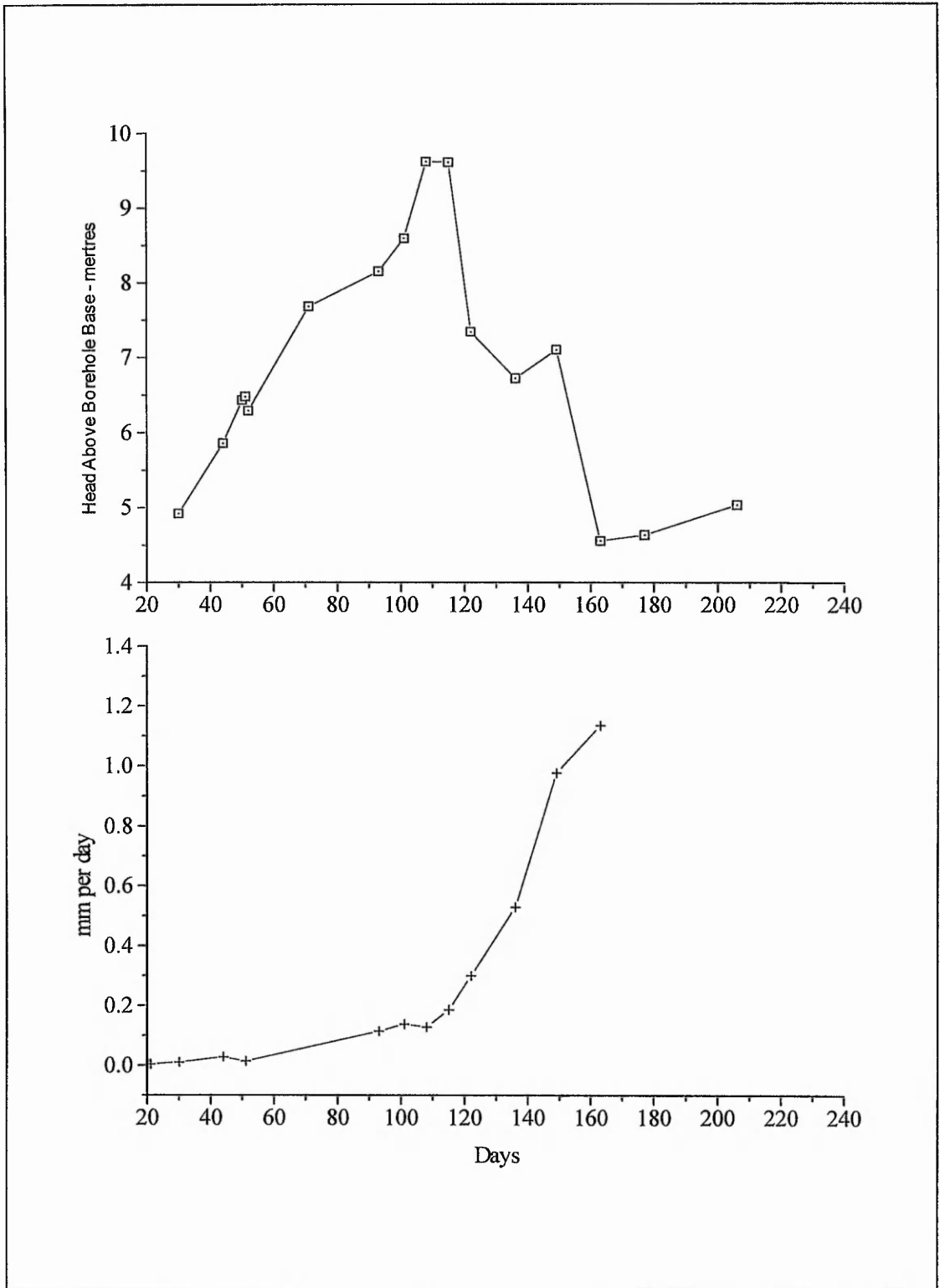


Figure 4.24 Dipped water level and displacement rate inclinometer 1

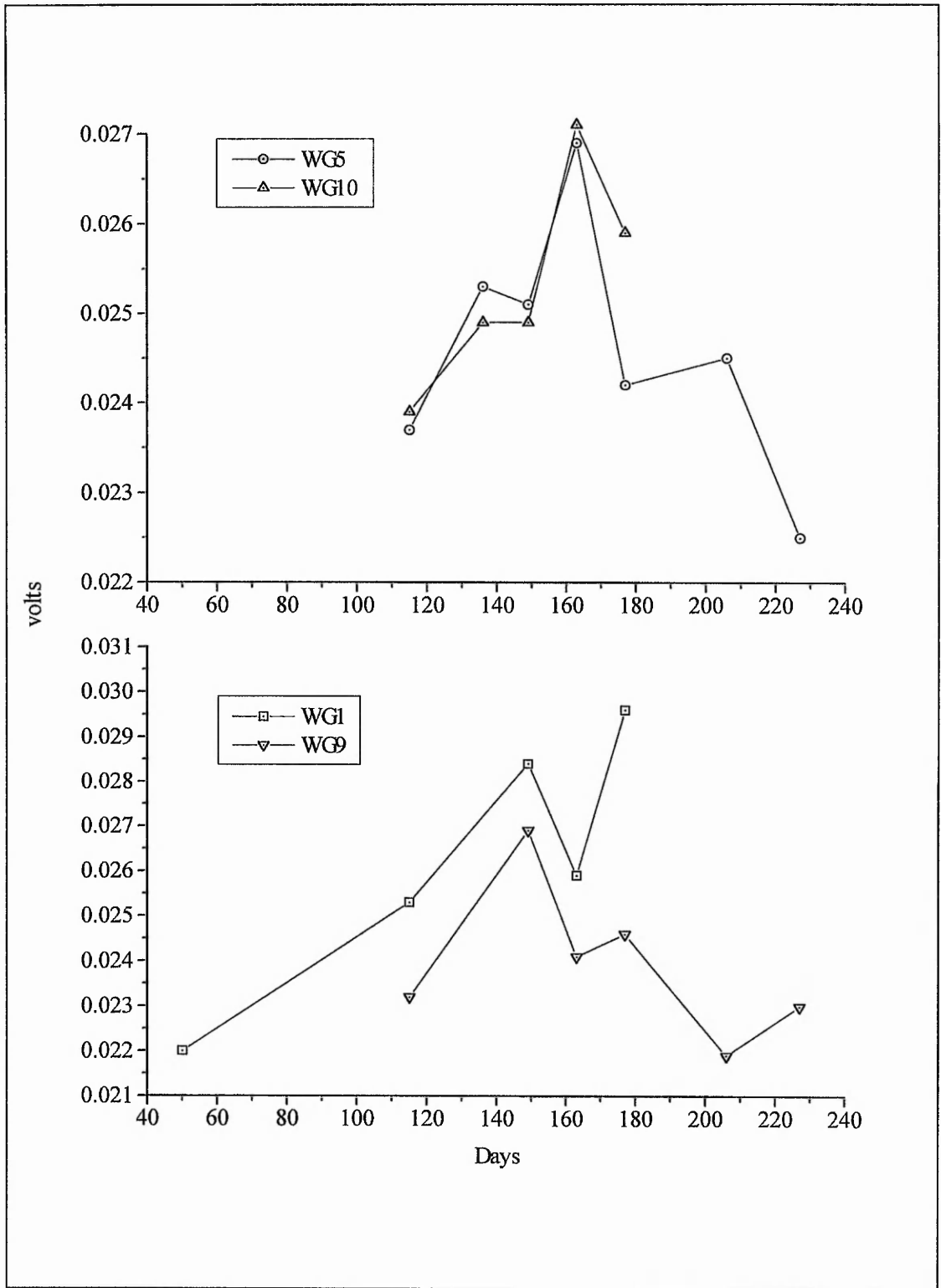


Figure 4.25 AE mean signal value WGs 1 & 9 and 5 & 10

Chapter 5

The Arlesey Large Scale Test

5.1 Introduction

The Arlesey large scale test was conceived as a means to supplement and complement the findings of the investigation at Cowden. Deformation at the BRE site was dependent upon natural processes and was, therefore, largely unpredictable in both extent and time scale. However at Arlesey the plan was to induce deformation of a slope by deliberately making a number of specific cuts. This enabled monitoring to take place as and when the equilibrium of the slope was being seriously affected and exerted some control over the extent and time scale of the deformation.

5.2 Site Description

The site was a working brick-pit (although 'moth-balled') where clay was dug for the making of bricks and for use in cat litter. It was owned by Butterley Brick and lay adjacent to a landfill site owned and worked by Shanks & M^eEwan. The pit, situated in the Bedfordshire town of Arlesey (figure 5.1), was approximately centred at Grid TL 185350.

The test site was a section of a cut slope situated entirely within the Gault Clay of the brick-pit and particulars of the test slope are described more fully in section 5.4.1. (Figure 5.2 illustrates the site and test slope after all cuts had been made). The Gault Clay, deposited in the Cretaceous Period (65-135 million years ago), is a heavily-overconsolidated dark blue-grey stiff to very stiff clay with closely spaced fissures (BS 5930). Some indication of the geotechnical characteristics of the Gault Clay are given in section 7.9.5 where the results of some triaxial tests carried out on reconstituted samples are discussed. Further information concerning the Gault Clay is provided by Samuels (1975) who reported the results of a number of laboratory tests conducted on samples of Gault Clay which were obtained as part of a site investigation in connection with the construction of a water tunnel in Essex.

There was much movement of traffic around the site including the arrival and departure of refuse vehicles and the continuous action of a bulldozer redistributing the recently deposited waste. Some 100 metres away from the slope face, a diesel pump was used throughout much of the winter period to drain a small pond of water which had accumulated at the bottom of the pit. Additionally, trains regularly passed by using the main London-Bedford rail line and light aircraft often flew over the site. Despite what would be perceived by most as a noisy environment, acoustic background noise was *not* (as will become evident) a problem. However, this serves to illustrate that examination of ultrasonic frequencies can be successfully conducted in such environments.

5.3 Site Instrumentation

5.3.1 Site Instruments

Seven wave guides and two inclinometers were installed at the site with the specifications as given in table 5.1. The instrument positions are shown in plan in figure 5.3.

5.3.2 Instrument Installation

Installation took place over a three week period between 19 September and 7 October 1994, although a number of days were lost due to bad weather. (Figure 5.4 shows the site shortly after installation had been completed. Note the very wet conditions). The instruments were installed using The Nottingham Trent University's B24 mobile rotary drilling rig.

Nine 150mm diameter boreholes were made to accommodate the instruments listed in table 5.1 using the continuous flight augering method.

Wave guides 1, 2, 3, 5 and 7 were assembled from 1.5 metre sections of 50mm diameter steel tubing screwed together (via couplers) into the required lengths and then inserted (in one piece) into the borehole. The borehole was then backfilled with either sand, gravel or grout. The grout was a 4:1 bentonite:cement mix.

Wave guide 4 was designed to be installed by being driven into the host soil and was formed from 1.5 metre sections of 50mm diameter solid steel bar. (This wave guide came in five 1.5 metre sections and was constructed at The Nottingham Trent University). Only two sections (which were screwed together) could be driven giving an instrument length of 3 metres. This was probably due to the frictional resistance generated between the wave guide and the Gault Clay.

Wave guide 6 was constructed from 3 sections of 3 metre length plastic drainage tubing which was assembled, waterproofed with denzo tape and sealant, and then inserted into a 9 metre deep borehole. The borehole was then backfilled with sand. This borehole was designed for use with a hydrophone. Unfortunately, readings obtained from the instrument proved erratic and unreliable, so no further consideration is given to wave guide 6 in this thesis.

No compaction technique was used on the sand and gravel backfills other than to tremie the fill into the borehole and to 'spiral' the wave guide in order to prevent 'bridging'.

All wave guides were cut down (if necessary) so that a maximum length of approximately 0.5 metres remained above ground. Table 5.1 shows the depths of the instruments below ground level.

The inclinometers were 9 metres in length and installation was carried out as described in section 4.3.2. Inclinometer 1 also doubled as a wave guide and was designated wave guide i.

5.3.3 The Control Wave Guide

Wave guide 7 was installed as a control wave guide (section 3.3). This instrument, from which base AE readings were taken, was installed approximately 16 metres from the face of the slope.

5.4 The Test

5.4.1 The Test Site

A section of slope entirely within the Gault Clay, approximately 16 metres in length and some 4.5 to 5.5 metres in height, was identified as being suitable for the test. The face of the slope, which made an angle of approximately 35° with the horizontal, was divided into six cuts and by the end of the test had been cut back by some 5.5 to 6.5 metres. Evidence of weathering, in the form of 'iron-staining', was confined solely to the exposed face of the slope except for some additional staining which was discovered along the shear plane of the 'small' pre-test failure which had occurred (section 5.4.3).

The extent of the test site, the instrument positions and the size of the six test cuts are illustrated in plan in figure 5.3. Figure 5.5 depicts the whole site in plan indicating a line of cross-section and, figure 5.6, the cross-section itself. Figure 5.7 illustrates a 3-D schematic of the six cuts and the profiles of either end of the site (showing the cuts) are illustrated in figure 5.8. Table 5.2 shows the approximate size, by volume, of the cuts. Figure 5.9 illustrates the test slope and the five marked cuts.

5.4.2 Instrument Monitoring

(i) Arlesey Standard Monitoring Routine

The monitoring system was largely derived from the experience gained at Cowden and is summarised as follows:-

- The AE data consisted of 2500 envelope waveform data points collected at 100kHz data sampling rate, every second for six minutes - i.e. a 2.5% sample resulting in a file consisting of 900,000 data points (3.6MB) or 9 seconds of data
- Total AE signal amplification of 96dB (x 63,096)
- Electrical ground (earth) connection through Landrover chassis
- Bipolar acquisition of signal envelope
- Monitoring method as outlined in section 3.5
- Threshold of 0.11V applied post-capture during data processing

It should be noted that none of the data files were lost due to incorrect grounding and all data was captured on a consistent basis making the database for Arlesey much larger than that for Cowden. Additionally, because of this experience and the reduced number of wave guides, it was also possible to increase the standard data file from 180,000 data points at Cowden to 900,000 data points at Arlesey.

The data files were named in accordance with the same convention as outlined for Cowden (section 4.4.1) except during the test period when (owing to multiple same day readings) it became necessary to add an extra identifying letter after the wave guide number.

(ii) The Inclinometers

The monitoring method, data processing and data interpretation is as outlined for Cowden in section 4.4.2 except the instrument length at Arlesey was 9 metres making the depth of the first reading 8.5 metres.

5.4.3 The Test - A Chronology

A site visit was made on 18 October 1994 and the gravel of wave guide 1, which had subsided by approximately 0.5 metres, was topped up.

Instrument monitoring commenced on 26 October 1994 (when the inclinometers were read twice in order to form the 'base' file) and completed on 12 April 1995. Pre-test readings were taken on ten occasions, between 26 October 1994 and 2 February 1995, and the first cut was made on Monday 6 February 1995. Cuts 2, 3 and 4 followed on the 7, 8 and 9 February 1995 respectively. (Figure 5.10 illustrates cut 2 in the process of being made). The test programme was interrupted because of the weekend (when the site was closed and access was not available) and cut 5 was carried out on 13 February 1995 with an intermediate reading taken on Friday 10 February 1995. Owing to the limited amount of deformation which had occurred (according to the inclinometers - section 5.5), it was subsequently decided to introduce a sixth cut which was carried out on 23 March 1995. Five days of intermediate readings were taken between cuts 5 and 6 and three days further readings were taken after cut 6 before the test was brought to an end. In all twenty-five separate days readings were taken usually involving one reading from each of the inclinometers and one six minute acquisition from each wave guide. However, during the test period, multiple readings were taken from many of the instruments.

The cuts were made by an excavator belonging to the plant hire company Blackwell and working under contract for Butterley Brick (this is also illustrated in figure 5.10).

On the 7 November 1994 a small failure was noted in the top centre of the slope, between inclinometer 2 and wave guide 4, where the level of the ground had dropped by about 0.75 metres. By the 16 November 1994 it was noted that the failure had moved downwards slightly and on the 23 November 1994 it was apparent that the failure itself had split into two parts; the left hand side of the slope progressing further down relative to the right hand side (looking down the slope). The final note on this minor failure was that, by 20 December 1994, the left hand side (again looking down slope) had extended further.

On the 16 February 1995 it was noted that the shallow failure described above had collapsed and, as such, the gradient of the slope had been reduced. On the 2 March 1995 it was, therefore, decided to remove the spill and restore the slope's previously steep profile. (Figure 5.11 depicts

the debris, arising from the collapse, prior to its removal and figure 5.12 illustrates the test site after cut 6, as the spoil is being levelled).

It should also be noted that the site, for the greater part of the monitoring period, was very wet. This, combined with the need to move the Landrover around, had the result in 'churning-up' the surface layers of the Gault Clay, making movement around (at times) extremely difficult. By way of example, the Landrover, in low differential gearing, became stuck on more than one occasion and required pulling out by site plant. In this respect there was only noticeable improvement from 23 March 1995 onwards.

Owing to the condition of the surface of the site, no noticeable effects (other than have already been mentioned), such as tension cracks etc., were observed. As such it is not possible to record a 'diary' of observations as it was for Cowden (section 4.4.3).

5.4.4 Instrument Monitoring History

The full AE and inclinometer monitoring history is presented in table 5.3 which gives the AE file identification suffices as well as the number of files acquired on each wave guide by day. The dates on which each of the cuts 1 to 6 were made are indicated by applying the cut number as a suffix to the appropriate date.

As with Cowden it is necessary to relate each AE acquisition with some time-scale. Unlike Cowden, however, multiple same-day readings of wave guides were taken, particularly at times when the slope had been cut away. It has, therefore, been necessary to set each AE file acquired a unique time in minutes. The first AE file captured was WG1.D1 on 26 October 1994 at 15:16 hours. The time is that as determined by the DOS clock and assigned to the file by DOS on completion of the acquisition routine. This particular time and date has been given the value 'zero' minutes. All times assigned to AE files thereafter (based on their DOS allocated times and dates) are relative to this.

The inclinometers were also subjected to same day multiple readings and, as such, it has been necessary to calculate a reference time in minutes for this data too. The base time is the same as

for the AE data but the time used to calculate the reference time for the inclinometer readings is that given by the datalogger.

Unfortunately a number of inclinometer readings were lost when it became apparent, through the generation of large face errors, that the torpedo was in need of re-calibration. For the short period while this was being done *Geotechnical Instruments Ltd.* kindly gave loan of a replacement.

The total number of AE files listed in table 5.3 is 246 but a further 12 'special' files were also captured to demonstrate (among other things) the effect of omitting the wave guide covers and to identify electronic noise. By way of information, the 258 AE files contain a total of 232,200,000 data points occupying 928.8MB.

The site was surveyed on 18 October 1994 and again, before the first cut was made, on the 3 February 1995.

5.5 Inclinometer Data Analysis

Figures 5.13 - 5.16 depict the change in mean deviation and displacement profiles for inclinometers 1 and 2. The largest recorded change in mean deviation for inclinometer 1 (at a depth of 1.5 metres) is 2.3mm and, for inclinometer 2 (at a depth of 0 metres) is 3.7mm. The equivalent figures for displacement profile are 13.6mm and 16.8mm (both at a depth of 0 metres) recorded for inclinometers 1 and 2 respectively. It should be noted, however, that for the latter part of the test, the greatest displacement profile recorded for inclinometer 1 occurred at a depth of 1 metre; only the final reading, taken on 22 May 1995, records a higher value at a depth of 0 metres. Whereas the right hand side of the slope (looking downslope) appears to be in the process of developing a shear zone at a depth of approximately 1.5m, the left hand side appears more to be failing by expansion due to stress relief leading to toppling. However, both inclinometers also indicate movement at a depth of approximately 5.5 - 6m.

As mentioned in section 5.4.3, conditions for much of the test were very wet and it is likely that water 'run-off' was responsible for causing the small failure (in the area of inclinometer 2) also described in that section. The inclinometer readings reflect this disparity between the two sides

of the site indicating that movement surrounding inclinometer 2 occurred primarily at the surface whereas that surrounding inclinometer 1 occurred primarily at a depth of 1.5 metres.

It proved beneficial to illustrate the Cowden inclinometer data in terms of rates of movement. Unfortunately the equivalent Arlesey data is of too low a magnitude to produce these figures with any degree of confidence. However, in order to relate the inclinometer data to the test, those depths recording the greatest change in mean deviation and displacement profile for both inclinometers 1 and 2 have been isolated and are plotted in figures 5.17 and 5.18. (Note that the displacement profile plotted for inclinometer 1 is that at a depth of 1.5m).

These figures show that movement across the first four cuts was virtually zero; the largest difference between any two recorded figures being 0.7mm for inclinometer 2's displacement profile. There is some greater activity after cut 5 but even this is only enough to increase movement across the whole test period to something in the order of 1-2mm. However it is fairly evident that after both cuts 5 and 6 movement rates increase. It is also evident that prior to cut 1 there was some activity around inclinometer 2 but no evidence of any around inclinometer 1. This compares well with the physical observations made of the site.

As the magnitudes of the movement are small it is difficult to be precise about the direction of the vectors. However, considering the larger values of displacement profile and change in mean deviation for inclinometer 1 reveals a general direction of movement of 340° – 350° . Similar consideration of the data for inclinometer 2 produces values of 0° – 15° . The measurement system makes 0° coincident with face A and points directly down slope. Angular measurements are then made in a clockwise direction which means that movement at Arlesey occurred downslope and inwards, towards the centre of the instrument array.

Face errors were typically in the range of 0.1 - 0.8mm.

Note also that the inclinometer data presented in figures 5.13 - 5.18 includes the extra reading taken on 22 May 1995 and for which there is no corresponding AE record.

5.6 Analysis and Interpretation of Field Acoustic Emission Data

5.6.1 Introduction

It should be considered that alternative wave guide designs may respond in different ways to a variety of deformation mechanisms and that alternative data processing techniques may isolate or accentuate different signal characteristics. This section examines the findings of both the Arlesey and Cowden studies in order to identify the mechanisms responsible for the generation of the acoustic emission. It also attempts to explain the effect of wave guide design and data processing technique in order to produce a descriptive model of field generated AE which is presented in Chapter 6.

The wave guide design parameters are identified as follows:-

- wave guide material
- wave guide backfill
- wave guide length
- position of wave guide relative to zone of deformation

Although the position of the wave guide will clearly affect the level of the emission it is not strictly speaking a design parameter as it is impossible to predict with any real accuracy where the slip plane will form (or, indeed, if it forms). (However, it is possible, in conjunction with a consideration of the prevailing geotechnical conditions, to make informed judgements as to the best positions for the wave guides - e.g. Cowden). Additionally, as the material of most of the wave guides employed consisted of 50mm diameter steel tubing, the bulk of both the Cowden and Arlesey tests are confined to examining the effect of wave guide backfill and length.

Two alternative forms of wave guide were also investigated at Arlesey. These were a grouted aluminium inclinometer casing and a driven solid steel bar.

The wave guide design parameters are, initially, dealt with separately because, given the available permutations of wave guide backfill, wave guide length and data processing technique (not to mention the position relative to any slip plane which may or may not develop), it is clearly impractical to discuss every combination; only the parameter in question, therefore, is

examined. The analysis then goes on to discuss the effects of different data processing techniques before concluding with some comment on the topics of control wave guide performance and background noise. Chapter 6 draws on the findings of these individual discussions in order to present a descriptive model of field generated AE from which custom-made monitoring systems can be designed to meet particular criteria.

Figures 5.19 - 5.24 compare the recorded mean signal values for each of wave guides 1, 2, 3, 4, 5 and i with that recorded for wave guide 7 (the control wave guide). The upper graph in each figure depicts the whole test period and the lower graph concentrates on cuts 1 to 5. In section 5.6.2 only mean signal value is considered in order to simplify discussion but it should be appreciated that this may not necessarily be the most productive data processing method. Figures 5.19 - 5.24 are reproduced here to serve as an introduction to the results. Where necessary, reference to specific figures is made later in section 5.6.

Note that, in the following graphs (as with the Cowden results), sets of AE data points are connected by lines. This is only to maintain clarity between individual sets of data points relating to different wave guides and is *not* meant to infer anything about the behaviour of the signal *between* data points.

5.6.2 Effect of Wave Guide Design

Traditionally the term 'wave guide' is used simply to refer to the metal rod inserted into the ground and which then 'guides' the 'wave' to the acoustic sensor. In fact, as has been seen in section 5.6.1, the level of the signal received is very much related to the design of the wave guide. The following sections attempt to isolate the effects of individual design parameters.

At Arlesey the wave guides were positioned in one line in an attempt to ensure that each suffered a similar amount and form of deformation. At Cowden, however, the relationship between slip plane and wave guide was more complicated.

(i) Wave Guide Backfill

Figure 5.25 compares the recorded mean signal values over the test period at Arlesey for each of wave guides 1 (gravel), 2 (sand) and 3 (grout) which were of equal design in all respects but backfill. It is evident that there were greater (but varying) levels of activity recorded during the test period and that differences existed between the responses of the wave guides to the cuts. Wave guide 1 indicated some determinable response to cuts 1, 4 and 5; wave guide 2 to cut 5 and wave guide 3 to cut 1. These results, where individual cuts have generated an AE response, should be considered in conjunction with the inclinometer data which determined that maximum movement across the first *five* cuts was in the order of 1-2mm and across the first *four* cuts was effectively zero.

It should also be noted that the high responses of wave guides 1 and 2 to cuts 4 and 5 were actually recorded some 24 hours after the cuts were made whereas the responses of wave guides 1 and 3 to cut 1 were recorded 0.5 and 4 hours (respectively) after the cut.

According to the inclinometer data, during the period between cuts 5 and 6, there was a steady increase in the amount of deformation to a total value in the order of 3mm (by displacement profile). This coincided with a period of increasing activity as recorded by wave guide 2 and, to a lesser extent, by wave guide 1 (figure 5.26). The tendency for sand backfilled wave guides to be more responsive in periods of gradual, prolonged deformation was first observed at Cowden where WG1 out-performed WG2 which, in turn, out-performed WG3 (section 4.5.2(ii), figures 4.19 & 4.23).

There appears to be an inconsistency between these findings and the lack of correspondence of the inclinometer and AE data for wave guide 2 (post cut 6) at Arlesey. Figure 5.27 shows that, although the inclinometer readings indicate a gradual increase in deformation shortly after cut 6, the AE data remained relatively flat and of low magnitude. However, according to the inclinometers, the rate of movement after this period greatly slowed down and it is likely that the AE readings reflected this. Unfortunately no intermediate readings were taken. However, this example supports the assertion that AE reflects the current state of instability whereas inclinometers only reflect the total deformation suffered to date.

(ii) Wave Guide Length

Intuitively it seems reasonable to expect (for a specific position in relation to a shear zone) that longer wave guides will be more responsive; passive wave guides would benefit from collecting AE over a greater volume (sections 2.4.5 and 3.3) and gauge wave guides would have a greater length over which to generate noise and/or a better chance of penetrating the shear zone (section 3.3). Indeed the only factors affecting the size of a wave guide (cost of materials and installation) have little to do with any philosophy concerning the science of AE field monitoring.

Figure 5.28 depicts the mean signal values for Arlesey wave guides 2 and 5 which were specifically designed to investigate this aspect. Unfortunately both wave guides also indicated little response to the cuts with each generating one good peak subsequent to cut 5. (This combination of wave guides is discussed further in section 5.6.3).

At Cowden the main instrument array was designed to examine the twin issues of wave guide backfill and length. Unfortunately, because the slip plane separated the two lines (figures 4.8 & 4.10), it is impossible to separate the effects of length and position relative to the slip plane.

There is, therefore, insufficient evidence from which to draw any conclusions.

(iii) Arlesey Wave Guide 4 - Solid Steel Driven Bar

Originally it had been intended to drive this wave guide to a depth commensurate with that of wave guides 1, 2 and 3. However it was only possible to reach a depth of under 3 metres. Figure 5.22 shows that the mean signal value generated was generally very low and rarely did it distinctly exceed the level recorded by the control wave guide. No large peaks are present on the plot although there does appear to be some increased activity after cut 5.

(iv) Arlesey Inclinator 1 - Use as Wave Guide

Unfortunately the monitoring record of inclinometer 1 as a wave guide is poor (figure 5.24). However the response of this wave guide is most interesting. Apart from two large responses to

cuts 4 and 5 the recorded mean signal level was distinctly lower than that recorded for the control wave guide.

5.6.3 Effect of Data Processing Technique

It has already been demonstrated in section 4.5.2(iv) concerning the Cowden test that different processing techniques can alter the apparent response of the AE. Clearly it is desirable to process the data in such a way that the results differentiate between those periods of inactivity and those in which some form of deformation is occurring. It may also be possible to differentiate between different types of deformation mechanism. This section examines the effects of different processing techniques. The relevance and interpretation of such effects is discussed in Chapter 6.

The somewhat disappointing results of the mean signal values of both wave guides 2 and 5 have already been seen in section 5.6.2 and figure 5.28. Consider figure 5.29 which depicts the standard deviation of the same data. It appears that this method of processing produces a better apparent signal response across the test period. Having said this, however, in fact the peak value for wave guide 2 (following cut 5) recorded a *mean* of 0.096 volts but a *standard deviation* of only 0.089 volts. Figure 5.30, which plots the mean, standard deviation and root means square for wave guide 2 indicates that the main reason for the apparent better response of standard deviation is because (generally) the level of the signal (during apparently inactive periods) was both low and consistent. From figure 5.30, it is evident that consideration of standard deviation (as opposed to arithmetic mean) produces a better determinable response record for wave guide 2 and the single high mean value following cut 5 is altered to a good response to cut 1, and two responses to each of cuts 4 and 5 (standard deviation). Note that standard deviation for wave guide 5 (figure 5.28) shows the first determinable response to cut 6. Also note that it is considered significant to discuss actual recorded and calculated voltages because, depending upon the final processing system decided upon, it may be more important to use large signal magnitudes (roots mean square) or large changes in the signal (standard deviation)

Interestingly, as figure 5.29 shows, the standard deviations recorded before the test period, for both wave guides 2 and 5, are remarkably similar. In fact, of the nine days of pre-test monitoring they share, eight days recorded coincident values for standard deviation. As figure 5.31 shows this is also true for wave guides 1, 2 and 3.

Another point worthy of note is that the steady increase in the mean signal value for wave guide 2 (figure 5.30) between cuts 5 and 6 (first identified in section 5.6.2) disappears when considering standard deviation.

When considering mean signal value the best response is recorded by wave guide 1 (figure 5.25). Even this, however, is improved by calculating the standard deviation of the same data (figure 5.31). It is evident that mean signal value generates responses to all five cuts but only those to cuts 4 and 5 are appreciably distinct measuring 0.091 volts and 0.102 volts respectively. Calculation of standard deviation also generates responses to all five cuts but records appreciably distinct values for cuts 1 (0.078v), 3 (0.049v), 4 (0.072v) and 5 (0.099v). As before, however, it is the relatively low and consistent value of standard deviation during periods of perceived inactivity which tends to accentuate these peaks.

A further step in the analysis is to introduce a *threshold*. Traditionally this is to eliminate background noise but, owing to the time required to process data sets containing 900,000 data points, a threshold of 0.11 volts is also used in order to reduce the data sets to a more manageable size.

Figures 5.32 and 5.33 illustrate the mean and standard deviation of the *post-threshold* data for wave guides 1 and 2, respectively. It is evident that the response record of the post-threshold mean values for both wave guides is greatly improved over their 'bulk' data counterparts and this is especially true of wave guide 2. From the graphs depicting the whole test period it is also interesting to note that (generally) the response *increases* across the test period from cut 1 to cut 5 when considering bulk data (e.g. figures 5.30 & 5.31) but *decreases* over the same period when considering post-threshold data. It is also interesting to note that all post-threshold analyses for these wave guides indicate a response to cut 6. Mean signal levels (post-threshold) vary from a general level of approximately 0.13 volts with peaks recording between (approximately) 0.15 and 0.28 volts (for both wave guides). Standard deviation (post-threshold) varies from a general level of approximately 0.03 volts with peaks recording between (approximately) 0.10 and 0.50 volts. Note also that both forms of processing technique (post-threshold) generate results which are, for the larger part of the pre-test period, coincident. Additionally it is also interesting to note that examining post-threshold data (particularly the standard deviation) appears to change the dominance across cuts 4 and 5 from wave guide 1 to wave guide 2.

The performance of wave guide 3 was generally poor, regardless of processing technique. Considering bulk data, the mean signal value (figure 5.21) records only one prominent peak of 0.088 volts following cut 1 whereas standard deviation records two prominent peaks; one just prior to cut 3 (0.059v) and one following cut 4 (0.036v). Standard deviation (figure 5.31) also indicates a third peak of 0.037 volts on Day 8 (10 January 1995), some twenty-six days before the first cut. An interesting point concerning the response of wave guide 3 is that, for both mean and standard deviation (bulk data), lower values than their control wave guide counterparts are generated for most of the readings from cut 5 to the test end. The post-threshold response is not much better with the mean producing one large peak immediately before cut 3 of 0.292 volts and indicating some increased activity between cuts 4 and 5. Calculation of post-threshold standard deviation produces a similar response.

Despite the fact that wave guide 4 (figure 5.22) does evidently generate some response, it is quite clearly the poorest performing of all wave guides. The largest peak, produced as the standard deviation of the post-threshold data, is only 0.237 volts and follows cut 4 (figure 5.34). This is the only wave guide which, across the whole test period, failed to produce a signal magnitude greater than the largest magnitude recorded for the control wave guide (assuming both data sets are processed in the same way).

When used as a wave guide, inclinometer 1 produced some interesting results despite the poor monitoring record. As figure 5.24 shows the majority of the bulk mean signal values are significantly below their control wave guide counterparts although two distinct peak magnitudes are recorded following cut 4 (0.057v) and cut 5 (0.078v). Considering the standard deviation of the data introduces a further peak following cut 2 and records a magnitude of 0.207 volts. The largest peak is obtained by calculating the standard deviation of the post-threshold data when the peak following cut 2 records a magnitude of 0.465 volts. Apart from this there is little improvement gained by the consideration of post-threshold data.

In an attempt to illustrate the effect of data processing more clearly, consider figure 5.35 which shows the bulk mean signal value and the post-threshold standard deviation for wave guide 2 on the same plot.

The control wave guide (wave guide 7) is dealt with separately in section 5.6.5.

5.6.4 Signal-Time Relationship - A Closer Look

Although it has been amply demonstrated that there is a good general correlation between the processed AE and the introduction of the cuts, the scale of the test period disguises the closer relationship that exists between the responses and the timing of the cuts. Figures 5.36 - 5.39 indicate the times and dates of all cuts and AE readings across all six test cuts. AE is represented by the standard deviation of the post-threshold data acquired from wave guide 1 (which has been selected because of the good response record).

As the figures indicate, the AE responses to cuts 1 and 2 were immediate but, by some 3 to 4 hours later, levels had reduced to those measured using the control wave guide. Cut 3 generated an immediate response which 0.5 hours later had reduced, once again, to background noise levels (as indicated by the control wave guide). However two subsequent readings, approximately 1.25 hours and 4.75 hours following cut 3, indicated increasing levels of activity. (In fact, this type of AE behaviour whereby an immediate response gradually decreases before increasing again was first demonstrated by Koerner *et al.*, 1978, and is shown as the response to cut 5 in figure 2.39). The wave guide was actually monitored while each of cuts 2, 3, 4, 5 and 6 were made and, as mentioned, AE readings made during cuts 2 and 3 indicated higher levels of activity. However those readings taken during cuts 4 and 5 indicate no increase whatsoever. In fact the first level of increased activity associated with cut 4 occurs some 24 hours later. Increased activity was recorded following cut 5 some 0.5 hours after the cut was made and again some 24 hours later. The AE response to cut 6 is also shown. The main point from this illustration is that there is a change in the general AE pattern, across cuts 1 to 5, from immediate responses to those which are more deferred.

5.6.5 The Control Wave Guide

It was appreciated at the outset that the acoustic sensor may respond to noise generated by sources other than those connected with the deformation of the slope and, in order to determine the level of this *background noise* (section 5.6.6), control wave guides were installed at both the Cowden and Arlesey sites. The principle of operation of the control wave guide is straightforward. The wave guide is installed well back from the face of the slope, and is unlikely to suffer any deformation. It can be postulated that the difference between the level of emission

captured from a wave guide within a zone of deformation and the level of emission captured from a control wave guide must, therefore, be due to deformation processes only.

It is fairly evident, however, from any of the figures 5.19 - 5.24 where the AE record of the control wave guide for Arlesey (wave guide 7) is displayed that it has responded to at least some of the test cuts, producing distinct peaks following both cut 3 and cut 6. Additionally, examination of post-threshold data indicates some response to both cuts 4 and 5. Note that the three peaks following cut 3 were all recorded within thirty-seven minutes of one another (although some 3 to 4 hours following the cut) and, as such, may incorrectly give the impression of there being a more sustained level of activity than there actually was. The peaks following cuts 4 and 5 both occurred some 24 hours after each cut and that following cut 6 some 2.5 hours following the cut.

At Cowden the original control wave guide (wave guide 7) had to be discounted in favour of wave guide 12 for reasons as explained in section 4.3.4. It is also fairly evident (from the observations discussed in section 4.5.2) that wave guide 12 responded to the deformation processes which affected the gauge wave guides. (There is a good correlation between increased levels of AE, the increase in movement rates and the rapid drop in water level measured in inclinometer 1 - section 4.5.3).

The main point arising from both Cowden and Arlesey (which is indisputable) is that, for the greater part, the control wave guides do produce distinctly lower levels of emission than their gauge counterparts. This lends support to the hypothesis that those wave guides within a zone of deformation do record some emission generated as a direct response of deformation of the slope.

5.6.6 Background Noise

Background noise refers to any extraneous noise arising through mechanisms not related to deformation (which is captured by the monitoring system) and it is considered that background noise may arise through one, some or all of three different sources identified as follows:-

(i) Airborne

This refers to noise generated by machinery, vehicles, activity, etc., in the form of acoustic (ultrasonic) waves through air (within the 15 - 45kHz bandwidth because of the electronic bandpass of the instrumentation).

The results of nine tests (between the Cowden and Arlesey sites) in which two consecutive readings of a wave guide were taken (one with and one without the wave guide covers) are shown in figure 5.40. This figure, which plots the mean signal value, indicates that in four of the tests absence of the wave guide covers did result in an increased level being recorded. However, in three of the tests, larger magnitudes were recorded with the wave guide covers in place while two tests produced more or less the same results. The figure also indicates which site the readings were taken from and the time interval between the sets of readings.

Additionally all Day 5 (30 November 1994) data was acquired without the wave guide covers in place. However, by reference to any of figures 5.19 - 5.24, it is evident that Day 5 data is entirely consistent with the recorded levels of other pre-test readings, regardless of which wave guide is examined or which processing technique is used.

(ii) Electronic

In sections 4.4.1 and 4.4.4 it was described how a large volume of the early Cowden data was lost due to poor grounding. This occurred because electronic interference overwhelmed and masked the genuine signal .

Three AE files were recorded (correctly grounded) at Arlesey with the input channel on the AET (section 3.2.3) switched off in order to obtain some idea of the level of electronic noise. The processed data is depicted along with the equivalent values for wave guide 7 in figure 5.41 (mean signal value bulk data) and figure 5.42 (standard deviation post-threshold data). It is evident that, in both cases, the magnitudes recorded in respect of electronic noise are small (less than 0.03 volts) and noticeably less than those recorded for wave guide 7.

(iii) Constructional

As has already been commented on in section 5.6.3 and illustrated in figure 5.24, when utilising inclinometer 1 as a wave guide it consistently generated readings which were of a smaller magnitude than those generated by the control wave guide. Inclinometer 1 was 9 metres long and situated in the deformation zone whereas wave guide 7 was only 3 metres long and situated some 16 metres from the face of the slope - yet wave guide 7 generated emission of a greater magnitude than the inclinometer. Additionally, as figure 5.24 shows, the inclinometer generally produced levels of emission of smaller magnitude within the test period than wave guide 7 did in the pre-test period. There is clearly some emission generated as a result of the constructional design of the wave guide.

Instrument Type	Instrument Code	Instrument Depth (mbgl)	Instrument Material	Instrument Backfill
Wave Guide	WG1	7.09	Steel Tubing	Gravel
Wave Guide	WG2	6.63	Steel Tubing	Sand
Wave Guide	WG3	7.09	Steel Tubing	Grout
Wave Guide	WG4	2.68	Steel Bar	Driven
Wave Guide	WG5	2.89	Steel Tubing	Sand
Wave Guide	WG6	6.69	Plastic Tubing	Sand
Wave Guide	WG7	2.84	Steel Tubing	Sand
Inclinometer	I1 & WGi	9.00	Aluminium	Grout
Inclinometer	I2	9.00	Aluminium	Grout

Table 5.1 Arlesey test site instrumentation (mbgl - metres below ground level). Inclinometer I1 was also utilised as a wave guide for a large part of the test.

Cut Number	Volume m ³	% of Total Volume Excavated	Cumulative % Excavated
1	2.4	1.3	1.3
2	5.7	3.2	4.5
3	9.1	5.1	9.6
4	13.0	7.3	16.9
5	38.3	21.5	38.4
6	110.0	61.6	100.0

Table 5.2 Size, by volume, of the six Arlesey test cuts

Date	Suffix	Number of AE files by Wave Guide									Inclinometer readings	
		1	2	3	4	5	6	7	i	Total	1	2
26 Oct 94	D1	1	1	1	1	1	1	1	0	7	2	2
7 Nov 94	D2	1	1	1	1	1	2	1	0	8	1	1
16 Nov 94	D3	1	1	1	1	1	1	1	0	7	1	1
23 Nov 94	D4	1	1	1	1	1	1	1	0	7	1	1
30 Nov 94	D5	1	1	1	1	1	0	1	0	6	1	1
1 Dec 94	-	-	-	-	-	-	-	-	-	0	1	1
21 Dec 94	D6	1	1	1	1	1	0	1	0	6	1	1
4 Jan 95	D7	1	1	1	1	0	0	0	0	4	1	1
10 Jan 95	D8	1	1	1	1	1	0	1	0	6	2	1
1 Feb 95	D9	1	1	1	1	1	1	1	1	8	1	1
2 Feb 95	X0	0	1	1	1	1	0	1	0	5	1	1
6 Feb 95 ¹	X1	2	4	3	1	1	2	3	1	17	3	3
7 Feb 95 ²	X2	5	3	3	2	1	3	3	1	21	3	3
8 Feb 95 ³	X3	4	2	2	2	2	2	4	1	19	2	3
9 Feb 95 ⁴	X4	3	2	2	2	1	3	1	1	15	2	2
10 Feb 95	X5	1	1	1	1	1	1	1	1	8	1	1
13 Feb 95 ⁵	X6	4	2	2	1	1	3	2	2	17	2	2
14 Feb 95	X7	1	1	1	1	1	1	1	1	8	1	1
16 Feb 95	X8	1	1	1	1	1	1	1	1	8	1	1
23 Feb 95	X9	1	1	1	1	1	0	1	0	6	1	1
2 Mar 95	V0	1	1	1	1	1	0	1	1	7	1	1
9 Mar 95	V1	1	1	1	1	1	1	1	1	8	1	1
23 Mar 95 ⁶	V2	7	2	2	2	2	2	2	1	20	2	2
24 Mar 95	V3	1	1	1	1	1	1	1	1	8	1	1
4 Apr 95	V4	1	1	1	1	1	1	1	2	9	1	1
12 Apr 95	V5	1	1	1	1	2	1	2	2	11	1	1
22 May 95	-	-	-	-	-	-	-	-	-	0	1	1

Table 5.3 Arlesey AE & inclinometer monitoring history



Figure 5.1 Geographical Position of Arlesey, Bedfordshire UK



Figure 5.2 Perspective view of test site which is the dark area to the fore of the landrover. Picture taken after cut 6.

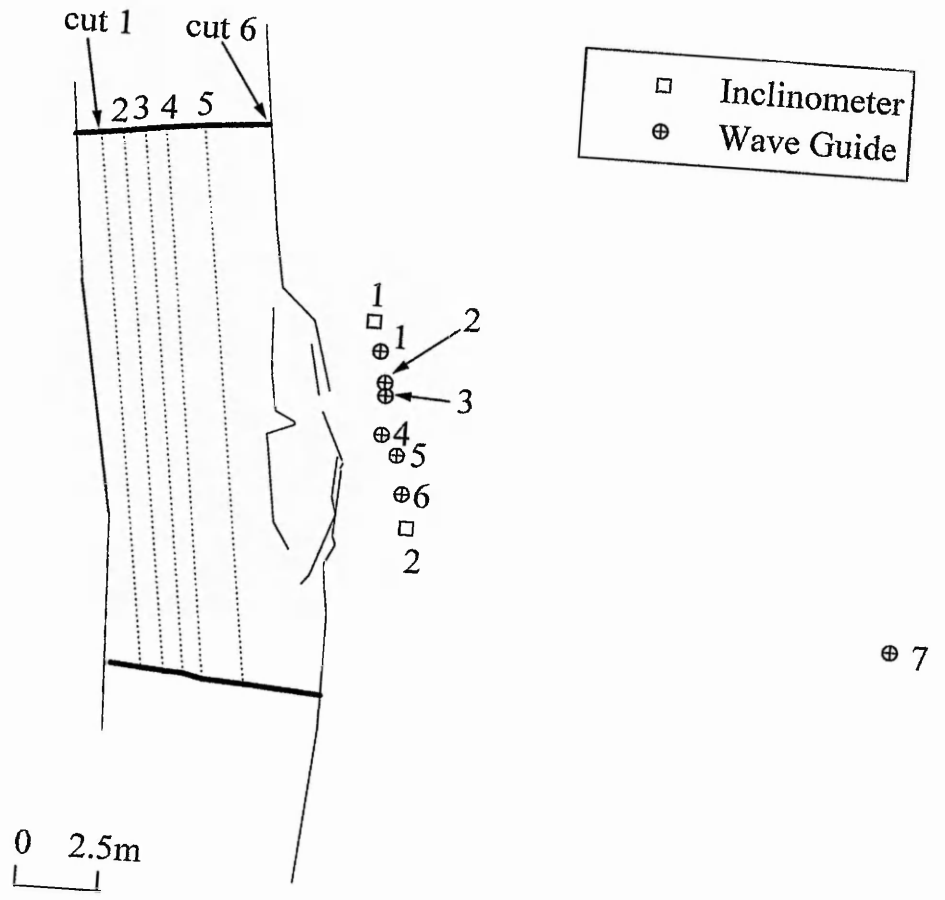


Figure 5.3 Arlesey test slope, instrument positions and six test cuts. The site and instrument positions were surveyed on 18 October 1994 and the cuts on 3 February 1995.

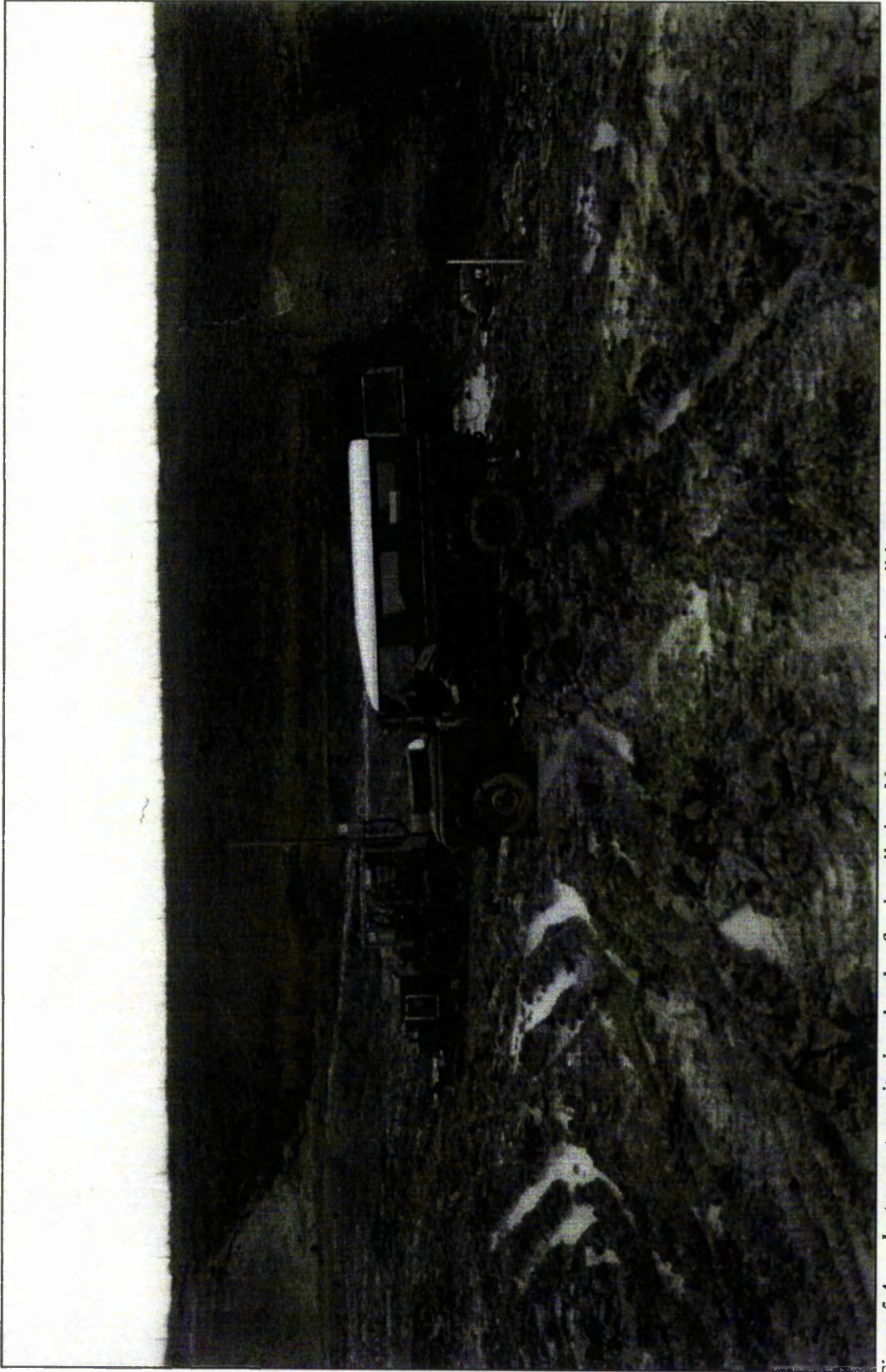


Figure 5.4 Instrument monitoring shortly after installation. Note very wet site conditions.

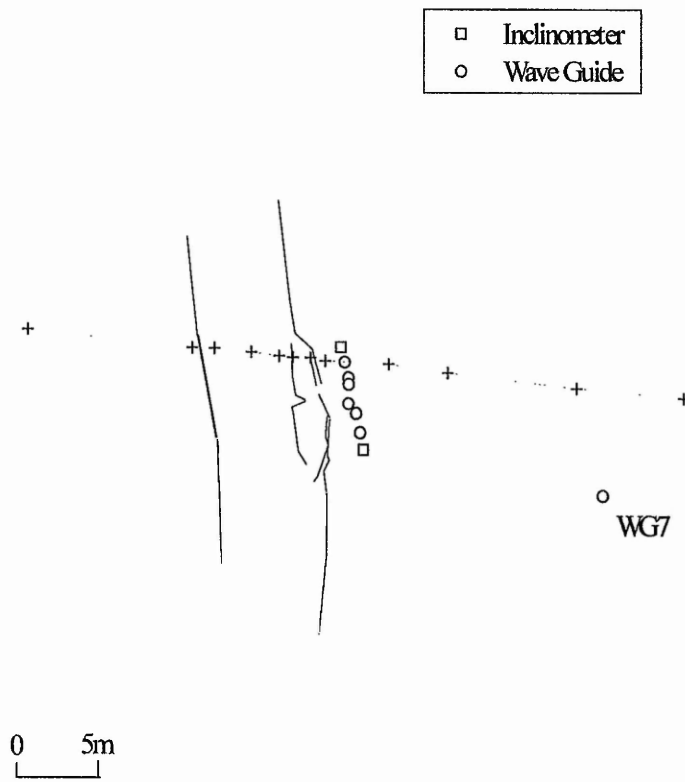


Figure 5.5 Site plan and line of section after survey 3 February 1995

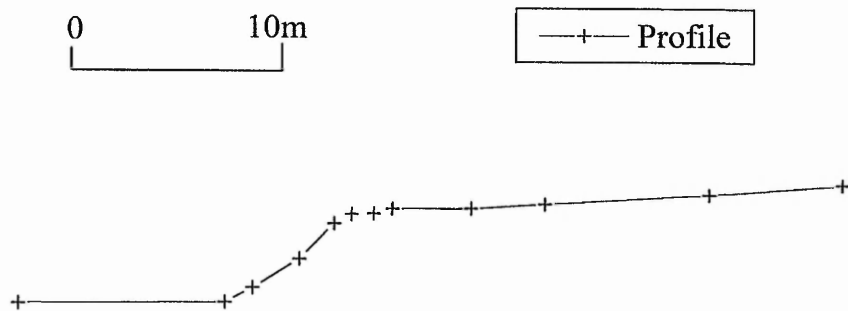


Figure 5.6 Slope profiles after survey 3 February 1995

Arlesey Test Cuts 1 to 6
All dimensions metres (not to scale)

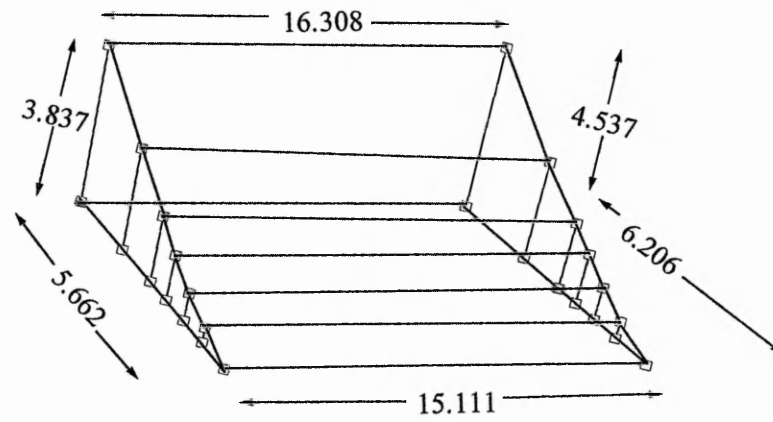


Figure 5.7 3-D schematic of test cuts after survey 3 February 1995

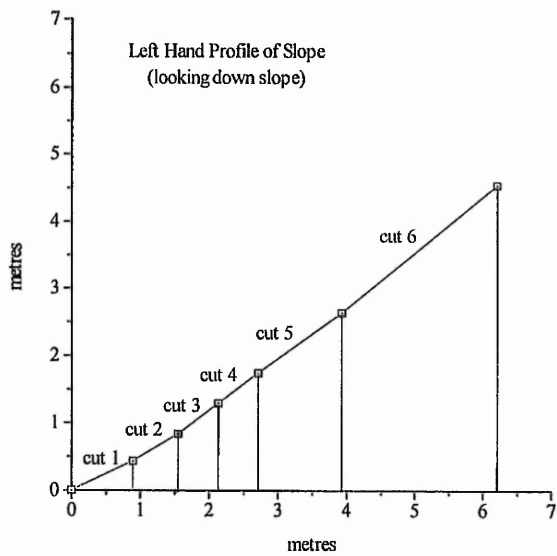
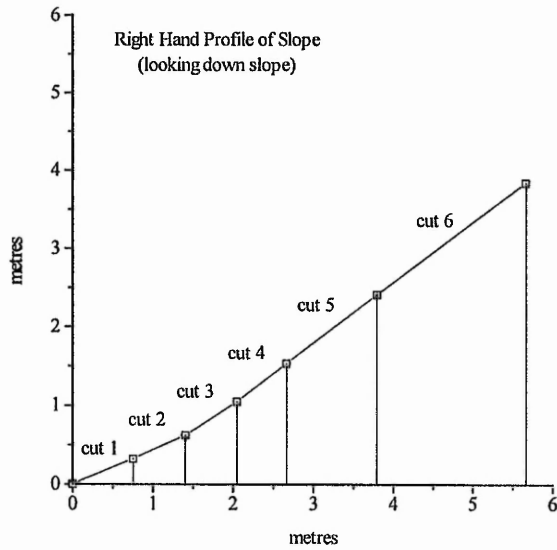


Figure 5.8 Slope profiles after survey 3 February 1995

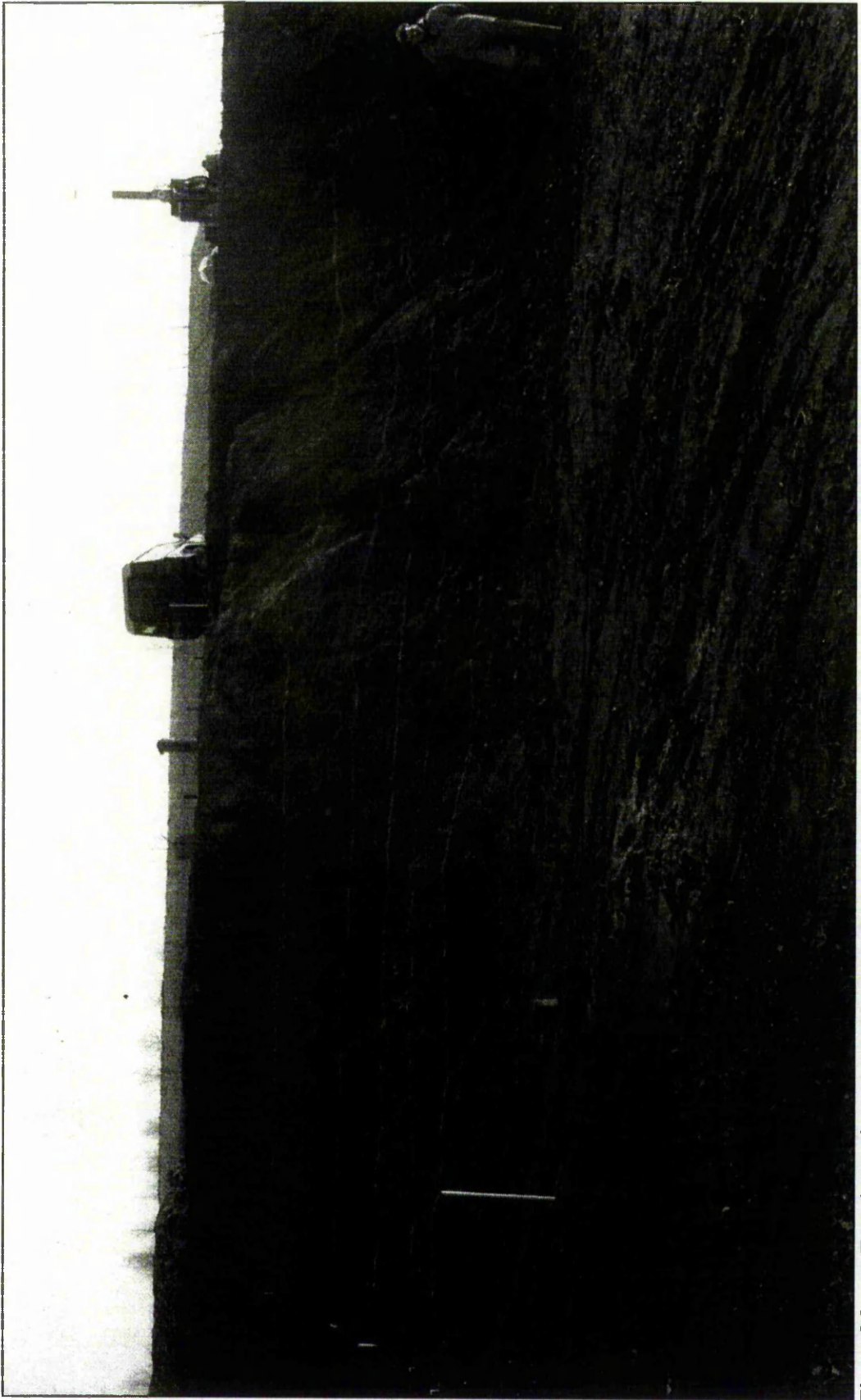


Figure 5.9 Test slope prior to cut 1. Note that five test cuts are marked and the sixth was in line with the top of the slope.

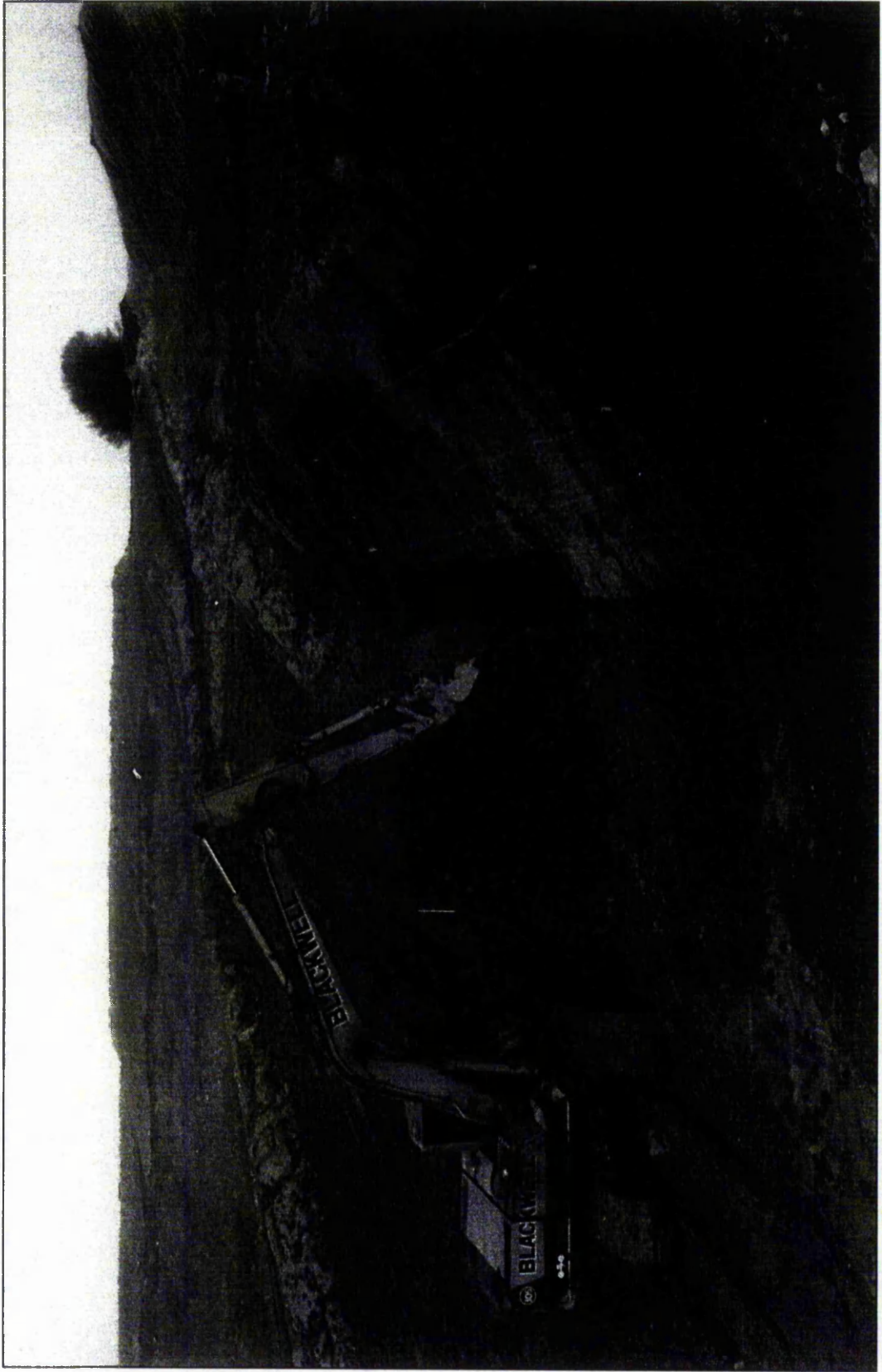


Figure 5.10 Test cut 2 in process of being made.



Figure 5.11 Failure which occurred after cut 5 but which was cleared before cut 6



Figure 5.12 Spoil from cut 6 being removed.

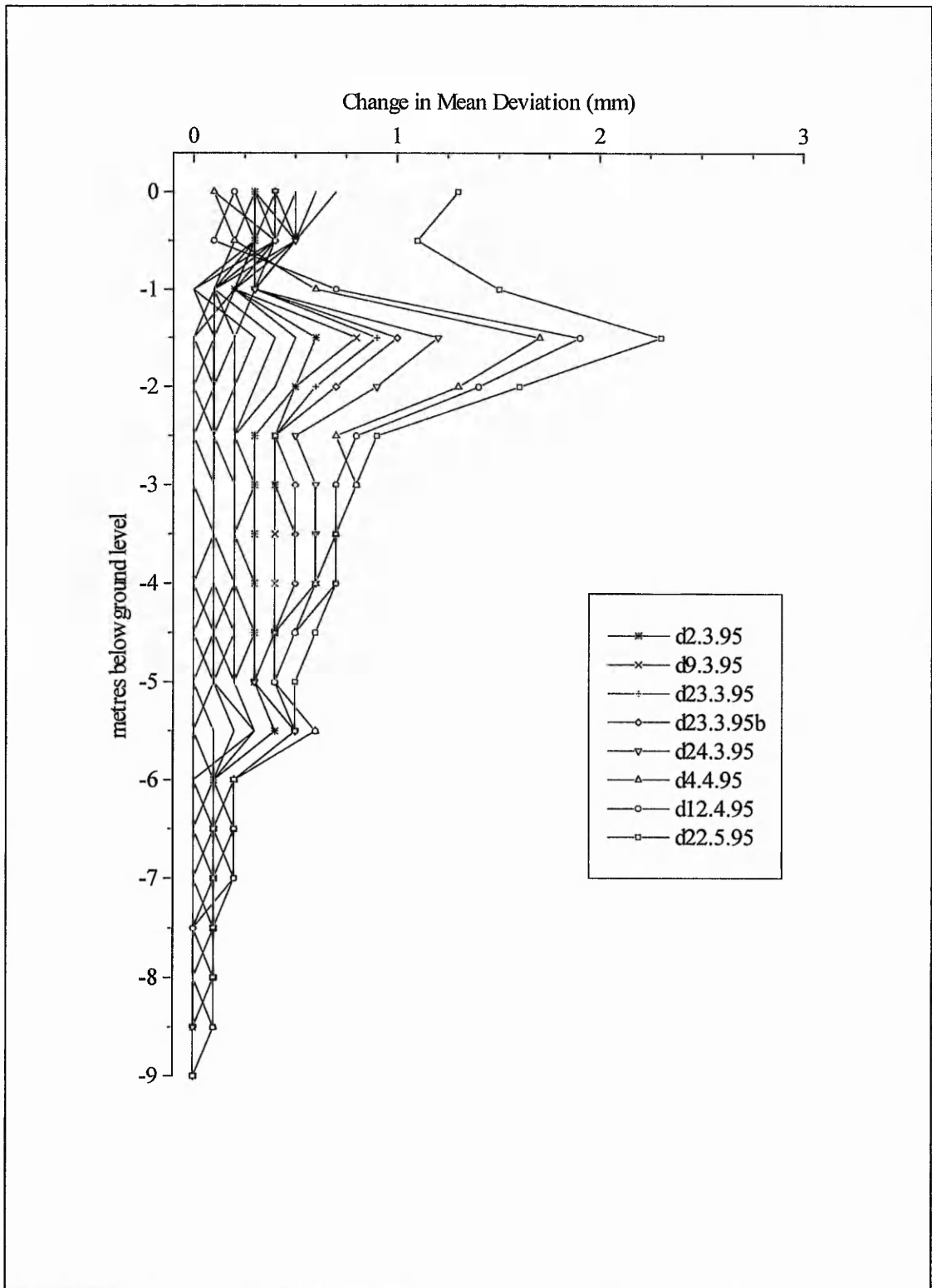


Figure 5.13 Arlesey Change in Mean Deviation Inclinometer 1

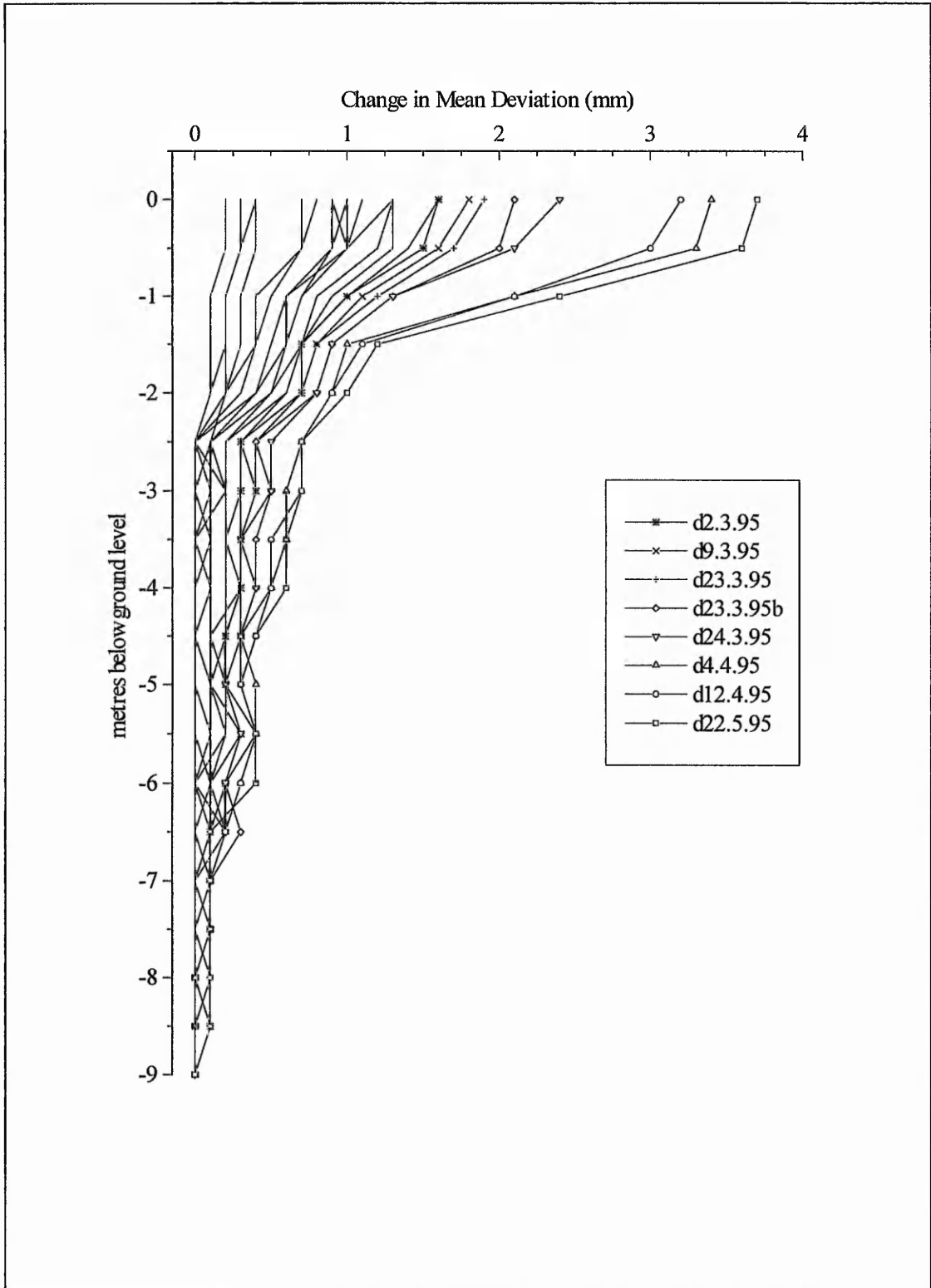


Figure 5.14 Arlesey Change in Mean Deviation Inclinometer 2

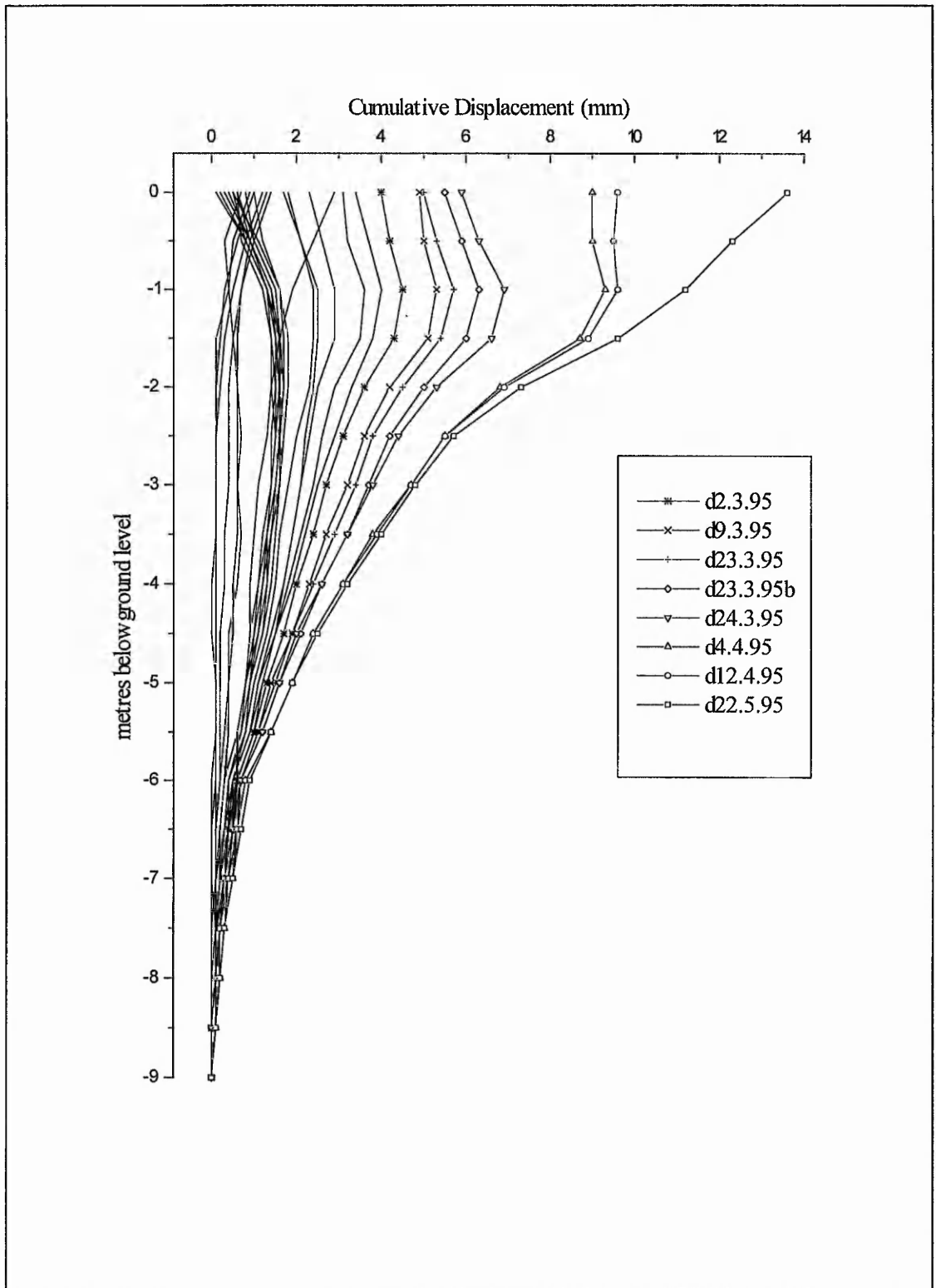


Figure 5.15 Arlesey Displacement Profile Inclinometer 1

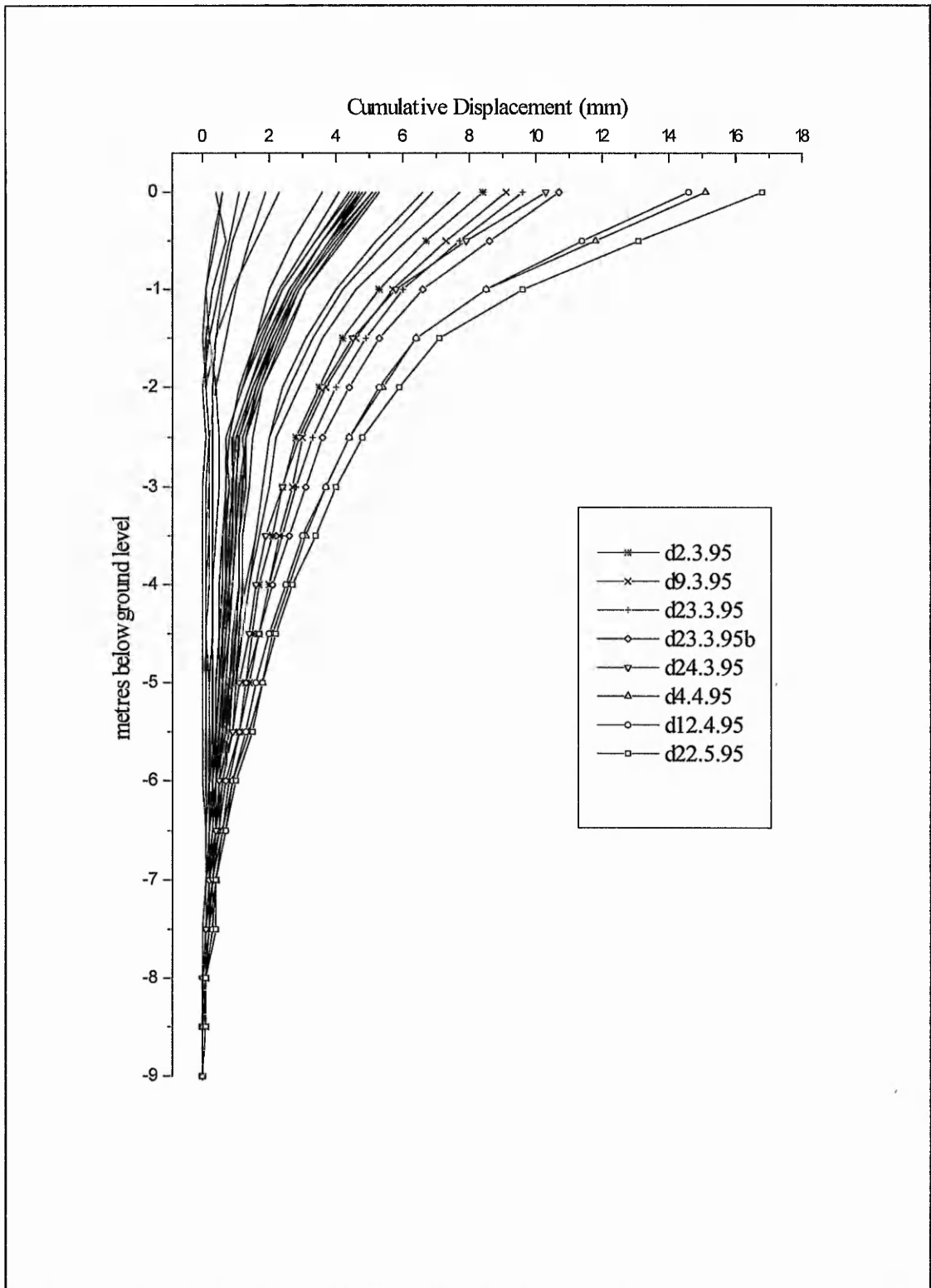


Figure 5.16 Arlesey Displacement Profile Inclinometer 2

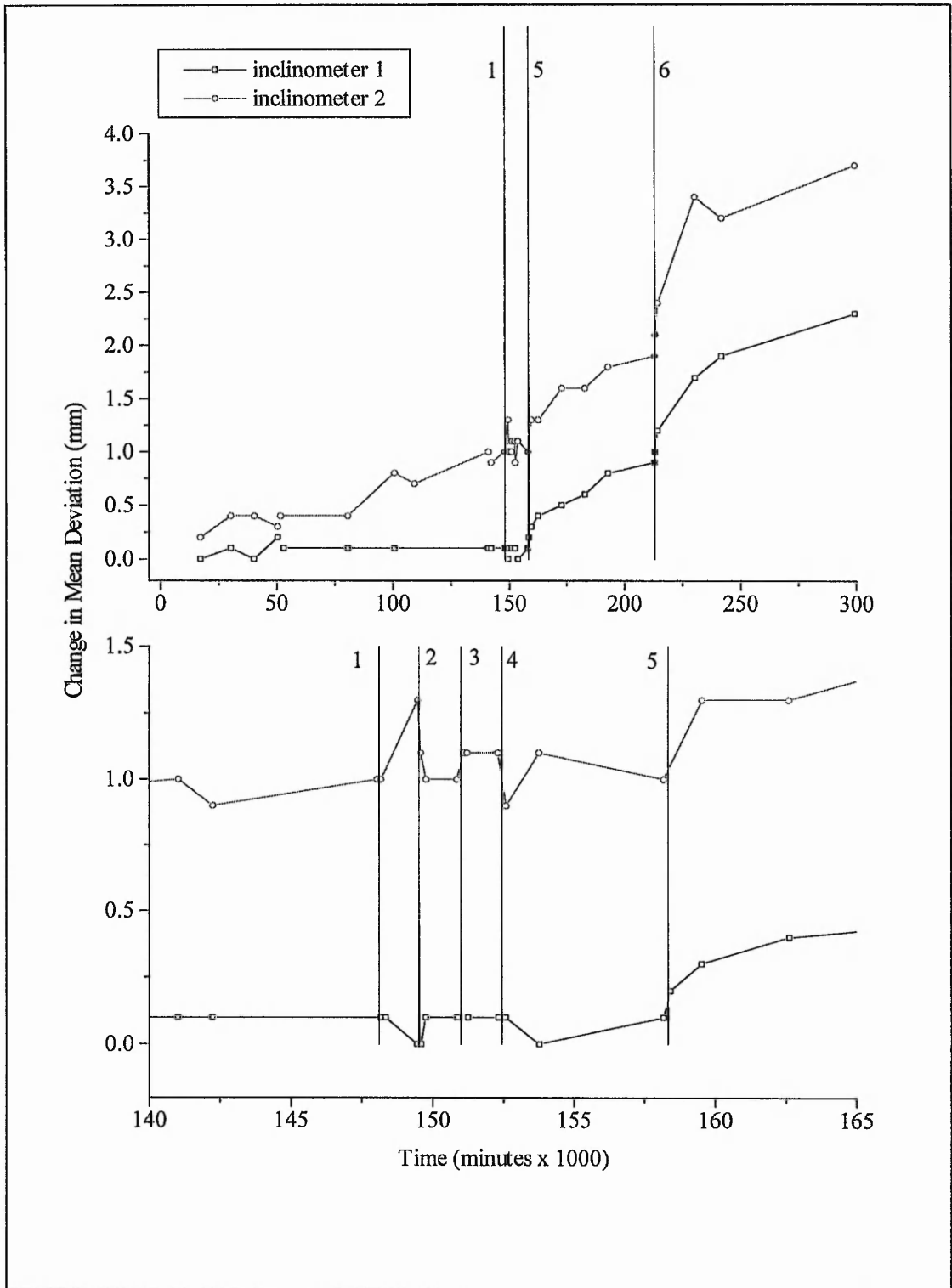


Figure 5.17 Arlesey change in mean deviation for inclinometer 1 (at depth 1.5m) and inclinometer 2 (at depth 0 metres). The upper plot illustrates the entire test period and indicates cuts 1, 5 & 6. The lower plot focuses on the main test period and indicates cuts 1, 2, 3, 4 & 5.

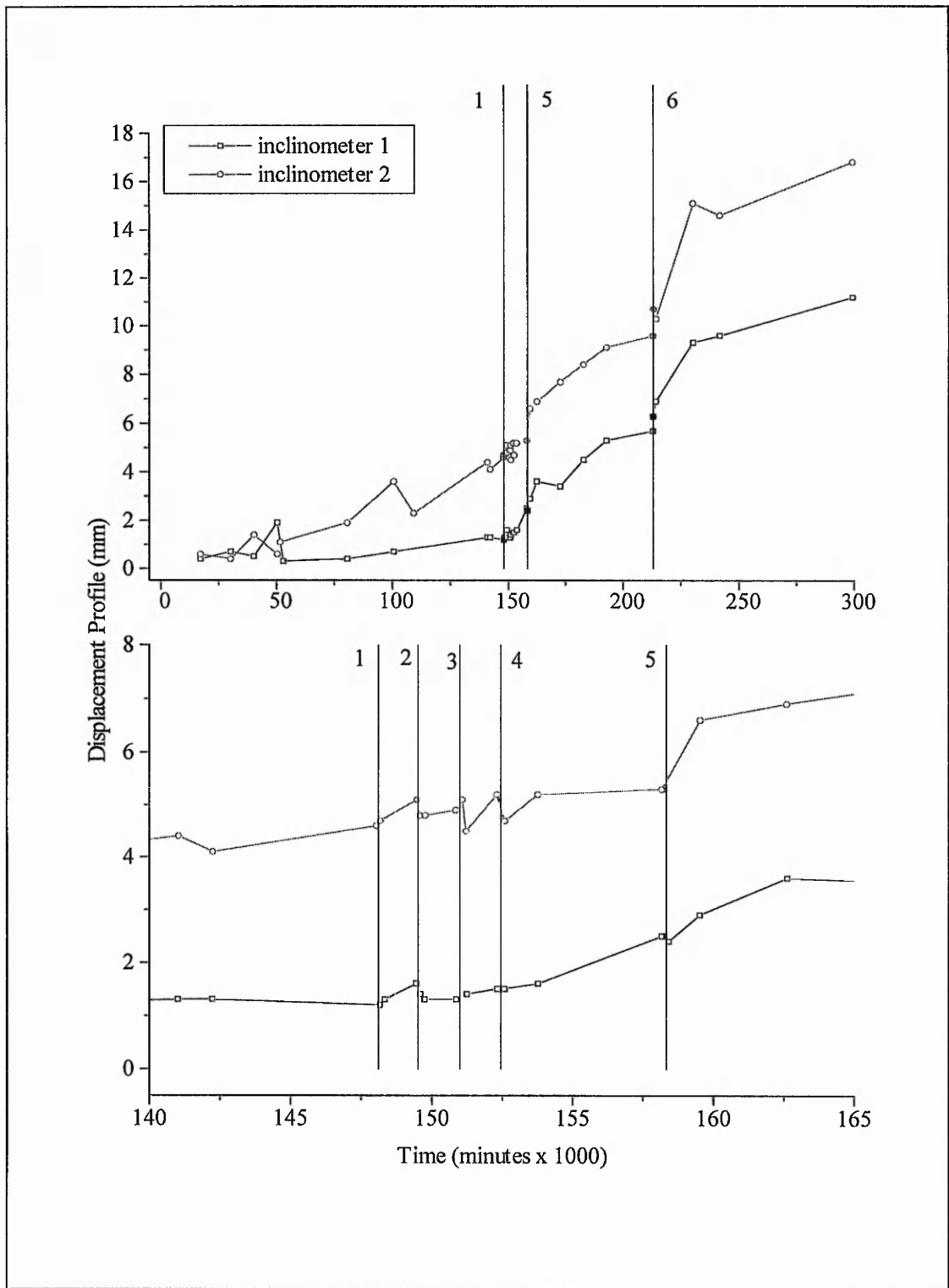


Figure 5.18 Arlesey displacement profile for inclinometer 1 (at depth 1.0m) and inclinometer 2 (at depth 0m). The upper plot illustrates the entire test period and indicates cuts 1, 5 & 6. The lower plot focuses on the main test period and indicates cuts 1, 2, 3, 4 & 5.

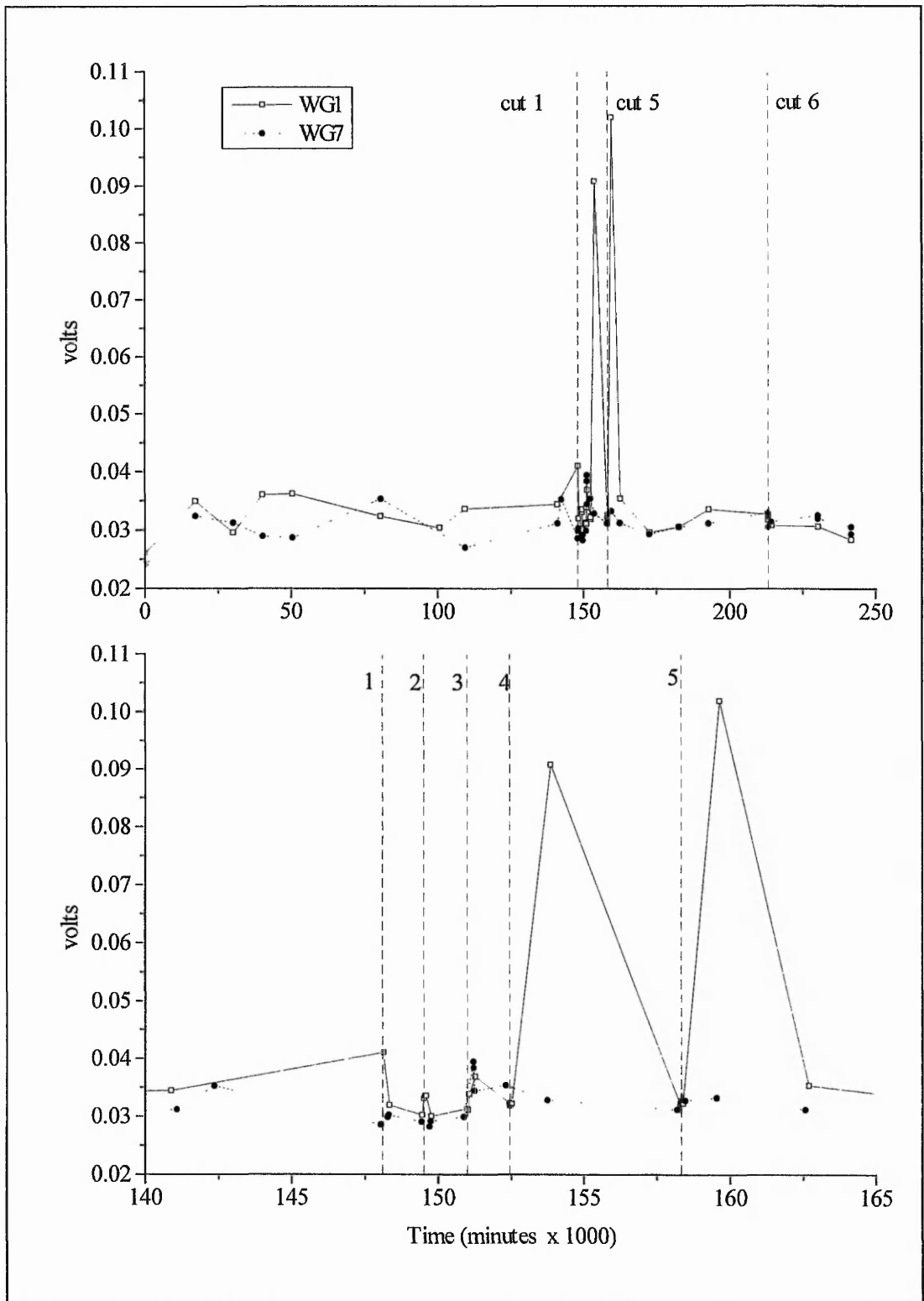


Figure 5.19 Arlessey AE mean signal value WGs 1 & 7. The upper plot illustrates the entire test period and indicates cuts 1, 5 & 6. The lower plot focuses on the main test period and indicates cuts 1, 2, 3, 4 & 5.

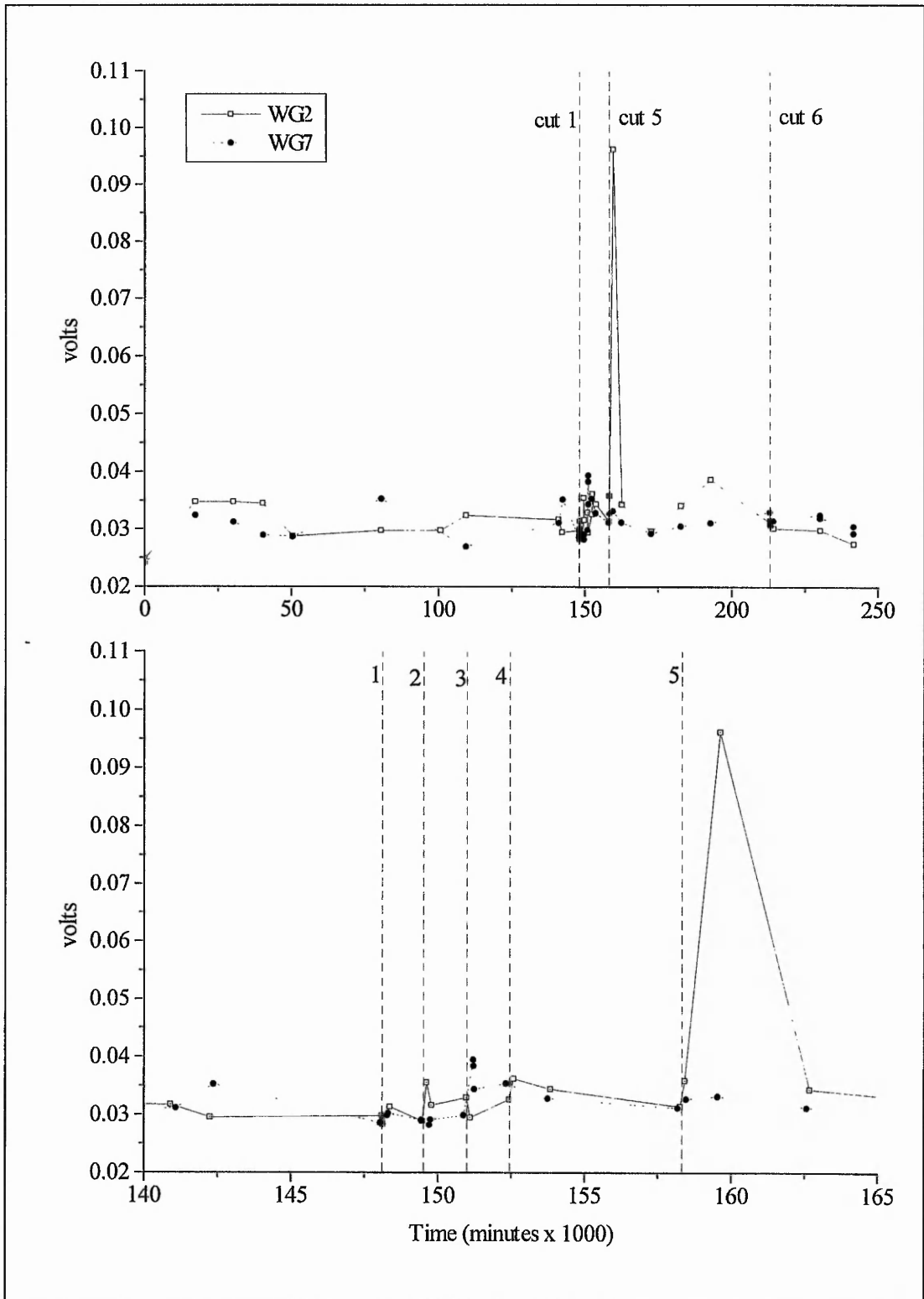


Figure 5.20 Arlesley AE mean signal values WGs 2 & 7. The upper plot illustrates the entire test period and indicates cuts 1, 5 & 6. The lower plot focuses on the main test period and indicates cuts 1, 2, 3, 4 & 5.

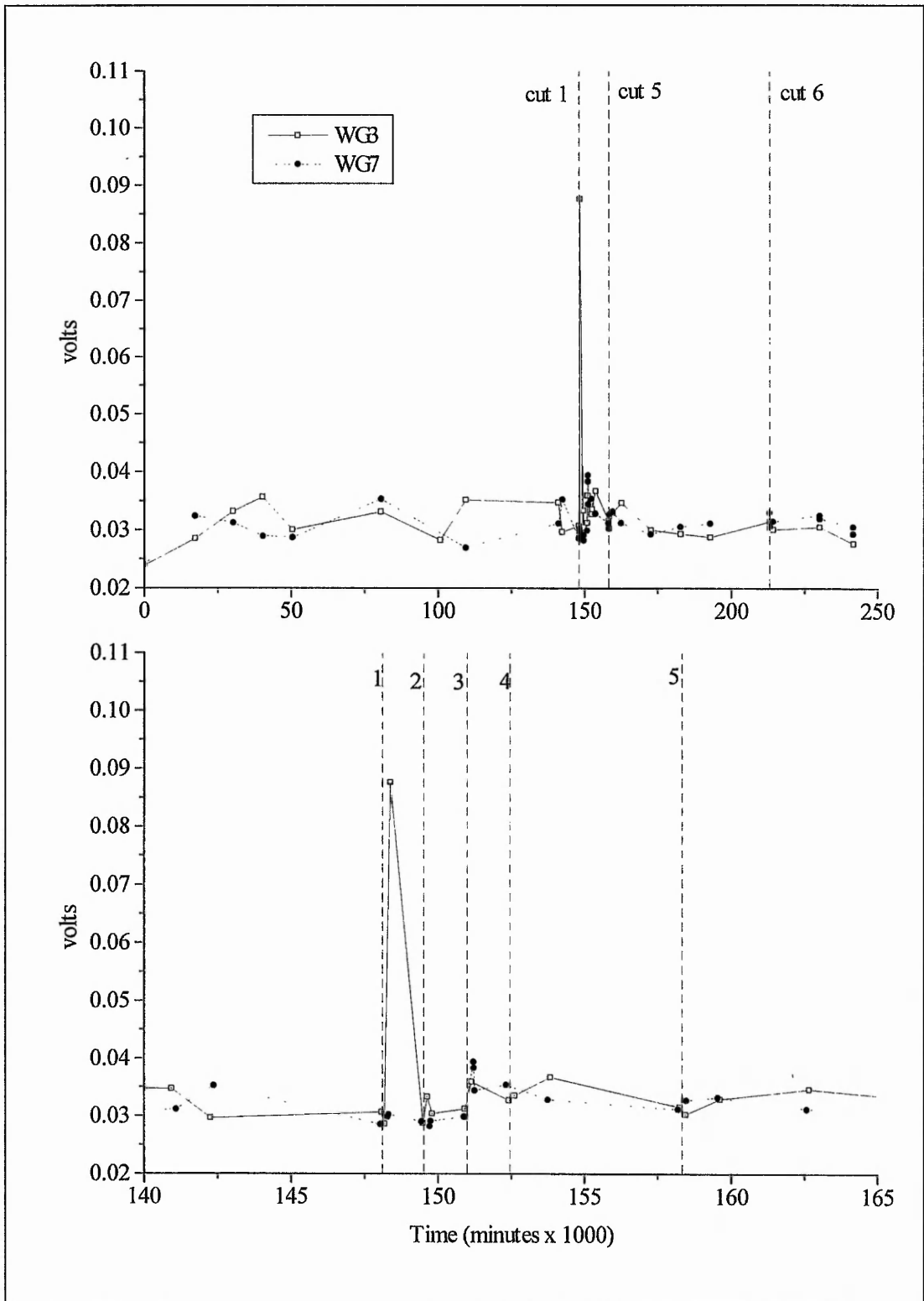


Figure 5.21 Arlesey mean signal value WGs 3 & 7. The upper plot illustrates the entire test period and indicates cuts 1, 5 & 6. The lower plot focuses on the main test period and indicates cuts 1, 2, 3, 4 & 5.

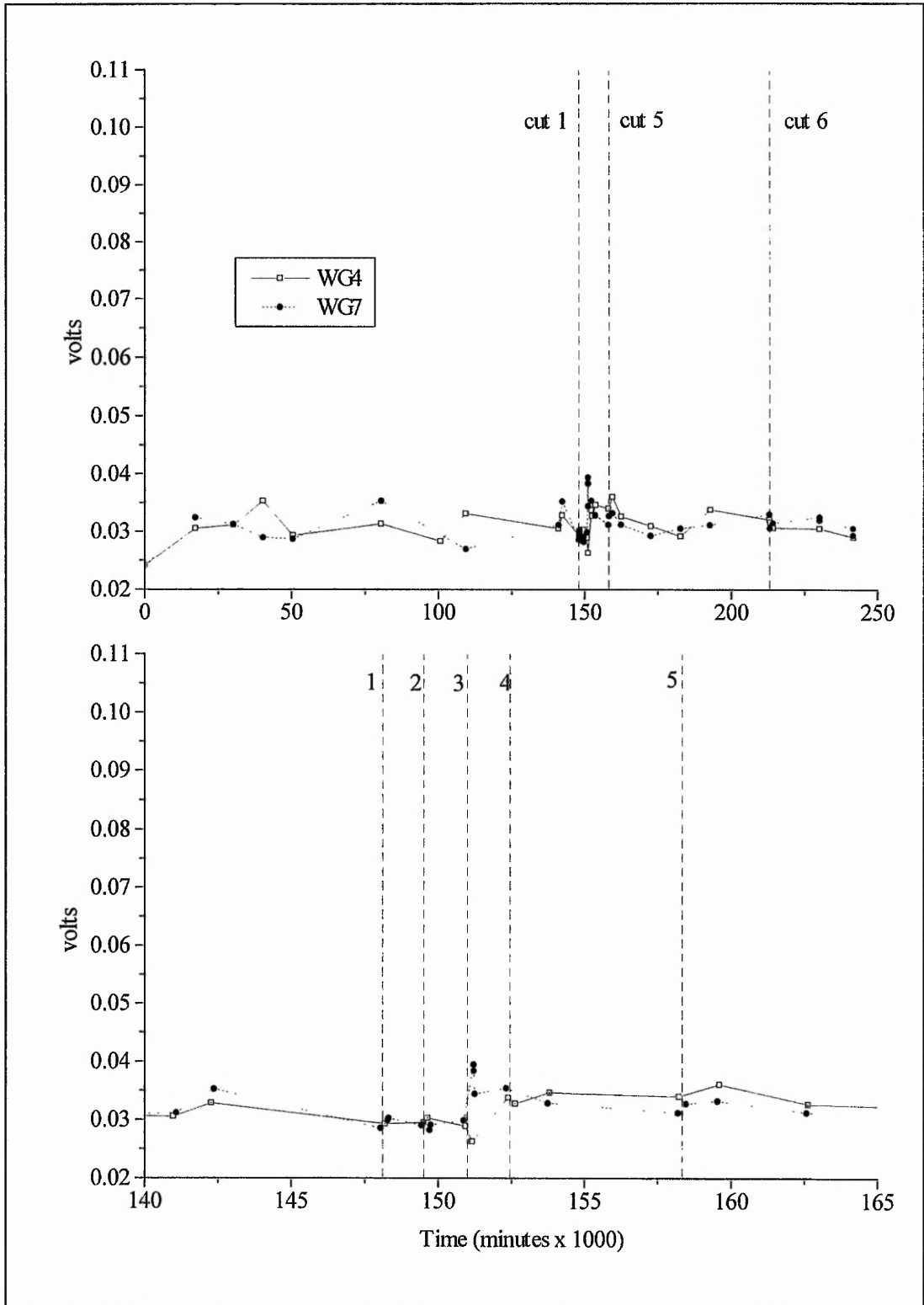


Figure 5.22 Arlesey AE mean signal value WGs 4 & 7. The upper plot illustrates the entire test period and indicates cuts 1, 5 & 6. The lower plot focuses on the main test period and indicates cuts 1, 2, 3, 4 & 5.

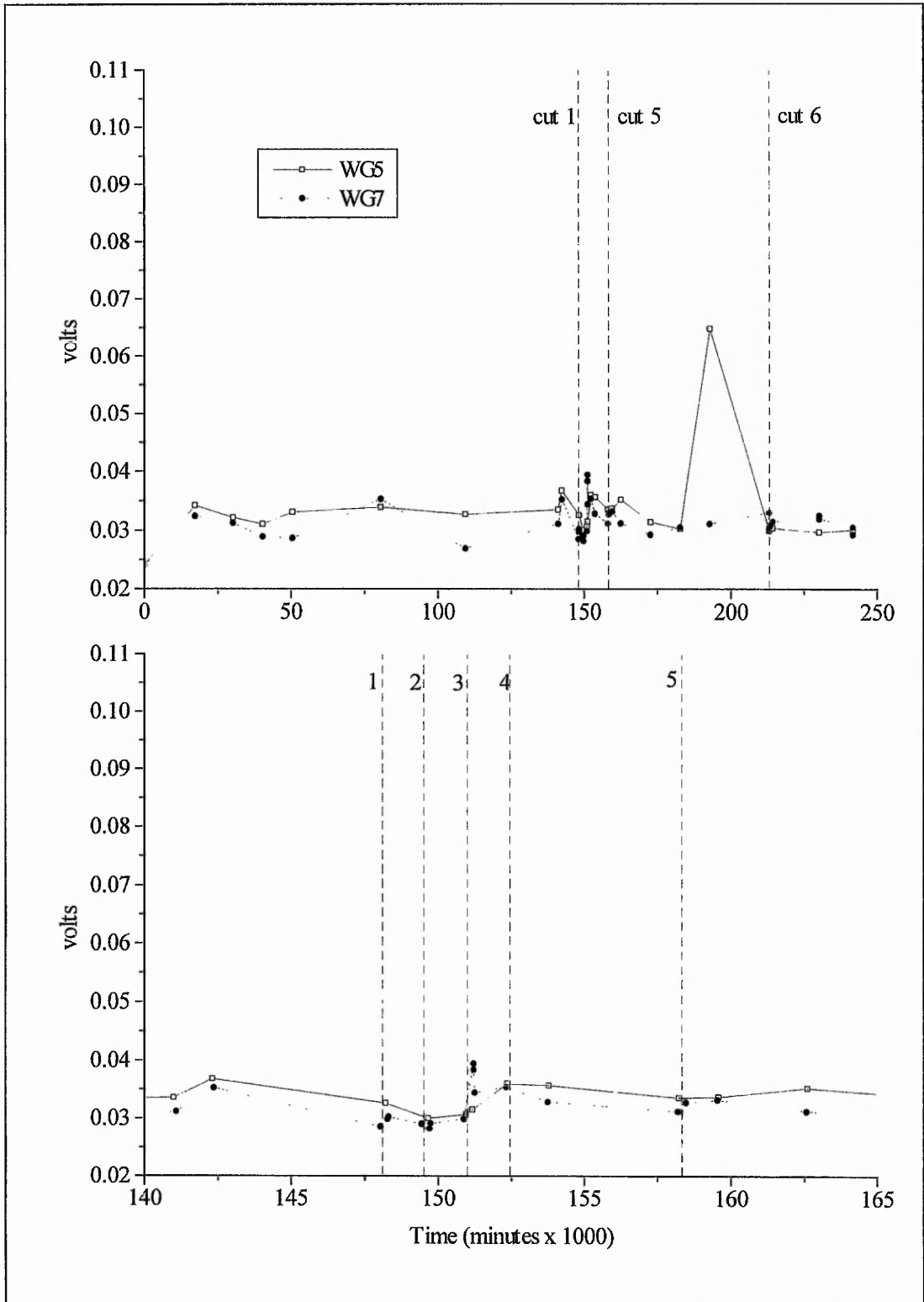


Figure 5.23 Arlesy AE mean signal value WGs 5 & 7. The upper plot illustrates the entire test period and indicates cuts 1, 5 & 6. The lower plot focuses on the main test period and indicates cuts 1, 2, 3, 4 & 5.

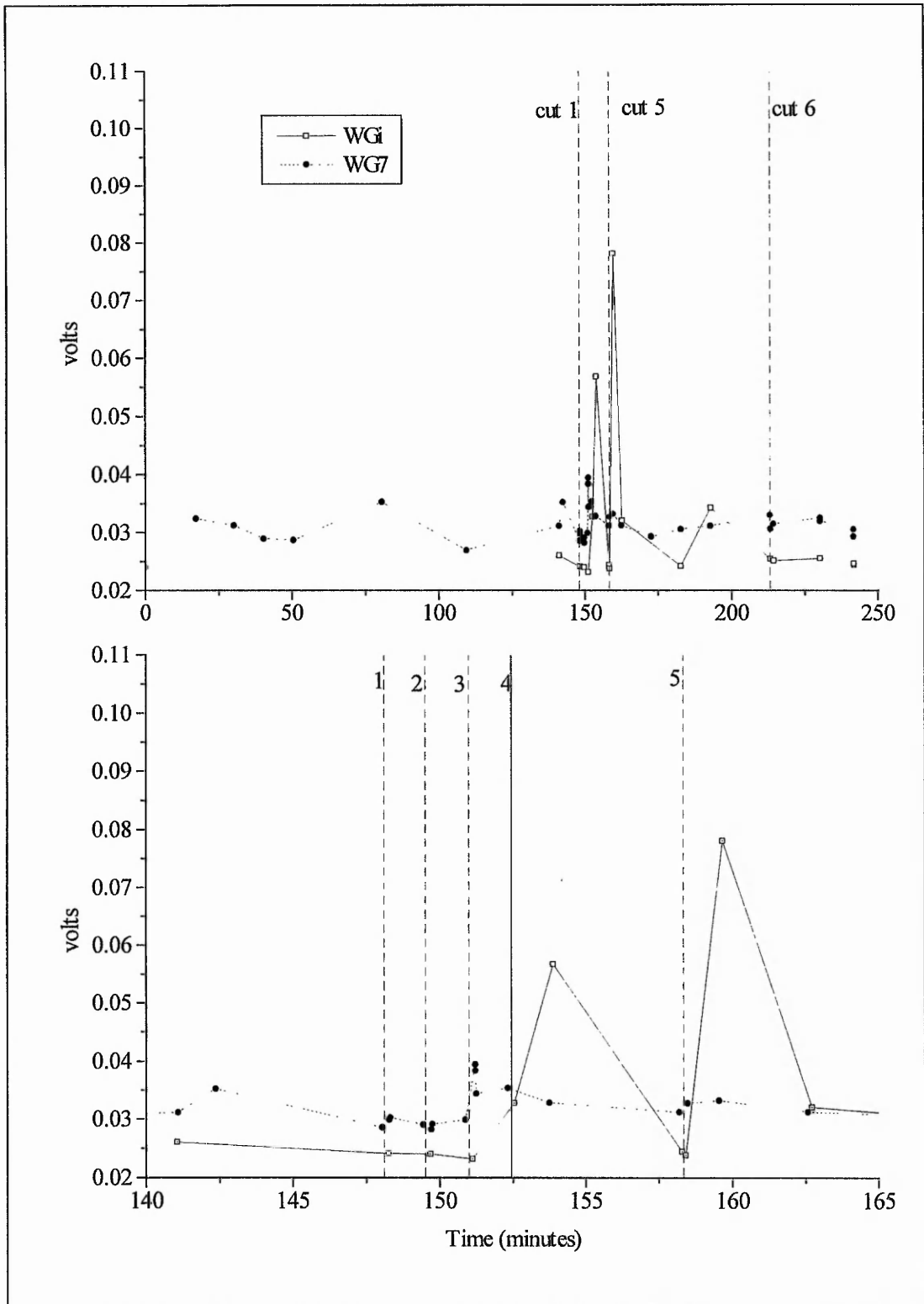


Figure 5.24 Arlesey AE mean signal value WGs i & 7. The upper plot illustrates the entire test period and indicates cuts 1, 5 & 6. The lower plot focuses on the main test period and indicates cuts 1, 2, 3, 4 & 5.

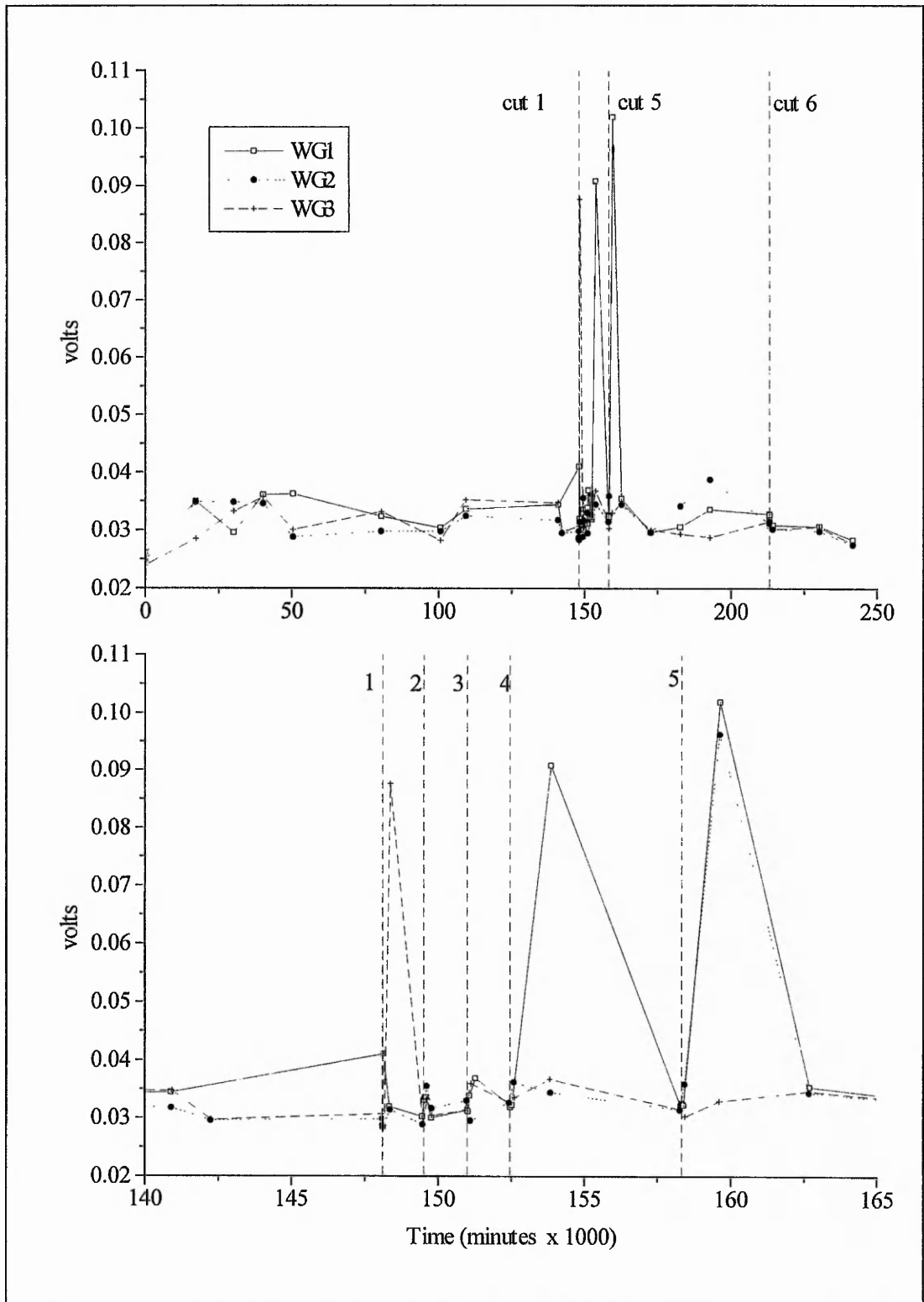


Figure 5.25 Arlesy AE mean signal values WGs 1, 2 & 3. The upper plot illustrates the entire test period and indicates cuts 1, 5 & 6. The lower plot focuses on the main test period and indicates cuts 1, 2, 3, 4 & 5.

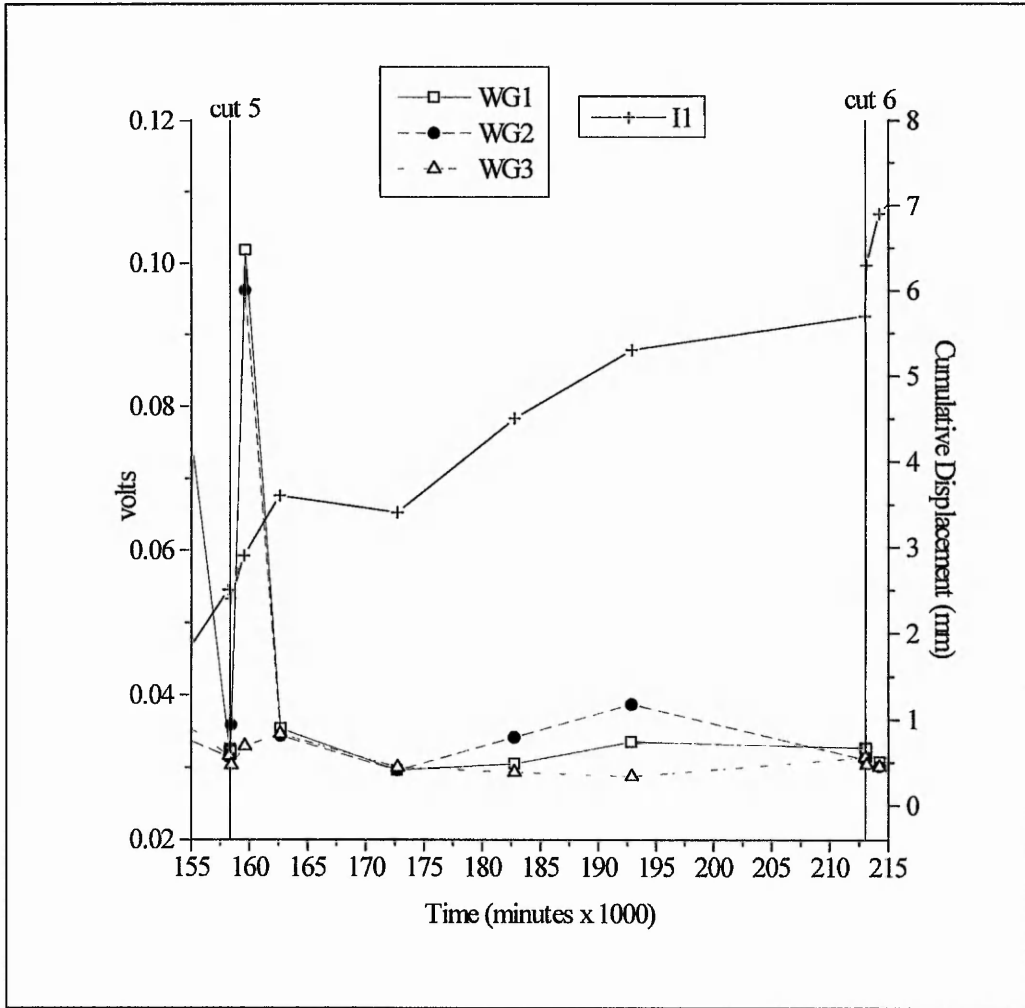


Figure 5.26 Arlesley AE mean signal values WGs 1, 2 & 3 and I1 displacement profile at 1.0 metre depth for period between cuts 5 & 6

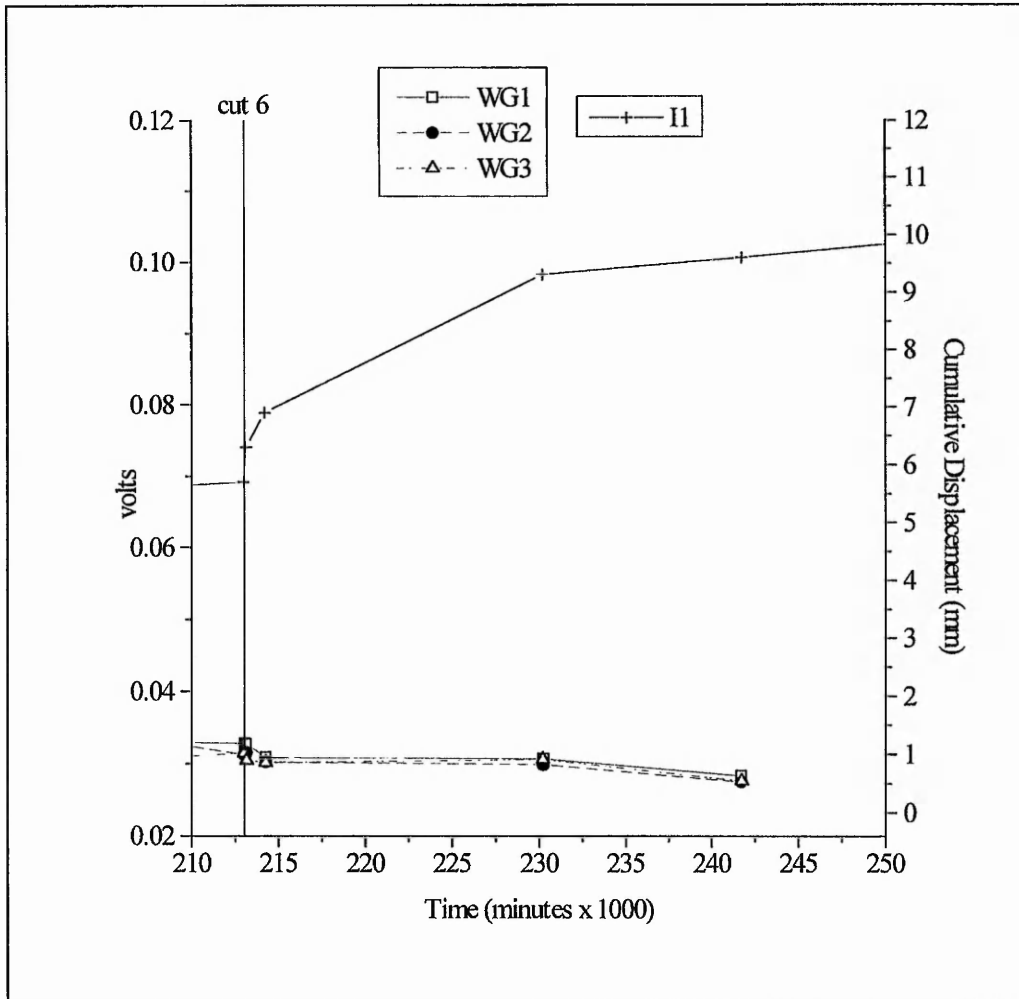


Figure 5.27 Arlesey AE mean signal values WGs 1, 2 & 3 and inclinometer 1 displacement profile depth 1.0 metre for period following cut 6

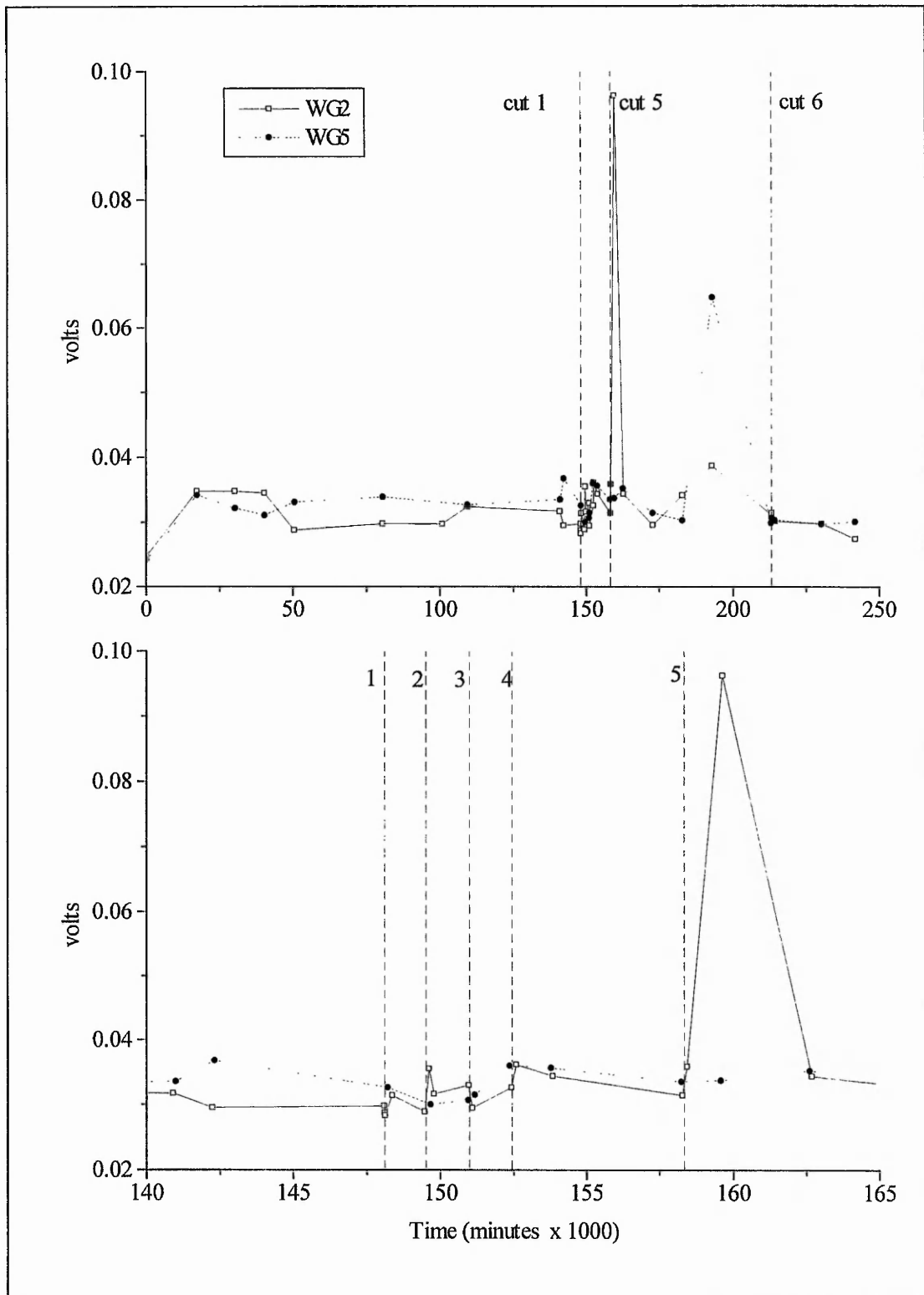


Figure 5.28 Arlesey AE mean signal values WGs 2 & 5. The upper plot illustrates the entire test period and indicates cuts 1, 5 & 6. The lower plot focuses on the main test period and indicates cuts 1, 2, 3, 4 & 5.

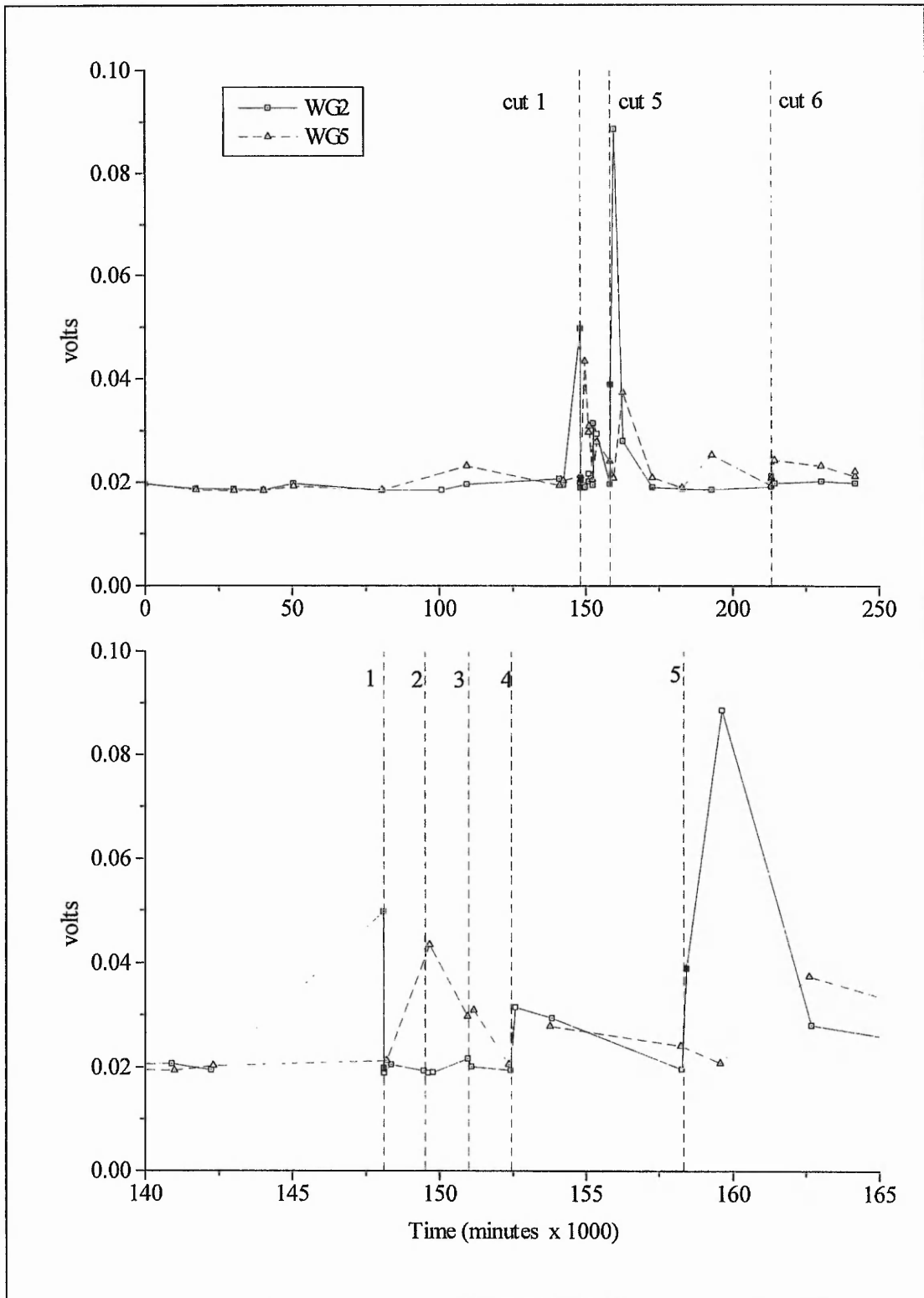


Figure 5.29 Arlesley AE standard deviation WGs 2 & 5. The upper plot illustrates the entire test period and indicates cuts 1, 5 & 6. The lower plot focuses on the main test period and indicates cuts 1, 2, 3, 4 & 5.

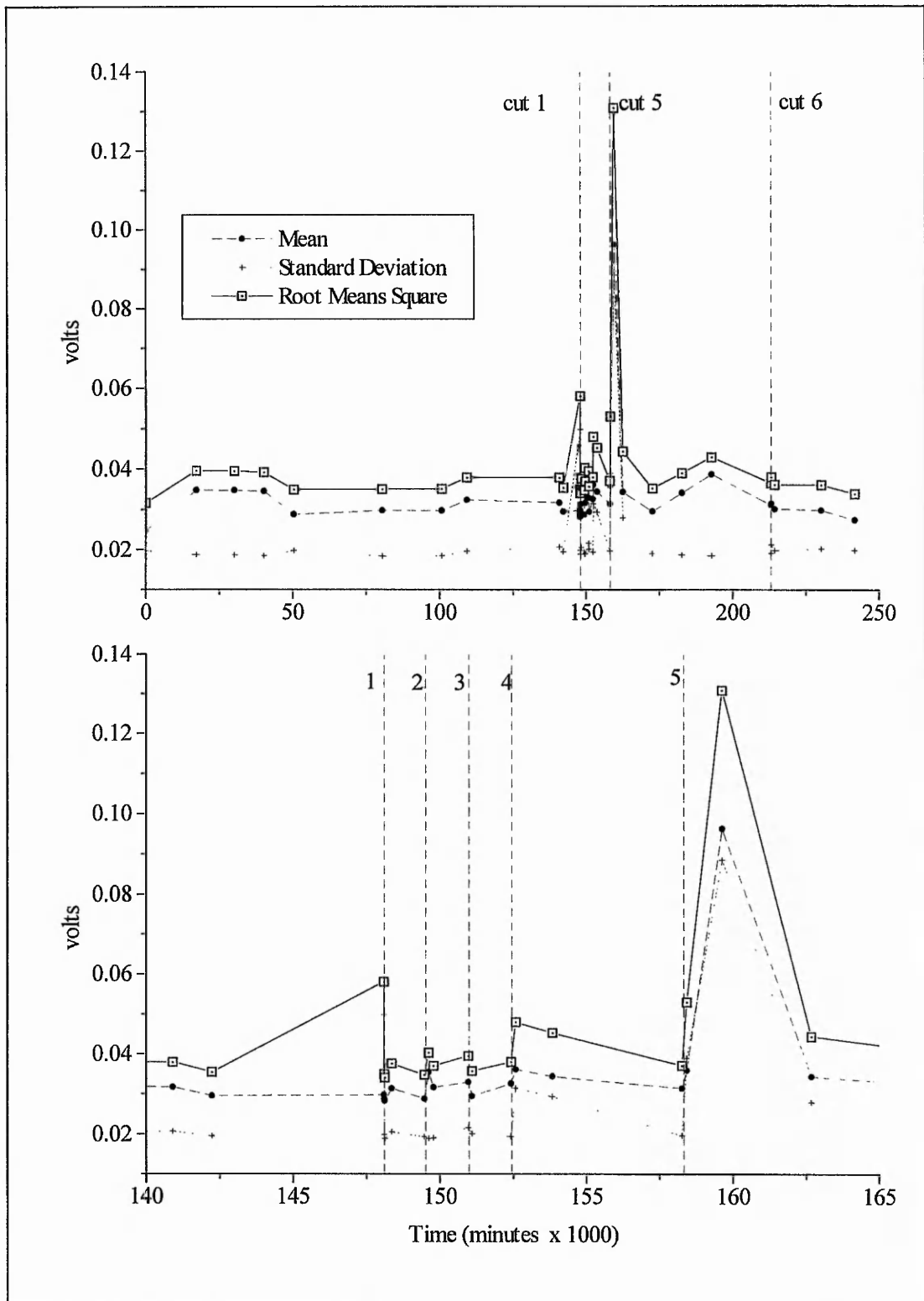


Figure 5.30 Arlesley AE mean signal value, standard deviation, root mean square WG2. The upper plot illustrates the entire test period and indicates cuts 1, 5 & 6. The lower plot focuses on the main test period and indicates cuts 1, 2, 3, 4 & 5.

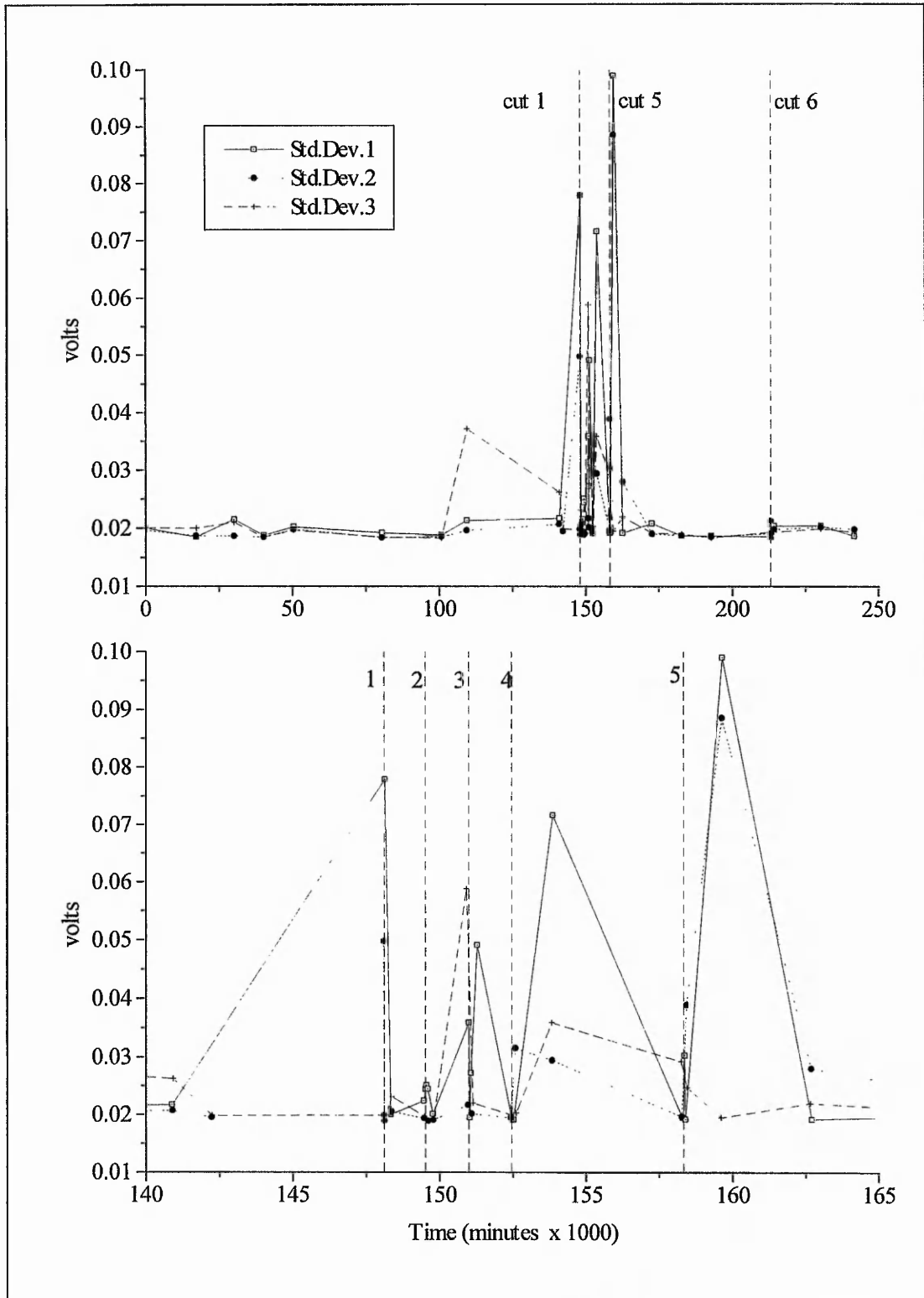


Figure 5.31 Arlesley AE standard deviation WGs 1, 2 & 3. The upper plot illustrates the entire test period and indicates cuts 1, 5 & 6. The lower plot focuses on the main test period and indicates cuts 1, 2, 3, 4 & 5.

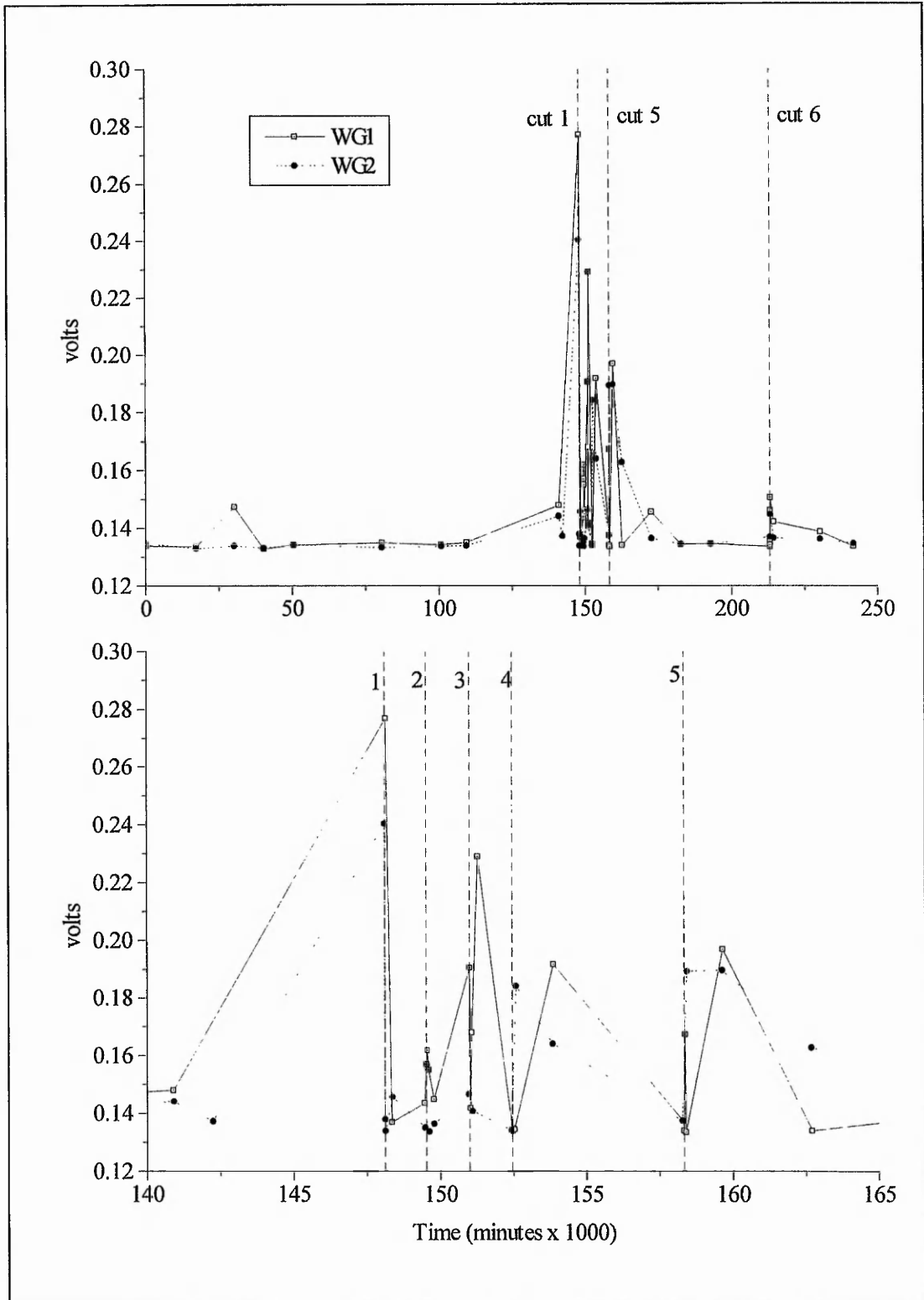


Figure 5.32 Arlesley AE mean signal values post-threshold WGs 1 & 2. The upper plot illustrates the entire test period and indicates cuts 1, 5 & 6. The lower plot focuses on the main test period and indicates cuts 1, 2, 3, 4 & 5.

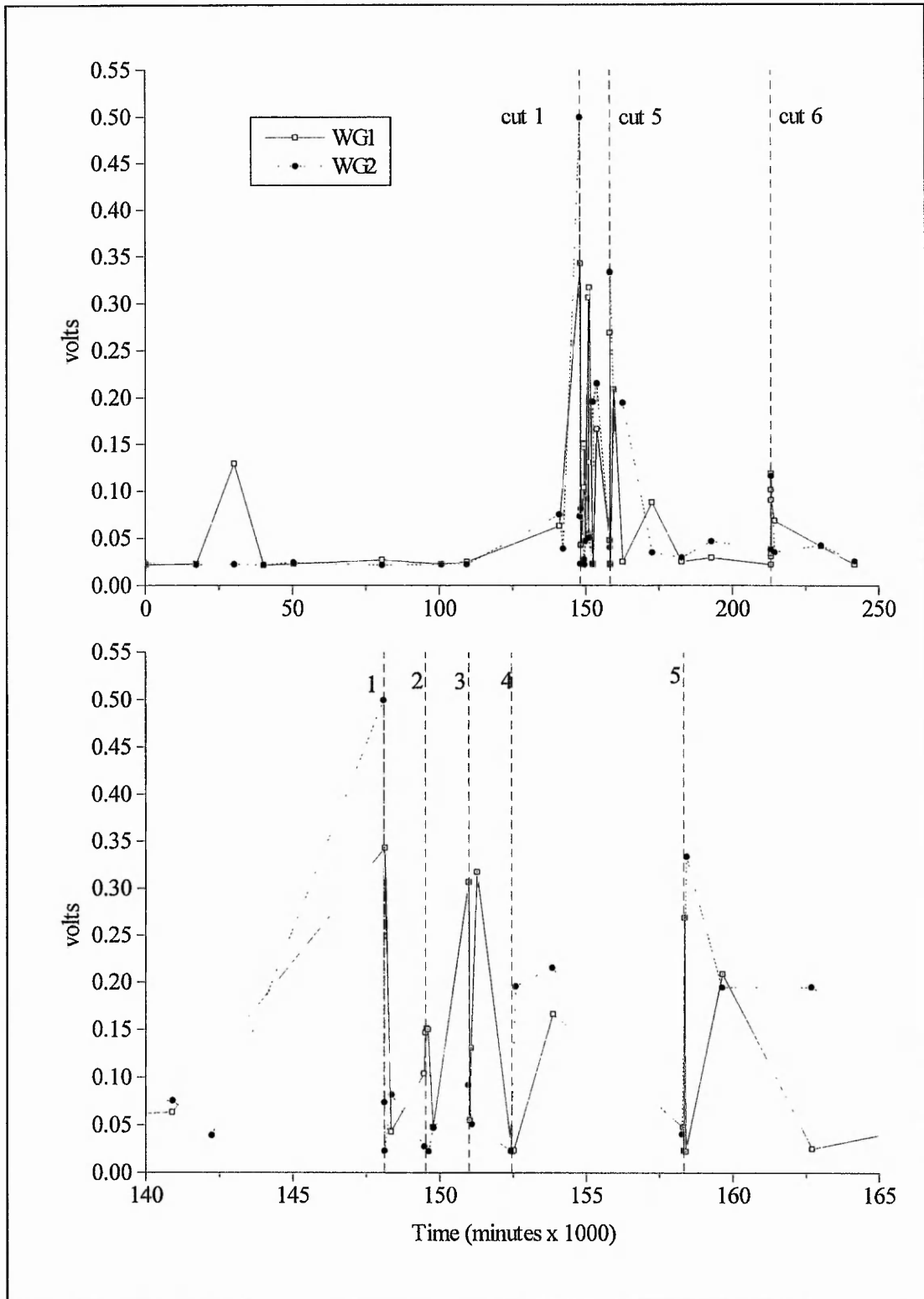


Figure 5.33 Arlesey AE standard deviation post-threshold WGs 1 & 2. The upper plot illustrates the entire test period and indicates cuts 1, 5 & 6. The lower plot focuses on the main test period and indicates cuts 1, 2, 3, 4 & 5.

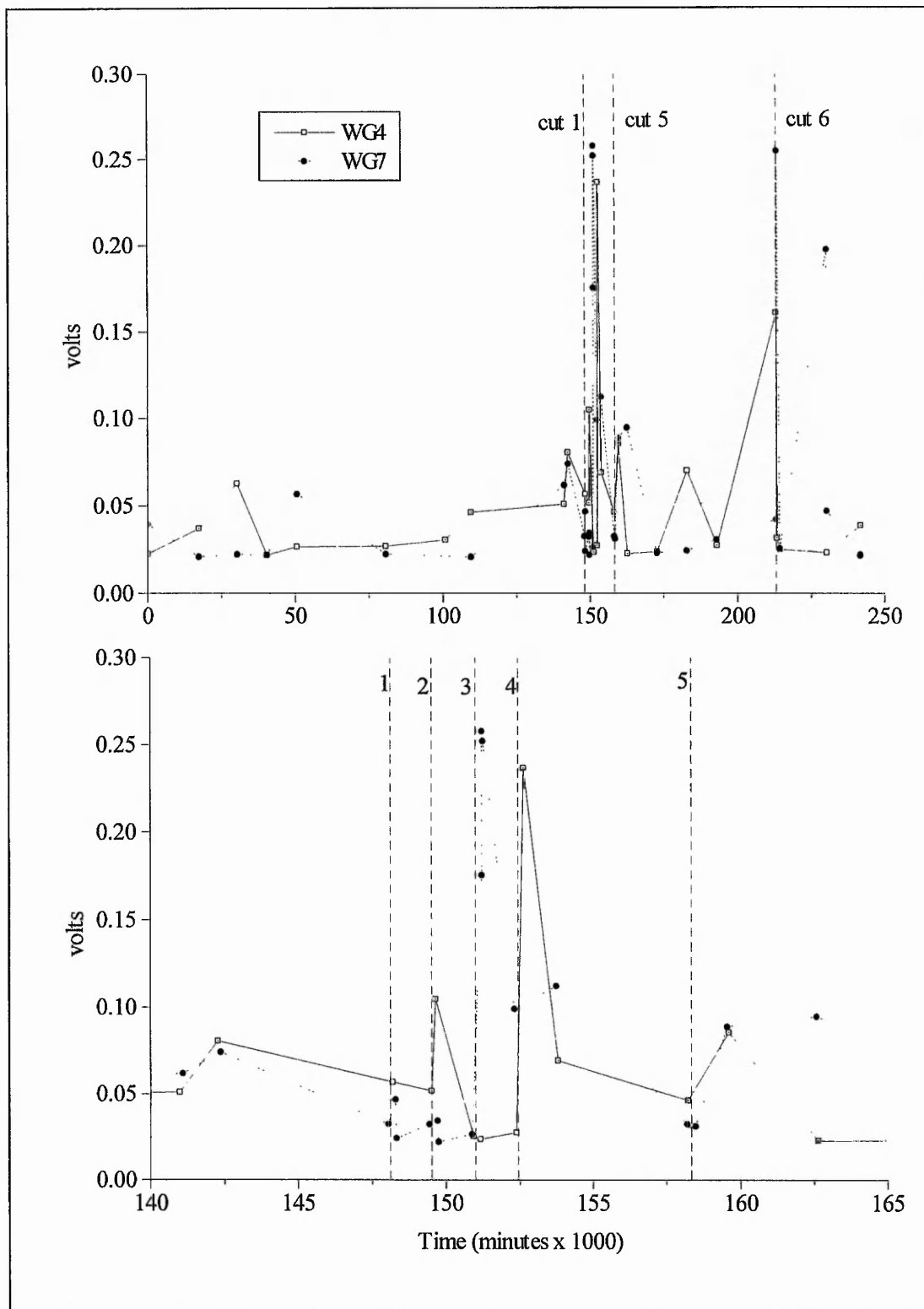


Figure 5.34 Arlesey AE standard deviation post-threshold WGs 4 & 7. The upper plot illustrates the entire test period and indicates cuts 1, 5 & 6. The lower plot focuses on the main test period and indicates cuts 1, 2, 3, 4 & 5.

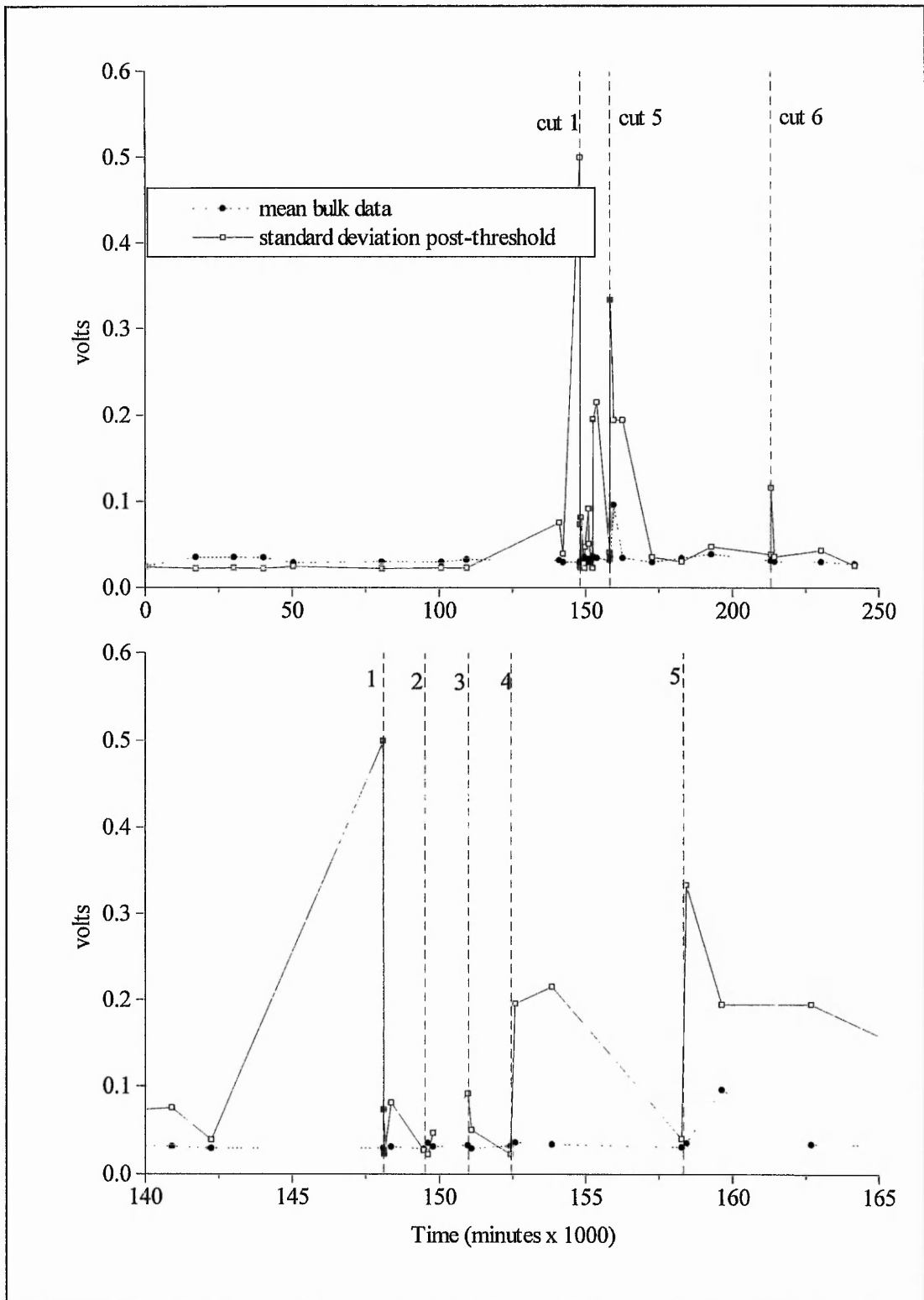


Figure 5.35 Arlesey mean signal value bulk data & standard deviation post-threshold WG2. The upper plot illustrates the entire test period and indicates cuts 1, 5 & 6. The lower plot focuses on the main test period and indicates cuts 1, 2, 3, 4 & 5.

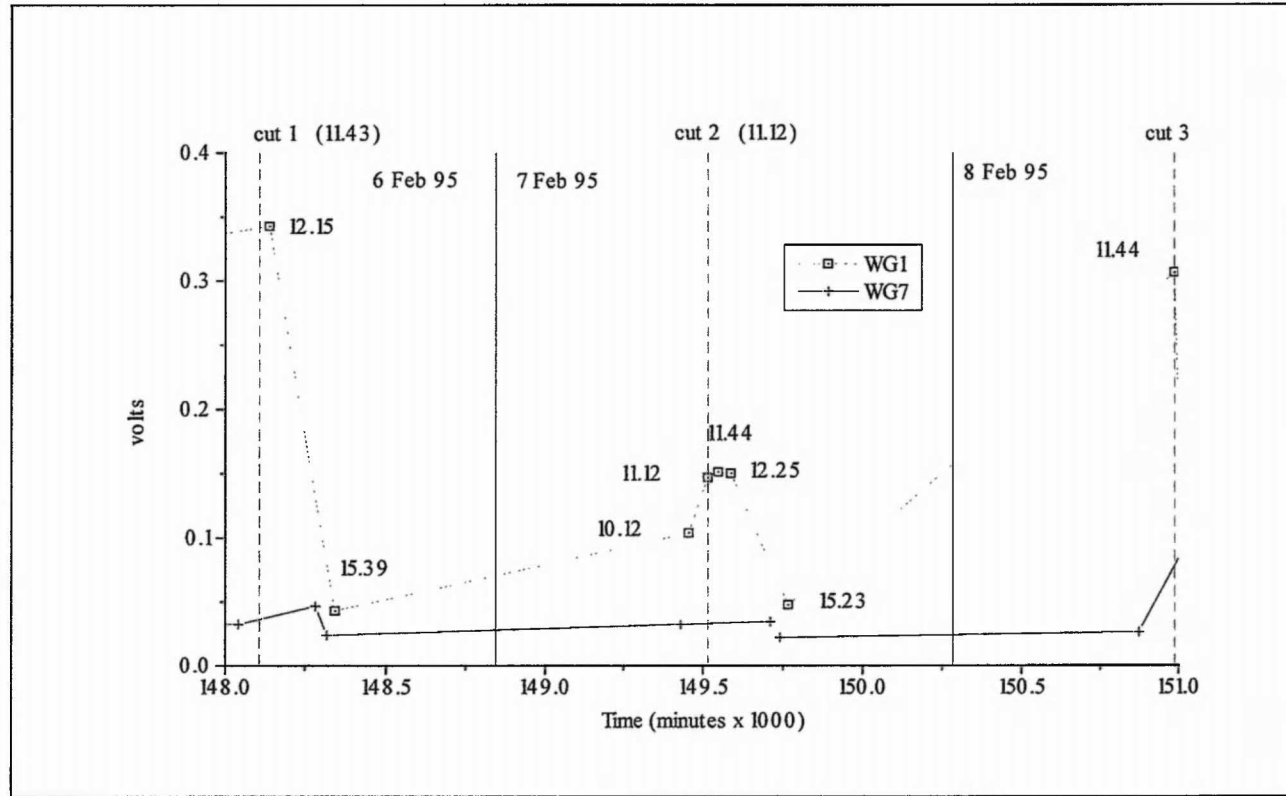


Figure 5.36 Arlesy AE standard deviation post-threshold WG1 Cuts 1-2

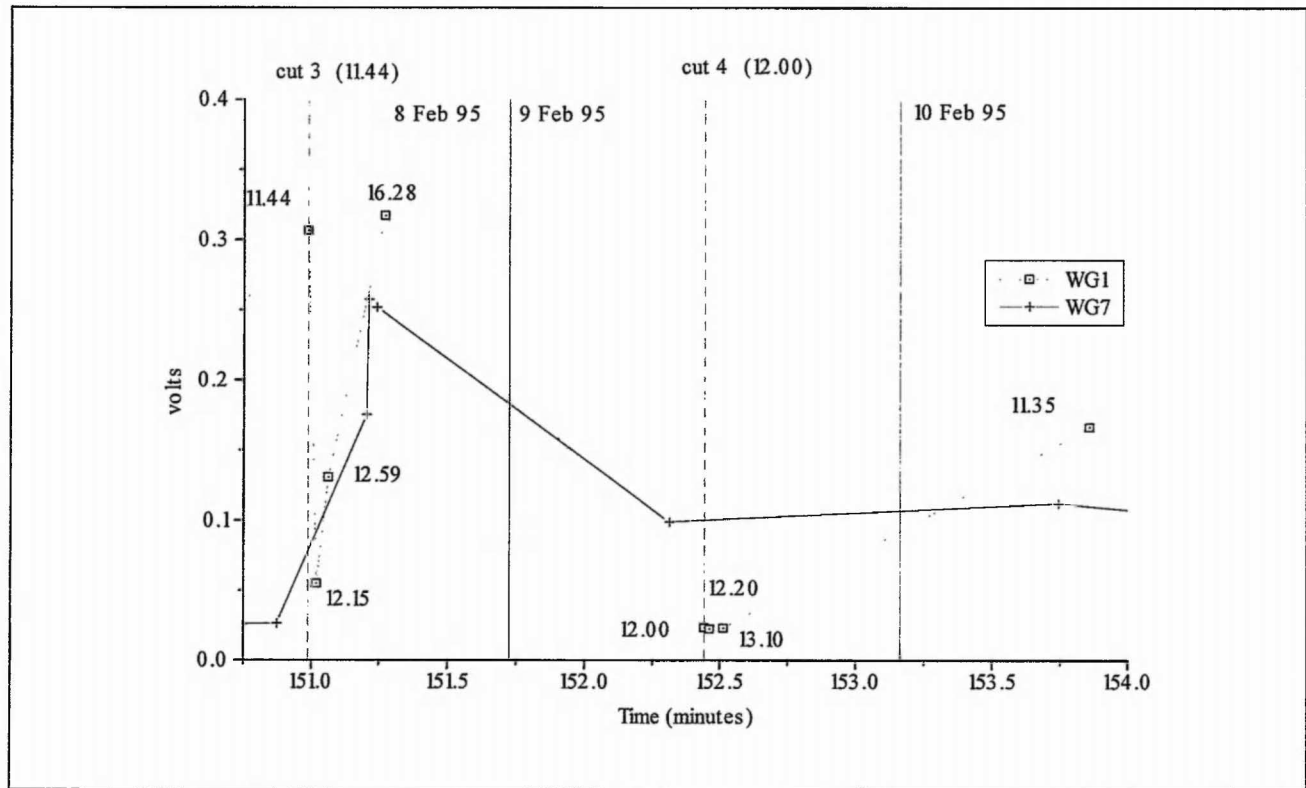


Figure 5.37 Arlesey AE standard deviation post-threshold WG1 cuts 3-4

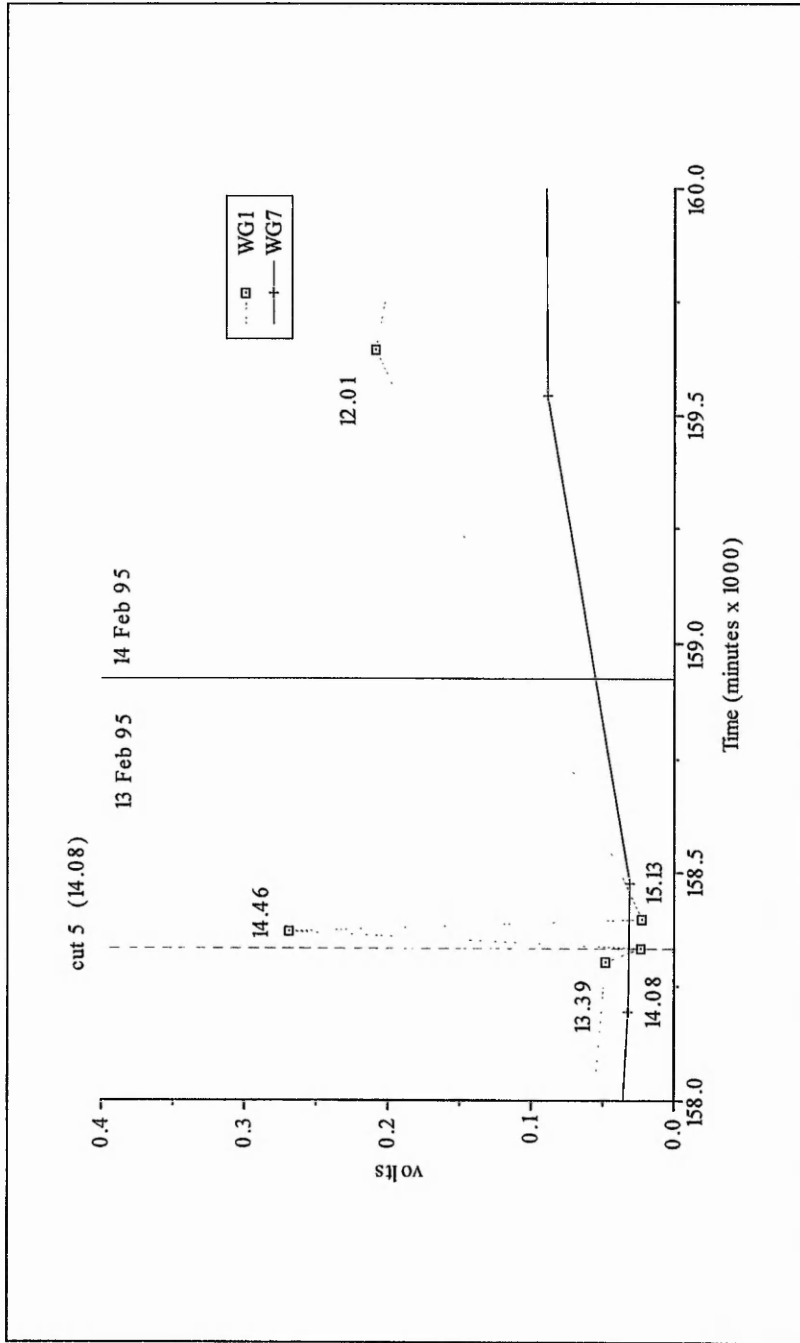


Figure 5.38 Arlesey AE standard deviation post-threshold data WG1 cut 5

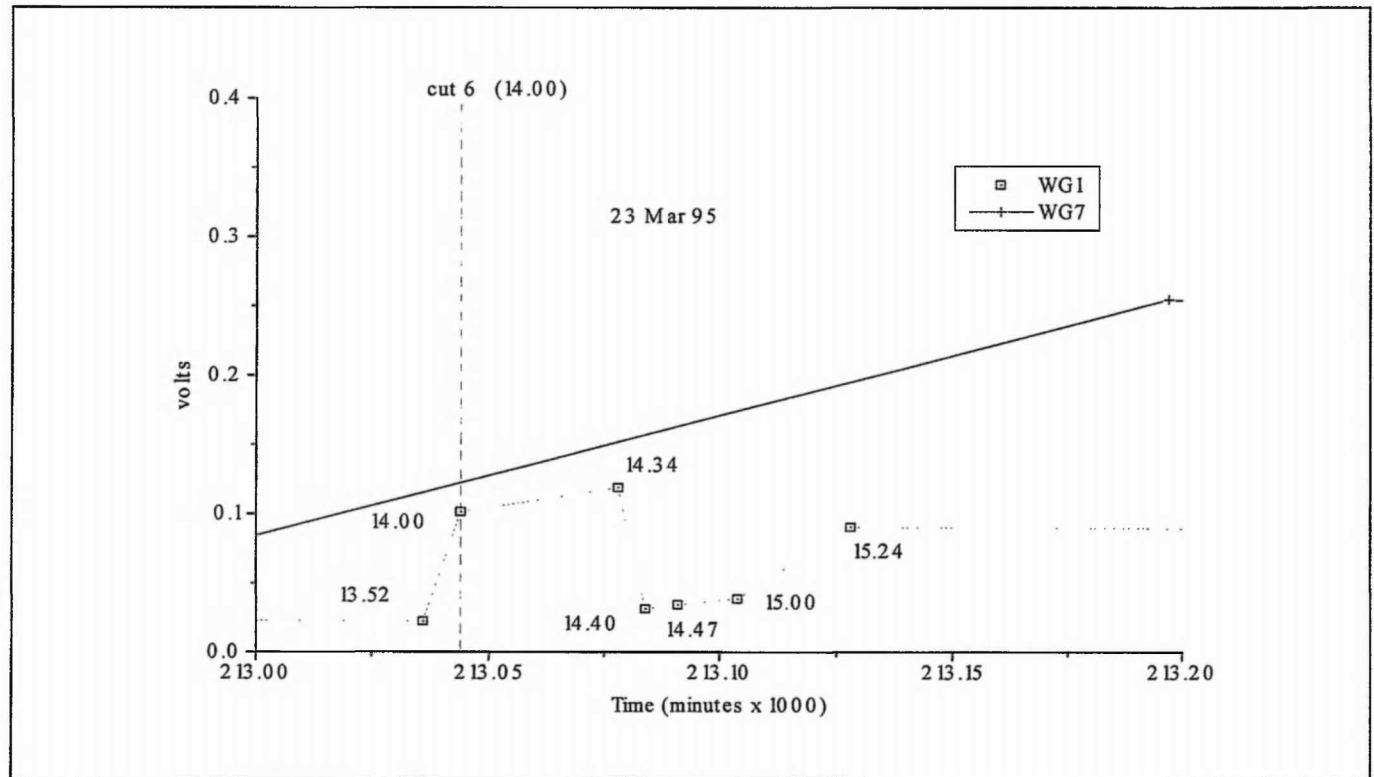


Figure 5.39 Arlesy AE standard deviation post-threshold data WG1 cut 6

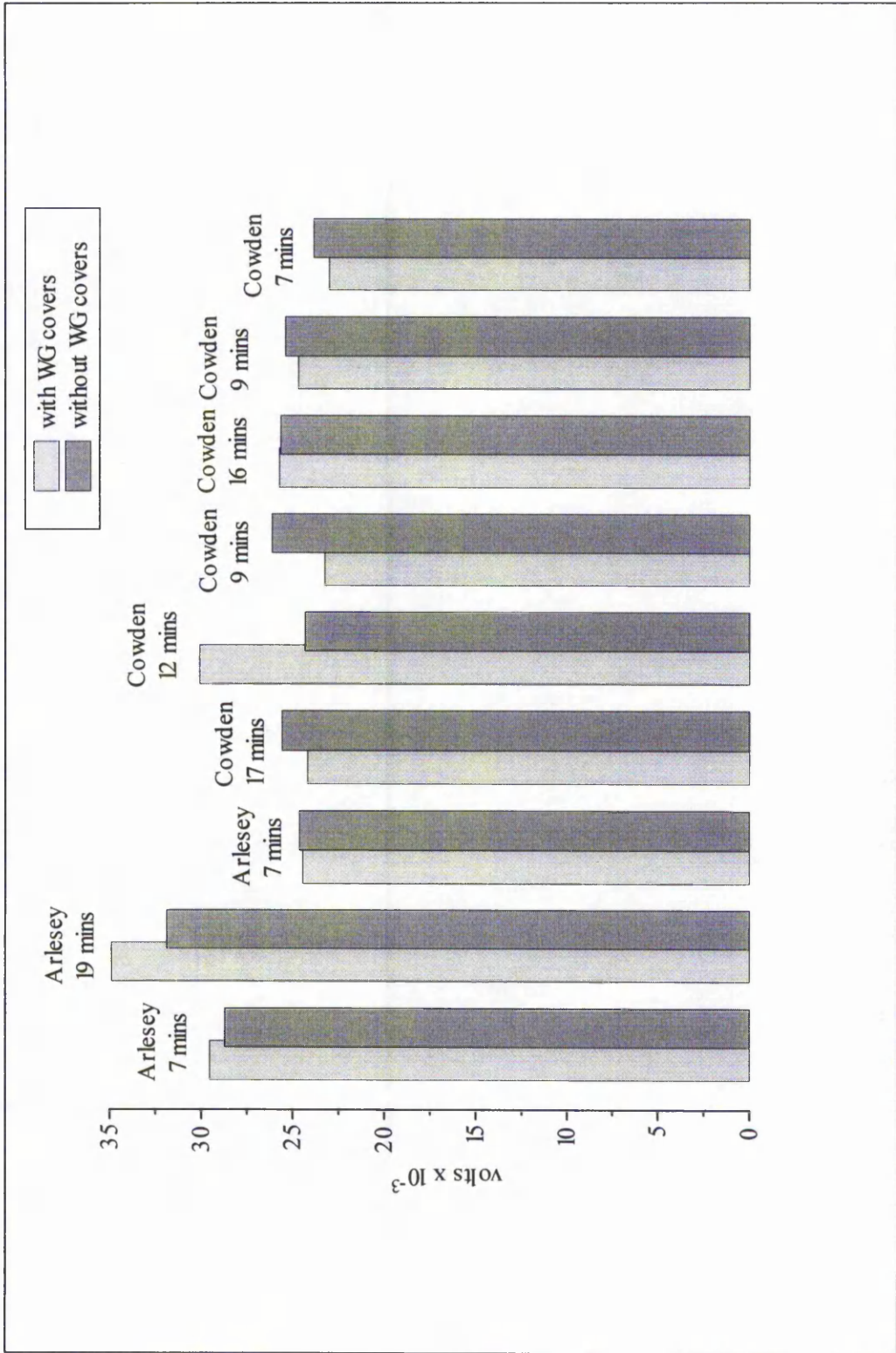


Figure 5.40 Arlesey & Cowden mean signal values - effect of wave guide covers

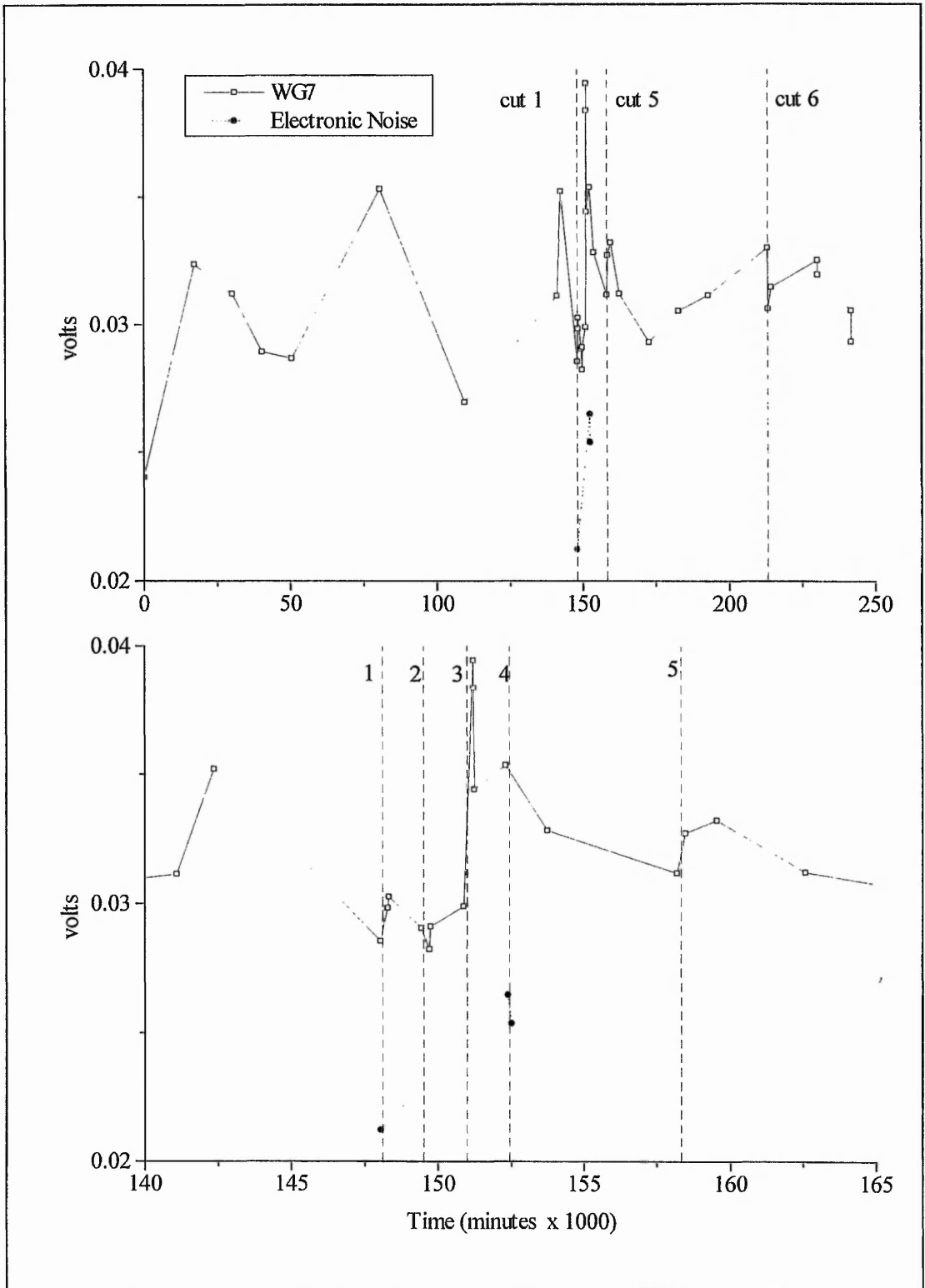


Figure 5.41 Arlesley AE mean signal values electronic noise & WG 7. The upper plot illustrates the entire test period and indicates cuts 1, 5 & 6. The lower plot focuses on the main test period and indicates cuts 1, 2, 3, 4 & 5.

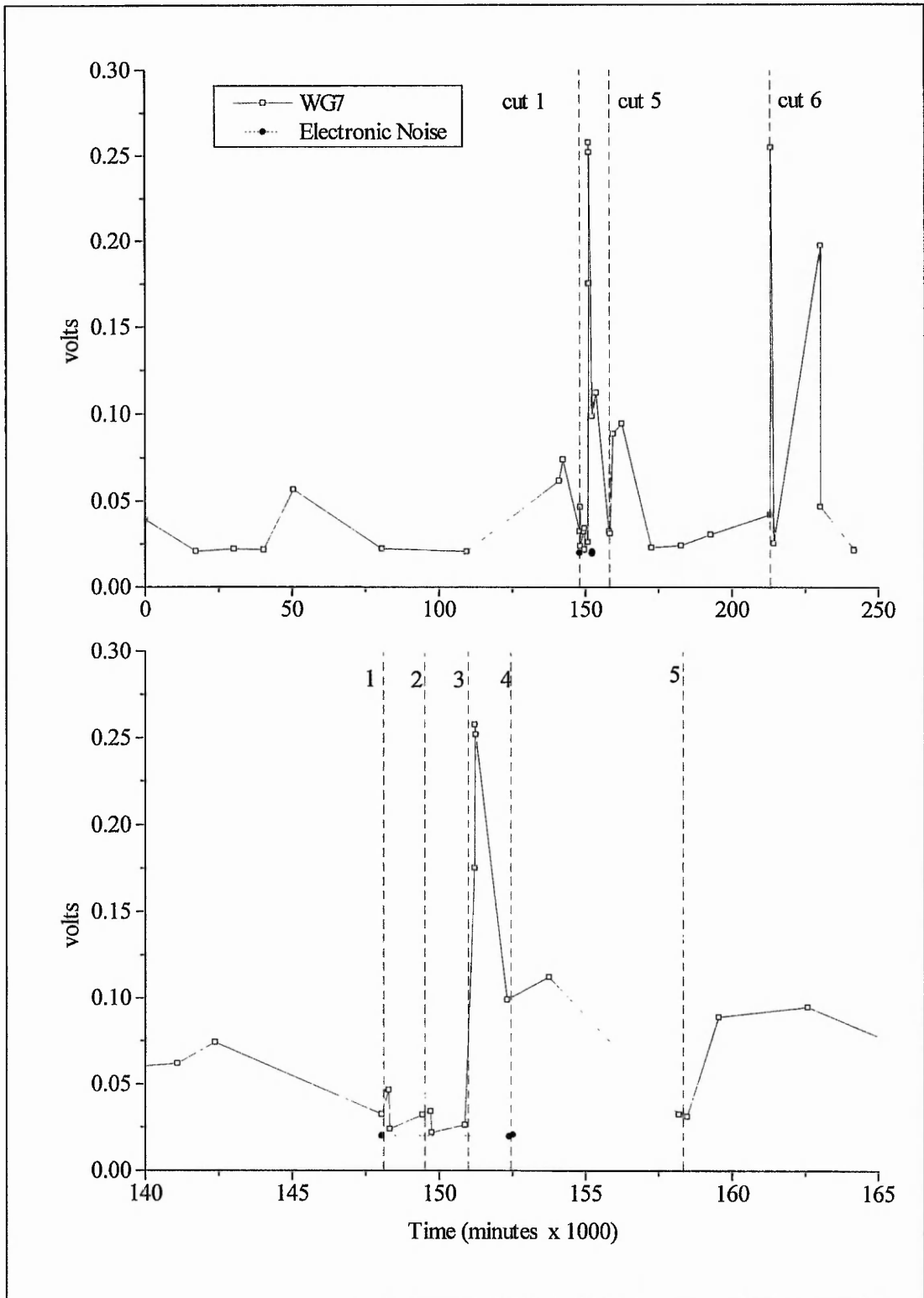


Figure 5.42 Arlesey AE standard deviation post-threshold electronic noise & WG7. The upper plot illustrates the entire test period and indicates cuts 1, 5 & 6. The lower plot focuses on the main test period and indicates cuts 1, 2, 3, 4 & 5.

Chapter 6

Implications of Cowden and Arlesey Results for Acoustic Emission Monitoring in the Field

6.1 Introduction

This chapter draws on the field test results obtained from both Cowden (Chapter 4) and Arlesey (Chapter 5). It attempts to amalgamate and explain the findings by the presentation of a single descriptive model.

Section 6.2 considers the nature of the emission (i.e. the constituent components of a captured emission) and section 6.3 discusses the evidence acquired in support of the active wave guide model. Section 6.4 examines the application of AE to deformation monitoring while section 6.5 considers the implications for AE generation mechanisms of the different results obtained by using different processing techniques. Finally, section 6.6 summarises the field test findings, describes the physical model and discusses some guidelines as to the design of AE monitoring systems tailored to suit particular geotechnical situations.

6.2 The Nature of the Emission

It is postulated that a captured emission consists of the combined effects of one or more of the following sources:-

- Airborne background noise
- Electronic noise and interference
- Noise due to the constructional features of the wave guide
- Emission related to deformation of the slope

Obviously it is only the final source which is of use, however it is important to appreciate the possible existence of the other three.

As has already been demonstrated airborne background noise does not appear to have presented a problem in this investigation (section 5.6.6) but it is important to appreciate that it *could*. Also, it may be suggested that the wave guide covers could have been dispensed with. However the wave guide covers did afford protection against wind blown debris striking the wave guide which, in turn, could have generated erroneous emission. In fact this would have been something of a problem at Cowden (where fragments of loose vegetation and particles of top-soil were blown about by coastal breezes) had the wave guide covers not been used.

It can only be speculated as to why the control wave guide at Arlesey regularly recorded mean signal values of greater magnitude in the *pre-test* period than was recorded from the inclinometer *during* the test period. The fact that the aluminium inclinometer consistently generated a lower magnitude emission than all the steel wave guides suggests that it may be a poorer generator (see part ii) and/or poorer propagator of sound. However the control wave guide was installed so far back from the face of the slope that it could not be suffering the effects of deformation and certainly not in the pre-test period. The question then arises as to how the control wave guide could at times generate more noise than other wave guides. This would suggest that some form of mechanism, as a result of the design of the wave guide, was responsible for generating this constructional noise. This could have been due to sporadic settlement of the control wave guide's sand backfill which was not compacted down (section 5.3.2) or, perhaps, to some interaction at the transducer-wave guide interface. It should be noted that, had the control wave guide been designed as a grout-backfilled aluminium inclinometer casing, then the *apparent* level of emission recorded by the gauge wave guides would have been inflated and would have been erroneously attributed to deformation.

If there was a genuine element of the emission generated due to some constructional feature of the wave guide then it is reasonable to expect differences in the magnitudes of the mean signal values recorded in the pre-test period for different wave guide designs. Of the eight pre-test readings for which there is a complete record the control wave guide produces a smaller magnitude mean signal value than wave guides 2 and 5 (both sand backfilled) on seven occasions; a smaller magnitude than wave guide 1 (gravel backfilled) on six occasions; a smaller magnitude than wave guide 3 (grout backfilled) on five occasions and a smaller magnitude than wave guide 4 (driven) on only four occasions. This would appear to lend support to the idea of constructional noise being generated as a result of a wave guide - backfill interaction. Unfortunately, however, due to the initial slope failure in the pre-test period (as detailed in

section 5.4.3), there is always the possibility that the gauge wave guides were subjected to some degree of deformation.

6.3 The Active Wave Guide Model

6.3.1 Evidence for the Active Wave Guide Model

In section 3.3 two models (*active* and *passive*), which have been used to explain the operational behaviour of the field wave guide, were described. This section examines some evidence which suggests that the active wave guide model (in this investigation) is the more appropriate.

In section 2.4.2 the results of previous studies into attenuation in soils were examined and, in particular, work by Nyborg *et al.* (1950) concentrated within the frequency range of 10 to 100kHz for a number of soil conditions. From figure 2.30, an ultra-conservative estimate of the attenuation suffered by a natural in-situ soil within this frequency range is 1dBcm^{-1} (100dBm^{-1} or 30dbft^{-1}). Additionally, examination of figure 4.9 (which depicts the Cowden site and developed shear plane) reveals that wave guides 5 and 12 (the control wave guide) lie along a line which is almost perpendicular to the shear plane where it cuts the surface. It has already been demonstrated (sections 4.5.2) that wave guide 12 at Cowden responded to deformation. (The good correlation between increased levels of AE, the increase in movement rates and the rapid drop in water level measured in inclinometer 1 - section 4.5.3). Wave guide 5 and wave guide 12 (which are of identical design) are separated by approximately 3m. If, therefore, the passive wave guide model were the more appropriate then an emission generated at the shear plane would need to propagate through the soil body to both wave guide 5 and 12. This would result in a reduction in the magnitude of a signal travelling between the two wave guides of some 300dB which, in turn, equates to a ratio between the magnitude of the signals passing each wave guide of 10^{15} !

Similar examples can be derived using wave guide 1 at Cowden and wave guides 2, 5 and 12 at Arlesey where the control wave guide is separated from the gauge wave guides by approximately 15 metres. Although the situation is complicated by (a) the existence of background noise, (b) periodic sampling of the signal and (c) the inability to monitor more than one wave guide at a time, the fact that the control wave guide has responded to ground deformations means that, had

the signal travelled through the soil as an acoustic medium, some very large signal magnitudes should have been recorded by those wave guides adjacent to a zone of deformation (passive model). This should have resulted in much of the data collected from gauge wave guides exceeding the 5 volt ceiling and 'washing-out' the signal. In fact, this only occurred very rarely at Cowden and never at Arlesey (it should also be noted that there is no reason why the active model should not generate signals which, similarly, exceed the 5 volt ceiling). It is this similarity between the magnitudes of signals recorded at gauge and control wave guides (especially when considering the very large attenuation in soil) which strongly suggests that the emission is generated locally (by an interaction between the metal of a wave guide and its backfill) and that the *active wave guide model* is the more appropriate.

6.3.2 Pedogenic Acoustic Emission

Despite the discussion of the previous section, it must be acknowledged that pedogenic AE (i.e. AE generated by the deforming host soil as a result of inter-particle action) probably exists and that the wave guides may also be capable of acting in accordance with the passive wave guide model. However, the findings of section 6.3.1 indicate that any such pedogenic AE (in this investigation) is either insignificant or goes undetected to the point where all detected AE can be explained by reference to the active wave guide model. One reason as to why pedogenic AE appears to be such an insignificant factor is the sensitivity of the acoustic sensor used (a 30kHz peak resonance piezoelectric acoustic transducer - section 3.2.1). Other investigations, for example Rouse *et al.* (1991a, 1991b) and Styles *et al.* (1988), used sensors sensitive to frequencies up to approximately 6kHz (section 2.5). The results of these investigations indicated that the passive wave guide model was the more appropriate.

As attenuation increases with increasing frequency (section 2.4.2), it is to be expected that increasing the frequency range examined would lead to a decrease in the level of pedogenic AE detected. This may serve to indicate the effect of examining different frequencies; a parameter not investigated in this study. However (when comparing field studies) it is difficult to consider this, or any other, individual aspect in isolation. Different soils suffer different levels of attenuation, so the nature of the host soil will exert some control over the capacity of a wave guide to detect pedogenic AE. Wave guide design also imposes considerable control over the ability of the wave guide to act either actively or passively. It has been shown that wave guides

designed as steel tubes with a sand or gravel backfill generate AE actively whereas it is likely that driven or grout backfilled wave guides (in clay soils) would be more receptive to pedogenic AE. (This is due to the good contact with the host soil afforded by driven wave guides and the similarity in propagating media for grout backfilled wave guides in clay soils). However, it should also be appreciated that wave guides designed to act passively are also capable of generating AE in accordance with the active wave guide model.

The *apparent* capacity of a wave guide to generate AE actively or capture it passively is, therefore, primarily dependent upon the design of the wave guide *and* the frequency bandwidth examined. (For example, examination of any of the grout backfilled wave guides in this investigation at a frequency of, say, 6kHz may have detected pedogenic AE). Whether a system is primarily concerned with the generation of active AE or the capture of passive AE is largely a matter of design. Ideally, active systems would employ noisy wave guide designs situated in (or close to) zones of deformation and higher frequency ranges would be examined; passive systems would employ quiet wave guide designs situated away from zones of deformation (making appropriate allowances for attenuation in the soil) and lower frequency ranges would be examined. Ultimately, which system is adopted is, currently, largely a case of personal preference. However site factors, such as ambient acoustic noise and the nature of the soil, will also influence the decision. (It should, however, be appreciated that nothing, as yet, is known of the frequency content of actively generated AE and all discussion of active AE is based on the findings of this investigation).

It is, therefore, possible that wave guides designed to generate active AE may detect spurious passive AE. However, based on the findings of this investigation, there is no evidence to suggest that this has occurred. There is also a possibility that passive AE may cause a disturbance to the backfill of a wave guide which could generate detectable active AE although, owing to the small wave amplitude of the passive AE, this is considered unlikely. Equally, passive wave guides may generate active AE but multi-channel approaches (where a number of wave guides are monitored concurrently) would enable removal of these spurious events.

The fact that wave guides probably have the capacity to both generate active AE and detect passive AE gives rise to the notion of a *hybrid* wave guide. Although no attempt at characterisation of the field captured AE (other than fairly rudimentary examinations of event magnitude and amplitude distributions) has been attempted by this investigation, other

investigations such as Rouse *et al.* (1991a, 1991b) and Styles *et al.* (1988) (section 2.5) have identified a number of different pedogenic AE events. If, therefore, active and passive AE can be both detected and distinguished then a hybrid wave guide may have some interesting applications. At this stage, however, any suggested use of such a hybrid wave guide would be highly speculative and it is likely that wave guide design would be tailored to restrict AE to either actively generated or passively acquired.

In section 2.5 a number of field investigations were summarised and it is interesting to reassess the findings in lieu of the above discussion. Unfortunately, there are few instances where wave guide design is detailed (particularly in terms of active/passive design) and there appears to have been little attempt to understand its operation in the field. From the available information, most investigations appear to have examined low frequency ranges (up to approximately 10kHz) and in soil which (generally) had a significant non-clay element. Without knowledge of the exact wave guide design it is difficult to comment on the origin of the AE but, despite the low frequencies examined, it is considered likely that the AE was generated actively (reflecting the significant non-clay element) and that this was the over-riding factor. Notable exceptions are the works by Rouse *et al.* (1991a, 1991b) and Styles *et al.* (1988), where a multi-channel approach facilitated the elimination of all but pedogenic AE. Additionally, the resin and glass fibre composite wave guide described by Nakajima *et al.* (1995) also generated AE actively.

Finally, it is interesting to note that no previous investigation appears to have utilised a control wave guide, except Fisher & Yorke (1964) who employed a 'reference' borehole (section 2.5).

The design of the active wave guide is discussed further in section 6.6.

6.4 Application of Acoustic Emission to Deformation Monitoring

It has been established that the AE is produced by an interaction between the metal of the wave guide and its backfill in response to the deformation of the slope within which it is installed. The wave guide assemblage therefore acts as a large strain-gauge with the deformation of the slope acting as the driving mechanism. From the results presented in the preceding sections it is evident that all wave guide designs are capable of producing a deformation induced emission. However it is equally evident, by considering signal magnitude and the response to the Arlesey

test cuts, that the sand and gravel backfilled wave guides produce the best responses. It can be envisaged that, following some disturbance to the equilibrium, the sand or gravel settles around the metal of the wave guide so generating an emission. It is also reasonable to suggest that, for a uniformly compacted backfill, the emission should initially be of a greater magnitude which gradually reduces with time to zero (as the backfill adjusts to the new equilibrium) unless there is another input from the deforming slope. (Although, in practice this may not be the case as a disturbance may cause the unravelling of voids etc., created when the backfill was first placed around the wave guide). Clearly sand and gravel particles, being hard and rigid, will generate emission of a greater magnitude through frictional contact with the metal wave guide than will the softer, more deformable, clay particles present in grout backfilled and driven wave guides.

There are two distinct applications for the use of AE to monitor the onset of slope instability:-

- As a means of routinely monitoring and measuring the gradual reduction in stability of the slope
- As a means of generating an immediate alarm in response to a severe disturbance to the stability of the slope

The Cowden study demonstrated the potential use of AE in routine monitoring where mean signal value (figure 4.19), standard deviation (figure 4.23 top) and cumulative area under the curve (figure 4.23 bottom) all depicted a generally rising trend, similar to that recorded by the inclinometers. Also, during the period between cuts 5 and 6 at Arlesey where a period of steady deterioration in the stability of the slope has already been identified, it has been demonstrated that the AE also reflects this rising trend; and, in both cases, it is the sand backfilled wave guides which appear to have responded the most appropriately in reflecting this gradual onset of instability. It has to be remembered that, because the interaction between wave guide and backfill (and hence the level of emission) will tend to diminish with time unless there is further input from the destabilising slope, that the level of recorded emission is highly dependent upon *when* the wave guide is monitored. At Cowden, for example, wave guides were generally read once a week. However the results in this respect are still promising but it is still (presently) a

purely qualitative indicator and quantification of the signal is beyond the scope of this investigation.

The Arlesey study demonstrates the way in which AE is capable of delivering an immediate response to sudden and severe changes in the stability of the slope. Section 5.6.4 has already looked at the relationship between the times of the AE response and the cuts where it was shown that, particularly for the first two cuts, there tended to be an immediate high response which gradually returned to background noise levels. This behaviour is consistent with the active wave guide model already described. In fact, for wave guide 2 (sand backfill), much higher levels of AE were recorded some 14 minutes *prior* to the first cut being made. This apparent anomaly can be explained by the presence of the excavator moving around at the base of the slope and provides a clue to one mechanism responsible for the generation of AE. In fact, it is suggested that low frequency vibrations generated by the excavator have propagated through the soil and disturbed the backfill causing some settlement (and therefore emission) to occur. This would also explain how the Arlesey control wave guide, some 16 metres away from the slope face, had also apparently suffered deformation. The diminished AE responses to cuts 2 and 3 can also be explained by this in conjunction with the active wave guide model. If vibration has caused settlement to occur around a wave guide then the capacity for further settlement has obviously been reduced. As a result, therefore, it is only AE captured *as* the early test cuts were being made (or immediately afterwards) that is likely to have been influenced by this vibration-induced settlement.

6.5 Data Processing Technique

Various data processing techniques are available but (as demonstrated) some appear to be better at distinguishing between periods of perceived activity and inactivity than others. Alternative processing techniques do, however, allow the same data to be viewed from a different perspective which, in turn, permits deductions to be made concerning the mechanism of AE generation.

Figures 6.1 - 6.4 depict the mean and standard deviation of both the bulk and post-threshold data for wave guides 1 and 2. It is evident that the mean signal value of the bulk data (figure 6.1) produces the poorest response but, nevertheless, there are still three very large peaks following

cuts 4 and 5. These values are calculated as the arithmetic mean of all 900,000 data points within a data set and, as a small number of genuine emission would fail to have much effect on the mean value, their relatively high magnitude clearly indicate a period of longer, more sustained activity. There is also a general contrast between the responses derived by the bulk and post-threshold analysis techniques. The bulk analyses (figures 6.1 & 6.2) produce a response profile which tends to increase across the test period cut 1 to cut 5, whereas the post-threshold analyses (figures 6.3 & 6.4) produce a response profile which tends to decrease across the same period. The post-threshold analyses also tend to produce distinctive responses to cut 6. (The post-threshold analyses are performed on data greater than or equal to 0.11 volts but this takes no account of the *number* of data points which fall into this category).

Calculation of the mean signal value of the post-threshold data (figure 6.3) produces a number of distinct peaks in response to the early test cuts which are indeterminable or non-existent from calculation of the bulk mean value (figure 6.1). This clearly indicates that the early test data contains a relatively small number of high value data points as opposed to the later test data which consists of a relatively large number of smaller magnitude data points.

6.6 Summary of Field Acoustic Emission Results

The relationship between the time of the response to the time of an Arlesey test cut has already been discussed in section 5.6.4 where it was demonstrated that this aspect also exhibited a change in nature across the test period. It should be appreciated, although only *one* mechanism (i.e. wave guide - backfill interaction) has been identified as being responsible for the generation of AE, that more than one mechanism may be responsible for creating such an interaction in the first place. If the findings of Chapters 4, 5 and 6 are combined then this produces a final descriptive model in which the AE response can be broadly grouped into two categories. These, together with a summary of the evidence for each, are as follows:-

- (a) Initial responses to early cuts which are possibly caused by vibrations from the excavator propagating through the soil but which could equally well have been caused by any sudden and major disturbance to the equilibrium of the slope. The emission tends to consist of intermittent bursts of relatively high value data immediately following a cut but only lasts for a limited period of time. It is likely that the emission is generated by the backfill settling around the metal

of the wave guide and so capacity for generation of this type of emission is limited. *Evidence: low mean value (bulk data), high mean value (post-threshold data), small number of post-threshold data points, close association of emission with an Arlesey test cut, tendency of emission to return to background noise levels relatively quickly.*

(b) Responses to later cuts and to slow natural degradation processes. The emission tends to consist of more sustained, relatively low value data and does not immediately follow a particular cut (Arlesey). *Evidence: high mean value (bulk data), low mean value (post-threshold data), high number of post-threshold data points, emission not immediately associated with a particular Arlesey test cut.*

The evidence from Cowden suggests that sand backfilled wave guides are more suited to conditions where there is a slow and gradual degradation in the stability of the slope. Although it is not clear from the Arlesey study there is some evidence to support this (see figure 6.4 where the dominant response across cuts 4 and 5 is given by wave guide 2). However it is evident that the best response to the early test cuts is generally provided by wave guide 1 (gravel backfill).

Figure 6.5 is an alternative look at the Arlesey data. This plots the average number of post-threshold data points per event against the total number of post-threshold data points and the numbers written beside some of the plotted data refer to the test cuts preceding their acquisition. (An event is defined as any number, including one, of consecutive data points greater than, or equal to, the threshold of 0.11 volts). The plot appears to separate out into two limbs. As is seen the upper limb (which is an extension of the majority of the data) consists mainly of data related to the earlier cuts whereas the lower limb consists of data mainly associated with later cuts. This is a very interesting result as it implies that, by collecting a specific number of post-threshold data points, it is possible to distinguish between the two proposed different causes of disturbance to the wave guide backfill by calculating the number of events within which the data points are contained. Essentially this is a simple measure of event magnitude, expressed in terms of the number of constituent data points in the event.

Figure 6.6 plots the same data as in figure 6.5 but in the form of number of events as a function of the number of post-threshold data points (plotted as \log_{10}). Although not as defined as figure 6.5, it is evident that the data plot onto two distinct gradients. The lower line, formed of responses to earlier test cuts, implies events consisting of (relatively) large numbers of data

points while the upper line, formed of responses to later test cuts, implies events consisting of (relatively) small numbers of data points.

Figure 6.7 shows the results of performing a similar calculation (as in figure 6.5) on fifty-one standard data sets (180,000 data points) captured at Cowden and it is evident that the points all follow a similar trend. Considering that the emission at Cowden is likely to have been generated in response to natural degradation of the slope (a single mechanism) this result is consistent with Arlesey. However it should be noted that the Arlesey sample is much bigger (900,000 data points) and the 0.11 volt threshold used for Arlesey compares with a 0.05 volt threshold used for the Cowden data. (Compare the scales of figures 6.5 and 6.7)

In fact an attempt at a direct comparison of the Arlesey and Cowden data can be made by multiplying the number of post-threshold data points acquired at Cowden by a factor of five. This has the effect of increasing the Cowden sample size of 180,000 data points to 900,000. However, the *average number of data points per event* will remain unchanged if, as is assumed, the original sample of 180,000 data points is a representative sample. This, therefore, merely has the effect of moving the Cowden data along the x-axis away from the origin. A plot, illustrating both the Arlesey and adjusted Cowden data, is shown in figure 6.8 from which it is seen that there is a reasonably good correlation between the Cowden data and the lower limb of that acquired from Arlesey.

The discrepancy in the value of the thresholds (mentioned above) reflects a general difference in the magnitudes of the emission captured from both sites. This is illustrated in figure 6.9 which plots the mean signal values of the control wave guides from both Cowden (wave guide 12) and Arlesey (wave guide 7). There is no apparent reason why this variance in the signal levels should exist. Airborne background noise has already been discounted and constructional noise should be consistent. In fact, pre-test noise levels at Arlesey should, if anything, be less than those at Cowden but, although this is true for two data points, the majority of the Arlesey magnitudes are much greater. It could be explained by a change in the sensitivity of the electrical system. However there is no evidence to suggest that any such change occurred part way through either the Cowden or Arlesey tests despite both lasting approximately six months; so there is no reason to suspect that it should change between tests. Note that the disparity in the number of bar graphs in figure 6.9 (between Arlesey and Cowden) reflects the difference in the number of data sets acquired from each control wave guide.

The results from Arlesey suggest that a gravel backfilled wave guide would best fulfil the role of delivering an immediate response to a sudden disturbance in the stability of the slope. This is because it appears to generate a (relatively) high magnitude emission of short duration (when compared to a sand backfilled wave guide). At Cowden, where deformation (due to natural processes) occurred at relatively slow but progressive rates, the sand backfill proved the most productive. However, this is probably because the sand backfill remained 'disturbed' and therefore emissive for a longer period of time. The gravel backfill may have produced high magnitude emission which went undetected because, as monitoring consisted of a three minute acquisition once a week, the operator simply was not there to capture it. This contrasts with the findings of the Arlesey test, where the monitoring routine was planned in conjunction with the cuts to the slope, which resulted in a better apparent response from the gravel backfilled wave guide.

Figure 6.10 depicts amplitude distributions of the event mean magnitude for wave guides 1 and 2 obtained from AE files acquired both immediately following cut 1 (day X1) and the day after cut 5 (day X7). It is evident that larger magnitude data were recorded from both wave guides in response to cut 1 than were recorded during the day following cut 5. However, it is also evident that much greater numbers of data were recorded during day X7 than were recorded following cut 1. This processing technique merely serves to emphasise much of what has already been determined and does not appear to reveal anything new. (i.e. there is no difference between the amplitude distributions of events captured in response to early test cuts and those captured in response to later test cuts).

It is envisaged that a practical AE system would need to monitor continuously and it must be recognised that this represents a significant departure from the monitoring philosophy employed in this investigation. However, it is possible to identify certain characteristics of an active wave guide system. It should generate emission in response to deformation either by a wave guide - backfill interaction (this investigation) or by some other mechanism (e.g. Nakajima *et al.* 1995). It has been demonstrated that the mineralogy and the particle size of the backfill affects the nature of the active AE and it is likely that the density to which it is compacted will affect it also. Finally, relatively high frequency bandwidths should be examined in order to reduce and minimise the effects of pedogenic AE and background noise. Active wave guide design is, therefore, based on a consideration of wave guide material, particle mineralogy and particle size (distribution) of backfill, density of backfill and monitoring frequency. (Note that the

performance of an active wave guide is also dependent upon the positioning of the wave guide relative to any zone of deformation). Using these parameters it is anticipated that wave guides can be designed to either (a) continuously monitor the onset of progressive failure or (b) to remain non-emissive until a disturbance of a sufficient (and predetermined) magnitude occurs.

The findings also suggest that it is possible to dispense with the need for a control wave guide. This has important implications because it means that a section of slope (such as a coastal cliff section or railway embankment etc.) can be instrumented with a line of active wave guides, each of which is monitored continuously by dedicated circuitry, and each of which is capable of generating an alarm to a remote monitoring station. Any one of the processing techniques considered could be utilised as an alarm . As an example, a potentially useful trigger is provided by a comparison of 'bulk' and post-threshold data standard deviations (figure 6.11) where it is seen that in the pre-test period the signals are coincident but diverge in the test period. (In fact, the standard deviation tends to offer the larger voltage ranges while root mean square offers the higher voltages).

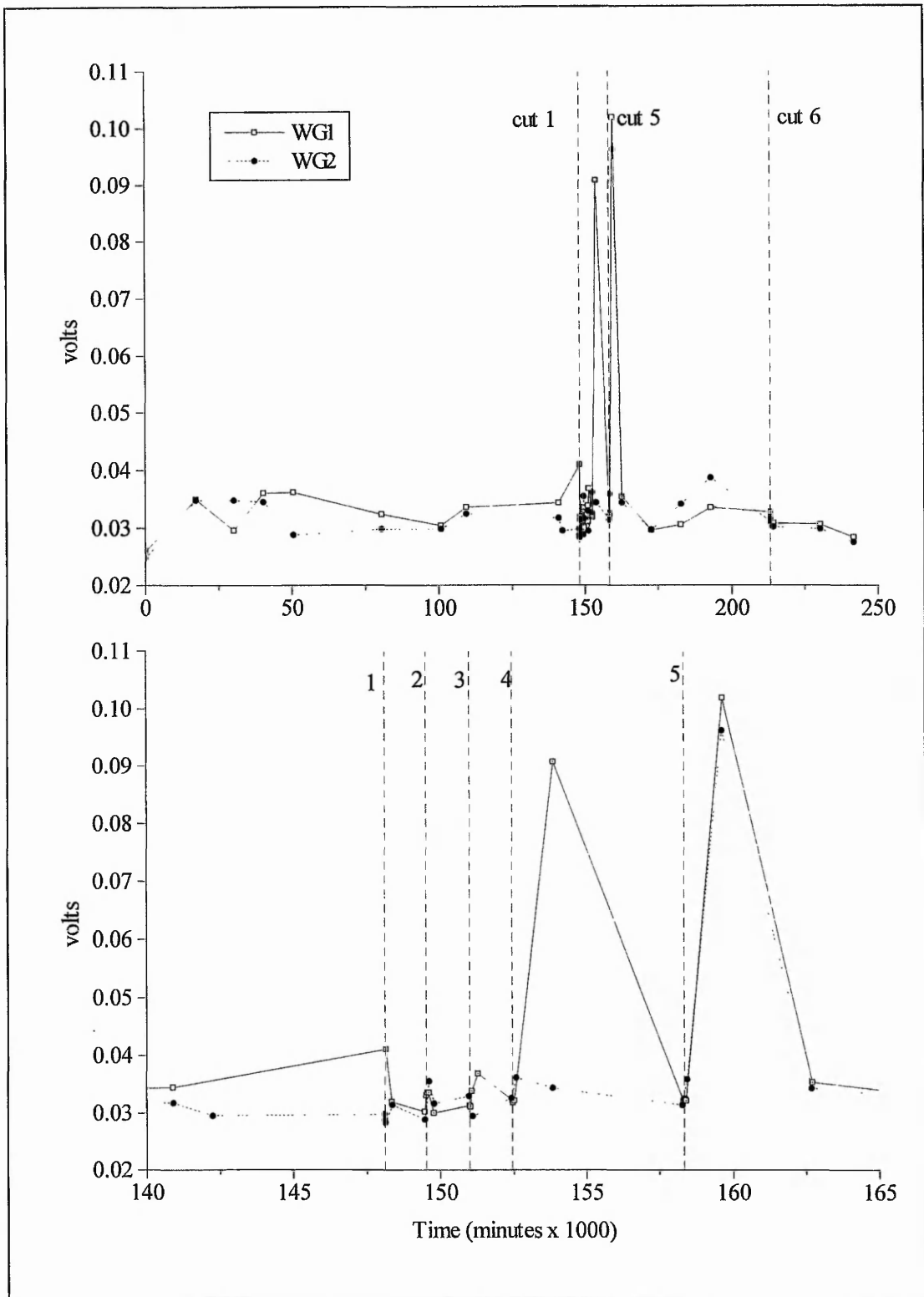


Figure 6.1 Arlesy AE mean signal values bulk data WGs 1 & 2. The upper plot illustrates the entire test period and indicates cuts 1, 5 & 6. The lower plot focuses on the main test period and indicates cuts 1, 2, 3, 4 & 5.

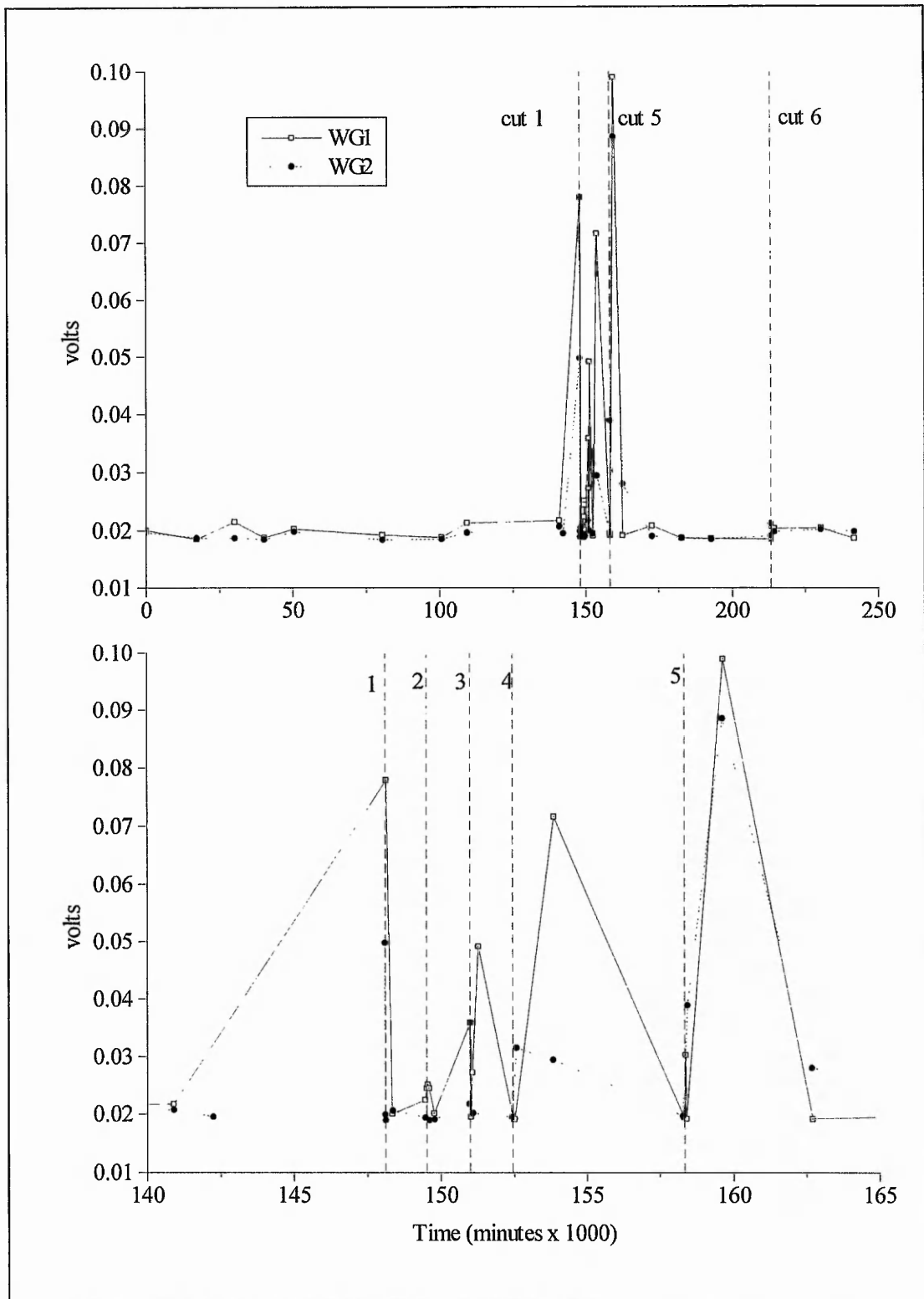


Figure 6.2 Arlesey AE standard deviation bulk data WGs 1 & 2. The upper plot illustrates the entire test period and indicates cuts 1, 5 & 6. The lower plot focuses on the main test period and indicates cuts 1, 2, 3, 4 & 5.

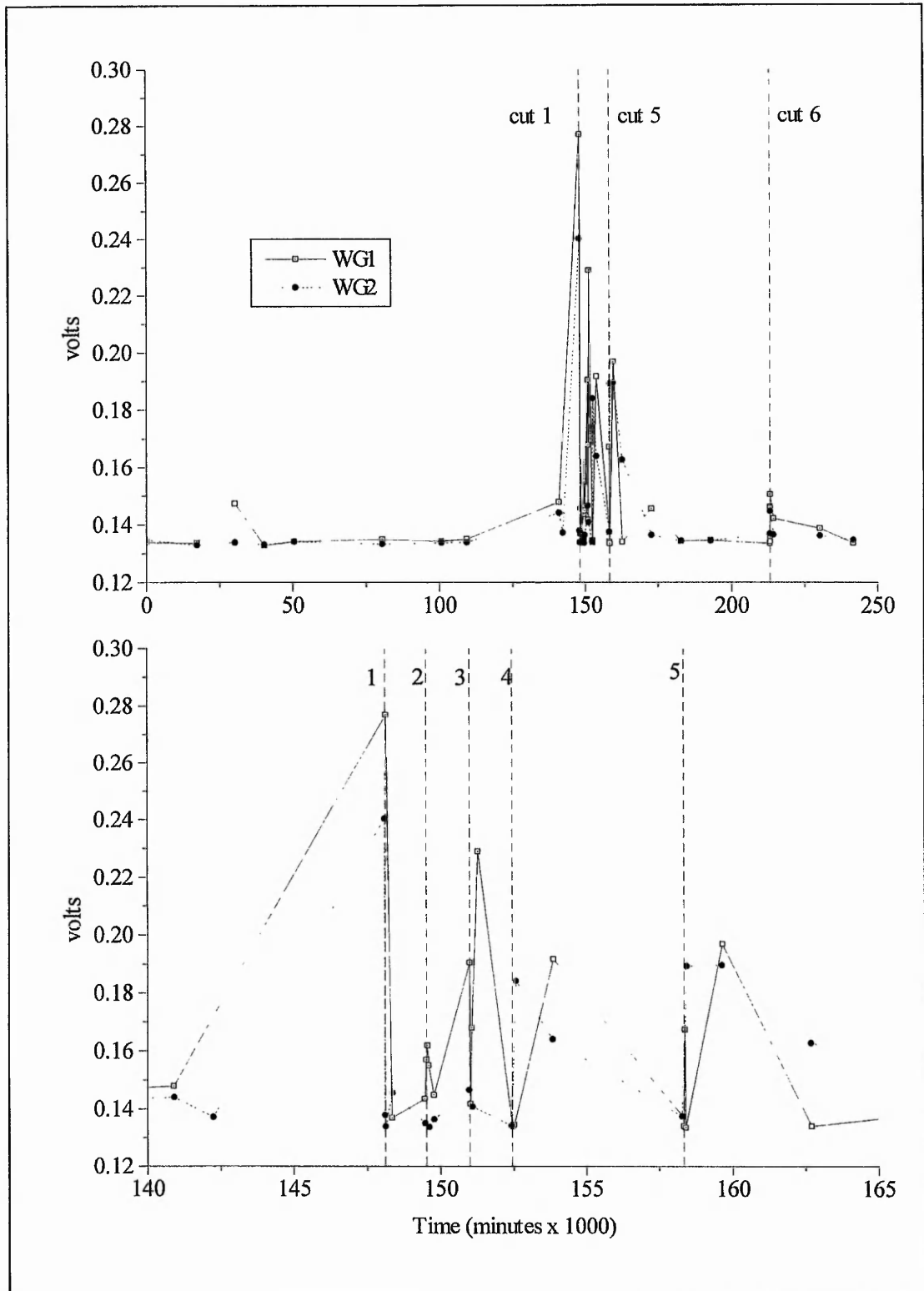


Figure 6.3 Arlesley AE mean signal values post-threshold WGs 1 & 2. The upper plot illustrates the entire test period and indicates cuts 1, 5 & 6. The lower plot focuses on the main test period and indicates cuts 1, 2, 3, 4 & 5.

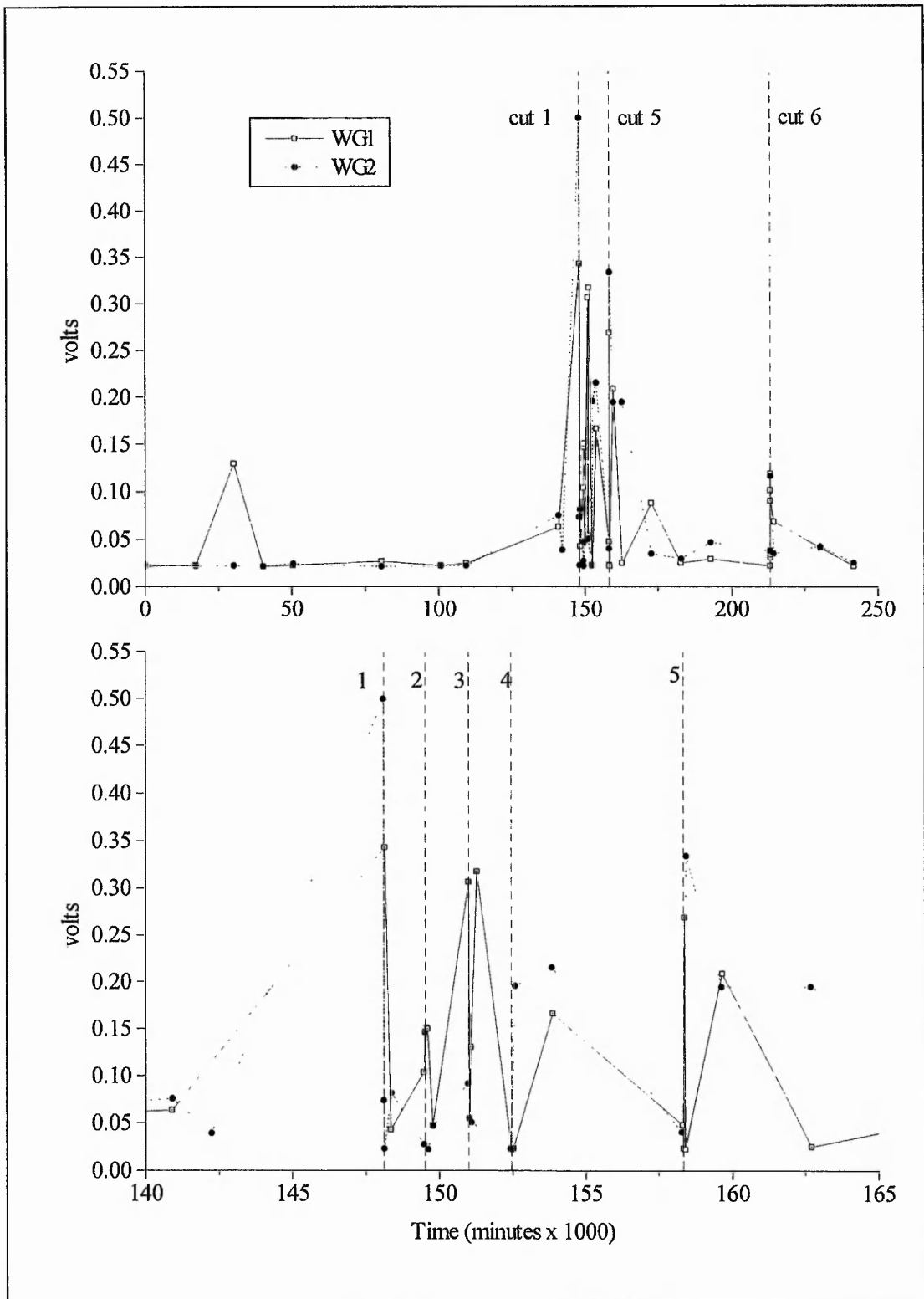


Figure 6.4 Arlesley AE standard deviation post-threshold WGs 1 & 2. The upper plot illustrates the entire test period and indicates cuts 1, 5 & 6. The lower plot focuses on the main test period and indicates cuts 1, 2, 3, 4 & 5.

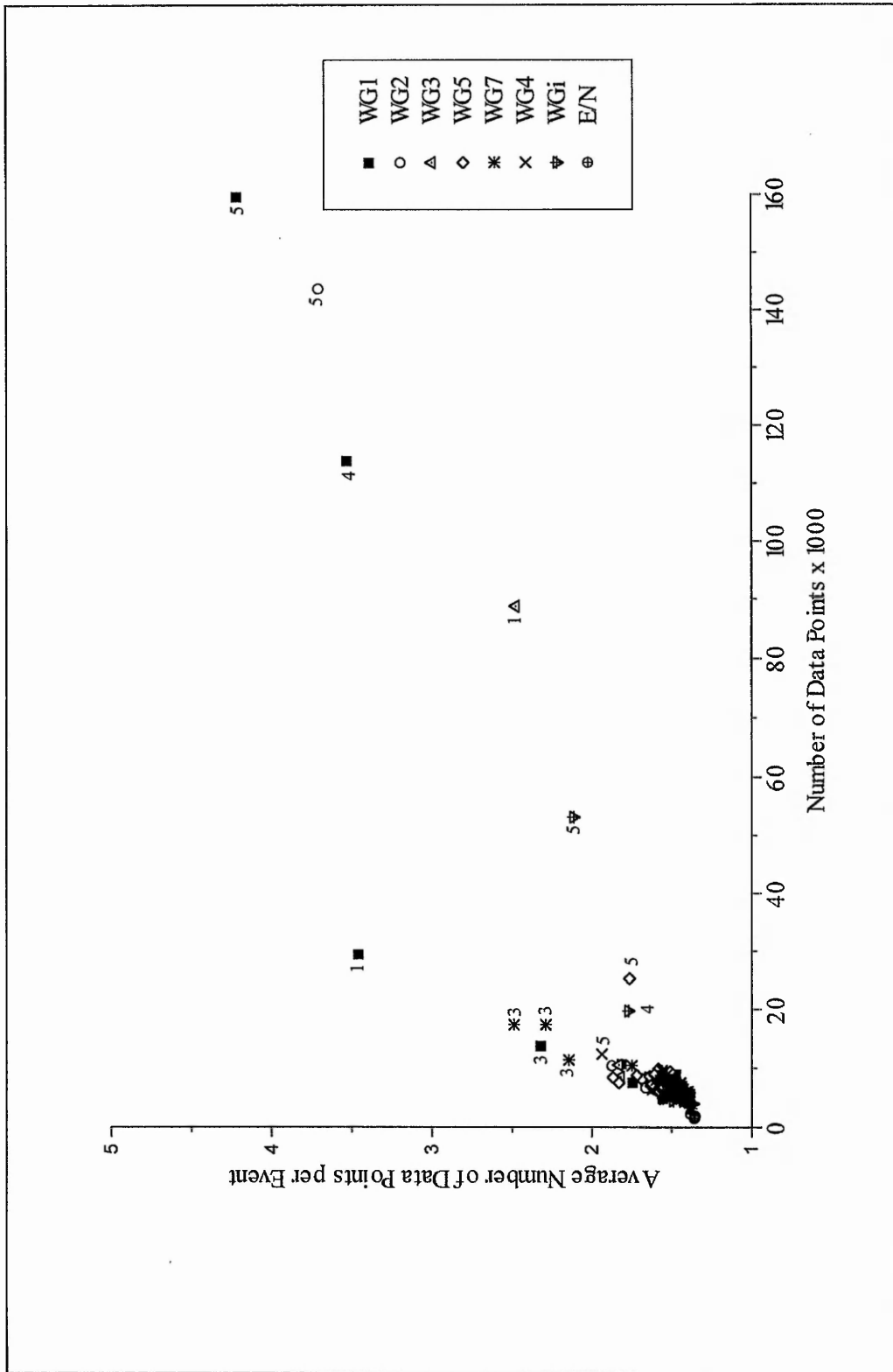


Figure 6.5 Arlesey number of post-threshold data points per event as a function of number of post-threshold data points - all WGs

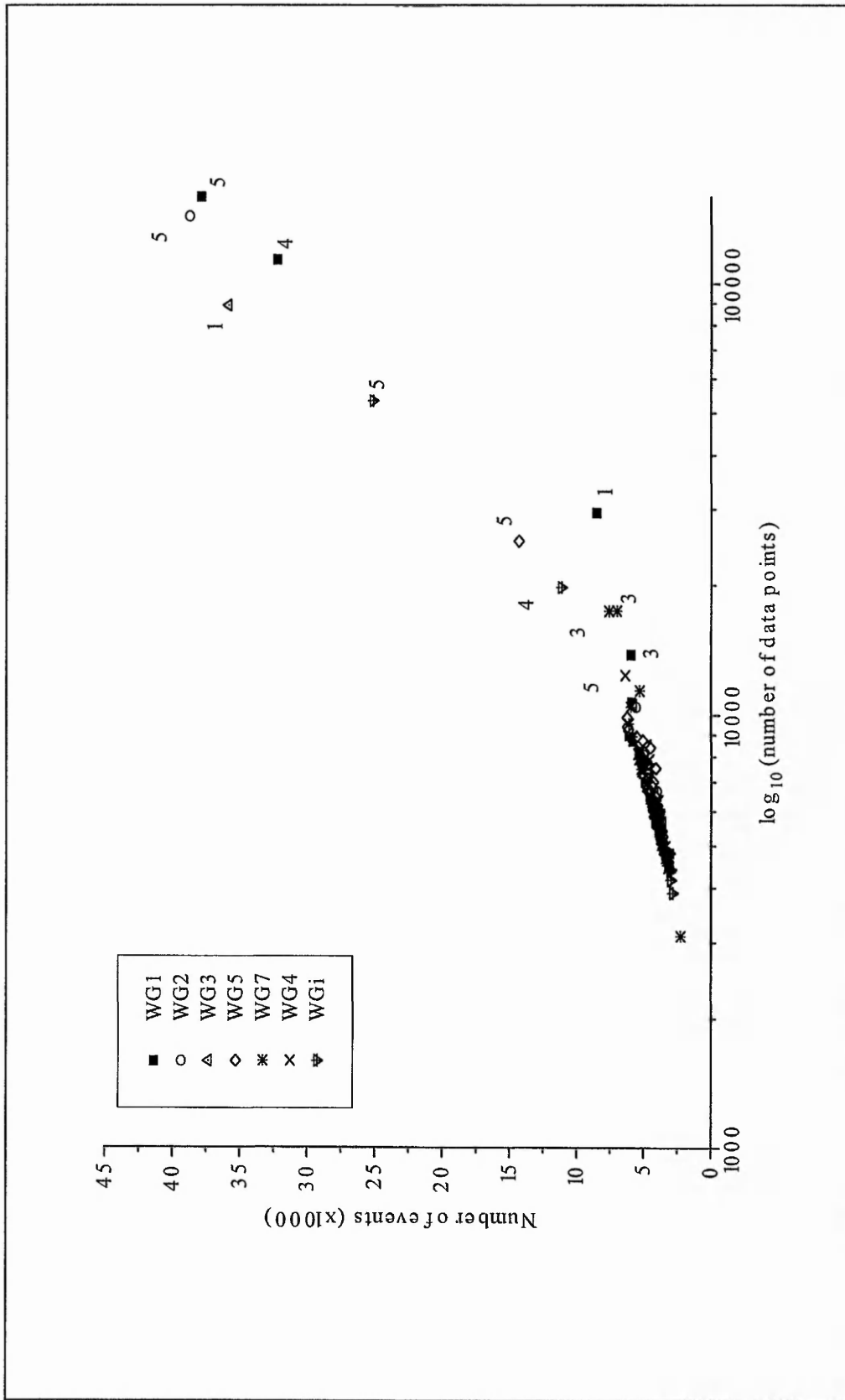


Figure 6.6 Arlesey number of events as a function of log₁₀ of number of data points - all WGs

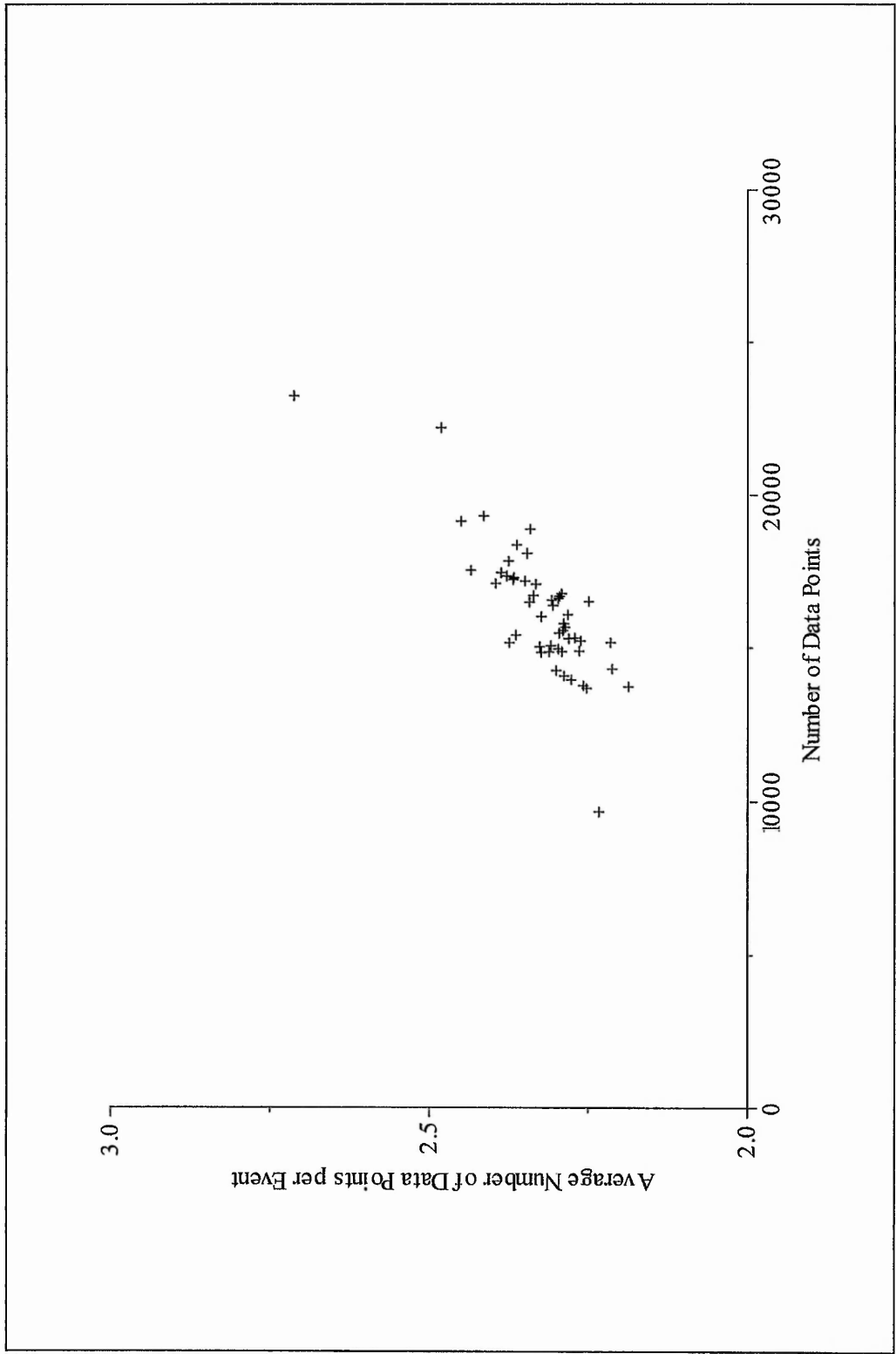


Figure 6.7 Cowden no. of post-threshold data points per event against number of post-threshold data points - all WGs

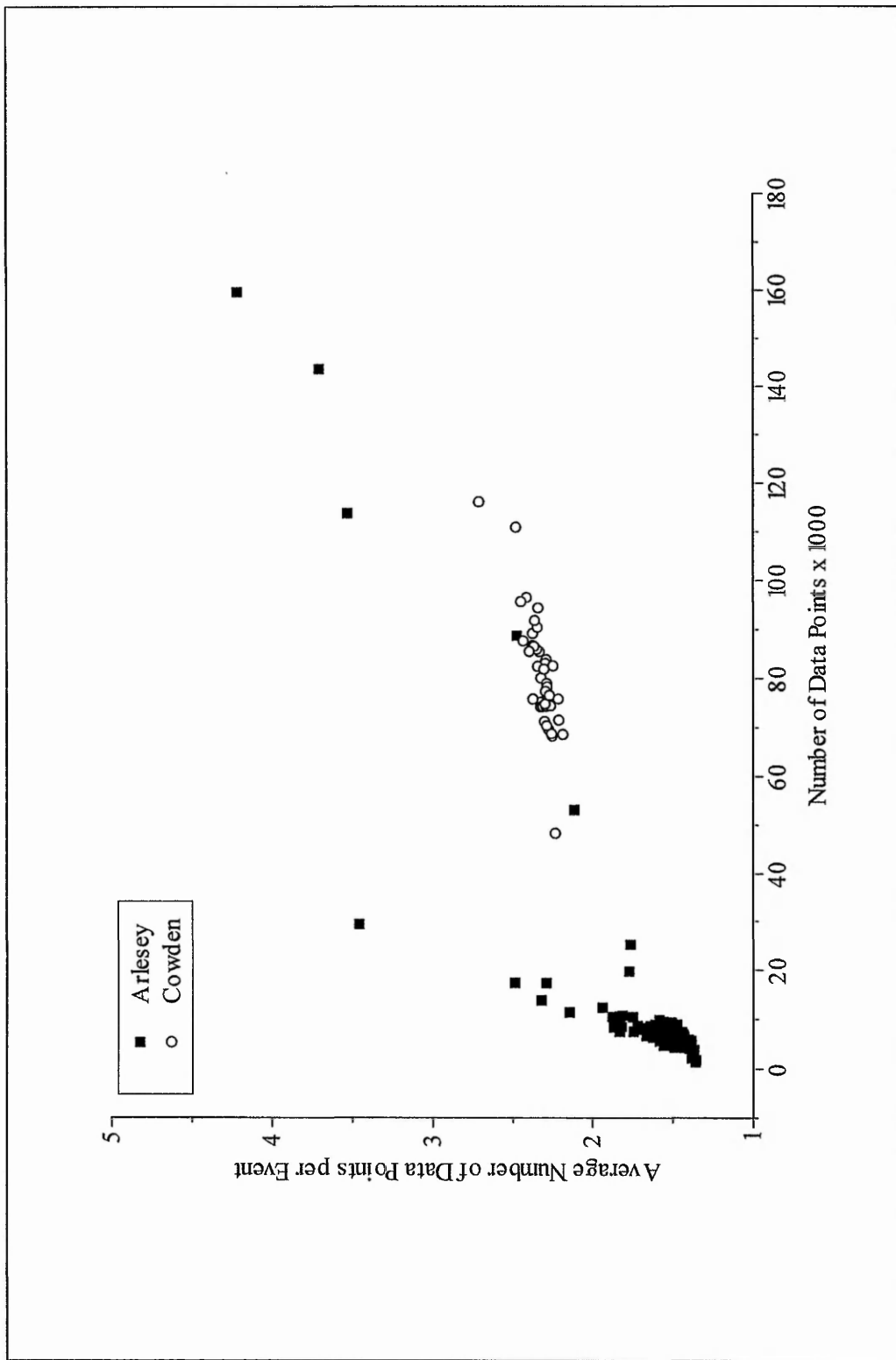


Figure 6.8 Arlesey & Cowden no. of post-threshold data points per event against number of post-threshold data points - all WGs

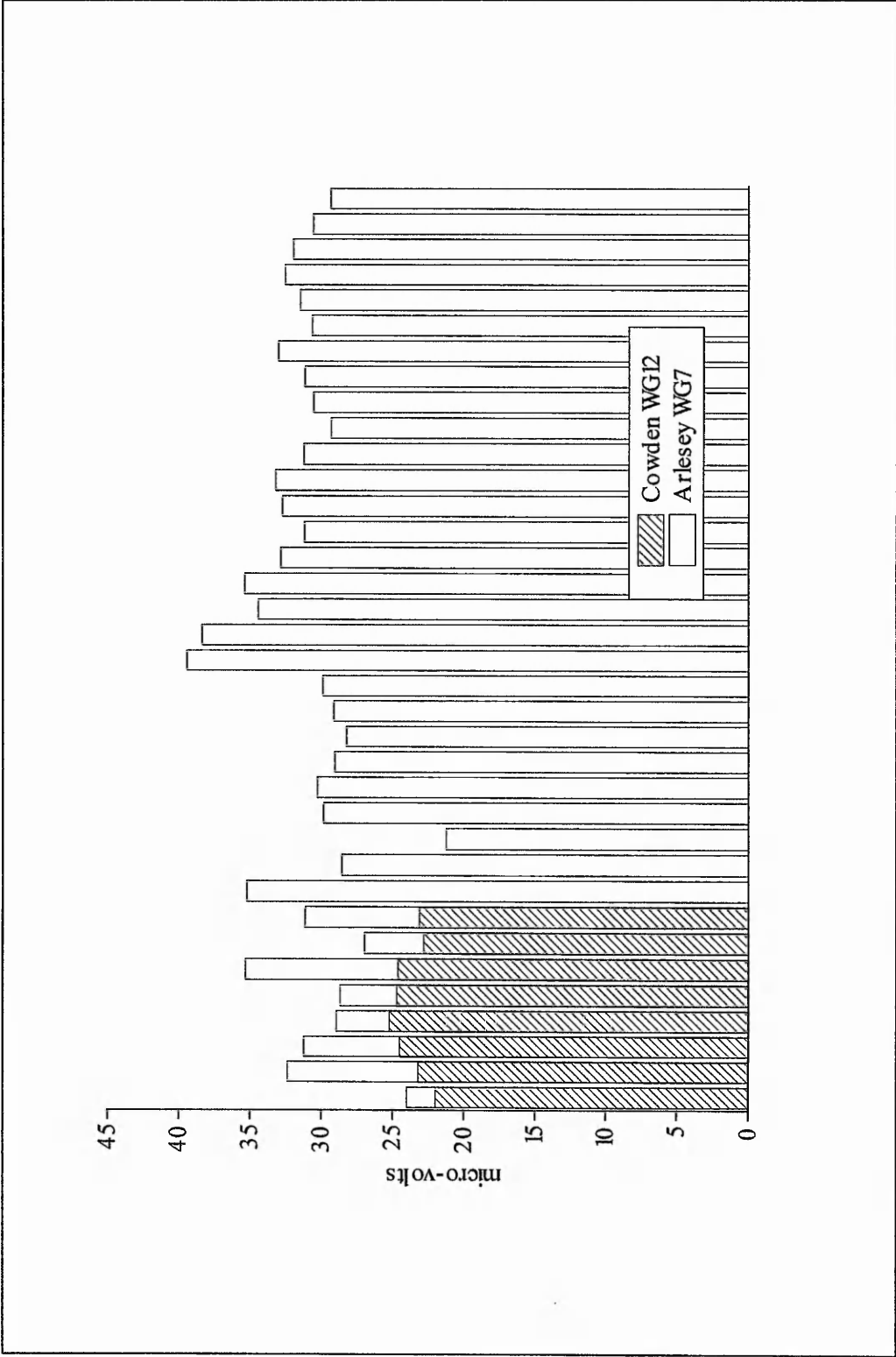


Figure 6.9 Comparison of control WGs Arleseey (WG7) & Cowden (WG12) mean signal values bulk data

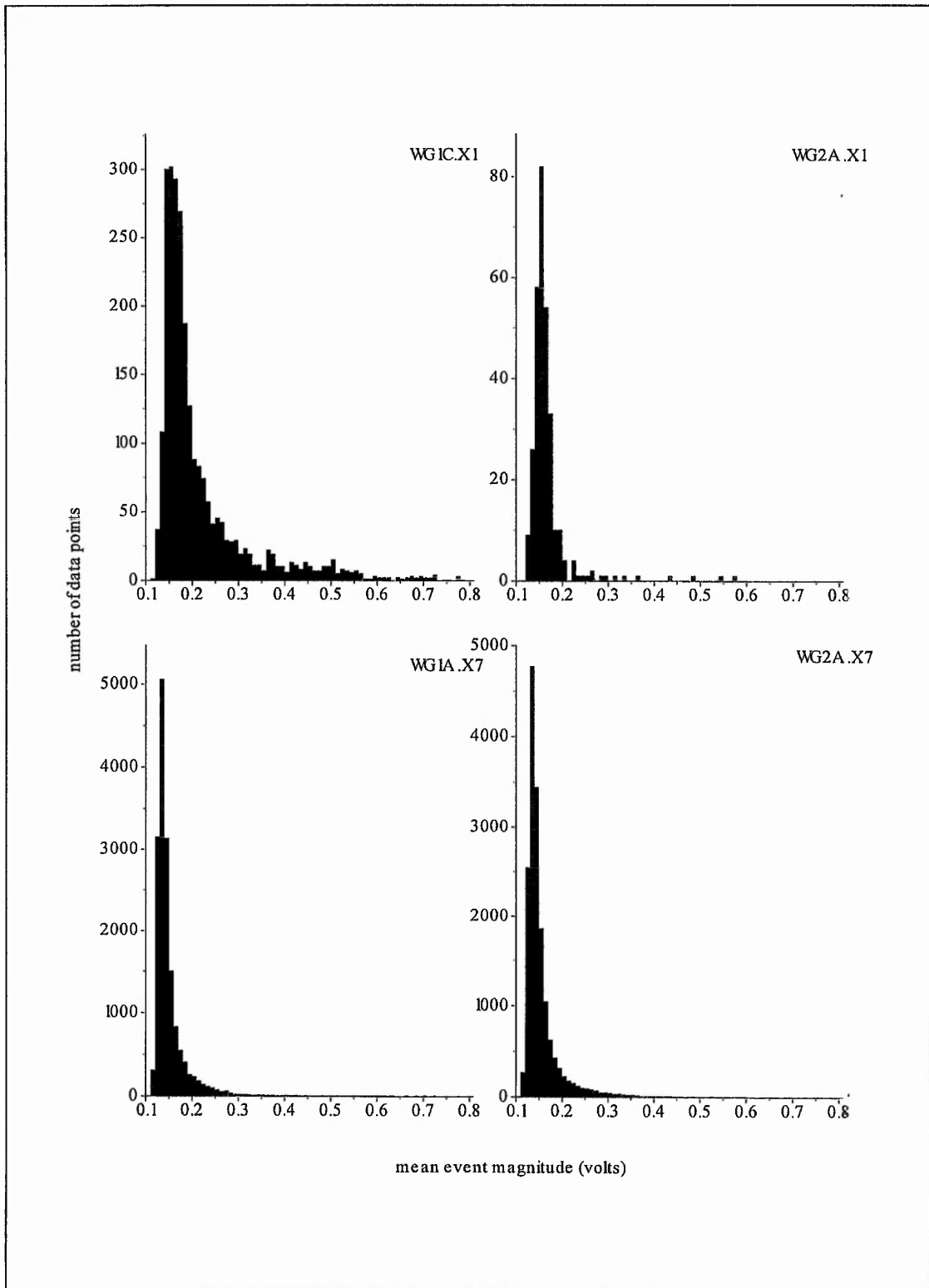


Figure 6.10 Event mean magnitude distributions for WGs 1 & 2 following days X1 & X7

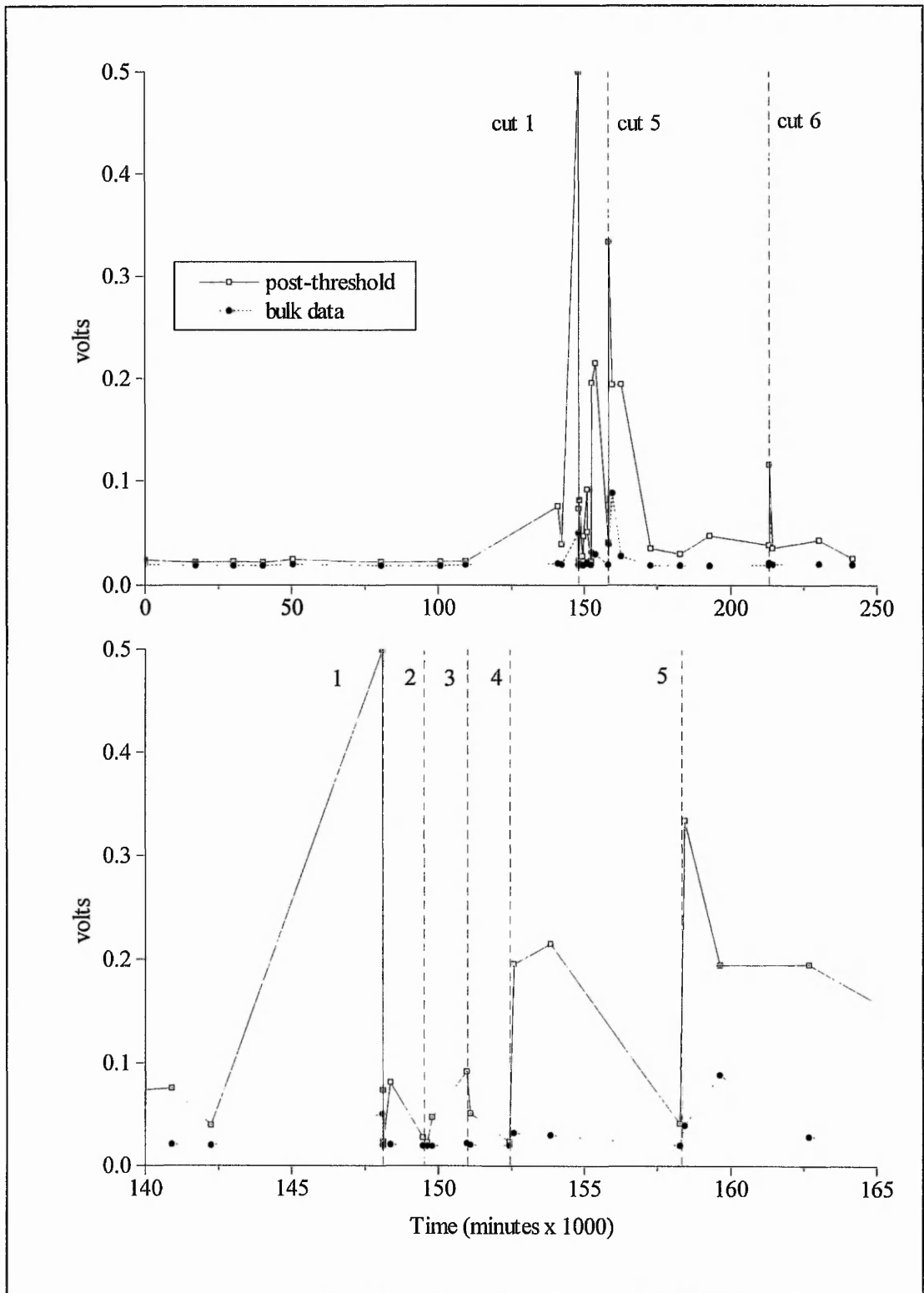


Figure 6.11 Arlesey AE standard deviation bulk & post-threshold data WG2. The upper plot illustrates the entire test period and indicates cuts 1, 5 & 6. The lower plot focuses on the main test period and indicates cuts 1, 2, 3, 4 & 5.

Chapter 7

The Laboratory Test Programme

7.1 Introduction

This chapter presents the results of a series of laboratory based experiments which attempt to explore the relationship between the deformation characteristics of a body of soil and the generated acoustic emission. The bulk of the programme involved the testing to failure of a number of soil types in triaxial compression at various cell pressures and under different drainage conditions. Section 7.2 describes the triaxial test apparatus, how it operated and how it interfaced with the AE capture system. Section 7.3 details the software components which drove and monitored the system. Section 7.4 deals with the test soils used and section 7.5 outlines the triaxial test procedure.

Consolidation tests (using the triaxial test apparatus) were also conducted in an attempt to demonstrate the *Kaiser effect* and the test procedure is dealt with in section 7.6. Additionally a number of 'box' tests have been carried out, in which it is attempted to replicate the perceived role of the wave guide (section 6.3) in the laboratory and these are described in section 7.7.

The results are presented and discussed in sections 7.8, 7.9, 7.10 and 7.11 before the main findings are summarised in section 7.12.

It should be appreciated at the outset that this investigation has been primarily concerned with field generated acoustic emission and, as such, the monitoring system employed has reflected this.

7.2 Triaxial Test Apparatus

7.2.1 The Acoustic Emission Triaxial Testing System

The AE capture system was identical to that described in section 3.2 with the exception that the DacPac was powered directly from a mains supply rather than using its own internal battery. A schematic of the monitoring system described in section 3.2 is shown as the lower half of figure 7.1 and the additional equipment required to conduct the compression tests is shown as the upper half of figure 7.1. This additional equipment comprised a Bishop and Wesley triaxial cell (figure 7.2), two GDS *digital controllers* (figure 7.3 depicts a digital controller) and another computer hereinafter referred to as the 'PC' in order to distinguish it from the notebook.

As the upper half of figure 7.1 indicates, a special base pedestal unit (constructed at The Nottingham Trent University) contained an AET 30kHz transducer (section 3.2.1) and the position of the transducer is also shown within the monitoring system in the lower half of figure 7.1 (in order to demonstrate how the two elements of the triaxial testing equipment combined).

A full description of the construction and use of the triaxial cell is given by Bishop and Wesley (1975). Menzies (1988) describes a system similar to that employed in this investigation whereby a Bishop and Wesley triaxial cell is driven by computer controlled digital controllers. As these two papers detail the design and operation of each system component, only a brief summary will be presented here.

Figure 7.2 depicts a schematic layout of the triaxial cell, in which a sample of soil was placed upon a piston which was capable of moving both upwards and downwards within the cell. Motion of the piston was effected by the hydraulic actuator connected to the pressure chamber and the cell pressure was generated and maintained by the hydraulic actuator connected to the cell (figures 7.1 and 7.3). As the piston was moved upwards the sample of soil was 'squeezed', generating both axial deformation and fluid pressure in the lower (pressure) chamber. The lower chamber pressure was recorded by the hydraulic actuator which, in turn, was read by the PC. This value was used to calculate the deviator stress, as shown in section 7.2.2. (An hydraulic actuator is a precision instrument which determines changes in the volume and pressure of a reservoir of fluid). The specific testing procedure used in this investigation is detailed in section 7.5.2.

7.2.2 Relationship between the Principal Stresses and the Lower Chamber Pressure

The relationship between the lower chamber pressure and the principal stresses acting on the soil sample is obtained by considering the static equilibrium of the cell and is expressed in the following equation, the derivation of which is given by Bishop and Wesley (1975):-

$$pa = \sigma_a A + \sigma_r (a - A) + Mg$$

where	p	Lower Chamber Pressure
	σ_a	Axial Stress
	σ_r	Radial Stress or Cell Pressure
	a	Bellofram Seal Area = 2,940mm ²
	A	Current Sample Cross-Sectional Area
	M	Mass of Piston and Sample
	g	Acceleration due to gravity (9.81 ms ⁻²)

Thus at any point in a test, and assuming that the sample deforms as a right regular cylinder, an equilibrium exists between the pressure in the lower chamber cell, the axial stress in the sample and the cell pressure acting over the balance of the *bellofram* seal area. The combined weight of the piston and sample is also included but, as its magnitude and the increase in magnitude it causes in the lower chamber pressure are both constant, its value can be regarded as zero providing that its effect on the lower chamber pressure is deducted. Once the lower chamber pressure has been determined (at a given strain), therefore, the axial and deviator stresses may be calculated.

7.2.3 Axial Strain Generation

As mentioned in section 7.2.1, the soil sample was 'squeezed' within the cell when fluid was pumped into the lower chamber by a hydraulic actuator. In fact, because the lower chamber effectively consisted of a cylinder of cross-sectional area 2,940mm², the magnitude of vertical strain (in mm) is simply calculated as the result of dividing the expelled volume (in mm³) by 2,940. This aspect was controlled by the 'PC' using specialist software written in 'HT BASIC'. Only two input parameters, the *target volume* and the *step*, were required. The target volume, input in mm³, controlled the maximum extent of the strain and the step, input in ms mm⁻¹,

controlled the rate of strain. Specific values of the input parameters are discussed in section 7.3.2.

7.2.4 Axial Ram Friction

As the piston (or ram) was driven upwards generating axial strain within the soil sample, friction, which opposed the motion of the ram, was also developed. As any frictional resistance would cause the pressure in the lower chamber to increase, it was necessary to determine its magnitude. This was achieved by driving the piston, without a soil sample and without filling the cell, both upwards and then downwards and recording the pressure reading in the lower chamber at the end of travel. With no cell pressure and no axial stress, but allowing for frictional resistance to upward motion of the piston (F), the equation given in section 7.2.2 can be rewritten as follows:-

$$p_1 a = Mg + F$$

However, for downward motion, this equation can be written:-

$$p_2 a = Mg - F$$

As the weight of the ram must be the same in both cases it is possible to rearrange and rewrite these equations as follows:-

$$p_1 a - F = p_2 a + F$$

$$2F = p_1 a - p_2 a$$

or, more simply

$$F = (p_1 - p_2)a/2$$

The bellofram seal area, a , is omitted from the final form of the equation in order to simplify it. This has the effect of expressing friction in the units of kPa.

A series of tests was conducted, forcing the ram to travel a variety of distances in both directions, to establish the magnitude of the friction. These results are presented in table 7.1.

As only compression tests were conducted it is the values for friction in the upward direction which are of primary importance but even these are considered acceptable enough to render consideration of friction unnecessary. It should also be noted that the magnitudes of ram travel quoted in table 7.1 are after the ram had already been raised through 3.4mm. This is because it was discovered that developed friction recorded much higher values when the ram was operated from the base of the lower chamber.

7.3 Computer Interface with Triaxial Tests

7.3.1 Standard Laboratory Acoustic Emission Monitoring Routine

As the A-to-D board (section 3.2.5) was incapable of triggering on the event it was essential to acquire as large a sample as possible and, for the laboratory tests, this constituted the major constraint (section 3.4). Some 72MB of hard disc space was available for data and this limited the volume acquired during a single test to a maximum of 18,000,000 samples. It was also necessary to fully process the data set and remove it from the hard disc before another test could be conducted.

The boards inability to trigger on the event and the restricted available hard disc space also made it desirable to condense the time period over which the test was conducted. This is because, for a fixed volume of disc space available for data storage, a reduction in the length of the test effectively increases the percentage size of the sample. For example, the standard test lasted fifteen minutes and, with total space available for 18,000,000 samples, this equates to a sample rate of 20,000 samples per second. Acquiring data at the board's maximum rate of 100kHz means that, by the end of the test, a sample representing 20% of the total data available had been captured. Had the tests lasted for, say, one hour then the equivalent figures would have been 5,000 samples per second and a 5% sample of the total available data. Clearly it is preferable to obtain as large a sample as possible. However, it is also desirable to lengthen the test in order to reduce the rate of strain to better reflect genuine field strain rates. This resulted in the

compromise standard test length of fifteen minutes which equated to a strain rate of 1.33mm per minute.

It is obviously necessary to relate the generated AE to the state of strain of the soil sample and this made it necessary to acquire the data in *real time*. This was not obligatory at either Cowden or Arlesey and, owing to the relatively small sample sizes, would not have been a problem anyway. However, in the laboratory tests, it necessitated the activation, in Viewdac, of the *Check Schedule Tolerance* toggle button and the input of a *latency* of 100 milli-seconds. This was a 'fail-safe' device which ensured that the data was acquired on-time (as specified in the capture routine), subject to a tolerance of 1/10 of a second. If the routine had failed to cope then an error was generated and the acquisition stopped.

7.3.2 Triaxial Cell Control and Monitoring

As mentioned in section 7.3.1, the duration of a standard triaxial test was adopted as fifteen minutes. It was also decided to shear all samples by 20% of their original length and, as samples were originally 100mm in length (section 7.5.1), this determined a ram movement of 20mm. The two 'PC' input parameters were, therefore, calculated as follows:-

Target Volume = $2,940 \times 20 = 58,800\text{mm}^3$ which is input as a negative value to instruct the hydraulic actuator that it is to expel that volume of water (into the lower chamber).

Step = $15 \times 60 \times 1000 / 58800 = 15$ milli-seconds per mm^3 (to the nearest integer).

The Laboratory *standard AE monitoring routine* can be summarised as follows:-

- The AE data consisted of 10,000 envelope waveform data points collected at a 100kHz data sampling rate, every one-half second for fifteen minutes - i.e. a 20% sample resulting in a file consisting of 18,000,000 data points (72MB) or 180 seconds of data
- Total signal amplification of 92dB (x 39,811)
- Unipolar acquisition of signal envelope
- A standard triaxial test which involved straining a sample by 20% over a fifteen minute period (equivalent strain rate 1.33mm per minute)
- Threshold applied post-capture during data processing of 2.5V (triaxial shear tests conducted on sands), 0.32V (triaxial shear tests conducted on clays) and 0.5V (box tests)

7.4 Test Soils

The main test soils used in this part of the investigation were three sands, whose particle size distribution (PSD) curves are shown in figure 7.4. The sands are identified as 'Red' (because of its colour), 'Arlesey' (because it was used as the wave guide backfill at Arlesey) and Leighton Buzzard (a standard laboratory testing soil). Table 7.2 presents values (based on the PSD curves) for D_{10} , D_{60} , and C_u . D_{10} is defined as the largest particle size of the smallest 10% of the sample, D_{60} as the largest particle size of the smallest 60% and C_u (called the uniformity coefficient) as D_{10}/D_{60} .

According to BS 5930, all three of the test sands are described as uniformly graded and each given the Group Symbol SPu. Despite this, however, it should be noted that there is a general trend of increasing particle size and decreasing uniformity coefficient from 'Red' to 'Arlesey' to Leighton Buzzard sand.

Two clays were also used in triaxial tests but, as will be seen in section 7.9.5, the results obtained were generally very poor. As such, the main purpose served by these tests is as a comparison with those conducted on samples of sand. It is not, therefore, considered necessary (or appropriate) to provide full descriptions (to BS 5930) of the clay samples. However, for the purpose of identification, one sample was a remoulded Mercia Mudstone and the other was remoulded Gault Clay (collected from the Arlesey site).

Box tests (sections 7.7 and 7.11) were also conducted using 'Arlesey' sand and a gravel (used as wave guide backfill at the Cowden site) in which over 82% of the particles were greater than 6.3mm.

7.5 Triaxial Test Procedures

7.5.1 Soil Sample Formation

All soil samples used in the triaxial tests were reconstituted or formed (as opposed to being taken from in situ samples) and consisted of cylinders of soil 100mm long by 50mm in diameter. There were three different methods of sample formation, reflecting the different soil properties, and these are detailed in the following paragraphs. It should be noted that this section should be read in conjunction with the next which deals with the triaxial test procedure.

Two of the sands, 'Arlesey' and Leighton Buzzard, permitted rapid drainage and it was necessary to form these samples under water. This (obviously) was done in situ and necessitated the use of a drainage base pedestal (constructed from brass at The Nottingham Trent University) which was placed on top of the base pedestal containing the transducer. Having done this, a sheath was stretched over the drainage pedestal (upon which had already been placed a porous stone) and an 'O-ring' clip used to secure the sheath to the base pedestal. A sample former was then placed over the sheath which was, in turn, stretched within the sample former and folded back along its outside edge; the effect being to make the sheath as a tight fitting inner skin to the sample former. The drainage tap was then opened, allowing water to flow into the sheath from a burette. The sand was then 'spooned' into the sheath and periodically 'tamped' down with a piece of wooden doweling. (Note that this light 'tamping' technique was used for all samples in order to maintain a constant degree of compaction). Once the sample had reached 100mm in length, the sample cap was placed on it and the sheath pulled off the sample former and over the cap. The sheath was then secured to the cap with an 'O-ring' clip. Finally the burette was lowered from its original position to apply a negative pore water pressure and the drainage tap closed in order to preserve it. The sample former was then removed.

As described in section 7.2.1, the triaxial base pedestal had to be modified in order to accommodate the transducer within it. However, this, in turn, necessitated the ducting of co-axial

cable from the transducer and *through* the side of the base pedestal. Unfortunately, the ducting interfered with the correct positioning of the sample former. The consequences of this were that it became impossible to ensure the accuracy of the sample height and diameter during formation. Furthermore, it was also difficult to 'tamp down' the upper surfaces of the sample as the action largely resulted in the displacement of sand particles. As such, it is likely that 'docking' of the sample prior to testing also caused some compression. It is very difficult to assign precise numbers to these effects but it is the author's opinion that both height and diameter of the sample could only be formed to an accuracy of within approximately 2 - 3mm.

Initially it was attempted to form samples of the 'Red' sand in exactly the same way as described for the other two sands. However, owing to its inability to facilitate drainage quickly enough (which probably reflects its smaller particle size and greater value of C_u), this proved impossible. Samples of this sand, therefore, were simply formed by compacting it directly into a sample former in air (using the same technique as used for the other two sands - but in air). The finished sample (which was reasonably robust without any support) was then placed on the porous stone over the drainage pedestal and the sample cap placed on top. Finally a sheath was secured around the sample using 'O-ring' clips. (Note that the drainage tap was kept closed to prevent the influx of water into the sample).

The bulk of the clay samples were formed by compacting the clay, in three stages, using a 2.5kg rammer in a *Proctor* mould (producing a sample 105mm in diameter). The first and second stages were each followed by 40 standard blows of the rammer and the third stage was followed by 65 standard blows. The resulting compacted clay was then cut down to the standard size (using a soil trimmer) and the sample set up on the base pedestal as described for 'Red' sand. (Note that this compaction method was arbitrarily decided upon for this investigation and was used to form all clay samples tested. Also note that samples were not compacted at specific moisture contents; this aspect was only determined from samples subsequent to testing).

7.5.2 The Triaxial Test Procedure

- 1 The soil sample was formed and installed as described in section 7.5.1. Note that after this stage, the tap controlling drainage to and from the sample was kept closed until stage 5 (below) was reached.

- 2 The lower chamber was connected to an hydraulic actuator, ensuring that no air entered the system (which contained de-aerated water only). The piston was then moved upwards a distance of 3.4mm by expelling $10,000\text{mm}^3$ from the actuator into the lower chamber. After verifying that the pressure in the lower chamber (as recorded by the actuator) was negligible, it was re-set to zero.
- 3 The cell was closed and filled with water. When full, the cell hydraulic actuator was positioned alongside the cell drainage tap and the cell pressure (relative to the actuator) set to zero. The actuator was then connected to the cell and the tap opened. At this point, the pressure readings of both cell and lower chamber actuators were generally in the region of 4 - 6kPa.
- 4 The sample was 'docked' and the remaining system components, as depicted in figure 7.1, activated. (Note that the actuators had already been switched on and allowed to 'warm-up' for two hours prior to being used).
- 5 The appropriate cell pressure was then generated by manually activating the cell hydraulic actuator. Thereafter, for undrained tests, the sample drainage tap remained closed until the test had been completed. For consolidated undrained tests, once the required cell pressure had been reached, the sample drainage tap was opened and excess pore water allowed to flow out of the sample. Once it had re-attained equilibrium, the tap was closed and kept that way for the duration of the test. For drained tests, the sample drainage tap was opened after the cell pressure had been applied and left open for the duration of the test. Note that the pore water was allowed to re-attain equilibrium before the test was started. (Equilibrium had been regarded as having been re-attained when the level of water in the burette had become stabilised).
- 6 The Viewdac acquisition routine was initiated and the appropriate parameters input into the PC (section 7.3.2). Both software elements were then activated simultaneously by the operator.

7.6 Consolidation Test Procedure

When a normally consolidated body of soil is subjected to some degree of stress, it responds by straining. As soil is inelastic, if the stress is subsequently removed, not all of the strain is recovered. Therefore if the stress is reapplied, *up to the point of previous maximum stress*, the soil body will be stiffer than it was initially (i.e. it will be over-consolidated). Beyond this point, however, it will behave as a normally consolidated body of soil. This difference in the stress-strain characteristics is also reflected in the generated acoustic emission in what is known as the *Kaiser* effect and four tests have been conducted to demonstrate this.

A sample of Leighton Buzzard sand was set up within the triaxial cell (as described in section 7.5.1), on the drainage pedestal, and the sample drainage tap left open. The piston was moved up by 3.4mm (without straining the sample) and the cell actuator ramped to a cell pressure of 25kPa. Four isotropic consolidation tests were then conducted by manually programming the cell actuator to ramp to a target cell pressure and back again (to the 25kPa cell pressure starting point) in a fifteen minute period. In each of the four tests the target pressure was 125, 225, 425, and 825kPa respectively. The same Viewdac routine as used for standard triaxial tests was employed and simultaneous activation with the manual ramping of the cell was, again, initiated by the operator. The fact that the Viewdac routine acquired the same number of samples over the same period of time but consolidation was made over an increasing stress range, has implications concerning the interpretation of the results. This is dealt with in more detail in section 7.10.

7.7 Box Tests

A number of tests were conducted in which it was attempted to simulate the behaviour of a metal wave guide interacting with a granular backfill. Figure 7.5 shows a schematic of the apparatus used in both plan and cross-section. Basically, a section of 50mm diameter steel tubing (as used in wave guides both at Cowden and Arlesey) had a piece of wooden doweling inserted through two holes drilled in one end. The assemblage was then installed into a rigid plastic box by positioning either end of the doweling through a hole drilled in either side of the box. The net effect was that the doweling acted as an axle, about which the section of steel tubing could rotate. The box was then filled (to the depth as shown in figure 7.5) with either 'Arlesey' sand or 'Cowden' gravel, as tests were conducted on both. (Note that the lower end of the steel tubing

was taped in order to prevent any backfill material rising upwards within it). Load was provided by means of a chord which passed through two holes drilled in the steel tubing (perpendicular to the direction of the axle) and to which was attached a load hanger. Weights were placed on the load hanger and the AE monitoring routine initiated (at the same time) by the operator. The AE routine was essentially the same as that used for previous consolidation and triaxial tests except that there was an in-built delay of 15 seconds between activation and acquisition of data. This was to allow for any extraneous noise generated by the addition of the weights etc., and permitted the operator to leave the sound-booth. A dial gauge, which had been positioned against one side of the steel tubing, was used to record movement at the end of the fifteen minute acquisition period.

7.8 Introduction to Triaxial Apparatus Test Results

Table 7.3 summarises all ninety-two tests (coded TR1 - TR92) conducted using the triaxial test arrangement. The table indicates for each test (where appropriate) the test code; the cell pressure; the maximum deviator stress at failure; the strain at which the maximum deviator stress is recorded; the mean spherical stress at failure; the work done on the sample (section 7.9.2 discusses this more fully); the statistical measures of the arithmetic mean, standard deviation and root means square computed on the bulk AE data; the number of post-threshold data points and the number of events; the type of test conducted; and the test soil used. Formulaic definitions (where appropriate) are provided at the bottom of table 7.3.

That part of the programme confined to the testing of soil samples in strain-controlled triaxial shear constitutes some sixty-eight tests performed on five different soil types and under three different drainage conditions. All tests, categorised by type and material, are summarised in table 7.4.

It is also pointed out that the work performed in deforming a sample is defined as the area under the force-deformation curve for 0 - 15% strain. Force is calculated as the product of the deviator stress and sample cross-sectional area, assuming that the sample deforms as a right regular cylinder and deformation is defined as the axial strain. Ideally, it would have been preferable to have used the effective stress by which to compare the acoustic emission of various soils as this would have been more consistent with the simple model of AE generation described in section

1.2. Unfortunately, it was not possible to monitor pore water pressures and, as most tests were conducted in the 'undrained' state, only 'total' stresses are usually available. The advantage which a consideration of work has over that of total stresses is (as will be seen in section 7.9.2) that work is dependent upon the deviator stress which is, in turn, dependent upon the effective stresses. Further discussion of the work equation is contained in section 7.9.2.

7.9 Results of Triaxial Shear Tests

7.9.1 Drained Triaxial Tests conducted on Leighton Buzzard Sand

Figure 7.6 plots the deviator stress (q) against strain for all eleven drained triaxial shear tests conducted on samples of Leighton Buzzard sand. It is evident that all, to a lesser or greater degree, have undergone *dilation*, generating peak strengths which reduce as the level of strain progresses until a continuous, or *critical*, strength is attained. There is also a clear relationship between the applied cell pressure and the developed shear strength which is better illustrated in the plots of the Mohr stress circles. Figure 7.7 plots the Mohr stress circles for all eleven tests and a general tangent fitted to the circles yields a value for ϕ'_{\max} of approximately 41° , although values vary from about 40° at high cell pressures to 47° at low cell pressures. (In fact, this behaviour is entirely as expected as the magnitude of dilation increases with *decreasing* effective stress).

It should be noted that, because these are drained tests, all stresses are *effective* and the circles relate to peak strengths. Also note that the fluctuation in the calculated magnitudes of q_{\max} is probably due to the presence of air bubbles in the water used to generate the cell pressure (which was not de-aerated). However, both figures 7.6 and 7.7 indicate that the test results are consistent and this would imply that the tests have been conducted in an acceptable manner.

Figure 7.8 plots q_{\max} against p' at failure and figure 7.9 plots q_{\max} against work. The similarity between the figures suggests that the substitution of p' by work is acceptable. The figures also indicate that each relationship can be considered to be approximately linear and 'best-fit' lines are drawn through each set of data.

Figure 7.10 plots the arithmetic mean, standard deviation and root means square (section 3.6) of the AE data acquired during the course of each drained test as a function of p' and figure 7.11 plots the same AE data as a function of work done. The graphs of arithmetic mean clearly indicate that there is a good linear correlation between the magnitude of the emission generated and the effective stresses acting on the soil skeleton. (Note that, in this instance, the magnitude of the emission is defined as the arithmetic mean of all the data points acquired during the course of an individual test - section 3.6). It should, however, be remembered that these 'bulk' statistics (i.e. based on all the acquired data with no consideration given to a threshold value) are derived from emission which is generated by a variety of deformation processes and may include (for a drained test) initial contraction, dilation followed by contraction around the shear zone and shearing at constant volume.

An alternative way of representing AE data is to plot an *event map* which describes some aspect of every event captured during the course of a test and relates it to the point in the test at which it was captured. Figure 7.12 depicts such a plot for TR50, 51, 54, 59 and 60. It represents *each event* with the mean magnitude (in volts) of the event's constituent data points and plots the mean against the axial strain recorded at the time of capture. The major finding from such a plot appears to be the indication that greater levels of stress (going down the graphs of figure 7.12 the test cell pressure increases) results in the generation of a greater number of similarly sized events rather than events of increased magnitude. This aspect is more clearly illustrated in figure 7.13 which shows frequency distribution curves of the mean event magnitude for all events (consisting of three or more data points) for the same tests. All plots depict a similar profile (but with increasing numbers of events with increasing test cell pressure) supporting the contention that increased effective stress produces a larger number of similarly sized events rather than events of increased magnitude.

7.9.2 Change in Sample Volume due to Drainage

As illustrated in figure 7.14, a determinable volume of water is capable of draining both into and out of a soil sample while it is being tested. This has implications for the calculation of the deviator stress and work done in deforming the sample. The deviator stress is obtained by periodically isolating the 'ram load' in the sample and dividing it by its current cross-sectional area, assuming that it deforms as a right regular cylinder. If drainage is monitored then the

sample volume at any point in a test can easily be determined as the sample volume at the test outset is known. The sample cross-sectional area is then simply calculated by dividing the adjusted sample volume by the new sample height (axial strain is continuously monitored). However, for the purposes of this investigation, volume change has been ignored.

A correctly formed soil sample, at the outset of a test, had a volume of $196,350\text{mm}^3$ and the largest recorded volume change was 12ml ($12,000\text{mm}^3$). This corresponds to a change in both the sample diameter and height in the order of $1\text{-}2\text{mm}$, which is considered to be beyond the tolerance of sample formation (section 7.5.1). Ignoring a volume change of this magnitude also has the effect of increasing the deviator stress by approximately 6% which, in the case of TR50 (cell pressure 100kPa), increases q_{max} by some 30kPa . Tests conducted at higher cell pressures generated smaller volume changes and, therefore, smaller percentage errors in the value of q . It should, however, be born in mind that, because the volume is continually changing during the course of a test, the change in the value of q will also continually change. Failing to take the volume change into account, therefore, means that the stress-strain plots have necessarily suffered some distortion.

The calculation for work done in deforming the sample, first described in section 7.8, is also in need of some adjustment to account for the change in volume. The work done in axially deforming the sample is, in fact, correct as it is derived from the 'ram load' in the sample which is independent of the cross-sectional area. Allowing for a change in volume, the work equation is correctly written as follows:-

$$W = q \cdot \epsilon_q + p' \cdot \epsilon_v$$

where

$$\epsilon_q = 2(\epsilon_1 - \epsilon_3)/3$$

$$\epsilon_v = \epsilon_1 + 2\epsilon_3$$

$$p' = (\sigma'_1 + 2\sigma'_3)/3$$

$$q = \sigma'_1 - \sigma'_3$$

and ϵ_1 , ϵ_3 and ϵ_v are the major principal, minor principal and volumetric strain components respectively; q , p' , σ'_1 and σ'_3 are the deviator stress, mean effective stress, major principal effective stress and minor principal effective stress respectively.

If, however, volume change is, or is assumed to be, zero then

$$\epsilon_v = 0$$

$$\epsilon_1 = -2\epsilon_3$$

and the work equation reduces to

$$W = q \cdot \epsilon_1$$

All drained tests resulted, due to dilation, in an increase in the sample volume (although the consolidation process would have initially resulted in a decrease in sample volume). As compression has been taken as positive this means that the adjustment due to volume change is negative, so the work figures quoted for drained tests are somewhat overstated. An indication of the magnitude of the error can be found by calculating the area under the $\epsilon_v - p'$ curve. For test TR60 this has the effect of reducing the work done in deforming the sample by just under 10Nm to approximately 34Nm. Similarly, for test TR50, the work done in deforming the sample is reduced by just under 4Nm to approximately 6Nm.

Despite this, for all drained tests the volumetric strain has been assumed to be zero primarily because, as the acquired AE is only a 20% sample of all the AE data generated during the course of a test, it is not considered to be of a sufficient resolution to justify more accurate calculations of q and work done. However it is important to appreciate that this adjustment has been omitted and to have some idea of its effect.

The same reasoning is applied to all consolidated undrained tests, in which the volume change on consolidation (not part of the work equation) is considerably smaller than that experienced in the drained tests.

7.9.3 Drained, Undrained & Consolidated Undrained Triaxial Shear Tests conducted on Leighton Buzzard Sand

Figure 7.15 plots q against axial strain for eight unconsolidated nominally undrained triaxial shear tests conducted on saturated samples of Leighton Buzzard sand (TR 44, 45, 48, 49, 53, 55, 61 & 62) and figure 7.16 plots their equivalent Mohr stress circles based on peak strengths. It is obvious that the sands have, in fact, been sheared in the drained state and the applied cell pressure has generated a corresponding increase in the effective stress. Typical results of undrained tests conducted on saturated soil should generate a horizontal failure envelope in which ϕ_{\max} is zero, as any increase in the total cell pressure should generate an equivalent increase in the pore water pressure, leaving the effective stresses unchanged. (Making the usual assumptions that the pore water and soil mineral material are incompressible). Briefly referring back to figure 7.15, it is evident that the sample in test TR62 was considerably stiffer than the others. Unfortunately, there is no obvious or apparent reason as to why this should be.

A general tangent fitted to the circles produces a value for ϕ_{\max} of approximately 46° , although values extend from approximately 59° at low stresses to approximately 40° at high stresses. This compares with an average value for ϕ'_{\max} of approximately 41° , as determined in section 7.9.1. The fact that ϕ_{\max} is greater than ϕ'_{\max} implies that negative pore water pressures were in force in the samples at the time of failure, despite the fact that the samples have evidently sheared in the drained state and dilated in the shear zone.

Bishop & Eldin (1950) conducted a number of undrained triaxial shear tests on *apparently* saturated sands and determined that it was possible to obtain appreciable non-zero values of ϕ_{\max} when considering a soil with a very low compressibility and a strongly dilatant structure. The authors attributed this to the samples not actually being fully saturated when sheared and suggested two possible explanations. Firstly the authors demonstrated '*that the slightest departure from full saturation leads to the measurement of very considerable angles of undrained shearing resistance, even in the case of clays*'; and, secondly, they pointed out that sufficiently large negative pore water pressures generated as a result of shear can cause *cavitation*, which is the formation of air and gas filled voids freed from solution.

Figure 7.17 plots q_{\max} as a function of p' for drained tests and as a function of p for consolidated nominally undrained and unconsolidated nominally undrained tests. The 'best-fit' line shown is

drawn only through the drained data (first plotted in figure 7.8) and indicates that there is a fairly good (but *not* true) linear relationship between the maximum recorded deviator stress and the mean effective stress. Those data points from nominally undrained tests which clearly do not plot on this line do not because values of q_{\max} are plotted against p rather than p' . An approximation of the mean effective stress acting on the soil skeleton at the point of failure (and also, therefore, the pore water pressures at that time) can be made by sliding each point horizontally until it intercepts the 'best-fit' line and reading the appropriate value for p' from the x-axis. The fact that the majority of these points plot above the line means that the effective stresses are greater than the total stresses and that negative pore water pressures were in force at the time of failure. This is in agreement with expectation and estimates of pore water pressures at the point of failure have been calculated as described and are listed in table 7.5. It is evident that the values vary considerably. Additionally, they should be considered in conjunction with the fact that performing the same operation on the drained data, through which the 'best-fit' line was drawn, produces estimated pore water pressures of up to 25kPa.

Figure 7.18 plots q_{\max} as a function of work and indicates a clear relationships between q_{\max} , and the work done in deforming the samples (and also, therefore, p').

The first graph depicting the AE response of the thirty-nine tests conducted on Leighton Buzzard sand (TR28 has been omitted as it's AE response is clearly anomalous) is depicted in figure 7.19, which plots the mean signal value against work. Although there is a good general correlation between the magnitude of the emission and the mean effective stress it is evident that there is a spread of the AE response. This may reflect differences in density and/or sample structure which, in turn, may have effected the way in which the sample had deformed. For example, one test (TR9), which failed by barrelling rather than by the development of a single good shear plane (as most did), produced a lower than average AE response.

Figure 7.20 plots the number of post-threshold data points against the number of events and supports the findings of the previous section that increasing mean effective stress generates more events of similar size, rather than larger events. Figure 7.21, which plots the mean signal value of the bulk data against the number of events, also demonstrates an approximate linear relationship. Finally, figure 7.22, plots frequency distribution curves for TR56 (consolidated nominally undrained), TR60 (drained) and TR62 (unconsolidated nominally undrained) and demonstrates that all tests (regardless of drainage conditions) exhibit similar distributions of event magnitude.

To summarise, therefore, the results of sections 7.9.1 and 7.9.3 indicate that the level of AE generated by Leighton Buzzard sand is related to the mean effective stress acting on the soil skeleton and is unaffected by drainage conditions. Increases in the level of AE are due to the generation of greater numbers of similarly sized events rather than events of larger size.

7.9.4 Triaxial Shear Tests conducted on Leighton Buzzard, 'Arlesey' and 'Red' Sand's

Figure 7.23 depicts the q - axial strain graphs for five unconsolidated nominally undrained triaxial shear tests (TR63, 64, 65, 66 & 67) and one drained triaxial shear test (TR68) conducted on nominally saturated samples of 'Arlesey' sand. Note that test result TR68 is considerably stiffer than the others. This is because, as a drained test conducted under a cell pressure of 500kPa, the mean effective stress at the start of the test would also have been 500kPa. This contrasts with the unconsolidated nominally undrained tests in which, at the test start, the mean effective stress would be merely due to the applied negative pore water pressure (probably in the region of -0.5 to -1.0kPa).

Figure 7.24 depicts the q - axial strain graphs for five unconsolidated nominally undrained triaxial shear tests (TR69, TR73, TR74, TR75 & TR76) conducted on samples of 'Red' sand. It should be evident that, whereas Leighton Buzzard and 'Arlesey' sands both regularly exhibit the 'classic' trait of a peak strength (associated with drained tests conducted on soils denser than critical), this is not the case for 'Red' sand in which q climbs to a constant maximum value.

The Mohr stress circles for 'Arlesey' and 'Red' sands are shown in figures 7.25 and 7.26 respectively. Again, differences in their responses to the imposed stress regimes are apparent in the graphs. A general tangent fitted to the nominally undrained 'Arlesey' data produces a value for ϕ_{\max} of approximately 44° , with magnitudes varying from between 53° at low stress values to 42.5° at high stress values. This contrasts with 'Red' sand in which it is possible to draw a single tangent to all the Mohr circles (in the main group) and which passes through the origin. This produces a single value for ϕ_{\max} of approximately 33° and it is likely that this also represents the value of ϕ'_{\max} . Clearly, whereas Leighton Buzzard and 'Arlesey' sands are dilating in the shear zone, 'Red' sand *appears* to contract and, as a result, its values of ϕ_{\max} and ϕ_{critical} are identical. The apparently anomalous behaviour of test TR69 is probably due to the fact that it was conducted several days before the main batch, when the 'Red' sand sample was much wetter. It

is likely that the greater moisture content prevented much of the applied cell pressure from generating an increase in the effective stress.

Figure 7.27 plots q_{\max} as a function of work for all thirty-nine tests conducted on Leighton Buzzard sand, all six tests conducted on 'Arlesey' sand and all five tests conducted on 'Red' sand. It is apparent that all, regardless of their respective characteristics, share the same q_{\max} :work relationship. However, it is evident from figure 7.28 (which plots the mean signal value of the bulk data as a function of work for the same tests) that the sands do produce differing levels of emission. It is clear that, per unit work done, Leighton Buzzard sand generates a higher magnitude emission than 'Arlesey' sand which (in turn) generates a higher magnitude emission than 'Red' sand (which is of very low magnitude and commensurate with background noise levels).

Figure 7.29 plots the total number of post-threshold data points against the total number of events for all tests and indicates that, despite being much less emissive, both 'Arlesey' and 'Red' sands generate events of a similar magnitude (in terms of data point size) to Leighton Buzzard sand. Figure 7.30 plots the mean signal value of the bulk data against the total number of events and, although there is a generally good agreement between the different sands, it is interesting to note that three results for 'Arlesey' sand do plot noticeably above the main body. This may suggest that, although 'Arlesey' sand is less emissive than Leighton Buzzard sand in terms of numbers of data points, that the magnitude of its constituent data points are somewhat higher. Figure 7.31, which plots the number of events as a function of work, clearly indicates that both 'Arlesey' and 'Red' sands produce much smaller number of events than Leighton Buzzard sand.

Figure's 7.32 and 7.33 depict frequency distribution curves for six tests conducted on 'Arlesey' sand and fifteen tests conducted on all three sands (five of each), respectively. All demonstrate similar distributions.

7.9.5 Triaxial Shear Tests Conducted on Clays

A small number of tests were conducted on two separate clays but, owing to the relatively low magnitude of the emission coupled with the periodic sampling technique used in this investigation, the results are generally poor.

Figure 7.34 illustrates the q - axial strain graphs for twelve unconsolidated undrained triaxial shear tests conducted on Gault Clay (TR77, 78, 80, 81, 82, 83, 84, 85, 86, 87, 88 & 89) and for four unconsolidated undrained tests conducted on Mercia Mudstone (TR36, 90, 91 & 92). It is evident that all exhibit the stress-strain characteristics in which no peak strength exists and q slowly climbs to a constant maximum value. This type of behaviour is typical of a soil which is sheared in the undrained state.

Mohr stress circles for sixteen tests conducted on clays are depicted in figure 7.35. Whereas the diameters of the Mohr circles for tests conducted on all sands increased with increasing normal stress, it is evident that there is no such normal stress dependent increase in the diameter of the clay Mohr circles. It is possible that the clay samples (of varying moisture content) were partially saturated when formed but became fully saturated after the application of the cell pressure. In figure 7.35, the larger Mohr circles were generated by the samples with the smaller moisture contents as a greater proportion of the applied cell pressure was transferred to the soil skeleton (in the form of an increase in the effective stress) before the sample became fully saturated. Conversely, the smaller Mohr circles (reflecting larger moisture contents) became saturated more quickly and less of the applied cell pressure was transferred to the soil skeleton.

This point is more clearly illustrated in figure 7.36 which plots q_{\max} as a function of moisture content for each clay test sample. It is evident that there is a distinct negative linear correlation between the maximum deviator stress and moisture content for each of the two clays. (A similar relationship exists between work and moisture content as is illustrated in figure 7.37). Figure 7.38 indicates the existence of a linear relationship between q_{\max} and the work done in deforming the sample.

(Note that moisture content is unavailable for TR88 and numbers of events/data points are unavailable for TR77, TR78 and TR79).

Figure 7.39 plots the AE mean signal value as a function of work done and reveals that little relationship has been established between the two parameters for a clay soil.

Figure 7.40 plots AE mean signal value against the number of events and figure 7.41 plots the number of post-threshold data points against the number of events. (Note that the threshold used

for all triaxial shear tests conducted on clays is 0.32 volts - reflecting the lower magnitude of the generated emission relative to the sands).

Figure 7.42 plots q_{\max} against the work done, figure 7.43 plots AE mean signal value against the work done and figure 7.44 plots the number of post-threshold data points against the number of events for the clay soils and for forty-eight tests conducted on sand.

7.10 The Consolidation Test

As described in section 7.6, a series of isotropic consolidation tests were conducted on a sample of Leighton Buzzard Sand. This involved four individual cycles of the application and removal of increases in the effective stress of magnitudes 100, 200, 400 and 800kPa respectively. Three graphs (figures 7.45 - 7.47) present the results. Note that each graph is divided into four quarters (one for each consolidation cycle) and that each quarter is subdivided into four sub-quarters. In the first cycle the first two sub-quarters represent virgin compression. However, in the final three cycles, the first sub-quarter represents the re-application of stress up to the maximum level of the previous cycle and it is only the second sub-quarter which represents virgin compression. For all cycles the last two sub-quarters represent the removal of the stress.

Figures 7.45 and 7.46 plot the event distribution with respect to each cycle and represent event magnitude in the form of mean event magnitude (in volts) and number of data points in event (respectively). It is fairly self evident that the sub-quarters which represent periods of virgin compression are also the most acoustically active. However, it is also clear that during those periods when load is being reapplied that emission is being generated. The Kaiser effect describes the particular situation where *no* emission is generated up to the point of previous maximum load. The case where emission is generated prior to this point is more correctly known as the *Felicity* effect (Bray & Stanley, 1997). Determination of the Felicity effect is usually used to infer the occurrence of structural damage. However, in the particular case of a sand, it is more likely due to the re-consolidation of soil elements (consisting of particles) which expanded when the stress was originally removed.

Figure 7.47 plots the same data in the form of cumulative post-threshold data points and, again, clearly illustrates the increased acoustic activity associated with periods of virgin compression.

Note that for this section a threshold value of 0.5 volts has been used to eliminate unwanted data. It should also be appreciated that, because the AE capture routine used was the same as that used in the triaxial shear tests, the data generated was only periodically sampled. Also, later cycles in the consolidation tests needed to be ramped at progressively faster rates in order to achieve their target pressures within the fifteen minute test period. Although it is likely that the increased rate of volumetric strain will, itself, lead to a greater level of emission, the graphs still clearly indicate that those periods of virgin compression are the more active.

7.11 Box Tests

As described in section 7.7, the main objective of the series of box tests was to simulate the (considered) behaviour of the wave guide in the field (sections 3.3 & 6.3). Eleven tests, denoted B1 - B11 inclusive, were conducted and are summarised in table 7.6.

Of the five noise tests (B1, B2, B3, B6 & B9) only two (B1 & B9) recorded any post-threshold (0.5 volts) data points and these numbered 221 and 51, respectively. This compares with the six load tests (B4, B5, B7, B8, B10 and B11) which recorded post-threshold data points of between 2,865 and 192,537.

Figures 7.48, 7.49 and 7.50 present the combined results of tests B4 and B5 (sand tests) in the form of event mean magnitude in volts, the number of data points per event and the cumulative number of post-threshold data points against time, respectively. It is evident that, not only did test B4 generate larger events than test B5, but that event size decreased within each test as it progressed. Figure 7.50 emphasises the decrease in acoustic activity as the backfill readjusted to a new equilibrium. However, considering the application of a load in test B4 immediately pulled the wave guide section through its maximum travel, it is interesting to note that there was still acoustic activity some two hours later.

Tests B7 and B8 (sand tests) were conducted using a smaller load than in test B4 in order to generate a slower, more controlled movement. Figures 7.51, 7.52 and 7.53 present the combined results of tests B7 and B8 in the form of event mean magnitude in volts, the number of data points per event and the cumulative number of post-threshold data points against time, respectively. Each plot also depicts the amount of movement recorded by the dial gauge. Note

that the large gap between the recorded movements at the end of test B7 and the beginning of test B8 occurs because movement (and AE) were only monitored after the load had been applied and a degree of equilibrium had been attained. Therefore, although the recorded movement during test B8 is relatively small, the larger level of AE (compared to test B7), is likely to reflect some element of the movement which had occurred between the tests. Again, however, it is noted how the magnitude of an event decreased as each test progressed. Figure 7.53 shows that, for test B7, there is an excellent correlation between the cumulative number of post-threshold data points and the recorded movement. In fact, as illustrated in figure 7.54, a similarly good relationship also exists for test B8.

Figures 7.55, 7.56 and 7.57 present the results of test B10 (gravel test) in the form of event mean magnitude in volts, the number of data points per event and the cumulative number of post-threshold data points against time, respectively. Again it is evident that the magnitude of an event decreased as the test progressed. However, there are two interesting points arising from this test conducted on 'Cowden' gravel. Firstly, as clearly illustrated in figures 7.55 and 7.56, there are periods (towards the end of the test) where no movement was recorded by the dial gauge and which corresponded to times when no AE was recorded either. Although the load used in test B10 was less than that used in the tests B4, B7 and B8, there is no indication of this type of behaviour having occurred in any of the tests conducted on sand. Secondly, the magnitudes of the events (both in terms of volts and number of constituent data points), are evidently larger for the gravel backfill than for the sand. Figure 7.58 plots event mean magnitude in volts for tests B8 and B10. Both recorded similar amounts of movement in the fifteen minute period (1.16mm for B8 and 1.03mm for B10) and similar numbers of post-threshold data points (38,620 for B8 and 42,762 for B10) but evidently test B10 generated events of a larger magnitude than did test B8. It should, however, be noted that this difference only manifests itself in a relatively small proportion of larger events; the bulk sharing a similar (although not identical) range. Further evidence of a difference in the character of generated AE is provided by considering the ratio's of the number of post-threshold data points to the number of events. For tests B4, B5, B7 and B8 (all sand backfilled) these are 3.731, 3.829, 3.545 and 3.679 (respectively) whereas for tests B10 and B11 (both gravel backfilled) they are 8.842 and 8.705 (respectively).

7.12 Laboratory Test Programme - Summary of Results

7.12.1 Triaxial Test Results

It is evident that the level of the acoustic emission is related to the magnitude of the effective stress acting on the soil skeleton (section 7.9.1). The relationship is dramatically illustrated in figure 7.59 which depicts the *event map* (mean magnitude of event in volts) of triaxial shear test TR11. In this test the drainage was changed part way through shearing and it is evident from the figure that a sharp increase in the deviator stress (and, therefore, the effective stress) was accompanied by a large increase in acoustic activity. Closer examination of the figure also reveals that (immediately prior to the sudden increase in deviator stress) a period of increased stiffness (when compared with the early stages of shearing) was also accompanied by increased AE activity. It is also evident that alternative soil minerals generate different levels of emission (sections 7.9.4 & 7.9.5), although there is no evidence to suggest that there is any fundamental difference in the character of the emission, as might be indicated by an amplitude distribution analysis.

This appears to be consistent with the simple model, outlined in section 1.2, in which the generation of AE was explained as being the result of inter-particle friction. It would appear reasonable, therefore, to expect that the magnitude of the generated emission ought to be related both to the frictional characteristics of the soil mineral and the effective stress under which it is being sheared. Unfortunately, the situation is not quite that straightforward. When subjected to shear, soil particles may slide but they can also roll and degrade (i.e. 'break-up'). Skinner (1969) reported an investigation into the effect of inter-particle friction on the shear strength of a random assembly of spherical particles. Using glass ballotini, the author demonstrated that the coefficient of friction could change by a factor of 'at least' five without significantly altering the shear strength of the assemblage. This was achieved by conducting shear box tests on dry glass ballotini (a low friction regime) and then glass ballotini which had been 'flooded' with distilled water (a high friction regime). Skinner (1969) concluded that under high friction regimes, particle rolling would become more dominant as opposed to low friction regimes which would tend to promote particle sliding.

Horn & Deere (1962) investigated the frictional characteristics of a number of minerals commonly found in rock and soil and concluded that the presence of fluid on the 'sliding surfaces' could have a 'profound' effect on the frictional coefficients.

If, therefore, the frictional coefficients of minerals can vary by a factor of 'at least' five and the presence of water have a 'profound' effect on their value, then clearly the interpretation of acquired AE data must take both these aspects into account. For example, two soils may exhibit similar stress-strain, but widely different AE, characteristics. Conversely, two soils generating similar levels of emission may (under identical stress regimes) suffer vastly different magnitudes of strain.

However, if increased effective stress and/or an increased coefficient of friction promotes greater particle rolling rather than sliding, then it may *not* be correct to expect simple relationships between the two factors and the level of generated emission to exist. However, as each of the mechanisms (sliding, rolling and degradation) may generate emission of different magnitude and/or different character, the use of AE as an investigative tool in the laboratory may have a lot to offer.

7.12.2 Box Test Results

In section 6.4 the Cowden and Arlesey field test results were considered together. It was suggested that the field wave guides generated noise as a result of an interaction between the metal tubing of the wave guide and its backfill. This, in turn, was caused by movement in the host slope (acting as an input) and the wave guide was described as acting like a *strain gauge* which simply responded to deformation within the slope. It was also suggested that, consequentially, noise generation would be greatest immediately after an input and would gradually reduce in magnitude until such time that equilibrium was re-attained (unless there was a further input) when it would cease. This is exactly the type of behaviour exhibited by all box tests.

It was also predicted that there should be a difference between the behaviour of sand and gravel backfills. It was suggested that gravel particles, being larger, would require greater inputs to cause them to slip and that slippage would occur over a much shorter time-scale but emission be

of a much greater magnitude than for sand particles. Clearly this exerts a fundamental control over the type of backfill most suited to a particular situation and this model was used to explain the apparently poor response of gravel backfilled wave guides used at Cowden. It has been clearly demonstrated by the box tests that gravel backfills do exhibit this type of behaviour. Whereas the sand backfill continuously generated emission, the gravel backfill did not; towards the end of the acquisition period there were distinct periods of zero movement accompanied by zero emission. It was also clearly demonstrated that the gravel backfill generated emission of a greater magnitude than did the sand backfill.

Magnitude of Ram Travel (mm)	Lower Chamber Pressure at End of Movement		Friction (kPa)
	Upwards (kPa)	Downwards (kPa)	
1.7	3.0	0.0	1.5
3.4	4.0	0.0	2.0
6.8	4.0	-1.0	2.5
10.2	3.0	-1.0	2.0
13.6	4.0	0.0	2.0
17.0	4.0	0.0	2.0

Table 7.1 Determination of axial ram friction

Sand	D ₁₀ (mm)	D ₆₀ (mm)	C _u
Red	0.077	0.187	2.4
Arlesey	0.187	0.375	2.0
Leighton Buzzard	0.305	0.495	1.6

Table 7.2 Test sand parameters from PSD curves (figure 7.4)

Test Code	Cell Pressure (kPa)	Max. Deviator Stress (kPa)	Strain @ Max. Deviator Stress %	Mean Spherical Stress @ Failure (kPa)	Work (N.m)	AE mean signal value (volts)	AE standard deviation (volts)	AE root means square (volts)	Number post-thres'd data points	Number of events	Test type	Test soil
TR1	100	578	4.50	293	13.90	0.21614	0.29532	0.36588	43807	6739	CU	LEB
TR2	200	828	3.88	476	20.85	0.24523	0.29302	0.38202	55484	15135	CU	LEB
TR3	300	1025	1.66	642	25.41	0.31972	0.40789	0.51823	122184	36258	CU	LEB
TR4	400	1774	3.38	991	42.92	0.34739	0.49604	0.60554	185499	44216	CU	LEB
TR5	100	572	5.24	291	14.13	0.23164	0.15794	0.28027	11255	2078	CU	LEB
TR6	200	1001	4.86	534	22.93	0.25763	0.27834	0.37921	43328	8662	CU	LEB
TR7	300	1406	5.81	769	35.08	0.30074	0.34325	0.45630	85700	26554	CU	LEB
TR8	400	1755	4.02	985	43.70	0.34473	0.45895	0.57394	162730	47676	CU	LEB
TR9	500	1816	4.36	1105	47.47	0.32846	0.40483	0.52127	125590	39504	CU	LEB
TR10	500	2010	4.25	1170	46.83	0.39081	0.56627	0.68798	251143	70793	CU	LEB
TR11	500	1414	6.02	971	26.74	0.38634	0.58345	0.69972	268006	70762	NOTE	LEB
TR12	100	428	4.34	243	10.54	0.22749	0.10244	0.24938	3268	907	CU	LEB
TR13	200	858	3.88	486	22.28	0.27240	0.24172	0.36409	36406	13681	CU	LEB
TR14	300	1195	4.50	698	29.90	0.26304	0.24424	0.35886	39835	12973	CU	LEB
TR15	100	450	6.97	250	10.13	0.23203	0.10705	0.25542	3533	1519	CU	LEB
TR16	100	735	4.09	345	16.33	0.23896	0.15306	0.28367	11445	4185	CU	LEB
TR17	200	1048	4.34	549	24.22	0.28384	0.28089	0.39924	53504	19304	CU	LEB
TR18	100	436	3.91	245	9.50	0.21480	0.09820	0.23607	3920	813	D	LEB
TR19	200	801	3.66	467	17.91	0.23822	0.15022	0.28152	11333	4396	D	LEB
TR20	300	1063	4.61	654	25.00	0.25309	0.22912	0.34130	28597	7724	D	LEB
TR21	300	1351	4.32	750	32.97	0.31745	0.38982	0.50266	112132	34991	CU	LEB
TR22	100	398	3.66	233	3.42	0.20993	0.06667	0.22014	99	341	NOTE	LEB
TR23	100	375	3.31	225	3.04	0.20953	0.05028	0.21536	580	100	NOTE	LEB
TR24	100	360	3.01	220	3.09	0.20836	0.05345	0.21499	1459	552	NOTE	LEB
TR25	100	408	3.48	236	3.40	0.28321	0.20768	0.35108	18765	7685	NOTE	LEB

TR26	100	394	4.69	231	2.88	0.27273	0.33701	0.43348	0157	9720	NOTE	LEB
TR27	100	396	4.13	232	3.23	0.21873	0.08439	0.23433	23086	9790	D	LEB
TR28	100	374	3.57	225	2.89	0.19619	0.05017	0.20240	433	141	D	LEB
TR29	100	389	4.60	230	3.28	0.23416	0.10257	0.25553	2229	1183	NOTE	LEB
TR30	100	382	4.37	227	2.92	0.23219	0.09649	0.25132	2183	808	NOTE	LEB
TR31	500	--	--	--	--	0.20268	0.02390	0.20397	14	10	NOISE	*
TR32	300	1380	4.79	760	31.61	0.27711	0.29116	0.40186	58206	19434	NOTE	LEB
TR33	300	1026	3.18	642	27.70	0.28893	0.32232	0.43279	73227	23282	NOTE	LEB
TR34	500	1891	4.38	1130	43.63	0.39322	0.58431	0.70425	266789	73850	NOTE	LEB
TR35	500	1806	6.49	1102	44.49	0.40677	0.55830	0.69071	250793	64683	NOTE	LEB
TR36	300	173	17.54	358	4.70	0.21906	0.03288	0.22139	44203	17346	UU	MEM
TR37	--	--	--	--	--	0.15118	0.03804	0.15586	2693	240	CLDT	LEB
TR38	--	--	--	--	--	0.15731	0.05409	0.16629	5158	633	CLDT	LEB
TR39	--	--	--	--	--	0.15866	0.08587	0.18034	15160	1656	CLDT	LEB
TR40	--	--	--	--	--	0.16144	0.13264	0.20889	40105	4303	CLDT	LEB
TR41	400	1443	3.84	881	32.24	0.35011	0.47200	0.58764	175550	49522	D	LEB
TR42	500	1904	3.95	1135	48.16	0.38975	0.53049	0.65822	226915	61854	D	LEB
TR43	400	1434	4.32	878	34.01	0.32277	0.36936	0.49046	99638	32323	CU	LEB
TR44	500	1825	5.54	1108	41.94	0.34023	0.43798	0.55455	143302	40983	UU	LEB
TR45	100	516	6.11	272	13.42	0.24959	0.11918	0.27647	4476	2060	UU	LEB
TR46	500	2034	5.22	1178	51.17	0.46489	0.68495	0.82777	375618	98797	CU	LEB
TR47	500	2024	4.68	1175	52.63	0.41869	0.60025	0.73181	283604	80136	CU	LEB
TR48	400	1812	5.97	1004	43.44	0.48587	0.74210	0.88697	444698	108645	UU	LEB
TR49	100	737	6.58	346	16.96	0.27988	0.25707	0.37993	41120	15355	UU	LEB
TR50	100	461	5.61	254	10.34	0.22599	0.10552	0.24929	4598	1018	D	LEB
TR51	200	847	4.11	482	19.18	0.25678	0.18151	0.31434	17705	6705	D	LEB
TR52	500	303	18.81	601	3.37	0.22046	0.13070	0.25618	10209	1685	D	LEB
TR53	200	1091	5.41	564	23.44	0.32155	0.37846	0.49656	102335	31866	UU	LEB
TR54	300	1185	3.63	695	27.28	0.31383	0.34367	0.46534	86187	29652	D	LEB
TR55	300	1233	5.25	711	27.35	0.36663	0.47844	0.60272	175707	51142	UU	LEB
TR56	500	2075	5.93	1192	48.56	0.51895	0.77171	0.92994	506848	127904	CU	LEB

TR57	400	413	4.59	538	7.06	0.20481	0.04361	0.20928	1004	285	NOTE	LEB
TR58	500	336	3.34	612	4.75	0.20651	0.05956	0.21481	1895	340	NOTE	LEB
TR59	400	1385	4.84	862	37.22	0.31993	0.39041	0.50470	109891	33273	D	LEB
TR60	500	1804	5.06	1101	44.04	0.41931	0.58865	0.72269	276091	72960	D	LEB
TR61	400	1732	5.47	977	37.56	0.35092	0.44024	0.56293	149084	48576	UU	LEB
TR62	500	1842	4.54	1114	46.12	0.42896	0.63871	0.76935	313419	77052	UU	LEB
TR63	100	739	4.36	346	17.56	0.23516	0.16660	0.28810	14955	2858	UU	ARL
TR64	200	1043	4.70	548	23.10	0.24803	0.18905	0.31177	20429	5204	UU	ARL
TR65	300	1111	5.68	670	26.93	0.32457	0.36845	0.49097	93637	27034	UU	ARL
TR66	400	1750	5.59	983	39.81	0.28177	0.33353	0.43655	65689	15568	UU	ARL
TR67	500	2090	5.52	1197	48.50	0.35752	0.42100	0.55226	126188	39448	UU	ARL
TR68	500	1925	3.79	1142	44.39	0.31139	0.32272	0.44837	67658	20381	D	ARL
TR69	100	53	1.05	118	0.92	0.20538	0.02324	0.20656	67	7	UU	RED
TR70	--	--	--	--	--	0.20918	0.02159	0.21016	0	0	NOISE	*
TR71	--	--	--	--	--	0.20882	0.02180	0.20983	0	0	NOISE	*
TR72	--	--	--	--	--	0.19361	0.01759	0.19430	0	0	NOISE	*
TR73	200	456	18.75	352	12.71	0.19952	0.09811	0.22223	5701	812	UU	RED
TR74	300	698	13.66	533	17.26	0.20254	0.08412	0.21920	4459	861	UU	RED
TR75	400	946	9.08	715	24.59	0.09549	0.12083	0.15398	4586	840	UU	RED
TR76	500	1159	18.50	886	28.73	0.20131	0.09067	0.22069	4908	942	UU	RED
TR77	100	61	2.73	120	0.74	0.19535	0.02106	0.19638	--	--	UU	GAC
TR78	500	54	2.29	518	0.86	0.20210	0.02397	0.20339	--	--	UU	GAC
TR79	300	81	3.66	327	1.78	0.20243	0.02112	0.20341	--	--	UU	GAC
TR80	300	151	17.11	350	3.68	0.19841	0.02398	0.19974	4509	3349	UU	GAC
TR81	100	136	11.78	145	3.18	0.20003	0.02247	0.20117	5113	3992	UU	GAC
TR82	200	164	17.43	255	3.60	0.20140	0.02025	0.20229	5239	4414	UU	GAC
TR83	400	232	17.86	477	5.22	0.19697	0.03476	0.19990	8136	3633	UU	GAC
TR84	500	209	11.58	570	5.41	0.19622	0.02880	0.19822	5516	2938	UU	GAC
TR85	300	233	17.79	378	4.78	0.19123	0.02386	0.19261	3246	1636	UU	GAC
TR86	200	233	17.97	278	4.83	0.19364	0.03837	0.19730	5403	2244	UU	GAC
TR87	100	219	14.48	173	4.70	0.19340	0.01908	0.19423	3063	1987	UU	GAC

TR88	500	270	17.70	590	6.32	0.19561	0.06908	0.20736	26200	6685	UU	GAC
TR89	300	275	19.16	392	6.09	0.20250	0.02341	0.20373	8621	7021	UU	GAC
TR90	500	75	18.04	525	1.40	0.19796	0.02002	0.19886	3814	3560	UU	MEM
TR91	300	75	10.35	325	1.36	0.19204	0.02312	0.19332	3932	2389	UU	MEM
TR92	100	87	12.12	129	1.65	0.19382	0.02680	0.19556	9359	3369	UU	MEM

Table 7.3 Summary of all ninety-two tests conducted using the triaxial test arrangement.

Definitions:-

- 1 Maximum deviator stress is the largest recorded value of $(\sigma_1 - \sigma_3)$ in a test.
- 2 Strain @ maximum deviator stress is the strain at which the largest recorded value of $(\sigma_1 - \sigma_3)$ occurred.
- 3 Mean spherical stress (p) @ failure is defined as $(\sigma_1 + 2\sigma_3)/3$ at the same point in the test identified in 1 & 2 above.
- 4 Work is calculated as the area under the force-strain graph for 0 - 15% sample deformation (see section 8.6).
- 5 AE mean signal value, standard deviation and root means square are calculated on the bulk data (see section 3.6 for definitions of statistical measures)
- 6 The number of post-threshold data points is based on a threshold value of 2.5 volts for all tests, except those conducted on samples of clay which are based on a value of 0.32 volts. The definition of an event is given in section 3.6.
- 7 Test types are divided into six categories:- drained (D), consolidated nominally undrained (CU), unconsolidated nominally undrained (UU), noise (to establish noise generated by the testing system), consolidation tests (CLDT) and those marked 'NOTE' (which are summarised in table 7.4).

8 Soil types are coded as follows:- Leighton Buzzard sand (LEB), 'Arlesey' sand (ARL), 'Red' sand (RED), Mercia Mudstone (MEM) and Gault clay (GAC).

Soil Type or Test Type	Triaxial Shear Tests Conducted on Soil Samples by Test Type			Other Tests	Total
	Drained	Consolidated Undrained (nominally)	Unconsolidated Undrained (nominally)		
Leighton Buzzard Sand	18, 19, 20, 28, 41, 42, 50, 51, 54, 59, 60 (11)	1, 2, 3, 4, 5, 6, 7, 8, 9, 10, 12, 13, 14, 15, 16, 17, 21, 43, 46, 47, 56 (21)	44, 45, 48, 49, 53, 55, 61, 62 (8)	-	40
Arlesey Sand	68 (1)	-	63, 64, 65, 66, 67 (5)	-	6
Red Sand	-	-	69, 73, 74, 75, 76 (5)	-	5
Gault Clay (remoulded)	-	-	77, 78, 79, 80, 81, 82, 83, 84, 85, 86, 87, 88, 89 (13)	-	13
Mercia Mudstone (remoulded)	-	-	36, 90, 91, 92 (4)	-	4
Noise Tests ¹	-	-	-	31, 70, 71, 72 (4)	4
Variable Drainage ²	-	-	-	11, 32, 33, 34, 35 (5)	5
Strain Rate ³	-	-	-	22, 23, 24, 25, 26, 29, 30 (7)	7
Consolidation ⁴	-	-	-	37, 38, 39, 40 (4)	4
Error ⁵	-	-	-	27, 52, 57, 58 (4)	4
<i>Total</i>	<i>12</i>	<i>21</i>	<i>35</i>	<i>24</i>	<i>92</i>

Table 7.4 Summary of laboratory tests using triaxial test rig (notes overleaf)

The numbers in table 7.4 refer to the test identification number (pre-fixed with TR) except those in brackets which indicate the total number of tests conducted within that particular category.

- 1 Noise tests in which triaxial shear tests were conducted with no soil sample in place in order to determine the level of system (background) noise.
- 2 Triaxial shear tests in which drainage conditions were changed part-way through the test.
- 3 Triaxial shear tests in which a non-standard rate of strain was adopted. (The results from this series of tests was very disappointing and are not considered in the text).
- 4 Consolidation tests conducted on Leighton Buzzard sand to illustrate the *Kaiser* effect.
- 5 Triaxial shear tests in which the stress-strain relationship obtained indicates that some degree of error was present.

Test Code	Cell Pressure (kPa)	Mean Spherical Stress at Failure (kPa)	Test Type	Approximate Sample Pore Water Pressure at Failure (kPa)
TR1	100	293	CU	-37.9
TR2	200	476	CU	-10.8
TR3	300	642	CU	31.5
TR4	400	991	CU	-87.2
TR5	100	291	CU	-36.1
TR6	200	534	CU	-61.6
TR7	300	769	CU	-79.8
TR8	400	985	CU	-81.7
TR9	500	1105	CU	0.5
TR10	500	1170	CU	-56.3
TR12	100	243	CU	5.8
TR13	200	486	CU	-19.7
TR14	300	698	CU	-18.3
TR15	100	250	CU	-0.5
TR16	100	345	CU	-83.9
TR17	200	549	CU	-75.4
TR21	300	750	CU	-63.8
TR43	400	878	CU	12.0
TR46	500	1178	CU	-63.2
TR47	500	1175	CU	-60.3
TR56	500	1192	CU	-75.2
TR44	500	1108	UU	-2.1
TR45	100	272	UU	-19.8
TR48	400	1004	UU	-98.4
TR49	100	346	UU	-84.4
TR53	200	564	UU	-87.7
TR55	300	711	UU	-29.3
TR61	400	977	UU	-75.2
TR62	500	1114	UU	-7.3

Table 7.5 Estimate of pore water pressures existing in samples at point of failure

Box Test	Description of Box Test
B1	A noise test, conducted with no fill in the box.
B2	A noise test, conducted with no fill in the box.
B3	A noise test, conducted with the box filled with 'Arlesey' sand and with the load hanger attached to the wave guide section (but no load).
B4	A load test, conducted with the box filled with 'Arlesey' sand. A 40N force was applied to the load hanger, which had the effect of pulling the wave guide section through its maximum travel (approximately 50mm).
B5	Test B4 was left standing for approximately two hours and test B5 conducted to investigate the noise levels being generated after some equilibrium of the backfill had been regained.
B6	A noise test, conducted with the box filled with 'Arlesey' sand.
B7	A load test, conducted with the box filled with 'Arlesey' sand. A 10N force was applied to the load hanger and readings noted from the dial gauge every 50 seconds.
B8	A continuation of test B7. Approximately one hour after test B7 had been concluded, an additional 10N force was applied to the load hanger (total load 20N) and, again, dial gauge readings were taken every 50 seconds.
B9	A noise test, conducted with no fill in the box.
B10	A load test, conducted with the box filled with 'Cowden' gravel. A 5N force was applied to the load hanger and readings noted from the dial gauge every 50 seconds.
B11	A continuation of test B10. Approximately one hour after test B10 had been concluded, an additional 5N force was applied to the load hanger (total load 10N). This had the effect of pulling the wave guide section through its maximum travel (approximately 50mm).

Table 7.6 Description of Box tests

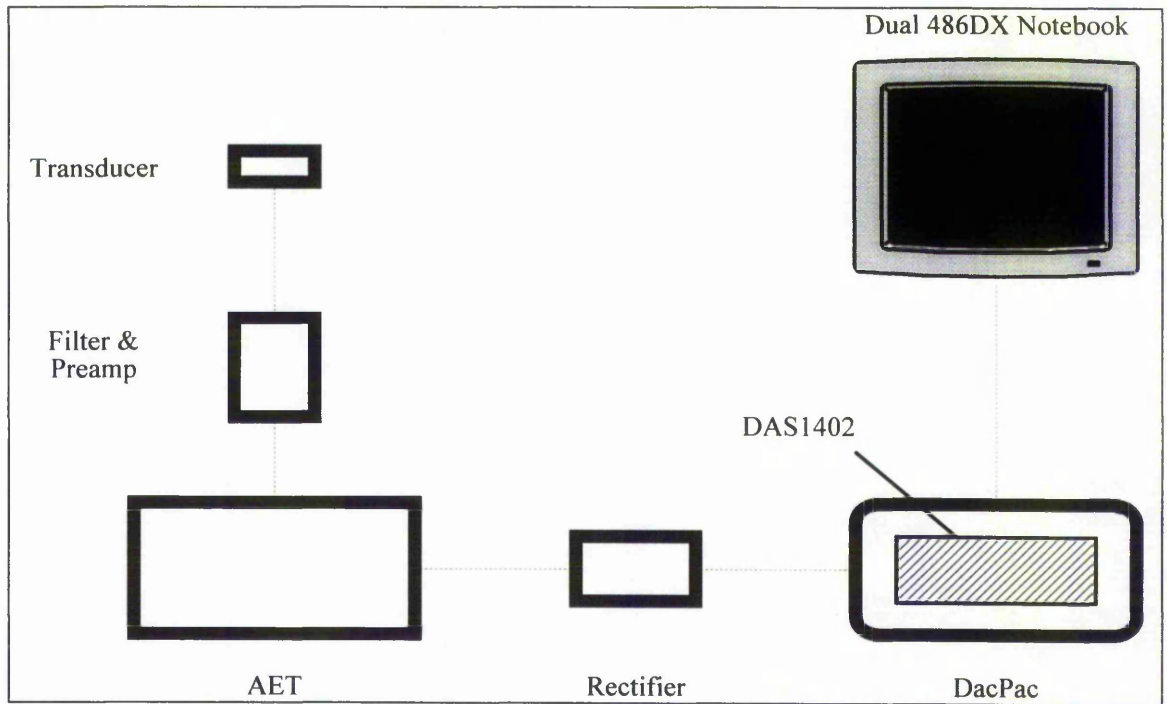
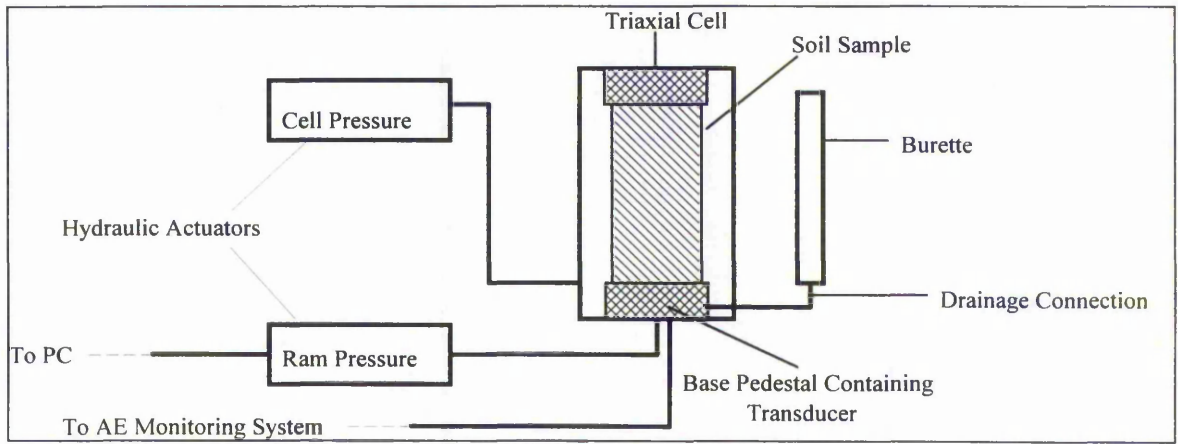


Figure 7.1 AE monitoring system (bottom) and additional triaxial testing equipment (top)

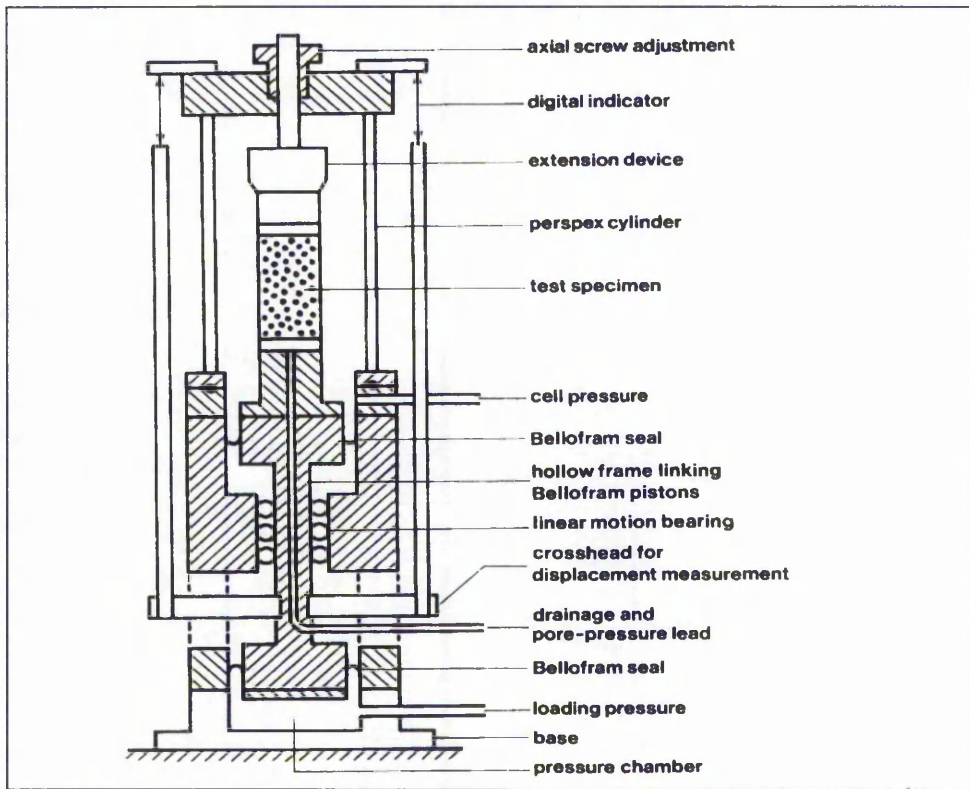


Figure 7.2 Schematic of Bishop & Wesley triaxial cell

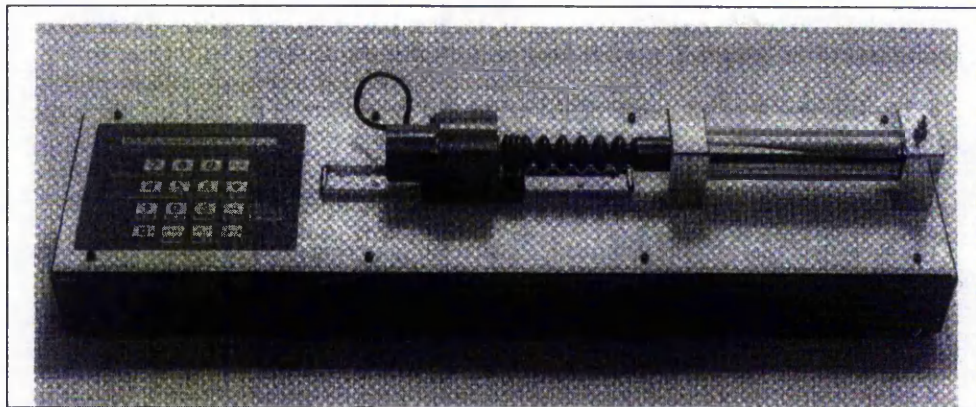


Figure 7.3 A GDS digital controller

(both figures after Menzies 1988)

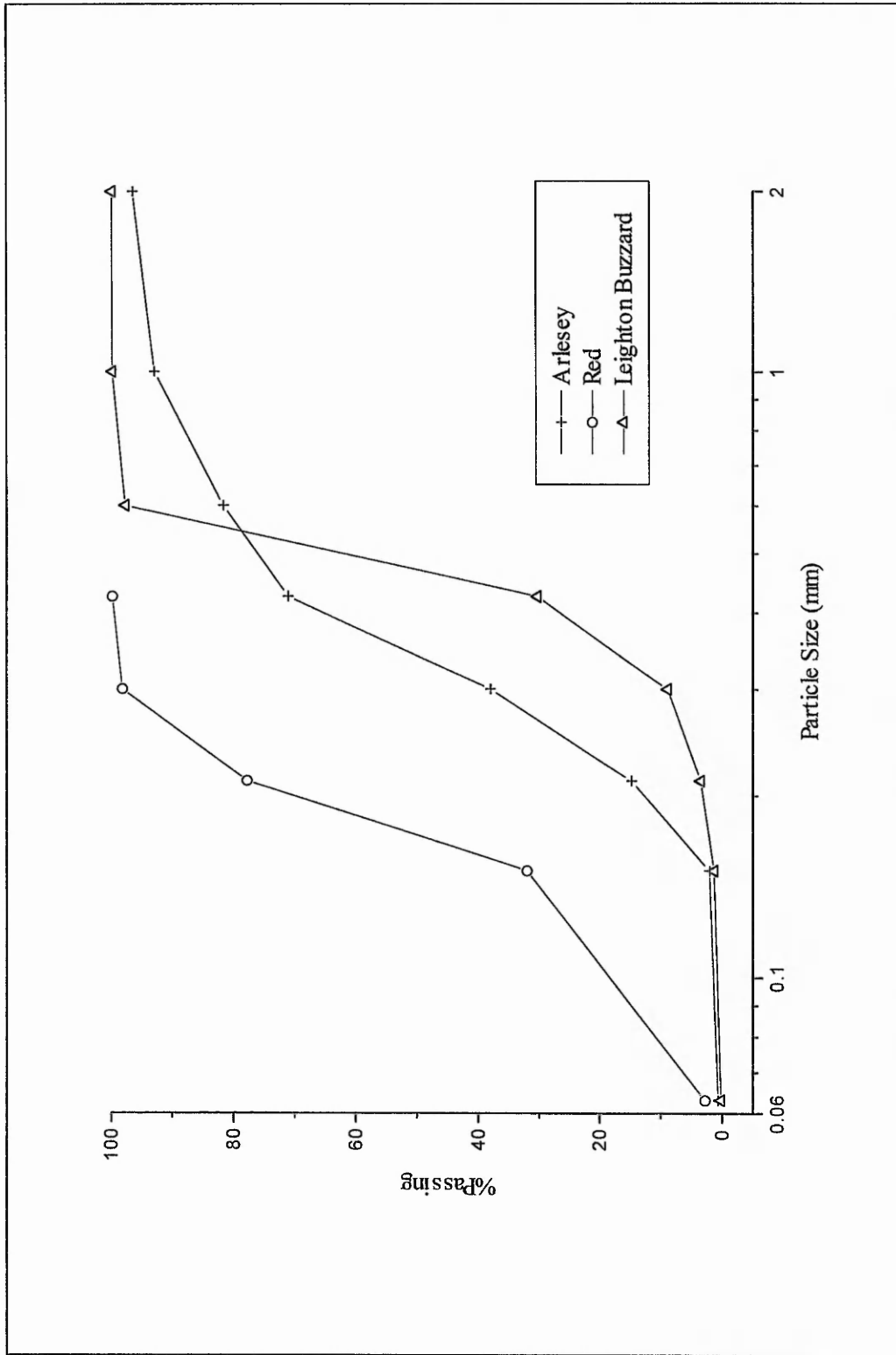


Figure 7.4 Particle Size Distribution (PSD) curves for 'Red', 'Arlesey' and Leighton Buzzard sands

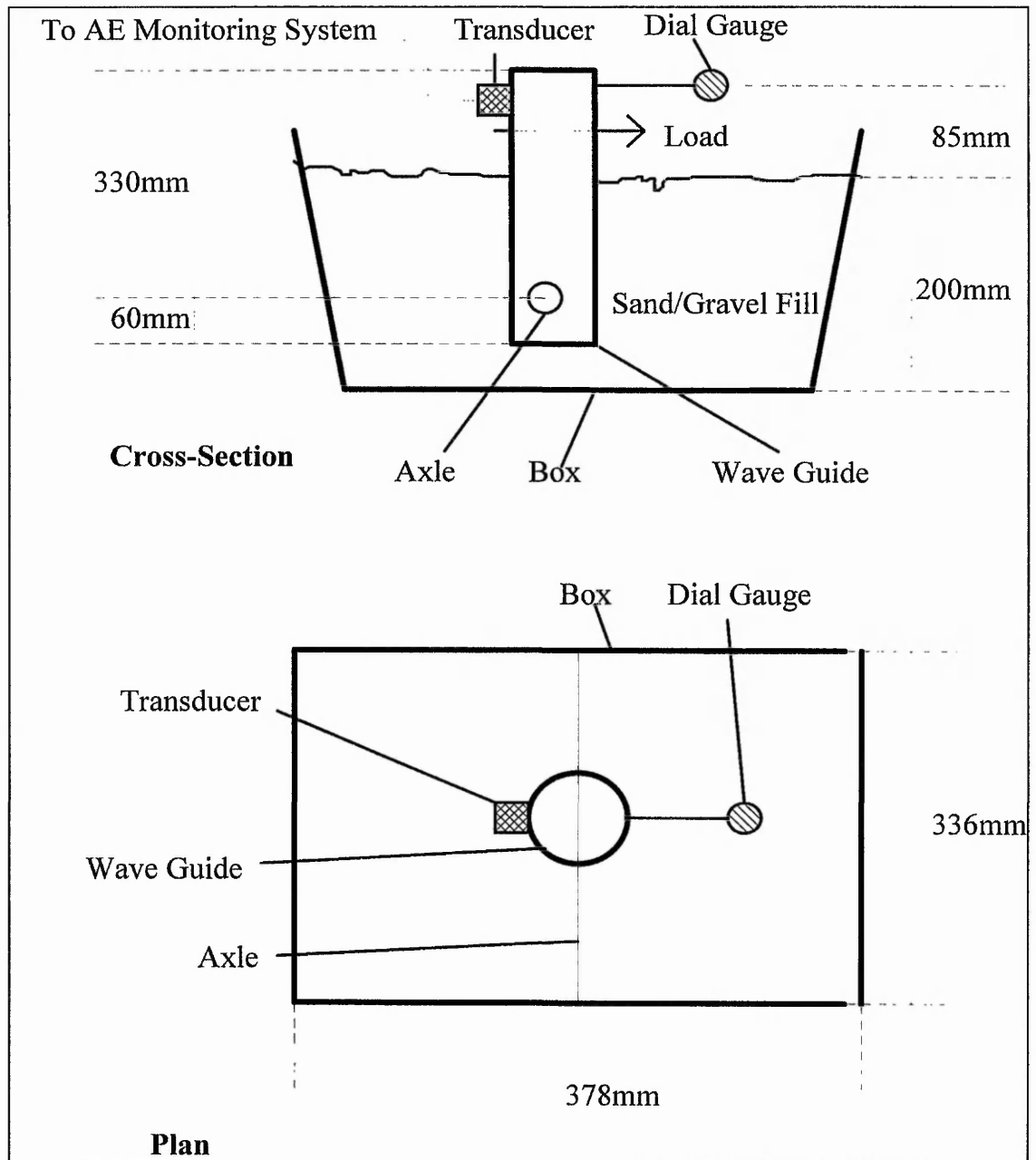


Figure 7.5 'Box' test equipment

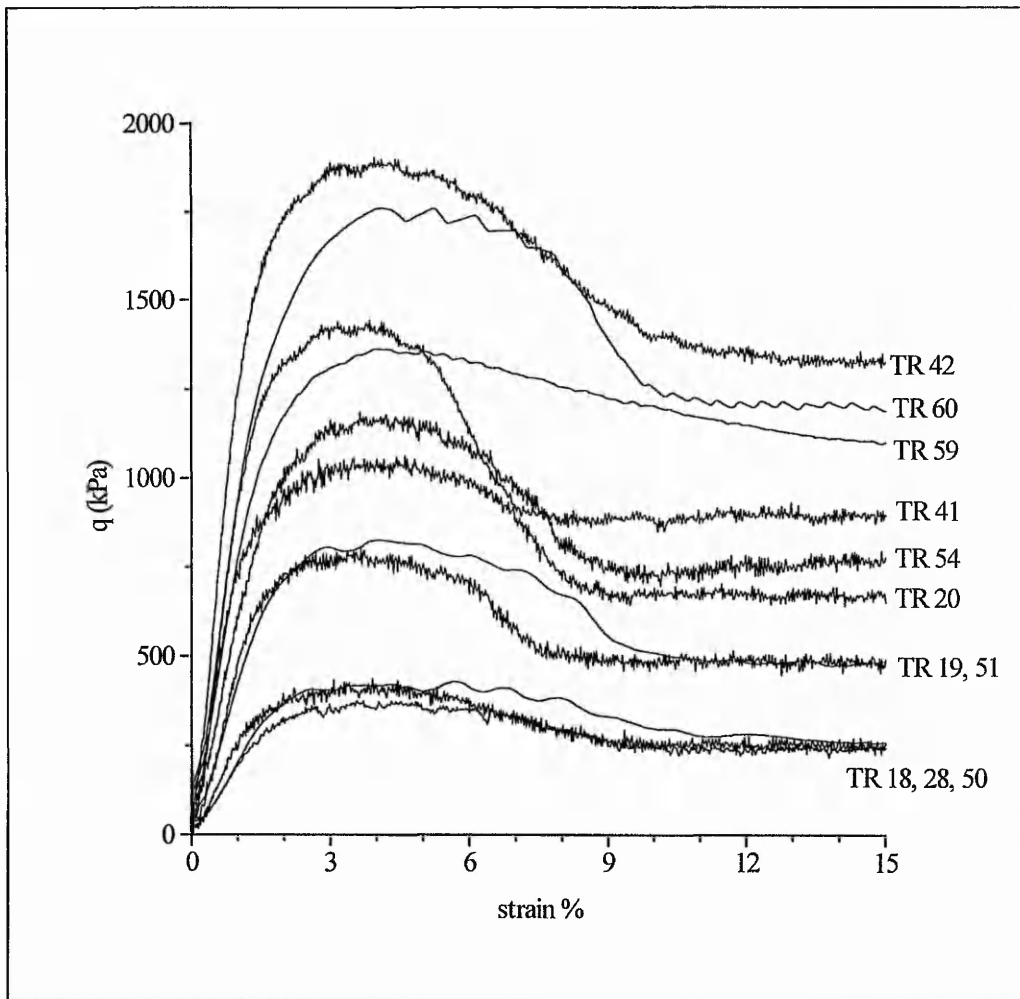


Figure 7.6 q vs axial strain for eleven drained triaxial shear tests conducted on samples of Leighton Buzzard sand.

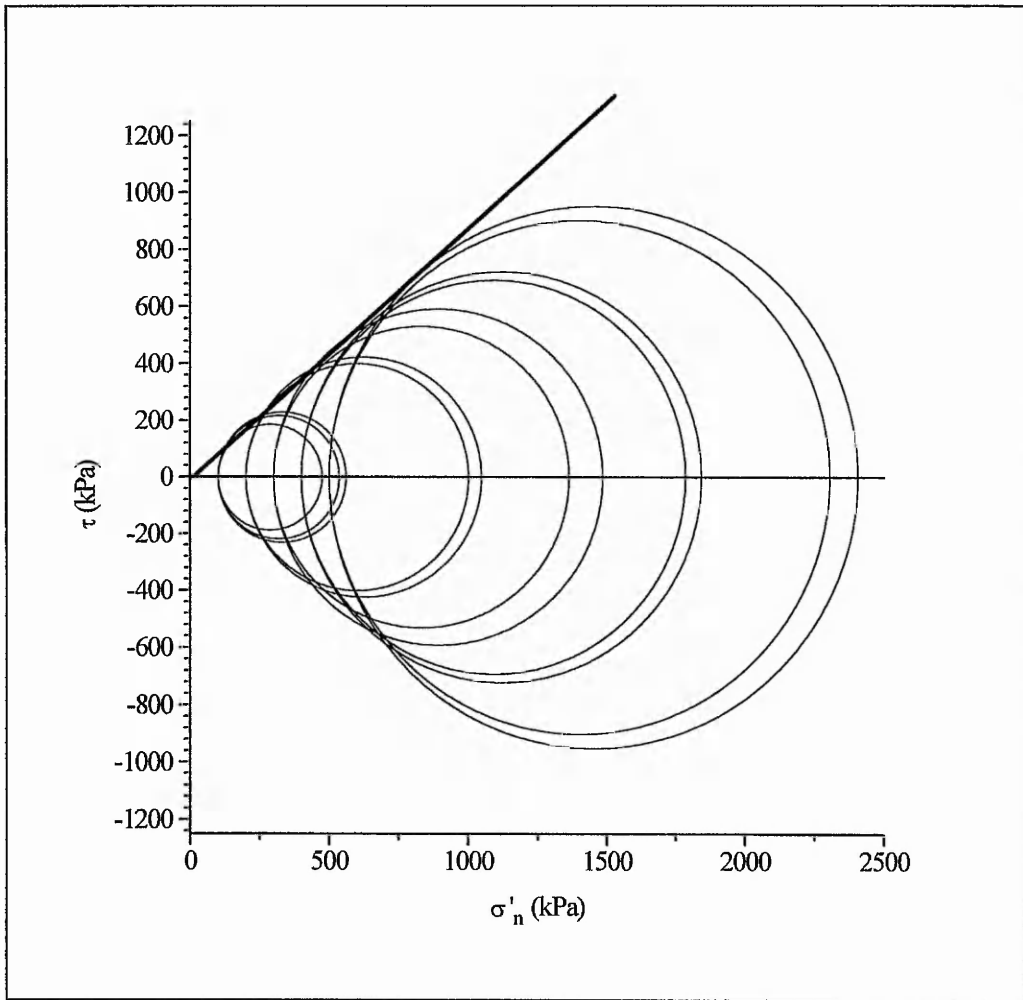


Figure 7.7 Mohr stress circles for eleven drained triaxial shear tests conducted on samples of Leighton Buzzard sand. A general tangent fitted to the circles produces a value for ϕ'_{\max} of approximately 41° . Note that, because these are drained tests, the normal stresses are *effective*.

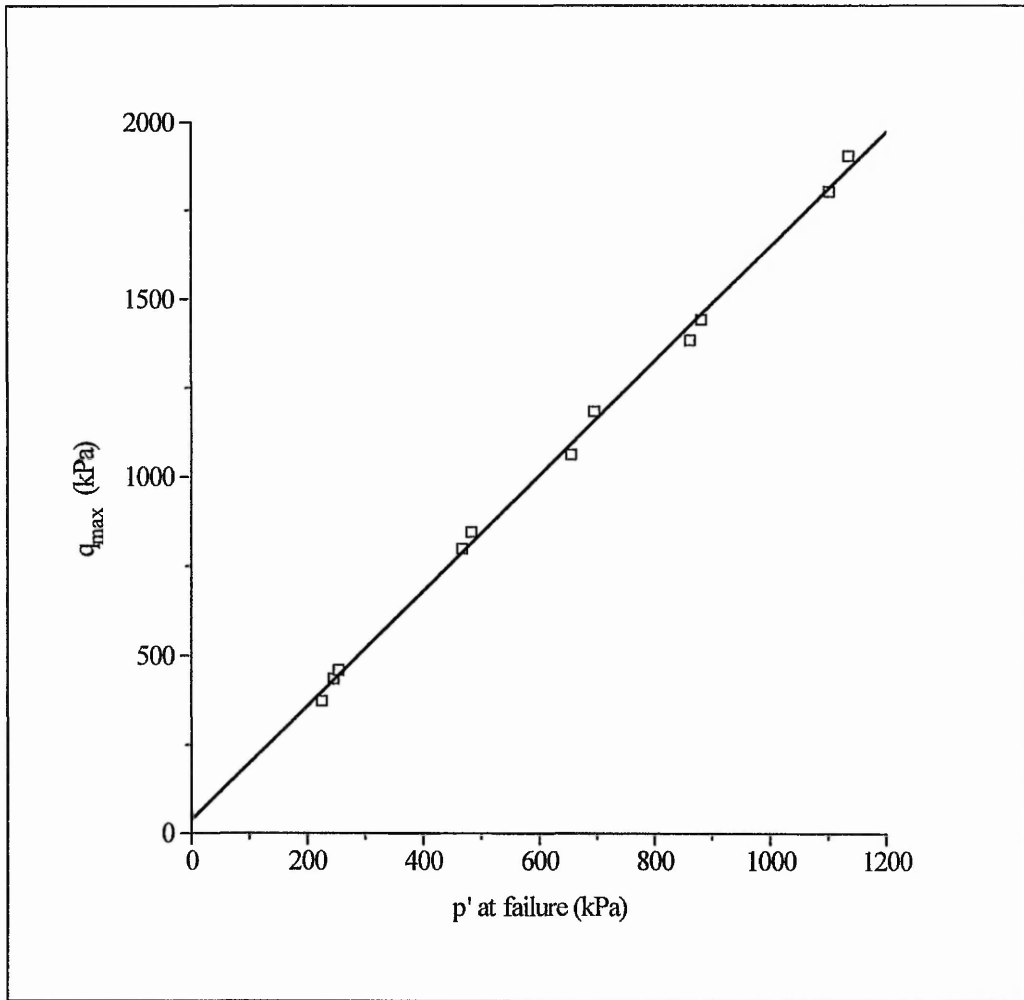


Figure 7.8 q_{max} vs p' at failure for eleven drained triaxial tests conducted on Leighton Buzzard sand (with a 'best-fit' line drawn through the data)

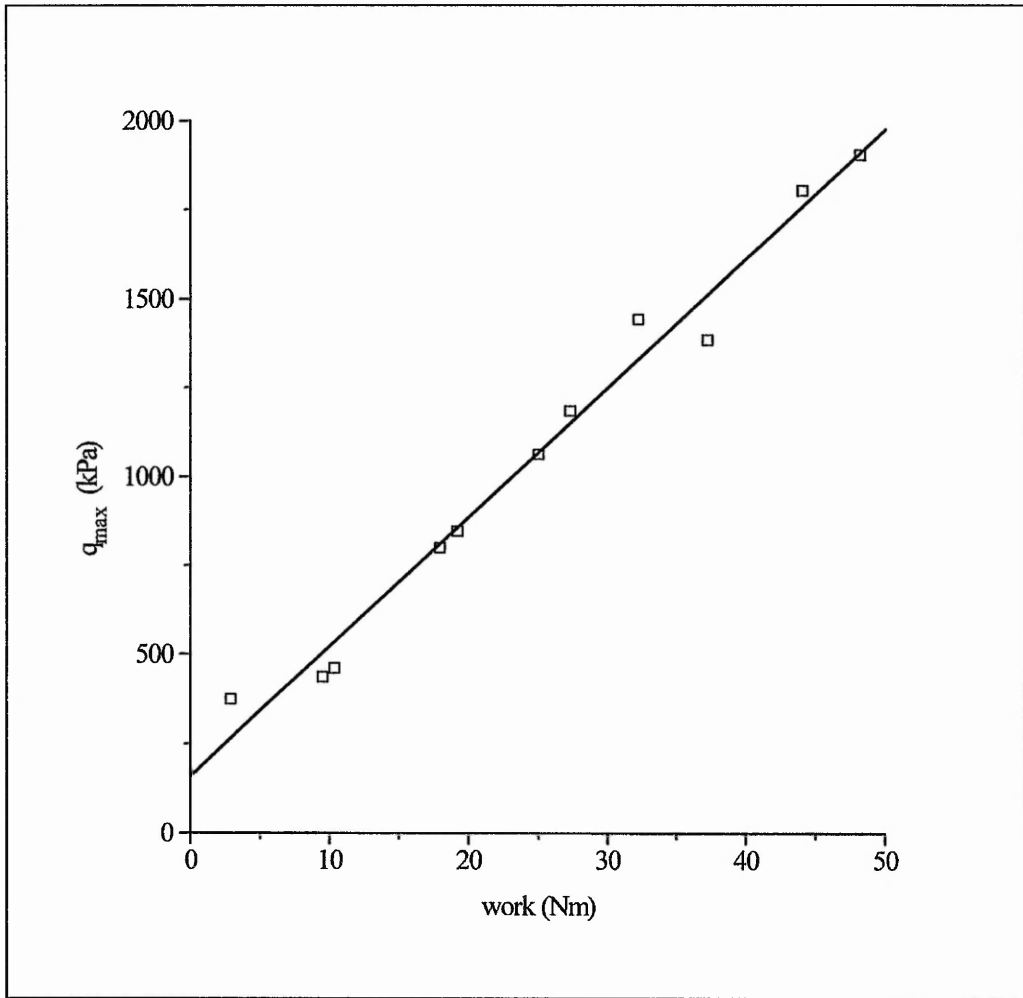


Figure 7.9 q_{\max} plotted as a function of work performed on the sample for eleven drained triaxial shear tests conducted on Leighton Buzzard sand (with a 'best-fit' line drawn through the data)

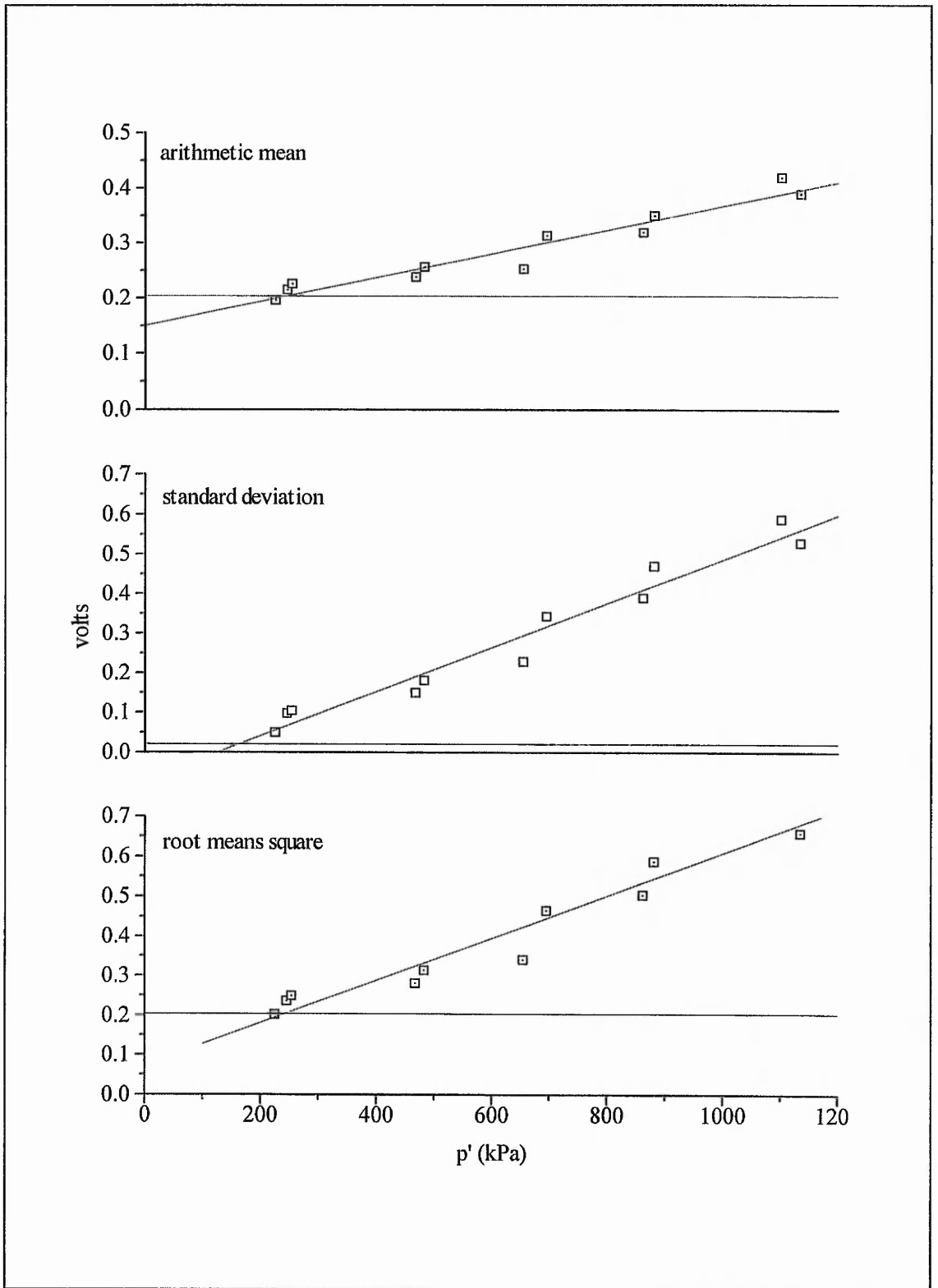


Figure 7.10 Bulk AE data acquired from 11 drained triaxial tests conducted on Leighton Buzzard Sand plotted against p' at failure. (Note that the average noise level is also shown)

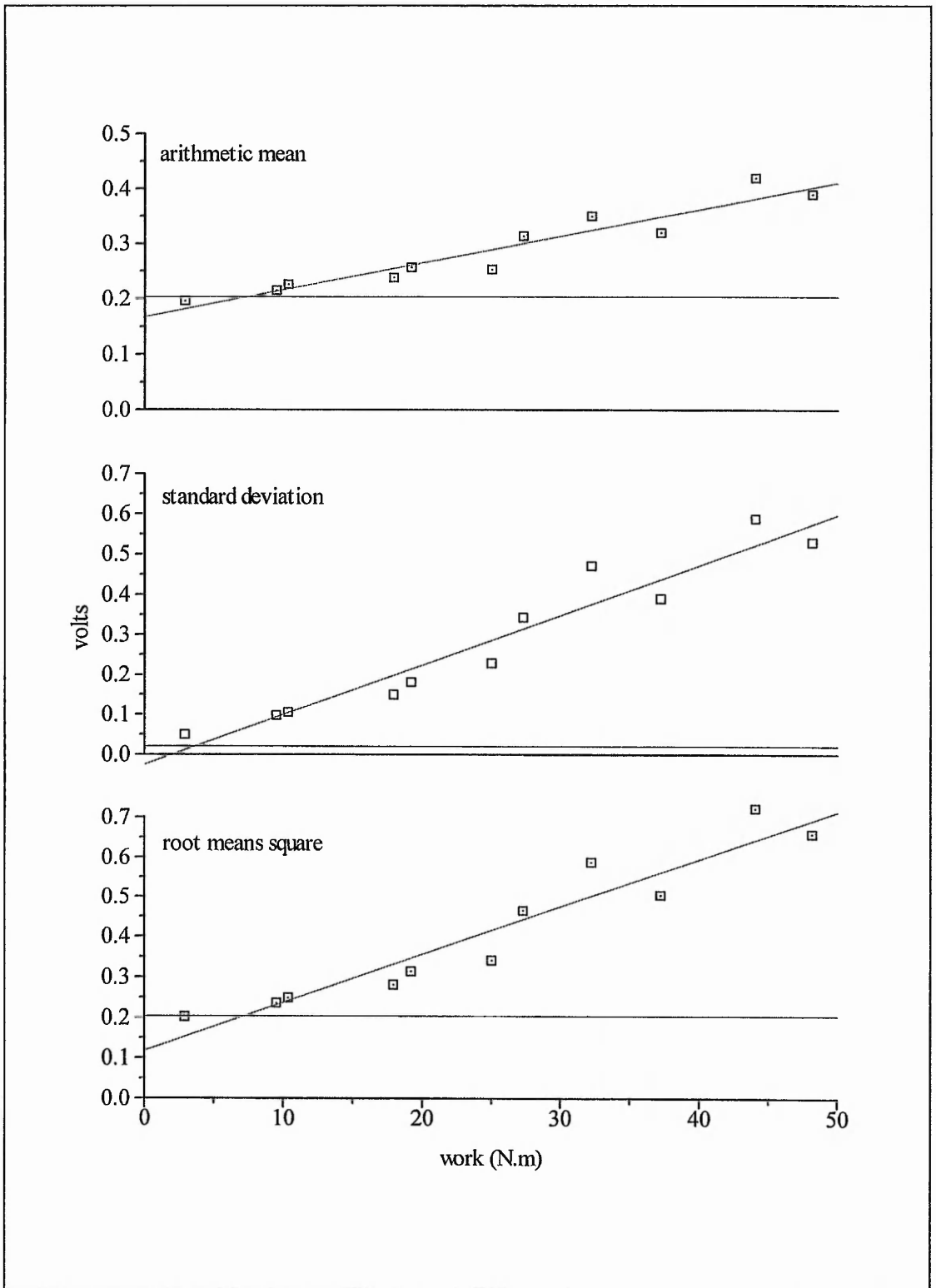


Figure 7.11 Bulk AE data acquired from 11 drained triaxial tests conducted on Leighton Buzzard Sand plotted against work. (Note the average noise level is also shown)

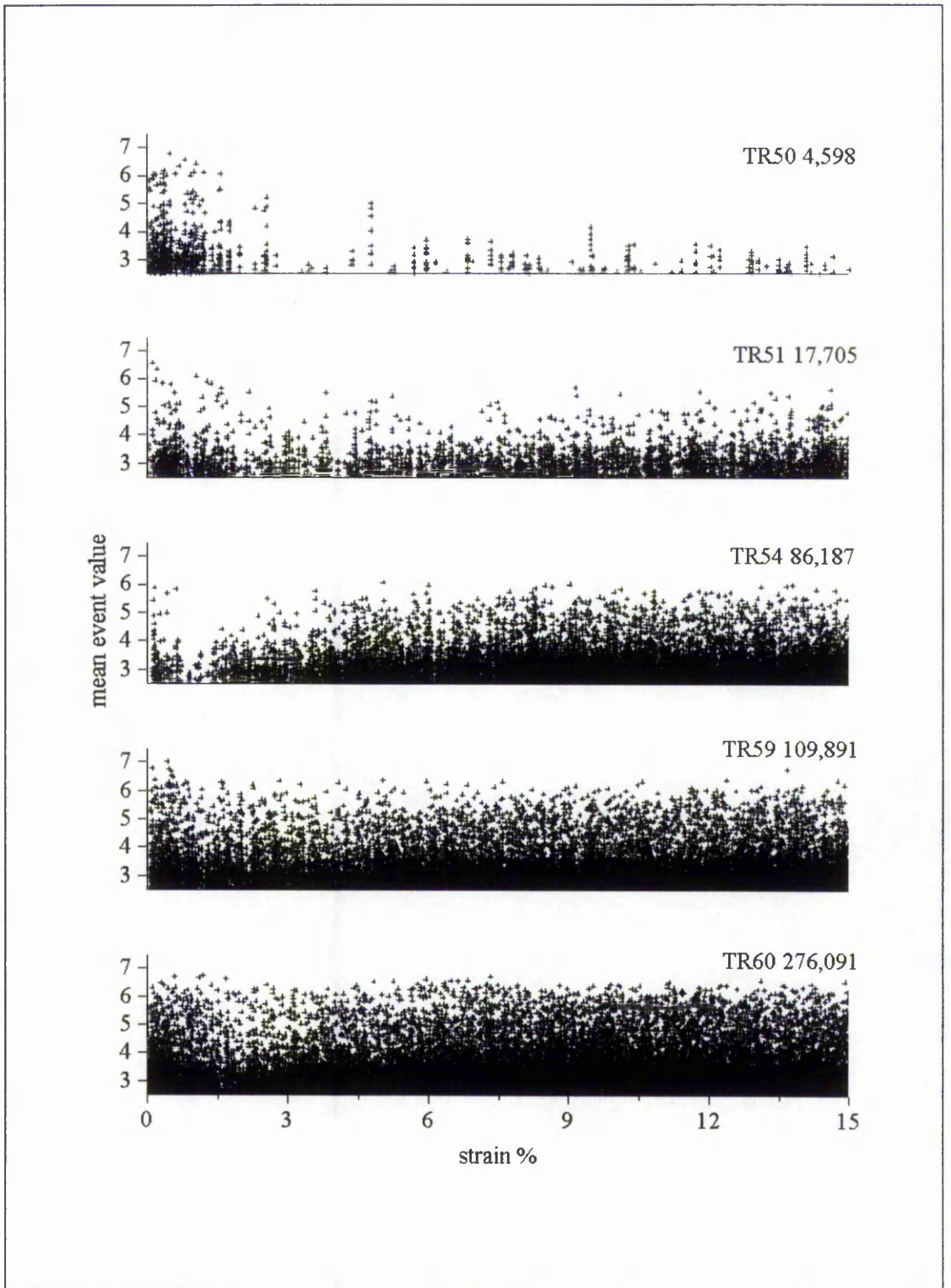


Figure 7.12 Event map depicting the mean magnitude of each event (in volts) against strain for TR50, 51, 54, 59 & 60. (Note that the total number of post-threshold data points for each test is also indicated in the graph)

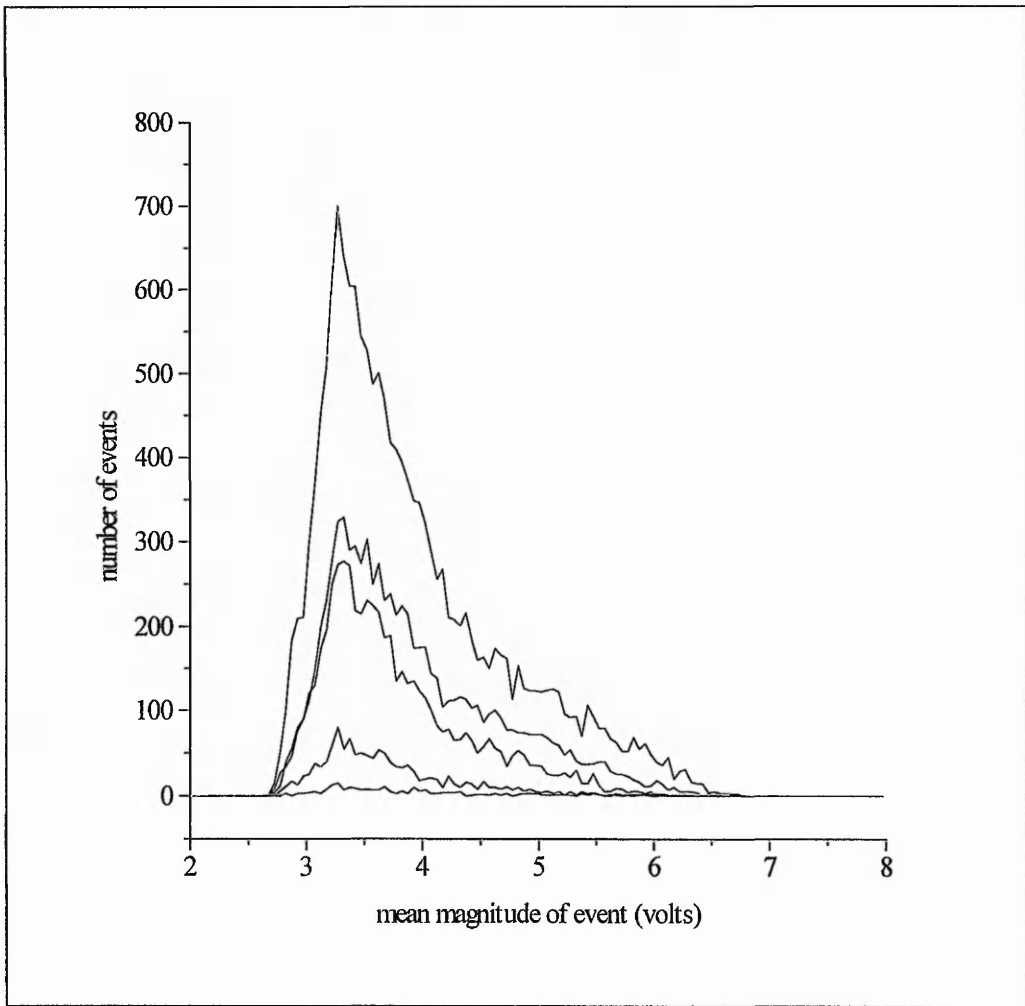


Figure 7.13 Frequency distribution of mean magnitude of event for all events with 3 or more data points for five drained triaxial shear tests conducted on Leighton Buzzard Sand (TR50, 51, 54, 59 & 60)

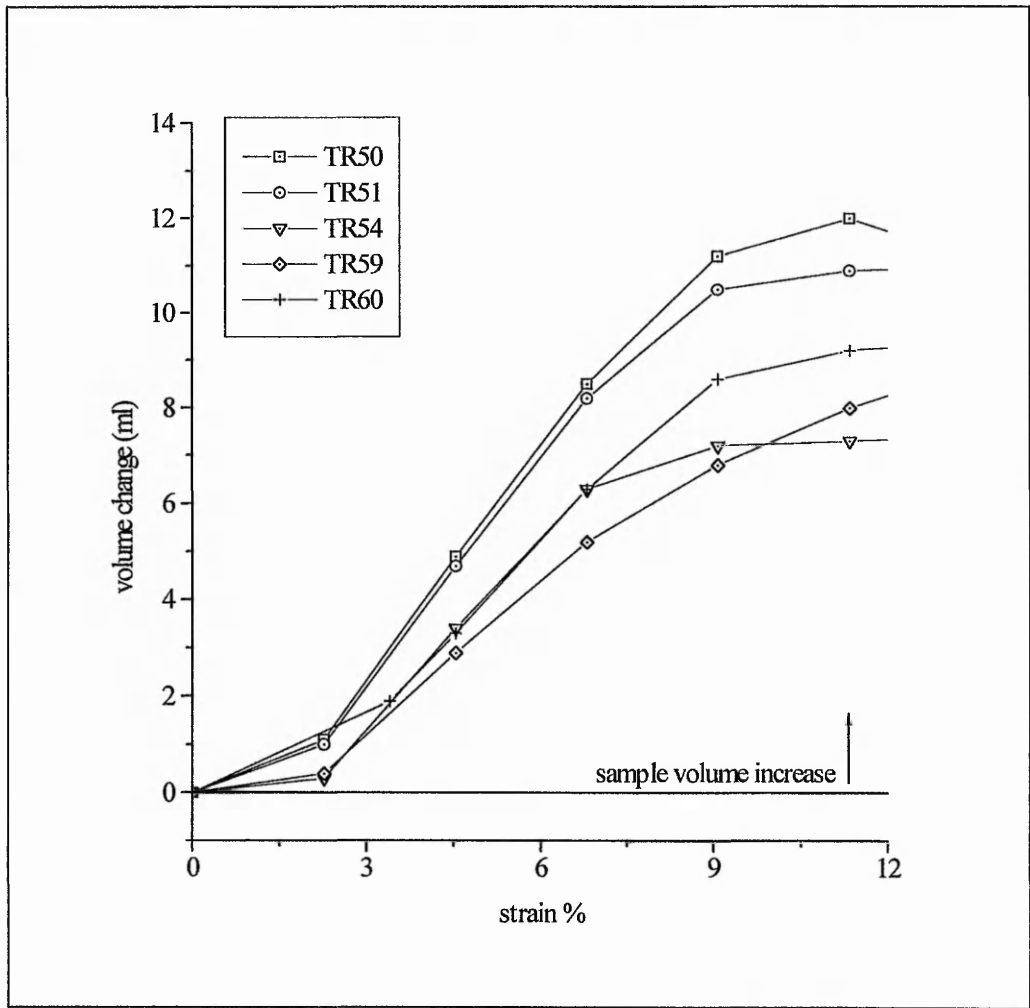


Figure 7.14 Change in sample volume, recorded for five drained triaxial shear tests conducted on Leighton Buzzard Sand, over the course of each test. TR 50, 51, 54, 59 & 60 equate to cell pressures (σ_3) of 100, 200, 300, 400 & 500kPa respectively.

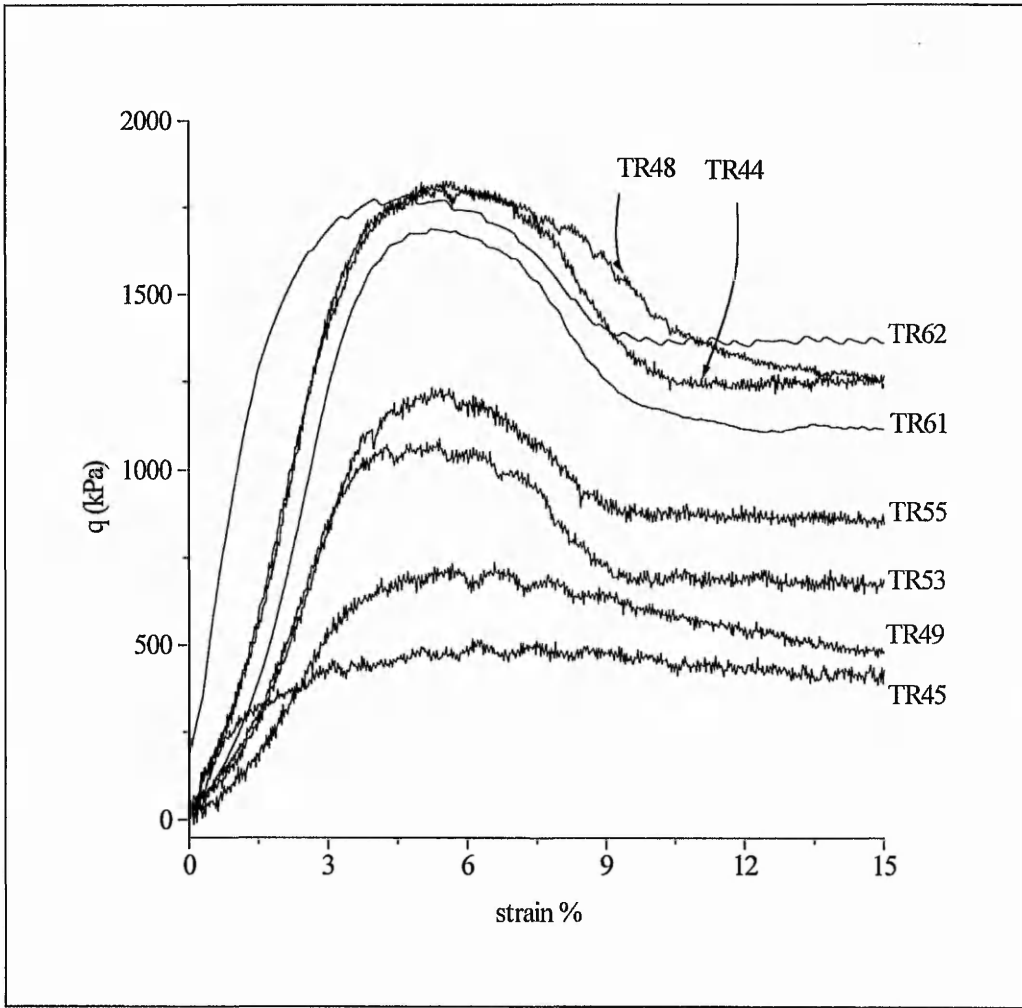


Figure 7.15 q vs axial strain for eight unconsolidated nominally undrained triaxial shear tests conducted on samples of Leighton Buzzard Sand.

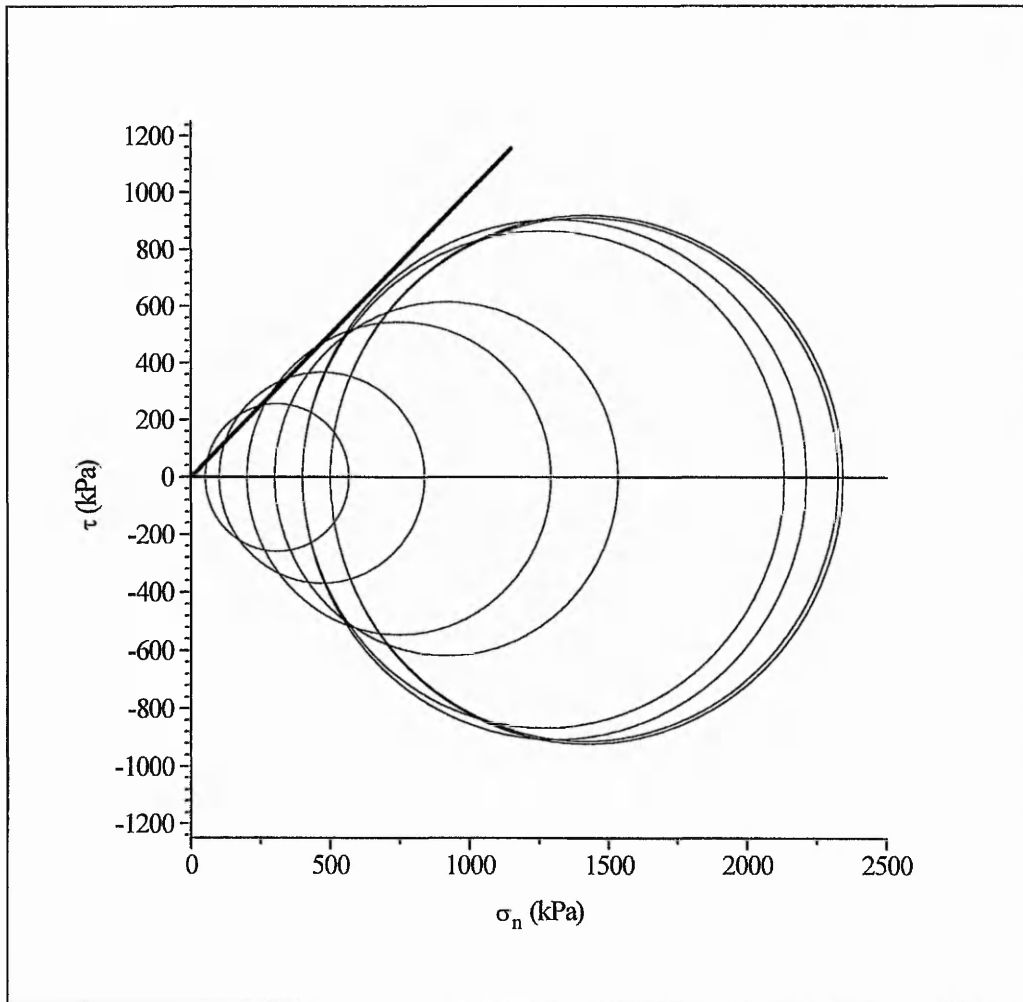


Figure 7.16 Mohr stress circles for eight unconsolidated nominally undrained triaxial shear tests conducted on samples of Leighton Buzzard Sand. A general tangent fitted to the circles produces a value for ϕ_{\max} of approximately 46° . Note that, because these are undrained tests, the normal stresses are *total*.

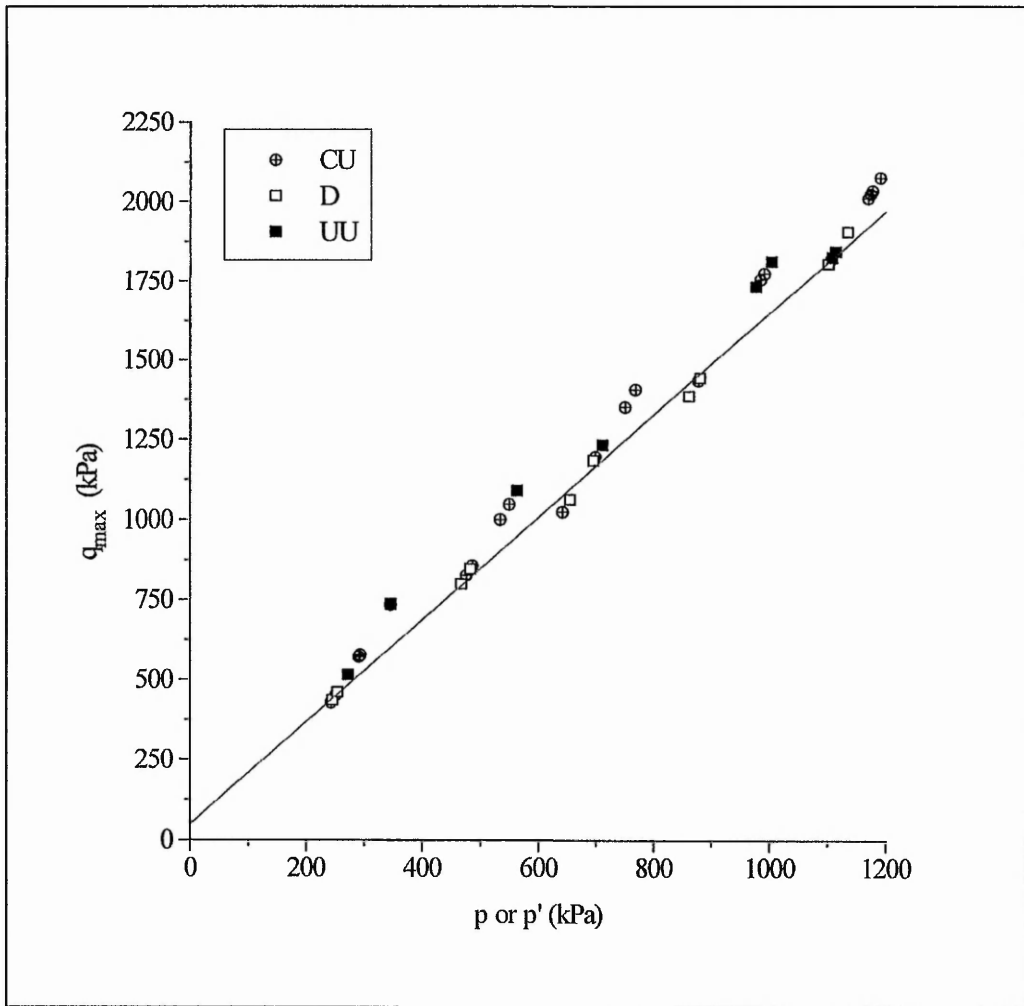


Figure 7.17 q_{max} plotted as function of p' for drained tests (D) and as a function of p for consolidated nominally undrained (CU) and unconsolidated nominally undrained tests (UU). Note that the 'best-fit' line is only drawn through the drained test results.

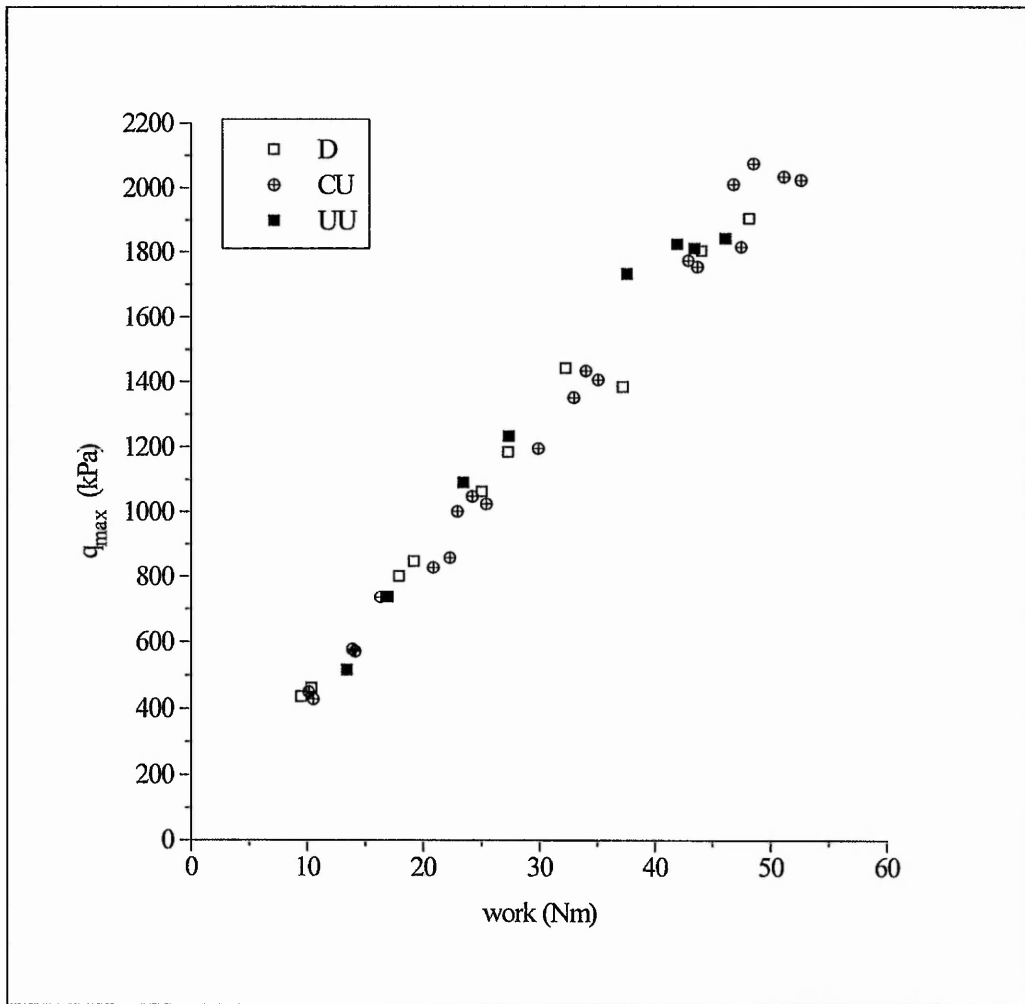


Figure 7.18 q_{max} as a function of work for a total of 39 drained (D), consolidated nominally undrained (CU) and unconsolidated nominally undrained (UU) triaxial shear tests conducted on Leighton Buzzard Sand.

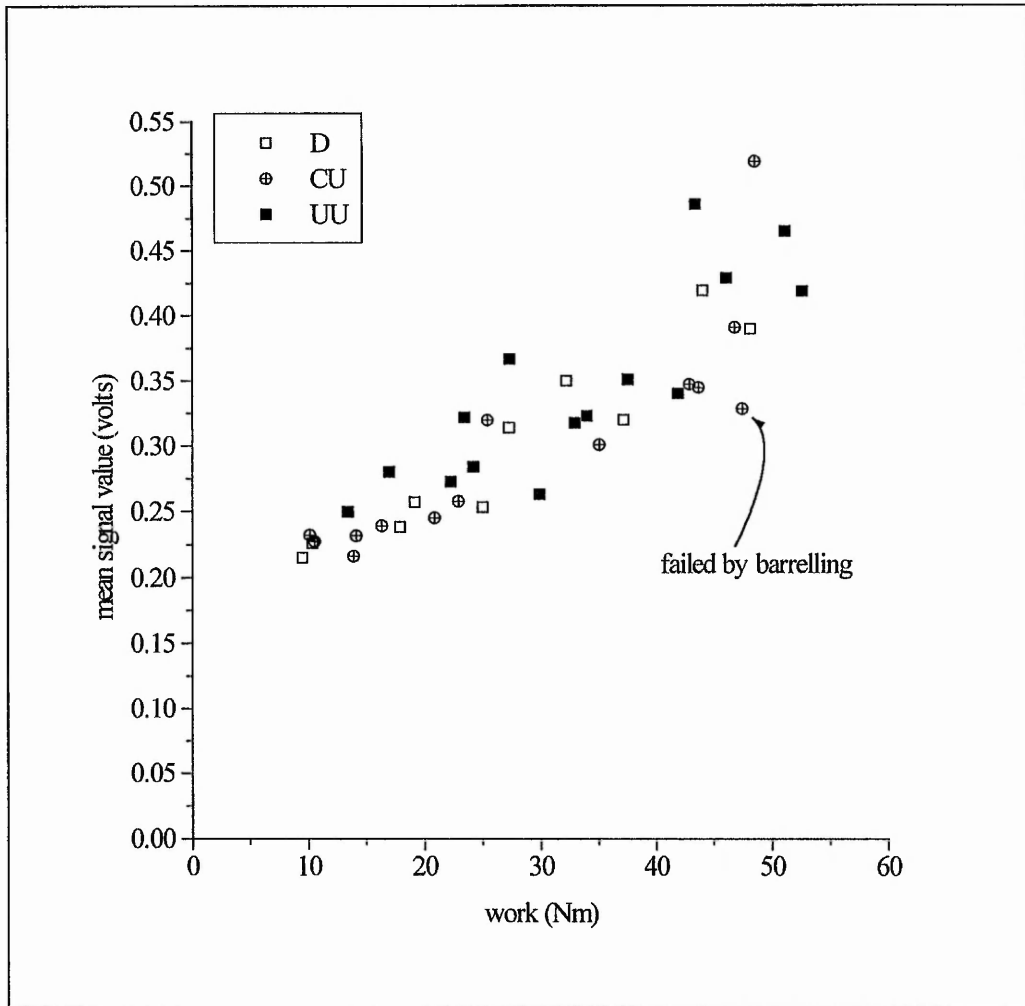


Figure 7.19 AE mean signal value as a function of work for a total of 39 drained, consolidated nominally undrained and unconsolidated nominally undrained triaxial shear tests conducted on Leighton Buzzard Sand.

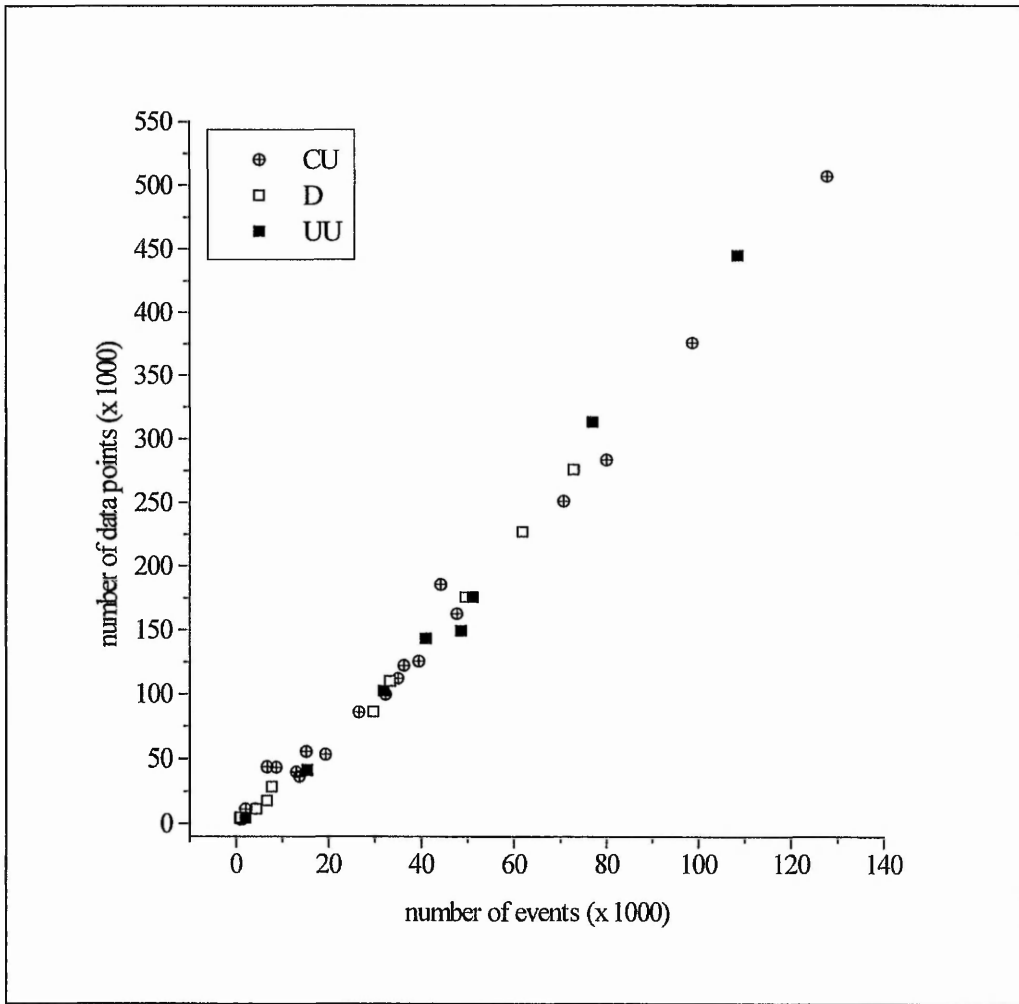


Figure 7.20 Number of post-threshold data points against number of events for a total of 39 drained, consolidated nominally undrained and unconsolidated nominally undrained triaxial shear tests conducted on Leighton Buzzard Sand.

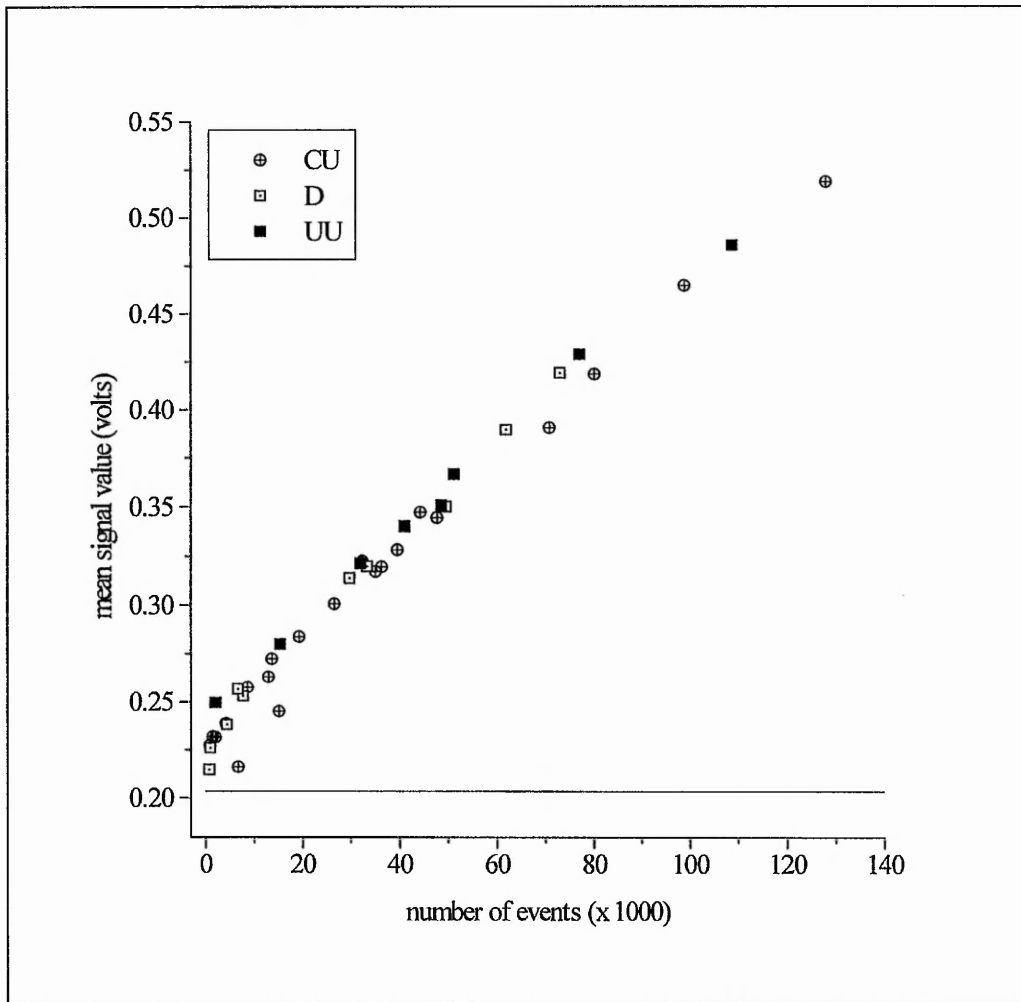


Figure 7.21 AE mean signal value against number of events for a total of 39 drained, consolidated nominally undrained and unconsolidated nominally undrained triaxial shear tests conducted on Leighton Buzzard Sand. (Note the average level of noise is also shown)

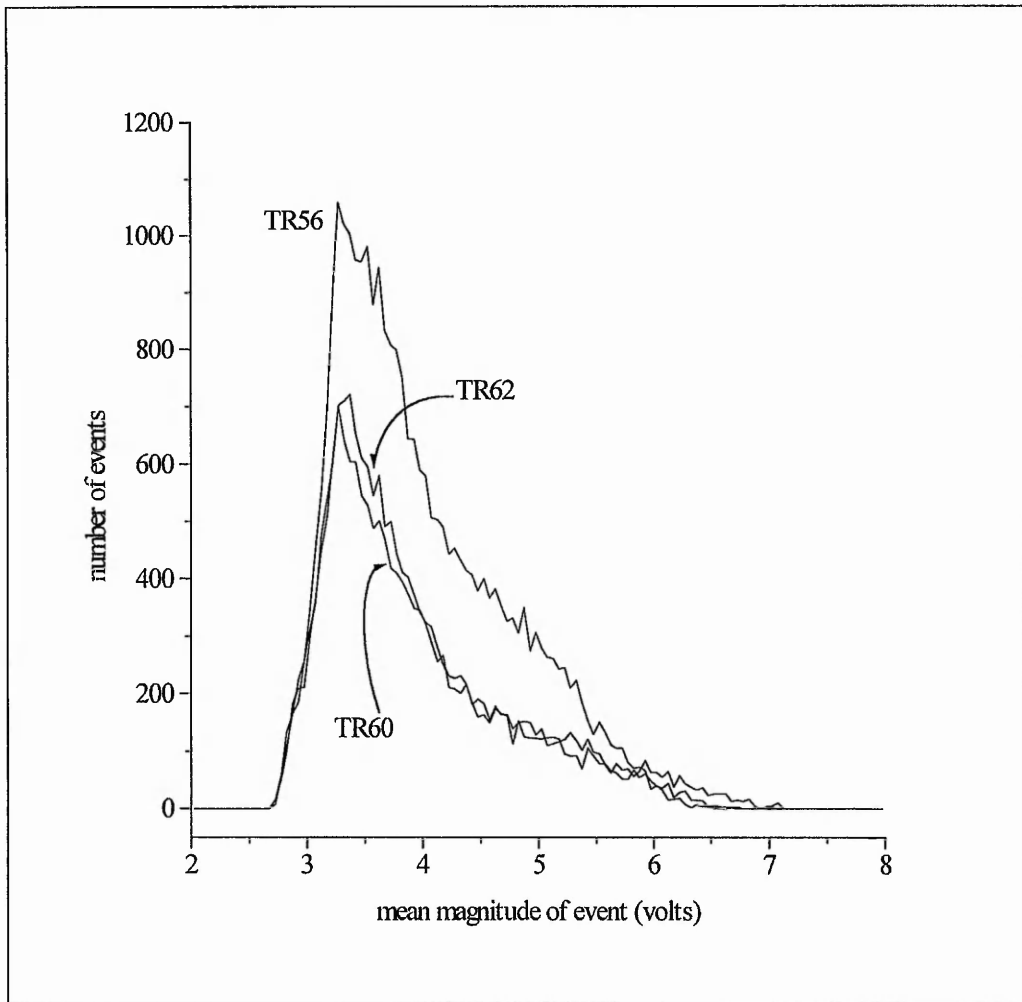


Figure 7.22 Frequency distribution of mean magnitude of event for all events with 3 plus data points for TR56 (consolidated nominally undrained), TR60 (drained), & TR62 (unconsolidated nominally undrained) derived from triaxial shear tests conducted on Leighton Buzzard Sand.

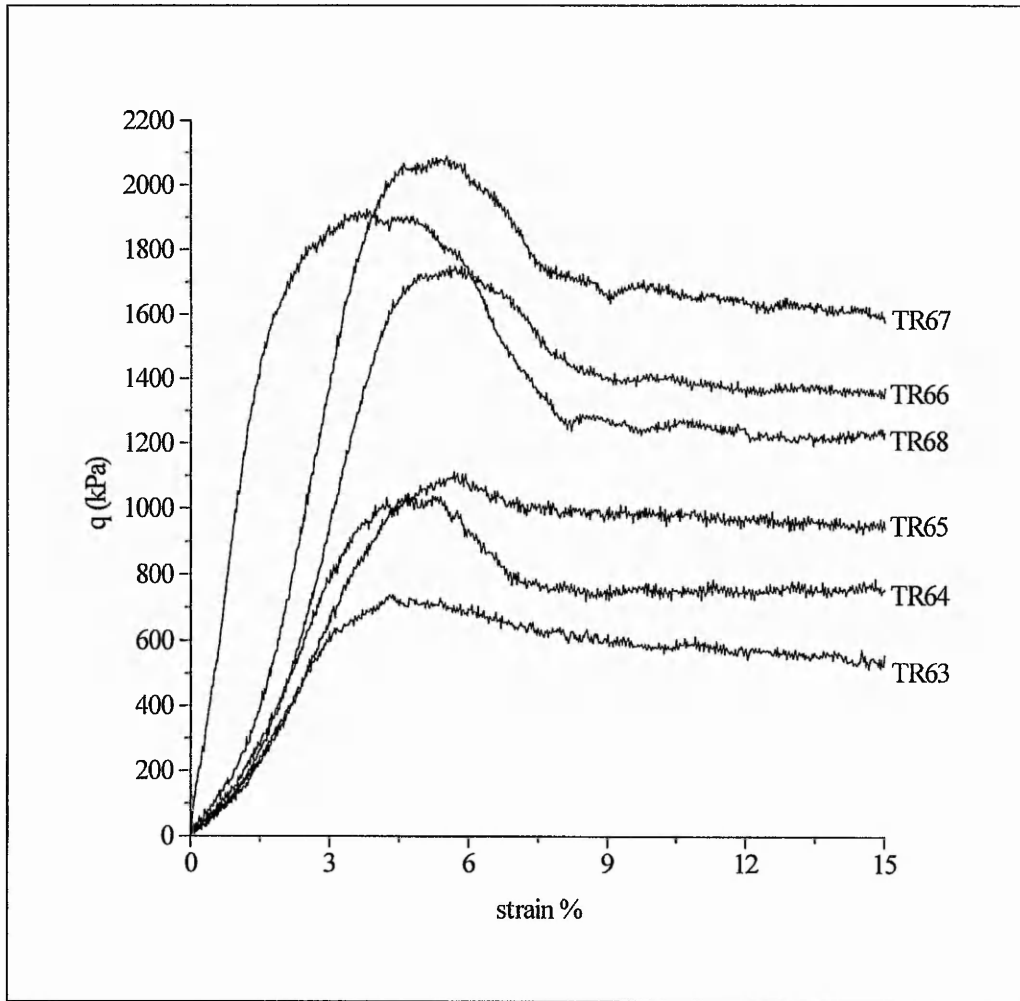


Figure 7.23 q vs axial strain for five nominally undrained (TR63, TR64, TR65, TR66 & TR67) and one drained (TR68) triaxial shear tests conducted on samples of 'Arlesey' sand.

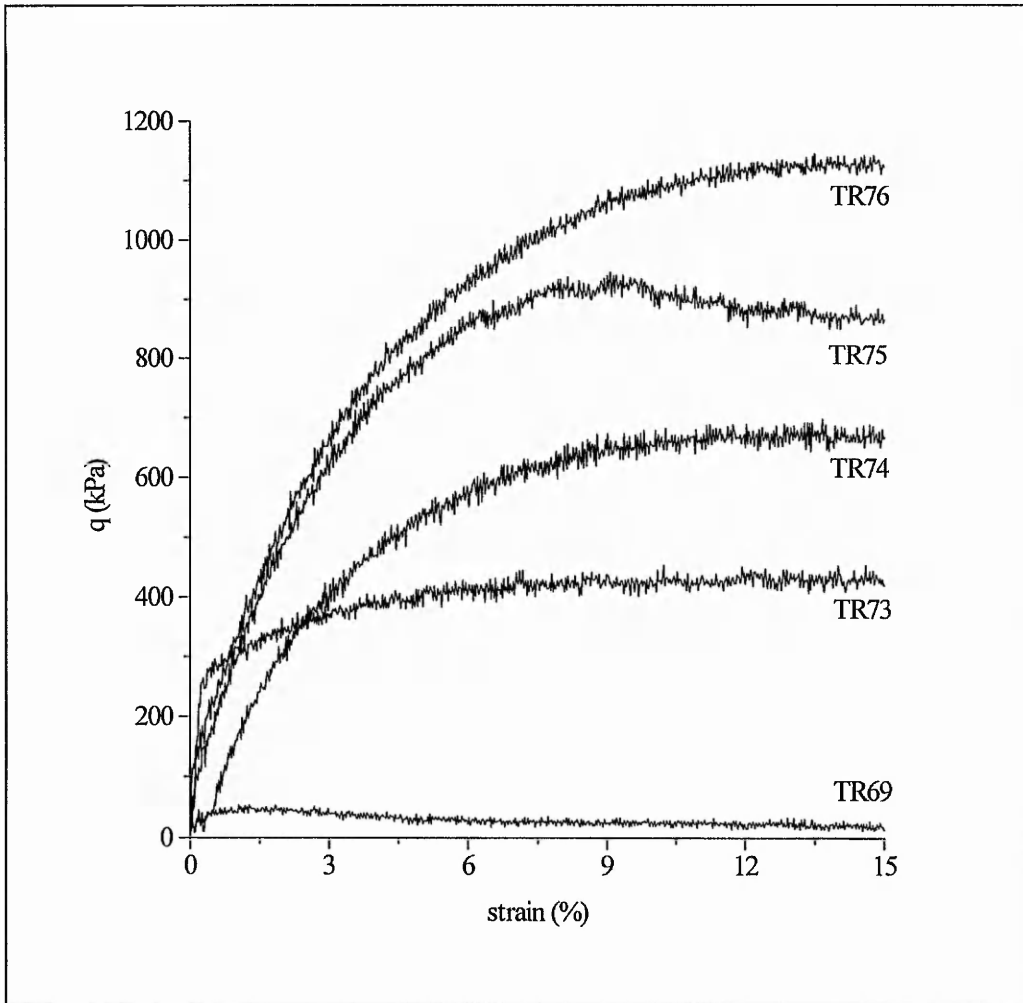


Figure 7.24 q vs axial strain for five nominally undrained (TR69, TR73, TR74, TR75 & TR76) triaxial shear tests conducted on samples of 'Red' sand.

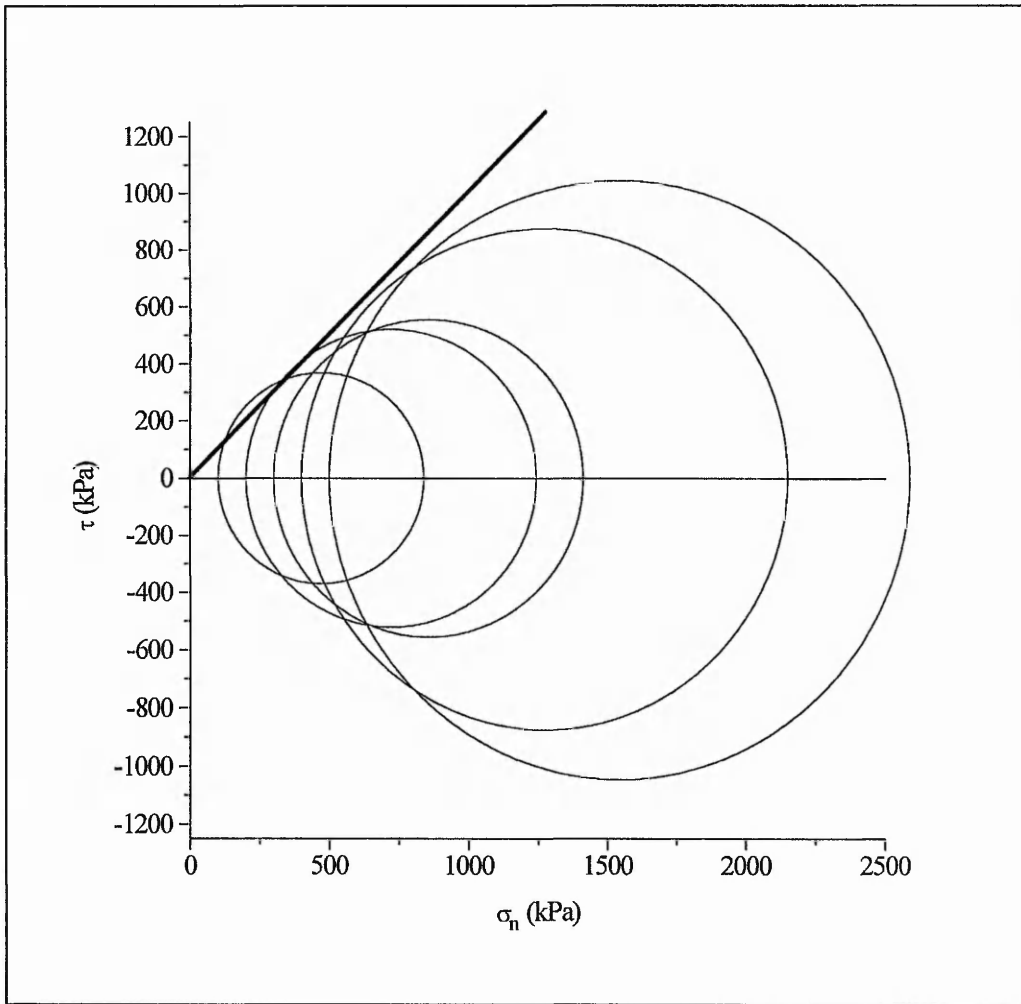


Figure 7.25 Mohr stress circles for five unconsolidated nominally undrained triaxial shear tests conducted on samples of 'Arlesey' sand. A general tangent fitted to the test circles produces a value for ϕ_{\max} of approximately 44° . Note that the normal stresses are *total*.

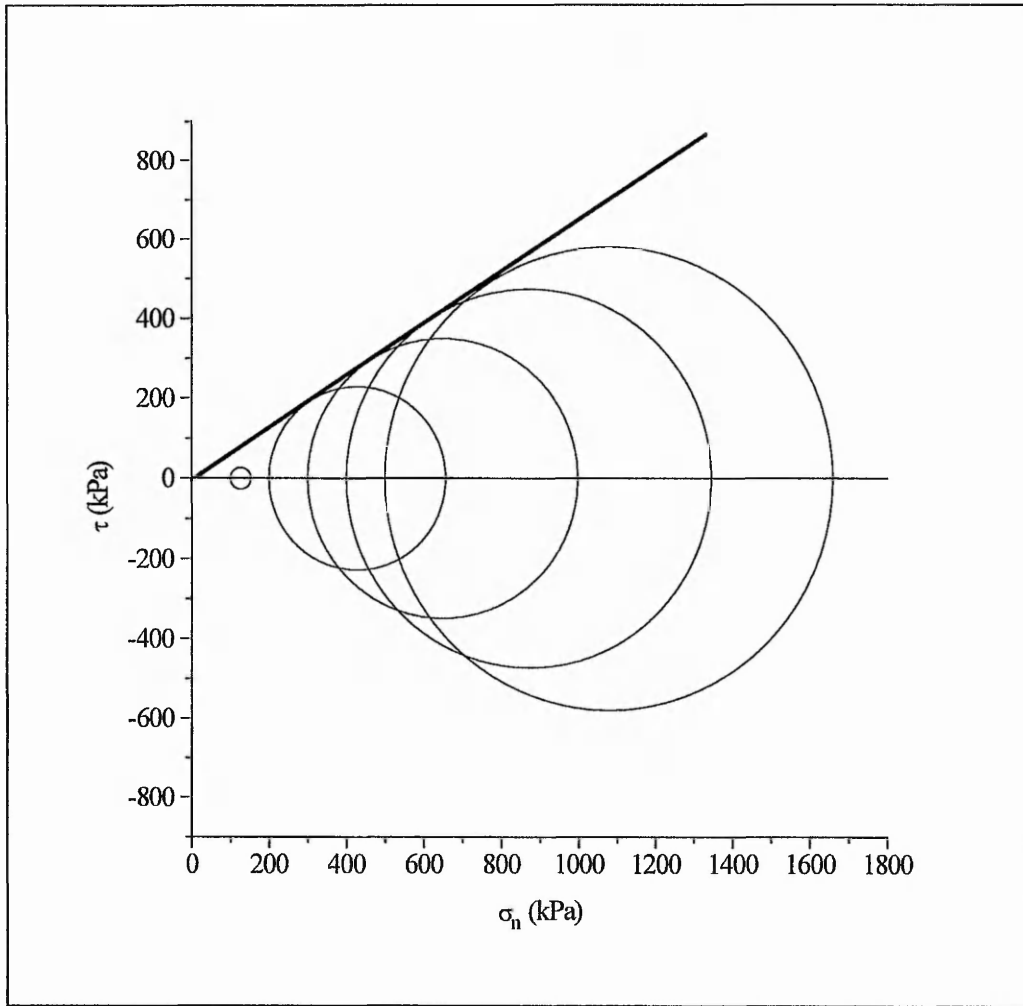


Figure 7.26 Mohr stress circles for five nominally undrained triaxial shear tests conducted on samples of 'Red' sand. A general tangent fitted to the circles (ignoring the first) produces a value for ϕ_{\max} of approximately 33° . Note that, because these are undrained tests, the normal stresses are *total*.

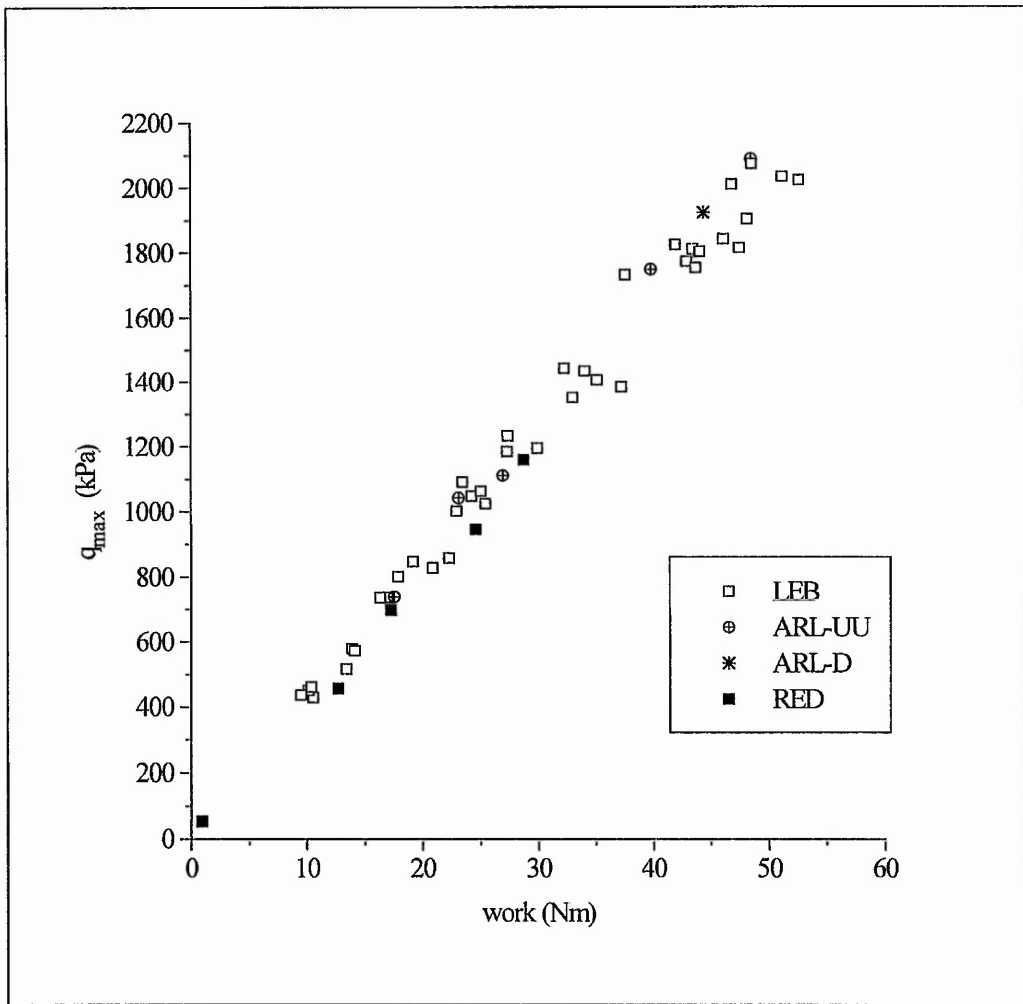


Figure 7.27 q_{max} vs work done for thirty-nine triaxial shear tests conducted on Leighton Buzzard sand, six triaxial shear tests conducted on 'Arlesey' sand and five triaxial shear tests conducted on 'Red' sand

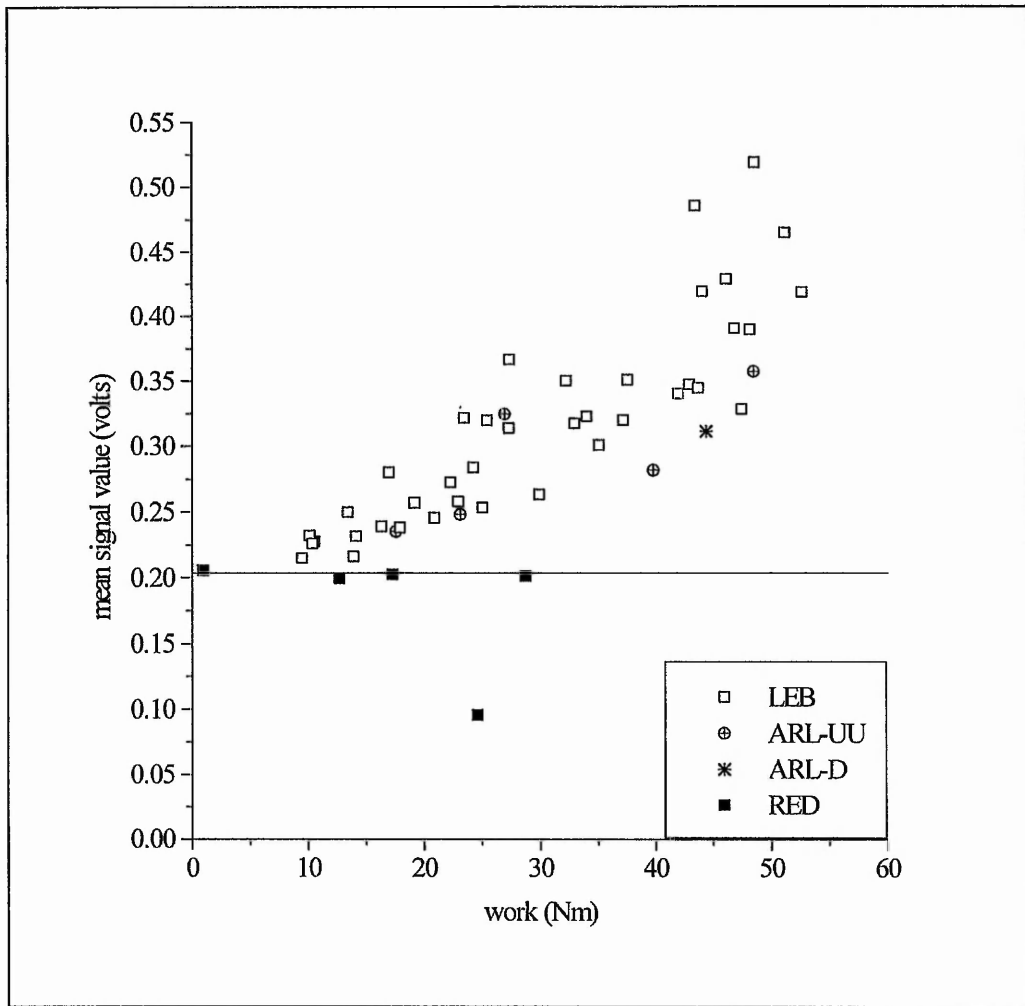


Figure 7.28 AE mean signal value (bulk data) as a function of work done on sample for thirty-nine triaxial shear tests conducted on Leighton Buzzard Sand, six triaxial shear tests conducted on 'Arlesey' sand and five triaxial shear tests conducted on 'Red' sand. (Note the average noise level is also shown)

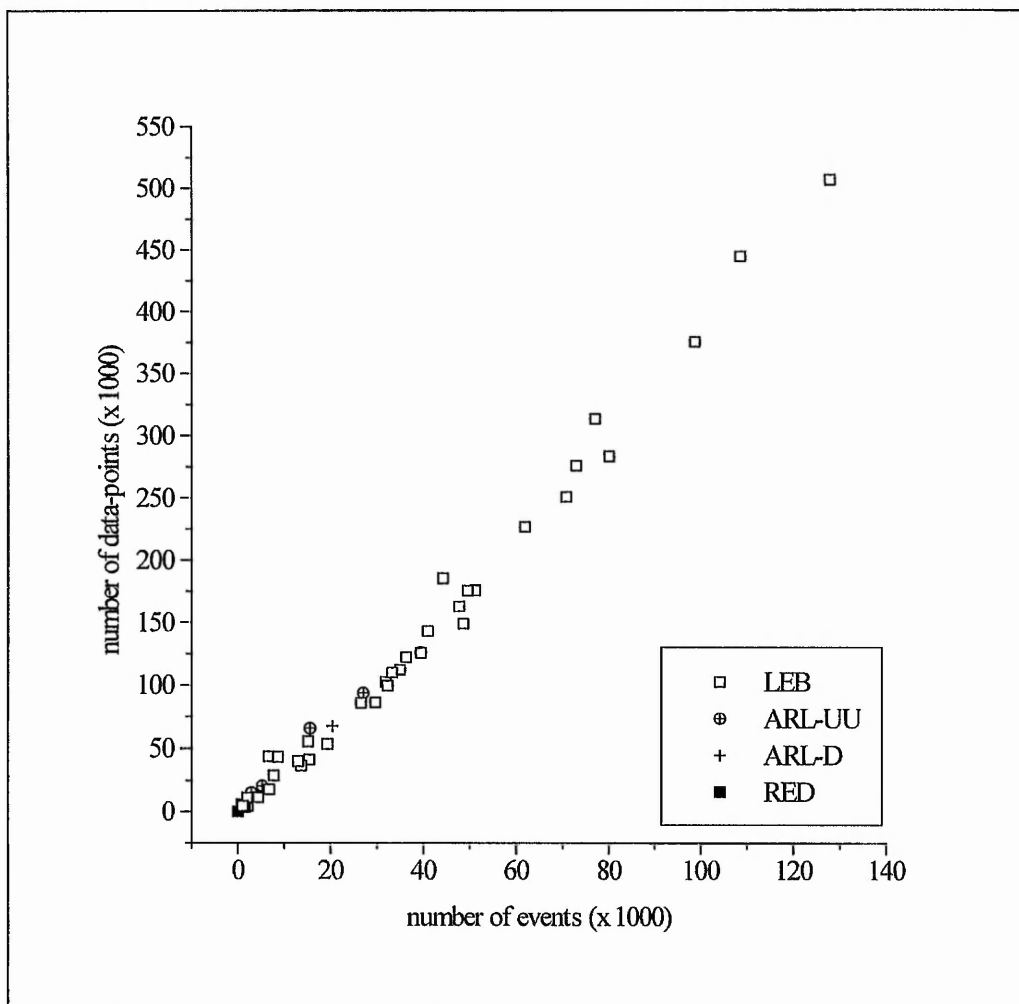


Figure 7.29 Number of post-threshold data points vs number of events for thirty-nine triaxial shear tests conducted on Leighton Buzzard sand, six triaxial shear tests conducted on 'Arlesey' sand and five triaxial shear tests conducted on 'Red' sand

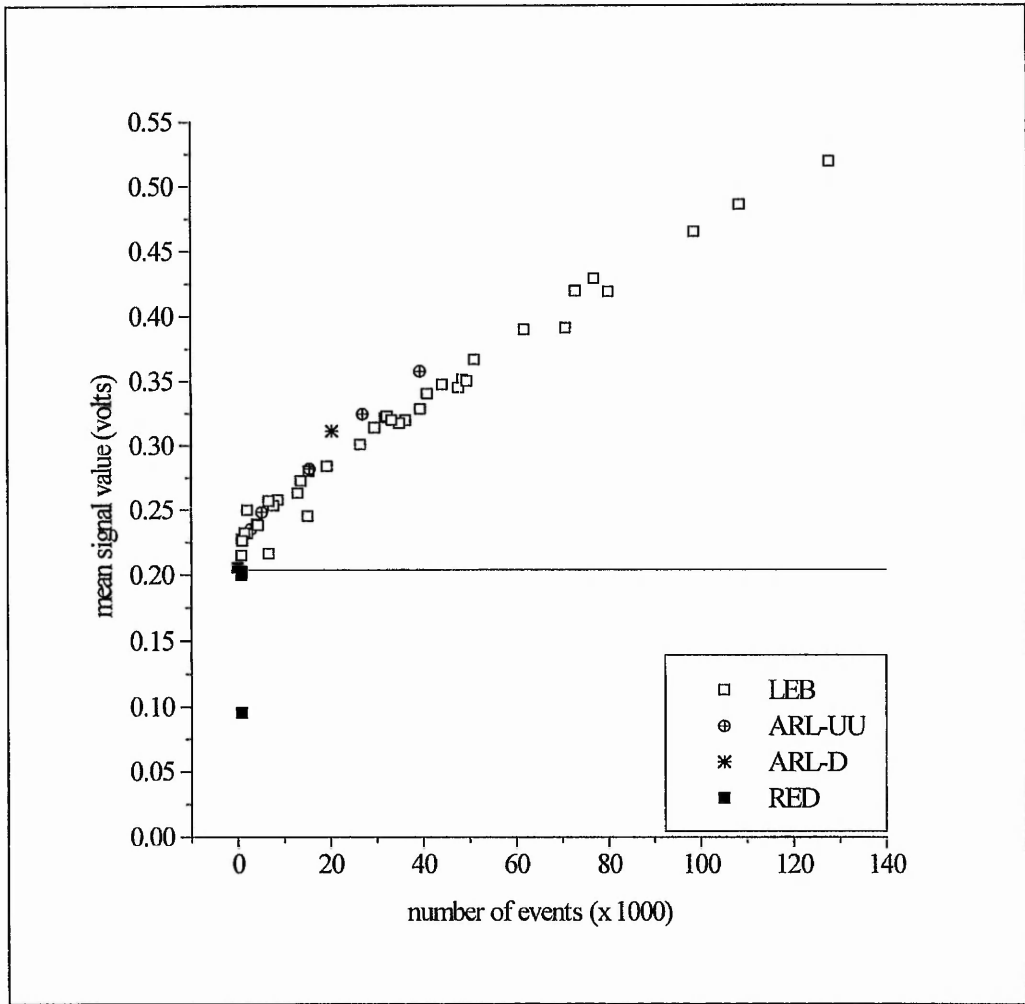


Figure 7.30 AE mean signal value vs number of events for thirty-nine triaxial shear tests conducted on Leighton Buzzard Sand, six triaxial shear tests conducted on 'Arlesey' sand and five triaxial shear tests conducted on 'Red' sand. (Note the average noise level is also shown)

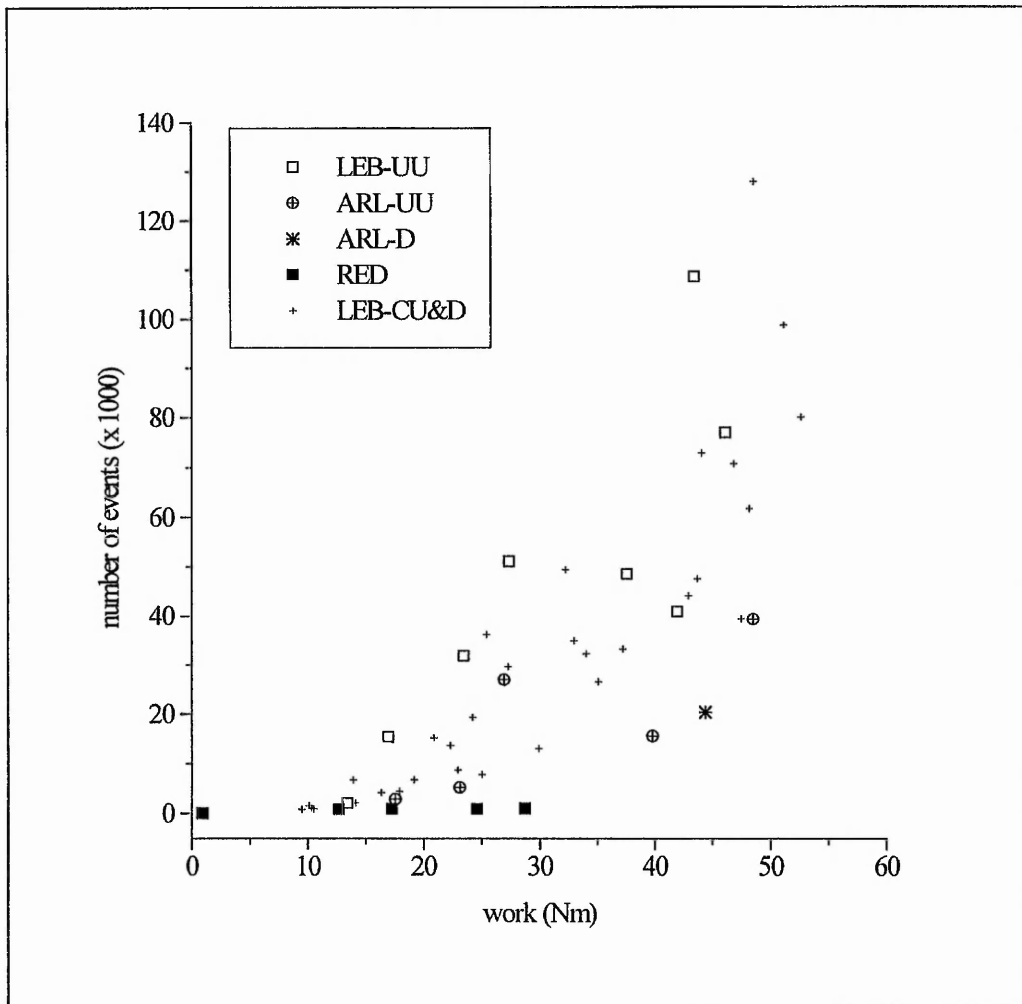


Figure 7.31 Number of events vs work done for thirty-nine triaxial shear tests conducted on Leighton Buzzard Sand, six triaxial shear tests conducted on 'Arlesey' sand and five triaxial shear tests conducted on 'Red' sand

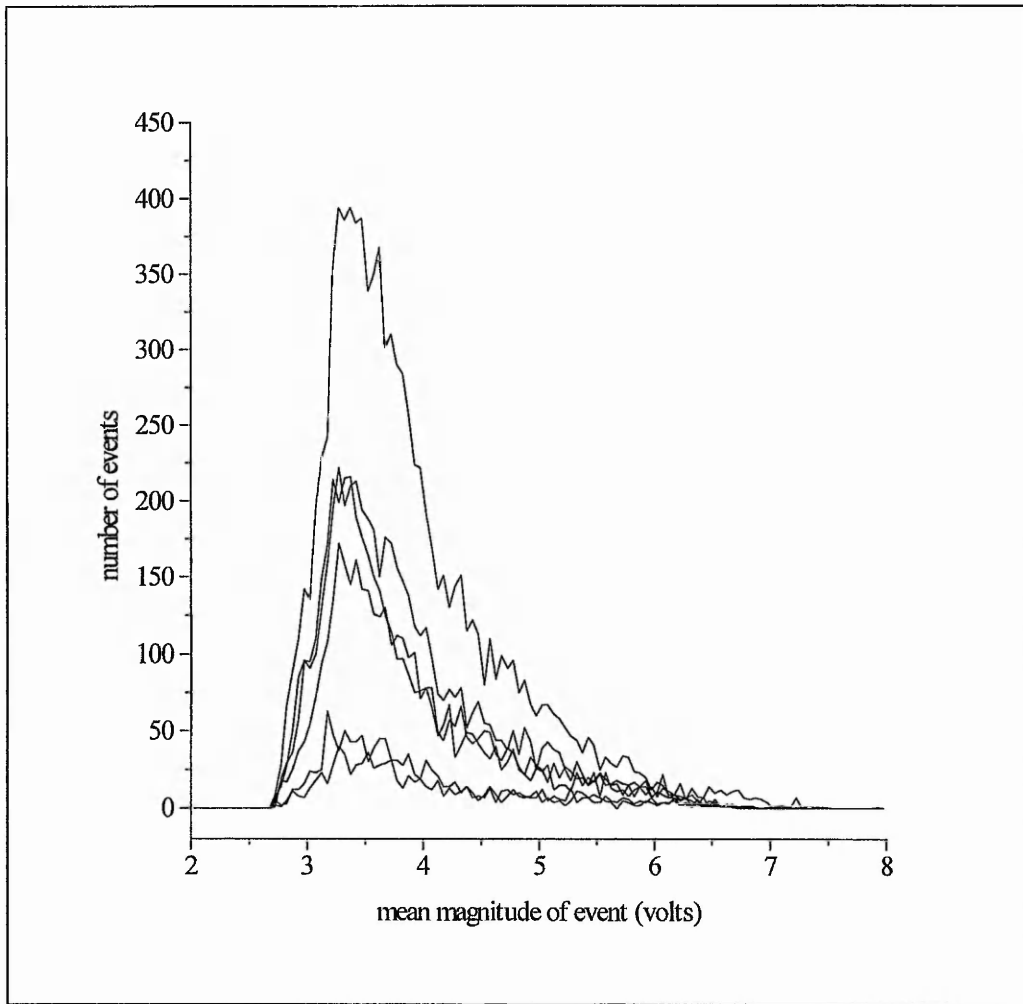


Figure 7.32 Frequency distribution of mean magnitude of event for all events with 3 plus data points for six triaxial shear tests conducted on samples of 'Arlesey' sand (TR63, 64, 65, 66, 67 and 68)

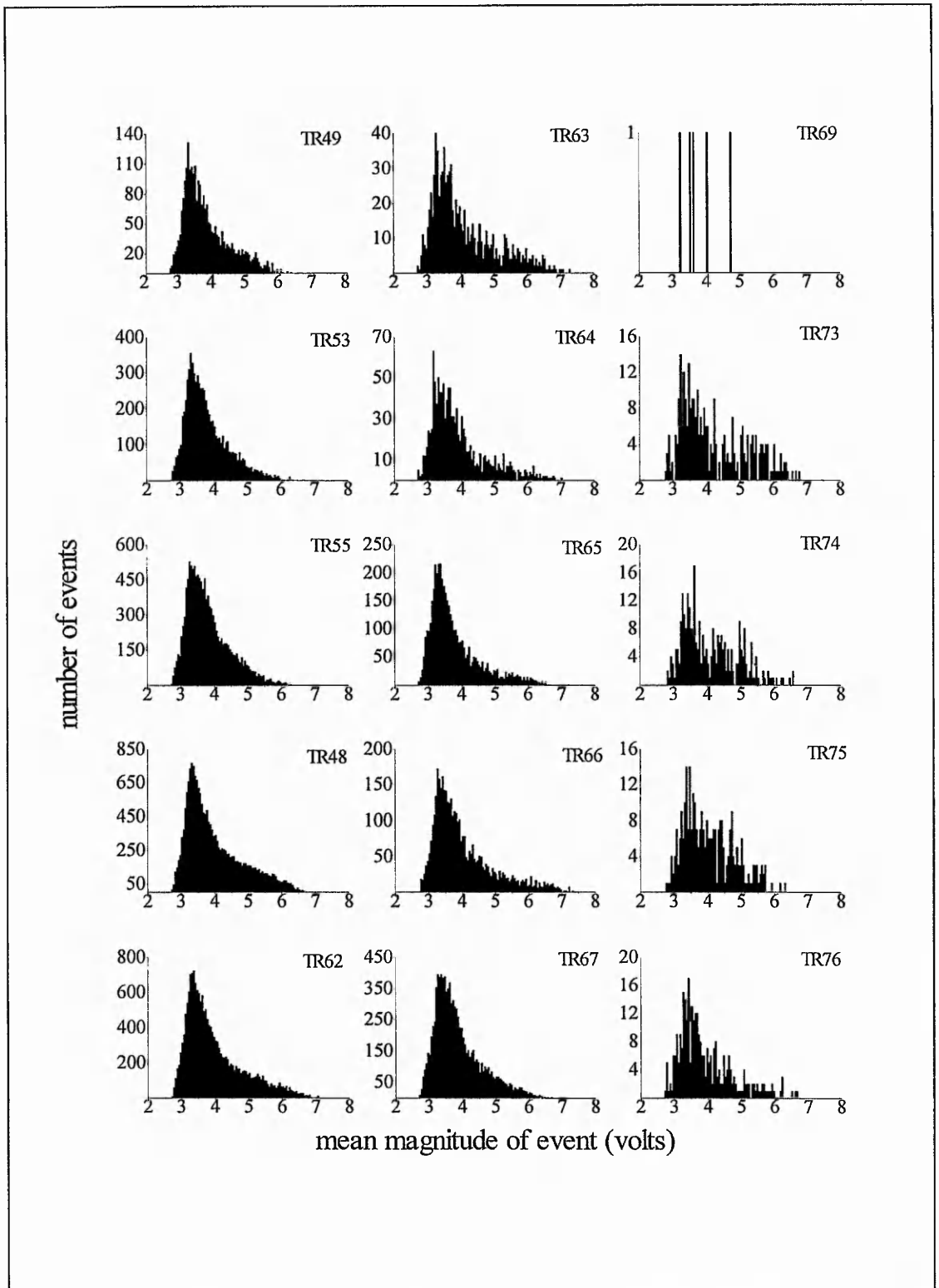


Figure 7.33 Frequency distribution curves for nine unconsolidated undrained triaxial shear tests (column 1 - Leighton Buzzard, column 2 - 'Arlesey', column 3 - 'Red')

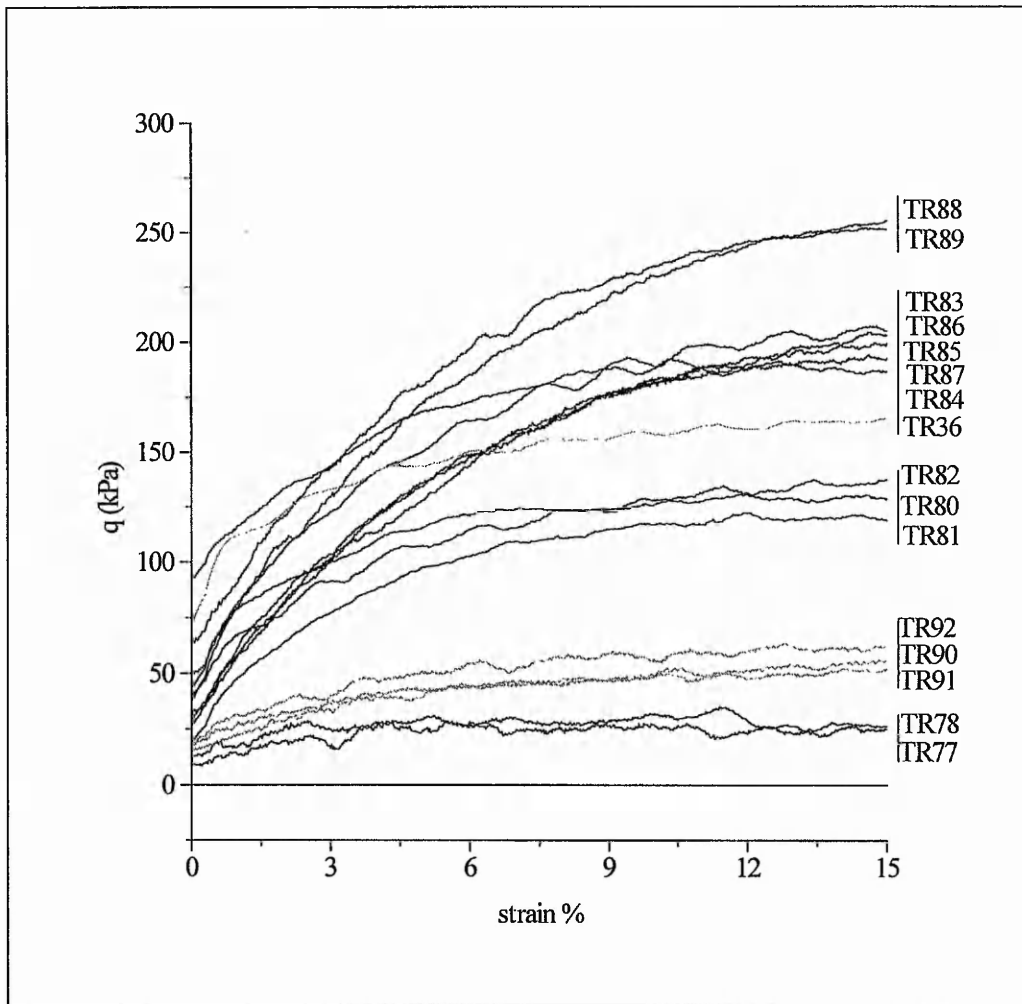


Figure 7.34 Graph of q against axial strain for twelve unconsolidated undrained triaxial shear tests conducted on samples of Gault Clay and for four unconsolidated undrained triaxial shear tests conducted on samples of Mercia Mudstone (shown in lighter type)

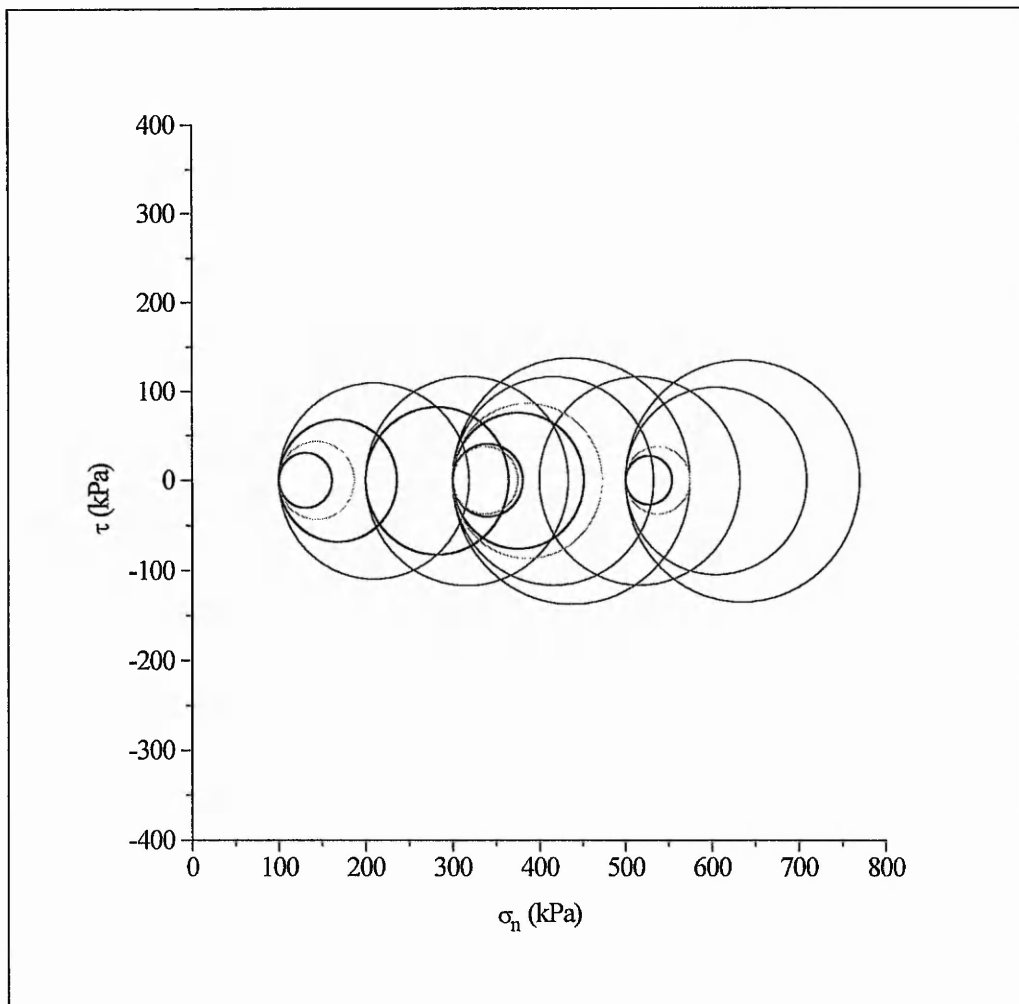


Figure 7.35 Mohr stress circles for twelve unconsolidated undrained triaxial shear tests conducted on samples of Gault Clay and for four unconsolidated undrained triaxial shear tests conducted on samples of Mercia Mudstone (shown in lighter type)

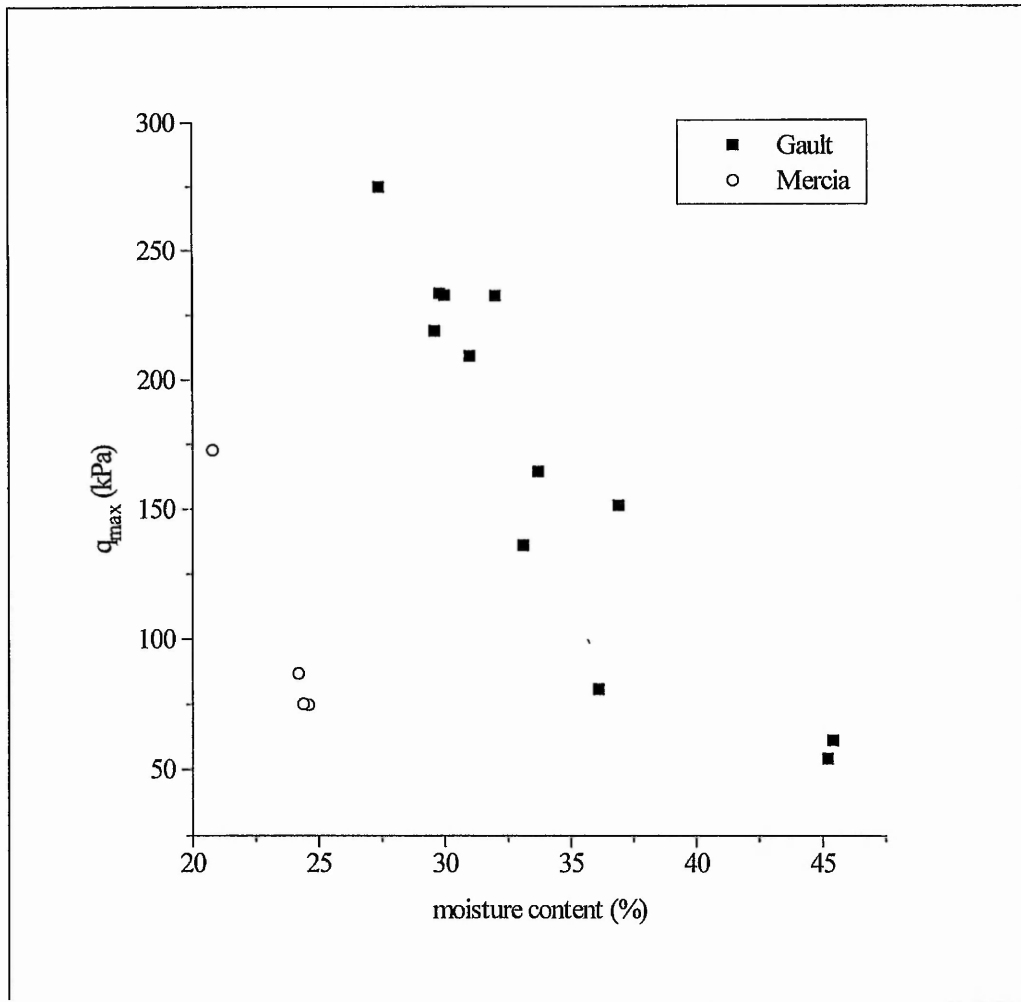


Figure 7.36 Graph of q_{max} against moisture content for twelve unconsolidated undrained triaxial shear tests conducted on samples of Gault Clay and for four unconsolidated undrained triaxial shear tests conducted on samples of Mercia Mudstone

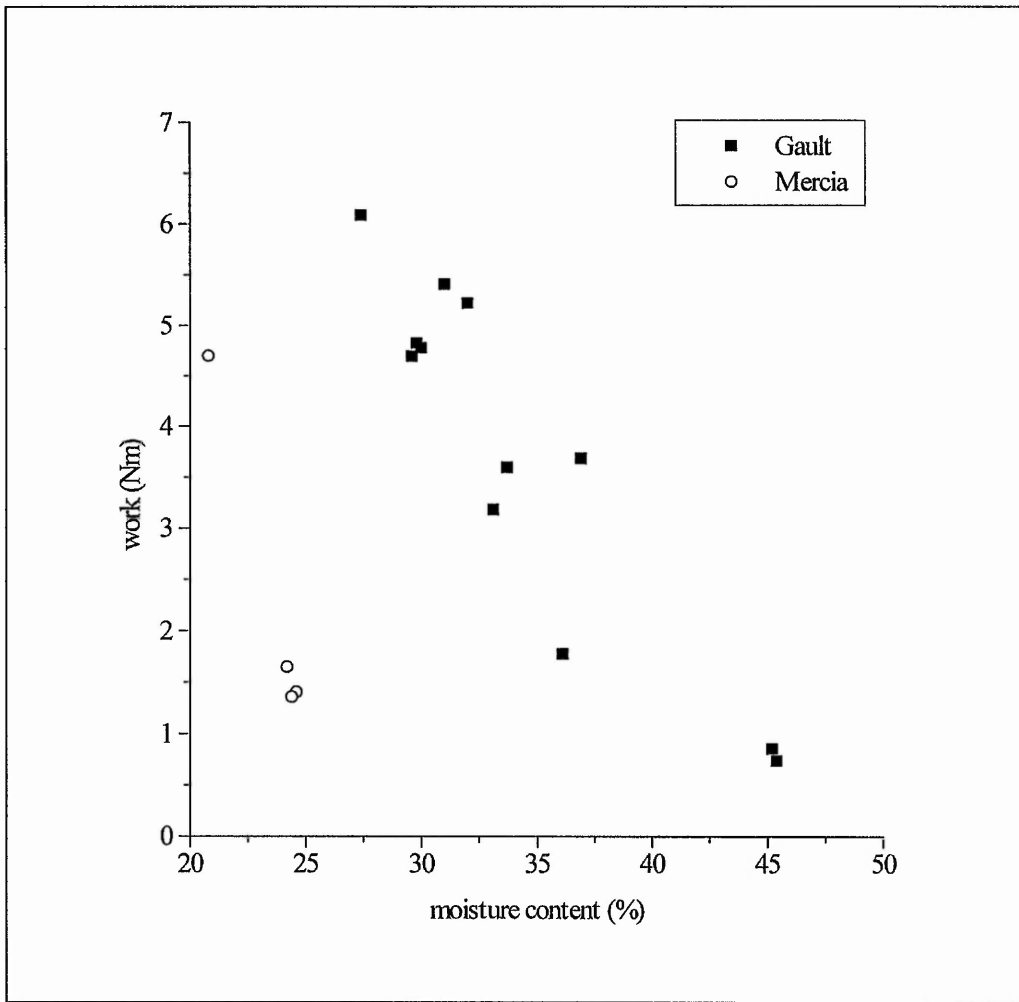


Figure 7.37 Graph of work done against moisture content for twelve unconsolidated undrained triaxial shear tests conducted on samples of Gault Clay and for four unconsolidated undrained triaxial shear tests conducted on samples of Mercia Mudstone

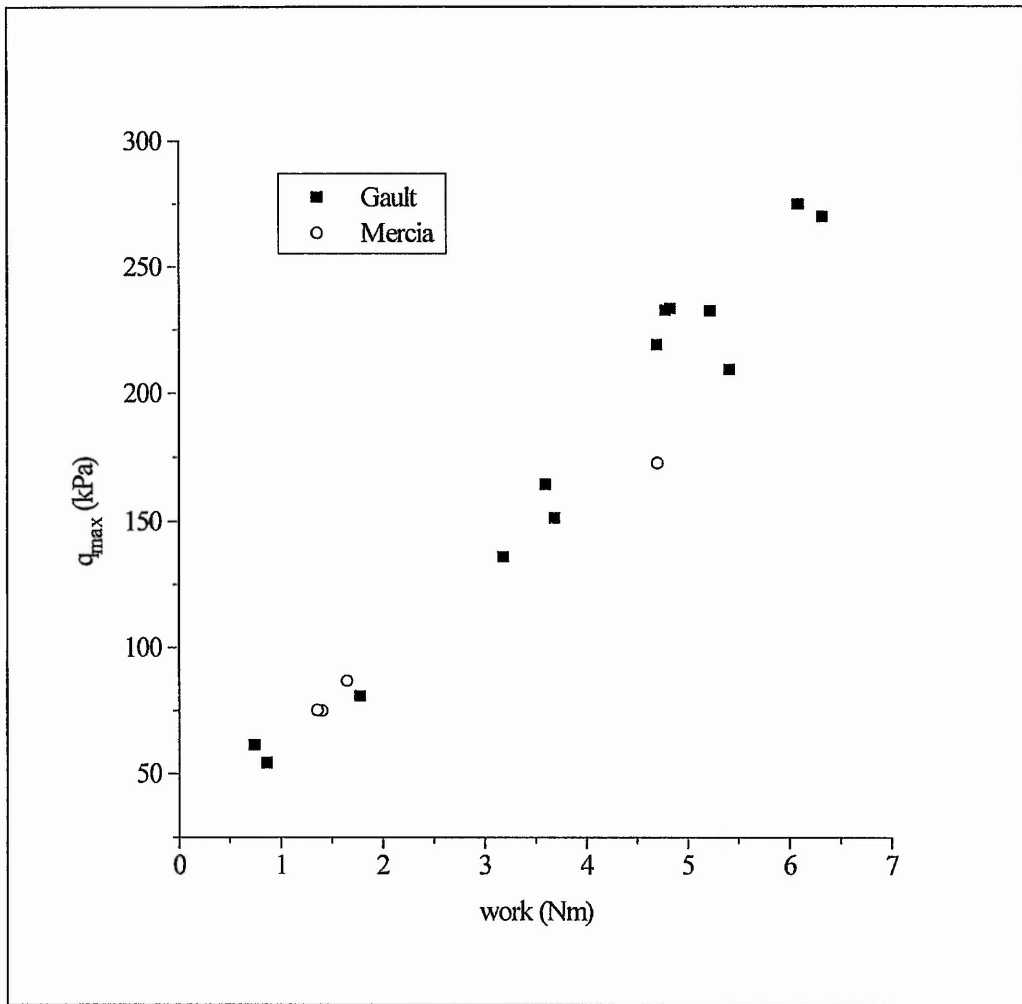


Figure 7.38 q_{max} against work done for twelve unconsolidated undrained triaxial shear tests conducted on samples of Gault Clay and for four unconsolidated undrained triaxial shear tests conducted on samples of Mercia Mudstone

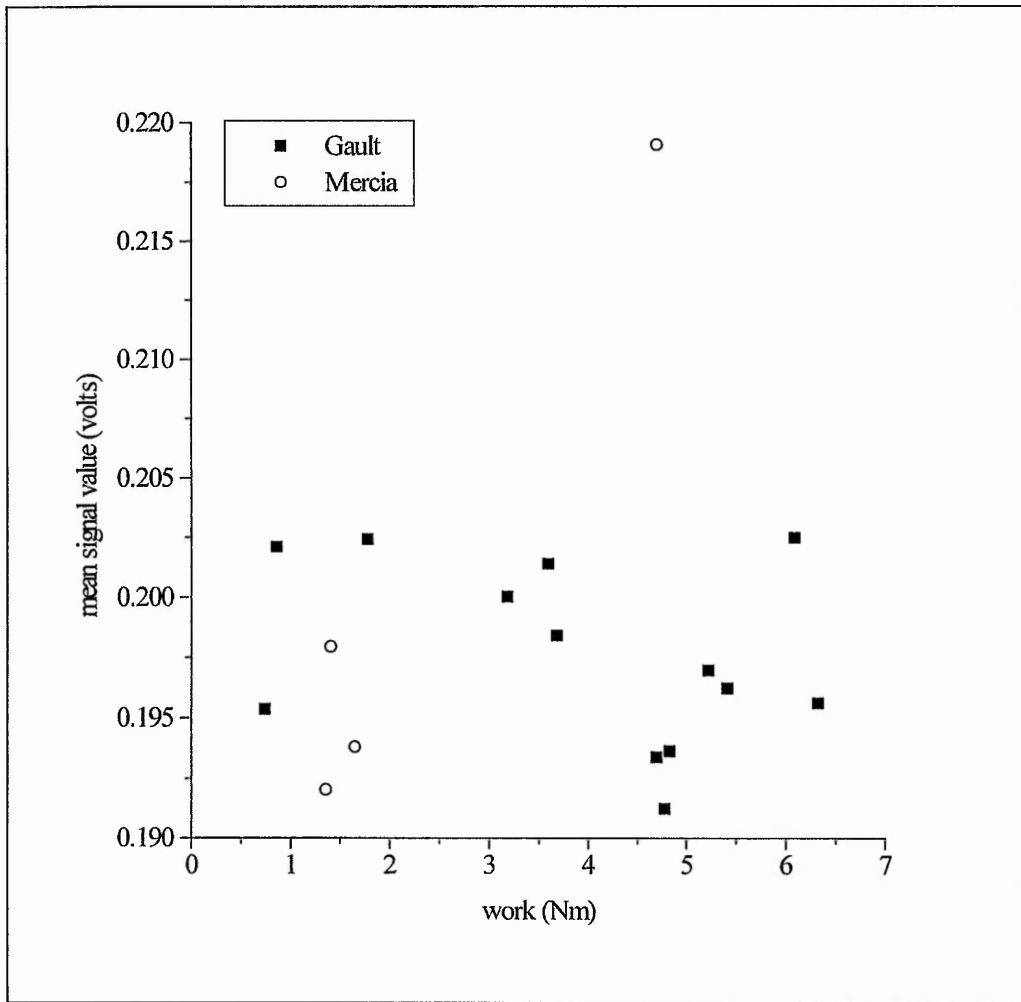


Figure 7.39 AE mean signal value as a function of work done for thirteen unconsolidated undrained triaxial shear tests conducted on samples of Gault Clay and for four unconsolidated undrained triaxial shear tests conducted on samples of Mercia Mudstone

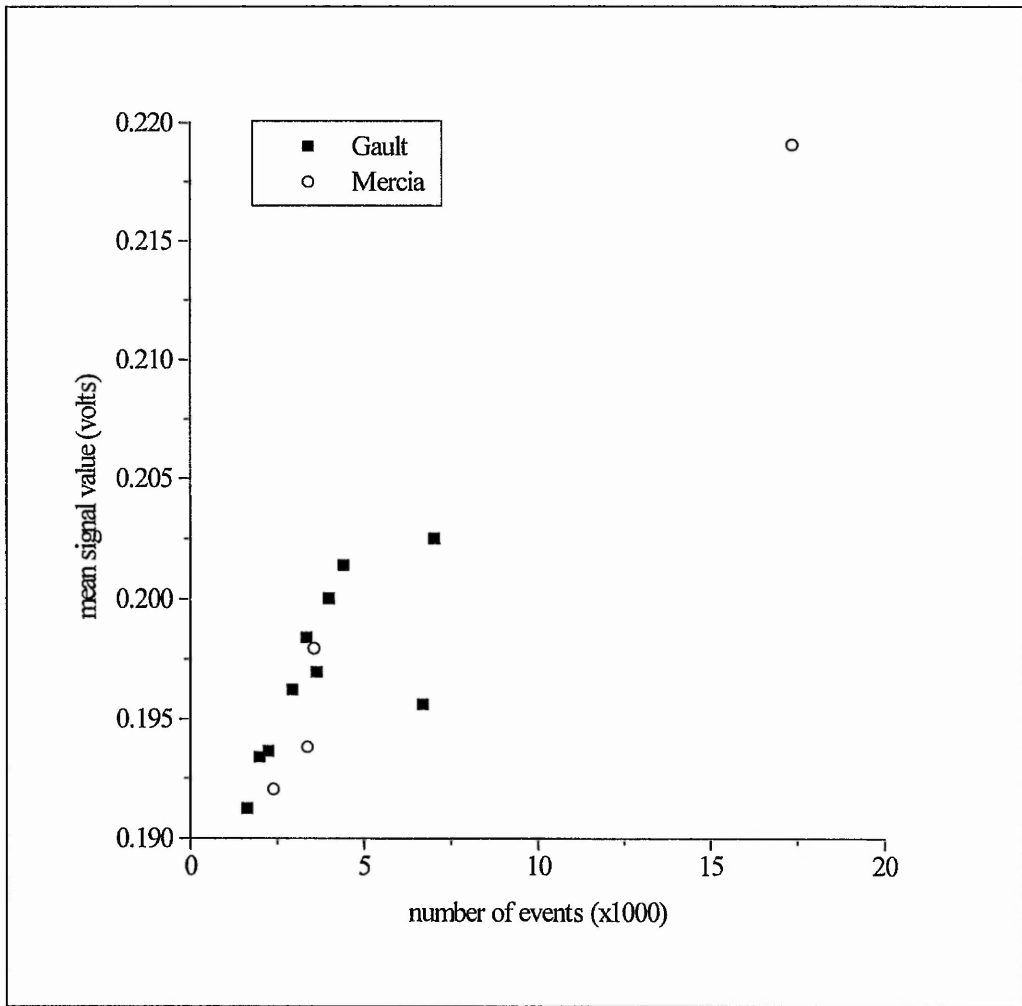


Figure 7.40 AE mean signal value as a function of number of events for ten unconsolidated undrained triaxial shear tests conducted on samples of Gault Clay and for four unconsolidated undrained triaxial shear tests conducted on samples of Mercia Mudstone

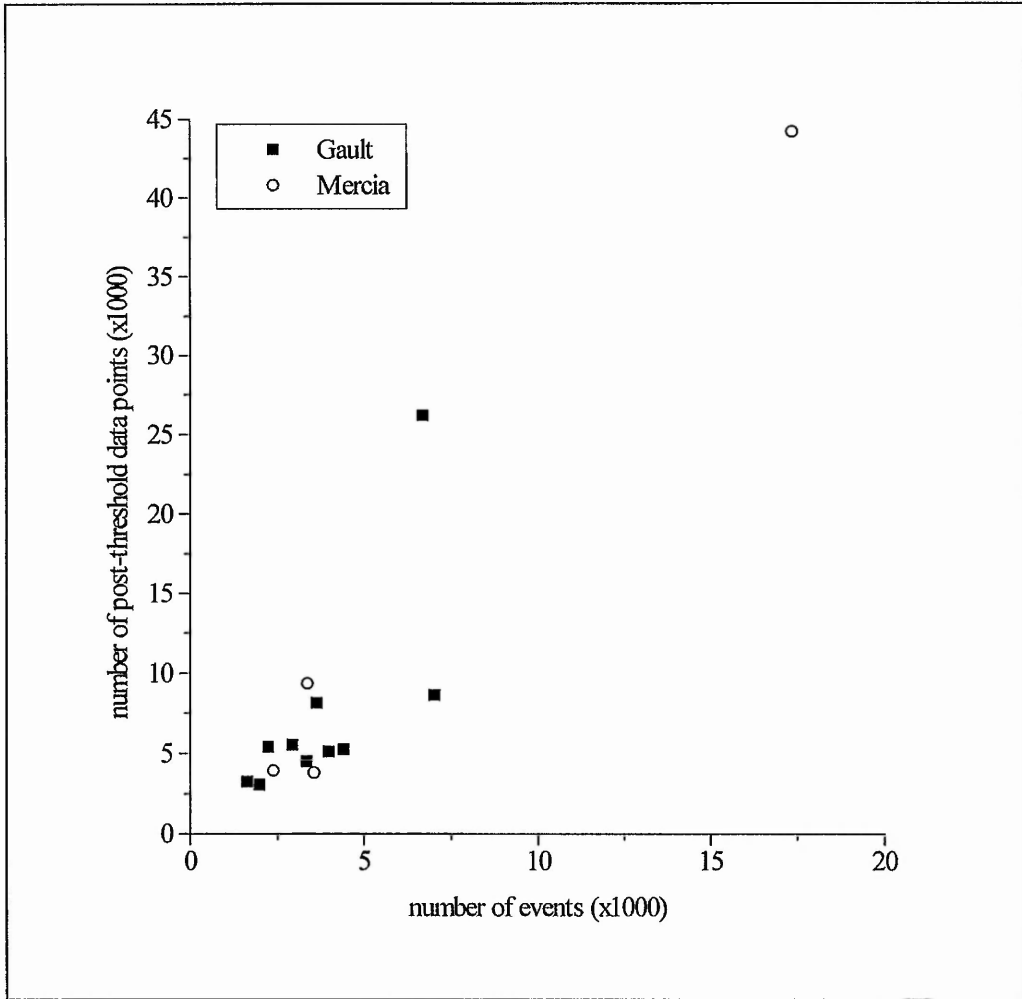


Figure 7.41 Number of post-threshold data points against number of events for ten unconsolidated undrained triaxial shear tests conducted on samples of Gault Clay and for four unconsolidated undrained triaxial shear tests conducted on samples of Mercia Mudstone (shown in lighter type)

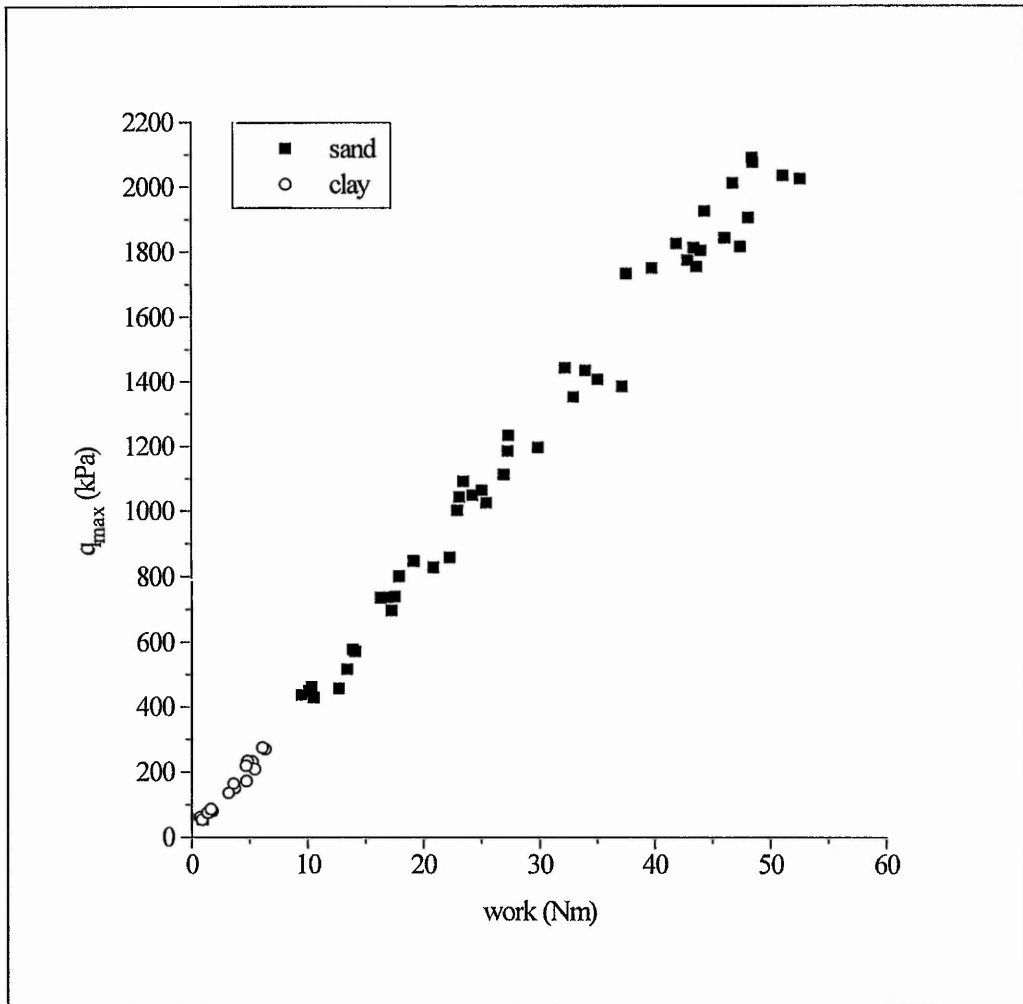


Figure 7.42 Graph of q_{\max} as a function of work for forty-eight triaxial shear tests conducted on sand and seventeen triaxial shear tests conducted on clay.

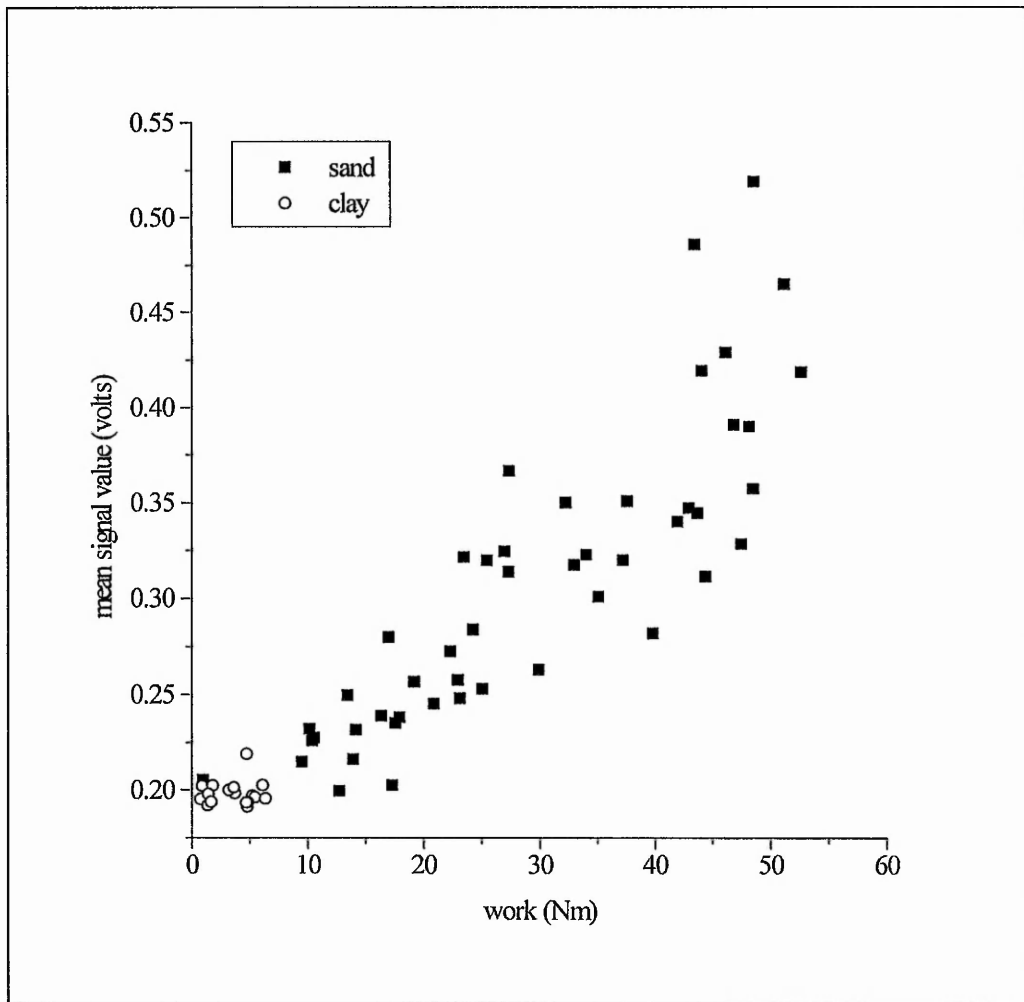


Figure 7.43 Graph of mean signal level (bulk data) as a function of work for forty-eight triaxial shear tests conducted on sand and seventeen triaxial shear tests conducted on clay.

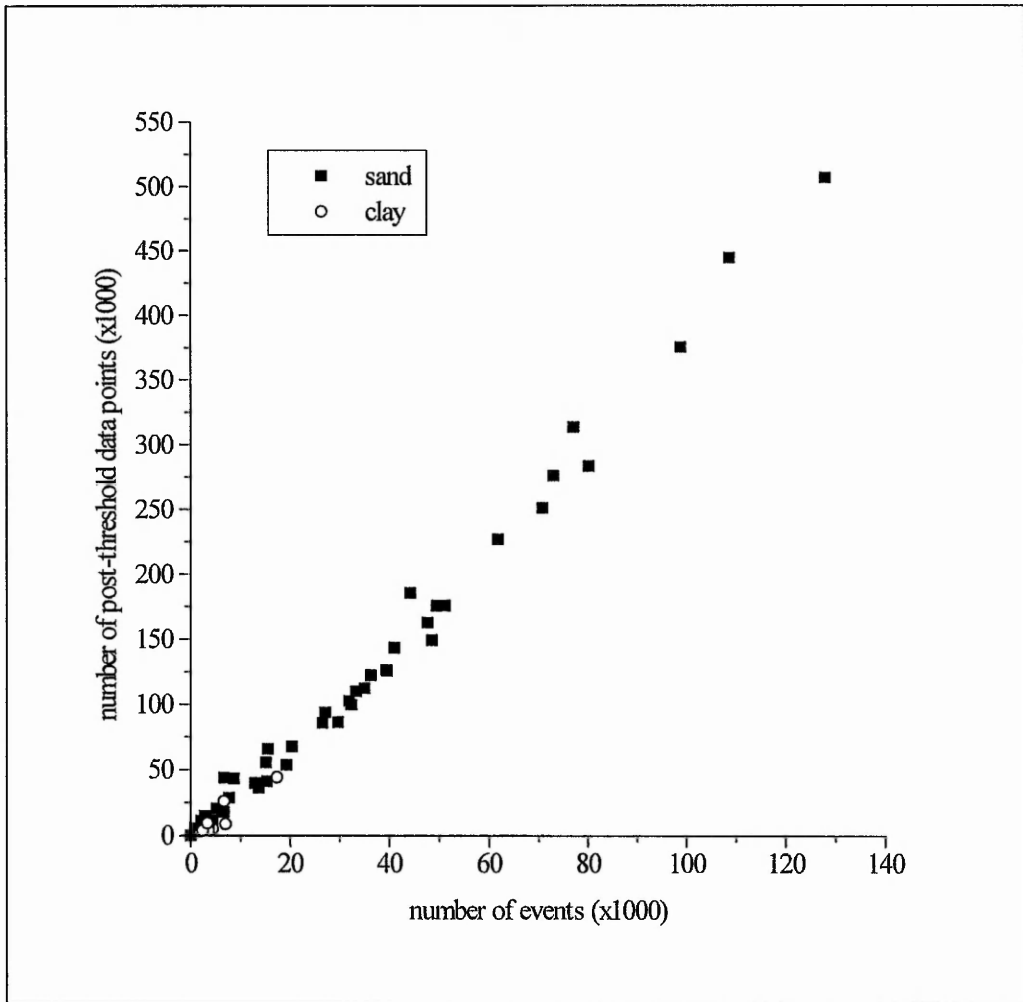


Figure 7.44 Number of post-threshold data points as a function of number of events for forty-eight triaxial shear tests conducted on sand and seventeen triaxial shear tests conducted on clay.

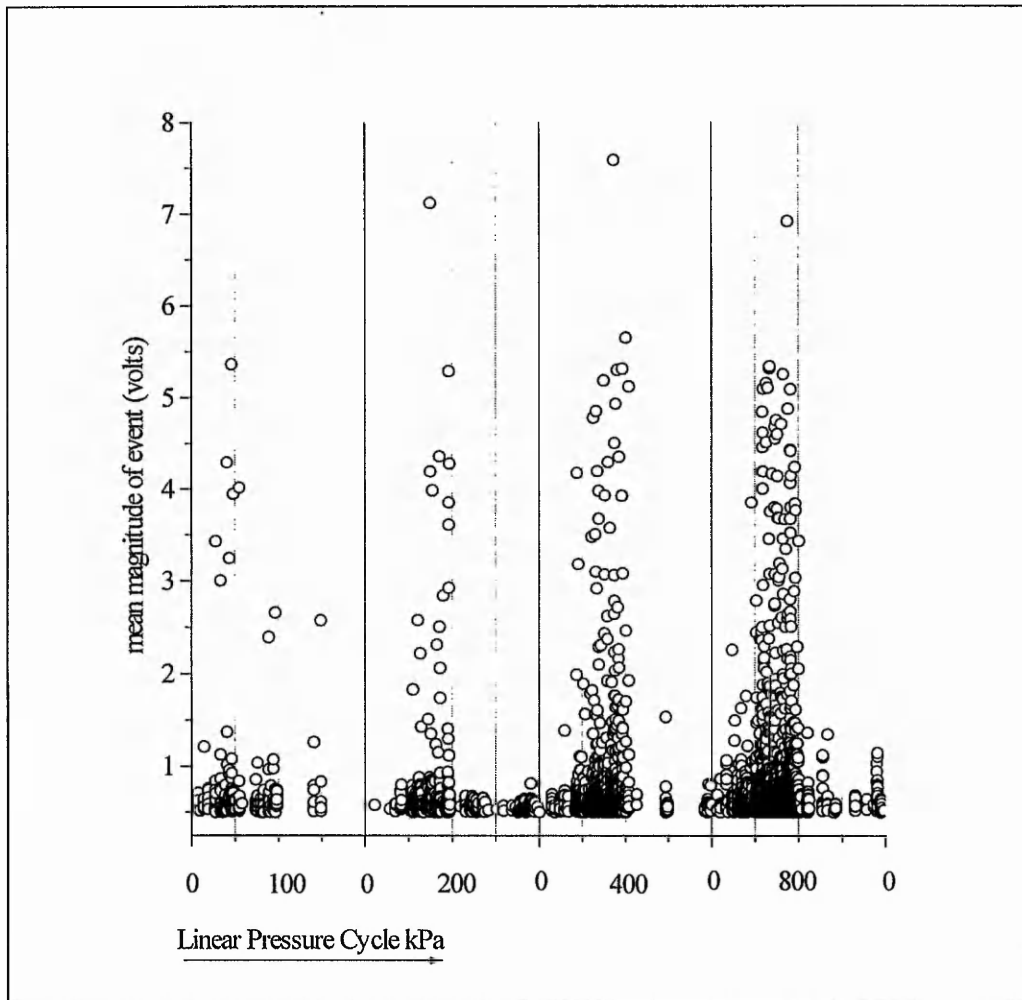


Figure 7.45 Event distribution (based on mean magnitude of event in volts) for four consolidation cycles.

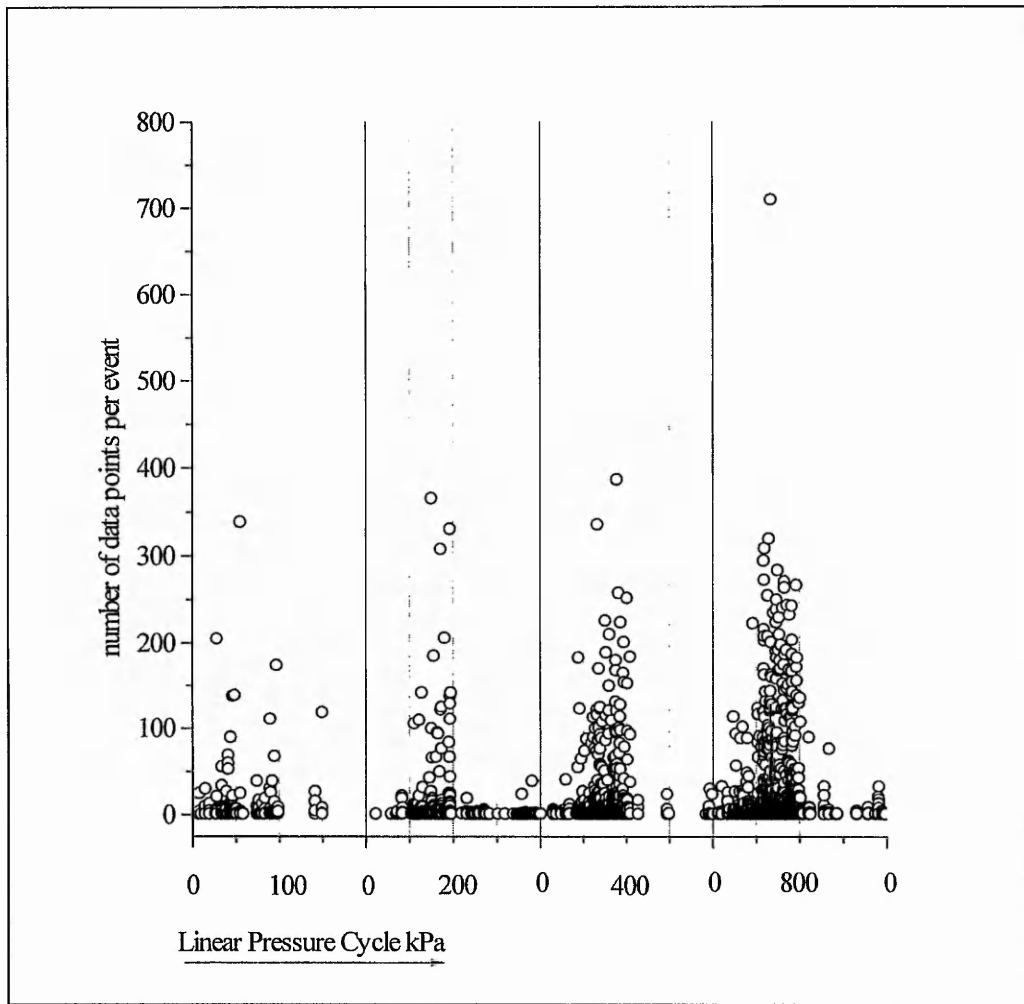


Figure 7.46 Event distribution (based on number of data points per event) for four consolidation cycles

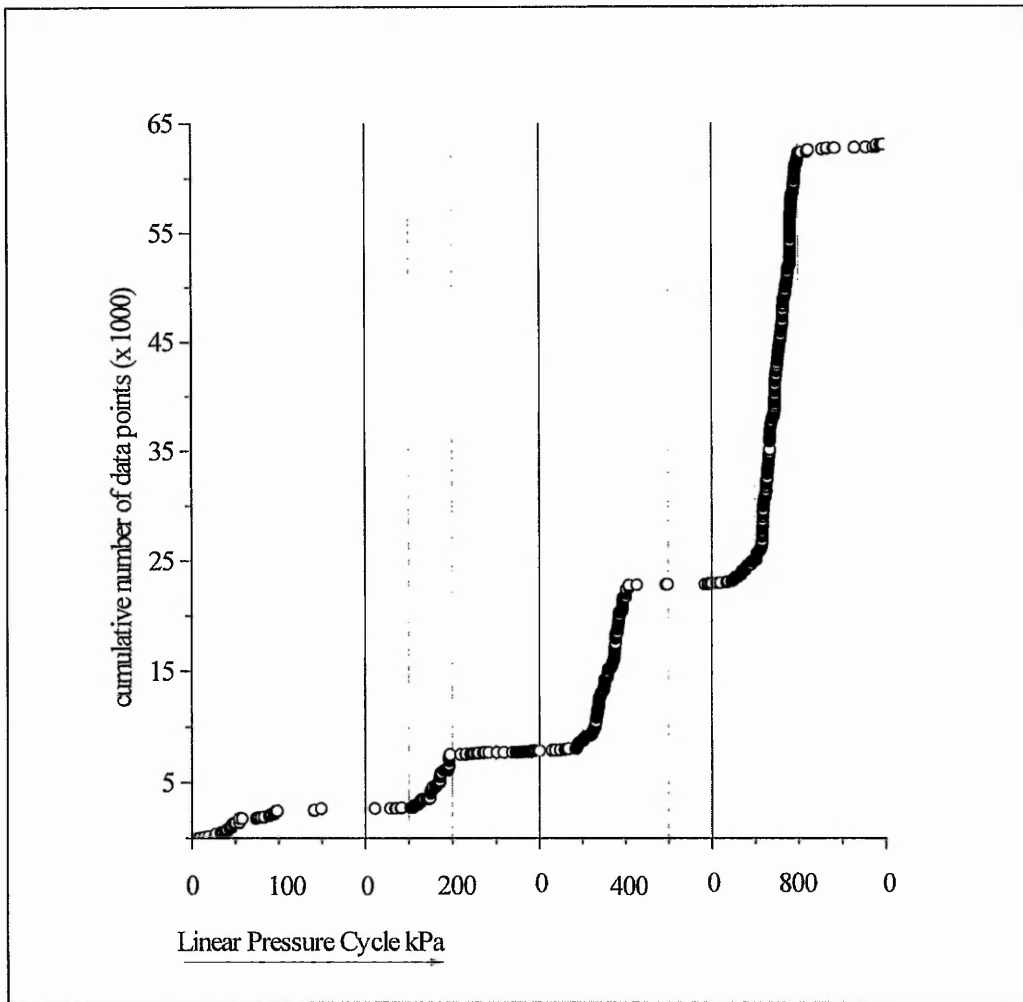


Figure 7.47 Cumulative number of post-threshold data points for four consolidation cycles

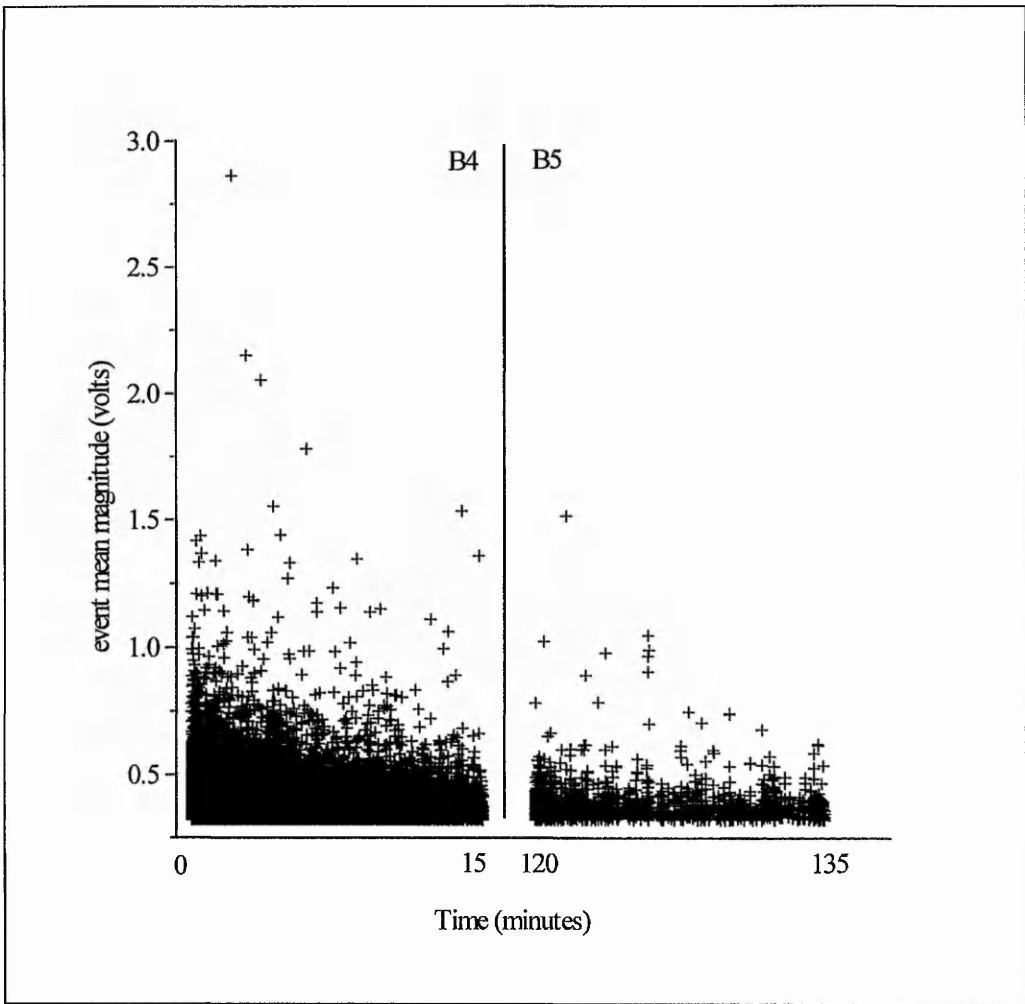


Figure 7.48 Box tests B4 and B5 by mean magnitude of event

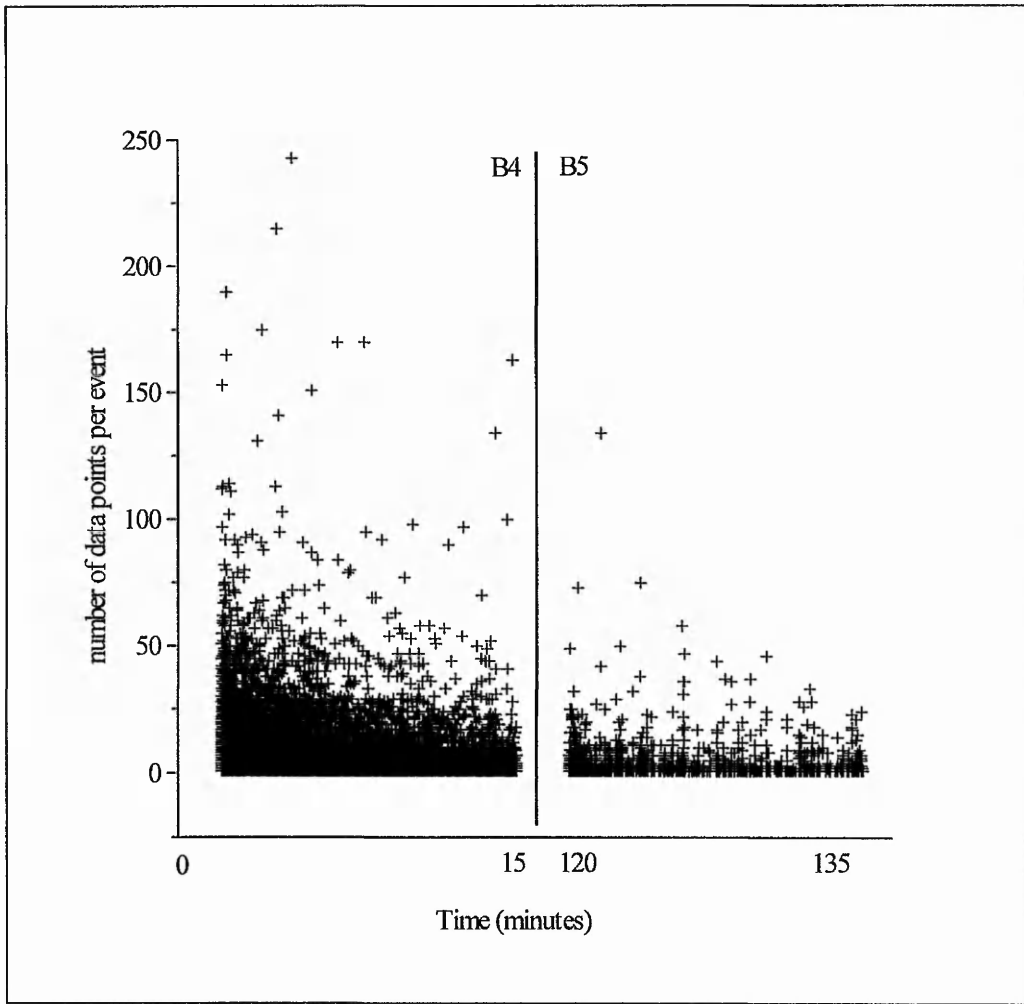


Figure 7.49 Box tests B4 and B5 by number of data points per event

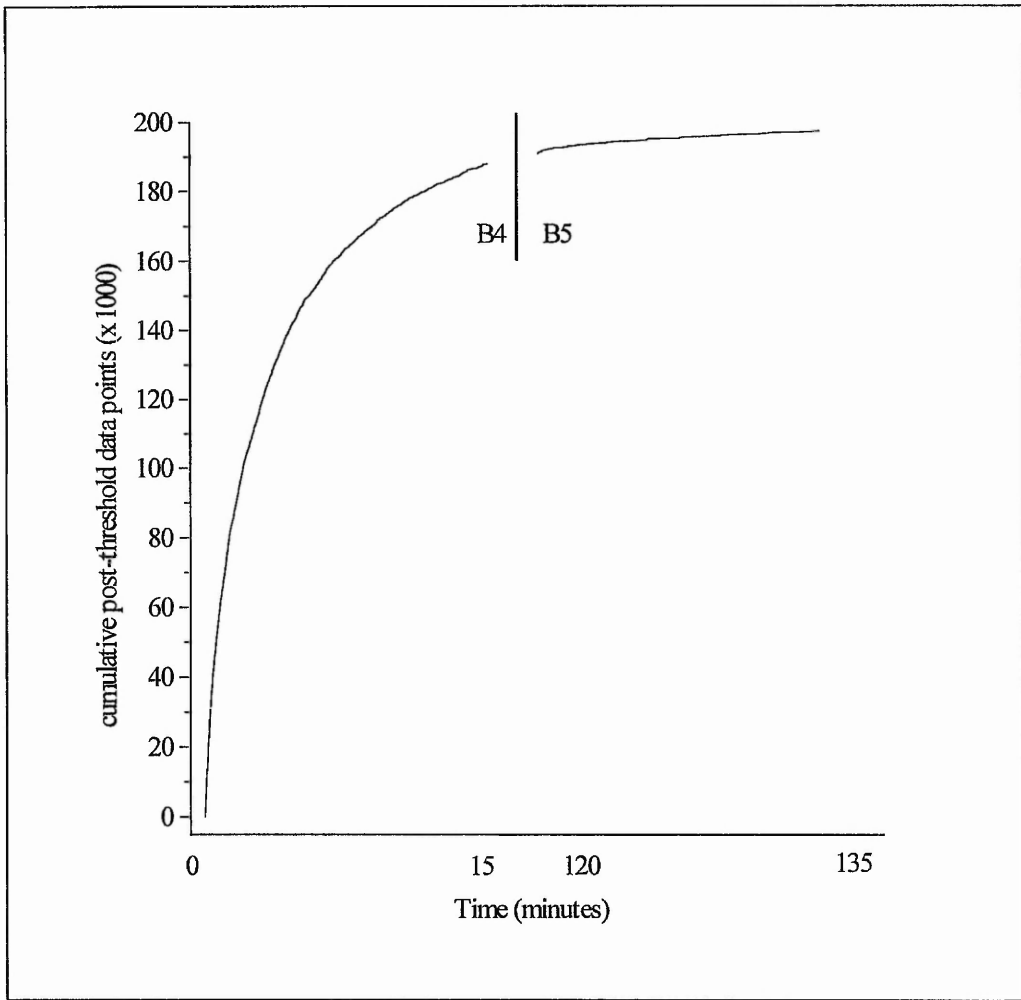


Figure 7.50 Box tests B4 and B5 by cumulative number of post-threshold data points

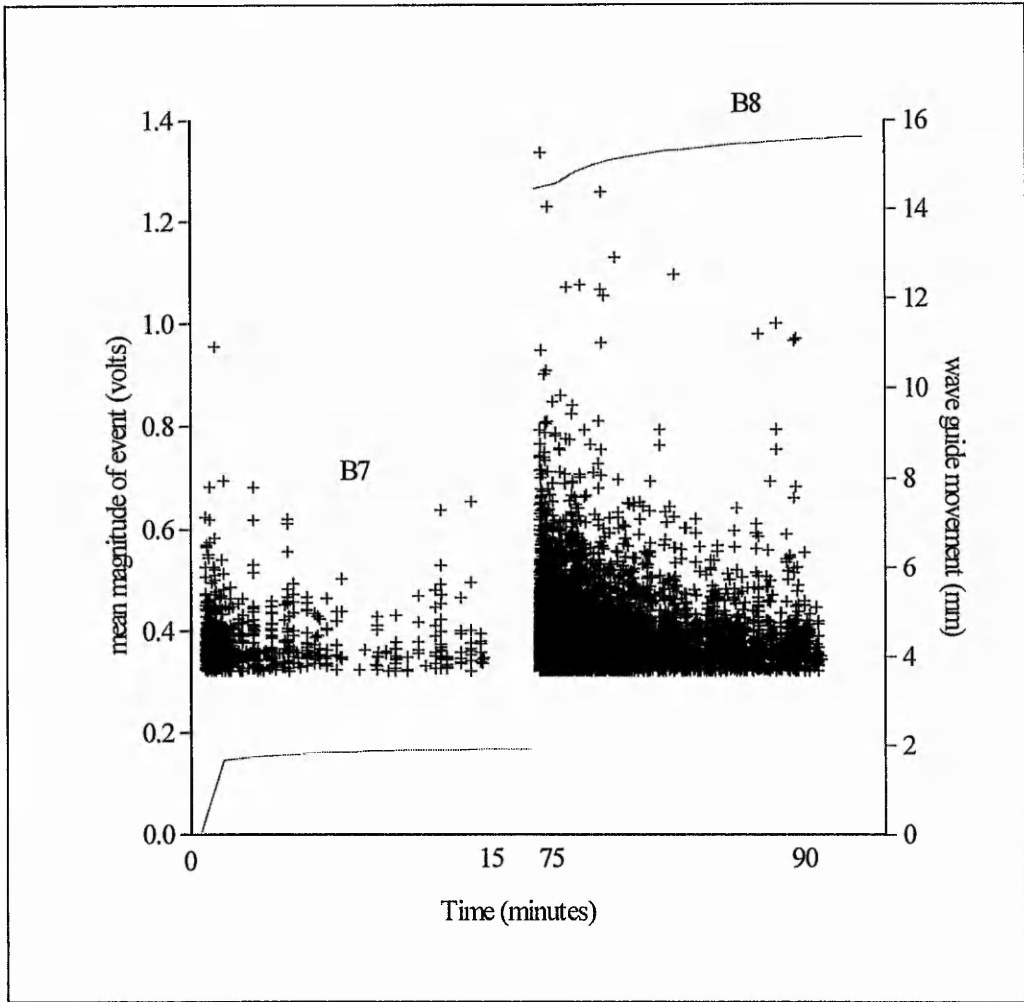


Figure 7.51 Box tests B7 and B8 by mean magnitude of event

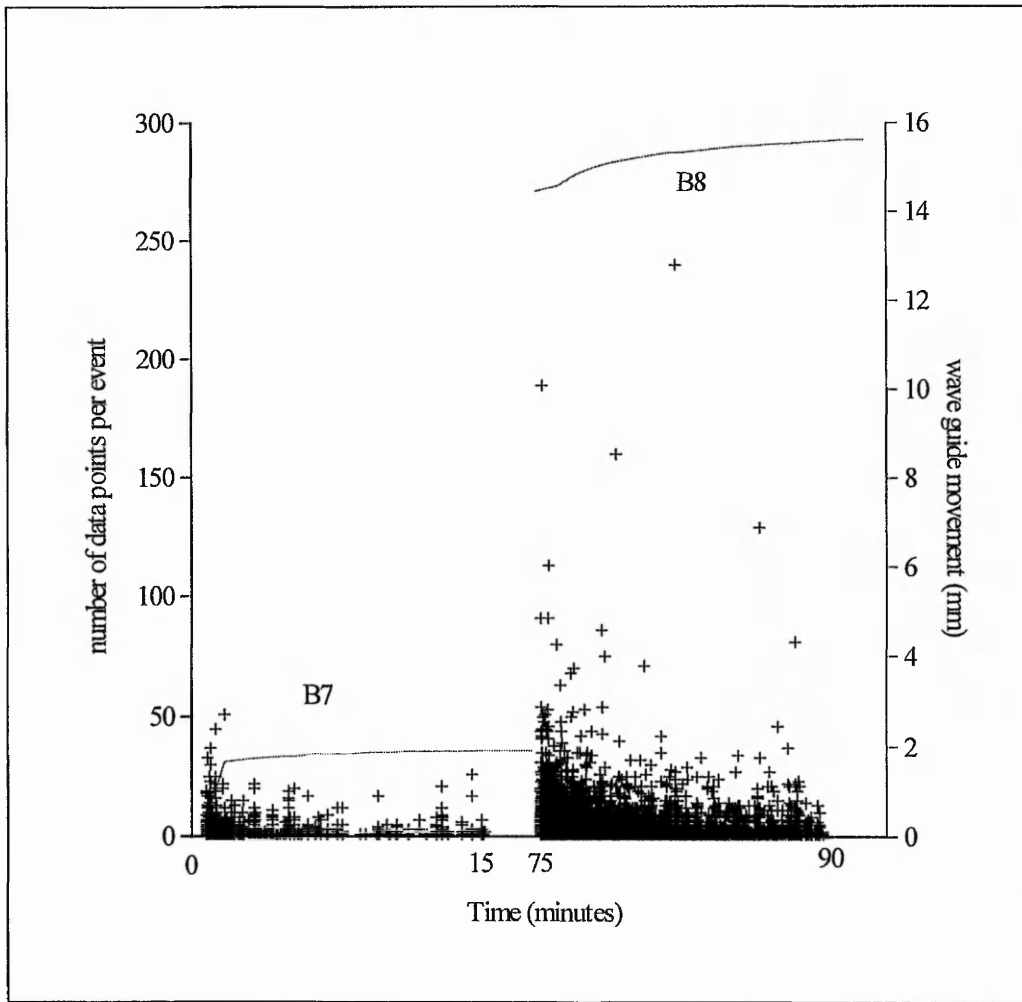


Figure 7.52 Box tests B7 and B8 by number of data points per event

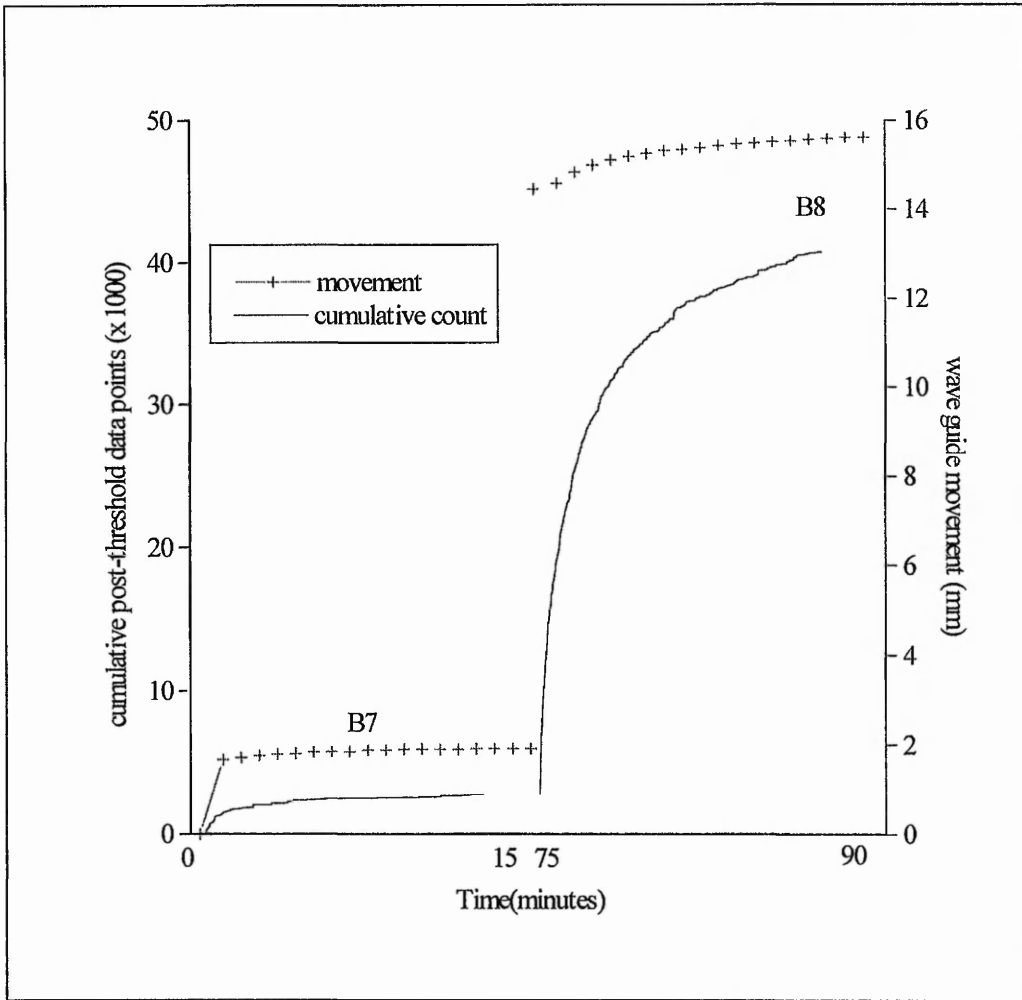


Figure 7.53 Box tests B7 and B8 by cumulative number of post-threshold data points

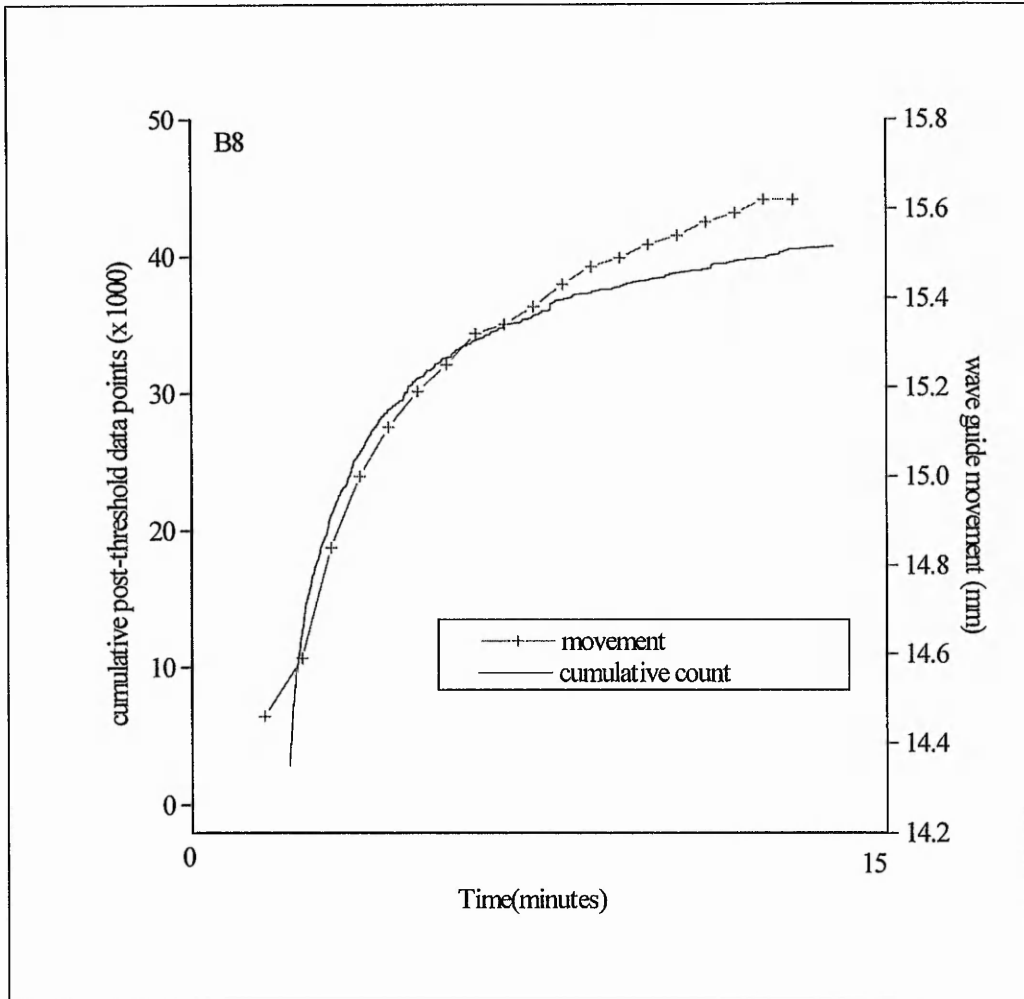


Figure 7.54 Box test B8 by cumulative number of post-threshold data points

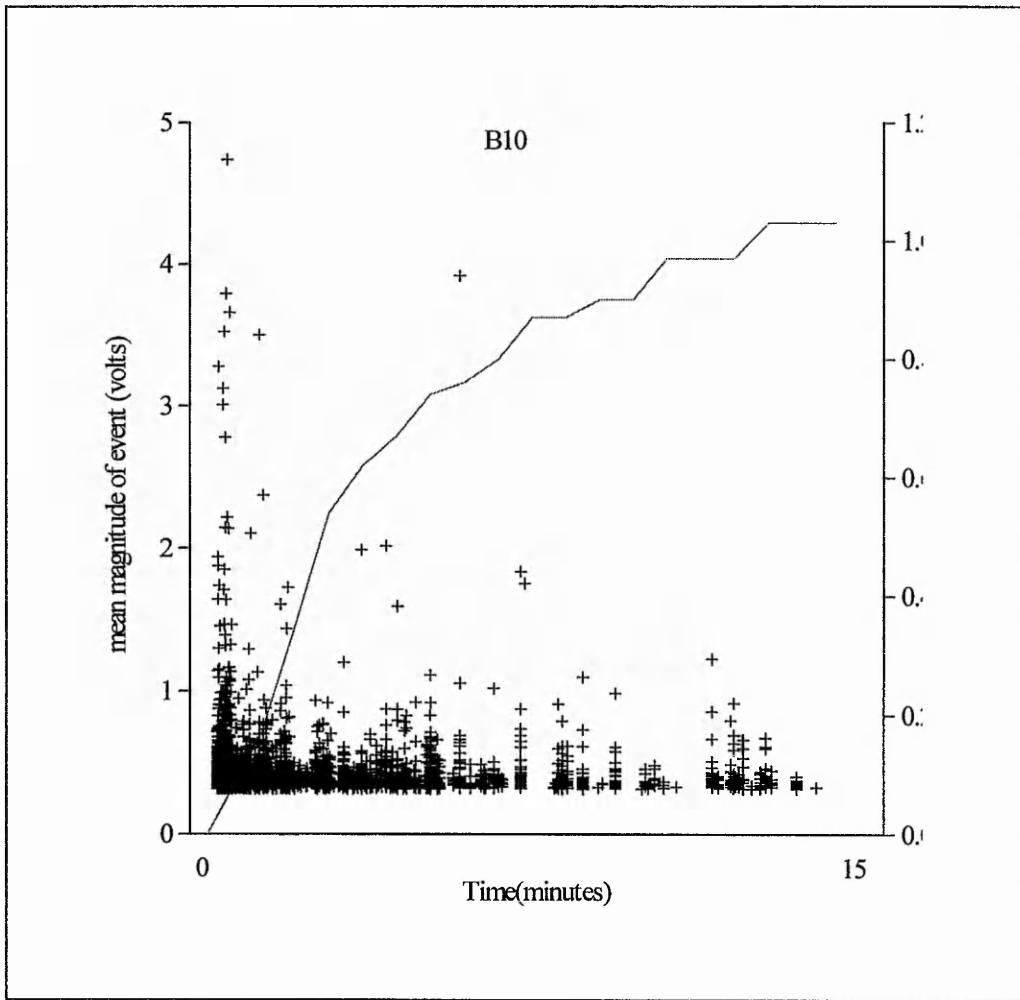


Figure 7.55 Box test B10 by mean magnitude of event

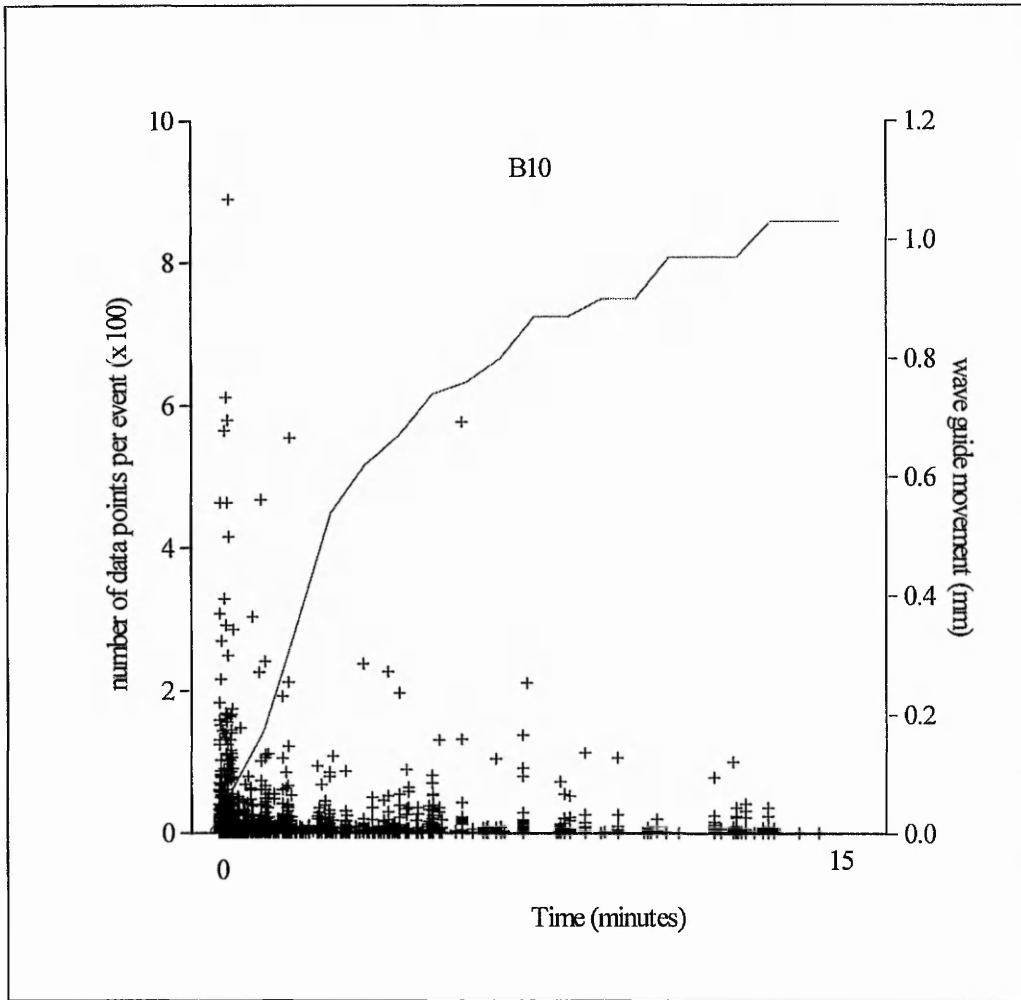


Figure 7.56 Box test B10 by number of data points per event

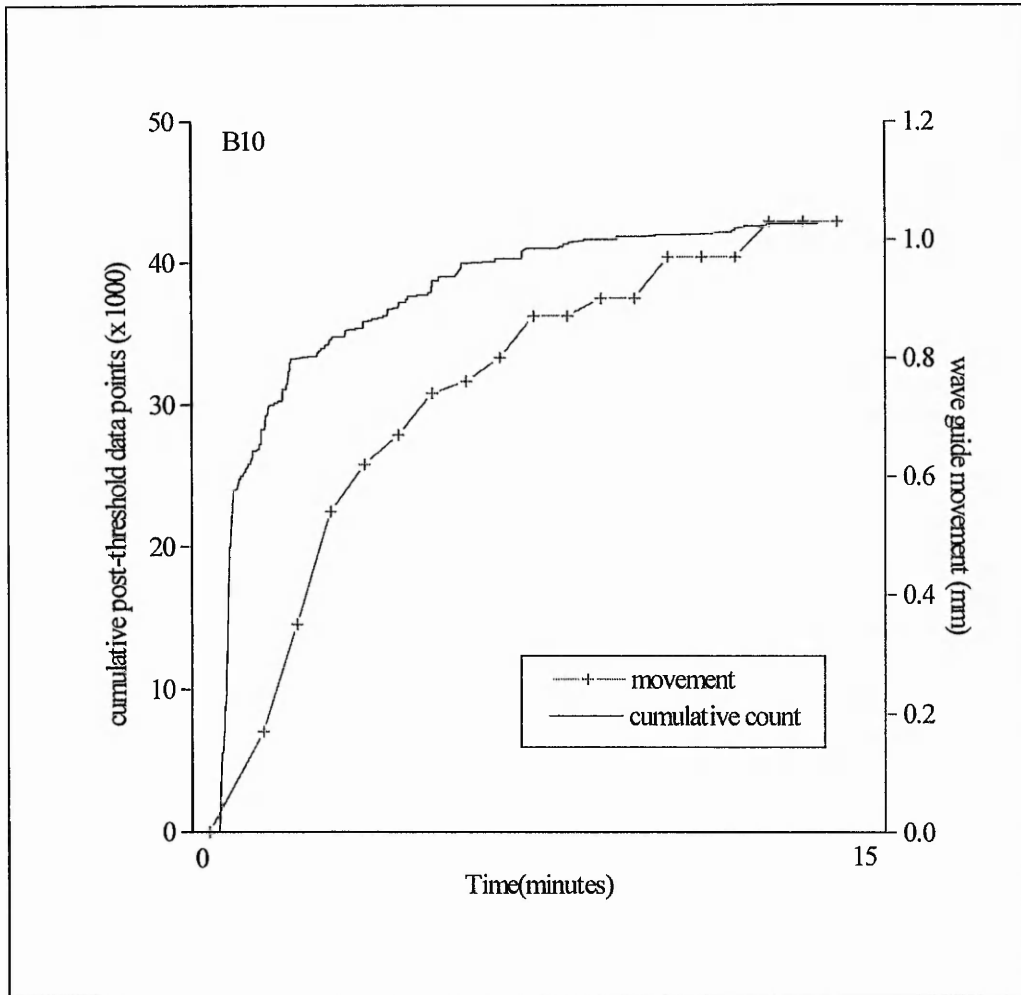


Figure 7.57 Box test B10 by cumulative number of data points

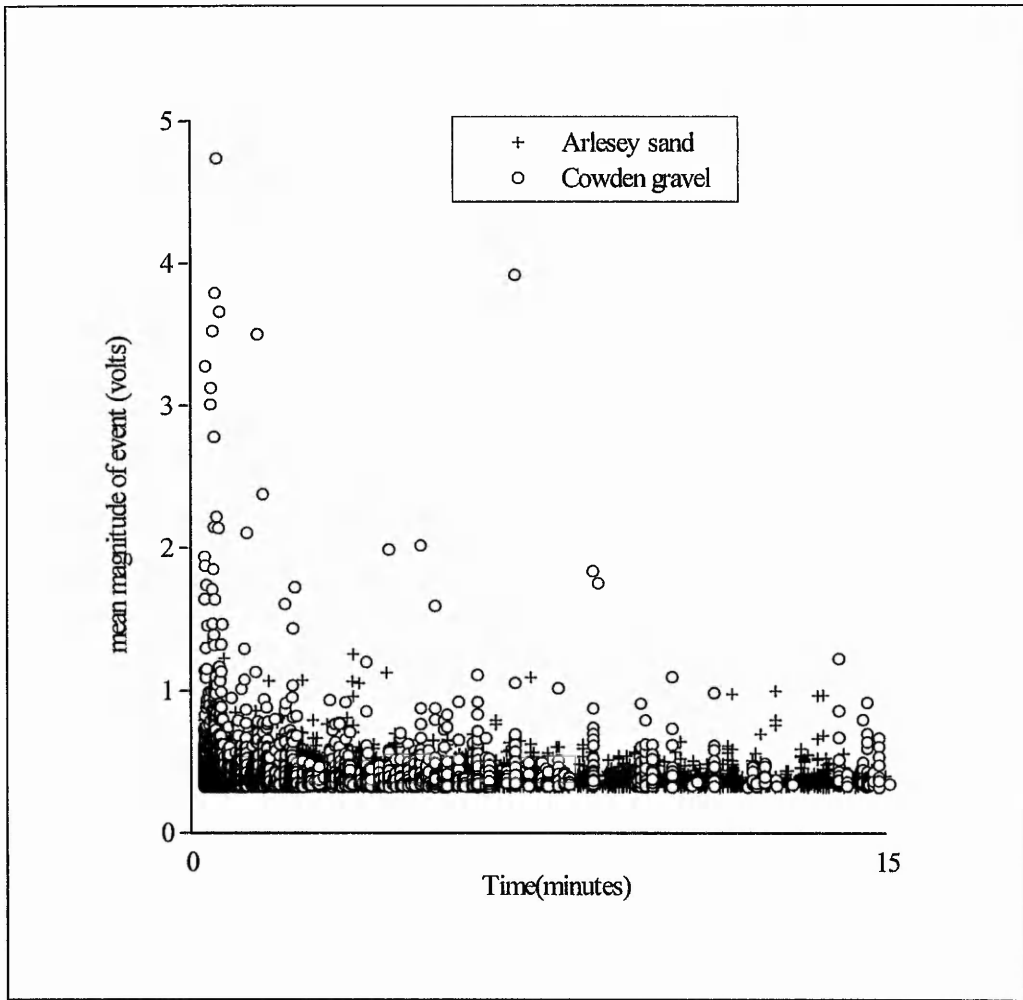


Figure 7.58 Box tests B8 and B10 by mean magnitude of event in volts

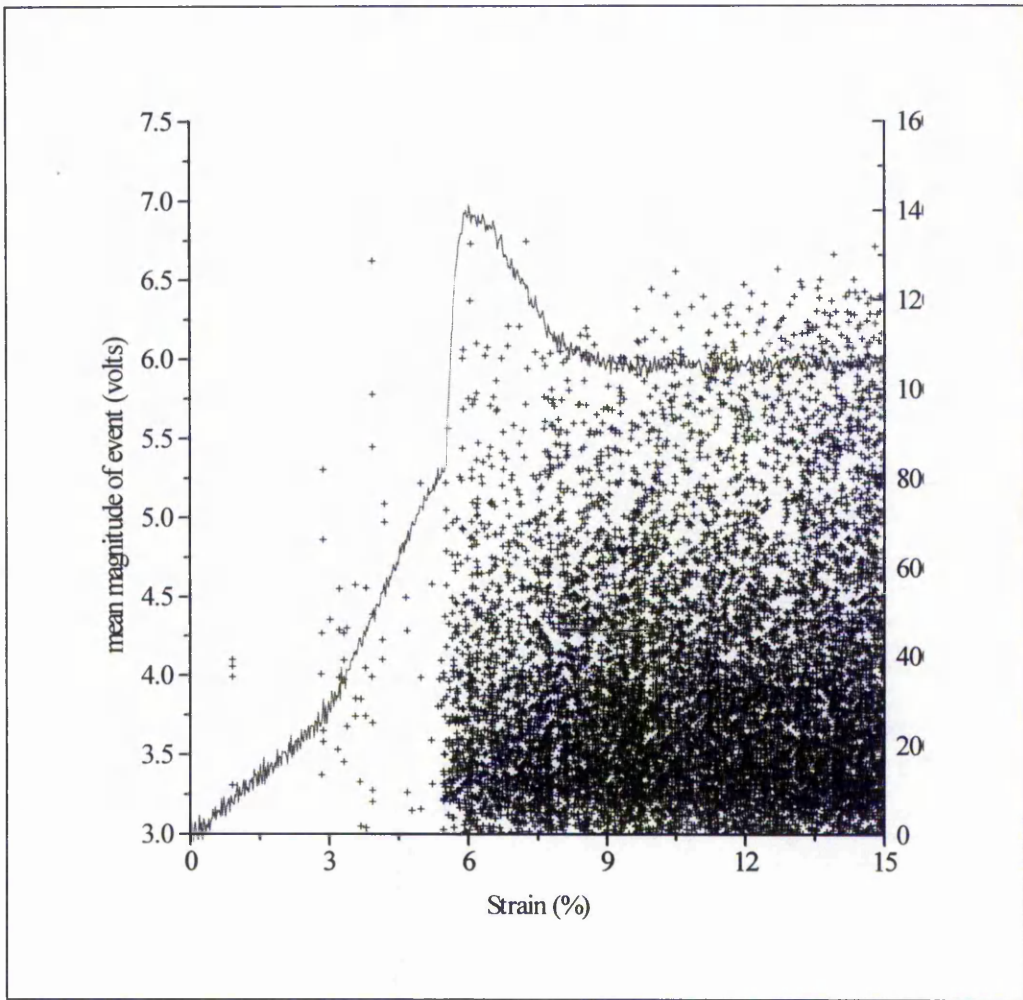


Figure 7.59 Triaxial shear test TR11 conducted on a sample of Leighton Buzzard Sand

Chapter 8

Conclusions

8.1 Field Investigations

This investigation has examined the feasibility of using the phenomenon of acoustic emission to detect and monitor first time deformation mechanisms in stiff, heavily over-consolidated clay soils. Primarily concerned with slope stability, the study has described a physical model which has attempted to explain the occurrence of the field generated acoustic emission. It has included a consideration of wave guide design and signal processing technique and has clearly demonstrated the use of an analogue-to-digital conversion board in the acquisition of soil generated acoustic emission.

Two field studies have been conducted. One was a naturally eroding section of coastal cliff at the Building Research Establishment's test site in Cowden and the other was an artificial large scale test in which a cut slope in a 'moth-balled' brickpit was destabilised by physically cutting the toe. The combined results from these two investigations suggest that the technique *can* be used to detect and monitor the development of first time deformation mechanisms.

It has been demonstrated that (for this investigation) the active wave guide model is the more appropriate when attempting to explain the generation of acoustic emission in the field. It is considered that this has implications for the design of wave guide most suited to a particular geotechnical situation. Sand and gravel backfilled wave guides were the most responsive. Although other wave guide designs generated acoustic emission, there was little correspondence with measured deformation. In particular, gravel backfilled wave guides appear to generate (relatively) high magnitude emission over a short time-scale whereas sand backfilled wave guides appear to generate (relatively) low magnitude emission over a long time scale. The results of a number of laboratory based 'box' tests, which were designed to replicate the perceived role of the active wave guide in the field, support these findings. Furthermore, it has been shown that acoustic emission can be used to detect, and differentiate between, a gradual deterioration in slope stability and a larger, more sudden

interference in the equilibrium of the slope. It is also evident that, while standard methods of deformation monitoring (i.e. inclinometers) indicate such small magnitudes of deformation have occurred as to be indistinguishable from instrument error, significant acoustic emission can be detected.

At each site a control wave guide was employed in order to determine the background noise level. The intention was to use the acquired background noise level to equilibrate AE data captured on different days in order that they would then be directly comparable. In fact both field studies indicated that (using a 30kHz peak resonant transducer) background noise was not a problem (although wind blown debris colliding with a wave guide and generating erroneous emission may be). This is an important finding as it implies that stability monitoring can be accomplished with reference to gauge wave guides only. It should be appreciated that it is still necessary to check (prior to acquisition) that the AE system's sensitivity has remained constant and other considerations (such as earthing conditions) are unaltered. However, this can be accomplished without the need to install and monitor a control wave guide outside the zone of deformation and eliminates the need to equilibrate alternate days AE data.

It was a consideration of acoustic emission detected from the control wave guide, in conjunction with that detected from the gauge wave guides, which lead to the identification of 'constructional' noise. This was generated as a result of the wave guide design and has nothing to do with slope deformation mechanisms.

It has also been clearly demonstrated that the technique used to process the acquired data could have a profound effect on the apparent response of the signal to periods of deformation. As with wave guide design, the technique used needs to reflect the geotechnical situation under consideration. It has been shown that the mean magnitude of a 'bulk' sample of acoustic emission data is sensitive to slow and gradual deformation, whereas the standard deviation of a 'post-threshold' data sample is most responsive to sudden disturbances in the equilibrium. Further forms of processing, such as amplitude distribution analysis, appear to confirm that a single mechanism (i.e. wave guide - backfill interaction) was responsible for the generation of the emission.

8.2 Laboratory Investigation

The main aim of the series of triaxial shear tests conducted was to characterise AE generated from soil material in a state of stress. It has been shown that the level of the acoustic emission is related both to the effective stress and the mineralogy and grading of the soil. However, it is likely that the relationship between these two factors and emission generation is highly complex owing to the behaviour of soil particles when subjected to shear. Using an analogue-to digital conversion board which *is* capable of triggering 'on the event', it should be possible to capture every emission and to relate it to the state of strain of the soil sample. Additionally, however, if alternative modes of particle response (to shear) generate emission which are of a different character then it would also be possible to determine the mode *and* relate it to the state of strain of the soil sample. In this respect, it is considered that acoustic emission has a great deal of potential as a research tool in the laboratory.

8.3 Future Work

In section 3.4, concerning monitoring philosophy, it was commented that ... *It is highly likely, therefore, that much deformation-related emission was not captured simply because no operator was present when it was generated.* This point acknowledged the fact that the method of making periodic site visits to acquire AE data probably effected the loss of a large volume of genuine deformation-related AE. It is fairly evident, therefore, that a major improvement would be the design of a *continuous* monitoring system, where all deformation-related AE would be captured. Such a system could be investigated using the findings of this research with the aim of developing the following applications.

- The provision of an immediate response (acting as an early warning system) to a sudden disturbance in the stability of a soil slope.
- A means of monitoring gradual changes in the stability of a soil slope.

The particular data processing technique used would be dependant upon the final capture system. However, the findings of this investigation suggest that it is possible to distinguish

between periods of activity and inactivity by processing AE data captured from a single wave guide in two alternate ways and comparing the results. This was illustrated in figure 6.11 which showed the standard deviation of both 'bulk' and 'post-threshold' data for Arlesey WG2. (Additionally, there are further examples where AE data captured from multiple wave guides has been shown to be coincident in the pre-test period but divergent within the test period. For example see figures 5.29 and 5.31)

Having determined that deformation *is* occurring, it may then be possible to distinguish the particular mechanism responsible by considering, for example, the mean value of the data ('bulk' or 'post-threshold') or the number of post-threshold data points. It should be appreciated that, at this stage, it is not possible to determine what constitutes a high or low mean value or a large or small number of data points. This, together with *quantification* of the AE data, requires further investigation if a working AE system is to be produced.

However the findings of this study suggest that it is possible to develop a system which, without reference to a control wave guide, would be able to indicate when activity was occurring and determine the mechanism responsible.

References

- Beard FD (1961). Predicting Slides in Cut Slopes. *Western Construction*, 72.
- Bell AG & Forster A (1991). The Geotechnical Characteristics of the Till Deposits of Holderness. *Quaternary Engineering Geology, Geological Society Engineering Geology Special Publication*, No. 7, 111-118.
- Bishop AW & Eldin G (1950). Undrained Triaxial Tests on Saturated Sands and their Significance in the General Theory of Shear Strength. *Géotechnique*, Vol 2, 13.
- Bishop AW & Wesley LD (1975). A Hydraulic Triaxial Apparatus for Controlled Stress Path Testing. *Géotechnique*, Vol 25, No. 4, 657-670.
- Blystra AR (1990). Using Acoustic Emission Testing in Seepage Investigations. *The International Joint Meeting, 1st Workshop on Acoustic Emission in Civil Engineering and 2nd Workshop on AE and Rock Fracture Mechanics*, Kumamoto, Japan, October, S49-S54.
- Blystra AR (1994). Acoustic Emission of Ground Water Flow. *Progress in Acoustic Emission VII, The Japanese Society for NDI*, Sapporo, Japan, 437-443.
- Bray D & Stanley RK (1997). Non-Destructive Evaluation, Revised Edition. *CRC Press*.
- Butcher AP (1991). The observation and analysis of a failure in a cliff of glacial till at Cowden, Holderness. *Slope Stability Engineering*, Thomas Telford, 271-276.
- Cadman JD & Goodman RE (1967). Landslide Noise. *Science*, Vol 15, 1182-1184.
- Chichibu A, Jo K, Nakamura M, Goto T & Kamata M (1989). Acoustic Emission Characteristics of Unstable Slopes. *Journal of Acoustic Emission* Vol 8, No. 4, 107-112.
- Coulomb CA (1776). Essais sur une application des regles des maxims et minimis a quelques problemes de statique relatifs a l'architecture. *Mémoires Académie Royale des Sciences*, Paris, 7:353A-353C.
- Deutsch WL, Koerner RM & Lord jnr AE (1989). Determination of Pre-Stress of In Situ Soils Using Acoustic Emissions. *Journal of Geotechnical Engineering*, Vol 115, No. 2, 228-245.
- Dixon N, Hill R & Kavanagh J. (1994). Acoustic Emission Techniques for Assessing Deformations in Soils. *International Symposium on Pre-Failure Deformation Characteristics of Geomaterials*, Sapporo, Japan, Vol 1, 253-258.
- Dixon N, Hill R & Kavanagh J (1996a). The Use of Acoustic Emission to Monitor the Stability of Soil Slopes. *International Conference on Advances in Site Investigation Practice*, ICE, London, March 1995, 739-749.
- Dixon N, Kavanagh J & Hill R (1996b). Monitoring Landslide Activity and Hazard by Acoustic Emission. *3rd Sino-British Geological Conference*, Taiwan, March, 40.

Evans BM (1981). AE Application to Civil Engineering Work. *Proc. 3rd Conference on Acoustic Emission/Microseismic Activity in Geological Structures & Materials*, Pennsylvania, 1981, 303-318.

Fisher CP & Yorke CA (1964). The Detection and Interpretation of Microseisms in Soil Masses. *Symposium on Soil Exploration, ASTM STP 351*, 121-131.

Garga VK & Chichibu A (1990). A Study of AE Parameters and Shear Strength of Sand. *Progress in Acoustic Emission V, The Japanese Society for NDI*, 129-136.

Goodman RE & Blake W (1966). Rock Noise in Landslides and Slope Failures. *Highway Research Record*, Vol 119, 50-60.

Hakuno M, Ogawara S & Hoshizume T (1968). Analysis of noise generated by sand particles when they slide. *Proc. Japan Society of Civil Engineers*, No. 164, 51-58.

Hardin BO & Richart FE (1963). Elastic Wave Velocities in Granular Soils. *Journal of the Soil Mechanics & Foundations Div., Proc. ASCE*, Vol 89, No. SM1, 33-65.

Hardin BO (1965). The Nature of Damping in Sands. *Journal of Soil Mechanics & Foundations Division, Proc. ASCE*, Vol 91, No. SM1, 63-97.

Hardy HR, Taioli F & Hager ME (1989). Use of Mechanical Waveguides and Acoustic Antennae in Geotechnical AE/MS Studies. *World Meeting on Acoustic Emission, Special Supplement, Journal of Acoustic Emission*, Vol 8, No. 1-2, S42-S48.

Hardy HR (1989). A Review of International Research Relative to the Geotechnical Field Application of Acoustic Emission/Microseismic Techniques. *Journal of Acoustic Emission*, Vol 8, Number 4

Hardy HR (1992). Laboratory Studies relative to the development of Mechanical Waveguides for Acoustic Emission Monitoring of Geologic Structures. *Italian Journal of Non-Destructive Testing & Diagnostics*, Vol XIII, No. 2, 32-38.

Hardy HR (1994). Geotechnical Field Applications of AE/MS Techniques at the Pennsylvania State University: a historical review. *NDT & E International 1994* Vol 27, No 4

Hill R, Dixon N & Kavanagh J (1994). Experience in Using Acoustic Emission to Monitor Soil Failure in the Laboratory and in the Field. *Progress in Acoustic Emission VII, Japanese Society for NDI*, Sapporo, Japan, S35-S39.

Horn HM & Deere DU (1962). Frictional Characteristics of Minerals. *Géotechnique*, Vol 12, 319-335.

Huck PJ, Koerner RM (1981). Acoustic Emission Monitoring of Soil and Rock Grouting. *Acoustic Emissions in Geotechnical Engineering Practice, ASTM STP 750, VP Drnevich & RE Gray Eds., American Society for Testing & Materials*, 155-163.

Jackson AL (1986). Acoustic Emission and Yield in Sand. *PhD Thesis at University of Aston, Birmingham*, (unpublished).

Koerner RM & Lord jnr AE (1972). Acoustic Emissions in Medium Plasticity Clayey Silt. *Journal Soil Mechanics & Foundations Division, Proc. ASCE*, Vol 98, No. SM1, 161-165.

Koerner RM & Lord jnr AE (1974). Acoustic Emissions in Stressed Soil Samples. *Journal Acoustical Society of America*, Vol 56, No. 6, 1924-1927.

Koerner RM, Lord jnr AE & McCabe WM (1975). Acoustic Emission Studies of Soil Masses in the Laboratory and Field. *Proc. of the 1st Conference on Acoustic Emission/Microseismic Activity in Geologic Structures & Materials*, 243-256

Koerner RM, Lord jnr AE, McCabe WM & Curran JW (1976). Acoustic Emission Behaviour of Granular Soils. *Journal of the Geotechnical Engineering Division, Proc. of the ASCE*, Vol 102, No. GT7, 761-773.

Koerner RM, Lord jnr AE & McCabe WM (1977). Acoustic Emission Behaviour of Cohesive Soils. *Journal of the Geotechnical Engineering Division, Proc. of the ASCE*, Vol 103, No. GT8, 837-850.

Koerner RM, Lord jnr AE & McCabe WM (1978a). Acoustic Emission Monitoring of Soil Stability. *Journal of the Geotechnical Engineering Div., Proc. ASCE*, Vol 104, No. GT5, 571-582.

Koerner RM, Lord jnr AE & McCabe WM (1978b). Acoustic Emission (Microseismic) Monitoring of Earth Dams. *Journal of the Geotechnical Engineering Div., Proc. ASCE*, Vol 104, No. GT5, 274-291.

Koerner RM, Reif JS & Burlingame MJ (1979). Detection Methods for Location of Subsurface Water and Seepage. *Journal Geotechnical Eng Div., Proc. ASCE*, Vol 105, No. GT11, 1301-1316.

Koerner RM, McCabe WM & Lord jnr AE (1981a). Acoustic Emission Behaviour and Monitoring of Soils. *Acoustic Emission in Geotechnical Practice, ASTM STP 750, American Soc. for Testing and Materials*, 93-141.

Koerner RM, McCabe WM & Baldivieso LF (1981b). Acoustic Emission Monitoring of Seepage. *Journal Geotechnical Eng., ASCE*, Vol 107, No. GT4, 521-526.

Koerner RM, Lord jnr AE & Deutsch WL (1984a). Determination of Prestress in Granular Soils Using AE. *Journal of Geotechnical Eng., ASCE*, Vol 110, No. 3, 346-358.

Koerner RM, Lord jnr AE & Deutsch WL (1984b). Determination of Prestress in Cohesive Soils Using AE. *Journal of Geotechnical Eng., ASCE*, Vol 110, No. 11, 1537-1548.

Koerner (1986). Acoustic Emission Monitoring of Land Subsidence. *Land Subsidence*, Vol 151, Ch 86, 225-234.

Lord jnr AE & Koerner RM (1974). Acoustic Emission Response of Dry Soils. *Journal of Testing and Evaluation*, Vol 2, No.3, 159-162.

- Lord jnr AE, Koerner RM, Curran JW (1977). Fundamental Studies of Acoustic Emissions in Soils. *Proceedings of 1st Conference on AE/MA in Geologic Structures and Materials*, Pennsylvania, June 1975, 135-148.
- Lord jnr AE & Koerner RM (1975). Acoustic emission in soils and their use in assessing earth dam stability. *Journal Acoustical Society America*, Vol 57, No. 2, 516-519.
- Lord jnr AE & Koerner RM (1979). Estimated Magnitude of Acoustic Emission in Soil. *Journal of the Geotechnical Engineering Div., Proc. ASCE*, Vol 105, No. GT10, 1249-1253.
- Lord jnr AE, Fisk CL & Koerner RM (1982). Utilisation of Steel Rods as AE Waveguides. *Journal of the Geotechnical Engineering Division, Proceedings of the ASCE*, Vol 108, No. GT2, 300-305.
- Lord jnr AE & Koerner RM (1983). An Acoustic Pressuremeter to Determine In Situ Soil Properties. *Journal of Acoustic Emission*, Vol 2, No. 3, 187-190.
- Lord jnr AE & Koerner RM (1985). Field Determination of Prestress (Existing Stress) in Soil and Rock Masses Using Acoustic Emission. *Journal of Acoustic Emission*, Vol 4, S11 - S16.
- Madgett PA & Catt JA (1978). Petrography, stratigraphy and weathering of late Pleistocene tills in east Yorkshire, Lincolnshire and north Norfolk. *Proceedings of the Yorkshire Geological Society*, 42, 55-108.
- Marsland A & Powell JJM (1985). Field and Laboratory Investigations of the Clay Tills at the BRE Test Site at Cowden, Holderness. *Proc. Int. Conference Construction in Glacial Tills*, Edinburgh.
- McCauley ML (1977). Monitoring Slope Stability with Acoustic Emission. *Proc. 1st Conference on Acoustic Emission/Microseismic Activity in Geologic Structures and Materials*, Pennsylvania, June 1975, 257-269.
- Menzies BK (1988). A Computer Controlled Hydraulic Triaxial Testing System. *Advanced Triaxial Testing of Soil and Rock, ASTM STP 977, Robert T Donaghe, Ronald C Chaney and Marshall L Silver Eds., American Society for Testing and Materials*, Philadelphia, 82-94.
- Mitchell RJ & Romeril PM (1984). Acoustic emission distress monitoring in sensitive clay. *Canadian Geotechnical Journal*, Vol 21, 176-180.
- Nakajima I, Negishi M, Ujihira M & Tanabe T (1995). Application of the Acoustic Emission Monitoring Rod to Landslide Measurement. *Proc. 5th Conference on Acoustic Emission/Microseismic Activity in Geologic Structures and Materials*, Pennsylvania, June 1991, 505-520.
- Nakamura Y (1977). Detection and Analysis of Acoustic Emission Signals. *Proc. of 1st Conference on Acoustic Emission/Microseismic Activity in Geologic Structures and Materials*, Pennsylvania, June 1975, 445-457.

- Naemura S, Tanaka M, Nishikawa S, Nakamura M, Jo K & Kishishita T (1990). Acoustic Emission of Penetration Experiments to Judge Soil Condition. *The International Joint Meeting, 1st Workshop on Acoustic Emission in Civil Engineering and 2nd Workshop on AE and Rock Fracture Mechanics*, Kumamoto, Japan, October, S55-S58.
- Nyborg WL, Rudnick I & Schilling HK (1950). Experiments on Acoustic Absorption in Sand and Soil. *Journal of the Acoustical Society of America*, Vol 22, No. 4, 422-425.
- Penning A, van der Kogel H, Koerner RM & Schenkeveld FM (1983). Acoustic Emissions During Slope Failure. *International Symposium on Field Measurements in Geomechanics*, Zurich, September, 749-763.
- Rouse C, Styles P & Wilson SA (1991a). Acoustic Emission from two Landslip Areas in South Wales. *Z. Geomorph. N.F., Suppl.-Bd.83*, 135-154.
- Rouse C, Styles P & Wilson SA (1991b). Microseismic emissions from flowslide-type movements in South Wales. *Engineering Geology*, 31, 91-110.
- Samuels SG (1975). Some Properties of the Gault Clay from the Ely-Ouse Essex water tunnel. *Géotechnique* 25, No. 2, 239-264.
- Shiotani T, Fujii K, Aoki T & Amou K (1994). Evaluation of Progressive Failure using AE Sources/Improved B-Value on Slope Model Tests. *Progress in Acoustic Emission VII, The Japanese Society for NDI*, Sapporo, Japan, S29-S34.
- Skinner AE (1969). A Note on the Influence of Interparticle Friction on the Shearing Strength of a Random Assembly of Spherical Particles. Technical Note *Géotechnique* (source details incomplete)
- Styles P, Rouse C & Wilson S (1988). Microseismic Monitoring of Landslip Movement in South Wales. *Welsh Office Research Contract Report: WEP/100/154/2*, 120 pages.
- Tanimoto K & Noda T (1977). A Study of Acoustic Emission from Sandy Soils. *Proc. 9th Int. Conference on Soil Mechanics & Foundation Eng.*, Vol 1, 315-318.
- Tanimoto K, Nishi M & Noda T (1978). A Study of Shear Deformation Process of Sandy Soils by the Observation of Acoustic Emission Response. *Proc. 2nd Conference. on Microzonation*, Vol 2, 971-982
- Tanimoto K, Nakamura J & Fudo R (1981). Application of Acoustic Emission in In-Situ Test. *Proc. 10th Int. Conf. on Soil Mech. & Found. Eng.*, Vol 2, 573-576.
- Tanimoto K & Nakamura J (1981a). Studies of Acoustic Emission in Soils. *Acoustic Emissions in Geotechnical Engineering Practice, ASTM STP 750, VP Drnevich & RE Gray, Eds., American Society for Testing & Materials*, 164-173.
- Tanimoto K & Nakamura J (1984). Use of AE Technique in Field Investigation of Soil. *3rd Conference on Acoustic Emission/Microseismic Activity in Geologic Structures & Materials*, Pennsylvania 1981, 601-612.

Villet WCB, Mitchell JK & Tringale PT (1981). Acoustic Emissions Generated During the Quasi-Static Cone Penetration of Soils. *Acoustic Emissions in Geotechnical Engineering Practice, ASTM STP 750, VP Drnevich & RE Gray, Eds., American Society for Testing & Materials*, 174-193.

Wood BRA & Harris RW (1990). Acoustic Emission Monitoring during Microseismic Activity Caused by Mine Subsidence. *The International Joint Meeting, 1st Workshop on Acoustic Emission in Civil Engineering and 2nd Workshop on AE and Rock Fracture Mechanics*, Kumamoto, Japan, October, S29-S34.

Yuda S, Hashimoto Y, Takahashi K, Kumagai DC, Doboku Chishitsu KK, Niitsuma H & Chubachi N (1984). Prediction of Slope Failure by Acoustic Emission Technique. *Proc 7th International AE Symposium*, Japan, 660-667.

Published Papers

The following five published papers relate to work described within this thesis

Dixon N, Hill R & Kavanagh J. (1994). Acoustic Emission Techniques for Assessing Deformations in Soils. *International Symposium on Pre-Failure Deformation Characteristics of Geomaterials*, Sapporo, Japan, September, Vol 1, 253-258.

Dixon N, Hill R & Kavanagh J. (1996). The Use of Acoustic Emission to Monitor the Stability of Soil Slopes. *International Conference on Advances in Site Investigation Practice, ICE*, London, March 1995, 739-749.

Dixon N, Kavanagh J & Hill R. (1996). Monitoring Landslide Activity and Hazard by Acoustic Emission. *3rd Sino-British Geological Conference*, Taiwan, March, 40

Hill R, Dixon N & Kavanagh J. (1994). Experience in Using Acoustic Emission to Monitor Soil Failure in the Laboratory and in the Field. *Progress in Acoustic Emission VII, Japanese Society for NDI*, Sapporo, Japan, 535-539.

Hill R, Dixon N & Kavanagh J (1996). Monitoring Deformation of Soil Slopes Using AE: Case Histories. *6th Conference on Acoustic Emission/Microseismic Activity in Geological Structures and Materials*, Pennsylvania, June, (In Press) [Not Included]

The five published papers pertaining to the work in this thesis present details of the field and laboratory studies conducted (predominantly by J Kavanagh) between September 1992 and September 1995. Data acquisition, data processing and interpretation of the results were primarily the responsibility of J Kavanagh and J Kavanagh was involved in the discussions with the other authors which resulted in the publications.